

add. No. C-3911

VOL. 31

INDIAN JOURNAL OF PHYSICS

No. 1

(Published in collaboration with the Indian Physical Society)

AND

VOL. 40

PROCEEDINGS

No. 1

OF THE

INDIAN ASSOCIATION FOR THE
CULTIVATION OF SCIENCE

JANUARY, 1957

PUBLISHED BY THE
INDIAN ASSOCIATION FOR THE CULTIVATION OF SCIENCE

JADAVPUR, CALCUTTA 32

BOARD OF EDITORS

R. K. ASUNDI	S. N. BOSE
K. BANERJEE	S. K. MITRA
D. M. BOSE	P. RAY
K. R. DIXIT	K. R. RAO
P. S. GILL	S. C. SIKKAR (<i>Secretary</i>)

B. N. SRIVASTAVA

EDITORIAL COLLABORATORS

PROF. D. BASU, Ph.D.

DR. A. BOSE, D.Sc.

DR. N. N. DASGUPTA, M.Sc., Ph.D.

PROF. A. K. DUTTA, D.Sc., F.N.I.

DR. S. GHOSH, D.Sc.

DR. S. R. KHASTOIR, D.Sc., F.N.I., F.R.S.E.

PROF. P. K. KICHLU, D.Sc., F.N.I.

PROF. D. S. KOTHARI, D.Sc., F.N.I.

DR. K. S. KRISHNAN, D.Sc., F.R.S.

PROF. B. D. NAG CHOWDHURY, Ph.D.

PROF. S. R. PALIT, D.Sc., F.R.I.C., F.N.I.

DR. S. PARTHASARATHY, D.Sc., F.N.I.

DR. H. RAKSHIT, D.Sc., F.N.I.

DR. R. GOPALAMURTY RAO.

DR. VIKRAM A. SARABHAI, M.A., Ph.D.

PROF. N. R. TAWDE, D.Sc., F.N.I.

ASSISTANT EDITOR

MR. A. N. BANERJEE, M.Sc.

Annual Subscription—

Inland Rs. 20

Foreign £ 2

NOTICE TO INTENDING AUTHORS

Manuscripts for publication should be sent to the Assistant Secretary, Indian Journal of Physics, Jadavpur, Calcutta 32.

The manuscripts submitted must be type-written with double space on thick foolscap paper with sufficient margin on the left and at the top. The original copy, and not the carbon copy, should be submitted. Each paper must contain an abstract at the beginning.

All references should be given the text by quoting the surname of the author, followed by year of publication, e.g., (Ghosh, 1954). The full reference should be given in a list at the end, arranged alphabetically, as follows: Ghosh, D. K., 1954, *Ind. J. Phys.*, 28, 485.

Line diagrams should be drawn on white Bristol board or tracing paper with black India ink, and letters and numbers inside the diagrams should be written neatly in capital type with India ink. The size of the diagrams submitted and the lettering inside should be large enough so that it is legible after reduction to one-third the original size. A simple style of lettering such as gothic, with its uniform line width and no serifs should be used, e.g.,

A·B·E·F·G·M·P·T·W·

Photographs submitted for publication should be printed on glossy paper with somewhat more contrast than that desired in the reproduction, and should, if possible, be mounted on thick white paper.

Captions to all figures should be typed in a separate sheet and attached at the end of the paper.

The mathematical expressions should be written carefully by hand. Care should be taken to distinguish between capital and small letters and superscripts and subscripts. Repetition of a complex expression should be avoided by representing it by a symbol. Greek letters and unusual symbols should be identified in the margin. Fractional exponents should be used instead of root signs.

INDIAN JOURNAL OF PHYSICS

VOL. 31

AND

PROCEEDINGS

OF THE

Indian Association for the Cultivation of Science, Vol. 40

(Published in Collaboration with the Indian Physical Society)

(With Twenty Plates)

Printed by Kalipada Mukherjee, Eka Press, 204/1. B. T. Road, Calcutta
and published by the Registrar, Indian Association for the Cultivation
of Science, Jadavpur, Calcutta 32

1957

Price Rs. 20 or £2

BOARD OF EDITORS

R. K. ASUNDI	P. S. GILL
K. BANERJEE	S. K. MITRA
D. M. BOSE	P. RAY
S. N. BOSE	K. R. RAO
K. R. DIXIT	S. C. SIKKAR (<i>Secretary</i>)
B. N. SRIVASTAVA	

EDITORIAL COLLABORATORS

PROF. D. BASU, Ph.D
DR. A. BOSE, D.Sc.
DR. N. N. DASGUPTA, M.Sc., Ph.D.
PROF. A. K. DUTTA, D.Sc., F.N.I.
DR. S. GHOSH, D.Sc
DR. S. R. KHASTGIR, D.Sc., F.N.I., F.R.S.E.
PROF. P. K. KICHLU, D.Sc., F.N.I.
PROF. D. S. KOTHARI, D.Sc., F.N.I.
DR. K. S. KRISHNAN, D.Sc., F.R.S.
PROF. B. D. NAG CHOWDHURY, Ph.D.
PROF. S. R. PALIT, D.Sc., F.R.I.C., F.N.I.
DR. S. PARTHASARATHY, D.Sc., F.N.I.
DR. H. RAKSHIT, D.Sc., F.N.I.
DR. R. GOPALAMURTY RAO.
DR. VIKRAM A. SARABHAI, M.A., Ph.D.
PROF. N. R. TAWDE, D.Sc., F.N.I.
DR. P. VENKATESWARLU.

ASSISTANT EDITOR

SRI. A. N. BANERJEE, M.Sc.

Annual Subscription—

Inland Rs. 20

Foreign £ 2

NOTICE

TO INTENDING AUTHORS

Manuscripts for publication should be sent to the Assistant Secretary, Indian Journal of Physics, Jadavpur, Calcutta 32.

The manuscripts submitted must be type-written with double space on thick foolscap paper with sufficient margin on the left and at the top. The original copy, and not the carbon copy, should be submitted. Each paper must contain an abstract at the beginning.

All references should be given in the text by quoting the surname of the author, followed by year of publication, e.g., (Ghosh, 1954). The full reference should be given in a list at the end, arranged alphabetically, as follows; Ghosh, D. K., 1954, *Ind. J. Phys.*, **28**, 485.

Line diagrams should be drawn on white Bristol board or tracing paper with black India ink, and letters and numbers inside the diagrams should be written neatly in capital type with India ink. The size of the diagrams submitted and the lettering inside should be large enough so that it is legible after reduction to one-third the original size. A simple style of lettering such as gothic, with its uniform line width and no serifs should be used, e.g.,

A·B·E·F·G·M·P·T·W·

Photographs submitted for publication should be printed on glossy paper with somewhat more contrast than that desired in the reproduction, and should, if possible, be mounted on thick white paper.

Captions to all figures should be typed in a separate sheet and attached at the end of the paper.

The mathematical expressions should be written carefully by hand. Care should be taken to distinguish between capital and small letters and superscripts and subscripts. Repetition of a complex expression should be avoided by representing it by a symbol. Greek letters and unusual symbols should be identified in the margin. Fractional exponents should be used instead of root signs.

INDIAN JOURNAL OF PHYSICS. VOL. 31, 1957

CONTENTS

No. 1. January

	PAGE
1. The Crystal Structure of Diphenyl at Different Temperatures —By G. S. R. Krishna Murti	1
2. The Equations of Motion of an Incompressible Viscous Fluid in the Parallel System of Coordinates—By Lakshmi Sanyal .	6
3. Ultraviolet Absorption Spectra of Isomeric Picolines in the Liquid and Solid States—By S. B. Banerjee	11
4. Fading and Random Motion of Ionospheric Irregularities—By S. N. Mitra and R. B. L. Srivastava	20
5. Recombination Coefficient and Electron Production Rate from total Electron Content in Unit Column below the Level of Maximum Ionisation—By S. Datta	43
6. Fast Coincidence with Fast Discriminators—By Rangalal Bhatta- charyya and Santimay Chatterjee	53

LETTERS TO THE EDITOR

1. Elastic and Inelastic Scattering of High Energy Electrons by some 2p-Shell Nuclei on the Intermediate Coupling Model—By M. K. Pal, S. Mukherjee and A. K. Saha	56
2. Dipole Moments of Tri-Substituted Benzenes Part II—By D. V. G. L. Narasimha Rao	60

No. 2. February

7. Electrical Oscillations in A. C. Discharge—By M. B. Karnik ..	61
8. Investigation of Discrete Sources of Radiation from Solar Eclipse Observations—By (Mrs.) Nilma Mitra	69
9. Further Studies on Asymmetrical Three Phase Oscillator for very Wide Frequency Deviation—By P. Kundu	83
10. Ultraviolet Absorption Spectra of a few Disubstituted Benzenes in Different States—By S. K. Sen	99
11. Variation in Lattice Constant in Thin Films of Gold—By S. N. Chatterjee	110
12. Epitaxial Growth of thin Evaporated Metallic Films on Cleavage Surfaces of Alkali Halides and other Crystals—By K. R. Dixit .	117

No. 3. March

13. R-C Network Analogue—By A. K. Choudhury and B. R. Nag ..	121
14. Ultraviolet Absorption Spectra of Ortho- and Para-Chloroanisole in the Liquid and Solid states—By S. B. Banerjee	135

15. X-Ray Analysis of Structure of Frozen Toluene and its Solution in Alcohol at -180°C —By S. G. Biswas and S. C. Sirkar ..	141
16. Transport Coefficients and Force between Unlike Molecules—By S. C. Saxena	146
17. Emission Spectra of Mixed Halogens. Part 1: ICl—By P. B. V. Haranath and P. Tiruvenganna Rao	156

LETTERS TO THE EDITOR

3. Study of Rectifying Characteristics of FeS_2 and Germanium Point Contact Rectifiers—J. N. Das	172
4. New Emission Spectrum of Chlorine in the Schumann Region—P. B. V. Haranath and P. Tiruvenganna Rao	175

No. 4. April

18. On the Ultraviolet Absorption Spectra of Frozen Solutions of Dichlorobenzenes in Isobutyl Alcohol—By S. B. Roy and S. C. Sirkar ..	177
19. On the Design of Four-Terminal Interstages for Pulse Application—By A. K. Choudhury and N. B. Chakrabarti	193
20. A Nuclear Induction Spin-Echo Apparatus—By B. M. Banerjee, S. K. Ghosh and A. K. Saha	211
21. Ultrasonic Velocity of Sodium Chloride Solution in Water-Dioxene Mixtures—By Srimbas Panda and Bibhuti Bhusan Deo ..	227
22. A New Method of Demodulation for Phase Frequency and Amplitude—By P. Kundu	231

No. 5. May

23. An Application of Lipson's Method in the Study of the Crystal System of BaBOF_3 —By D. M. Chackraburttty	235
24. Sommerfeld's Fine-Structure Formula from Five Dimensional Wave-Equation—By C. C. Banerjee	242
25. Apparent Separation and Intensity Ratio of Close Spectral Lines—By K. C. Chaturvedi	247
26. Dipole Moments of some Substituted Benzenes and Pyridines. Part I—Fluorotoluenes—By C. R. K. Murty	256
27. Improved Performance of Photomultipliers in Scintillation Counters—By A. Ashmore, B. Collinge and S. K. Sen	261
28. Spin Echoes with Four and More Pulses—By T. Ghose, S. K. Ghosh and D. K. Roy	265
29. Slots in an Imperfectly Conducting Waveguide—By B. Chatterjee ..	278

LETTER TO THE EDITOR

5. Dipole Moments of Some Esters—K. V. Gopala Krishna ..	283
--	-----

Contents

iii

No. 6. June

30. Measurement of Thermal Neutron Absorption Cross Section using Spherical Symmetry Method—By A. M. Ghosh and N. K. Ganguly	285
31. Models of the Lower Ionosphere as may be inferred from Absorption Results—By P. Bandyopadhyay	297
32. Solar Eclipse of 30th June, 1955 and its Effect upon the Ionosphere—By S. N. Mitra	309
33. X-Ray Diffraction Study of the Heat Treatment of Kaolinite — By G. B. Mitra	324
34. Branching Ratio for Slow Neutrons—By Madan Lall Sehgal	329

LETTERS TO THE EDITOR

6. Induction Drag—K. P. Chopra	332
7. Dipole Moments of Tri-Substituted Benzenes. Part III—D. V. G. L. Narasimha Rao	334

BOOK REVIEW

1. Relaxation Spectrometry—By E. G. Richardson	335
2. Progress in Cosmic Ray Physics, Vol. III—By J. G. Wilson	335

No. 7. July

35. Charge Transfer Reactions—By S. N. Ghosh and W. F. Sheridan	337
36. The Crystal Structure of <i>p</i> -Nitroaniline at Different Temperatures—By G. S. R. Krishna Murti	353
37. Electronic Spectra of Benzylamine and Isobutyl Benzoate in Different States at Different Temperatures—By S. B. Banerjee	359
38. Emission Spectra of Mixed Halogens. Part II. IBr and BrCl—By P. B. V. Haranath and P. Tiruvenganna Rao	368
39. Excitation of the Spectrum of the Sunlit Aurora—By Prabhat K. Sen Gupta	376

LETTERS TO THE EDITOR

8. A New Particle Accelerator—Yatendra Pal Varshni	384
9. The Ultraviolet Absorption Spectra of <i>o</i> , <i>m</i> , <i>p</i> -Fluoriodo-and Bromochlorobenzenes—S. L. N. G. Krishnamachari	387

BOOK REVIEW

3. Techniques Generales du Laboratoire de Physique—By J. Surugue	390
--	-----

No. 8. August

40. A Note on the Validity of the Revised Rotational Structure Constants of Green-Yellow System of VO Bands—By N. R. Tawde and N. Sreedhara Murthy	391
41. Raman Spectra of Isomeric Picolines in Different States and in Solutions of Ethyl Alcohol at Different Temperatures—By G. S. Kastha	395

42. Force Constants for like Molecules on Exp-Six Model from Thermal Conductivity—By K. P. Srivastava	404
43. n-p and p-p Scattering from Case-Pais Model in the Energy-Range 91 Mev to 437 Mev—By S. Mukherjee and M. K. Pal	415
44. Analysis of Cathode-Coupled free Running Multivibrator—By D. C. Sarkar	431

No. 9. September

45. A Deviation from Wilkinson's Theory of Discharge Spread in Geiger-Counters—By Satyapal Puri	441
46. Analysis of the Near Ultraviolet Absorption Spectra of Ortho, Meta and Para-Fluorochlorobenzene Vapours—S. L. N. G. Krishnamachari	447
47. Crystal Structure and Magnetic Susceptibility of Rectifying Cuprous Oxides—By K. R. Dixit and V. V. Agashe	466
48. Electronic Spectra of Trichlorobenzenes in the Liquid State and in the Solid State at -180°C —By S. B. Banerjee	483

No. 10. October

49. Theoretical Calculations of Transition Probabilities in the First Negative ($\delta^4\Sigma_g \rightarrow \alpha^4\Pi_u^-$) Bands of O_2^+ —By S. P. Rao and J. D. Ranade	491
50. Analysis of the Near Ultraviolet Absorption Spectra of α - and β -Fluoronaphthalenes—By S. Ramamurty, M. Jagannadha Rao and V. Ramakrishna Rao	497
51. On the p-p Scattering at High Energies—By A. Das	511
52. Solar Tidal Effects in the F_2 -Region of Ionosphere over Delhi—By C. S. Raghavendra Rao	516
53. Anomalous Magnetic Moments of Proton and Neutron—By S. K. Kundu	526
54. Design of Continuous Baffle in a Short Lens Beta-Ray Spectrometer—By P. N. Mukherjee, M. K. Pal, M. K. Banerjee and A. K. Saha	531

LETTER TO THE EDITOR

10. On Optical Method of Measuring Convective Air Velocity—H. N. Patil	539
--	-----

No. 11. November

55. An Accurate Phase Meter for Four-Terminal Networks—By B. Chatterjee	541
56. Scattering of 9.5 Mev Protons by Nitrogen—By Anwar Hossain and A. N. Kamal	553

Contents

v

57. Ultrasonic Velocity in Cobalt and Cadmium Sulphate Solutions at Different Temperatures and Concentrations—By Srinibas Panda and Braja Sundar Mohanty	560
58. Photoionization versus Photoelectric Effect for Discharge Spread and Output Pulse Measurements in G-M Counters—By P. S. Gill and S. P. Puri	564
59. On the X-Ray Diffraction Pattern and Micellar Dimensions of some Substitutes of Jute Fibre—By S. K. Chowdhury	572
60. Absorption Spectra of Chloroanilines—By P. B. V. Haranath and K. Sree Ramamurthy	577
61. Ultraviolet Absorption Spectra of 1, 3, 5-Trichlorobenzene and 1, 3, 5-Trimethyl-Benzene in Different Solvents and at different Temperatures—By S. B. Roy	588

No. 12. December

62. Thermal Conductivity of Binary and Ternary Mixtures of Helium, Argon and Xenon—By S. C. Saxena	597
63. Optical and Electrical Methods of Measuring Thicknesses of Thin Metallic Films—By Y. G. Naik and E. M. Balsara	607
64. The Crystal Structure of Anthranilic Acid at Different Temperatures—By G. S. R. Krishna Murti	611
65. Analysis of the Near Ultraviolet Absorption Spectrum of para-Chloroanisole—By V. Suryanarayana and V. Ramakrishna Rao	619
66. Measurement of Thermal Neutron Activation Cross-section—By M. L. Sehgal	630
67. Raman Spectra of Frozen Solutions of some Monosubstituted Benzene Compounds in Ethyl Alcohol—By G. S. Kastha	635
68. On the Structure of Alphoncellose and Holocellulose obtained from Jute Fibres—By S. K. Chowdhury	639

LETTER TO THE EDITOR

11. Space Group of Anthrone—S. N. Srivastava	644
--	-----

BOOK REVIEW

4. Physicochemical Calculations—By E. A. Guggenheim and J. E. Pure	646
--	-----

AUTHOR INDEX

AUTHOR	SUBJECT	PAGE
Agashe, V. V.	see Dixit, K. R.	466
Ashmore, A., Collinge B. and Sen, S. K.	Improved performance of photo- multipliers in scintillation counters	261
Balsara, E. M.	see Naik, Y. G.	607
Bandhyopadhyay, P.	Models of lower ionosphere as may be inferred from absorption results	297
Banerjee, B. M., Ghosh, S. K. and Saha, A. K.	A nuclear induction spin-echo appa- ratus.	211
Banerjee, C. C.	Sommerfield's fine structure formula from five dimensional wave equation.	242
Banerjee, M. K.	see Mukherjee, P. N.	531
Banerjee, S. B.	Ultraviolet absorption spectra of isomeric picolines in the liquid and solid states.	11
	Ultraviolet absorption spectra of ortho and chloroanisole in the liquid and solid states.	135
	Electronic spectra of benzylamine and isobutyl benzoate in different states at different temperatures.	359
	Electronic spectra of trichloro- benzene in the liquid and solid states at -180°C .	483
Bhattacharyya, R. and Chatterjee S.	Fast coincidence with fast discrimi- nators.	53
Biswas, S. G. and Sirkar, S. C.	X-ray analysis of structure of frozen toluene and its solution in alcohol at -180°C .	141
Chakraburttty, D. M.	An application of Lipson's method in the study of the crystal system of BaBOF_3 .	235
Chakrabarti, N. B.	see Choudhury, A. K.	193
Chatterjee, B.	Slots in an imperfectly conducting wave guide.	278
	An accurate phase-meter for four- terminal net-works,	541
Chatterjee, S.	see Bhattacharyya, R.	53
Chatterjee, S. N.	Variation in lattice constants in thin films of gold.	110

AUTHOR	SUBJECT	PAGE
Chaturvedi, K. C.	Apparent separation and intensity ratio of close spectral lines.	247
Chopra, K. P.	Induction drag (I).	332
Choudhury, A. K. and N. B. Chakravarti	On the design of four-terminal inter-stage for pulse application.	193
Choudhury, A. K. and Nag. B. R.	R—C network analogue.	121
Chowdhury, S. K.	On the X-ray diffraction patterns and miceller dimensions of some substituted jute fibres.	572
	On the structure of alphacellulose and holocellulose obtained from jute fibres	639
Collinge, B.	see Ashmore, A.	261
Das, A.	On the p-p scattering at high energies	511
Das, J. N.	Study of rectifying characteristics of FeS_2 and germanium point-contact rectifiers.	172
Datta, S.	Recombination coefficient and electron production rate from total electron content in unit column below the level of maximum ionisation.	43
Deo, B. B.	see Panda, S.	227
Dixit, K. R.	Epitaxial growth of thin evaporated metallic films on cleavage surfaces of alkali halides and other crystals.	117
Dixit, K. R. and Agashe, V. V.	Crystal structure and magnetic susceptibility of rectifying cuprous oxides	466
Ganguly, N. K.	see Ghosh, A. M.	285
Ghose, T., Ghosh, S. K. and Ray, D. K.	Spin-echoes with four and more pulses.	265
Ghosh, S. K.	see Ghosh, T. K.	265
Ghosh, S. K.	see Banerjee, B. M.	21
Ghosh, A. M. and Ganguly, N. K.	Measurement of thermal neutron absorption cross-section using spherical symmetry method.	285
Ghosh, S. N. and Sheridan, W. F.	Charge transfer reactions.	337

Author Index

ix

AUTHOR	SUBJECT	PAGE
Gill, P. S. and Puri, S. P.	Photoionization versus photoelectric effect for discharge spread and out-put pulse measurements in G-M counters	564
Gopalakrishna, K. V.	Dipole moments of some esters (L)	283
Haranath, P. B. V. and Rao, P. T.	Emission spectra of mixed halogens, Part I, ICl.	156
	Emission spectra of mixed halogens, Part II, IBr and BrCl.	368
Haranath, R. B. V.	New emission spectrum of chlorine in Schumann region (L).	175
and Ramamurthy, K. S.	Absorption spectra of chloroanilines.	577
Hossain, A. and Kamal, A. N.	Scattering of 9.5 Mev protons by nitrogen.	553
Kamal, A. N.	see Hossain, A.	553
Karinik, M. B.	Electrical oscillations in A. C. discharge.	61
Kastha, G. S.	Raman spectra of isomeric picolines in different states and in solutions of ethyl alcohol at different temperatures.	395
	Raman spectra of frozen solutions of some mono-substituted benzene compounds in ethyl alcohol.	635
Krishnamachari, S. L. N. C.	The ultraviolet absorption spectra of <i>o</i> , <i>m</i> , and <i>p</i> -fluoriodo and bromochlorobenzene (L).	387
	Analysis of near ultraviolet absorption spectra of ortho, meta and para fluorochloro benzene vapours.	447
Krishna Murti, G. S. R.	The crystal structure of diphenyl at different temperatures,	1
	The crystal structure of <i>p</i> -nitro-aniline at different temperatures.	353
	The crystal structure of anthranilic acid at different temperatures.	611
Kundu, P.	Further studies on asymmetrical three-phase oscillator for very wide frequency deviation.	83
	A new method of demodulation for phase frequency and amplitude.	231

AUTHOR	SUBJECT	PAGE
Kundu, S. K.	Anomalous magnetic moments of proton and neutron.	526
Mitra, G. B.	X-ray diffraction study of heat treatment of kaolinite.	324
Mitra, Nilima (Mrs.)	Investigation of discrete sources of radiation from solar eclipse observations.	69
Mitra, S. N.	Solar eclipse of 30th June, 1955 and its effect upon the ionosphere.	309
Mitra, S. N. and Srivastava, R. B. L.	Fading and random motion of ionospheric irregularities	20
Mohanty, B. S.	see Panda, S.	560
Mukherjee, P. N., Pal, M. K., Banerjee, M. K. and Saha, A. K.	Design of continuous baffle in a short lens betaray spectrometer	531
Mukherjee, S.	see Pal, M. K.	56
Mukherjee, S. and Pal, M. K.	n-p and p-p scattering from Case-Pais. model in energy range 91 Mev to 437 Mev	415
Murty, C. R. K.	Dipole moments of some substituted benzenes and pyridines. Part I. Fluorotoluene	256
Nag, B. R.	see Choudhury, A. K.	121
Narasinha Rao, D. V. G. L.	Dipole moments of tri-substituted benzenes.. Part II (L).	60
	Dipole moments of tri-substituted benzenes, Part III.	334
Nayak, Y. G. and E. M. Balsara	Optical and electrical methods of measuring thickness of thin metallic films.	607
Pal, M. K.	see Mukherjee, P. N.	531
Pal, M. K. and S. K. Mukherjee and A. K. Saha	Elastic and inelastic scattering of high energy electrons by some 2 p-shell nuclei on the intermediate coupling model (L).	56
Pal, M. K.	see Mukherjee, P. N.	415
Panda, S. and B. B. Deo	Ultrasonic velocity of sodium chloride solution in water-dioxene mixtures.	227
Panda, S. and B. S. Mohanty	Ultrasonic velocity in cobalt and cadmium sulphate solutions at different temperatures and concentrations.	560

AUTHOR	SUBJECT	PAGE
Patil, H. N.	On optical method of measuring convective air velocity (L).	539
Puri, S. P.	A deviation from Wilkinson's theory of discharge spread in Geiger counters	441
Puri, S. P.	see Gill, P. S.	564
Ramamurty, S., Rao M. J. and Rao V. R.	Analysis of new ultraviolet absorption spectra of α - and β -fluoronaphthalenes	497
Ranade, J. D.	see Rao S. P.	491
Rao, C. S. R.	Solar tidal effects in the F_2 -region of ionosphere over Delhi.	516
Rao, M. J.	see Ramamurty, S.	497
Rao, P. T.	see Haranath, P. B. V.	156
	"	175
	"	368
Rao, S. P. and Ranade J. D.	Theoretical calculations of transition probabilities in the first negative $b^4\Sigma_g^- \rightarrow a^4\Pi_u^-$ bands of O_2^+ .	491
Rao, V. R. and V. Suryanarayan	Analysis of near ultraviolet spectrum of parachloroanisole	619
Rao, V. R.	see Ramamurty, S.	497
Ray, D. K.	see Ghose, T.	265
Roy, S. B.	Ultraviolet absorption spectra of 1, 3, 5-trichlorobenzene and 1, 3, 5-trimethyl benzenes in different solvents and at different temperatures.	588
Ray, S. B. and S. C. Sirkar	On the ultraviolet absorption spectra of frozen solutions of dichlorobenzenes in iso-butyl alcohol	177
Saha, A. K.	see Banerjee, B. M.	211
"	see Mukherjee, P. N.	531
"	see Pal, M. K. (L).	56
Sanyal, Lakshmi	The equation of motion of an incompressible viscous fluid in the parallel system of co-ordinates.	6
Sarkar, D. C.	Analysis of oathode coupled free running multivibrator.	431
Saxena, S. C.	Transport coefficients and force between unlike molecules.	146

AUTHOR	SUBJECT	PAGE
Saxena, S. C.	Thermal conductivity of binary and ternary mixtures of helium, argon and xenon.	597
Sehgal, M. L.	Branching ratio of slow neutrons	329
Sehgal, M. L.	Measurement of thermal neutron activation cross section.	630
Sen, S. K.	Ultraviolet absorption spectra of a few disubstituted benzenes in different states.	99
Sen, S. K.	see Ashmore, A.	261
Sengupta, P. K.	Excitation of the spectrum of sunlit aurora.	376
Siheridan, W. F.	see Ghosh, S. N.	337
Sirkar, S. C.	see Roy, S. B.	177
"	see Biswas, S. G.	141
Sreedhara Murthy, N.	see Tawde, N. R.	391
Sree Ramamurthy, K.	see Haranath, P. B. V.	577
Srivastava, K. P.	Force constants for like molecules on exp-six model from thermal conductivity.	404
Srivastava, R. B. L. and Mitra S. N.	Fading and random motion of ionospheric irregularities.	20
Srivastava, S. N.	Space group of anthrone (L)	644
Suryanarayan, V. and Rao, V. R.	Analysis of near ultraviolet spectrum of parachloro anisole.	619
Tawde, N. R. and Murthy, N. S.	A note on the validity of revised rotational structure of constants of green yellow system of VO bands.	391
Varshni, Y. P.	A new π -particle accelerator.	384

SUBJECT INDEX

SUBJECT	AUTHOR	PAGE
Alphacellulose and holocellulose obtained from jute fibres. On the structure of	S. K. Chowdhury	639
Asymmetrical three-phase oscillator. Further studies on	P. Kundu	83
Charge transfer reactions	S. N. Ghosh and W. F. Sheridan	337
Close spectral lines. Apparent separation and intensity ratio of	K. C. Chaturvedi	247
Continuous baffle in a short lens beta-ray spectrometer. Design of	P. N. Mukherjee, M. K. Pal, M. K. Banerjee and A. K. Saha	531
Convective air velocity. On optical method of measuring (L)	H. N. Patil	539
Crystal structure of anthranilic acid at different temperatures. The	G. S. R. Krishna Murti	611
Crystal structure of diphenyl at different temperatures. The	G. S. R. Krishna Murti	1
Crystal structure and magnetic susceptibility of rectifying cuprous oxides.	K. R. Dixit and V. V. Agashe	466
Crystal structure of <i>p</i> -nitroaniline at different temperatures. The	G. S. R. Krishna Murti	353
Demodulation for phase, frequency and amplitude. A new method of	P. Kundu	231
Dipole moments of trisubstituted benzenes. Part II (L)	D. V. G. L. Narasinha Rao	60
„ Part III (L)	„ „	334
Dipole moments of some substituted benzenes and pyridines. Part I—Fluorotoluenes	C. R. K. Murty	256
Dipolements of some esters.	K. V. Gopalakrishna	283
Elastic and inelastic scattering of high-energy electrons by some 2 <i>p</i> -shell nuclei on the intermediate coupling model. (L)	M. K. Pal, S. Mukherjee and A. K. Saha	56
Electrical oscillations in A. C. discharge	M. B. Karnik	61

SUBJECT	AUTHOR	PAGE
Expitaxial growth of thin evaporated metallic films on cleavage surfaces of alkali halides and other crystals	K. R. Dixit	117
Equation of motion of an incompressible viscous fluid in the parallel system of co-ordinates. The	Lakshmi Sanyal	6
Fast coincidence with fast discriminators	Ranglal Bhattacharyya and Santimay Chatterjee	53
Force-constants of like molecules on exp-six model from thermal conductivity	K. P. Srivastava	404
Four-terminal interstages for pulse applications. On the design of	A. K. Choudhury and N. B. Chakravarti	193
Imperfectly conducting waveguide. Slots in an	B. Chatterjee	278
Induction drag (L)	K. P. Chopra	332
Ionospheric irregularities. Fading and random motion of	S. N. Mitra and R. B. L. Srivastava	20
Lattice constants in thin films of gold. Variation in	S. N. Chatterjee	110
Lipson method in the study of crystal system of BaBOF_3 . An application of	D. M. Chakraburttty	235
Magnetic moments of proton and neutron. Anomalous	S. K. Kundu	526
Models of lower ionosphere as may be inferred from absorption results.	P. Bandyopadhyay	297
Multivibrator. Analysis of cathode-coupled free running	D. C. Sirkar	431
New particle accelerator. A (L)	Yatendra Pal Varshni	384
n-p and p-p scattering from Case-Pais model in energy range 91 Mev to 437 Mev	S. Mukherjee and M. K. Pal	415
Nuclear induction spin-echo apparatus. A	B. M. Banerjee; S. K. Ghosh and A. K. Saha	211

Subject Index

rv

SUBJECT	AUTHOR	PAGE
Optical and electrical methods of measuring thickness of thin metallic films	Y. G. Naik and E. M. Balsara	607
Phase meter for four terminal networks. An accurate	B. Chatterjee	541
Photoionization versus photoelectric effect for discharge spread and out-put pulse measurements in G-M Counters	P. S. Gill and S. P. Puri	564
Photomultipliers in scintillation counters. Improved performance of	A. Ashmore, B. Collinge and S. K. Sen	261
p-p scattering at high energies. On the	A. Das	511
Radiation from solar eclipse observations. Investigation of discrete sources of	(Mrs.) Nilima Mitra	69
R-C network analogue	A. K. Choudhury and B. R. Nag	121
Recombination coefficient and electron production rate from total electron content in unit column below the level of maximum ionisation	S. Datta	43
Rectifying characteristics of FeS_2 and germanium point contact rectifiers. Study of (L)	J. N. Das	172
Revised rotational structure constant of green-yellow system of VO bands. Note of the validity of the	N. R. Tawde and N. Sreedhara Murthy	391
Scattering of 9.5 Mev protons by nitrogen.	Anwar Hossain and A. N. Kamal	553
Slow neutrons. Branching ratio for	Madan Lall Sehgal	329
Solar eclipse of 30th June, 1955 and its effect upon the ionosphere.	S. N. Mitra	309
Solar tidal effects in the F_2 -region of ionosphere over Delhi.	C. S. Raghavendra Rao	516
Sommerfeld's fine structure formula from five dimensional wave-equation	C. C. Banerjee	242

SUBJECT	AUTHOR	PAGE
SPECTRA :		
Space group of anthrone (L)	S. N. Srivastava	644
Absorption spectra of chloroanilines	P. B. V. Haranath and K. Sree Ramamurthy	577
Analysis of near ultraviolet absorption spectrum of para-chloroanisole	V. Suryanarayan and V. R. Rao	619
Electronic spectra of benzyaniline and iso-butyl benzoate in different states and at different temperature	S. B. Banerjee	359
Electronic spectra of trichlorobenzenes in the liquid and solid states at 180°C	S. B. Banerjee	483
Emission spectrum of chlorine in the Schumann region. New	P. B. V. Haranath and P. Tiruvenganna Rao	175
Emission spectra of mixed halogens. Part I. ICl		156
Emission spectra of mixed halogens. Part II. IBr and BrCl		368
Excitation of spectrum of sunlit aurora	Prabhat K. Sengupta	376
Raman spectra of frozen solutions of some monosubstituted benzene compounds in ethyl alcohol	G. S. Kastha	636
Raman spectra of isomeric picolines in different states and in solutions of ethyl alcohol at different temperatures	G. S. Kastha	395
Ultraviolet absorption spectra of <i>o</i> , <i>m</i> , <i>p</i> -fluoroiodo and bromobenzenes. The (L)	S. L. N. G. Krishnamāchari	387
Ultraviolet absorption spectra of ortho and para-chloroanisole in the liquid and solid states.	S. B. Banerjee	135
Ultraviolet absorption spectra of isomeric picolines in the liquid and solid states.	S. B. Banerjee	11

Subject Index

xvii

SUBJECT	AUTHOR	PAGE
Ultraviolet absorption spectra of a few disubstituted benzenes in different states	S. K. Sen	99
SPECTRA :		
Ultraviolet absorption spectra of frozen solution of dichlorobenzenes in isobutyl alcohol. On the	S. B. Roy and S. C. Sirkar	177
Ultraviolet absorption spectra of ortho, meta and para fluorochlorobenzene vapours. Analysis of near	S. L. N. G. Krishnamachari	447
Ultraviolet absorption spectra of α - and β -fluoronaphthalenes. Analysis of near	S. Ramamurty., M. Jagannadha Rao and V. Ramakrishna Rao	497
Ultraviolet absorption spectra of 1, 3, 5-trichlorobenzene and 1, 3, 5-trimethyl benzene in different solvents at different temperatures.	S. B. Roy	588
Spin-echoes with four and more pulses.	T. Ghosh, S. K. Ghosh and D. K. Roy	265
Thermal conductivity of binary and ternary mixtures of helium, argon and xenon.	S. C. Saxena	597
Thermal neutron absorption cross-section using spherical symmetry method. Measurement of	A. M. Ghosh and N. K. Ganguly	285
Thermal neutrons activation cross-section. Measurement of	M. L. Sehgal	630
Transition probabilities in the first negative ($b^4\Sigma_g^- \rightarrow a^4\pi^-_{u1}$) bands of O_2^+ . Theoretical calculation of	S. P. Rao and J. D. Ranade	491
Transport coefficient of force between unlike molecules	S. C. Saxena	146
Ultrasonic velocity of sodium chloride solution in water-dioxane mixtures	Srinibas Panda and Bibhuti Bhusan Deo	227

SUBJECT	AUTHOR	PAGE
Ultrasonic velocity in cobalt and cadmium sulphate solution at different temperatures and concentrations.	Srinibas Panda and Braja Sundar Mohanty	560
SPECTRA :		
Wilkinson's theory of discharge spread in Geiger-counters. A deviation from	Satyapal Puri	441
X-ray analysis of structure of frozen toluene and its solution in alcohol at -180°C	S. G. Biswas and S. C. Sirkar	141
X-ray diffraction pattern and micellar dimensions of some substituted jute fibre. On the	S. K. Chowdhury	572
X-ray diffraction study of the heat treatment of kaolinite	G. B. Mitra	324

THE CRYSTAL STRUCTURE OF DIPHENYL AT DIFFERENT TEMPERATURES*

G. S. R. KRISHNA MURTI

OPTICS DEPARTMENT, INDIAN ASSOCIATION FOR THE CULTIVATION OF SCIENCE,
JADAVPUR, CALCUTTA-32

(Received for publication September 13, 1956)

Plate I

ABSTRACT. The dimensions of the unit cell of the crystal of diphenyl at 32°C and -180°C were determined by taking the Debye-Scherrer patterns at those temperatures. The unit cell dimensions at 32°C are $a = 8.29$ A.U., $b = 5.82$ A.U., $c = 9.48$ A.U., and $\beta = 94^\circ 41'$; and at -180°C, $a = 7.98$ A.U., $b = 5.70$ A.U., $c = 9.37$ A.U. and $\beta = 95^\circ 21'$. The coefficients of expansion α_a , α_b and α_c along the three crystallographic axes a , b and c in the range -180°C to 32°C are 18.33×10^{-5} , 9.93×10^{-5} and 5.54×10^{-5} respectively. The small change in the angle of β at -180°C is attributed to a small rotation of molecules in the unit cell. It is pointed out that the larger contraction along a -axis is consistent with the orientation of the molecules in the unit cell.

INTRODUCTION

The space group to which the crystal of diphenyl at room temperature belongs was determined by several previous workers. Hengstenberg and Mark (1929) took rotation photographs about a and b axes and found the space group to be C_{2h}^5 , the unit cell dimensions of the crystal being $a = 8.22$ A.U., $b = 5.69$ A.U., $c = 9.50$ A.U. and $\beta = 94^\circ 8'$. Next Clark and Pickett (1930) arrived almost at the same values by taking the rotation, oscillation and Laue photographs of the crystal. Later, Dhar (1932) repeated the investigation in order to find the positions of atoms in the molecule in the unit cell and he reported the unit cell dimensions to conform to $a = 8.38$ A.U., $b = 5.82$ A.U., $c = 9.47$ A.U. and $\beta = 95^\circ 18'$. These values are slightly higher than those reported by previous workers. He further reported that the molecule is inclined to the cell faces and no crystallographic axis is in the plane of the molecule, but the two benzene rings are flat regular hexagons lying in one plane.

The ultraviolet absorption spectra of diphenyl in the liquid state at 80°C and in the solid state at 30°C and -180°C, were studied by Deb (1953). He pointed out that the very broad band observed in the liquid state is split up into two broad bands when the liquid is solidified and kept at 30°C and when the solid is cooled to -180°C, these bands become sharper and are resolved into nine distinct bands. It has been pointed out by him that these results can be inter-

*Communicated by Prof. S. C. Sirkar

preted on the assumption that the excited state electronic energy level is split up into three components when the crystal is cooled to -180°C .

It was not known whether the crystal structure of diphenyl changes when the temperature is lowered to -180°C . So it was thought worthwhile to study the Debye-Scherrer patterns of the crystal at room temperature and at -180°C to find out whether there is any change in the structure of the crystal with the lowering of temperature.

EXPERIMENTAL

Chemically pure diphenyl was taken from the original packing of Merck's and was redistilled under reduced pressure. The specimen for Debye-Scherrer pattern was prepared as described in an earlier paper (Krishna Murti and Sen, 1956). The diameter of the specimen used was about 0.03 cms.

A Seifert X-ray tube operating at 26 mA, 32 KV was used and an exposure of about $2\frac{1}{2}$ hours was sufficient to record the Debye-Scherrer patterns with moderate densities. Copper radiation filtered through a nickel filter to cut off $K\beta$ lines was used to photograph the patterns. The distance from specimen to the film was measured accurately by taking the Debye-Scherrer pattern of rocksalt. The distance was 5.20 cms.

The Debye-Scherrer pattern of the crystal at -180°C was recorded by using the low temperature camera described earlier by Krishna Murti and Sen (1956). Several photographs under the same conditions were taken to verify the genuineness of the results. Spacings were calculated from the diameters of the rings which could be measured correct to about 0.05 mm.

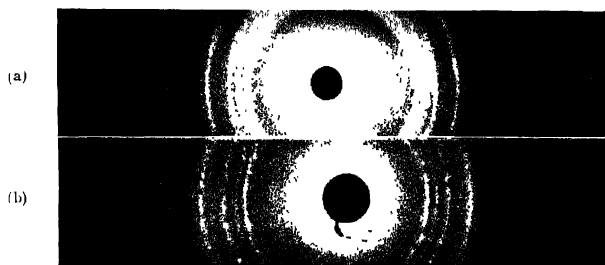
RESULTS & DISCUSSION

The spacings corresponding to the rings observed for the crystal at different temperatures are given in Table I in which the spacings calculated from the data of previous workers are also given for comparison. The intensities of Debye-Scherrer rings are indicated in parentheses. Some of the representative patterns are reproduced in Plate I.

It can be seen from Table I that the spacings observed for the crystal at room temperature (32°C) are slightly larger than the corresponding spacings calculated from the data of Hengstenberg and Mark (1929) and Clark and Pickett (1930). This clearly points to slightly larger values for the unit cell dimensions. The indices of different rings observed in the Debye-Scherrer pattern are assigned with the help of the intensities of the planes given by Hengstenberg and Mark (1929).

The dimensions of the unit cell calculated from some of the intense rings observed in the case of the crystal at 32°C are

$$a = 8.29 \text{ A.U.}, b = 5.82 \text{ A.U.}, c = 9.48 \text{ A.U.}, \text{ and } \beta = 94^{\circ}41'.$$



Debye-Scherrer patterns of diphenyl at different temperatures.

- (a) Specimen at 32°C
(Radius of the camera = 5.04 Cms)
- (b) Specimen at -180°C
(Radius of the Camera = 5.20 Cms)

TABLE I
Spacings of the crystal of diphenyl

Planes	Calculated spacings from the data of			Observed 32°C	spacings -180°C
	Murk & Hengstenberg (1929)	Clark and Pickett (1930)	Dhar (1932)		
001	9.470	9.540	9.430	9.450 (m)	9.340 (m)
011	4.880	4.880	4.950	4.955 (vw)	4.862 (vw)
002	4.730	4.770	4.715	4.725 (vs)	4.665 (vs)
111	4.270	4.250	4.350	4.330 (s)	4.242 (s)
200	4.100	4.040	4.170	4.130 (w)	3.980 (vw)
201	3.880	3.830	3.950	3.900 (vs)	3.790 (s)
012	3.640	3.650	3.660	3.670 (m)	3.605 (w)
112	3.410	3.405	3.450	3.435 (vw)	3.385 (vw)
210	2.325	2.290	3.390	3.360 (vw)	3.260 (vw)
211	3.205	3.170	3.270	3.240 (vs)	3.158 (vs)
211	3.070	3.050	3.120	3.110 (w)	3.012 (w)
020	2.845	2.835	2.910	2.910 (vw)	2.850 (vw)
113	2.675	2.680	2.690	2.685 (w)	2.655 (w)
203	2.610	2.600	2.630	2.627 (w)	2.575 (w)
022	2.440	2.440	2.480	2.460 (m)	2.430 (m)
203	2.405	2.410	2.410	2.425 (m)	2.350 (m)
004	2.390	2.385	2.360	2.355 (w)	2.330 (vw)
221	2.240	2.230	2.280	2.275 (vw)	2.220 (vw)
114	2.150	2.160	2.160	2.158 (vw)	2.130 (vw)
023	2.110	2.110	2.140	2.140 (vw)	2.100 (vw)
400	2.050	2.020	2.085	2.060 (w)	1.990 (w)
401	1.970	1.950	1.990	1.984 (w)	1.946 (w)
410	1.930	1.900	1.960	1.948 (vw)	1.880 (w)
214	1.880	1.880	1.870	1.860 (vw)	1.835 (vw)
024	1.820	1.825	1.830	1.834 (w)	1.802 (vw)
115	1.730	1.740	1.720	1.730 (m)	1.702 (m)
403	1.660	1.650	1.670	1.660 (m)	1.610 (m)

These values of a , b and c are higher than those reported by Hengstenberg and Mark (1929) and by Clark and Pickett (1930). The values of b and c agree with those reported by Dhar (1932) but the value of β given by Dhar is much higher than that reported by previous workers. The value $94^{\circ}41'$ for β observed in the present investigation agrees closely with value given by Groth (1919) and also by Hengstenberg and Mark (1929). So, it appears that the value of the product $a \sin \beta$ given by Dhar is almost correct but the individual values of a and β given by him are too high.

It can be further seen from Table I that the spacings observed for the crystal at -180°C are smaller than the corresponding spacings in the crystal at 32°C . As no disappearance of any of the rings is observed with lowering of temperature of the crystal it can be concluded that mere contraction of the unit cell takes place with the lowering of the temperature to -180°C . Thus there is no change in the crystal structure when the crystal is cooled to -180°C and the space group C_{5h}^{2h} is retained even at -180°C .

The dimensions of the unit cell of the crystal at -180°C have been calculated from the observed intense rings and these are found to be

$$a = 7.98 \text{ A.U.}, b = 5.70 \text{ A.U.}, c = 9.37 \text{ A.U. and } \beta = 95^{\circ}21'.$$

So, it seems that the spatial configuration of the molecules in the unit cell of the crystal at room temperature changes a little when the crystal is cooled to -180°C and the slightly different value of β may indicate a rotation of molecules at low temperatures which may also be responsible for producing different amounts of contraction along the three directions. The small change in the value of β indicates a small rotation of the molecules in the unit cell. The structure of the molecule in the unit cell seems to remain unaltered with the lowering of temperature to -180°C . So the changes in the ultraviolet absorption spectrum observed by Deb (1953) are not due to any change in the structure of the crystal.

The coefficients of expansion α_a , α_b and α_c along the three directions of crystallographic axes a , b and c in the range -180°C to 32°C , were calculated and the values were found to be $\alpha_a = 18.33 \times 10^{-5}$, $\alpha_b = 9.93 \times 10^{-5}$ and $\alpha_c = 5.54 \times 10^{-5}$.

According to Dhar (1932) the molecule lies nearer to the bc plane than to the ac plane. Also the length of the molecule lies almost along the c -axis and the thickness would be almost at right angle to bc plane, i.e. almost along a -axis. Since the contraction along the a -axis is found to be largest at low temperatures, it seems that some forces of attraction between the neighbouring molecules act at right angles to the plane of the molecule at low temperatures to bring them closer together. These forces may be due to formation of virtual bonds between the molecules which brings out the splitting of the absorption bands observed at -180°C .

ACKNOWLEDGMENT

The author is indebted to Professor S. C. Sirkar, D. Sc., F.N.I. for his kind help and guidance during the progress of the work.

REFERENCES

- Clark, G. L. and Pickett, L., 1930, *Proc. Nat. Acad. Sci.*, **16**, 20.
Deb, A. R., 1953, *Ind. J. Phys.*, **27**, 305
Dhar, J., 1932, *Ind. J. Phys.*, **7**, 43.
Groth, P., 1919, *Chem. Kristal.*, Vol. 5, 4.
Hengstenberg, J. and Mark H., 1929, *Z. Krist.*, **70**, 283.
Krishna Murti, G. S. R. and Sen, S. N., 1956, *Ind. J. Phys.*, **30**, 242

THE EQUATIONS OF MOTION OF AN INCOMPRESSIBLE VISCOUS FLUID IN THE PARALLEL SYSTEM OF COORDINATES

LAKSHMI SANYAL

APPLIED MATHEMATICS DEPARTMENT, CALCUTTA UNIVERSITY

(Received for publication September 7, 1956)

ABSTRACT For a rigorous deduction of the equations of three-dimensional boundary layer on a given surface, the Stokes-Navier equations of motion of an incompressible viscous fluid under no body forces have been transformed in the parallel system of coordinates.

INTRODUCTION

In this paper, the Stokes-Navier equations of motion (in non-dimensional form) of an incompressible viscous fluid under no body forces have been transformed in the parallel system of coordinates. This has been done with a view to the deduction of the equations of three-dimensional boundary layer on a given surface in a rigorous manner. The system of parallel coordinates is defined as follows

Let S_0 be a given analytic regular surface possessing at each point non-zero principal radii of curvature and let the lines of curvature on S_0 be taken as the coordinate curves $\xi = \text{constant}$ and $\eta = \text{constant}$. Let $\xi(x, y, z) = \text{constant}$ be a system of surfaces parallel to S_0 , ξ being the perpendicular distance of the point (x, y, z) from S_0 . The system of parallel surfaces and the developables of the congruence of normals to these surfaces along the lines of curvature form a triply orthogonal system of surfaces. ξ, η, ζ are therefore the coordinates of a point in the parallel system of coordinates.

Let (x_0, y_0, z_0) be the cartesian coordinates of the foot of the perpendicular from the point (x, y, z) on S_0 . Then the first fundamental quadratic form of the surface is

$$Ed\xi^2 + Gd\eta^2 \quad \dots (1)$$

where

$$E = \Sigma \left(\frac{\partial x_0}{\partial \xi} \right)^2, \quad G = \Sigma \left(\frac{\partial x_0}{\partial \eta} \right)^2. \quad \dots (2)$$

Let X, Y, Z be the direction cosines of the normal to the surface S_0 at the point (x_0, y_0, z_0) . Then

$$\Sigma X \frac{\partial x_0}{\partial \xi} = 0, \quad \Sigma X \frac{\partial x_0}{\partial \eta} = 0 \quad \dots (3)$$

Equations of Motion of an Incompressible Viscous Fluid, etc. 7

Since the lines of curvature on S are the coordinate curves, the second fundamental quadratic form of the surface is

$$Ld\xi^2 + Nd\eta^2 \quad \dots \quad (4)$$

where
$$L = \sum X \frac{\partial^2 x_0}{\partial \xi^2}, \quad N = \sum X \frac{\partial^2 x_0}{\partial \eta^2}, \quad \dots \quad (5)$$

The principal radii of curvature corresponding to the curves $\eta = \text{const.}$ and $\xi = \text{const.}$ are respectively given by

$$\frac{1}{R_1} = \frac{L}{E}, \quad \frac{1}{R_2} = \frac{N}{G} \quad \dots \quad (6)$$

If $h_1 d\xi, h_2 d\eta, h_3 d\zeta$ be the elements of length in the directions ξ, η, ζ ,

$$h_1^2 = \sum \left(\frac{\partial x}{\partial \xi} \right)^2, \quad h_2^2 = \sum \left(\frac{\partial x}{\partial \eta} \right)^2, \quad h_3^2 = \sum \left(\frac{\partial x}{\partial \zeta} \right)^2 \quad \dots \quad (7)$$

Now
$$x = x_0 + \xi X, \quad y = y_0 + \zeta Y, \quad z = z_0 + \xi Z \quad \dots \quad (8)$$

Then
$$h_1^2 = E + 2B\xi + C\xi^2 \quad \dots \quad (9)$$

where
$$B = \sum \frac{\partial X}{\partial \xi} \frac{\partial x_0}{\partial \xi}, \quad C = \sum \left(\frac{\partial X}{\partial \xi} \right)^2 \quad \dots \quad (10)$$

Differentiating the first equation of (3) with respect to ξ and using the first equation of (5), we get $B = L$. Differentiating

$$X^2 + Y^2 + Z^2 = 1$$

with respect to ξ , we see that $\frac{\partial X}{\partial \xi}, \frac{\partial Y}{\partial \xi}, \frac{\partial Z}{\partial \xi}$ are the direction numbers of a vector tangential to S_0 . Such a vector is therefore a homogeneous linear function of the two tangential orthogonal vectors

$$\left(\frac{\partial x_0}{\partial \xi}, \frac{\partial y_0}{\partial \xi}, \frac{\partial z_0}{\partial \xi} \right) \quad \text{and} \quad \left(\frac{\partial x_0}{\partial \eta}, \frac{\partial y_0}{\partial \eta}, \frac{\partial z_0}{\partial \eta} \right) \quad \dots \quad (11)$$

so that
$$\frac{\partial X}{\partial \xi} = a \frac{\partial x_0}{\partial \xi} + b \frac{\partial x_0}{\partial \eta} \quad \dots \quad (12)$$

with similar expressions for $\frac{\partial Y}{\partial \xi}, \frac{\partial Z}{\partial \xi}$. Multiplying these by $\frac{\partial x_0}{\partial \xi}, \frac{\partial y_0}{\partial \xi}, \frac{\partial z_0}{\partial \xi}$

and adding and using the value of B , we get $a = -\frac{L}{E} = -\frac{1}{R_1}$.

Multiplying the equations by $\frac{\partial x_0}{\partial \eta}$, $\frac{\partial y_0}{\partial \eta}$, $\frac{\partial z_0}{\partial \eta}$ respectively and adding and observing that the vectors (11) are right angles, we get

$$bG = \Sigma \frac{\partial X}{\partial \xi} \frac{\partial x_0}{\partial \eta}.$$

Differentiating the second equation of (3) with respect to ξ and observing that the coordinate curves are lines of curvature and therefore $\Sigma X \frac{\partial^2 x_0}{\partial \xi \partial \eta} = 0$,

we get $b = 0$. Therefore $C = \frac{L^2}{E} = \frac{E}{R_1^2}$

Substituting in the expression for h_1 , we get $h_1 = \sqrt{E} \left(1 - \frac{\xi}{R_1} \right)$... (13a)

Similarly $h_2 = \sqrt{G} \left(1 - \frac{\xi}{R_2} \right)$. .. (13b)

Further it is seen at once that $h_3 = 1$.

EQUATIONS OF MOTION

Stokes-Navier equations of motion of an incompressible viscous fluid under no body forces in dimensionless form can be written as

$$\frac{\partial \vec{V}}{\partial t} - [\vec{V} \cdot \vec{\Omega}] = \text{grad} \left(\frac{p}{\rho} + \frac{1}{2} V^2 \right) - \frac{1}{R} \text{rot} \vec{\Omega} \quad \dots (14)$$

where R is the Reynolds' number of the flow, $\vec{\Omega} = \text{rot} \vec{V}$ and $[\vec{V} \cdot \vec{\Omega}]$ denotes the vector product of \vec{V} and $\vec{\Omega}$.

Introducing parallel system of coordinates defined in the preceding section and denoting by u, v, w the components of velocity in the directions ξ, η, ζ , and by $\vec{i}, \vec{j}, \vec{k}$ unit vectors in these directions, we have

$$\vec{\Omega} = \text{rot} \vec{V} = \begin{vmatrix} \vec{i} & \vec{j} & \vec{k} \\ h_2 h_3 & h_3 h_1 & h_1 h_2 \\ \frac{\partial}{\partial \xi} & \frac{\partial}{\partial \eta} & \frac{\partial}{\partial \zeta} \\ h_1 u & h_2 v & h_3 w \end{vmatrix} \quad \dots (15)$$

Equations of Motion of an Incompressible Viscous Fluid, etc. 9

Using the values of h_1, h_2, h_3 obtained before, we get for the components of $\vec{\Omega}$

$$\begin{aligned} & \frac{R_2}{\sqrt{G(R_2 - \xi)}} \left(\frac{\partial w}{\partial \eta} + \frac{\sqrt{G}}{R_2} v \right) - \frac{\partial v}{\partial \xi}, \quad - \frac{R_1}{\sqrt{E(R_1 - \xi)}} \left(\frac{\partial w}{\partial \xi} - \frac{\sqrt{E}}{R_1} u \right) + \frac{\partial u}{\partial \xi}, \\ & \frac{R_1}{\sqrt{E(R_1 - \xi)}} \frac{\partial v}{\partial \xi} - \frac{R_2}{\sqrt{G(R_2 - \xi)}} \frac{\partial u}{\partial \eta} + \frac{R_1 R_2}{\sqrt{E G (R_1 - \xi)(R_2 - \xi)}} \\ & \times \left[v \frac{\partial}{\partial \xi} \left\{ \sqrt{G} \left(1 - \frac{\xi}{R_2} \right) - u \frac{\partial}{\partial \eta} \left\{ \sqrt{E} \left(1 - \frac{\xi}{R_1} \right) \right\} \right] \end{aligned}$$

Also the components of $-\vec{V} \cdot \vec{\Omega} \mid \frac{1}{2} \text{ grad } V^2$ are

$$\begin{aligned} & \frac{R_1 u}{\sqrt{E(R_1 - \xi)}} \left(\frac{\partial u}{\partial \xi} - \frac{\sqrt{E}}{R_1} w \right) + \frac{R_2 v}{\sqrt{G(R_2 - \xi)}} \frac{\partial u}{\partial \eta} + w \frac{\partial u}{\partial \xi} \\ & + \frac{R_1 R_2}{\sqrt{E G (R_1 - \xi)(R_2 - \xi)}} \left[u v \frac{\partial}{\partial \eta} \left\{ \sqrt{E} \left(1 - \frac{\xi}{R_1} \right) \right\} - v^2 \frac{\partial}{\partial \xi} \left\{ \sqrt{G} \left(1 - \frac{\xi}{R_2} \right) \right\} \right], \dots (16) \\ & \frac{R_2 v}{\sqrt{G(R_2 - \xi)}} \left(\frac{\partial v}{\partial \eta} - \frac{\sqrt{G}}{R_2} w \right) + \frac{R_1 u}{\sqrt{E(R_1 - \xi)}} \frac{\partial v}{\partial \xi} + w \frac{\partial v}{\partial \xi} \\ & + \frac{R_1 R_2}{\sqrt{E G (R_1 - \xi)(R_2 - \xi)}} \left[u v \frac{\partial}{\partial \xi} \left\{ \sqrt{G} \left(1 - \frac{\xi}{R_2} \right) \right\} - u^2 \frac{\partial}{\partial \eta} \left\{ \sqrt{E} \left(1 - \frac{\xi}{R_1} \right) \right\} \right], \\ & \frac{R_1 u}{\sqrt{E(R_1 - \xi)}} \left(\frac{\partial w}{\partial \xi} + \frac{\sqrt{E}}{R_1} u \right) + \frac{R_2 v}{\sqrt{G(R_2 - \xi)}} \left(\frac{\partial w}{\partial \eta} + \frac{\sqrt{G}}{R_2} v \right) + w \frac{\partial w}{\partial \xi}. \end{aligned}$$

The equations of motion in parallel system of coordinates are therefore

$$\begin{aligned} & \frac{\partial u}{\partial t} + \frac{R_1 u}{\sqrt{E(R_1 - \xi)}} \left(\frac{\partial u}{\partial \xi} - \frac{\sqrt{E}}{R_1} w \right) + \frac{R_2 v}{\sqrt{G(R_2 - \xi)}} \frac{\partial u}{\partial \eta} + w \frac{\partial u}{\partial \xi} \\ & + \frac{R_1 R_2}{\sqrt{E G (R_1 - \xi)(R_2 - \xi)}} \left[u v \frac{\partial}{\partial \eta} \left\{ \sqrt{E} \left(1 - \frac{\xi}{R_1} \right) \right\} - v^2 \frac{\partial}{\partial \xi} \left\{ \sqrt{G} \left(1 - \frac{\xi}{R_2} \right) \right\} \right] \\ & = - \frac{R_1}{\sqrt{E(R_1 - \xi)}} \frac{\partial p}{\partial \xi} - \frac{1}{R} (\text{rot } \vec{\Omega})_{\xi} \dots (17a) \end{aligned}$$

$$\begin{aligned}
& \frac{\partial v}{\partial t} + \frac{R_2 v}{\sqrt{G(R_2 - \xi)}} \left(\frac{\partial w}{\partial \eta} - \frac{\sqrt{G}}{R_2} w \right) + \frac{R_1 u}{\sqrt{E(R_1 - \xi)}} \frac{\partial v}{\partial \xi} + w \frac{\partial v}{\partial \xi} \\
& + \frac{R_1 R_2}{\sqrt{E G (R_1 - \xi) (R_2 - \xi)}} \left[u w \frac{\partial}{\partial \xi} \left\{ \sqrt{G} \left(1 - \frac{\xi}{R_2} \right) \right\} - u^2 \frac{\partial}{\partial \eta} \left\{ \sqrt{E} \left(1 - \frac{\xi}{R_1} \right) \right\} \right] \\
& - \frac{R_2}{\sqrt{G(R_2 - \xi)}} \frac{\partial p}{\partial \eta} - \frac{1}{R} (\text{rot } \vec{\Omega})_\eta \quad \dots \quad (17b)
\end{aligned}$$

$$\begin{aligned}
& \frac{\partial w}{\partial t} + \frac{R_1 u}{\sqrt{E(R_1 - \xi)}} \left(\frac{\partial w}{\partial \xi} + \frac{\sqrt{E}}{R_1} u \right) + \frac{R_2 v}{\sqrt{G(R_2 - \xi)}} \left(\frac{\partial w}{\partial \eta} + \frac{\sqrt{G}}{R_2} v \right) + w \frac{\partial w}{\partial \xi} \\
& = - \frac{\partial p}{\partial \xi} - \frac{1}{R} (\text{rot } \vec{\Omega})_\xi \quad \dots \quad (17c)
\end{aligned}$$

where the components of $\text{rot } \vec{\Omega}$ are obtained from the components of $\vec{\Omega}$ given in (16) by replacing u, v, w by $\Omega_t, \Omega_\eta, \Omega_\mu$ respectively.

The equation of continuity of an incompressible fluid

$$\frac{\partial}{\partial \xi} (h_2 h_3 u) + \frac{\partial}{\partial \eta} (h_3 h_1 v) + \frac{\partial}{\partial \zeta} (h_1 h_2 w) = 0$$

become in parallel coordinates,

$$\begin{aligned}
& \frac{\partial}{\partial \xi} \left\{ \sqrt{G} \left(1 - \frac{\xi}{R_2} \right) u \right\} + \frac{\partial}{\partial \eta} \left\{ \sqrt{E} \left(1 - \frac{\xi}{R_1} \right) v \right\} + \frac{\partial}{\partial \zeta} \left\{ \sqrt{E G} \left(1 - \frac{\xi}{R_1} \right) \left(1 - \frac{\xi}{R_2} \right) w \right\} \\
& = 0 \quad \dots \quad (18)
\end{aligned}$$

ACKNOWLEDGMENTS

The author wishes to express her thanks to Dr. S. Ghosh for helpful suggestions.

ULTRAVIOLET ABSORPTION SPECTRA OF ISOMERIC PICOLINES IN THE LIQUID AND SOLID STATES*

S. B. BANERJEE

OPTICS DEPARTMENT, INDIAN ASSOCIATION FOR THE CULTIVATION OF SCIENCE,
JADAVPUR, CALCUTTA-32.

(Received for publication August 21, 1956)

ABSTRACT. The ultraviolet absorption spectra of α -, β - and γ -picoline have been investigated in the liquid state and in the solid state at -180°C . The results have been compared with those observed for the substances in the vapour state by previous workers.

All the three compounds exhibit two systems of bands in the vapour state, the first system being attributed to $n \rightarrow \pi^*$ transition (Transition I) and the other system to $\pi \rightarrow \pi^*$ transition (Transition II). It is observed, however, that in the liquid and solid states these substances yield only one system of bands corresponding to Transition II. The ν_0 -band in each case is found to undergo large shift towards longer wavelengths with liquefaction of the vapour. With solidification and lowering of temperature to -180°C the bands get a little sharper and the ν_0 -bands are further displaced slightly towards longer wavelengths. The results have been interpreted on the assumption that in the condensed phases the molecules of picolines form associated groups probably through the nitrogen non-bonding electron and a hydrogen atom of neighbouring molecules.

INTRODUCTION

It was suggested by Kasha (1950) that in the spectra of N-heterocyclic compounds like pyridine there may be two systems of bands, the excitation of a nitrogen non-bonding electron into the π -orbital of the ring being responsible for the occurrence of System I ($n \rightarrow \pi^*$ transition) and the other system resulting from the excitation of the π -ring electron ($\pi \rightarrow \pi^*$ transition). The investigation of the ultraviolet absorption spectrum of pyridine vapour by Sponer and Stücklen (1946) and a further re-examination of it by Rush and Sponer (1952) showed that the substance gives two systems of bands with the ν_0 bands at 34769 cm^{-1} and 38350 cm^{-1} , which correspond to the $n \rightarrow \pi^*$ and $\pi \rightarrow \pi^*$ transitions respectively. Rush and Sponer (1952) also studied the absorption spectra of the three isomeric picolines (methyl pyridines) in the vapour state and observed the two transitions for these substances. One of these near 35500 cm^{-1} was interpreted as an allowed $A_1 - B_2$ transition due to the excitation of an sp^2 non-bonding electron of the nitrogen atom into the first π -orbital of the ring and the other stronger system at 38500 cm^{-1} as an allowed $A_1 - B_1$ transition resulting from the excitation of π -ring electron.

*Communicated by Prof S. C. Sirkar

In an investigation of the ultraviolet absorption spectra of pyridine in the liquid state and in the solid state at -180°C reported in an earlier paper (Banerjee, 1956b) it was observed that one of the two systems of bands observed in the case of the vapour disappears when the vapour is liquefied. This fact was explained on the assumption that in the liquid and solid states the pyridine molecules form associated groups through the nitrogen non-bonding electron and a hydrogen atom of neighbouring molecules. The present work was undertaken to study the ultraviolet absorption spectra of α -, β -, and γ -picoline in the liquid and solid states in order to investigate the changes which may take place in the spectra of these substituted pyridine compounds with the changes of state. It was also intended to find out whether the changes in the absorption spectra of the picolines which might take place with lowering of temperature give us any clue to the proper analysis of the bands.

EXPERIMENTAL

Chemically pure samples of the picolines were distilled under reduced pressure before use. Very thin films of the liquids of thickness of the order of a few microns were found to produce absorption bands instead of continuous absorption shown by slightly thicker films. Thicker films of the liquids were also used in order to find out whether a second system of bands was exhibited. Aluminium foils of different thicknesses were used as distance pieces in the absorption cell in order to get films of different thicknesses. Spectrograms were taken on Ilford HP 3 films with a Hilger E 1 spectrograph. Iron arc spectrum was taken on each spectrogram as comparison. Microphotometric records of the bands were taken with a Kipp and Zonen type self recording microphotometer. The frequencies of the absorption bands were determined with the help of microphotometric records of iron arc spectrum in the same way as described in an earlier paper (Banerjee, 1956a).

RESULTS AND DISCUSSION

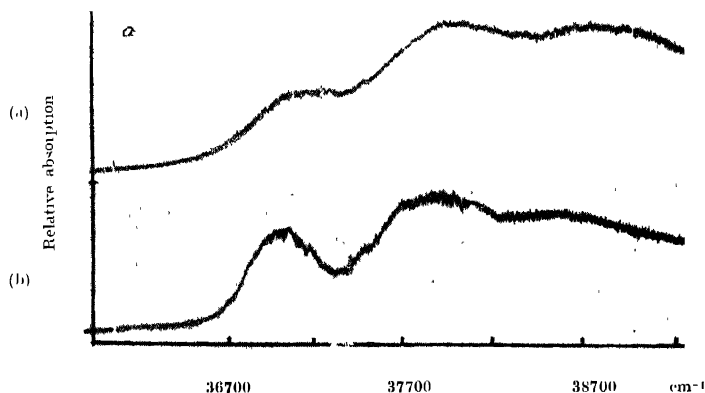
The microphotometric records of the absorption spectra of the picolines have been reproduced in figures 1, 2 and 3. The frequencies in cm^{-1} of the bands and then probable assignments are given in Tables I, II and III.

As the complete analysis of the absorption spectra of the compounds in the vapour state had already been reported by Rush and Spomer (1952), the spectra of these in the vapour state were not studied in the present investigation. The bands due to the vapours were found to consist of two systems corresponding to $n \rightarrow \pi^*$ and $\pi \rightarrow \pi^*$ transitions and were designated by the authors as Transition I and Transition II respectively. The assignments of the bands given by Rush and Spomer have been included in the Tables I, II and III for comparison.

TABLE I

 Absorption bands of α -picoline

Vapour Rush and Spomer (1952)		Liquid at 32°C Present author		Solid at -180°C Present author	
cm ⁻¹ & Intensity	Assignment	cm ⁻¹ & Intensity	Assignment	cm ⁻¹ & Intensity	Assignment
37450 vw		37074 m	ν_0	36971 m	ν_0
37530 w		37997 s	$\nu_0 + 923$	37767 s	$\nu_0 + 796$
37620 m	ν_0 (0-0)	38914 s	$\nu_0 + 2 \times 923$	37939 s	$\nu_0 + 968$
38250?m				38725 m	$\nu_0 + 796$
38430?s	$\nu_0 + 810$				+ 968
38580 vs	$\nu_0 + 960$				
39200 s	$\nu_0 + 2 \times 810$				
39500 s	$\nu_0 + 2 \times 960$				
40100?mw	$\nu_0 + 2 \times 810 + 960$				


 Fig. 1. Microphotometric records of the ultraviolet absorption spectra of α -picoline
 (a) Liquid at 32°C (b) Solid at -180°C

α -Picoline

The ultraviolet absorption spectrum of α -picoline in the vapour state shows two systems of bands (Rush and Spomer, 1952) corresponding to Transition I ($n \rightarrow \pi^*$) and Transition II ($\pi \rightarrow \pi^*$). The first system on the longer wavelength

side (corresponding to Transition I) consists of weak and narrow bands with the ν_0 -band at 34753 cm^{-1} and the second system on the shorter wavelength side (Transition II) consists of stronger bands with the ν_0 -band at 37620 cm^{-1} . In the case of the liquid state only one system of broad bands probably corresponding to the $\pi \rightarrow \pi^*$ transition has been observed in the present investigation while the bands due to the other transition could not be detected. The ν_0 -band in the case of the liquid is found to be at 37074 cm^{-1} . So it is displaced by 546 cm^{-1} towards longer wavelengths from its position in the spectrum due to the vapour state. This suggests that in the liquid state the excited electronic state of the α -picoline molecule is lowered considerably by the intermolecular field and this happens probably due to formation of associated groups. The absence of the bands of Transition I may also be attributed to formation of associated groups of molecules in the pure liquid through the nitrogen non-bonding electron and the hydrogen atom of neighbouring molecules. This result confirms the view mentioned in the case of pyridine in an earlier paper (Banerjee, 1956b) that the first system of bands exhibited by pyridine and substituted pyridines in the vapour state is due to $n \rightarrow \pi^*$ transition and that it disappears in the liquid state owing to formation of associated groups.

The spectrum due to the liquid contains two other broad bands besides the ν_0 -band which can be assigned to progressions of the frequency 923 cm^{-1} . In the case of the vapour state reported by Rush and Sponer (1952) the spectrum contains several transitions which can be represented in terms of frequencies 960 cm^{-1} and 810 cm^{-1} (Table I). Probably, the band corresponding to the assignment $\nu_0 + 923$ observed in the case of the liquid is formed by the broadening of the bands $\nu_0 + 810$ and $\nu_0 + 960$ given by the vapour state. As these bands become much broader with liquefaction of the vapour they are not resolved from each other and they overlap each other to produce a maximum lying between the two bands corresponding to the excited state frequencies 810 cm^{-1} and 960 cm^{-1} respectively. Such broadening of the bands in the spectrum due to the liquid is due probably to fluctuation of the intermolecular field caused by some sort of movements of the molecules. In the solid state such movements cease altogether. When the liquid is solidified and cooled to -180°C the ν_0 -band is found to be at 36971 cm^{-1} and the bands become sharper. They can be assigned as $\nu_0 + 796$, $\nu_0 + 968$ and $\nu_0 + 796 + 968$. Thus the bands corresponding to excited state frequencies 810 and 960 cm^{-1} observed in the case of the vapour are again resolved in the case of the solid state with the frequencies changed slightly.

β -Picoline

As reported by Rush and Sponer (1952) the absorption spectrum of β -picoline vapour consists of two systems of bands corresponding to Transition I ($n \rightarrow \pi^*$) and Transition II ($\pi \rightarrow \pi^*$) with the ν_0 -bands at 34684 cm^{-1} and 37380 cm^{-1}

TABLE II
 Absorption bands of β -picoline

Vapour Rush and Spomer (1952)		Liquid at 32°C Present author		Solid at -180°C Present author	
ν in cm ⁻¹ & Intensity	Assignment	ν in cm ⁻¹ & Intensity	Assignment	ν in cm ⁻¹ & Intensity	Assignment
36475 w		36930 m	ν_o	36862 m	ν_o
36585 vw	Transition 1	37087 m	ν_o +157	37519 m	ν_o + 657
36645 vw	Transition 1	37582 s	ν_o + 652	37845 s	ν_o + 984
36745 mw	Transition 1	37910 s	ν_o + 980	38509 s	ν_o + 984
36800 mw	Transition 1 ? ν_o - 3 \times 190	38568 s	ν_o + 980 + 652		+ 657
36935 ms	ν_o - 445				
36995 w	ν_o - 2 \times 190				
37100 w					
37190 ms	ν_o - 190				
37380 s	ν_o (0-0)				
37540 ms	ν_o + 160				
	ν_o + 600 - 445				
37770 m	ν_o + 390				
37980 ms	ν_o + 600				
38090 mw	ν_o + 710				
38180 s	ν_o + 800				
	ν_o + 1020 - 190				
38320 vs	ν_o + 940				
38400 vs	ν_o + 1020				
38540 m	ν_o + 160 + 1020				
	ν_o + 160 + 940				
38760 mw	ν_o + 390 + 940				
	ν_o + 390 + 1020				
38970 m	ν_o + 600 + 940				
	ν_o + 600 + 1020				
39190 ms	ν_o + 800 + 1020				
	ν_o + 2 \times 1020 - 190				
39310 s	ν_o + 2 \times 940 ?				
	ν_o + 940 + 1020				
39540 m	ν_o + 160 + 2 \times 1020				
39760 m	ν_o + 390 + 2 \times 940				
	ν_o + 390 + 2 \times 1020				
39960 m	ν_o + 600 + 2 \times 940				
	ν_o + 600 + 2 \times 1020				

respectively. In the liquid and solid states this substance also gives only one system of bands corresponding to Transition II. In the spectrum due to the liquid state five broad bands are observed (figure 2). The first band is broad and seems to consist of two maxima separated by 157 cm^{-1} . If the first maximum on the longer wavelength side at 36930 cm^{-1} be taken as the ν_0 -band it is found that the ν_0 -band is displaced by 450 cm^{-1} from its position in the spectrum due to the vapour. Thus in this case also the molecules seem to become strongly associated with liquefaction of the vapour as in the case of α -picoline. Assuming the band at 36930 cm^{-1} to be the ν_0 -band for liquid state, the other bands can be assigned as $\nu_0 + 157$, $\nu_0 + 652$, $\nu_0 + 980$ and $\nu_0 + 980 + 652$. When the liquid is solidified and cooled to -180°C the ν_0 band shifts to 36862 cm^{-1} and it becomes sharp. Also, the band which was assigned as $\nu_0 + 157\text{ cm}^{-1}$ in the case of the liquid disappears. The other bands in the case of the solid can be expressed in terms of vibration frequencies 657 cm^{-1} , 984 cm^{-1} and their combinations

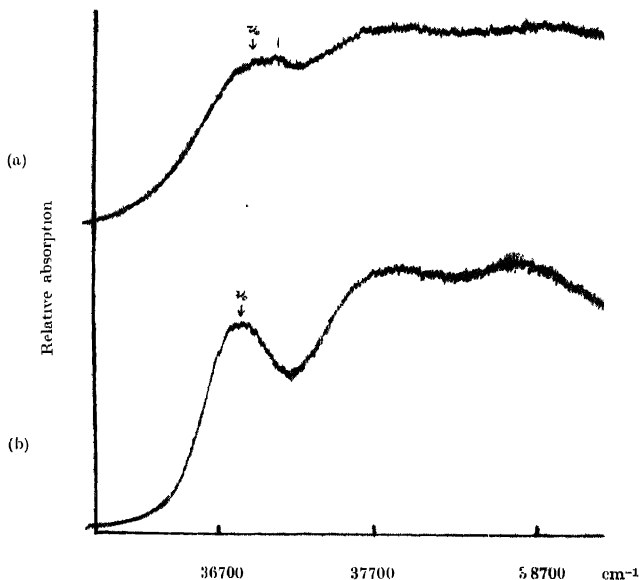


Fig. 2. Microphotometric records of the ultraviolet absorption spectra of β picoline.
(a) Liquid at 32°C (b) Solid at -180°C

The disappearance of the band mentioned above at low temperature is significant. While analysing the bands due to the vapour state Rush and Spomer (1952) observed progressions of vibrational frequencies 160 , 390 , 600 , 800 , 940 and 1020 cm^{-1} . Of these the frequency 160 cm^{-1} was assigned as a combination

frequency (600-445) cm^{-1} (Table II). This implied a transition from an excited vibrational state of frequency 445 cm^{-1} in the ground state to another excited vibrational state of frequency 600 cm^{-1} . According to such an interpretation of the band it would be expected that at low temperatures this band would disappear, because the number of molecules in the excited vibrational state corresponding to vibrational frequency 445 cm^{-1} would be negligible. Since it is observed in the present investigation that the band disappears at -180°C it is evident that this band is produced by a transition in which an excited vibrational state is involved. These results thus confirm this assignment made by Rush and Sponer (1952).

γ -Picoline :

In the classification of the absorption spectrum of γ -picoline vapour given by Rush and Sponer (1952) the ν_0 band of Transition I was assumed to be at 35165

TABLE III
Absorption bands of γ -picoline

Vapour Rush and Sponer (1952)		Liquid at 32°C Present author		Solid at -180°C Present author	
Wave No (cm ⁻¹) & Intensity	Assignment	Wave No. (cm ⁻¹) & Intensity	Assignment	Wave No. (cm ⁻¹) & Intensity	Assignment
38220 <i>mw</i>		38033 <i>ms</i> <i>ν</i> ₀		37969 <i>ms</i> <i>ν</i> ₀	
38320 <i>m</i> <i>ν</i> ₀ (0-0)?		38800 <i>s</i> <i>ν</i> ₀ 1-767		38558 <i>ms</i> <i>ν</i> ₀ + 586	
38570 <i>m</i>		39560 <i>s</i> <i>ν</i> ₀ + 2 × 767		38921 <i>s</i> <i>ν</i> ₀ + 952	
38920 <i>ms</i> <i>ν</i> ₀ + 600				39513 <i>msb</i> <i>ν</i> ₀ + 952 + 586	
39240 <i>s</i> <i>ν</i> ₀ + 920					
39500 <i>s</i> <i>ν</i> ₀ + 1180				39876 <i>msb</i> <i>ν</i> ₀ + 2 × 952	
<i>ν</i> ₀ + 2 × 600					
39800 <i>ms</i> <i>ν</i> ₀ + 600 + 920					
40120 <i>ms</i> <i>ν</i> ₀ + 2 × 920					
40410 <i>m</i> <i>ν</i> ₀ + 920 + 1180					
<i>ν</i> ₀ + 920 + 2 × 600					
41140 ? <i>m</i>					
41360 ? <i>mw</i> <i>ν</i> ₀ + 2 × 920 + 1180 ?					

cm^{-1} and this system of bands is not observed in the spectrum due to the substance in the liquid and solid states as in the case of the α - or β -compounds. The bands of Transition II in the case of the vapour are diffuse and the probable

position of the ν_0 -band is taken at 38320 cm^{-1} (Rush and Sponer, 1952). The spectrum due to the substance in the liquid state consists of three broad bands, the ν_0 -band being at 38033 cm^{-1} and the other bands representing progressions of frequency 767 cm^{-1} . Thus with liquefaction of vapour the ν_0 -band shifts towards longer wavelengths by 287 cm^{-1} . When the liquid is frozen five absorption bands are observed and the ν_0 -band is found to be at 37969 cm^{-1} . So only a small displacement of about 64 cm^{-1} towards longer wavelengths takes place in the position of the ν_0 -band with solidification. The bands due to the solid state represent transitions $\nu_0 + 586$, $\nu_0 + 952$, $\nu_0 + 952 + 586$ and $\nu_0 + 2 \times 952$. The bands are rather broad even at -180°C and those corresponding to frequencies $\nu_0 + 586$ and $\nu_0 + 952 + 586$ are just resolved from the adjacent bands.

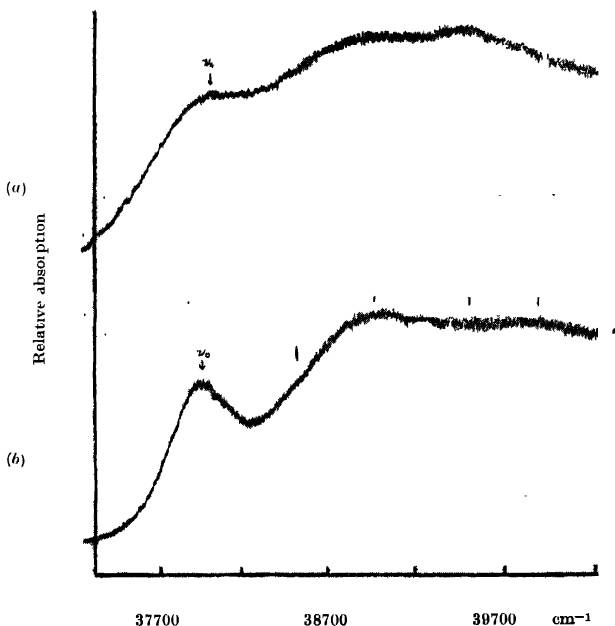


Fig.3. Microphotometric records of the ultraviolet absorption spectra of γ picolno.
(a) Liquid at 32°C (b) Solid at -180°C

The band $\nu_0 + 767\text{ cm}^{-1}$ observed in the case of the liquid probably does not represent an excited state vibration frequency but it is probably produced by the overlapping of the bands $\nu_0 + 600$ and $\nu_0 + 920$ observed in the spectrum of the vapour each of which becomes broader and merges into the other when the vapour is liquefied. This result is similar to that observed in the case of

α -picoline and indicates that in the liquid state the motion of the molecules causes a fluctuation of intermolecular field which is responsible for the broadening of the bands. When the liquid is solidified and cooled to -180°C the bands become a little sharper owing to cessation of some motions of the molecules and the bands involving excited state frequencies 600 and 920 cm^{-1} due to the vapour are found to be just resolved from each other

From the above discussions it can be seen that the molecules of each of the three isomeric picolines are probably linked with each other through the nitrogen non-bonding electron and a hydrogen atom of neighbouring molecule in the state of aggregation. In all the three cases it is found that in the liquid state the bands become broad due to fluctuation of intermolecular field and when the liquids are solidified and cooled to -180°C the bands become sharper. But the sharpening of the bands is not as pronounced as is usually observed in the case of halogen substituted benzene compounds

ACKNOWLEDGMENT

The author is indebted to Professor S. C. Sirkar, D. Sc., F. N. I., for his helpful guidance during the progress of the work.

REFERENCES

- Banerjee, S. B., 1956a, *Ind. J. Phys.*, **30**, 106.
 " 1956b, *Ind. J. Phys.*, **30**, 480.
Kasha, M., 1950, Discussions of the Faraday Society, No. **9**, 14.
Rush, J. H., and Sponer, H., 1952, *J. Chem. Phys.*, **20**, 1847.
Sponer, H. and Stuecklen, H., 1946, *J. Chem. Phys.*, **14**, 101.

FADING AND RANDOM MOTION OF IONOSPHERIC IRREGULARITIES.

S. N. MITRA AND R. B. L. SRIVASTAVA

ALL INDIA RADIO, NEW DELHI

(Received for publication June 15, 1956)

ABSTRACT: The paper describes the results of the statistical analysis of fading curves obtained at Delhi on transmission from the medium wave transmitter at Lucknow operating on 1020 Kc/s. The different types of fading commonly experienced and their possible causes are discussed. The irregular types of fading, which formed the material for analysis, are shown to be caused by either a random motion of the ionospheric irregularities or by superposition of a steady signal upon the randomly varying one. It has been shown that the probability distribution of the former is given by a Rayleigh curve and that of the latter by a normal law of error. The relative proportion of the random and the steady components in the case of a Gaussian distribution of amplitude has been calculated. The 'time-analysis' of the fading curves reveals the r.m.s. velocity in the line-of-sight of the random motion of the ionospheric irregularities and is found to be between 4 and 25 m/sec. Booker, Ratcliffe and Shinn had studied the problem of fading from a diffraction process of an irregular screen representing the ionosphere. Their analysis has been used in the present paper to deduce the r.m.s. velocity of the ionospheric irregularities based on auto-correlation function and the power spectrum of the received wave. It is found that the values of the r.m.s. velocity deduced from the two methods are in substantial agreement. The effect of steady drift, location and the dimension of irregularities in the ionosphere causing the irregular fading have also been discussed.

1. INTRODUCTION

It is well known that the fading of a downcoming wave from the ionosphere is often caused by motion of ionospheric irregularities, from which the incident wave is diffractively scattered. The downcoming wave may be considered as the resultant of a large number of scattered wavelets having different phases. As the scattering centres change their position the resultant wave will fade. This motion may be imparted either by a steady drift in the ionosphere or random motion of ionospheric irregularities. Statistical analysis of such fading curves has already been reported by Mitra (1949a) and McNicol (1949). Ratcliffe (1948) has shown how, from a consideration of the scattered power, the root mean squared value of the random velocity of the irregularities can be evaluated. The steady drift can be determined by employing the familiar spaced receiver technique (Mitra, 1949b).

When a fading curve of a received signal is taken on continuous wave transmissions, there are causes other than drift to produce fading. For example, the interference between multiple-hop transmissions will produce amplitude fluctuation.

tuation of the received signal. But the predominant cause of fading even on such transmissions is the drift of ionospheric irregularities. There are, however, some peculiar types of fading known as 'Surge' and 'Flutter' commonly experienced in South India whose origin is not yet clearly understood.

Excepting surge and flutter, the short period fading has been known to possess similar characteristics both on short and medium waves. While some amount of work in the nature of statistical analysis has been carried out on fading on short wave transmissions taken on pulses and continuous wave, the fading on medium waves has not received serious attention. The present paper will deal mostly with medium wave fading. It will be shown in the paper that similar types of statistical analysis can be applied to fading curves taken on medium wave transmissions to evaluate the random motion of the ionospheric irregularities. It will also be shown in the paper that in some cases the analysis reveals that a steady signal was superimposed upon a randomly varying one. The ratio between the steady and the random component has been evaluated from the analysis.

We shall first concentrate upon the distribution of the resultant amplitude from its temporal variation. The shape of the distribution curve will indicate whether the fading has been caused by random motion of the ionospheric irregularities or by the addition of a steady signal upon a randomly varying one. We shall next evaluate the ratio between the steady and the random signals. A 'time analysis' of the fading curve will enable us to evaluate the r.m.s. value of the random velocity. In many aspects, the problem is similar to the analysis of random electrical noise as developed by Rice (1944, 1945) and later extended by Fürth and MacDonald (1947).

Booker, Ratcliffe and Shinn (1950) have studied the problem from its optical analogy. The irregularities in the ionosphere have been considered in terms of an irregular diffracting screen illuminated by a source of radiation and the diffraction pattern studied in terms of its 'auto-correlation' function and angular spectrum. We shall use some of their results and show that the deductions made from both the above methods are very nearly the same.

The possibility of the fading being caused by a steady ionospheric drift blowing the irregularities unchanged in form cannot be excluded. Investigation of such drift from fading curves indicates that where the steady drift is the predominant factor, the fading is usually quasi-periodic in nature (Mitra, 1949b) and the rate of fading slow. The rapid types of fading are usually caused by random motion of the ionospheric irregularities. In this paper, we shall make no assumption regarding the nature of the ionospheric irregularities and their origin.

2 EXPERIMENTAL PROCEDURE

Some fading records on medium wave transmissions from Lucknow (Lat. $26^{\circ}55'$ N Long $80^{\circ}55'$ E) on 1020 Kc/s were taken at the Research Department, All India Radio, New Delhi (Lat. $28^{\circ}35'$ N, Long. $77^{\circ}5'$ E) during the months of March and April, 1955. An RCA field strength meter with a built-in D.C. amplifier was used. The output from the second detector of the receiver in the field strength meter was passed on to the D.C. amplifier which actuated a pen-and-ink recorder. The receiver was found to be fairly linear in the range through which the fading curves were recorded. Experiments were conducted in the night from 2230 to 2400 IST ($5\frac{1}{2}$ hours ahead of G.M.T.). A typical fading curve is shown in figure 1. These curves have been analysed statistically

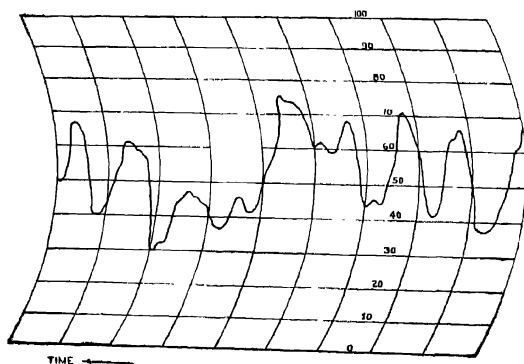


Fig. 1. Typical fading curve
(Lucknow 1020 Kc/s Recorded at Delhi on 7.4.55 at 2240 HRS I.S.T.)

and the results described in the following sections. The total number of records analysed is 46. On an earlier occasion about 200 fading records were taken on vertical incidence pulsed transmissions on frequencies of 4.8, 5.4, 6.0 and 7.5 Mc/s. A simple analysis of these records for evaluating the r.m.s. velocity of ionospheric irregularities has been included in the paper.

3. AMPLITUDE ANALYSIS

When the scattering centres are moving in a random manner, the resultant amplitude of the received signal at any instant may be thought of as due to the sum of a large number of vectors (each vector corresponding to a wave scattered from a centre) each having random phase. The problem, therefore, becomes similar to one of 'random walk' and Lord Rayleigh (1899) has given the mathematical expression for the probability of occurrence of the resultant vector. Let

R be the resultant amplitude in the received signal at any instant. Then the probability $P(R)dR$ of finding an amplitude R within the range of amplitudes R and $R+dR$ is given by

$$P(R)dR = \frac{R}{\psi} e^{-\frac{R^2}{2\psi}} dR \quad \dots (1)$$

where
$$\int_0^\infty P(R)dR = 1 \quad \dots (2)$$

and
$$\psi = \int_0^\infty W(f) df \quad \dots (3)$$

$W(f)$ being the density in the power spectrum.

ψ is also related to the mean value \bar{R} and the mean squared value \bar{R}^2 by the following equations

$$\bar{R} = \int_0^\infty P(R)RdR = \left(\frac{\pi\psi}{2} \right)^{1/2} \quad \dots (4)$$

$$\bar{R}^2 = \int_0^\infty P(R)R^2dR = 2\psi \quad \dots (5)$$

Similarly, R_m , i.e. that value of R for which $P(R)$ is maximum is given by

$$R_m = \psi^{1/2} \quad \dots (6)$$

It is sometimes convenient to evaluate ψ in the following way

$$\log \frac{P(R)}{R} = \log \frac{1}{\psi} - \frac{R^2}{2\psi} \quad \dots (7)$$

The plot of $\log \frac{P(R)}{R}$ against R^2 is, therefore, a straight line, the slope of which is $-\frac{1}{2\psi}$ and the intercept $\log \frac{1}{\psi}$.

4. ADDITION OF A STEADY SIGNAL

When a steady signal in the form of a wave specularly reflected from the ionosphere or in the form of a ground wave is superimposed upon the randomly varying signals, the distribution of the envelope due to such addition is as follows (Rice, 1945) :

Suppose $B \cos pt$ represents the steady signal and Q is the resultant amplitude of the envelope at any instant. Then the probability density $P(Q)$ is given by

$$P(Q) = \frac{Q}{\psi} \exp \left[-\frac{Q^2 + B^2}{2\psi} \right] I_0 \left(\frac{QB}{\psi} \right) \quad \dots (8)$$

where I_0 is the Bessel function of zero order with imaginary argument. The mean squared value of Q is given by

$$\begin{aligned} \bar{Q}^2 &= \int_0^\infty \frac{Q}{\psi} \exp \left[-\frac{Q^2 + B^2}{2\psi} \right] I_0 \left(\frac{QB}{\psi} \right) Q^2 dQ \\ &= B^2 + 2\psi = B^2 + R^2 \end{aligned} \quad \dots (9)$$

Let us put $b = \frac{B}{\psi}$, = ratio between the amplitude of the steady signal and the most probable value of the random signal. Curves for various values of b (-0, 1, 2, 3, ...) have been plotted by Rice. When b is small compared to unity,

$$P(Q) \simeq \frac{Q}{\psi} \exp \left(-\frac{Q^2}{2\psi} \right) \quad \dots (10)$$

which gives a Rayleigh distribution (1). When b is large compared to unity, we may replace $I_0 \left(\frac{QB}{\psi} \right)$ by its asymptotic expression and (8) becomes

$$\begin{aligned} P(Q) &\simeq \left(1 + \frac{1}{8QB/\psi} \right) \left(\frac{Q}{2\pi B\psi} \right)^{1/2} \exp \left[-\frac{(Q-B)^2}{2\psi} \right] \\ &\simeq \frac{1}{\sqrt{2\pi\psi}} \left(\frac{Q}{B} \right)^{1/2} \exp \left[-\frac{(Q-B)^2}{2\psi} \right] \end{aligned} \quad \dots (11)$$

Thus, $P(Q)$ follows a normal distribution. McNicol (1949) has shown that the expression (11) may be rewritten in the form

$$P(Q) \simeq \frac{1}{\sqrt{2\pi\psi}} \exp \left[-\frac{(Q-Q_m)^2}{2\psi} \right] \quad \dots (12)$$

within an accuracy of about 1%. Q_m is given by

$$Q_m = [\psi(b^2 + 1)]^{1/2} \quad \dots (13)$$

In actual analysis, however, those fading curves whose amplitude distribution is normal in shape can be represented by equation (12). Then a plot of $\log P(Q)$

against $(Q-Q_m)^2$ gives a straight line whose slope is given by $\frac{1}{2\psi}$. Knowing ψ and Q_m one can evaluate b which represents the relative proportion between the steady and the random signals in the received wave.

In recent years some workers have indicated (C.C.I.R. 1953) that the amplitude analysis of their fading curves represents a distribution which is of normal logarithmic in character. The distribution is

$$P(R) = \frac{1}{\sqrt{2\pi}\sigma} \int_{\log R}^{\infty} \exp\left(-\frac{R-R_m}{2\sigma}\right)^2 dR \quad \dots (14)$$

It may, however, be pointed out that (14) is very similar to (12) and such a distribution is probably due to the addition of a steady signal upon a randomly varying one.

5. ANALYSIS OF EXPERIMENTAL RESULTS

The amplitude analysis of the records was carried out in the following way. Equidistant lines at a very small interval of time (1 second) were drawn across the records and the amplitude read off at each interval. Curves were then plotted showing the probability of occurrence of an amplitude against the range of amplitude. In some cases, Rayleigh distribution was evident and in others, Gaussian. In both cases ψ was determined by the methods mentioned above and the values of b were also calculated.

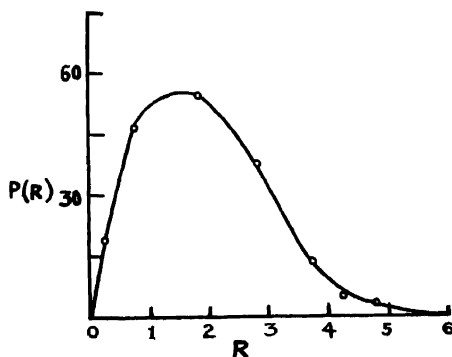


Fig. 2 (a). Amplitude analysis (Rayleigh) (Fading Curve No. 7)

Two typical cases are shown in figures 2 and 3. Figure 2(a) shows the Rayleigh distribution and figure 2(b) the corresponding plot of $\log \frac{P(R)}{R}$

against R^2 . Figure 3(a) shows a typical normal distribution which is due to the addition of a steady signal upon a random one. Figure 3(b) shows the corresponding plot of $\log P(Q)$ against $(Q - Q_m)^2$.

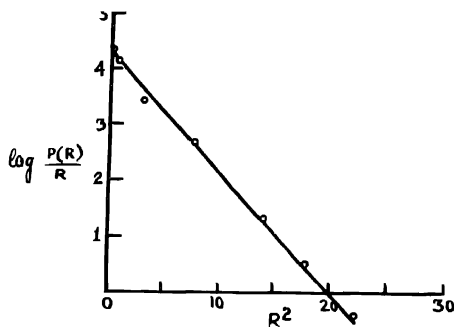


Fig. 2(b). Log plot of Fig. 2(a).

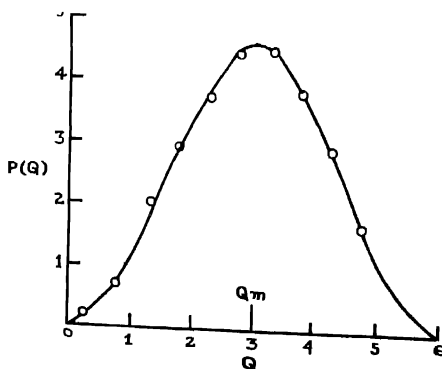


Fig. 3(a). Amplitude analysis (Gaussian) (Fading Curve No. 11)

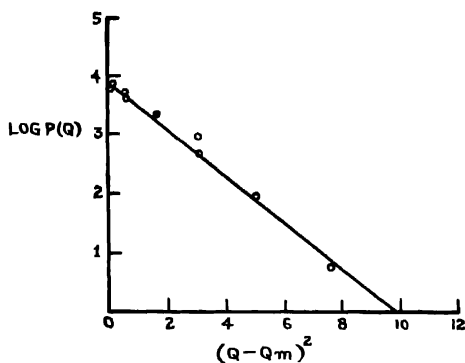


Fig. 3(b). Log plot of Fig. 3(a).

The results of analysis of the fading curves taken at Delhi on the medium wave transmissions from Lucknow on 1020 Kc/s are shown in Table I.

TABLE I

No.	Station	Frequency	Time IST	Date	Nature of distribution	ψ	b
1.	Lucknow	1020 Kc/s	2235	5 4.55	Rayleigh	3.28	.71
			2250	6 4.55	"	3.11	.92
3.			2250	7 4.55	"	3.33	1.34
4.			2305	7.4.55	"	2.98	1.25
			2250	8 4.55	"	3.5	1.67
			2255	8.4.55	"	2.97	.6
			2245	10.4.55		2.21	.6
			2310	10 4.55		1.19	—
			2315	10.4.55	"	2.39	1.0
10.			2245	5.4.55	Normal	1.2	2.3
11.			2255	5.4.55	"	1.28	2.5
12.			2300	5.4.55	"	1.57	2.4
13.			2240	6.4.55	"	.29	2.1
14.			2255	6.4.55	"	1.08	2.2
15.			2300	6.4.55	"	.95	2.64

It will be noted from the above table, that whenever b exceeds 2, the distribution of the resultant amplitude becomes a normal curve. But for b less than 2 the distribution is given by a Rayleigh one. In other words, when the strength of the steady signal in the fading curve is more than twice that of the random component, a normal distribution of the resulting envelope is obtained. McNicol has also obtained this transition from Rayleigh to normal curve for $b \geq 2$. Thus, the theory predicted by Rice (1945) is found to agree with the experimental results.

6. COMBINATION OF SEVERAL WAVES

In the previous sections we have considered the cases where either only the random signal or a combination of a steady signal with a random component is present in the received wave. It is of interest to enquire what happens when several sky-wave components are present in the downcoming wave. It is quite likely that on C. W. transmissions under suitable conditions (specially during night when absorption is low) multiple-hop components are simultaneously received. A steady signal in the form of a ground wave (when the distance between the transmitter and the receiver is small) or a specularly reflected component may also be present.

We shall first consider the superposition of a number of random components. de Boer (1931) has worked out individual cases when the number n varies from 1, 2, 3, ... We assume that the amplitudes of the different components are all equal, the variation is only in the phase. This assumption is well justified in the case of an isotropic ionosphere where the scattering centres are evenly distributed in all directions. The different sky waves will undergo the same scattering process and the amplitude of the different components may be regarded as equal.

A convenient measure for describing the situation is by means of 'percentage of scattering'. This is given by

$$\text{Percentage of scattering} = \frac{\bar{R}^2}{\bar{R}^2} \cdot \frac{\sigma}{R} \cdot 100$$

de Boer has calculated from theoretical grounds, the values of the percentage of scattering for various values of n (1, 2, 3, ...). He finds that the percentage scattering approaches asymptotically a value of 21% for $n \geq 4$. This value is obtained from a Rayleigh distribution. It is, therefore, found that even for several components, each varying randomly, the resulting distribution essentially remains a Rayleigh one. In the present analysis, the percentage scattering has been calculated for each of the 9 fading curves mentioned in Table I. The values are shown in Table II.

TABLE II

No.	Fading curve	Percentage scattering
1.		22.7
2.		25.4
3.		16.0
4.		11.5
5.		15.7
6.		24.3
7.		23.7
8.		27.5
9.		30.5

We shall now discuss the case when both the amplitude and the phase in the individual components are varying. Pearson (1906) has worked out the exact mathematical expression for $n = 1, 2, 3, \dots$. For practical purposes, however, the following expression for the probability distribution of the resultant amplitude r is a good approximation.

$$P(r) = \frac{2r}{\bar{n}\bar{r}^2} \exp\left(-\frac{r^2}{\bar{n}\bar{r}^2}\right) \quad \dots (15)$$

which is again a Rayleigh distribution. The percentage of scattering is nearly the same as we get for phase variations alone, namely 21.5%.

In the case of several random components being present together with a steady signal the distribution of the envelope will be either a Rayleigh or a normal one depending upon the relative proportion of the steady signal.

We therefore find that the amplitude distribution of a rapid type of fading pattern taken either on medium wave or on short wave transmissions, when given by a Rayleigh curve, is predominantly due to the addition of a large number of random vectors arising from diffractive scattering from ionospheric irregularities. When the distribution is given by a normal law of error, a comparable amount of steady signal in the form of either a ground wave or a specularly reflected component is superimposed upon the randomly varying signal. It is possible to evaluate the relative proportion of the steady signal and the random component from the parameters of the normal distribution curve. When several sky-wave signals, each varying independently in phase and amplitude, are present the distribution of the envelope is still a Rayleigh one.

7 TIME ANALYSIS

It has been mentioned in the introduction that when fading is due to random motion of ionospheric irregularities it is possible to evaluate the r.m.s. value of the random velocity. The analysis is similar to the case of random noise arising from a resistor kept at certain temperature.

In this section we shall discuss the problem in some detail.

Let us assume that the ionospheric irregularities are moving with a random velocity v in the line of sight and v_0 is its r.m.s. value. The scattering centres can be assumed to be in random motion much like the gas molecules in thermal agitation and the distribution of v (in one dimension) may be expressed by the following normal law

$$P(v) = \frac{1}{\sqrt{2\pi}v_0} \cdot \exp\left(-\frac{v^2}{2v_0^2}\right) \quad \dots (16)$$

$$\text{where} \quad \int_{-\infty}^{\infty} P(v)dv = 1 \quad \dots (17)$$

The wave-frequency scattered from each irregularity will undergo a Doppler shift due to its motion and the shifted frequency f will be given by

$$f = f_0 \left(1 + \frac{2v}{c}\right) \quad \dots (18)$$

where f_0 is incident wave frequency

Combining (16) and (18), we have,

$$P(f) = \frac{1}{\sqrt{2\pi}v_0} \cdot \frac{c}{2f_0} \exp\left[-\frac{c^2(f-f_0)^2}{8f_0^2v_0^2}\right] \quad \dots (19)$$

$$\text{Writing} \quad \sigma = \frac{2f_0v_0}{c} = \frac{2v_0}{\lambda} \quad \dots (20)$$

(19) becomes

$$P(f) = \frac{1}{\sqrt{2\pi}\sigma} \exp\left[-\frac{(f-f_0)^2}{2\sigma^2}\right] \quad \dots (21)$$

Thus the Doppler shifted frequencies are also distributed in terms of a normal law of error with the standard deviation σ

Now the phases of the scattered waves from the individual irregularities are distributed at random since the scattering centres are themselves displaced in

a random manner. Powers due to each contribution add up and the power spectrum $W(f)$ may be expressed by

$$W(f) = \frac{\psi}{\sqrt{2\pi}\sigma} \exp\left[-\frac{(f-f_0)^2}{2\sigma^2}\right] \quad \dots \quad (22)$$

where $\psi = \int_0^\infty W(f)df = \text{total energy in the power spectrum.}$

The fading of the resultant wave at the ground is, therefore, seen to be due to the addition of a large number of scattered signals whose frequencies are distributed in accordance with (19) and powers in accordance with (22). The situation is similar to the case when random noise is passed through a filter whose band-pass characteristic is given by a normal expression of the type represented by (22).

Furth and MacDonald (1947) have shown, from an extension of Rice's theory, that when random noise having a Rayleigh amplitude distribution is passed through a band pass filter whose power-pass characteristic is given by (22), then the probability distribution of v_τ , the successive difference between two amplitudes within a small interval of time, is also given by the following normal law

$$P(v_\tau)dv_\tau = \frac{1}{\sqrt{\pi}} e^{-x^2} dx \quad \dots \quad (23)$$

$$\text{where,} \quad x = \frac{v_\tau}{2\pi\sigma\tau\sqrt{2\psi}} \quad \dots \quad (24)$$

From (23) and (24)

$$\begin{aligned} \overline{\left[\frac{v_\tau}{\tau}\right]} &= \frac{2}{\tau} \int_0^\infty P(v_\tau)v_\tau dv_\tau \\ &= \sqrt{2\pi\psi} \cdot 2\sigma \\ &= 4R\sigma \text{ from (4)} \\ &= \frac{8v_0R}{\lambda} \text{ from (20)} \quad \dots \quad (25) \end{aligned}$$

where λ is the wavelength of the radio wave. $\overline{\left[\frac{v_\tau}{\tau}\right]}$ has been called the "speed of fading" and is seen to be inversely proportional to the wavelength of the radio wave.

There is another method of calculating v_0 . From equation (23),

$$v_{\tau}^2 = \int_0^{\sigma} P(v_{\tau}) v_{\tau}^2 dv_{\tau} \\ \frac{1}{2}(2\pi\sigma\tau\sqrt{2}\psi)^2 \\ = \frac{16\pi^2 v_0^2 \tau^2}{\lambda^2} \cdot \psi \quad (26)$$

v_0 can be calculated from a knowledge of v_{τ}^2 , τ , ψ and λ .

Thus from a fading record whose amplitude distribution is given by a Rayleigh law and v_{τ} -distribution by a normal curve the value of v_0 , the r.m.s. velocity in the line of sight of the random motion of the ionospheric irregularities can be determined with the help of equations (25) and (26).

It should, however, be remembered that the above analysis refers to a random velocity v in the line of sight. For oblique incidence transmissions, the situation may be described by means of an ellipsoid passing through the scattering centres and with the transmitter and the receiver at the two foci. Then the component of the velocity along a direction normal to the ellipsoid will only be effective in producing a Doppler shift. When the scattering centres are located at the point of reflection of the incident wave, then the line-of-sight velocity will be $v \cos \phi$ where ϕ is the angle of incidence.

The speed of fading will therefore become,

$$\frac{|v_{\tau}|}{\tau} = \frac{8v_0 R \cos \phi}{\lambda} \quad \dots (27)$$

The value of ϕ can be determined from a knowledge of the distance between the transmitter and the receiver and by assuming a certain height of reflection. The speed of fading on oblique incidence will, however, be less by a factor $\cos \phi$ than that for the equivalent normal incidence transmission.

There is, however, a simple but approximate method of evaluating v_0 . Rice has shown that if σ is the standard deviation of the power spectrum of the received signal, then the number N of maxima per second of the fading record is given by

$$N = 2.52\sigma \\ \text{i.e.,} \quad v_0 \approx \frac{N\lambda}{5} \quad \dots (28)$$

This method of evaluating v_0 has been adopted in the fading records taken in February, 1952 on short wave pulsed transmissions at vertical incidence.

8. CALCULATION OF v_0

(a) *Medium wave.*

The medium wave fading curves as indicated in Table I were analysed for v_r -distribution. Only those curves were selected whose amplitude distribution obeyed Rayleigh's law. A typical v_r -distribution is shown in figure 4 where

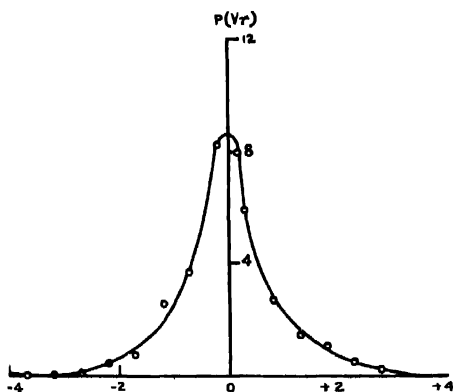


Fig. 4. v_r Distribution (Gaussian)

$\tau = 1$ second. A perusal of Table I shows that only 9 such curves are available. Table III below shows the values of v_0 determined from these fading curves by employing equation (27).

TABLE III

Fading curve No.	v_0 (m/s)
1	20.5
2	14.24
3	5.18
4	5.7
5	3.9
6	4.52
7	10.16
8	25.1
9	15.66

It would be seen from the above table that v_0 was varying between 3.9 and 25.1 m/s

(b) *Short waves.*

We had taken about 200 fading curves on an earlier occasion on vertical incidence pulsed transmissions on 4.8, 5.4, 6.0 and 7.5 Mc/s (Mitra, 1953). These fading curves were taken by employing a peak amplitude recorder (Mazumdar & Mitra, 1954) and were taken for five minutes at a stretch successively on the four frequencies mentioned above from 1230 to 1730 I.S.T. centred on each half hour. The records taken for 8 days from 21st to 29th February have now been utilised to calculate v_0 in the following way.

The speed of fading has been evaluated from each record by counting the number of maxima per minute. The average speed of fading has been calculated for all the fading records at each hour for the eight-day period. Table IV below gives the average hourly values of v_0 over the eight-day period (21st to 29th Feb.), calculated from the speed of fading by employing equation (28) for the different short wave frequencies at different hours of the day

TABLE IV

Time I S T	Values of v_0 in m/s on			
	4.8 Mc/s 62.5m	5.4 Mc/s 55.5m	6.0 Mc/s 50.0m	7.5 Mc/s 40.0m
1230	1.4	-	-	-
1300	1.2	1.2	1.3	.8
1330	1.2	1.2	.9	.6
1400	1.5	1.2	.8	.5
1430	1.7	1.1	1.3	.6
1500	1.6	1.0	.9	.7
1530	1.3	1.1	.9	.6
1600	1.2	1.0	.9	.6
1630	1.0	.8	.9	.5
1700	1.0	.8	.7	.5
1730	1.1	.9	.6	.3
Average	1.3	1.0	.9	.6

A curve is plotted showing the variation of v_0 with wavelength and is shown in figure 5. The curve is a straight line indicating the validity of equations (25) and (28).

The higher values of v_0 found in our analysis of medium wave fading curves (shown in Table III) are, therefore, to be expected according to the theory

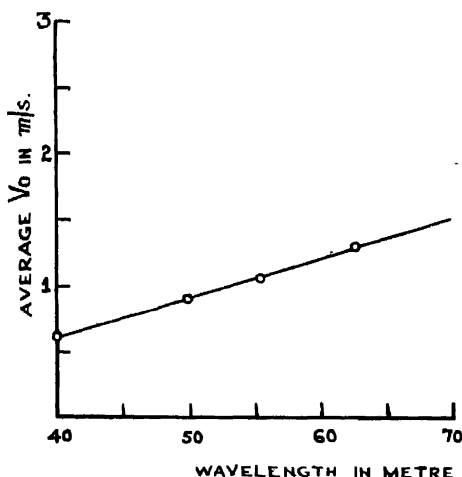


Fig. 5. Variation of v_0 with wavelength.

described above. In experiment too we have found higher values of v_0 from an analysis of the m.w. fading records (Table III).

9. RIGOROUS ANALYSIS

A detailed statistical analysis of similar fading curves (Mitra, 1949a) has revealed that the normal distribution of v_r is rather an approximation. An accurate distribution of v_r based on the standard statistical test known as the 'goodness of fit' (χ^2 -test) has been found to be a type VII distribution of Pearson and is given by

$$P(v_r) = A \left(1 + \frac{v_r^2}{a^2} \right)^{-m} \quad \dots (29)$$

$$\text{where,} \quad A = \frac{1}{a} \cdot \frac{\overline{m}}{\sqrt{\pi} \overline{m} - \frac{1}{2}} \quad \dots (30)$$

$$m = \frac{5\beta_2 - 9}{2(\beta_2 - 3)} \quad \dots (31)$$

$$\text{and} \quad a^2 = \frac{2\mu_2\beta_2}{\beta_2 - 3} \quad \dots (32)$$

μ_2 and β_2 are the corrected second order moment' and the 'co-efficient of excess' in the distribution. Physically the type VII distribution appears similar to a normal curve except that it is narrower at the maximum and wider at the skirts. In the present case also, we found a distribution (figure 4) which will be better represented by a type VII curve. But for all practical purposes where the main object is to calculate v_0 the normal distribution for v_r is a good approximation.

The significance of this departure of v_r -distribution from a normal one has been explained in the following way. We have assumed that the line of sight velocities of the irregularities are distributed according to a normal law of error. But the Doppler shift in frequency will depend upon the total change in the path due to the motion of the irregularities. Now, for the irregularities moving overhead, the Doppler shift in frequency will be smaller than for those situated at a distance. Smaller Doppler shifts indicate large occasions when v_r will be zero, and therefore, the v_r -distribution will have too many values near the peak. We, therefore, find that for a large number of irregularities moving at random in the horizontal reflecting plane of the ionosphere, a more accurate v_r -distribution will be given by a type VII distribution curve of Pearson. Banerji (1953) has, however, pointed out that the distribution of v_r is independent of the power spectrum of the returned wave and will remain Gaussian for any shape of the power spectrum. There are reasons to believe that the distribution of v_r and the power spectrum are interdependent and detailed statistical consideration is being worked out (to be published later) which will show that a type VII distribution is a better representation of the distribution of v_r as obtained in experiment.

10 EFFECT OF SLOWLY VARYING COMPONENTS

So far we have discussed the effect of the addition of a large number of component waves having random amplitudes and phases. Occasions may arise when, downcoming wave consists in the addition of two magneto-ionic components from the ionosphere. When both the components are fading independently and each component is the resultant of a large number of waves scattered from ionospheric irregularities, the fading will be irregular and the amplitude distribution of the resultant wave will be given by Rayleigh's law.

In the absence of irregularities, the two magneto-ionic components will have specular reflections from the ionosphere and their resultant will show amplitude variation due to a temporal variation between the phases of the two components. In such cases, the amplitude variation is periodic in nature (Mitra, 1950).

In general, it may be concluded that when the fading of the received signal is irregular in nature, it is either due to the addition of a large number of waves diffractively scattered from the ionospheric irregularities having random motion amongst themselves, or due to the superposition of a steady signal upon a randomly

varying component wave. The methods of analysis outlined in the previous sections can be employed to determine the r.m.s. value of the random velocity and the relative proportion of the steady signal present in the fading wave.

II. FADING AND CORRELATION FUNCTION

We have assumed that the fading is produced by diffractive scattering from a large number of ionospheric irregularities and the scattered wavelets having random amplitudes and phases combine at the ground to give a resultant signal at any instant. The signal will vary when the scattering centres are in motion. The fluctuating signal may be considered similar to 'random noise' produced when a resistor is kept at a temperature equilibrium.

The problem may also be looked upon from its optical analogy. We may visualise the situation in terms of an irregular diffracting screen replacing the irregular structure of the ionosphere illuminated by a point source of radiation representing the transmitter at the ground. We may replace the problem of irregular reflection in the ionosphere by means of a transmission one when the transmitter is located on the other side of the screen and study the distribution of the wave-field produced at the ground. The wave-field at any instant may be completely described from a knowledge of the nature of the diffracting screen. The instant-to-instant variations in the diffraction pattern will have some statistical properties in common so long as we deal with a 'stationary state.' An important statistical property of such variation is the auto-correlation function, which indicates the degree of correlation between the two values of the wave-field made at time separated by a series of time intervals. Rice (1945) has developed the theory of random noise based on the auto-correlation function. Wang and Uhlenbeck (1945) have used this function while describing the Brownian motion in liquids. Booker, Ratcliffe and Shinn (1950) have discussed the problem of ionospheric diffraction in terms of "angular spectrum" and auto-correlation function. We shall use some of their results in our analysis.

In our experiments, when the irregular screen is illuminated by plane waves, we get a temporal variation of the resulting e.m.f. of the wave-field on the ground. Let $\rho R(\tau)$ represent the autocorrelation function of the amplitude R of the fluctuating e.m.f. $\rho R(\tau)$ is given by

$$\rho R(\tau) = \frac{\int_{-\infty}^{\infty} R(t)R(t+\tau)dt - \left[\int_{-\infty}^{\infty} R(t)dt \right]^2}{\int_{-\infty}^{\infty} [R(t)]^2dt - \left[\int_{-\infty}^{\infty} R(t)dt \right]^2} \quad \dots \quad (33)$$

We have already seen that the Doppler-shifted frequency f in the returned wave (due to random motion of the irregularities) is distributed (c.f. equation 21) with a probability $P(f)$ given by

$$P(f) = \frac{1}{\sqrt{2\pi}} \frac{\lambda}{2v_0} \exp \left[-\frac{\lambda^2}{8v_0^2} (f - f_0)^2 \right] \quad \dots (34)$$

The same expression also gives the 'power-spectrum' of the returned wave.

Now, by well-known Wiener's theorem, the auto-correlation function is proportional to the Fourier transform of the distribution of power in the power-spectrum. Therefore

$$\begin{aligned} \rho R(\tau) &\propto \frac{\left| \int_{-\infty}^{\infty} W(f - f_0) \exp(2\pi i f \tau) df \right|^2}{\left[\int_{-\infty}^{\infty} W(f) df \right]^2} \\ &\propto \left[\int_{-\infty}^{\infty} \exp\left(-\frac{f^2 \lambda^2}{8v_0^2}\right) \exp(2\pi i f \tau) df \right]^2 \\ &\propto \left[\exp\left(-\frac{8\pi^2 \tau^2 v_0^2}{\lambda^2}\right) \right]^2 \\ &\propto \exp\left(-\frac{16\pi^2 v_0^2 \tau^2}{\lambda^2}\right) \quad \dots (35) \end{aligned}$$

We thus find that the auto-correlation function falls to e^{-1} after a time $\tau = \frac{\lambda}{4\pi v_0}$

which can be conveniently called the 'fading time' since it will, on the average, represent the time that has elapsed before the received signal has altered appreciably.

For oblique incidence v_0 should be replaced by $v_0 \cos \phi$ and the auto-correlation function becomes

$$\rho R(\tau) \propto \exp\left(-\frac{16\pi^2 v_0^2 \tau^2 \cos^2 \phi}{\lambda^2}\right) \quad \dots (36)$$

The fading of a doubly reflected wave from the ionosphere has been similarly dealt with. If $\rho R_1(\tau)$ and $\rho R_2(\tau)$ are the auto-correlation functions for the first and second reflections respectively, then,

$$\rho R_2(\tau) = [\rho R_1(\tau)]^2 \quad \dots (37)$$

In other words, if the ionospheric irregularities are moving with the same horizontal velocity at the two points of reflection the rate of fading for the second reflection will be less than that for the first reflection as given by the above formula.

We shall now proceed to the determination of $\rho_R(\tau)$ from one of the fading curves. We have analysed one fading curve (No. 5 in Table 1) for obtaining $\rho_R(\tau)$ from a series of values of τ . Figure 6 shows the auto-correlogram where

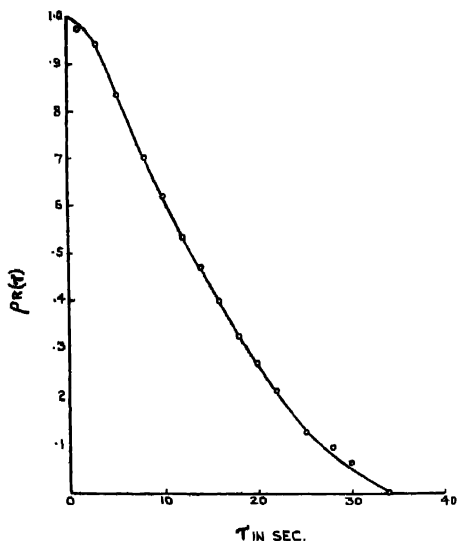


Fig. 6. Autocorrelation function of fading curve No. 5.

$\rho_R(\tau)$ has been plotted against τ . The curve is normal in shape and the value of τ for which $\rho_R(\tau)$ falls to e^{-1} is about 16.5 seconds. We can now employ the relation $\tau = \frac{\lambda}{4\pi v_0}$ for this value of τ . λ is 204.1 m in the present case. v_0 therefore, works out to about 3.3 m/sec. This value of v_0 compares favourably with that obtained from time-analysis (3.9 m/sec).

12. STEADY DRIFT, LOCATION AND DIMENSION OF IRREGULARITIES

In the case of a steady ionospheric drift blowing the randomly spaced irregularities unchanged in form the fading patterns at two spaced receivers will be similar in nature although they are irregular individually. Ratcliffe and Pawsey (1933) and Pawsey (1935) have shown that the fading patterns taken at two receivers

separated by about a wavelength remain sensibly similar. The effect of the ionospheric drift causes the pattern at one receiver to be displaced with respect to the other by a time-interval depending upon the velocity of the drift, while the dissimilarity between the two fading patterns indicates the presence of the random motion of the irregularities. This is, of course, true when the random motion is smaller than the steady drift and available experimental evidence indicates that it is so except during ionospheric disturbances when the random motion predominates. Briggs, Phillips and Shinn (1950) have developed a method by which both the steady drift and the random motion could be determined from a consideration of the correlation functions of the fading curves taken at three receiving points. But it is not possible to evaluate the steady drift from the analysis of a fading curve taken at a single receiver.

The wave diffraction at the ground could be produced by reflection or from transmission through an irregular part of the ionosphere and it is difficult to locate the system of irregularities. Available experimental evidence indicates that the system of irregularities is mostly situated at or below the E layer (Mitra, 1952).

In order to become efficient scattering centres, the dimension of the irregularities should be of the order of a wavelength used. In an earlier experiment Mitra (1953) has shown that the horizontal length of an irregularity was about 1 Km (Wavelength used was 75 m) and the diameter of the first Fresnel zone was found to be about 9 Km.

13. SUMMARY AND CONCLUSION

It has been mentioned in the introduction that in studying the different processes that are assumed to cause the fading of a downcoming wave, we shall not make any assumption regarding the nature of the ionospheric irregularities. We assume that the irregularities exist in a horizontal plane and their steady drift as well as random motion cause the fading. These irregularities may, however, be in the form of densely ionised clouds whose ionic densities are greater than the 'back ground' ionisation of the ionosphere. What causes them to be formed and to persist over a period of time are still not fully known.

It has been shown in the paper that the distribution of resulting amplitude in a fading wave taken on medium wave transmissions obeys either a Rayleigh's curve or a normal law of error. The former is obtained when the fading is caused by irregular diffractive scattering of the incident radio wave from local irregularities existing in a horizontal plane in the ionosphere and moving at random amongst themselves, the latter when there is a steady signal in the nature of a specularly reflected component present along with the scattered waves. The analysis further reveals how to calculate the proportion of steady signal from a Gaussian amplitude distribution. It has also been stated that superposition

of several waves, each fading randomly, does not alter the amplitude distribution which remains essentially a Rayleigh one

A time analysis of the fading curves would enable one to determine v_0 , the r.m.s. value of the random motion of the irregularities in the line of sight. For this purpose, only those fading curves could be considered whose amplitude distribution obeys a Rayleigh law. It has been found from the time analysis of 9 such fading curves that v_0 varies between 3.9 and 25.1 m/sec. A more rigorous time-analysis indicates somewhat different distribution and its possible ionospheric causes have been discussed. Utilising a simple method of determining v_0 about 200 fading curves taken on short waves of different frequencies on an earlier occasion have been analysed and it has been shown that the linear relationship between v_0 and wavelength is obeyed

v_0 can also be determined from auto-correlation function of the fading curve, a method due to Booker, Ratcliffe and Shinn (1950). It has been found that v_0 determined from a consideration of the auto-correlation function agrees fairly well with the value obtained from time analysis.

The effect of a steady drift, location and dimension of the ionospheric irregularities have also been discussed in the paper.

ACKNOWLEDGMENT

The work described in the paper forms part of a programme of ionospheric research of All India Radio and is published by permission of Mr. B. V. Baliga, Chief Engineer, All India Radio. The authors wish to thank Mr. S. Thiruvengkatachari, Research Engineer, All India Radio, for helpful discussions. The summary of the paper was read in July, 1955 at the symposium on Ionospheric Drift organised by the Radio Research Committee of the Council of Scientific and Industrial Research.

REFERENCES

- Banerji, R. B., 1953, *Proc. Phys. Soc. B*, **66**, 105.
Booker, H. G., Ratcliffe, J. A., and Shinn, D. H., 1950, *Phil. Trans. Roy. Soc. A*, **262**, 579.
Briggs, B. H., Phillips, G. J., and Shinn, D. H., 1950, *Proc. Phys. Soc. B*, **53**, 106.
C. C. I. R., 1953, Document No. 22 (Study Group VI).
de Boer., 1931, *Tijds. Ned. Rad.*, **5**, 1.
Furth, R., and MacDonald, D. K. C., 1947, *Proc. Phys. Soc.*, **59**, 388
McNicol, R. W. E., 1949, *Proc. I.E.E.* Pt. III, **93**, 517.
Mazumdar, S. C., and Mitra, S. N., 1954, *Ind. J. Phys.*, **28**, 251.
Mitra, S. N., 1949a, *Proc., I.E.E.*, Pt. III, **93**, 505.
Mitra, S. N., 1949b, *Proc. I.E.E.*, Pt. III, **93**, 441.
Mitra, S. N., 1950, *Ind. J. Phys.*, **24**, 197.
Mitra, S. N., 1952, *J. Sci. Ind. Res.* **11B**, 453.

- Mitra, S. N. 1953, *J. Sci. Ind. Res.* **12A**, 319.
Mitra, S. N. 1953, *Ind. J. Phys.* **27**, 561.
Pawsey, J. L., 1935, *Proc. Camb. Phil. Soc.*, **31**, 125.
Pearson, K. 1906, A mathematical theory of random migration, London.
Rutcliffe, J. A., 1948, *Nature*, **162**, 9.
Ratchiffe, J. A. and Pawsey, J. L. 1953, *Proc. Camb. Phil. Soc.*, **29**, 301
Rice, S. O., 1944, *Bell Syst. Tech. J.*, **23**, 282.
Rice, S. O. 1945, *Bell Syst. Tech. J.*, **24**, 46.
Rayleigh, Lord. 1899, *Collected Works*, I, 495.
Wang M. O. and Uhlenbock G. E. 1945, *Rev. Mod. Phys.*, **17**, 323.

RECOMBINATION COEFFICIENT AND ELECTRON PRODUCTION RATE FROM TOTAL ELECTRON CONTENT IN UNIT COLUMN BELOW THE LEVEL OF MAXIMUM IONISATION

S. DATTA

INSTITUTE OF RADIO PHYSICS AND ELECTRONICS, UNIVERSITY COLLEGE OF TECHNOLOGY, 92, UPPER CIRCULAR ROAD, CALCUTTA-9

(Received for publication September 26, 1956)

ABSTRACT. The paper describes the results of computation of the mean recombination coefficient ($\bar{\alpha}$) and the mean electron production rate (\bar{q}) in the F region on quiet days. The diurnal variation of n , the total number of electrons in a column of unit cross section extending from the "bottom" to the maximum ionization density height of the same region is utilised for the purpose. The values of n and its diurnal variation, in their turn, are computed from the $P'-f$ records of the automatic ionospheric recorder installed at Haringhata (Calcutta).

Night-time average values of $\bar{\alpha}$ obtained by the same method, show a marked seasonal change, the maximum being in December ($\bar{\alpha} = 10.8 \times 10^{-10}$ c.c. per sec. per electron) and the minimum in June ($\bar{\alpha} = 2.2 \times 10^{-10}$ c.c. per sec. per electron). Assuming that the recombination coefficient falls off at an exponential rate, $\alpha_m e^{-pz}$ (where z is the reduced height, α_m is the recombination coefficient at the maximum ionization height and p is a constant), a method has been suggested for determining the value of p from the recombination rate in the unit column and that at the maximum ionization density height.

INTRODUCTION

Recombination coefficient (α_m) and electron production rate (q_m) at the height of maximum electron density in the F region have been determined by several authors (Appleton, 1937; Bajpai, 1938; Bhar, 1939; Seaton, 1947; Baral and Mitra, 1950) from the diurnal variation of the maximum electron density (N_m) governed by the equation,

$$\frac{dN_m}{dt} = q_m - \alpha_m N_m^2 \quad \dots (1)$$

α_m and q_m so determined have, however, sometimes negative and zero values which cannot be interpreted. This happens specially for equatorial stations where midday dip of maximum ionization density occurs. In view of this, Skinner and Wright (1954) have suggested the determination of α_m and q_m from the diurnal variation of the total number of electrons (n) in the F region in a column of unit cross section extending from the "bottom" to the height of maximum ionization density of the layer. This is because the diurnal variation of n has no midday dip

(Ratcliffe, 1951). Skinner and Wright (1955) have obtained from the diurnal variation of n , the annual mean day time variations of $\bar{\alpha}$ and \bar{q} in the F region at Ibadan on magnetically quiet and disturbed days. The mean electron production rate \bar{q} is defined by $\bar{q} \cdot \bar{y}_m = \int_{h_0}^{h_m} q dh$ and the mean recombination coefficient $\bar{\alpha}$ is defined by $\bar{\alpha} \left(\frac{n}{y_m} \right)^2 \cdot y_m = \int_{h_0}^{h_m} \alpha N^2 dh$ where y_m is the height from the "bottom" (h_0) to the level of maximum ionization of the layer (h_m).

THE METHOD

If the electrons disappear by recombination, the variation of n with time is governed by the equation.

$$\frac{dn}{dt} = \bar{q} \cdot y_m - \bar{\alpha} \left(\frac{n}{y_m} \right)^2 \cdot y_m \quad \dots (2)$$

where \bar{q} and $\bar{\alpha}$ are the mean electron production rate and mean recombination coefficient as defined earlier.

If \bar{q} and $\bar{\alpha}$ are assumed to vary symmetrically about midday, we have

$$\bar{q} = \frac{n_2^2 \left(\frac{dn}{dt} \right)_1}{y_{m_1} (n_2^2 - \alpha^2 n_1^2)} \cdot \alpha n_1^2 \left(\frac{dn}{dt} \right)_2 \quad \dots (3)$$

$$\text{and} \quad \alpha = \frac{\alpha y_{m_1} \left\{ \alpha \left(\frac{dn}{dt} \right)_1 - \left(\frac{dn}{dt} \right)_2 \right\}}{(n_2^2 - \alpha^2 n_1^2)} \quad \dots (4)$$

where $\alpha = \frac{y_{m_2}}{y_{m_1}}$ and suffixes 1 and 2 refer to conditions before and after midday.

At night, $\bar{q} = 0$, hence

$$\frac{dn}{dt} = -\bar{\alpha} \left(\frac{n}{y_m} \right)^2 \cdot y_m \quad \dots (5)$$

In an ionized region where the electron density may be assumed to vary parabolically with height, the electron density, N at any height, h is given by (9)

$$N = N_m \left(1 - \frac{Z^2}{4} \right) \quad \dots (6)$$

where $Z = \frac{h-h_m}{H}$, N_m = maximum ionization density at the height, h_m ($Z=0$) and H = scale height,

In such a region, if the electrons disappear by recombination

$$\bar{\alpha} \left(\frac{n}{y_m} \right)^2 \cdot y_m = \frac{8}{15} \alpha_m N_m^2 \cdot y_m \quad \dots (7)$$

It has been shown by Ratcliffe (1951) that for a parabolic region,

$$n = 2/3 \cdot N_m \cdot y_m \quad \dots (8)$$

So, for parabolic distribution,

$$\alpha_m = \frac{\bar{\alpha}}{1.2} \quad \dots (9)$$

Similarly, for such a region when the total electron production rate and total recombination rate in the unit column are equal, i.e. near noon,

$$\bar{q} \cdot y_m = \frac{8}{15} \alpha_m N_m^2 \cdot y_m \quad \dots (10)$$

Hence

$$q_m = \frac{15}{8} \cdot \bar{q} \quad \dots (11)$$

where q_m — electron production rate at the maximum ionization height under quasi-equilibrium conditions.

The values of $\bar{\alpha}$ have been determined by utilising equation (4) for day time conditions and equation (5) for night time conditions. The values of \bar{q} have been obtained by using equation (3).

If the recombination coefficient falls off exponentially with height, $\alpha_m e^{-pz}$ where α_m is the value of the recombination coefficient at the maximum ionization level ($Z = 0$), then the total recombination rate in the unit column of a parabolic region is given by

$$H \int_{-2}^0 \alpha_m e^{-pz} \cdot N_m^2 \left(1 - \frac{Z^2}{4} \right)^2 \cdot dz = H \alpha_m N_m^2 \cdot f(p) \quad \dots (12)$$

where

$$f(p) = p^{-3} \cdot e^{2p} (2 - 3p^{-1} + 1.5p^{-2}) - p^{-1} (1 - p^{-2} + 1.5p^{-4}) \quad \dots (13)$$

Variation of $f(p)$ with p ($1 < p < 2.0$) is shown in figure 3. At night,

$$\frac{dn}{dt} = -H \alpha_m N_m^2 f(p) \quad \dots (14)$$

So,

$$f(p) = \frac{\left(\frac{dn}{dt} \right)}{H \cdot \left(\frac{dN_m}{dt} \right)} = \frac{2}{3} \left[2 + \frac{N_m}{H} \cdot \frac{dy_m}{dN_m} \right] \quad \dots (15)$$

Since $\frac{dN_m}{dt} = -\alpha_m N_m^2$ and $n = \frac{2}{3} N_m \cdot y_m$.

From the diurnal variations of n and N_m , the values of $f(p)$ and hence, of p may be obtained

It is worth mentioning that theoretical considerations show that the electron distribution can not be parabolic if the recombination coefficient is dependent exponentially with height

RESULTS

Ionospheric records ($P'-f$) at 30 minutes interval on international magnetically quiet days for the months of March and April, 1955, obtained at the Ionosphere Field Station, Haringhata (Lat. $22^{\circ}56'$ N, 28 miles north of Calcutta) of the Institute of Radio Physics and Electronics, University of Calcutta, were utilised for obtaining the values of n . List of five international magnetically quiet days for each of the months of March and April were obtained from the "Ionospheric Data" published by the Central Radio Propagation Laboratory, Washington, D.C.

Half hourly values of n were determined from the ($P'-f$) records by Ratcliffe's method on the assumption of a parabolic electron density distribution

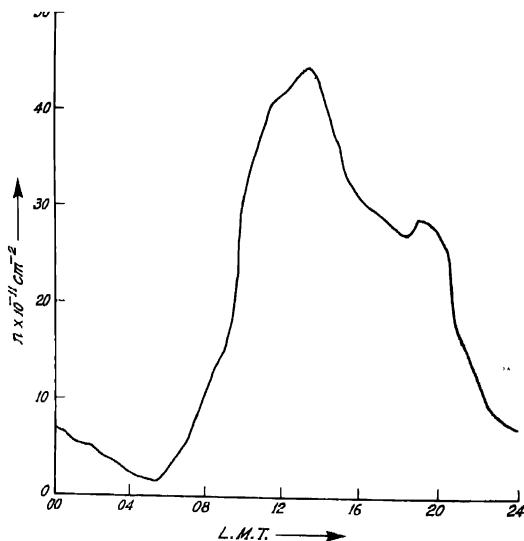


Fig. 1. Mean quiet day diurnal variation of n for the months of March and April.

in the layer. Figure 1 shows the mean quiet day diurnal variation of n for the months of March and April, 1955.

To obtain the values of $\left(\frac{dn}{dt}\right)$, a linear change of n between the half hourly values was assumed. Figure 2 shows the persistent midday dip with maxima at

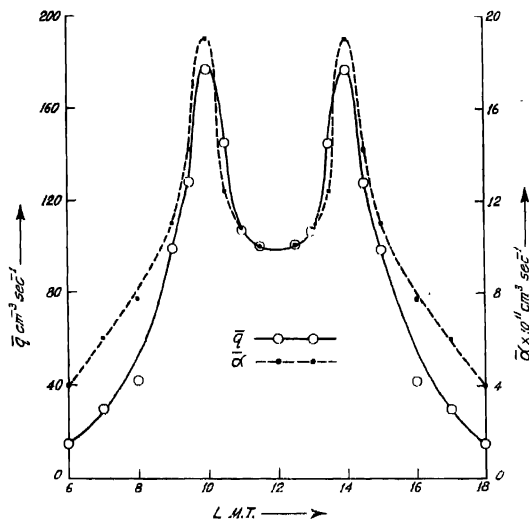
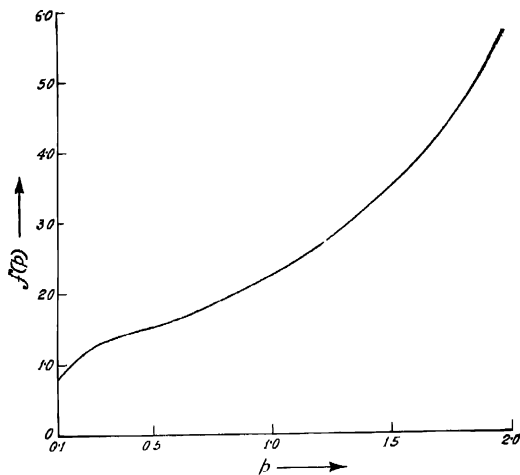
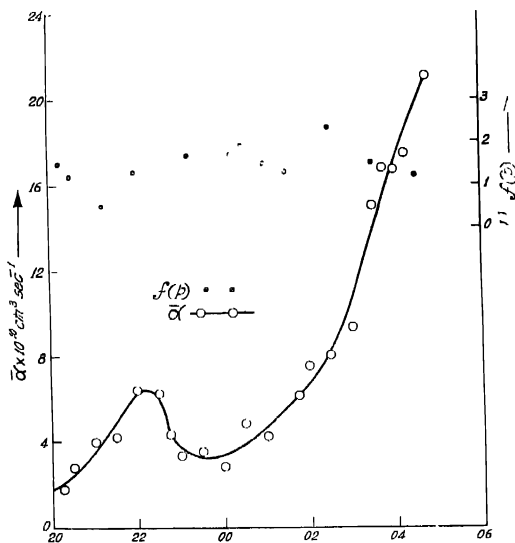


Fig. 2. Mean quiet day diurnal variation of $\bar{\alpha}$ and \bar{q} for the months of March and April.

10 hrs. and 14 hrs. (L.M.T.) in variation of $\bar{\alpha}$ and \bar{q} for F_2 region obtained from quiet day ionospheric records at Haringhata (Lat. $22^{\circ}56'$ N). Similar, but more pronounced dip has also been obtained by Skinner and Wright in the variation of $\bar{\alpha}$ and \bar{q} computed from ionospheric data at Ibadan (Lat. $7^{\circ}22'$ N). Table I shows the mean hourly values of α_m and q_m for the months of March and April at day time obtained from the value of $\bar{\alpha}$ and \bar{q} respectively.

Figure 4 shows the mean quiet day nocturnal variation of α in the F region for the same months. Figure 4 also shows the plots of night time values of $f(p)$ obtained from the observed values of $\left(\frac{dn}{dt}\right)$ and $\left(\frac{dN_m}{dt}\right)$. Experimental values of $f(p)$ are widely scattered. The experimental value of $f(p)$ is found to be of the order 1.70 at midnight. From figure 3 this corresponds to the value, $p = .66$ approximately. Variation of the recombination coefficient with the reduced

Fig. 3. Variation of $f(p)$ with p ($1 < p < 2.0$)Fig. 4. Mean quiet day nocturnal variation of α and plots of $f(p)$ for the months of March and April.

height Z at midnight ($\alpha_m = 3.2 \times 10^{-10} \text{ cm}^3 \text{ sec}^{-1}$) when $p = .66$ is shown in figure 5. It will be noted that with $p = .66$ the value of the recombination coefficient at the bottom of the F region is $1.2 \times 10^{-9} \text{ cm}^3 \text{ sec}^{-1}$ at midnight.

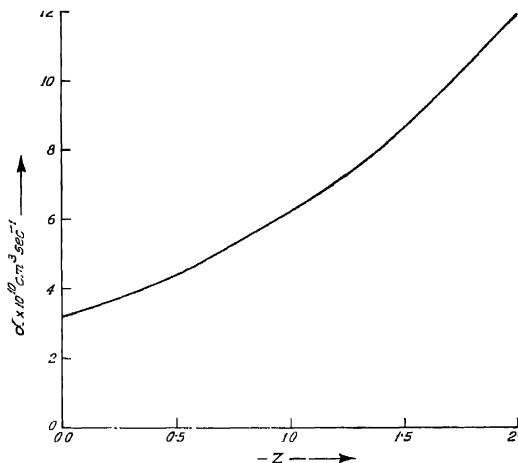


Fig. 5. Variation of recombination coefficient with reduced height (Z) at midnight when $\alpha_m = 3.2 \times 10^{-10} \text{ cm}^3 \text{ sec}^{-1}$ and $p = .66$.

TABLE I

Mean hourly values of α_m and q_m obtained from $\bar{\alpha}$ and \bar{q} .

Time (L. M. T.)	α_m $\text{cm}^3 \text{ per elec-}$ tron per sec.	q_m $\text{Per cm}^3 \text{ per}$ sec.
0600 1800	3.3×10^{-11}	28
0700 1700	5.0×10^{-11}	56
0800 1600	6.4×10^{-11}	79
0900 1500	9.2×10^{-11}	185
1000 1400	15.8×10^{-11}	332
1100 1300	9.0×10^{-11}	200
1200	8.3×10^{-11}	188

Figure 6. Shows the seasonal variation of the average night time $\bar{\alpha}$ for the year of 1954

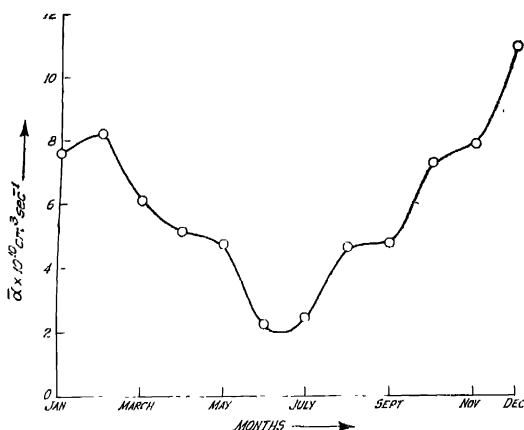


Fig. 6 Seasonal variation of average night time $\bar{\alpha}$ in the F region over Calcutta.

DISCUSSIONS

The anomalous negative and zero values of α_m and q_m that are sometimes obtained when they are computed from the diurnal variation of N_m , disappear when computed from the diurnal variation of n (total electron content). This is presumably due to the fact that in such computation any change in the thickness of the layer due to the vertical ionic drift or thermal expansions and contractions is taken into account. (There is, of course, the proviso that the fraction of the total ionization below the level of maximum ionization density does not change). Both methods of computation, however, have the common drawback that they assume a symmetrical variation of the recombination coefficient and electron production rate about noon. In connection with the computation from the diurnal variation of n , it is to be noted that the anomaly of the midday dips in the diurnal variations of α_m and q_m persists even with this computation, though less markedly. Two suggestions have been put forward to explain this anomaly. According to Skinner and Wright the midday dips in $\bar{\alpha}$ and \bar{q} are to be ascribed to the change caused by the vertical ionic drift in the fraction of the total ionization which lies below the level of maximum ionization density. This change affects the computed values of n and the method of determining $\bar{\alpha}$ and \bar{q} from the diurnal variation of n , and so leads to anomalous results.

According to Lepechinsky (1951) the diurnal temperature cycle may also contribute partly to the midday dip of q_m . Thus, if q_{m_1} and q_{m_2} be the maximum electron production rates when the solar zenithal angles are χ_1 and χ_2 , and the corresponding temperatures are $T_1^\circ\text{K}$ and $T_2^\circ\text{K}$ respectively, then

$$\frac{q_{m_1}}{q_m} = \frac{T_2 \cos \chi_1}{T_1 \cos \chi_2} \quad \dots (16)$$

Hence assuming that the temperature variation only is responsible for the midday dip, it is found from the values of q_m given in Table I that the midday temperature is nearly twice of that at 10 and 14 hrs (L.M.T.) in the F_2 region over Haringhata. Such large diurnal temperature variation between morning and noon hours appears to be doubtful.

It is interesting to note in this connection that plausible theoretical expressions for the recombination coefficient (α) depending on temperature and pressure may be utilised for estimating temperature variation in the ionospheric regions. Thus, according to Thompson and Thomson?

$$\alpha = \alpha_0 \left(\frac{P}{P_0} \right) \left(\frac{T_0}{T} \right)^3 \quad \dots (17)$$

where P = gas pressure

T = gas temperature, $r \propto \frac{1}{T}$

and α_0 , P_0 , T_0 are the recombination coefficient, pressure and temperature respectively corresponding to reference conditions. If $\left(\frac{P}{P_0} \right)$ be considered unity for ionospheric conditions

$$\alpha = \alpha_0 \left(\frac{T_0}{T} \right)^3 \quad \dots (18)$$

Seaton (1948) has utilised this expression for the study of worldwide temperature variations in different ionospheric regions. We have also utilised it to determine seasonal variation of temperature from the computed values of $\bar{\alpha}$ for different seasons. It was found that in F region the average night time temperatures for summer (June-July) and equinox (March-September) are 1.58 and 1.20 times respectively that of winter (December-January).

Since, H the scale height is proportional to T , the measurement of H also permits an estimation of the temperature. Thus from scale height measurements,

Baral and Mitra found that the F-region temperature over Calcutta varies from 700°K in winter to 1200°K in summer (for the period of high solar activity) and 500°K in winter to 900°K in summer (for the period of low solar activity).

ACKNOWLEDGMENTS

The work forms part of the programme of the Radio Research Committee of the Council of Scientific and Industrial Research, Government of India, and the author wishes to express his thanks to the Council for financial assistance.

The author is indebted to Professor S. K. Mitra for his guidance and interest throughout the process of the work.

The author is grateful to Dr. J. N. Bhar for his interest and encouragement and to Dr. S. S. Baral for helpful discussions and suggestions.

REFERENCES

- Appleton, E. V., 1937, *Proc. Roy. Soc. A*, **162**, 451.
 Bappu, R. R. and Pant, B. D., 1938, *Ind. Jour. Phys.*, **12**, 211.
 Bhar, J. N., 1939, *Ind. Jour. Phys.*, **13**, 253.
 Seaton, S. L., 1947, *Phys. Rev.*, **72**, 712.
 Baral, S. S. and Mitra, A. P., 1950, *Jour. Atmos. Terr. Phys.*, **1**, 95.
 Skinner, N. J. and Wright, R. W., 1954, *Jour. Atmos. Terr. Phys.*, **5**, 290.
 Ratchiffe, J. A., 1951, *Jour. Geophys. Res.*, **56**, 487.
 Skinner, N. J. and Wright, R. W., 1955, *Jour. Atmos. Terr. Phys.*, **7**, 105.
 Mitra, S. K., 1952, *The Upper Atmosphere*, Asiatic Society, Calcutta.
 Ratchiffe, J. A., 1951, *Jour. Geophys. Res.*, **56**, 463.
 Lepochumsky, 1951, *Jour. Atmos. Terr. Phys.*, **1**, 278.
 Thompson, J. J. and Thompson, G. P., *Conduction of Electricity through Gases*, 3 Gd., Cambridge University Press, 491.
 Seaton, S. L., 1948, *Jour. Met.*, **5**, 204.

FAST COINCIDENCE WITH FAST DISCRIMINATORS*

RANGALAL BHATTACHARYYA AND SANTIMAY CHATTERJEE

INSTITUTE OF NUCLEAR PHYSICS, CALCUTTA

(Received for publication August 18, 1956)

ABSTRACT. A simple arrangement using fast discriminators with fast coincidence circuit has been described. With this a resolving time of ten milli-microseconds can be easily obtained. The main features of this arrangement are its stability and simplicity

INTRODUCTION

Use of amplitude discriminators employing conventional circuitry preceding coincidence circuit is restricted to a resolving time much longer than what present day coincidence circuits can yield, unless the slow-fast arrangement (Bell *et al*, 1952) is utilised. The limit is actually set by the slow rise-time of the anode pulses of the discriminators which, in such experimental arrangements, are often necessary for amplitude selection in both channels. A fast discriminator can, however, be conveniently used in each of the channels giving equalised output pulses for input pulses above the desired level and with these equalised pulses the coincidence circuit gives a well defined and stable resolving time. Such an arrangement, to be described here, has the advantage that the elaborate assembly in the slow-fast type can be avoided.

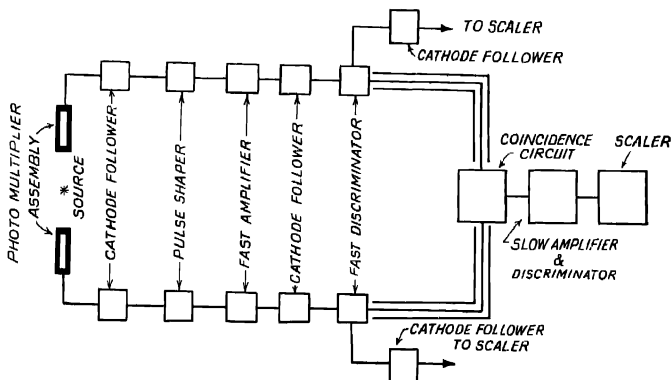


Fig. 1. Block diagram of the experimental arrangement.

*The paper in a modified form was reported at the Indian Science Congress in January, 1956.

EXPERIMENTAL ARRANGEMENT AND OBSERVATIONS

Figure 1 shows the experimental arrangement. The fast coincidence circuit similar to that evolved by Garwin (1950) has been used for its inherent stability and simplicity. The fast discriminator in the two channels have been constructed after Moody *et al* (1952) using the secondary emission pentode type EFP 60 in the trigger current. Other components of figure 1 being self-explanatory have not been described. The characteristics of this discriminator as regards the suitability of its use in a coincidence channel have been studied and are given below.

(a) Input sensitivity of 0.25 volt has been attained for input pulse width of 25 milli-microseconds. The stability of that level being not very good, working region has to be much higher.

(b) Plate pulse widths from 0.1 microsecond to 0.5 microsecond have been obtained with different values of dynode load and feedback capacitor, the amplitude is about 20 volts for a plate load of 100 ohms. The rise time of the plate pulse is $1 \cdot 10^{-8}$ sec. The lowest width quoted has been selected in order to handle adequate counting rate. The plate pulse has been clipped to a width of 20 milli-microseconds before being fed to the coincidence circuit.

(c) The circuit triggering delay should be small and uncertainty in triggering should be much smaller than the resolving time aimed at. It has been observed that for input pulse height above 1.2 volts (input pulse width 25 milli-microseconds), the triggering delay remains nearly 3 to 5 milli-microseconds.

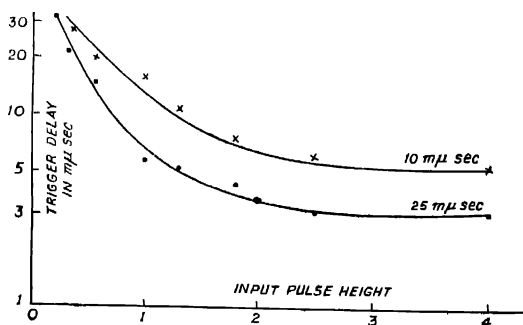


Fig. 2 Curve showing the variation of triggering delay with input pulse height.

However, the triggering delay increases as the input pulse height decreases to the extent of 30 milli-microsecond for 0.2 volt input pulse height. This is shown in figure 2.

To ensure that the majority of the photo-multiplier pulses are amplified to at least 1.2 volts, video amplifier of 30 Mc/s bandwidth have been used.

A resolving time of 2×10^{-8} secs. has been obtained with this arrangement. Plastic phosphors in conjunction with RCA 5819 type photo-multipliers have been used as detectors. Figure 3 shows the prompt coincidence curve obtained with Co^{60} .

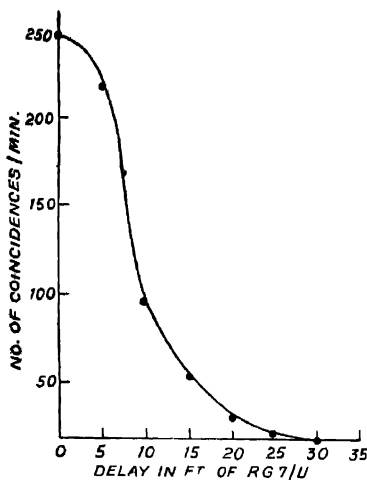


Fig. 3. Prompt coincidence curve obtained with Co^{60} .

For detection of coincident events from nuclei, fast coincidence with or without delay between the channels are very often utilised. Although the above method does not seem to be capable of yielding a resolving time limit reached otherwise, the simplicity of the arrangement advocates its use for a resolving time near 10 milli-microseconds. The method, however, has enabled us to obtain a stable resolving time without getting much trouble in the adjustments of the coincidence circuit. As the minimum triggering sensitivity of this discriminator changes with input pulse width, the input pulse needs to be properly shaped.

ACKNOWLEDGMENT

The authors are indebted to late Prof. M. N. Saha for his interest in the work. They are also thankful to Prof. A. K. Saha for his helpful discussions.

REFERENCES

- Boll, R. E., Graham, R. L., Potch, H. E., 1952, *Canad. J. Phys.*, **30**, 35.
 Garwin, R. L., 1950, *R. S. I.*, **21**, 569.
 „ 1953, *R. S. I.*, **24**, 618.
 Moody N. F., MacLusky, G. J. R., Deighton, M. O., 1952 *Electronic Engg.*, **24**, 214.

Letters to the Editor

The Board of Editors will not hold itself responsible for opinions expressed in the letters, published in this section. The notes containing reports of new work communicated for this section should not contain many figures and should not exceed 500 words in length. The contributions must reach the Assistant Editor not later than the 15th of the second month preceding that of the issue in which the Letter is to appear. No proof will be sent to the authors.

1

ELASTIC AND INELASTIC SCATTERING OF HIGH ENERGY ELECTRONS BY SOME 2p-SHELL NUCLEI ON THE INTERMEDIATE COUPLING MODEL

M. K. PAL, S. MUKHERJEE AND A. K. SAHA

INSTITUTE OF NUCLEAR PHYSICS, CALCUTTA

(Received for publication November 12, 1956)

In recent years a considerable amount of data has accumulated on scattering of high energy electrons by different nuclei. The collective model and the independent particle model of the nucleus have been used by different workers to explain these data. We have worked out the scattering formulae for 2p-shell nuclei by using the 'Intermediate Coupling' model. In this note we report the results of our preliminary calculations with these formulae on elastic and inelastic scattering by Be^9 and C^{12} .

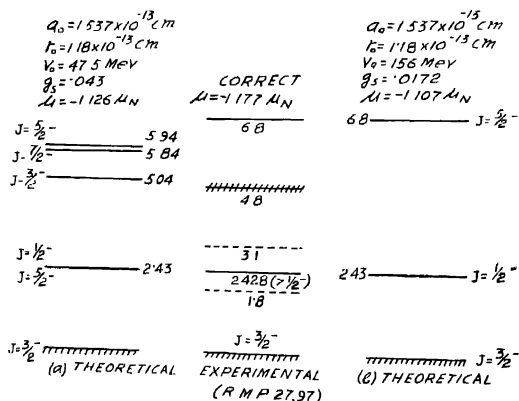


Fig. 1 Calculated and observed energy level diagrams of Be^9 .

For Be^9 we have assumed a deliberately simplified form of nuclear Hamiltonian with a strong Majorana central interaction and comparatively weak tensor and spin-orbit interactions. This reduces the number of LS-coupling states whose superposition is required to construct the wavefunctions of the lowest few energy levels of the nucleus. The resultant energy levels are shown in figure 1. The oscillator well-parameter, a_0 , has been chosen equal to 1.537×10^{-13} cm. in accordance with Swiatecki's (1951) formula. We have calculated the scattering cross-sections corresponding to the energy level diagram (a). The results are presented in figure 2. It is seen that though the elastic curve agrees fairly well with the experimental data, the inelastic curves are considerably below the experimental ones on a logarithmic plot.

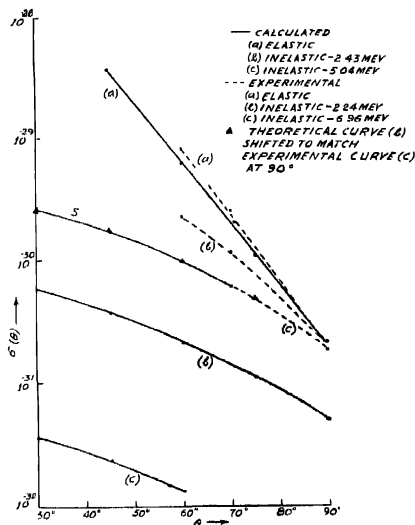


Fig. 2. Elastic and inelastic differential cross-section curves for Be^9 . Theoretical curves correspond to energy level diagram (a) of Fig. 1.

One of the predictions from our theory is that for different inelastic scattering with change of total angular momentum J , the $\sigma(\theta)$ vs. θ curves will run parallel on a logarithmic plot. This has been corroborated by the inelastic curves for C^{12} of Fregeau and Hofstadter (1955). The inelastic curves of McIntyre, Rahn, and Hofstadter (1954) for Be^9 , however, do not conform to this conclusion. It may be pointed out that these curves do not show the experimental errors, and hence no definite inference can be made from them. For Be^9 our inelastic curves can be shifted vertically to match exactly the lower experimental inelastic curve.

The upper one can be matched if we choose $a_0 = 2.0 \times 10^{-13}$ cm., but then the agreement of the elastic curve becomes poorer

In case of C^{12} we have chosen $a_0 = 1.582 \times 10^{-13}$ cm. as it gives a better fit with the curves for 4.43 and 9.61 Mev levels of figure 10' of Fregeau *et al* than the Swiatecki-value $a_0 = 1.692 \times 10^{-13}$ cm. With same value of a_0 we have plotted the square of the function

$$C' = \frac{K'^2}{6} e^{-K'^2/4} \quad (K' = a_0 K, \quad K = \text{change of momentum of the electron})$$

in figure 3. From our theory this curve should have ordinates related by a constant factor to the corresponding ones of the experimental curve of Fregeau *et al*

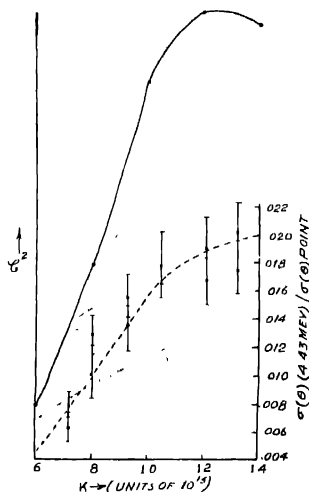


Fig. 3. Comparison of C'^2 vs. K curve for C^{12} with the experimental $\sigma(\theta)(4.43 \text{ Mev})/\sigma(\theta)$ point vs. K curve of Fregeau and Holstadter.

shown in the same figure. This is actually the case, the factor being 1.8, except for points above $K \approx 1.2 \times 10^{13}$. But here again the large experimental uncertainties do not allow us to make a definite conclusion.

In figure 4 we have plotted for C^{12} the inelastic curve with change of J . A constant multiplicative factor has been chosen so that the curve matches at $\theta = 90^\circ$ the experimental points on curve D in figure 4 of Fregeau *et al*. The agreement with the experimental data is fairly good.

So far we have attempted to verify if, without making detailed wavefunction calculations, we can get any evidence that forces us to reject the theory. For-

unately, we do not get any such evidence. Detailed calculations of the wavefunctions of O^{12} with a nuclear Hamiltonian that satisfies two-body data on bind-

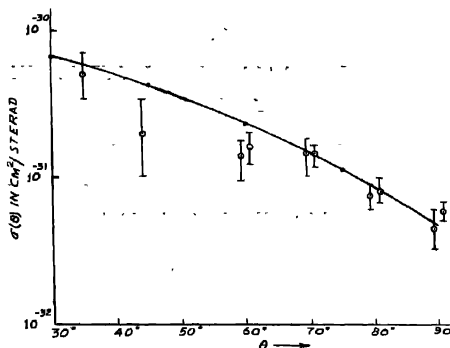


Fig. 4. Comparison of inelastic ($J' \neq J$) $\sigma(\theta)$ vs. θ curve for O^{12} with experimental data of Fregeau and Hofstadter.

ing and scattering are in progress. With such wavefunctions we expect to make definite conclusions as to the quantitative agreements of the theory, especially the high inelastic cross-sections. That work will be reported elsewhere in due time.

REFERENCES

- Fregeau, J. H. and Hofstadter, R., 1955, *Phys. Rev.*, **99**, 1503.
 McIntyre, J. A., Hahn, B. and Hofstadter, R., 1954, *Phys. Rev.*, **94**, 1084.
 Swiatecki, W. J., 1951, *Proc. Roy. Soc. A*, **205**, 238.

2.

DIPOLE MOMENTS OF TRI-SUBSTITUTED BENZENES. PART II

D V G L NARASIMHA RAO

PHYSICS DEPARTMENT, ANDHRA UNIVERSITY, WALTAIR

(Received for publication October 12, 1956)

In continuation of the work (Rao, 1956) on tri-substituted benzenes, the dipole moment values are reported in this article for some more similar molecules containing an amino group. The observations are carried out in benzene solution at 30°C. The calculated values are also given in the following table. In these calculations the dipole moment vector of the amino group is taken as making an angle of 38° with the C-N bond which links the group to the benzene ring, following Marsden and Sutton (1936) in their treatment of some substituted anilines. The polarisability of the NH₂ group used is 1.97×10^{-24} , calculated from the refraction of the group extrapolated to infinite wavelength using the values at various wavelengths (Landolt-Bornstein, *Physikalisch-Chemischen Tabellen*, 5th edition, Berlin, 1923, Page 985).

TABLE

Compound	μ	
	observed	calculated
2 Chloro 4 Toluidine	2.35 D	2.44
2 Chloro 6 Toluidine	2.81	2.87
4 Chloro 2 Toluidine	3.07	3.04
3 Chloro 2 Toluidine	2.08	2.62
5 Chloro 2 Toluidine	3.20	3.10

Details will be communicated shortly

REFERENCES

- Narasimha Rao, D. V. G. L., 1956, *Ind. J. Phys.*, In press.
 Marsden, R. J. B., and Sutton, L. E., 1936., *Jour. Chem. Soc.*, 599.

ELECTRICAL OSCILLATIONS IN A. C. DISCHARGE

M. B. KARNIK

THE INSTITUTE OF SCIENCE, BOMBAY

(Received for publication September 4, 1956)

ABSTRACT : R. f. oscillations have been detected in A. C. discharge. A large number of r. f. components are observed to be simultaneously present. These components are modulated with the supply frequency of 50 c/s. Two new methods have been employed for measuring these frequencies. In one method the Lissajous figures produced on a C. R. O. are utilised. In the other, a superheterodyne frequency meter is used. The values of the frequencies of the r. f. components observed do not appear to change appreciably with different parameters, particularly E/P, gas, and circuit constants.

INTRODUCTION

While studying the effect of irradiation on the electrodeless discharge Joshi (1945), Tiwari (1948) and von Engel and Harries (1951) have observed some pulses in the discharge. The existence of a large number of discrete frequencies of R. F. oscillations in A.C. silent discharge has been studied by Khastgir and others (1952, 53, 54). We describe here what are apparently some similar pulse oscillations in a 50 c/s A.C. discharge. We have determined the pulse frequencies and studied the effect of different parameters like E/P, nature of the gas, circuit constants and the nature and the geometry of the tube on the values of the observed radio frequencies.

METHODS OF MEASUREMENTS

The type of wave-form which had to be analysed is shown in figure 1. The streaks represent high frequency compounds developed in the tube due to elec-

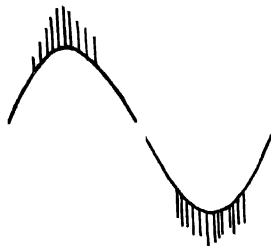


Fig. 1. Current oscillogram showing pulses on 50 cycle curve.

trical discharge. There are inherent difficulties in the measurement of the frequencies of these streaks. Firstly, there are a number of components in the

radio frequency region simultaneously present. Secondly, on all these components which are very weak, is superimposed a strong 50 c/s modulation from the supply voltage. Hence the methods suitable for measuring unmodulated signals with very wide separation in their frequencies cannot be employed here. We have, therefore, devised two methods, employing a cathode ray oscillograph and a superheterodyne circuit. The method employing the cathode ray oscillograph is based on the following consideration. When two sine voltages are applied to the deflecting plates of a cathode ray oscillograph, we can see closed Lissajous figures if the two frequencies involved can be expressed by a ratio of integers. The exact configuration of the pattern depends upon the frequency ratio and upon the relative phases of the two waves. The ratio of the horizontal to vertical frequency is the number of times the pattern touches a vertical line divided by the number of times it touches a horizontal line. This deciphering is at its best with a difference in phase of 90° between the components. As all the unknown frequencies we have to measure are modulated, they cannot be coupled with an unmodulated known frequency to produce a Lissajous pattern. With one modulated and one unmodulated frequency applied to the plates of the cathode ray oscillograph there is only a luminous patch seen on the screen; but if both the frequencies are modulated and if one of the two modulating frequencies is an integral multiple of the other we can observe a Lissajous figure, provided the primary (i.e. carrier) frequencies are equal to one another. The Lissajous figures in this case will be similar to those produced by the modulating frequencies alone. In our work the unknown frequencies which are modulated with 50 c/s are applied to the X-plate of the oscillograph, while to the Y-plates is connected an r.f. oscillator, the output of which is modulated with a fixed frequency of 400 c/s. As the ratio of the modulating frequencies is 400:50 i.e. 8:1, its Lissajous pattern will be a pattern of 8 loops (figure 2). The locked pattern is identical

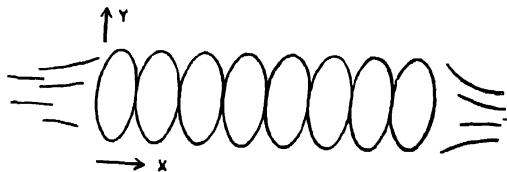


Fig. 2 Lissajous figure showing eight loops. Along X is the out-put of the discharge tube modulated with 50 c/s, while along Y is the output of the r.f. oscillator modulated with 400 c/s.

with the pattern one would obtain from 50 c/s plus 400 c/s when both are without carrier frequencies; but there is a small fuzzy background. This of course is natural considering the large number of frequencies which are present and which at the same time produce a faint moving pattern. This pattern will remain stationary and will be observed only when one of the unknown frequencies is the same as that given by the r.f. oscillator. The readings on the oscillator

are taken whenever the steady pattern of eight loops appears on the screen of the cathode ray oscillograph. This method is suitable for our work because only one unknown frequency is utilised at a time to lock up the pattern of eight loops. Thus we can measure the values of all the r.f. components present simultaneously. This method has proved to have a good resolving power, resolution of course depending on the "band spread" resolution of the r.f. oscillator used as known frequency source.

In the second method a superheterodyne circuit is employed. The output of the discharge tubes, containing unknown frequencies, is fed to the antenna coil of the superheterodyne circuit (figure 3.) In the circuit after the detection

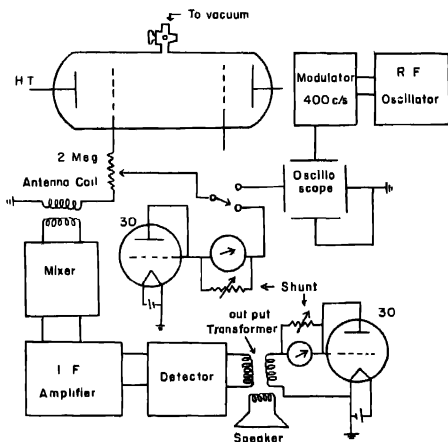


Fig. 3 Block diagram for the position E_1 in the case of the internal electrode tube with the cathode ray oscillograph, the superheterodyne circuit and the current measuring unit.

stage, a power tube with an output transformer is employed. The output of its secondary is rectified by a triode 30 converted to a diode and the rectified voltage is fed to the micro-ammeter (or a mirror galvanometer). The setting giving maximum current is determined by a resonance curve. This setting gives the value of the unknown frequency. Here, however, the resolution is much less than that obtained with a C.R.O.

The above two methods were supplemented by an absorption wave-meter. At the output of the wave-meter there is a germanium crystal in series with a mirror galvanometer for detecting very weak signals.

EXPERIMENTAL

The presence of electrical oscillations has been investigated in three types of discharge tubes. They are (1) an internal electrode discharge tube, (2) a flat glass electrode discharge tube and (3) an ozoniser type. The internal electrode tube (figure 3) consists of a pyrex glass tube with two aluminium electrodes each of diameter 30 mm. They are separated by a distance of 151 mm. Between the two electrodes two square grid-like probes are introduced. The probes are not symmetrically situated. The probe No. 1 is at 40 mm from one aluminium electrode while probe No. 2 is at 31 mm. distance from the other aluminum electrode. Thus the two probes are separated by a distance of 80 mm. With the help of this construction three different electrode gap separations of value 40 mm. (E_1), 120 mm. (E_2) and 151 mm. (E_3) were available. The two probes P_1 and P_2 constituted the grids² between the electrodes separated by 120 mm and 111

TABLE I
Internal electrode tube

Method	Range	Total no. of readings for each column	air	argon	hydrogen	oxygen	mercury vapour
↑ Cathode Ray Oscillograph ↓	Kc. sec	1936	100±1.1	101±1.5	107±2	106±2.5	110±3
		299	—	655±7	654±8	665±15	650±0
		1573	1190±49	1240±52	—	—	—
	Me. sec	1478	2.06±0.05	2.05±0.01	—	—	—
		191	2.30±0.07	2.20±0.01	2.22±0.04	2.27±0.02	—
		167	—	2.36±0.04	2.40±0.0	2.40±0.0	—
		173	—	—	2.61±0.02	2.6±0.01	2.64±0.04
		2091	2.74±0.03	2.72±0.06	2.77±0.02	2.77±0.02	2.8±0.0
		267	—	7.4±0.1	7.5±0.08	7.4±0.07	7.5±0.1
		1793	11.6±0.2	11.3±0.5	10.3±0.3	10.6±0.1	10.1±0.0
		2093	14.2±0.3	14.2±0.1	13.5±0.3	13.7±0.4	—
		1413	15.7±0.2	15.7±0.1	15±0.2	14.9±0.3	14.7±0.4
		2072	25.9±0.2	25.6±0.4	—	26.0±0.0	25.5±0.0
		2319	27.1±0.3	26.8±0.4	26.8±0.2	26.8±0.2	26.5±0.0
Super het. fre- quency meter	Kc. sec	54	672±50	686±51	—	—	—
Wave meter	Mc. sec	nil	nil	nil	nil	nil	nil

mm. respectively. Thus with this arrangement we have taken three diodes (E_1 , E_2 and E_3) and two triodes (E_1 and P_2) of different dimensions. The flat glass electrode tube consists of a pyrex glass tube with flat ends of diameter 50 mm. separated by a distance of 58 mm. This tube is held coaxially between two metallic discs of diameter 160 mm. The large diameter of the disc gives a uniform electric field. In the ozoniser type discharge tube there are two test tubes of pyrex glass fused together at the necks, with a small gap of 4.1 mm. between

TABLE II
Flat-glass electrode tube

Method	Range	Total no. of readings for each column	air	argon	hydrogen	oxygen
Cathode Ray Oscillograph ↑ ↓	Kc. sec.	198	103±2	106±2	105±3	103±4
		193	658±9	654±5	670±13	656±7
	Mc. sec.	180	2.14±0.02	2.23±0.05	2.10±0.02	2.24±0.09
		190	2.6±0.01	2.61±0.02	2.56±0.06	2.63±0.02
		185	2.80±0.02	2.78±0.08	2.79±0.01	2.79±0.02
		162	3.1±0.03	3.1±0.0	3.1±0.0	3.1±0.05
		175	7.50±0.14	7.50±0.05	7.47±0.05	7.42±0.05
		194	10.7±0.4	10.6±0.3	11.0±0.6	11.0±0.2
		206	14.0±0.2	13.75±0.25	14.1±0.3	13.9±0.23
		182	15.0±0.6	14.8±0.2	15.3±0.5	15.0±0.2
		228	26.0±0.17	26.0±0.1	26.0±0.1	26.0±0.2
		199	27.0±0.2	27.0±0.0	27.0±0.0	27.0±0.0
Super hot frequency meter	Kc. sec.	20	670±53	668±45	-	-
Wave meter	Mc. sec.	nil	nil	nil	nil	nil

them. The internal surface of the smaller tube and the external surface of the bigger tube act as glass electrodes with an area of about 1000 sq. cm. In order to feed electric potential to this tube, the internal tube is filled with acidulated water, in which the H.T. terminal from a transformer is immersed. The L. T. terminal is prepared by immersing the whole assembly in a glass vessel containing acidulated water.

The supply of the electrical energy is taken from a commercial A.C. point of 230 volts and 50 c/s frequency. We have used two H.T. transformers of output

TABLE III
 Ozoniser type tube

Method	Range	Total no. of readings for each column	air	argon	hydrogen	oxygen
← Cathode Ray Oscillograph → ↑	Kc. sec.	195	714 ± 14	714 ± 15	717 ± 15	707 ± 8
		181	961 ± 10	953 ± 7	952 ± 9	955 ± 11
		193	1025 ± 25	1020 ± 34	1040 ± 7	1040 ± 30
	Mc. sec.	169	2.04 ± 0.05	2.04 ± 0.01	2.02 ± 0.02	2.01 ± 0.01
		116	2.25 ± 0.01	2.30 ± 0.02	2.24 ± 0.1	2.34 ± 0.1
		74	2.76 ± 0.08	2.8 ± 0.0	2.8 ± 0.0	—
		153	3.1 ± 0.1	3.2 ± 0.2	3.13 ± 0.05	3.17 ± 0.05
		187	7.5 ± 0.16	7.5 ± 0.1	7.5 ± 0.1	7.6 ± 0.2
		192	10.6 ± 0.8	10.6 ± 0.6	10.6 ± 0.1	10.6 ± 0.05
		191	14.1 ± 0.1	14.0 ± 0.02	14.6 ± 0.1	14.0 ± 0.0
		193	15.3 ± 0.3	15.5 ± 0.6	15.3 ± 0.2	15.1 ± 0.1
		209	26.5 ± 0.5	26.2 ± 0.2	26.1 ± 0.2	26.0 ± 0.0
		174	27.2 ± 0.2	27.0 ± 0.0	27.0 ± 0.0	26.75 ± 0.25
Super hot frequency meter	Kc. sec.	20	680 ± 56	—	—	680 ± 53
Wave Meter	Mc. sec.	59	1.5 ± 0.7	1.45 ± 0.8	1.42 ± 0.9	1.42 ± 0.8

40 KV and 4KV. In the external circuit two carbon resistances of values 9 megohms and 2 megohms are alternately employed.

Our experiments consisted of measurements of current and frequency. The currents were measured by rectifying the fall of potential across the series resistance with the help of a triode 30 used as a diode. The rectified current was measured by a mirror galvanometer. The observations were taken in air, hydrogen, oxygen, commercial argon and mercury vapour. The gas pressures were varied from 0.01 mm. to 750 mm.

It was observed from the current oscillogram that the high frequency streaks were very prominent in the cases of the flat glass electrode discharge tube and the ozoniser type discharge tube. In the case of the internal electrode tube the streaks were less conspicuous. In the use of an absorption wavemeter, it was observed that the readings were possible only for the ozoniser type discharge tube, while for the remaining tubes, radiations were too weak to energize the wavemeter.

OBSERVATIONS

The observations may be divided into two parts, the current measurement and the frequency measurements.

1. *Current Measurements:* Typical graphs of mean discharge current for the internal electrode tube, plotted in microamperes, versus E/P in volts/cm/mm. Hg, are shown in figure 4. For the E positions, the graphs are like those for a

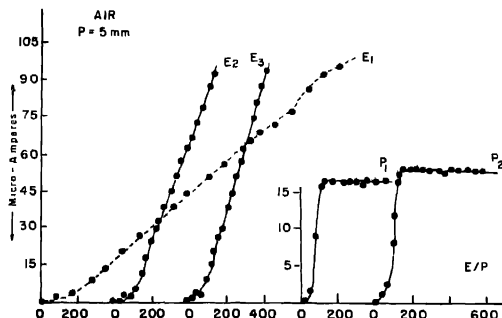


Fig. 4. Current graphs for the internal electrode tube E_1 E_2 and E_3 are the graphs for the diode positions while P_1 and P_2 are the graphs of the grid currents in the triode positions of the tube.

gas-filled diode, and for the P positions like those of grid current versus anode potential for gas-filled triodes. In the remaining tubes the electrode also act like the electrodes of a diode and the current against E/P curves are also similar to those of a gas-filled diodes. Our graphs are like those for multigrid tubes observed by Emeleus and others (1951) who found that the form of the graphs was independent of noise level of disturbances. Our graphs, likewise, do not show any obvious effect due to intensity and frequencies of the electrical oscillations.

2. *Frequency Measurements:* The main result obtained has been that the frequencies observed cluster round certain values, by whichever methods they were measured, and whichever tubes and discharge parameters were employed. The megacycle oscillations only appear prominently, however, at the high pressures, and for these the individual band-widths were greater than for the lower frequency oscillations. The frequency readings are summarised in Tables I, II and III.

It is natural to suspect that some of the observed frequencies could be produced by the external circuit of the discharge tube. We have, however, varied the circuit inductances and resistances very widely without effect on our results, whilst the capacities of the tube are different. We are therefore led to the conclusion

that the discrete frequencies observed are peculiar property of the discharge under consideration

ACKNOWLEDGMENT

The author wishes to acknowledge his grateful thanks to Prof. K. R. Dixit, formerly Head of this Department and now Principal of Gujarat College, Ahmedabad for suggesting the problem and for valuable guidance throughout the work. He also thanks Prof. K. G. Emelcus, Queen's University, Belfast for valuable suggestions

REFERENCES

- Emelcus, K. G., Neill, T. R. Armstrong, E. B., 1951, *Proc. Royal. Irish. Acad.*, **54A**, No. 18, 201.
 Joshi, S. S., 1945, *Curr. Science*, **14**, 67.
 Khastgir and Setty, 1952, *Curr. Science*, **21**, 197.
 Khastgir and Setty, 1953, *Proc. Nat. Inst. Sci. (India)*, **19**, No. 5, 631.
 Khastgir and Setty, 1953, *Science and Culture*, **18**, 435.
 Khastgir and Suvastava, 1954, *Proc. Nat. Inst. Sci. (India)*, **22**, No. 3, 290.
 Tiwari, S. N., 1948, *Ind. J. Phys.*, **22**, 553.
 von Engel, A. and Haines, W. L., 1951, *Proc. Phys. Soc. (London)* **B64**, 916.

INVESTIGATION OF DISCRETE SOURCES OF RADIATION FROM SOLAR ECLIPSE OBSERVATIONS

(Mrs.) NILIMA MITRA

ALL INDIA RADIO, NEW DELHI

(Received for publication June 30, 1956)

ABSTRACT. Ionospheric observations during the partial solar eclipse (89.5%) of 20th July, 1944 have been critically examined in order to determine whether the reduction of ion-density of the E layer with the progress of the eclipse follows Chapman's theory of layer-formation based on a homogeneous distribution of radiation across the solar disc. The observed time-difference of 10 minutes between the maximum of the eclipse and the minimum of the ion-density gives the value of effective recombination coefficient as $\alpha = .56 \times 10^{-8}$ by employing Appleton's 'sluggishness' formula. α is also calculated from the variation of N_p around local noon during the control period, which gives α as $.55 \times 10^{-8}$. The variation of the observed and computed values of J , the ion-production function, indicates that there must have been some discrete sources of radiation on the east limb of the sun causing the asymmetry in the variation of N_p with the progress of the eclipse. Various models of the sun are then assumed from known variations of the obscuration functions of the disc and limb and the values of J calculated for different values of contributions from the east and west limbs of the sun. By a series of trials, a suitable model is worked out which fits well with the observed variation of J . This model, when compared with the sun-chart of the eclipse day, is found to be a representative one. There were some prominences of the east limb which were possibly causing extra ionisation of the E layer before the maximum of the eclipse. This indicates that, in addition to a homogeneous distribution of radiation across the solar disc, discrete sources on the limb play an important part in causing the ionisation of the E layer.

1. INTRODUCTION

Chapman's theory of formation of ionospheric layers assumes a homogeneous distribution of ionising radiation across the solar disc. This theory has been found to generally agree with observations specially for the E and F₁ layers. However, critical examination of the changes in ionisation density during the progress of a solar eclipse has often indicated that discrete sources of radiation on the solar disc produce considerable effect on the ionosphere (Wilkes, 1937, Mitra, 1953; Minnis, 1955). In the present paper one such observation during the partial solar eclipse of 20th July, 1944 (Baral and Mitra, 1944-45) has been examined in detail. It is shown that radiation from discrete sources on the solar disc was playing an important part in the production of the E layer. We have selected ionospheric investigations during this particular eclipse, since 1944 was the year of minimum solar activity. One would, therefore, expect few discrete sources on the sun. Even then we have found that the density of ionisation in

the E layer was influenced by radiations coming from a few discrete sources from an apparently undisturbed sun.

The observation of inhomogeneous radiation causing ionisation of the E layer is of importance since the hitherto known theories assume the production of the E layer by a homogeneous distribution of radiation across the solar disc. E layer is also known to behave in a regular manner although there are quite a few phenomena like E_s , E_2 etc., which are not yet completely understood. It is felt that any observed irregularity in the E layer and a possible explanation of its origin will be of help in understanding the behaviour of the region as a whole.

Another important feature of the analysis is the determination of the effective recombination coefficient in the E layer of the ionosphere from the reduction of the ionisation density during the progress of the eclipse. Similar attempts in the past have indicated that α is of the order of 10^{-8} cm³/sec. Our investigation has revealed that a value of α of about 6×10^{-8} cm³/sec fits in fairly accurately with the observations.

2. EXPERIMENTAL RESULTS

It has been mentioned in section 1 that the experimental observations during the eclipse of 20th July, 1944 have been utilised in the present investigation. The experimental procedure and the results obtained are briefly described below.

The ionospheric observations were made at the University College of Science, Calcutta (Lat. 22°33' N, Long. 88°22' E). The circumstances of the eclipse are given in Table 1.

TABLE 1

Circumstances of the eclipse of 20th July, 1944 at Calcutta

Eclipse starts	0923 L.M.T.
Eclipse maximum	1113 L.M.T.
Eclipse ends	1303 L.M.T.
Magnitude	89.5%

Observations of the critical frequency of E and F₂ layers were made during the progress of the eclipse. The measurements were started one hour before the commencement of the eclipse and were continued at intervals of 20 minutes upto one hour after the eclipse was over. The observations were made more frequently about the middle of the eclipse. Measurements were also made 3 days before the eclipse and 3 days after it during the same local hour to check the average condition of the ionosphere. Figure 1 depicts the changes in the ionisation density (f_oE^2) of the E layer on the eclipse day and during the control period. The same figure also shows the percentage obscuration of the solar disc with the progress of the eclipse. It would be noted from the

figure that there was an appreciable reduction in the ionisation density of the E layer on the eclipse day. The minimum of ionisation was attained about 10 minutes after the maximum of the eclipse. We shall utilise the above observations in our further investigations.

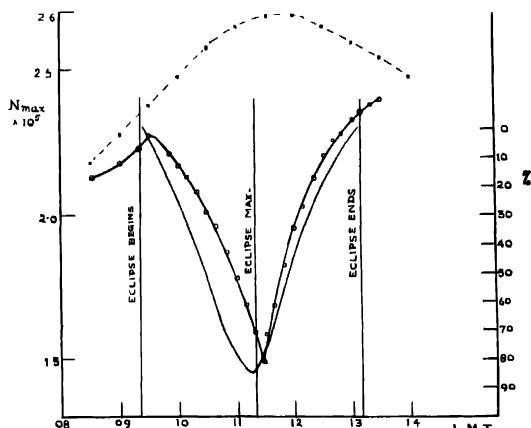


Fig. 1. Variation of E-layer ion-density during solar eclipse of 20th July, 1944. \circ - \circ - \circ Eclipse Day. \circ - \circ - \circ Control period. — Percentage obscuration of solar disc.

3. ANALYSIS OF OBSERVATIONS

(a) Control Period

The observations during the control period provide an approximate check whether Chapman's theory of layer formation was generally obeyed. According to this theory the ions and electrons produced by solar radiation disappear by recombination. There may be different processes by which recombination takes place. Taking α as the recombination coefficient giving the resultant effect of all the processes, we can write

$$\frac{dN_e}{dt} = q - \alpha N_e^2 \quad (1)$$

where α is the effective recombination coefficient,

N_e is the number density of electrons (ions) at any instant at any particular height,

q is the rate of ion production.

Under equilibrium conditions i.e. at midday,

$$\frac{dN_e}{dt} = 0$$

$$\text{and} \quad q = \alpha N_e^2 \quad \dots (2)$$

$$\text{Now} \quad q = \beta I_0 \text{Ch}(\chi) / H \exp l \quad \dots (3)$$

where β is the number of ions produced by absorption of unit quantity of radiation, I_0 is the intensity of radiation before it enters the atmosphere, $\text{Ch}(\chi)$ is the Chapman function for solar zenith angle χ , H is the scale height.

$\text{Ch}(\chi)$ is equal to $\cos \chi$ for $\chi \leq 85^\circ$

or,

$$N_e = \text{Const.} (\cos \chi)^{\frac{1}{2}} \quad \dots (4)$$

In order to verify the above relation, the observed value of N_e (figure 1) and of $\cos(\chi)$ have been plotted in a logarithmic scale in figure 2. The slope of the straight line gives the value of the exponent of $\cos \chi$. This exponent comes out to be .54 from figure 2 which is in fairly good agreement with the theoretical value of .5

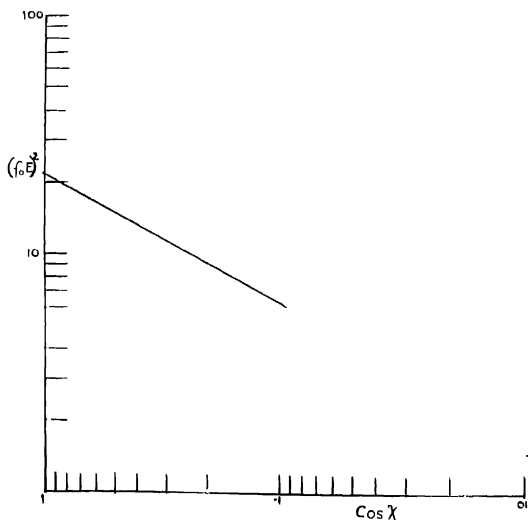


Fig. 2. Variation of E-layer ion-density with solar zenith angle (Control period)

(b) *Evaluation of the Recombination Coefficient*

The observations during the eclipse can be utilised in different ways for determining α in the E layer. The simplest method is from the 'sluggishness effect'

(Appleton 1953) in which there should be a time-lag between the maximum of ion production and the maximum of the ionisation density. Applying this principle to the case of eclipse observation one should expect a time-difference between the maximum of the eclipse and the minimum of the ionisation density. Some workers in the past have observed such time-lags but attempts to evaluate the recombination coefficient were not made since the principle was not known at the time. In our observations we have observed a time-difference of 10 minutes.

Using the familiar relation

$$\Delta t = \frac{1}{2\alpha N} \quad \dots (5)$$

α comes out to be $.56 \times 10^{-8}$ cm³/sec and is in fairly good agreement with the generally accepted value of α in the E layer

We shall now proceed to determine α by other methods from our observations

It is possible to evaluate α from the measurements carried out during the control period. In figure 1 we have selected two points *A* and *B* equally spaced around noon from the diurnal variation of the ionisation density. Assuming the values of α and q to be the same at *A* and *B*.

$$q_A = q_B = \frac{\left[(N_e)^2_B \left(\frac{dN_e}{dt} \right)_A - (N_e)^2_A \left(\frac{dN_e}{dt} \right)_B \right]}{(N_e)^2_B - (N_e)^2_A} \quad \dots (6)$$

Taking similar points at equal distances at an interval of 15 minutes around noon a series of values of q are found out. These values have been plotted against the spacings around noon and q at midday determined by extrapolation. These values can be taken as q_0 , the maximum rate of ion production. In the present case q_0 comes out to be 405 ions/cc/sec. From equation (2), i.e. under equilibrium condition and putting q_0 as 405, α comes out to be $.55 \times 10^{-8}$ cm³/sec. This value of α is in very good agreement with that determined from the 'sluggishness effect' α during the eclipse can be determined from the reduction of the ionisation density in the following way. If the fraction of the disc exposed is given by A at any instant and χ , the solar zenith angle, then the rate of electron decay is given by

$$\frac{dN_e}{dt} = Aq_0 \cos \chi - \alpha N_e^2 \quad (7)$$

$\frac{dN_e}{dt}$ is known from the measurements shown in figure 1. A is known from the characteristics of the eclipse. Similarly, q_0 and $\cos \chi$ are also known.

We have thus calculated N_e^2 by assuming different values of α . Then a series of curves were drawn showing the variation of N_e with time for different values of α . These curves were compared with observed variation as could be seen in figure 3. The curve that fits best the observed variation of N_e gives the

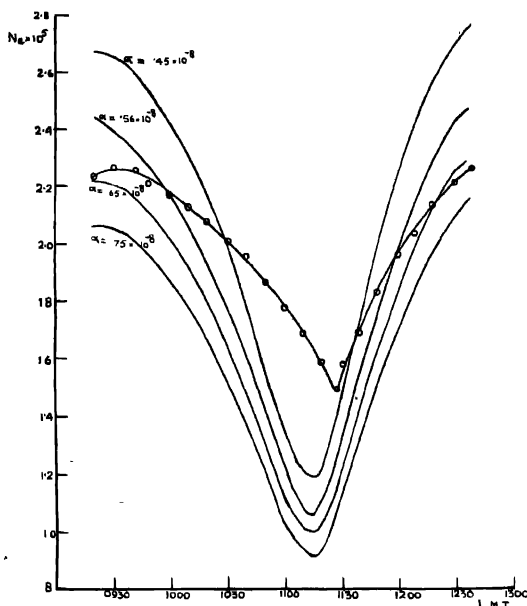


Fig. 3. Comparison between observed values of E-layer ion-density and those calculated theoretically assuming uniformly radiating disc.

value of α for the E layer. It would be seen from figure 3 that the theoretical curves do not agree with observed variation but the curves with $\alpha = .65 \times 10^{-8}$ and $\alpha = .56 \times 10^{-8}$ appear to be the nearest approach. There is considerable asymmetry between the observed and calculated variations during the first half of the eclipse. The reduction in ionisation density was much too slow and gradual in the first half compared to that after the maximum of the eclipse. This clearly indicates that the distribution of radiation is not homogeneous across the solar disc and the asymmetry is probably due to some discrete sources of ionising radiation on the sun which were left exposed during the first half of the eclipse and occulted after the maximum of the eclipse. We shall deal with this point more fully in the next section.

4. NON-HOMOGENEOUS DISTRIBUTION OF SOLAR RADIATION

We have seen from figure 3 that with a value of $\alpha = .56 \times 10^{-8}$ the theoretical curve of N_e gives an asymmetry in the first half of the eclipse. It fits fairly well with the other half. If α is dependent upon pressure and temperature it is unlikely that it will vary during the progress of the eclipse and the asymmetry from the beginning till the maximum of the eclipse is most probably due to some discrete sources of radiation which were left unobscured in the beginning but became occulted later during the eclipse. This can also be proved in the following way.

We write from equation (1)

$$\frac{dN_e}{dt} = Aq_0 \text{Ch}(\chi) - \alpha N_e^2 \quad \dots (8)$$

where A is the fraction of the solar disc unobscured.

q_0 is the maximum value of q .

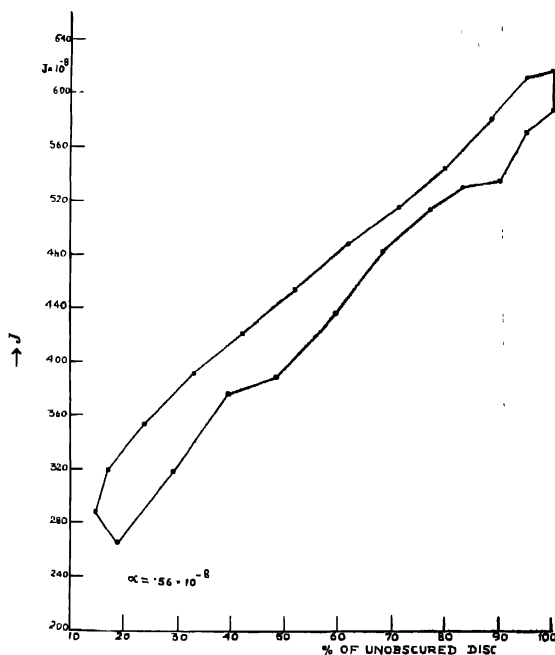


Fig. 4. Variation of J with unobscured area of solar disc

$\text{Ch}(\chi)$ is the Chapman function which can be written as $\cos \chi$ for $\chi \leq 85^\circ$. Therefore,

$$Aq_0 = J = \left(N_e^2 + \frac{1}{\alpha} \frac{dN_e}{dt} \right) \sec \chi \quad \dots (9)$$

J can be appropriately called the function for ion production. We have evaluated J every 10 minutes from our experimental results assuming $\alpha = .56 \times 10^{-8}$. The values of J in units of 10^8 (electrons/cc) have been plotted in figure 4 against the percentage area of the unobscured disc

If the ionisation in the E layer were caused by uniform radiation coming from different parts of the solar disc one would expect that the values of J would be the same at intervals equally spaced around the maximum of the eclipse and

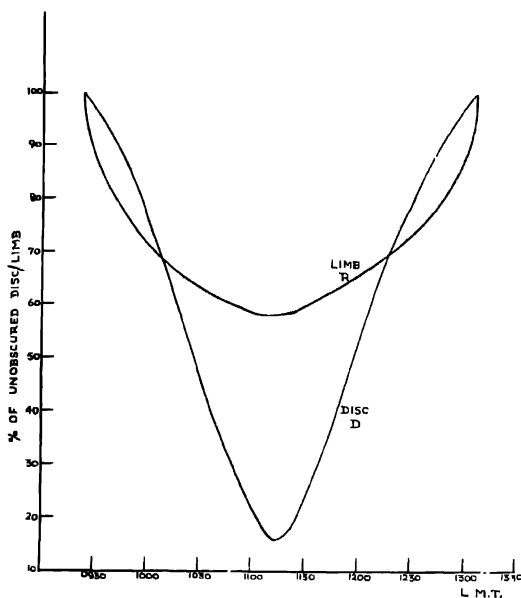


Fig. 5. Obscuration function of disc and limb.

figure 4 should become a straight line. The circumstances of the eclipse indicated that the west limb of the sun was largely obscured before the maximum of the eclipse while the east limb was left exposed. This relation was reversed after the maximum of the eclipse. Figure 4 indicates that there must have been intense local sources on the east limb of the sun which gave higher values of J before

the maximum of the eclipse than after it. These radiations were stronger than the corresponding ones in the west limb.

We shall now analyse our observations further with a view to obtaining a variation of J which would fit the observed values (figure 3). We shall evaluate separately the contributions to J due to uniform disc and the limb and those due to discrete radiations from the limb. We shall then attempt to determine a model of the sun which would explain the observed variations. This model will be compared with known prominences on the limb and also with the $H\alpha$ -dark markings which were prominences projected on the disc.

The obscuration functions of the disc and the limb are plotted in figure 5. Figure 6 indicates the progress of the eclipse at different selected times. The ion-

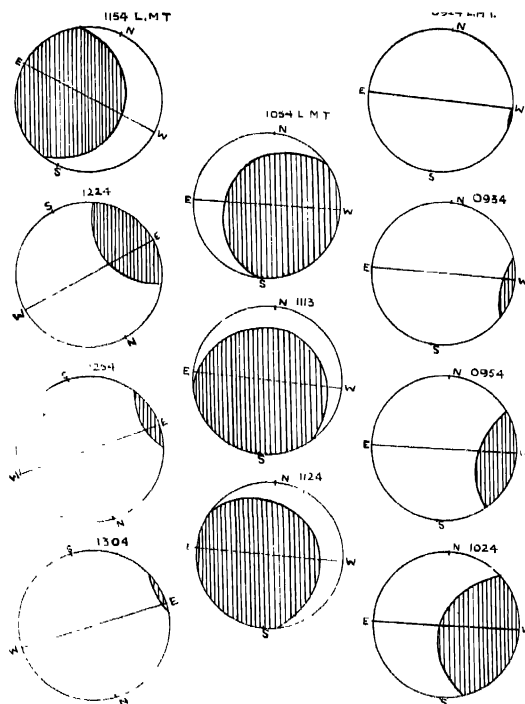


Fig. 6. Appearance of the sun during the progress of the solar eclipse of July 20, 1944, at Calcutta.

production function J can be written as $J_0 = J_D + J_R$ in the absence of contributions from the limbs. J_D is the contribution due to the disc and J_R that due to the

limb. It would be seen from figure 4 that our observed value of the maximum of J i.e. J_0 is about 630 and J_R which is given by the minimum value of J is about 290. Had the eclipse been total J_R would have been zero. We have seen that discrete sources on the east limb were giving higher values of J before the maximum of the eclipse than during the later period. These extra radiations were also contributing to the total value of J_0 . Denoting J_E and J_W as contributions from the east and west limbs respectively, figure 4 indicates that $J_E - J_W$ is of the order of 30. This value is, however, only for $\alpha = .56 \times 10^{-8}$. If we take some other value of α then $J_E - J_W$ will be different indicating its dependence upon α alone.

Now, if the sun were radiating uniformly, the value of J_0 ($= J_D + J_R$) would have been somewhat lower than that found from figure 4, i.e. 630. An approximate estimate of this quantity under the condition of a homogeneous distribution of radiation can be obtained by averaging the observed values of J_D and J_R . This comes out to be 460. One should add to this quantity the extra contributions from the limbs in order to obtain the values of J_0 under actual circumstances. Thus

$$J_0 = J_D + J_R + J_E + J_W$$

Taking J_0 as 630, $J_D + J_R$ as 460 and $J_E - J_W$ as 30, we have calculated a series of values of J_0 at different instants for different independent values of J_D , J_R , J_E and J_W assuming different models.

Table II below gives some models for calculating J consistent with the above representative values.

TABLE II
Models for J , $\alpha = .56 \times 10^{-8}$

	J_D	J_R	J_E	J_W	J_0
Model I	300	160	100	70	630
Model II	400	60	100	70	630
Model III	350	110	100	70	630

From the above models, the values of J_D and J_R at different instants of time were calculated from figure 5. We have not studied the variation of J_E and J_W independently with time since $J_E - J_W$ is a function of α alone. The values of J_0 at different times were next evaluated. A series of curves were plotted with the above models showing the variation of J with time. That model which best fits the observed values of J was considered to be representative of the contributions coming from the sun and responsible for production of the E layer.

Figure 7 shows the variation of J with time as observed and as computed from model I. It would be seen from this figure that the model I gives a very good agreement between the observed and computed values and can be taken as representative of the discrete sources of radiation coming from the sun as assumed in constructing the model.

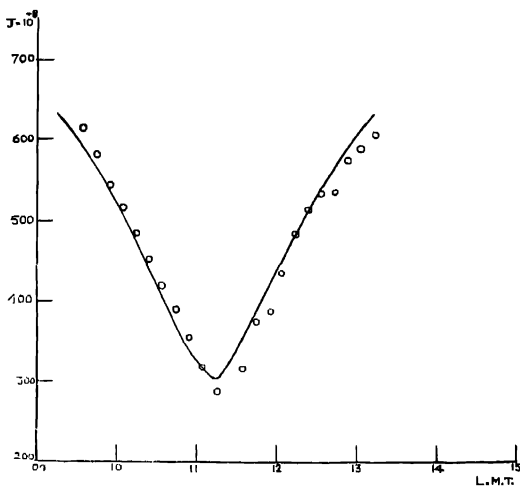


Fig. 7. Variation of J with time for E layer. o o o observed values of J . — Computed from model.

We next turn to a discussion of the model considered for representing the observed variation of J . Our model has been based on the assumption of some discrete sources of radiation from the east limb of the sun which, by their obscuration only during the second part of the eclipse, were giving rise to an asymmetry in the value of N_e and J .

Figure 8 shows a Sun-chart prepared for July 20, 1944 containing the sketches of the prominences on the limb and also the $H\alpha$ dark markings. Since 1944 was the year of minimum solar activity the sun was comparatively free from a great many prominences. The position of the observed prominences can be read off the chart in terms of the position angles or latitudes and longitudes as one desires. A weak sunspot group was present on the disc near the west limb (Lat. $25^{\circ}20'S$, Long. $60^{\circ}E$) but it appeared at about 1800 L.M.T. long after the eclipse was over. The relevant details of the spot group taken from Greenwich and Zurich records are entered on the same figure. Records of Kodaikanal, Greenwich and Zurich observatories do not show that any flare occurred on the visible hemisphere.

It would be seen from figure 8 that there were some prominences on the east limb of the sun between 15° and 45°N . As we shall presently see, these prominences were mainly responsible for the observed asymmetry in the variation of

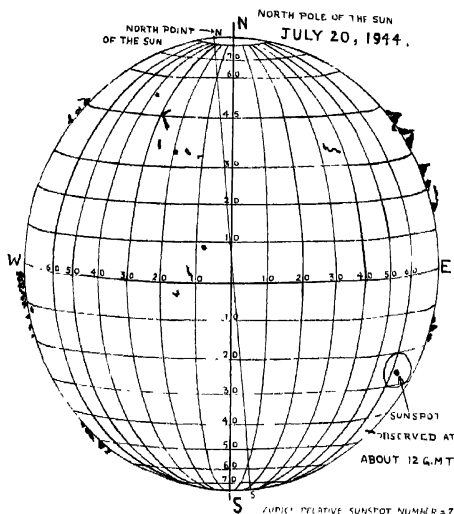


Fig. 8. Sun chart

Greenwich area of umbra = 3

" " " whole spot = 12

Millionth's of Sun's visible hemisphere.

the ionisation density of the E layer during the progress of the eclipse. A reference to figure 6 would indicate that the portion of the east limb where these prominences appeared was left uncovered from the beginning to the maximum of the eclipse. The intense radiation from these sources was, therefore, coming till about 1124 L.M.T. and thereby causing extra ionisation in the E layer during this period. Had these sources been absent there would have been a more rapid reduction in the ionisation density of the E layer as more and more area of the sun was being obscured with the progress of the eclipse. The variation of N_e would, therefore, have agreed with one of the theoretical curves in figure 3 depending upon the value of α . As a result of extra ionising radiation from these sources the reduction of N_e became more gradual from the beginning till the maximum of the eclipse and its value at any instant higher than the one theoretically calculated.

After the maximum of the eclipse, the east limb of the sun began to be obscured and the west limb slowly exposed. The prominences

on the east limb were mostly obscured between 1124 and 1224 L.M.T. The rise in the ionisation density of the E layer during this part of the eclipse was, therefore, due to a uniform radiation from the solar disc and the variation of N_e fits in fairly closely with the theoretical curves as could be seen from figure 3. The slight departure from the theoretical variation may be due to the contribution from some minor prominences as could be seen from figure 8.

The close agreement between the observed and calculated values of J (figure 7) based on a suitable model of the sun, where the contributions from the disc and the limbs were separately considered, encourages us to believe that in addition to the homogeneous distribution of radiation across the solar disc discrete sources on the limb play an important part in causing the ionisation of the E layer. Such asymmetries, if observed, in the variation of the ionisation density of the E layer (figure 3) during the progress of any eclipse can, therefore, be explained in terms of extra ionising radiation from discrete sources on the sun.

SUMMARY AND CONCLUSION

The results obtained in the present investigation can be summarised as follows

The value of the effective recombination coefficient in the E layer found by different methods from the experimental data on solar eclipse of 20th July, 1944 is of the order of $.56 \times 10^{-8} \text{ cm}^3/\text{sec}$.

The E layer is generally found to follow Chapman's theory where the source of ionising radiation is assumed to be homogeneously distributed across the solar disc. This has also been borne out from the measurements during the control period. But while considering the observations of the reduction in the ionisation density with the progress of the eclipse it is found that there is a remarkable asymmetry in the variation of the ion-production function. This can be attributed to radiation from discrete sources on the sun. Taking the contributions from the disc and limb separately, it is found that J_E is greater than J_W . It is also seen from the sun-chart that there were some prominences on the east limb. The asymmetry in the series of curves giving the variation of N_e with time for different values of α is maximum between 1030 and 1130 L.M.T. The progress of the eclipse together with the sun-chart indicates that during this time the prominences on the east limb were left exposed. The radiation from these sources is quite likely to produce appreciable ionisation of the E layer. In model I, $J_E = 100$, $J_W = 70$, and $\alpha = .56 \times 10^{-8}$. The values of J computed from this model are found to agree fairly well with the observed variations in the ion-production function.

It is possible to have an approximate idea of the recombination process in the E layer from the value of α . For radiative recombination, α is of the order of

10^{-12} cm³/sec (pressure taken as 10^{-3} mm). For dielectronic recombination process, α is also of the order of 10^{-12} cm³/sec. If the recombination is by the process of mutual neutralisation then α is of the order of 10^{-7} cm³/sec. But for dissociative recombination $\alpha \simeq 10^{-8}$ cm³/sec. Our value of α is $.56 \times 10^{-8}$ and therefore, the process of dissociative recombination is indicated.

ACKNOWLEDGMENTS

This author is deeply indebted to Mr. S. Basu, Director General of Observatories for kindly supplying her with the details of the circumstances of the eclipse, obscuration of the disc and the limb and the Sun-chart reproduced in the paper. Her grateful thanks are due to Mr. S. N. Mitra for suggesting the problem, making available the eclipse observations and for valuable help in the preparation of the paper.

The paper was read at the technical convention of the Institution of Telecommunication Engineers held in New Delhi on 30th December, 1956.

REFERENCES

- Apploton, E. V., 1953, *J. Atmosph. Terr. Phys.*, **3**, 282.
 Baral, S. S. and Mitra, S. N., 1944-45, *Science & Culture*, **10**, 175.
 Minnis, C. M., 1955, *J. Atmos. Terr. Phys.*, **6**, 91.
 Mitra, S. N., 1953, *J. Sci. Ind. Res.*, **12A**, 319.
 Wildes, M. V. 1939, *Proc. Phys. Soc.*, **51**, 138.

FURTHER STUDIES ON ASYMMETRICAL THREE PHASE OSCILLATOR FOR VERY WIDE FREQUENCY DEVIATION

P. KUNDU

INDIAN INSTITUTE OF TECHNOLOGY, KHARAGPUR.

(Received for publication September 26, 1956)

ABSTRACT. A three stage oscillator is described here which has been developed on the principle of asymmetrical three phase oscillator. Like a conventional system, only three stages are used here, each of which produces a phase shift, but unlike it, only one stage is used as an amplifier to produce the loop gain required by the system to oscillate. The performance of this oscillator has been found to be more uniform and the adjustment less critical for optimum operating condition, unlike the other types of RC oscillator. Oscillations of quite good waveform have been obtained over a frequency range of few hundred cycles to few tens of megacycles.

This system has been investigated from the point of view of producing very wide frequency deviation with uniformity of performance over a wide frequency range. The conditions for linearity and freedom from amplitude modulation have also been derived for different operating conditions. A maximum frequency deviation of about four to one has been achieved over a frequency range of few Kc/s to few Mc/s without necessitating any adjustments other than the tuning capacitances.

INTRODUCTION

The principle of asymmetrical three phase oscillator (Kundu, 1955) was already described and its linearity of frequency deviation with the mutual conductance of the modulator tubes was shown to point out its comparative suitability as a frequency modulated source. In a recent communication (Kundu, 1956) it was also shown that the overall performance may be greatly improved by modifying the system in such a way that the loop gain of the oscillator is less dependent on the frequency selective elements. The present paper gives full details of the work.

The need of a wide deviable source is felt over a frequency spectrum from very low to very high frequencies in the diverse fields of applications of frequency modulation. In sub-carrier current communication a maximum linear frequency deviation of about 40% of the mean carrier is required over a frequency range of few Kc/s to few hundred Kc/s. The requirement is, however, much less in F.M. broadcasting or in frequency shift telegraphy, but it is a few percent of the mean carrier in V.H.F. multichannel communication using F.M., in measuring apparatus for observing transmission frequency characteristics of a system and also in telemetering systems for guided missiles. A system would be more

useful for the above requirements if the modulation could be directly impressed anywhere in the frequency spectrum according to the different applications.

The basic requirement for a system to be suitable for all the above applications are met if the system is capable of wide frequency deviation having a uniformity of operation over a frequency spectrum from very low to very high frequencies.

The performance of the asymmetrical oscillator (figure 1) described previously falls short of the above requirements due to the fact that the frequency

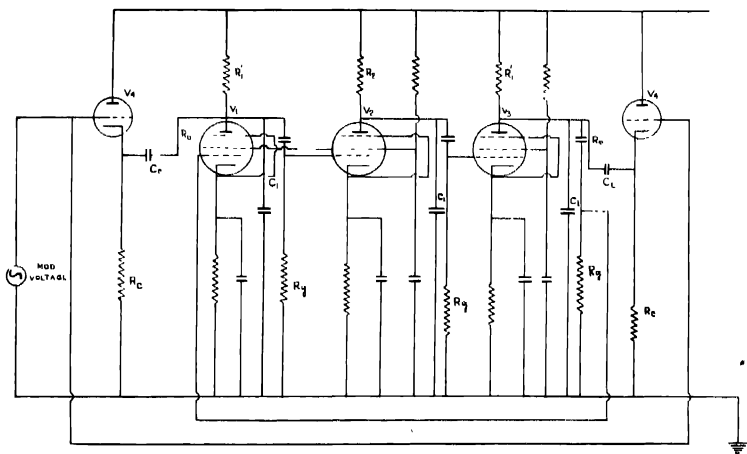


Fig. 1. Frequency modulated asymmetrical 3-phase system

variation necessitated a corresponding variation of the anode loads of the two stages. As a result, the loop gain is subjected to wide variation as can be seen from the equation (6iii) of the paper (*loc cit*) given as

$$A = \frac{g_m^3 R_1^3}{2 \left(1 + 2 \frac{R_1}{R_p} \right)}$$

where R_1 = effective anode load and $R_1 \ll R_p$, and the optimum operating condition, which L , is rather critical, is thereby disturbed. In order to eliminate this difficulty, it is therefore necessary to use the frequency selective network in such a way that its variation has minimum effect on the loop gain of the system (Kundu, 1951). The two anode loads were therefore connected to the cathodes of the two amplifier stages. Like a conventional three phase system, only three stages are used here, each of which produces a phase shift, but unlike it, only one of the stages is an amplifier which produces the necessary

gain. Here an inherent asymmetry is introduced by the amplifier stage while the phase shift due to the load of each of the stages may be similar or otherwise as the case may be.

The performance of this oscillator has been found to be more uniform and the adjustment much less critical for optimum operation unlike the other types of RC oscillators. A maximum frequency deviation of about 4 : 1 has been obtained over a frequency range of few Kc/s to few Mc/s simply by varying the grid bias of the cathode follower stages. The variation of frequency is quite linear over a range required for the applications mentioned above. The lower frequency of operation is limited due to the unwanted phase shift and attenuation introduced by the coupling, decoupling and the power supply-capacitances, while the dissimilar stray capacitance effect across the load resistances and the grid cathode capacitances of each stage affects the performance at the h.f. range.

This system may be compared with that developed by Ames (1949) modifying a phase shift oscillator (Hollingsworth, 1941) having replaced the resistances of the RC ladder networks with the output impedances of cathode follower stages. There a frequency deviation of about one octave has been reported using about 8 to 10 tubes to obtain optimum performance. The present system is basically a 3-phase oscillator and is capable of producing wider frequency deviation with uniformity of performance over the 1f to r.f. range. With proper asymmetry in the phase shift produced by one of the stages compared to the two similar stages, higher linearity in frequency deviation may be obtained over wider range. A further advantage lies in the simplicity of technique and in the economy of components.

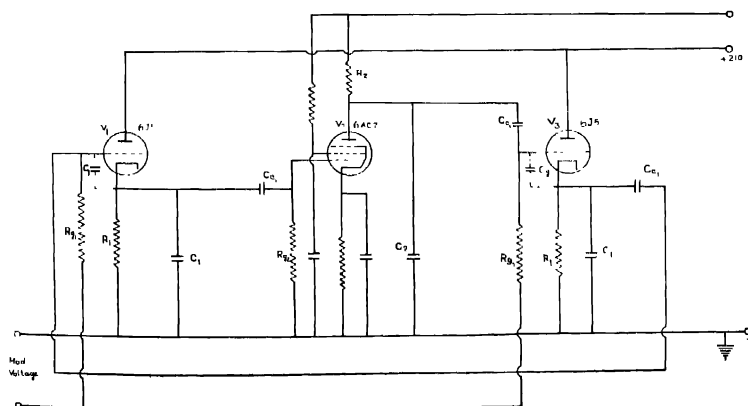


Fig. 2. Modified asymmetrical 3-phase system.

A basic design principle is presented here from an analytical point of view. The condition for linearity and freedom from spurious amplitude modulation have been discussed so that the components may be selected properly to obtain most satisfactory results. Experimental curves are also drawn to corroborate the theoretical conclusions

THEORETICAL CONSIDERATIONS

The complete oscillator is illustrated in the figure 2. The gain of each of the cathode follower stages is given by (Eq. 6A, appendix)

$$A_1 = \frac{g_{m1} + j\omega C_u}{G + j\omega C} \quad \dots (1)$$

where

$$G = g_m + \frac{1}{r_{p1}} + \frac{1}{R_1}$$

and

$$C = C_1 + C_g$$

and that of the amplifier is

$$A_2 = \frac{gm_2 R_2}{1 + j\omega C_2 R_2} \quad \dots (2)$$

Hence the loop gain of the system is given by

$$A = A_1^2 A_2 \quad \dots (3)$$

In deriving the equation for the gain A , the input impedances of the two cathode follower stages have been assumed to be very high.

The input admittance of the cathode follower stage is

$$Y_{in} = -\frac{1}{R_i} + j\omega C_i \quad \dots (4i)$$

where

R_i = input resistance

C_i = input capacitance

The values are given by (appendix eqn. 12A & 13A)

$$R_i = -\frac{1 + g_{m1}^2 / \omega C_1^2}{g_{m1} C_g / C_1} \quad \dots (4ii)$$

and

$$C_i = C_{gp} + C_g \frac{1 + g_{m1} R_1 + \omega^2 C_1^2 R_1^2}{(1 + g_{m1} R_1)^2 + \omega^2 C_1^2 R_1^2} \quad \dots (4iii)$$

The values of the input resistance and the capacitance are not constant but depend on the circuit parameters and also on the frequency. The above

equation for gain A is then valid so long as the shunting effect of the input negative resistance of the cathode follower is negligible, the input capacity being accounted for by the shunting capacity of the load. Besides, an assumption has also been made that the voltage developed across the cathode follower load is fed back between grid and cathode, in other words, the grid cathode impedance is very high.

Under these conditions the complex gain of the system is given by :

$$A = \frac{g_{m_2} R_2 [(g_{m_1}^2 - \omega^2 C_g^2) + 2j\omega g_{m_1} C_g]}{[(G^2 - \omega^2 C^2 - 2\omega^2 G C C_2 R_2) + j\omega(G^2 C_2 R_2 - \omega^2 C^2 C_2 R_2 + 2GC)]} \quad (5i)$$

$$= g_{m_2} R_2 \frac{a + jb}{c + jd} \quad \dots (5ii)$$

$$\text{or,} \quad A = |A| \angle \phi \quad \dots (5iii)$$

$$\text{where } |A| = \frac{g_{m_1}^2 + \omega^2 C_g^2}{(G^2 + \omega^2 C^2)} \times \frac{g_{m_2} R_2}{(1 + \omega^2 C_2^2 R_2^2)^{\frac{1}{2}}} \quad \dots (5iv)$$

$$\text{and} \quad \phi = \tan^{-1} \frac{b}{a} = \tan^{-1} \frac{d}{c} \quad \dots (5v)$$

For oscillations to be maintained $\phi = \phi_A + 2\phi_c = 0$

$$\text{i.e. } \omega^4 C_g^2 C^2 - \omega^2 g_{m_1}^2 C^2 \left(1 + \frac{C_g^2 G^2}{C^2 g_{m_1}^2} + 2 \frac{C_g^2 G}{C C_2 g_{m_1}^2 R_2} - \frac{2C_g}{C_2 g_{m_1} R_2} - \frac{4C_g G}{C g_{m_1}} \right) \\ + g_{m_1} G^2 \left(1 + \frac{2C}{C_2 G R_2} - \frac{2C_g G}{C g_{m_1} R_2} \right) = 0.$$

$$\text{Let} \quad g_{m_1} R_2 \gg C_g / C \quad \text{and} \quad C_g / C < < 1$$

$$\text{Then} \quad \omega^4 C_g^2 C^2 - \omega^2 g_{m_1}^2 C^2 + g_{m_1}^2 G^2 \left(1 + \frac{2C}{C_2 G R_2} \right) = 0$$

$$\text{or} \quad \omega^2 g_{m_1}^2 C^2 \left(\frac{\omega^2 C_g^2}{g_{m_1}^2} - 1 \right) + g_{m_1}^2 G^2 \left(1 + \frac{2C}{C_2 G R_2} \right) = 0$$

Assuming that

$$\omega C_g / g_{m_1} < < 1$$

the equation is reduced to

$$\omega^2 g_{m_1}^2 C^2 = g_{m_1}^2 G^2 \left(1 + \frac{2C}{C_2 G R_2} \right)$$

Then the frequency of oscillation is given by

$$\omega = \frac{G}{C} \sqrt{1 + \frac{2C}{C_2 G R_2}} \quad \dots (6)$$

The gain required for maintenance of oscillations at this frequency should be (from equation 5 iv)

$$A = g_{m_2} R_2 \frac{g_{m_1}^2}{G^2(4 + 2G R_2 C_2/C + 2C/C_2 G R_2)} \quad \dots (7i)$$

When

$$g_{m_1} \approx G \text{ and } C_2 = C$$

$$A = g_{m_2} R_2 \frac{1}{G^2(4 + 2g_{m_1} R_1) + \frac{2}{g_{m_2} R_2}} \quad \dots (7ii)$$

Conditions for oscillations as given in the equation (6) & (7) are of similar nature as those obtained previously for figure 1. But the main point of difference here is that the effect on the loop gain due to the variation of frequency with g_{m_1} is considerably less, and may be negligible over a certain range as is seen from the equation. Amplitude of oscillations, however, remains constant when frequency is varied by varying C and C_2 so that C_2/C always remains constant

The above equations are, however, restricted by the condition that the frequency of oscillation ω must be $<< g_{m_1}/C_g$

$$\text{i.e. } \frac{C_g}{C} << \left(1 + \frac{2}{g_{m_1} R_2}\right)^{-\frac{1}{2}}$$

Hence C_g/C must be $<< 1$ when $g_{m_1} R_2 >> 1$

and C_g/C must be $<< \sqrt{g_{m_1} R_2}$ when $g_{m_1} R_2 << 1$

Under this condition all other assumptions made before are also satisfied simultaneously

OTHER MODE

As in all multiphase oscillators, this system may also oscillate with more than one frequency. Here the interstage coupling network may produce the necessary phase lead for the system to oscillate at a different frequency similar to the phase shift type of oscillator (Ginzton, 1941), with the difference that the ladder network has been isolated from each other by the cathode follower stages as shown in the figure 3.

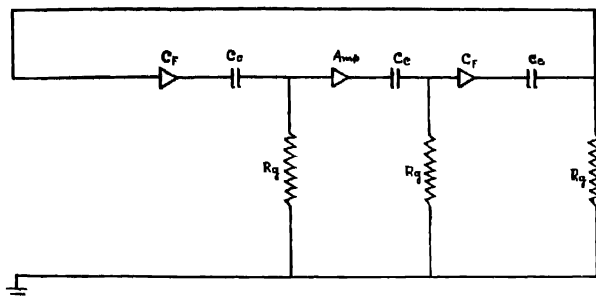


Fig. 3.

Assuming that all the networks are of same value and have no loading effect on the previous stages, the condition for gain and frequency for oscillations to be maintained are respectively given by

$$A = g_{m_2} R_2 \frac{1}{8 \left(1 + \frac{1}{g_{m_1} R_1} \right)} > 1 \quad \dots \quad (8i)$$

$$\text{and} \quad \omega = \frac{1}{\sqrt{3 C_E R_g}} \quad \dots \quad (8ii)$$

When the values of the $C_E R_g$ are different from one another, the attenuation becomes more and the anode load needed for the oscillations is also more.

PERFORMANCE OF THE SYSTEM

(a) As an Oscillator

It has been observed that even when the maintenance condition satisfies simultaneously for the above two cases, the high frequency mode was only maintained over a range of critical maintenance condition. With the increase of the loop gain, both the oscillations are generated simultaneously. With further increase, the higher frequency mode is interrupted over a cycle of lower frequency mode giving rise to similar type of oscillations as is found in the squegging of a LC oscillator.

Suppression of the low frequency mode has, however, been completely assured here, by wide separation of the two oscillating frequencies and by so proportioning the successive coupling network that there is more attenuation and phase shift in one of the networks compared to the other two.

When the low frequency mode is completely suppressed, this oscillator has been found to be capable of generating quite stable sinusoidal oscillations of good

waveform over a frequency range of few hundred cycles to few tens of megacycles. The entire frequency range may be covered in steps by changing the three capacitances simultaneously, and continuously varying the grid bias of the cathode follower stages. The range of variation may be seen from the curves in figures 4 a,b. The frequency at the high frequency end may, however, be varied

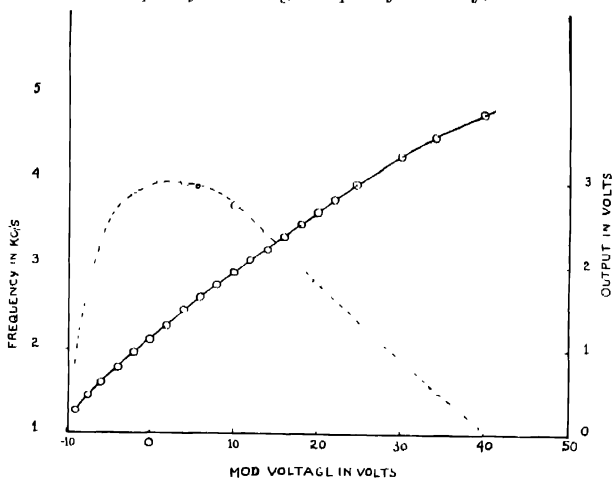


Fig. 4a

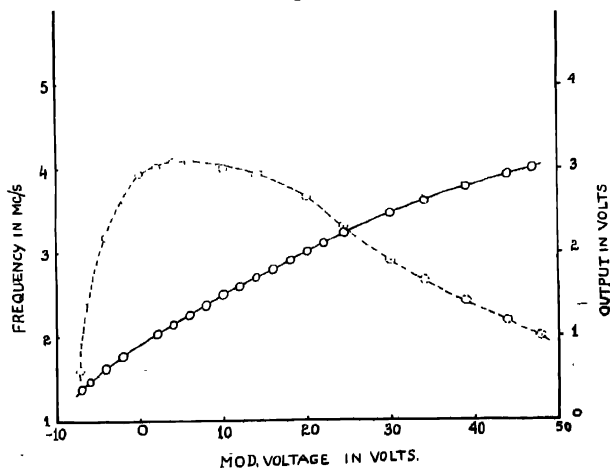


Fig. 4b.

continuously over a ratio of 10 : 1 by a three gang condenser. In order to maintain a constant output for a continuous coverage of frequency, some form of gain stabilisation should be incorporated. As regards the overall ratio of frequency variation in one set up, it may be pointed out that a maximum variation of about four times may be obtained over a range of few Kc/s to few Mc/s. But the ratio decreases at higher frequencies. This is due to the fact that the stray capacitances which are inherently present become increasingly important with the decrease of the shunting capacitances C_1 and C_2 and affect the stages differently and thereby introduce more attenuation. At higher frequencies, however, the ratio may be increased by increasing the loop gain, the resulting distortion being negligible due to the filtering action of the network.

(ii) *As a Deviable source*

The frequency deviation that may be obtained in this system is considerably more than that is usually required for the diverse fields of applications of frequency modulation. Two important characteristics that ought to be satisfied are, however, the linearity of modulation and freedom from spurious amplitude modulation. The suitability of this system has, therefore, been studied from the point of view of the different conditions under which the above requirements may be fulfilled.

(a) *Linearity*.

In the present system, the frequency deviation is several times the mean carrier frequency and the limit of variation of $g_{m1}R_2$ is $1 > g_{m1}R_2 \gg 1$. The frequency variation with g_{m1} is essentially non-linear in the region $g_{m1}R_2 \leq 1$ and is given by

$$f = \frac{g_{m1}}{2\pi C} \left(1 + \frac{2}{g_{m1}R_2} \right)^{1/2} \quad \dots \quad (9i)$$

when

$$g_{m1} \leq G \text{ and } C = C_2$$

The variation of f vs g_{m1} is, however, paractically linear in the region when $g_{m1}R_2 \gg 1$ and the frequency is given by :

$$f = \frac{1}{2\pi} \left(\frac{g_{m1}}{C} + \frac{1}{C_2R_2} \right) \quad \dots \quad (9ii)$$

But the main requirement is to obtain a linear variation of frequency with the modulating voltage. The nature of variation of the $g_{m1} \sim v_g$ curve of the modulator tubes should then be according to the region of working as was pointed out earlier by Kundu (1955).

In the region of non-linear relationship between f and g_{m1} as in equation (9i), the linearity of frequency deviation with a modulating voltage may only be ob-

tained if the non-linearities of the f vs gm_1 and gm_1 vs v_g curves cancel each other. But in the case when $gm_1 R_2 \gg 1$, the amplifier phase shift is maximum and is about 90° and it becomes independent of frequency, and the rate of change of phase shift of the cathode followers remains constant at the oscillating condition $\phi_A + 2\phi_C = 0$. The slope of frequency with modulating voltage should, therefore, remain constant so long as $gm_1 \sim v_g$ is linear as was shown in the case of figure 1. The modulating tubes in this case should then be so selected that there is a square-law relation between its plate current and grid cathode voltage v_g .

Here then lies the advantage of the asymmetrical system in which frequency may be varied linearly with gm_1 over a wide range. A further advantage of the present system compared to the one discussed previously, lies in the less amplitude variation as may be seen from the equations for loop gain of the two cases as well as less distortion due to the inherent degenerative feed-back in the cathode follower stages.

A further possibility of maintaining linearity over a greater range lies in maintaining the phase shift of all the three stages constant by maintaining $gm_1 R_2$ constant. This necessitates R_2 to be varied in inverse proportion to gm_1 so that the frequency varies linearly with gm_1 . But in the applications, as stated before, the required percentage deviation from the carrier is considerably less than what is obtainable here. It may therefore be preferable to work on the region where linearity is more conveniently obtained with minimum spurious amplitude modulation.

(b) *Amplitude modulation* :

From the equation (7ii) it may be seen that the loop amplification is maximum when $gm_1 R_2 = \frac{1}{gm_1 R_1}$, i.e., $gm_1 R_2 = 1$

and is given by
$$A = \frac{gm_2 R_2}{8} \quad (10i)$$

This is also the condition for minimum variation of gain with the variation of gm_1 . In the case when $gm_1 R_2 \ll 1$

$$A = \frac{1}{2} gm_1 gm_2 R_2^2 \quad \dots (10ii)$$

and the gain should vary proportionately with gm_1 in this region.

When $gm_1 R_2 \ll 1$,
$$A = \frac{gm_1}{2gm_2} \quad \dots (10iii)$$

In this case of when $gm_1 R_2$ is maintained constant, the amplitude variation with gm_1 can only be avoided if gm_2 (the mutual conductance of the amplifier) is varied proportionately with gm_1 .

EXPERIMENTAL OBSERVATION

Experimental curves are drawn to study the performance of the system under different conditions as discussed above. The first set of observations is made to study the nature of variation of frequency and amplitude as well as the range of deviation with the grid voltage variation of the two cathode follower stages over the frequency spectrum from few Kc/s to few Mc/s. The second observation is made to see the increase in deviation ratio at the h.f. range by increasing the loop gain.

The last set of measurements is taken to see the nature of variation of frequency with the mutual conductance under truly asymmetrical condition of operation having $C_2 > C$ and $g_{m1} > \frac{1}{R_2}$

TABLE 1

$C_{c_1} = .101\mu F$	$C_{c_3} = .101\mu F$	$V_1, V_3 = 6J5$
$R_{g_1} = 500K\Omega$	$R_{g_3} = 800K\Omega$	$V_3 = 6AO7$
$C_{c_2} = .001\mu F$	$R_1 = 7K\Omega$	
$R_{g_2} = 100K\Omega$		

1	(a) $C = C_2 = .011\mu F$	Fig. 4a
	(b) $C = C_2 = 100PF$	Fig. 4b
2	$C = C_2 = 25PF$	Fig. 5
	(a) $R_2 = 2.2K\Omega$	
	(b) $R_2 = 15.2K\Omega$	
3	$R_2 = 17.2K\Omega$	Fig. 6
	$C_2 = 10PF$	

DISCUSSION

The experimental curves are shown to study the basic principle of operation of the system. The first set of curves (figures 4a. and 4b) shows the nature of variation of frequency and amplitude with the input voltage to the cathode followers in the region $g_{m1}R_2 \geq 1$. The variation of frequency is seen to be practically linear over a considerable range even including the region of non-linear relationship between $f \sim g_{m1}$, as given in equation (9i). This is because the non-linearities of the g_{m1} vs v_g characteristic of 6J5 tubes and f vs v_g of the equation

(9i) are cancelling each other, as was also observed by Rakshit and Sarkar (1950) in the case of a symmetrical system. A minimum variation in amplitude is also obtained from 2 to 2.8 Kc/s in figure 4a and 1.8 to 2.6 Mc/s in figure 4b satisfying the condition for negligible spurious amplitude modulation as was discussed in the earlier section.

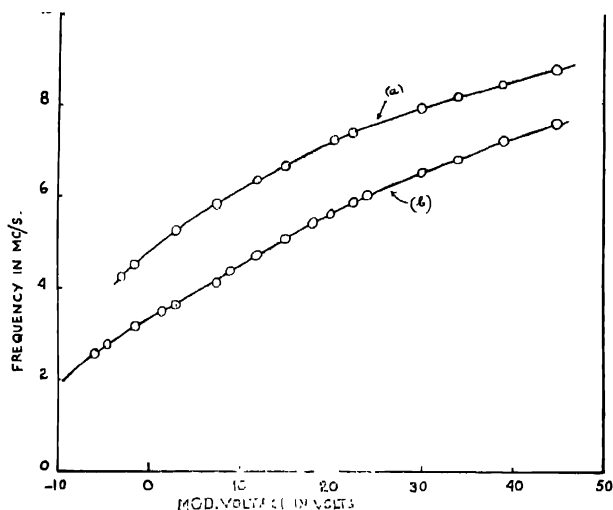


Fig. 5

In the second set of curves it is seen that in figure 5, curve (a) the overall frequency deviation is reduced when the physical capacitances are comparable to the stray and interelectrode capacitances, which are inherently present across each of the load are not same, become of increasing importance with the reduction of C_1 and C_2 . As a result, it affects the stages differently and thereby introduces attenuation and the system fails to maintain oscillations at low values for g_{m1} . The loop gain may, however, be increased by increasing the anode resistance R_2 to increase the range as is seen in curve (b) in figure 5.

Finally the effect of asymmetry may best be studied from the figure 6. Here the variation of frequency with g_{m1} is shown having no physical capacitances for C_1 . The slight discrepancy in the expected linearity for the high values of g_{m1} may be due to the corresponding reduction of r_p so that $g_{m1} \neq G$. The variation in amplitude, however, is much less than is expected from the equation and this is due to the negative input resistance of the cathode follower stages at this frequency which increases the gain of the system. This property may then be utilised to avoid the amplitude variation in this region.

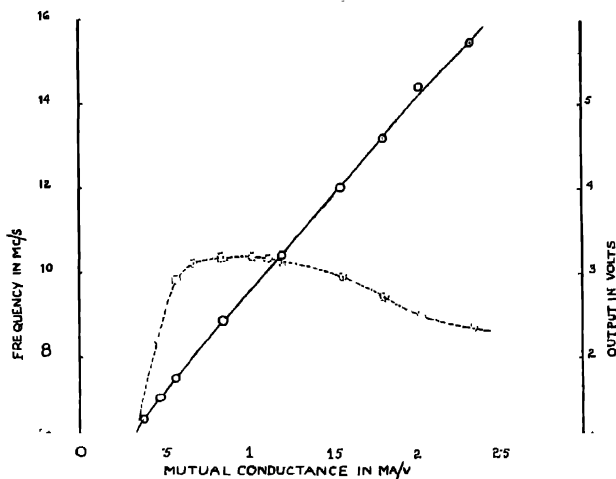


Fig. 6.

The above observations have been restricted by the condition $\omega < g_{m1}/C_g$. In the present set up having $C_g = 4PF$ and with $g_{m \min}$ as $5mA/V$, the minimum frequency must be $f_{\min} < 20$ Mc/s. The frequency limit may, however, be increased by selecting tubes with greater figure of merit.

CONCLUSION

The modified three phase asymmetrical system has been studied here analytically and experimental curves are also obtained which closely follow the theoretical conclusions. The performance of this system shows its comparative suitability as a very wide deviable source from the point of view of linearity, freedom from amplitude modulation and uniformity of operation over a wide frequency range. The analysis of the system and the experimental investigations have been restricted within the assumption of very high input impedance of the cathode follower stages. Further work is on progress so as to utilise this negative resistance of a cathode follower as a load of an amplifier stage to develop a deviable source.

ACKNOWLEDGMENT

The author records his grateful thanks to Prof. H. Rakshit for his kind interest in the work and for very helpful discussions.

REFERENCES

- Ames 1949, *Electronics*, **22**, 96.
 Gunston and Hollingsworth, 1941, *Proc. I.R.E.*, **29**, 43.
 Kundu, P. 1951, *Brit. I.R.E.*, **II**, 6, 233.
 Kundu, P. 1951, *Ind. Jour. Phys.*, **29**, 151.
 Kundu, P. 1956, *Proc. Ind. Sc. Cong. Part III* : 465.
 Rakshit, H. and Sarkar, N. 1950, *Ind. Jour. Phys.*, **24**, 107.

APPENDIX

The Response of the Cathode follower.

A generalised treatment of a cathode follower circuit is given by taking into consideration the different impedances so that the response may then be deduced under any condition

The equivalent circuit as shown in figure 7a, with a source of signal e_i having zero internal impedance. The assumption of zero source impedance is justifiable so long as the impedance remains so high that all the output voltage is fed back between the grid to cathode. The effect of finite input impedance, however, only modifies the input voltage e_i , which is the output voltage of the previous stage in this case.

Applying Kirchhoff's laws (figures 7a, 7b)

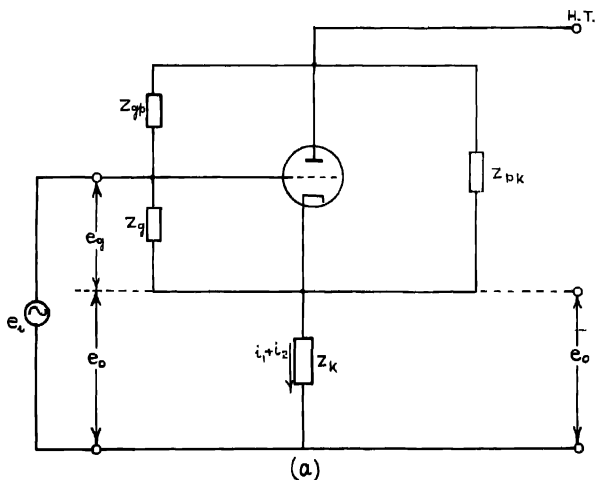
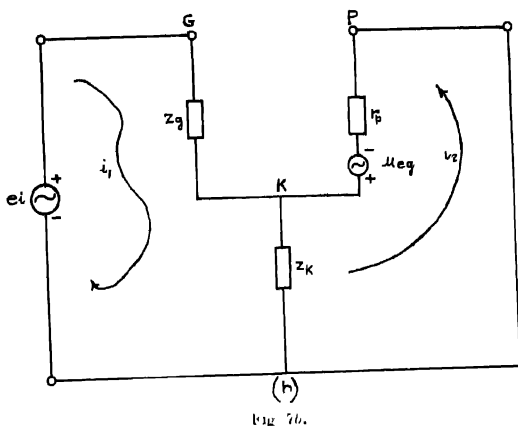


Fig. 7a, Cathode follower and its equivalent circuit.



$$e_i = e_g + e_0 \quad (1A)$$

$$\mu e_g = e_0 + i_2 r_p \quad (2A)$$

But

$$e_0 = (i_1 + i_2) z_k$$

On

$$i_2 = \frac{e_0}{z_k} - i_1 = \frac{e_0}{z_k} - \frac{e_g}{z_g} \quad (3A)$$

Substituting the values of i_2 in the equation (2A) we get

$$e_g(\mu + r_p/z_g) = e_0(1 + r_p/z_k)$$

or

$$(e_i - e_0)(\mu + r_p/z_g) = e_0(1 + r_p/z_k)$$

$$A = \frac{e_0}{e_i} = \frac{\mu + r_p/z_g}{\{(1 + \mu) + r_p(1/z_g + 1/z_k)\}} \quad (4A)$$

In this particular case

$$z_k = R_1(1 + j\omega C_1 R_1) \text{ and } z_g = 1/j\omega C_g$$

where C_1 = effective capacity connected across the load.

R_1 = resistance at the cathode

C_g = grid to cathode capacity.

Then

$$A = \frac{g_{m1} + j\omega C_g}{(g_{m1} + 1/r_{p1} + 1/R_1) + j\omega(C_1 + C_g)} \quad (5A)$$

$$\text{or} \quad A = \frac{gm_1 + j\omega C_g}{G + j\omega C_g} \quad (6A)$$

$$\text{where} \quad G = gm_1 + 1/r_p + 1/R_1$$

$$\text{and} \quad C = C_1 + C$$

Input Impedance of the cathode follower :

$$\text{From the figure 7b :} \quad e_i = i_1 z_g + i_1 z_k + i_2 z_k \quad (7A)$$

$$\text{and} \quad \mu e_g = i_2 r_p + (i_1 + i_2) z_k \quad (8A)$$

$$\therefore \quad i_2 = \frac{\mu e_g}{r_p + z_k} - \frac{i_1 z_k}{r_p + z_k} \quad (9A)$$

$$\text{Hence} \quad e_i = i_1 z_g + i_1 \left[\frac{r_p z_k}{r_p + z_k} + \mu i_1 \frac{z_g z_k}{r_p + z_k} \right] \quad (10A)$$

$$\text{Then} \quad y_{in} = \frac{i_1}{e_i} = \frac{r_p + z_g}{z_g(r_p + z_k) + z_k r_p + \mu z_g z_k} \quad (11A)$$

Substituting the values of z_k and z_g , we get

$$y_{in} = j\omega C_g \frac{(1 + R_1/r_p) + j\omega C_1 R_1}{(1 + gm_1 R_1) + j\omega C_1 R_1} \quad (12A)$$

$$\text{which yields} \quad R_i = - \frac{1 + gm_1^2 / \omega^2 C_1^2}{gm_1 C_g / C_1^2} \quad (13A)$$

$$\text{Since} \quad C_g / C \ll 1 \text{ and } gm_1 R_1 > C_g / C$$

$$\text{and} \quad C_1 = C_{gp} + C_g \frac{1 + gm_1 R_1 + \omega^2 C_1^2 R_1^2}{(1 + gm_1 R_1)^2 + \omega^2 C_1^2 R_1^2} \quad (14A)$$

ULTRAVIOLET ABSORPTION SPECTRA OF A FEW DISUBSTITUTED BENZENES IN DIFFERENT STATES*

S. K. SEN

(OPTICS DEPARTMENT, INDIAN ASSOCIATION FOR THE CULTIVATION OF SCIENCE,
JADAVPUR, CALCUTTA-32

(Received for publication October 1, 1956)

ABSTRACT. The near ultraviolet absorption spectra of *p*-dimethoxy benzene, *m*-dichlorobenzene and *m*-bromotoluene in the liquid and solid states at low temperatures have been investigated and the results have been compared with those for the vapour state of the substances and also with those for other such molecules. Absorption spectra of *p*-dimethoxy benzene and *m*-bromotoluene in the vapour state have also been studied and the bands have been analysed

Two broad bands have been observed in the spectrum due to liquid state of *p*-dimethoxy benzene with the 0,0 band at 33309 cm^{-1} . The 0,0 band shifts by 534 cm^{-1} towards longer wavelengths with the change from vapour to liquid state. The broad bands are replaced by eight sharper bands when the liquid is solidified and kept at room temperature, the 0,0 band being displaced further by 457 cm^{-1} towards longer wavelengths. On cooling down the crystals to -180°C the bands become sharper and two more bands appear, but the position of the 0,0 band remains unaltered.

The spectrum due to liquid state of *m*-dichlorobenzene gives four broad bands, the 0,0 band being at 35826 cm^{-1} . It is displaced by 360 cm^{-1} towards longer wavelengths with liquefaction of the vapour. In the solid state at -180°C the excited electronic state is observed to be split up into three components.

Similar results are observed in the case of *m*-bromotoluene, the 0,0 band of the liquid being at 36197 cm^{-1} .

INTRODUCTION

Swamy (1952, 1953a) observed in the near ultraviolet absorption spectra of crystals of *p*-xylene and *p*-dichlorobenzene at low temperatures, a number of bands which could be assigned to excited state vibrational frequencies of the molecules. The number of bands observed in the latter case, however, is larger than that in the former case. In order to find out whether the influence of intermolecular field on the electronic state depends on the nature of the substituent group in such para disubstituted benzenes, the ultraviolet absorption spectra of *p*-dimethoxy benzene $\text{C}_6\text{H}_4(\text{OCH}_3)_2$ in different states have been studied in the present investigation and the results have been compared with those due to *p*-xylene and *p*-dichlorobenzene.

*Communicated by Prof. S. C. Sarkar

Splitting of the electronic energy levels into three components was observed by Swamy (1953a, 1953b) in the absorption spectra of *o*-dichlorobenzene and *o*-bromotoluene at low temperatures, although no such splitting was observed in the case of para compounds. This indicates that probably the intermolecular field created by polar molecules in the crystal produces such a splitting of the electronic energy level while in the case of non-polar molecules such splitting does not take place. In order to verify this conclusion the ultraviolet absorption spectra of *m*-dichlorobenzene and *m*-bromotoluene in the liquid and solid states have been investigated. Further, the absorption spectrum of *m*-bromotoluene in the vapour state has been studied as no data for the vapour state were available for comparison. The results have been discussed and compared with those for isomeric dichlorobenzenes and bromotoluenes respectively.

EXPERIMENTAL

Chemically pure samples of *p*-dimethoxybenzene obtained from Scherring-Kahlbaum, Berlin, *m*-dichlorobenzene obtained from Theodor Schuchardt-München and *m*-bromotoluene from City Chemical Corporation, U.S.A., were distilled several times before being used in the present investigation.

The experimental arrangement was the same as that employed in an earlier investigation by the author (Sen, 1955). Spectrograms were taken on HP3 films with a Hilger E1 quartz spectrograph having a dispersion of 3 Å.U. per mm in the region 2600 Å. The absorption spectrum of *p*-dimethoxybenzene in the vapour state at room temperature was photographed with a sealed absorption tube of length 50 cm and of diameter 14 mm, quartz windows being cemented to the ends of the tube with Araldite and the substance being contained in a bulb attached to the tube. The spectrum of *m*-bromotoluene in the vapour state was recorded with a similar absorption tube which was kept at 55°C by means of electric heater, the bulb containing the liquid being kept at a temperature of 45°C by means of another electric heater. The time of exposure required to record the spectra due to vapour state was about an hour. Very thin films of thickness of the order of a few microns were required to obtain absorption bands due to the liquid and solid states. Interference fringes were exhibited by the absorption spectra of crystals owing to passage of light through thin crystalline films. The time of exposure varied from 20 minutes to about an hour.

Iron arc spectrum was photographed on each spectrogram as comparison. Microphotometric records were obtained with a self-recording microphotometer supplied by Kipp and Zonen. The frequencies of the bands were measured from the records as explained earlier (Sen, 1956b).

RESULTS

The microphotometric records of the spectrograms due to the substances in the liquid, solid and vapour states are given in figures 1, 2 and 3. The frequencies

of the bands due to vapour state are entered in Tables I and IV. Such data for the liquid and solid states are given in Tables II, III and V. The relative intensities of the bands are indicated as usual by the letters (vs), (s) (m) (w) and (vw). The bands have been assigned to particular transitions and these are given in the last column of each table.

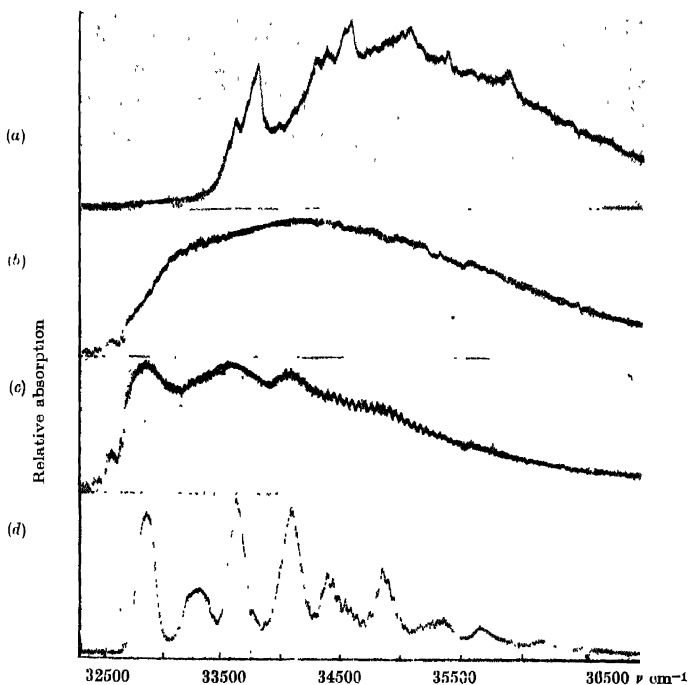


Fig. 1. Microphotometric records of the ultraviolet absorption spectra of *p*-dimethoxy benzene (a) Vapour at 32°C, (b) Liquid at 60°C, (c) Crystal at 32°C, (d) Solid at -180°C.

TABLE I

Absorption bands of *p*-dimethoxybenzene in the vapour state at 32°C

Wave No cm ⁻¹	Assignment	Wave No cm ⁻¹	Assignment	Wave No. cm ⁻¹	Assignment
33752 (vw)	0 - 271	34779 (w)	0 - 243 - 689	35943 (m)	0 - 586 - 756 × 2
33642 (w)	0 - 201	34845 (w)	$\left\{ \begin{array}{l} 0 - 1002 \\ 0 - 243 - 756 \end{array} \right.$	36012 (w)	$\left\{ \begin{array}{l} 0 - 1002 - 1161 \\ 0 - 171 - 385 - 804 \\ \times 2 \end{array} \right.$
33735 (m)	0 - 108	34946 (w)	$\left\{ \begin{array}{l} 0 - 1103 \\ 0 - 171 - 243 - 689 \end{array} \right.$	36063 (w)	0 - 304 - 689 - 1228
33789 (m)	0 - 54	35004 (w)	$\left\{ \begin{array}{l} 0 - 1161 \\ 0 - 117 - 304 - 689 \end{array} \right.$	36142 (w)	$\left\{ \begin{array}{l} 0 - 304 - 689 - 1299 \\ 0 - 304 - 385 - 804 \end{array} \right.$
33843 (vs)	0,0				
34014 (w)	0 - 171				
34086 (w)	0 - 243	35071 (m)	$\left\{ \begin{array}{l} 0 - 1228 \\ 0 - 171 - 243 - 304 \\ \quad \quad \quad - 504 \end{array} \right.$	36180 (w)	$\left\{ \begin{array}{l} 0 - 243 - 586 - 756 \\ \quad \quad \quad \times 2 \end{array} \right.$
34147 (w)	0 - 304				
		35142 (s)	0 - 1299	36242 (w)	$\left\{ \begin{array}{l} 0 - 1103 - 1299 \\ 0 - 304 - 586 - 756 \end{array} \right.$
34228 (w)	0 - 385				
		35224 (w)	0 - 689 × 2		
34347 (m)	0 - 504				
		35311 (w)	0 - 171 - 1299	36297 (w)	$\left\{ \begin{array}{l} 0 - 1161 - 1299 \\ 0 - 1228 \times 2 \end{array} \right.$
34429 (m)	0 - 586				
		35379 (w)	0 - 304 - 1228		
34532 (s)	0 - 689			36313 (w)	$\left\{ \begin{array}{l} 0 - 171 - 1002 - 1299 \\ 0 - 171 - 689 - 804 \\ \quad \quad \quad \times 2 \end{array} \right.$
		35450 (m)	0 - 804 × 2		
34599 (s)	0 - 756			36445 (w)	0 - 1299 × 2
		35511 (w)	0 - 504 - 1161	36526 (w)	$\left\{ \begin{array}{l} 0 - 385 - 1002 - 1299 \\ 0 - 171 - 243 - 756 \\ \quad \quad \quad \times 3 \end{array} \right.$
34647 (vs)	0 - 804			36652 (w)	0 - 756 × 2 - 1299
		35646 (w)	0 - 504 - 1299	36744 (w)	0 - 304 - 1299 × 2
34700 (w)	0 - 171 - 689				
		35733 (w)	0 - 856 - 1299	36798 (w)	$\left\{ \begin{array}{l} 0 - 243 - 304 - 804 \\ \quad \quad \quad \times 3 \end{array} \right.$
		35791 (w)	0 - 385 - 756 - 804		
		35870 (w)	0 - 804 - 1228	36908 (w)	$\left\{ \begin{array}{l} 0 - 171 - 385 - 804 \\ \quad \quad \quad \times 3 \end{array} \right.$

TABLE II

 Absorption bands of *p*-dimethoxybenzene in the liquid and solid states

Liquid at 60°C		Crystal at 32°C		Solid at -180°C	
Wave No. cm ⁻¹	Separation cm ⁻¹	Wave No. cm ⁻¹	Assignment	Wave No. cm ⁻¹	Assignment
33309 (s, vb)	985	32852 (s, b)	0,0	32844 (s)	0,0
		33345 (m, b)	0+493	33319 (m)	0+475
34294 (s, vb)		33624 (s, b)	0+772		
		34119 (s, b)	0+1267	33624 (s)	0+780
		34395 (m, b)	0+772×2	34105 (s)	0+1261
		34893 (m, b)	0+772+1267	34407 (m)	0+780×2
		35387 (w)	0+1267×2	34579 (m)	0+475+1261
		35665 (w)	0+493+772×3		
				34881 (m)	0+780+1261
				35362 (w)	0+1261×2
				35665 (w)	0+780×2+1261
				36149 (w)	0+780+1261×2

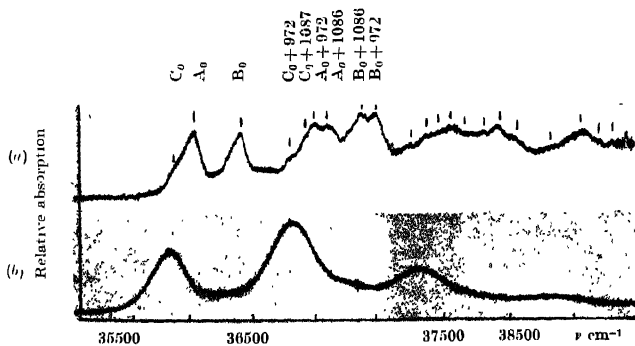

 Fig.2. Microphotometric records of ultraviolet absorption spectra of *m*-dichlorobenzene
 (a) Solid at -180°C (b) Liquid at 32°C

TABLE III

Absorption bands of *m*-dichlorobenzene in the liquid and solid states

Liquid at 32°C		Solid at -180°C	
Wave No. cm ⁻¹	Assignment	Wave No. cm ⁻¹	Assignment
35826 (s, b)	0,0	35853 (m)	
36829 (s, b)	0 + 1003	36022 (s)	
37830 (m, b)	0 + 1003 × 2	36418 (s)	
38838 (w, b)	0 + 1003 × 3	36825 (w)	C ₀ + 972
		36939 (m)	C ₀ + 1086
		36994 (s)	A ₀ + 972
		37108 (s)	A ₀ + 1086
		37390 (s)	B ₀ + 972
		37504 (s)	B ₀ + 1086
		37796 (w)	C ₀ + 972 × 2
		37910 (w)	C ₀ + 972 + 1086
		37968 (w)	A ₀ + 972 × 2
		38080 (m)	A ₀ + 972 + 1086
		38192 (w)	A ₀ + 1086 × 2
		38361 (w)	B ₀ + 972 × 2
		38479 (m)	B ₀ + 972 + 1086
		38590 (w)	B ₀ + 1086 × 2
		38883* (m)	C ₀ + 972 × 2 + 1086
		39050 (m)	A ₀ + 972 × 2 + 1086
		39165 (w)	A ₀ + 972 + 1086 × 2
		39280 (w)	A ₀ + 1086 × 3

TABLE IV

 Absorption bands of *m*-bromotoluene in the vapour state at 55°C

Wave No. cm ⁻¹	Assignment	Wave No. cm ⁻¹	Assignment
36356 (m)	0—170	37886 (w)	$\left\{ \begin{array}{l} 0+1360 \\ 0+303+461+601 \end{array} \right.$
36526 (vs)	0,0	37900 (w)	0+601+834
36829 (w)	0+303	38200 (w)	0+834×2
36987 (m)	0+461	38317 (w)	0+834+966
37127 (w)	0+601	38420 (w)	0+461+601+834
37360 (s)	0+834	38458 (m)	0+966×2
37492 (vs)	0+966	38553 (w)	0+461+601+966
37730 (m)	0+1204	38658 (w)	0+461+834×2
		38703 (w)	0+966+1204
		38850 (w)	0+966+1360

TABLE V

 Absorption bands of *m*-bromotoluene in the liquid and solid states

Liquid at 32°C		Solid at -180°C		
Wave No. cm ⁻¹	Assignment	Wave No. cm ⁻¹	Designation	Assignment
36197 (s, vb)	0, 0	36136 (w)	C ₀	
37223 (s, v)	0+1026	36570 (s)	B ₀	
38247 (m, vb)	0+1026×2	37004 (vs)	A ₀	
		37122 (w)	C ₁	C ₀ +988
		37554 (s)	B ₁	B ₀ +988
		37992 (vs)	A ₁	A ₀ +988
		38112 (w)	C ₂	C ₀ +988×2
		38538 (w)	B ₂	B ₀ +988×2
		38982 (s)	A ₂	A ₀ +988×2

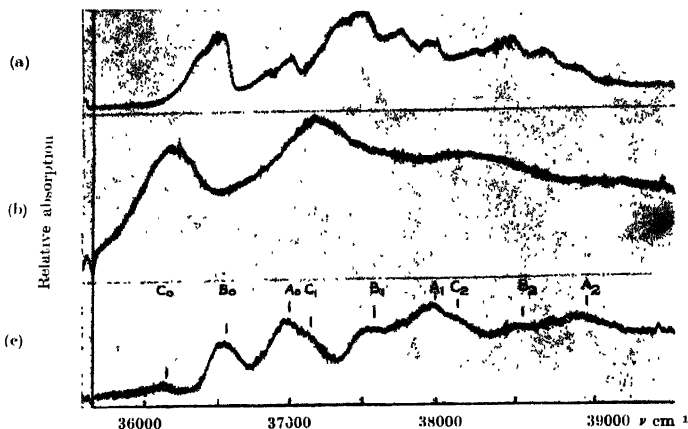


Fig. 8. Microphotometric records of the ultraviolet absorption spectra of *m*-bromotoluene

DISCUSSION

Para-dimethoxybenzene :

The absorption spectrum of *p*-dimethoxybenzene in the vapour state was reported earlier by Sreeramamurty (1950). As the data were not available the spectrum due to the vapour state was reinvestigated. A probable assignment has been made, the 0,0 band being assumed to be at 33843 cm^{-1} . The ground state vibration frequencies 201 and 271 cm^{-1} derived from the bands on the longer wavelength side of the 0,0 band agree with the Raman frequencies of the molecule (Magat, 1936). The bands displaced by 54 and 108 cm^{-1} from the 0,0 band towards longer wavelengths may be due to $v \rightarrow v$ transitions. The other bands show progressions of excited state frequencies $171, 243, 304, 385, 504, 586, 689, 756, 804, 1002, 1103, 1161, 1228$ and 1299 cm^{-1} respectively. The corresponding probable ground state frequencies observed in the Raman spectrum are $201, 270, 371, 403, 516, 635, 705, 791, 818, 1030, 1165, 1181, 1261$ and 1310 cm^{-1} respectively. The upper state vibration frequency 1297 cm^{-1} observed by Sreeramamurty, as mentioned by Suryanarayana and Rao (1956), agrees well with the frequency 1299 cm^{-1} observed in the present investigation. The upper state fundamental frequency 1297 cm^{-1} was accounted for by Sreeramamurty as due to CH_3 bending vibration—a symmetric vibration outside the phenyl ring and was also found in the spectra of anisole and other substituted anisoles. This assignment is probably not acceptable because in the case of *p*-dichlorobenzene also, an excited state frequency 1255 cm^{-1} is observed (Sponer, 1942; Swamy, 1953a). On the other hand, the mode ν_{13} of benzene ring in the ground state

has a frequency 1478 cm^{-1} (Herzberg, 1946) and in the excited state this may be lowered to a value between 1250 and 1300 cm^{-1} .

The spectrum due to the liquid state gives two very broad bands with their centres separated by a distance of 985 cm^{-1} and the 0,0 band is assumed to be at 33309 cm^{-1} . The 0,0 band is thus found to shift by 534 cm^{-1} towards longer wavelengths on liquefaction of vapour. In the case of *p*-xylene and *p*-dichlorobenzene (Swamy, 1952, 1953a) the bands are sharper. The shift of the 0,0 band in the present case is larger than in the case of *p*-xylene and *p*-dichlorobenzene. Thus the influence of intermolecular field is larger in the present case. The molecules in this case may execute angular oscillation and the intermolecular field acting on the molecules may fluctuate more widely than in the case of *p*-xylene and *p*-dichlorobenzene—resulting in larger broadening of electronic energy levels. Hence the intense bands appear as broad bands in the present case, and the feeble bands are not resolved.

In the solid state at room temperature, the broad bands become a little sharper so that eight sharper bands are observed. The strongest band at 32852 cm^{-1} has been taken as the 0,0 band. The 0,0 band thus shifts by 457 cm^{-1} further towards longer wavelengths probably due to the formation of virtual bonds through strongly associated neighbouring molecules and thus lowers the excited electronic energy state. Sharpening of the bands may be due to cessation of lateral motion of the molecules. The excited state frequencies observed in the case of the crystal are 493 , 772 and 1267 cm^{-1} . The frequency 1267 cm^{-1} may correspond in the excited state to the upper state fundamental frequency 1299 cm^{-1} for the vapour.

When the solid is cooled to -180°C the bands become still sharper and ten sharp bands are observed. The position of the 0,0 band remains unchanged with respect to that of 0,0 band of the solid state at room temperature as observed also in the case of *p*-dichlorobenzene. The excited state frequencies 475 , 780 and 1261 cm^{-1} are given by the bands due to the crystal at -180°C . These do not change much with the lowering of the temperature of the crystal. It is concluded that the formation of virtual bonds through association of neighbouring molecules is more or less complete in the solid state at room temperature and therefore no further shift of the 0,0 band takes place with lowering of temperature. The amplitude of angular oscillation of the molecules in the lattice diminishes with lowering of temperature and the fluctuation of the intermolecular field diminishes. Consequently, the bands become sharper at low temperatures.

m-Dichlorobenzene.

The spectrogram published by Spomer (1942) for the absorption spectrum of *m*-dichlorobenzene in the vapour state shows that the 0,0 band is at 36186 cm^{-1} . There are also other prominent bands at 36564 , 37147 , 37276 , 37290 and 38107 cm^{-1} which can be assigned as $0+378$, $0+960$, $0+1090$, $0+1104$ and

S. K. Sen

$0 + 960 \times 2 \text{ cm}^{-1}$. These correspond to the Raman lines at 398, 1000, 1070 and 1126 cm^{-1} respectively.

The spectrum due to the liquid state gives four broad bands and the 0,0 band is observed at 35826 cm^{-1} . The frequency difference between the succeeding bands is 1003 cm^{-1} . The 0,0 band thus shifts by 360 cm^{-1} towards longer wavelengths on liquefaction of vapour. The same shift is observed in the case of *o*-dichlorobenzene (Swamy, 1953a) also.

The spectrum due to the solid state at -180°C appears to be quite different from that due to the liquid. The first strong band due to the liquid is replaced by two intense bands and a weaker band on the longer wavelength side when the liquid is solidified and cooled to -180°C . The results can be interpreted only on the assumption that the excited state electronic energy level is split up into three components as in the case of *o*-dichlorobenzene (Swamy, 1953a). The splitting may occur due to asymmetric distribution of dipoles around each molecule in the lattice. In the case of *o*-dichlorobenzene, the principal band is accompanied by two weaker components whereas in the case of the meta compound two strong bands are accompanied by a weaker band. Thus the difference in position of the substituent halogen atoms produces a difference in the relative intensities of the components. It is concluded that splitting depends not only on the nature and position of substituents but also on the presence or absence of permanent electric moment, as no such splitting was observed in the case of *p*-dichlorobenzene (Swamy, 1953a).

m-Bromotoluene :

From Table IV we find that the absorption spectrum of *m*-bromotoluene in the vapour state shows the 0,0 band at 36526 cm^{-1} . The ground state vibration frequency 170 cm^{-1} corresponds to a Raman frequency (Magat, 1936). The bands show progression of excited state frequencies 303, 461, 601, 834, 966 and 1204 cm^{-1} . The corresponding ground state frequencies may be 378, 518, 667, 915, 990 and 1365 cm^{-1} respectively.

The spectrum due to the liquid state gives three broad bands with the 0,0 band at 36197 cm^{-1} and the frequency difference between the succeeding bands is 1026 cm^{-1} . The 0,0 band thus shifts by 329 cm^{-1} towards longer wavelengths. In the case of *o*-bromotoluene the corresponding shift of the 0,0 band is 404 cm^{-1} (Swamy, 1953b).

The spectrum due to the solid state at low temperatures exhibits altogether nine bands, each of the three bands due to the liquid state being replaced by three bands. The first band at 36136 cm^{-1} is very weak and the next one at 36570 cm^{-1} is stronger and the third one at 37004 cm^{-1} is still stronger. So it appears that in this case also splitting of the energy level takes place and assignment of the bands has been made accordingly. As the relative intensities of the

three components into which each band is split up depend on the relative positions of the substituents it appears that the splitting is due to formation of some actual bonds between neighbouring molecules and not due to general distribution of dipoles around each molecule.

A comparison of the results obtained in this investigation in the case of the meta compounds and also for the ortho compounds reported earlier by Swamy (1953a, 1953b) with those for other disubstituted benzenes not containing halogen atom show that in the case of the polar molecule containing halogen atoms, some fundamental change takes place in the excited electronic state at low temperatures. This change is different from Davydov splitting because in the latter case the effect depends only on the distribution of electric charges around a molecule and not on the nature of the substituent atom.

ACKNOWLEDGMENT

The author is indebted to Professor S. C. Sirkar, D.Sc., F.N.I. for his kind interest and constant guidance throughout the progress of the work.

REFERENCES

- Herzberg, G., 1946, *Infra red and Raman spectra of Polyatomic molecules*, **118**, 364.
Magat, M., 1936, Numerical data on Raman Effect.
Sen, S. K., 1955, *Ind. J. Phys.*, **29**, 561.
Sen, S. K., 1956b, *Ind. J. Phys.*, **30**, 553.
Sponor, H., 1942, *Rev. Mod. Phys.*, **14**, 224, 229.
Sreeramamurty, K., 1950, D.Sc. Thesis submitted to the Andhra University.
Suryanarayana, V., and Rao, V. R., 1956, *Ind. J. Phys.*, **30**, 126.
Swamy, H. N., 1952, *Ind. J. Phys.*, **26**, 233.
" 1953a, *Ind. J. Phys.*, **27**, 55.
" 1953b, *Ind. J. Phys.*, **27**, 119.

VARIATION IN LATTICE CONSTANT IN THIN FILMS OF GOLD

S. N. CHATTERJEE

INSTITUTE OF NUCLEAR PHYSICS, CALCUTTA-9.

(Received for publication, August 27, (1956))

Plate II

ABSTRACT. Lattice constants of gold for films of different thicknesses ($3-120\text{\AA}$) were determined by the electron diffraction technique. It was found that for thin films of gold ($1-10\text{\AA}$) the lattice constant increases by about 5% over the value of the constant for films ($40-120\text{\AA}$) thick.

INTRODUCTION

Lennard Jones (1930) predicted theoretically that the lattice constant for non-ionic crystals should increase with the decrease of crystal size. For crystals comprising 125 and 300 atoms respectively, this constant was expected to be 7 and 5 per cent greater than that for a massive crystal, on theoretical grounds.

Finch and Fordham (1936) obtained, in case of $3-10\text{\AA}$ thin nickel films, a deviation from the usual lattice constant which varied from 0.2 to 1.0 per cent for different reflections. Dankov and Shisakov (1939) reported an increase of the lattice parameter for small crystals in case of $\alpha\text{-Fe}$. Boswell (1951) found that for crystal sizes less than 100\AA , the lattice constants of the alkali halides were less than the X-ray values by an amount dependent on the crystal size. He also obtained a similar decrease in the lattice constant for thin gold, silver and bismuth films. Lafourcade (1953) obtained a decrease in the lattice parameter for thin films ($1-10\text{\AA}$) of gold. Recently Pinsker revealed an increase of the lattice parameter (1.2 to 1.5 per cent) taking place during condensation of the copper on a hot face of NaCl. There is, therefore, differences of opinion about the nature of the change of lattice constant with crystal size. The present work was under taken with the purpose of examining this point critically with the help of electron diffraction technique.

EXPERIMENTAL

(a) *Electron diffraction arrangement :*

The diffraction photographs reproduced below were taken with the electron microscope assembled at the Institute of Nuclear Physics (Das Gupta *et al.* 1948).

Figure 1a gives the sectional diagram of the electron microscope together with the diffraction specimen holder. The electron-optical ray diagram for diffraction

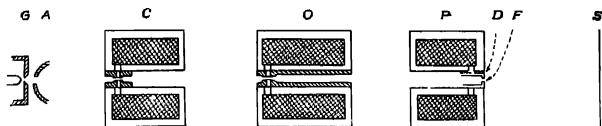


Fig. 1a. Sectional diagram of the electron microscope.

is shown in figure 1b. In order to obtain large diffraction angle (greater number of rings) and high resolution, the diffraction specimen contained in a special adapter was placed in the position *D* after the projector lens. As usual the condenser lens formed an image of the cross-over *X* from the electron gun. The position of

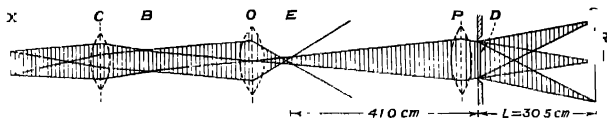


Fig. 1b. Electron optical ray path for diffraction.

this image can be varied by varying the condenser current. The smallest cross section *B* of the beam from the condenser lens is focussed by the objective in front of the projector lens at *E*. This is again focussed by the projector on the final screen in order to obtain sharp diffraction rings. By varying the condenser and the objective currents, the position and the size of the electronic spot at *E* could be altered. As will be shown later this controls the resolution of the diffraction photographs.

(b) Resolution of the electron diffraction arrangement.

By the resolving power of a diffraction arrangement is meant, up to which difference Δd between two grating constants d and $d + \Delta d$, the diffraction rings formed can still be differentiated. This is measured by the expression $d/\Delta d$.

From the equation $2d \sin \theta = \lambda$ and $2 \sin \theta \approx 2\theta = \frac{R}{L}$

$$\text{one obtains} \quad \frac{d}{\Delta d} = \frac{L\lambda}{d\Delta R} = \frac{L\lambda}{d\delta} \quad \dots (1)$$

where $\Delta R \approx \delta$ = diameter of the central spot. (Figure 2).

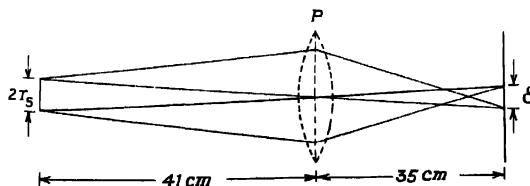


Fig. 2. Estimation of the spot size.

It will be seen from figure 2, that in the present case, if r_s be the radius of the effective source in front of the projector lens P , then the diameter of the spot on the photographic plate,

$$\delta = \frac{35}{41} \cdot 2r_s = 1.7r_s \quad (2)$$

δ was estimated by calculation. From the previously measured diameter of the electron cross-over near the anode 300μ (De, 1950), and the calculated values of the focal lengths of the condenser and objective lenses for different currents, $2r_s$ was calculated to be 57μ . Hence $\delta = 48.5\mu$.

Now from equation (1), with $L = 30.48$ cm, $\lambda = .06 \text{ \AA}$ for 40 Kv. and $d = 1 \text{ \AA}$,

we get for the resolving power $\frac{d}{\Delta d} = 380$.

The current in the lens coils is supplied by an electronically regulating unit, and the high tension is stabilised to a very high degree. The degrees of stabilisation were measured previously (De, 1951) and were as follows :

Power supply	Fluctuations
Condenser lens	$\Delta I_c/I_c = 1.0 \times 10^{-3}$
Objective lens	$\Delta I_o/I_o = 5.5 \times 10^{-5}$
Projector lens	$\Delta I_p/I_p = 1.3 \times 10^{-4}$
High tension	$\Delta V/V = 1.0 \times 10^{-4}$

These fluctuations in lens currents and high tension are too small to affect the resolving power calculated above.

(c) *Films for electron diffraction studies :*

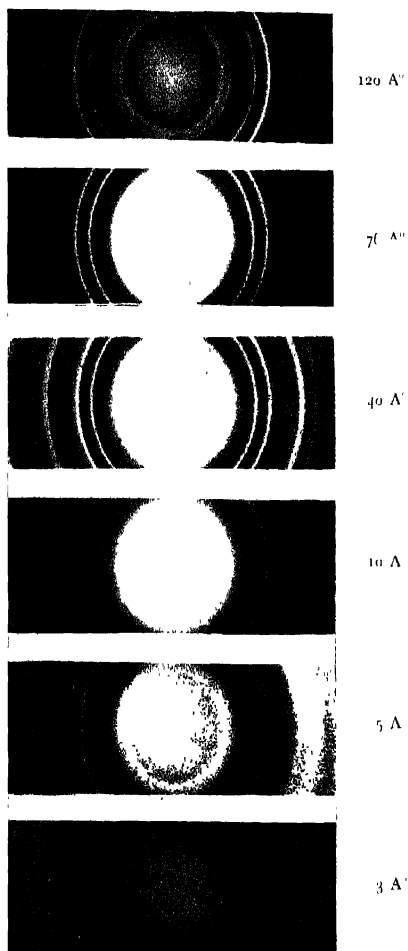
The metallic films used in the diffraction study varied in thickness from 3 to 120 \AA . Such films were deposited on a substrate of collodion (thickness $50\text{--}100 \text{ \AA}$) by evaporation in vacuum. The thickness t of the deposited metal film was estimated from the relation,

$$t = \frac{3}{4} \frac{1}{4\pi\rho} \times \frac{Mh}{r^2} \quad \dots \quad (3)$$

where ρ and M were the density and mass of evaporated metal, r and h the distance and height of the metal from the film support. With $\rho = 19.3$ for gold this reduces to

$$t = 310 \frac{Mh}{r^2} \text{ \AA} \quad (4)$$

where M is expressed in milligrams. The formula (4) was deduced on the basis of uniform evaporation in all directions. To test the validity of the formula,



Diffraction photographs of gold films of different thickness

the apparatus was calibrated by measuring the weight of the deposited metal for thick films with the help of a micro-balance. A graphical method for rapid estimation of film thickness for different metals and evaporating conditions have been described by Nandi (1954).

(d) *Electron diffraction photographs for thin films.*

Gold film of different thickness deposited on collodion films were interposed in the path of the electron beam and the photographs were taken. The constant of the apparatus $L\lambda$ was determined from the measured values of the radii r for diffraction rings for a film thickness (40-76 Å) and the standard values of the lattice constant of gold (Hall, 1953).

The ring diameters were measured with the help of a comparator reading in microns. For each diffraction photographs a number of clearly distinguishable sharp rings were chosen for the measurement of diameters. The lattice constant was calculated separately for each ring and the mean of them was taken to correspond to the particular film thickness.

Microphotometer traces of the diffraction photographs were also obtained with an approximate 7 fold magnification. Each negative was scanned diametrically and the distances between the peaks in the traces gave the ring diameters on the magnified scale. From such microphotometer traces values of the lattice constants could be obtained.

RESULTS

Plate II shows the diffraction photographs reproduced in the order of increasing film thickness. The microphotometer traces are shown in figure 3. The length R represents the radius of 1.11 ring in each case.

Table I gives the film thickness as deduced from equation (4) in column 1, column 2 and 3 contain the indices for different rings and the measured diameters in millimeters. The values of the lattice constants, as deduced from these measurements are given in column 4. The mean values of a are contained in the last column of Table I.

The table shows a marked increase in the lattice constant for very thin films of gold (≤ 10 Å). No gradual change in lattice constant with film thickness could be concluded for insufficiency of data. For very thin films (≤ 10 Å) it is found $\Delta a = +0.203$ Å (approximately +5%). This increase is also confirmed directly by the micro-photometric records.

This positive deviation is in qualitative agreement with the theoretical prediction of Lennard Jones (1930). The general features of the diffuseness of the ring, the increase of the continuous background and the changes in the relative

TABLE I

Measured values of lattice constants with film thickness.

Thickness in (\AA)	Ring index (h k l)	Diameter (mm)	a in (\AA)	Mean a (\AA)
3	111	15.137	4.186	4.186
	111	15.073	4.195	
5	113	28.960	3.180	4.186
	220	24.638	4.183	
	111	15.160	4.171	
10	200	17.380	4.207	4.189
	220	24.130	4.181	
	113	29.149	4.198	
	111	15.818	3.999	
	200	18.379	3.995	
40	220	25.941	3.986	3.987
	113	30.497	3.977	
	331	39.977	3.980	
	420	40.912	3.985	
	111	15.839	3.999	
	200	18.268	4.009	
76	220	25.876	3.996	4.001
	113	30.260	4.007	
	331	39.881	3.996	
	420	40.744	4.001	
	111	15.905	3.980	
	200	18.327	3.991	
	220	25.978	3.981	
120	113	30.379	3.994	3.984
	331	40.045	3.981	
	420	41.020	3.987	
	422	45.029	3.977	

intensities of 200 and 111 rings with the decrease of film thickness are in agreement with the observations of Lafourcade (1953).

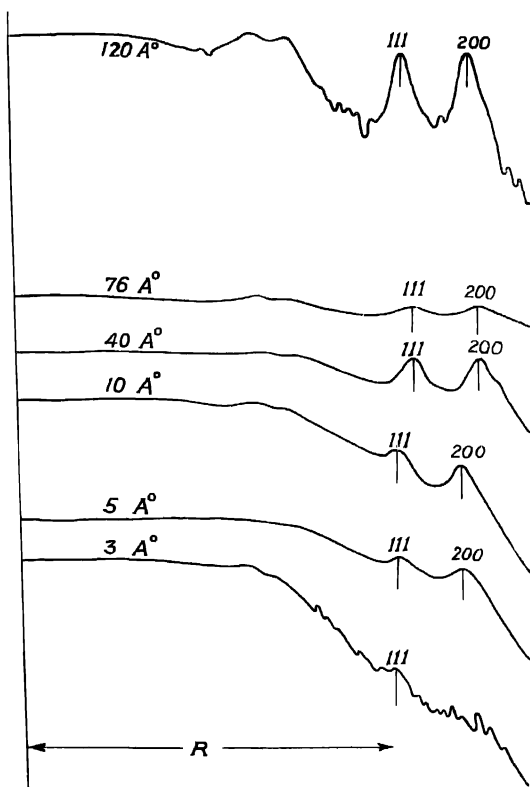


Fig. 3. Microphotometric analysis of diffraction figures.

CONCLUSION

The present investigation reveals that for thin films of gold ($1-10 \text{ \AA}$), the lattice constant increases by about 5% over the value of the constant for films ($40-120 \text{ \AA}$) thick.

ACKNOWLEDGMENTS

The author wishes to express his indebtedness to Prof. N. N. Das Gupta for encouragement and advice all through the work, to Dr. K. Das Gupta for

help in the microphotometer analysis and to Sri M. L. De for design of the diffraction adapter, and for valuable discussions. The author is also indebted to the Ministry of Education, Govt. of India, for financial assistance.

REFERENCES

- Boswell, F. W. C. 1951, *Proc. Phys. Soc. (A)*, **64**, 465.
Dankov, P. D and Shusakov, N. A. 1939, *C. R. Acad. Sci. U.S.S.R.*, **24**.
Das Gupta, N. N *et al*, 1948, *Ind. Jour. Phys.* **22**, 497-513.
De, M. L., 1950, *Ind. Jour. Phys.* **24**, 303-308.
De, M.L., 1951, *Unpublished*
Finch and Fordham, 1936, *Proc Phys. Soc.*, **48**, 85-94.
Hall, C. E., 1953, *Introduction to Electron Microscopy*, McGraw Hill, Book Co., New York.
Lafoureaud, L. and Larroue, P , 1953, *Ann. Fac. Sci.*, **17**, 143-228.
Lonnard Jones, J. E., 1930, *Z. Kristallogr.*, **75**, 215.
Nandy, K. P. 1954, *Rev. Sci. Inst.*, **25**, 523-524.
Pinsker, Z. G., 1953, *Electron Diffraction*, Chap 9, London.

EPITAXIAL GROWTH OF THIN EVAPORATED METALLIC FILMS ON CLEAVAGE SURFACES OF ALKALI-HALIDES AND OTHER CRYSTALS.*

K. R. DIXIT

GUJARAT COLLEGE, AHMEDABAD.

(Received for publication December 24, 1956)

ABSTRACT. The paper gives a theory of epitaxial growth of evaporated metal atoms. It is shown that the observed crystal structure and the orientation will be the combined result of the forces of temperature orientation and the attractive forces of the van der Waals' type.

The term epitaxy was introduced by Royer to denote the phenomenon of the oriented growth of one crystal upon another. Various attempts have been made to explain the occurrence of epitaxy. All these are based on the concept of a geometrical fitting between the lattices of the substrate and the overgrowth. Royer (1928) put forward three rules for epitaxial growth. According to him oriented growth occurs only when it involves the parallelism of two lattice planes, with almost identical spacings. The percentage misfit between the spacings of the substrate and the deposit is regarded as the main factor which governs the epitaxial growth. Bruck attempted to explain the results by assuming that the orientation of the deposit is such as to make the sum of the distances of the substrate ions from the deposit atoms a minimum when considered only over a unit cell. This restriction to unit cell appears to be arbitrary and further the effect of both the positive and the negative ions present has to be considered. This was done by Engel (1952). According to Engel, the orientation depends upon the possibility of suitable ionisation and the degree of misfit. Menzer (1938) also put forward a theory which depends upon the degree of misfit. The degree of misfit is sometimes calculated with the length of a unit cell, and sometimes even with the length of two and three cells. The theory put forward by Frank and van der Merwe (1949) requires certain critical misfits to produce orientations.

All the theories of epitaxial growth put forward so far either assume that a small misfit is an essential condition for the occurrence of an oriented overgrowth or they are based on the concept of basal plane pseudo-morphism. According to Pashley (1956) the present experimental evidence does not completely support any of these assumptions. The degree of misfit, however, does appear to have some significance. In the light of this an attempt is made here to put forward a theory of oriented growth on oriented substrate. This theory is essentially an

*(Presidential address, read before the Indian Physical Society's annual meeting, Calcutta, January 1957).

extension of the theory put forward (Dixit, 1933) for oriented growth on amorphous surfaces.

Thin films were then prepared by evaporating metal atoms on flat amorphous surfaces. The electron diffraction study of these films showed fibrous orientations, which in their turn showed a characteristic dependence on the temperature of the substrate. This was explained by assuming that the atoms in such a layer behave like a two dimensional gas and obey an equation similar to the van der Waals' equation. We have in this case

$$\pi A = RT$$

where π is the two dimensional pressure (surface tension)

A is the area occupied by the atom on the substrate

R is the gas constant

T is the absolute temperature

In the present case metal atoms are also evaporated on flat surfaces. But the flat surfaces are now the cleavage planes of crystals.

This introduces a significant difference in our considerations. An amorphous flat surface only serves as a reasonably flat support for the two dimensional gas and there is no interaction between the atoms of the substrate and the atoms in the gas. In the present case the cleavage surface not only serves as a flat support, but there will also be a force of attraction between the ions of the substrate and the deposited neutral metal atoms. As before, we shall consider the formation of the first atomic layer only. The upper layers will be assumed to have the same structure. The additional force of attraction, which now manifests itself between the ions of the substrate and the deposited neutral metal atoms can be reasonably assumed to be of the polarisation or of van der Waals' type. This force will introduce an additional term in the equation already given which will depend on the van der Waals' energy and the area occupied by the atom. The equation thus becomes

$$\pi A + AC/r^6 = RT$$

where r is the distance between the two atoms, one of the substrate and the other of the deposit,

or

$$r^2 = r_1^2 + r_2^2 + l^2$$

where r_1 is the atomic distance for the substrate,

r_2 is the atomic distance for the deposit,

and l is the distance between the two planes, namely, the substrate plane and the deposit plane.

In the above equation if the term AC/r^6 is absent we get the same relation as before, showing orientation as a function of the temperature. The effect of this term is to effectively reduce the term RT on the right hand side, i.e. the

temperature at which any particular orientation occurs in the presence of the attractive force of the substrate is less than the temperature at which the same orientation would occur in the absence of the attractive force, or the epitaxial temperature will be less than the amorphous orientation temperature. Further even here as before

$$A_{111} < A_{100} < A_{110}$$

and therefore

$$T_{111} < T_{100} < T_{110}.$$

Both these conclusions appear to agree with experimental observations. This will be seen if we compare the behaviour of evaporated silver atoms on amorphous substrates (Dixit, 1933) on calcite (Rudigar, 1937) and on alkali halides (Shirai, 1943). This convinces us of the reasonableness of our modification and we can proceed further with the consideration of this equation. We shall consider how the modifying term ACr^{-6} could be written.

$$\begin{aligned} ACr^{-6} &= A' (r_1^2 + r_2^2 + l^2)^{-3} \\ &= A' r_1^{-6} \left\{ \frac{r_2^2 + r_1^2}{r_1^2} + 2 + \frac{l^2}{r_1^2} \right\}^{-3} \\ &= A' r_1^{-6} \left\{ \left(\frac{r_2 + r_1}{r_1} \right) \left(\frac{r_2 - r_1}{r_1} + 2 \right) + 2 + \frac{l^2}{r_1^2} \right\}^{-3} \\ &= A' r_1^{-6} \left\{ \text{misfit}(\text{misfit} + 2) + 2 + \frac{l^2}{r_1^2} \right\}^{-3} \end{aligned}$$

l^2/r_1^2 will be of the order of unity. Introducing A_1 and A_2 which are the areas occupied by the atoms in the substrate and deposit respectively. These areas will be proportional to r_1^2 and r_2^2 , and we get

$$A_2/A_1 = r_2^2/r_1^2 = \text{misfit}(\text{misfit} + 2) + 1.$$

Now writing $\text{misfit}(\text{misfit} + 2) = x$, we get

$$ACr^{-6} \sim \frac{CA_1^{-2}}{27} \left(1 + \frac{x}{3} \right)^{-3} (1+x).$$

If the misfit is small, $x = 2 \text{ misfit}$, which is also small and to a first approximation we get that ACr^{-6} will depend on $A_1^{-2}(1+2 \text{ misfit})$ if we neglect $x/3$ or $1/3^2(1-4/3 \text{ misfit}^2)$ if we neglect powers of x higher than the first.

This indicates that the effect of the additional force of attraction can be expressed in terms of the area occupied by an atom in the cleavage plane of the sub-

strate or its lattice constant and orientation. In addition, it depends on the misfit. This also appears to agree with the general experimental observations.

In deriving these relations we have not made any arbitrary assumptions about the misfit or the extent of the misfit or about basal plane pseudo-morphism. All the experimental observations appear to follow as a natural consequence of the two dimensional behaviour of a van der Waals' gas, subjected to the polarisation forces in addition to the forces of a two dimensional pressure. Most of the experimental observations on the epitaxial growth of evaporated metals on cleavage surfaces, appear to agree at least qualitatively with this theory.

REFERENCES

- Bruck, L., 1936, *Ann. Phys.* **26**, 233.
 Dixit, K. R., 1933, *Phil. Mag.*, **16**, 1049.
 Engel, O. G., 1952, *J. Chem. Phys.*, **20**, 1174.
 " 1953, *J. Res. Nat. Bur. Stand. Wash.*, **50**, 249.
 Frank F. C. and van der Merwe, J. H. 1949, *Proc. Roy. Soc. (London)* **198**, 205 and 216;
 and **200**, 125
 Menzer, G., 1938, *Naturwissenschaften* **26**, 385.
 " 1938, *Z. Kristallogr.*, **99**, 378 and 410
 Pashley, D. W., 1956 *Advances in Physics* **5**, 173.
 Royer, L., 1928, *Bull. Soc. Franc. Mineral.*, **51**, 7.
 " 1932, *C. R. (Paris)* **194**, 1088.
 " 1935, *Ann. Phys.* **23**, 16.
 " 1937, *C. R. (Paris)* **205**, 1418.
 " 1948, *C. R. (Paris)* **226**, 95 and 262.
 " 1954, *Bull. Soc. Franc. Mineral.*, **77**, 1004.
 Rudiger, O., 1937, *Ann. Phys.* **30**, 505.
 Shirai, S., 1943, *Proc. Phys. Math. Soc. Japan*, **25**, 633.

R-C NETWORK ANALOGUE

A. K. CHOUDHURY AND B. R. NAG

INSTITUTE OF RADIOPHYSICS AND ELECTRONICS, CALCUTTA UNIVERSITY

(Received for publication, August 27, 1956)

ABSTRACT. An R-C analogue for obtaining the steady state and transient response of networks is described. The zeroes and poles of the network function are realised by a system of cascade feedback amplifiers, the input and feedback networks of the amplifiers being so arranged that the zeroes and poles of the transfer function of the system are identical with those of the network function. The root loci of a few basic networks for the feedback amplifiers have been studied. A method of solving polynomial equations using the analogue is also described.

INTRODUCTION

The location of zeroes and poles of a network function in the complex frequency plane determines completely the steady state and transient response of a network. The response of a network can, therefore, be determined by an analogue system realising the poles and zeroes of the network function in an equivalent complex frequency plane. In potential analogue method of network analysis or synthesis (Boothroyd, Cherry and Makar, 1949) the zeroes and poles of the network function, are realised by placing current sources and sinks in an electrolytic tank and the potential distribution in the tank gives the frequency response of the network.

In the present work, the zeroes and poles of the network function are realised by using feedback amplifiers. The feedback and input networks of the amplifier are composed of resistance and capacitance only. For the sake of convenience of adjustment of the location of zeroes and poles, a small number of zeroes and poles are realised at each stage. The complete network function is realised by putting a number of feedback amplifiers in cascade so that the transfer function of the whole system has poles and zeroes identical with those of the network function excepting a constant scaling factor in amplitude and frequency. Since the zeroes and poles of the R-C feedback and input networks become the zeroes and poles of the feedback amplifier transfer function, study has been made of the root-loci of a few basic R-C networks, which are used as feedback and input networks.

As an example of the above, the steady state response of third order Butterworth function has been measured using R-C feedback amplifiers.

A method of solving a polynomial using the R-C analogue is also described

1. INTERPRETATION OF THE NETWORK FUNCTION IN THE COMPLEX FREQUENCY PLANE

The network function $Z(P)$ of a physically realisable network can be written

$$Z(P) = H \cdot \frac{(P+P_1)(P+P_3)\dots\dots\dots N(P)}{(P+P_2)(P+P_4)\dots\dots\dots D(P)}$$

where P is the complex frequency and H is an arbitrary constant. P_2, P_4, \dots are the poles (natural modes) and P_1, P_3, P_5, \dots are zeroes (infinite loss points) of the network function. The steady state response of the network is obtained from the expression for $Z(P)$ when P is substituted by $j\omega$. The transient response will be given by the sum of terms of the form $A_2 e^{P_2 t}$ where A_2 is the residue of the function $Z(P)$ at the pole P_2 . The steady state and transient responses of the network are completely determined by the zero-pole locations and are uniquely related to each other.

For a physically realisable network, there are certain restrictions on the location of the zeroes and poles of $Z(P)$. If $Z(P)$ be the driving-point impedance function of a network, the zeroes and poles of $Z(P)$ must be on the left half of the complex frequency plane and $Z(P)$ must be positive real. If $Z(P)$ be the transfer function of the network, $Z(P)$ need not be positive real but none of the poles can be on the right half side of the complex frequency plane. There is no restriction, in general, on the zeroes excepting the upper limit of the order of numerator polynomial

2. TRANSFER FUNCTION OF A FEEDBACK AMPLIFIER

Transfer function of feed-back amplifier as shown in the figure 1 is

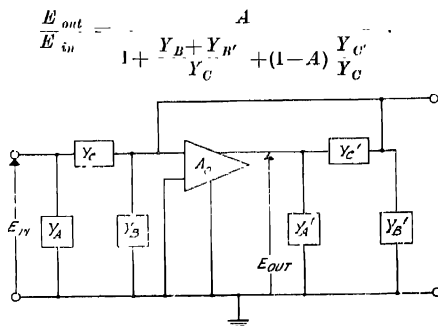


Fig. 1. Feedback amplifier.

is the open loop gain of the amplifier. Input and feedback networks are shown in the π form. For two-terminal networks $Y_B = Y_{B'} = 0$. For four-terminal networks also effect of Y_B and $Y_{B'}$ will, in general, be small when A is large except when $\frac{Y_B + Y_{B'}}{A}$ is comparable to Y_C . So, neglecting Y_B and $Y_{B'}$, the transfer function can be simplified to

$$\frac{E_{out}}{E_{in}} = \frac{A}{1 + (1-A) \frac{Y_C}{Y_C}}$$

If Y_{12} and Y_{12}' denotes the short circuit transfer admittances of the networks, then Y_C and Y_C' of the equivalent π are respectively equal to Y_{12} and Y_{12}' ; and the transfer function becomes in general

$$\frac{E_{out}}{E_{in}} = \frac{A}{1 + (1-A) \frac{Y_{12}'}{Y_{12}}}$$

which for large values of A simplifies to

$$\frac{E_{out}}{E_{in}} = -Y_{12}' \frac{1}{Y_{12}} \quad (1)$$

The zeroes of the transfer function are the zeroes of Y_{12} , and $\frac{1}{Y_{12}'}$ and the poles

are the poles of Y_{12} and Y_{12}' . It will be seen that if there be a pole of the network function on the real frequency axis, the value of the transfer function of the feedback amplifier should be infinite at that frequency. In practice, the transfer function will have a value equal to the gain of the amplifier under open loop condition, at that frequency. But this is of little consequence since in practice poles of a network due to inherent dissipation, will never be located on the real frequency axis.

R-C feedback and input networks are used to obtain the proper pole and zero location. The limitations on the short circuit transfer admittance function (Y_{12}) of R-C network have been discussed by Guillemin (1949). The results are stated here: Poles of Y_{12} must be simple and real negative, zeroes of Y_{12} can be real or complex. The degree of numerator polynomial of Y_{12} can be equal to or greater by one than the degree of the denominator.

So, using R-C network as the input network real negative poles and real or complex zeroes can be realised. Using the same network as the feedback network, real negative zeroes and real or complex poles can be realised. Also,

if n poles are to be realised using R-C network as the feedback network, there will be n or $(n-1)$ zeroes associated with n poles and hence the input network should be designed to cancel these zeroes.

3. INPUT AND FEEDBACK NETWORKS

(a) Network for a real pole :

The short circuit transfer admittance function Y_{12} of the network of figure 2 is given by $Y_{12} = \frac{x+\alpha}{R}$ where $x = PCR$ is the normalised value of frequency, normalised with respect to $1/CR$.

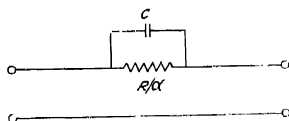


Fig. 2 A network for a real pole or zero. $Y_{12} = \frac{x+\alpha}{R}$, $x = PCR$

When this network is used as the feedback element and a resistance $\frac{R}{2}$ as the input element as shown in figure 3, the transfer function of the amplifier becomes

$$\frac{V_{out}}{V_{in}} = - \frac{v}{x+\alpha}$$

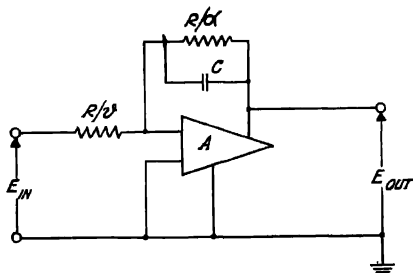


Fig. 3. Feed back amplifier for real pole. $\frac{E_{out}}{E_{in}} \approx \frac{v}{x+\alpha}$

Pole of the transfer function is at α and is real negative. Different values of α can be obtained by keeping C fixed and varying the resistance R/α and in fact this resistance can be calibrated to read directly α . However, exact position of

the pole for an amplifier having non-infinite gain will be slightly different since the exact expression for transfer function is given by

$$\frac{E_{out}}{E_{in}} = - \frac{A}{1-A} \frac{\frac{\nu}{x+\alpha} + \frac{\nu}{1-A}}{\frac{\nu}{x+\alpha} + \frac{\nu}{1-A}}$$

This deviation is very small for values of $A > 1000$.

(b) *Networks for a complex pole :*

(1) The short circuit transfer admittance of the network of figure 4 is given by

$$Y_{12} = \frac{\beta}{R} \frac{x^2 + \frac{1}{\beta}}{x + \frac{\alpha}{4\beta^2}} = \frac{N(x)}{D(x)}$$

where

$$x = PCR.$$

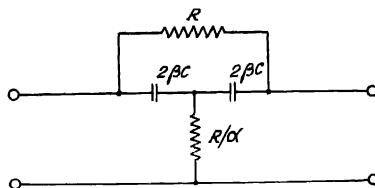


Fig. 4. Network (1) for complex poles or zeroes. $Y_{12} = \frac{\beta}{R} \frac{x^2 + \frac{1}{\beta}}{x + \frac{\alpha}{4\beta^2}}$.

With this network as the feedback element and a resistance R/β as the input element as shown in figure 5, the transfer function of the amplifier becomes [neglecting the effect of $Y_{B'}$ (cf. figure 1), and A , the finite value of the gain of the amplifier]

$$\frac{E_{out}}{E_{in}} = - \frac{x + \alpha'}{x^2 + \frac{1}{\beta} x + \frac{\alpha}{4\beta^2}} \quad \dots (2)$$

where

$$\alpha' = \frac{\alpha}{4\beta}.$$

This transfer function has a zero at α' , and a pair of poles at $\eta e^{\pm j\theta}$, where

$$\eta e^{\pm j\theta} = \frac{1}{2\beta} [-1 \pm j\sqrt{\alpha-1}].$$

Poles are conjugate complex when $\alpha > 1$. Modulus of the poles is $\eta = \frac{\sqrt{\alpha}}{2\beta}$ and also the arguments are $\theta = \pm \tan^{-1} \sqrt{\alpha-1}$.

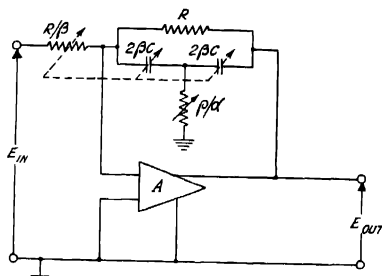


Fig. 5. Feedback amplifier for complex poles using network shown in Fig. 4.

$$\frac{E_{out}}{E_{in}} \sim - \frac{x + \alpha'}{x^2 + \frac{\alpha}{\beta} + \frac{\alpha}{4\beta^2}} ; \alpha' = \frac{\alpha}{A\beta}$$

The value of the argument of the poles depends only on α and hence by varying α alone argument θ can be set to any value, and θ can be read from a calibrated scale. Another scale calibrated in terms of $\sqrt{\alpha}$, will give the modulus of the roots when $\beta = 1$. Any modulus other than $\frac{\sqrt{\alpha}}{2}$ for any value of $\theta = \tan^{-1} \sqrt{\alpha-1}$ can be obtained by varying β , keeping α fixed. For any value of $\beta \neq 1$, modulus can be obtained multiplying the modulus dial reading by $1/\beta$, β being obtained from a calibrated dial.

When the effect of Y_B' and A , are taken into account, transfer function of the amplifier becomes [figure 5].

$$\begin{aligned} \frac{E_{out}}{E_{in}} &= - \frac{x + \frac{\alpha}{4\beta}}{\frac{1-A}{A} \left[\frac{1}{1-A} \left\{ x \left(1 + \frac{\alpha}{2\beta} \right) + \frac{\alpha}{4\beta} \right\} + (x + \eta e^{j\theta})(x + \eta e^{-j\theta}) \right]} \\ &= - \frac{x + \eta \frac{\sqrt{\alpha}}{2}}{\frac{1-A}{A} \left[x^2 + x \left\{ 2\eta \cos \theta + \frac{1}{1-A} \left(1 + \frac{\alpha}{2\beta} \right) \right\} + \eta^2 + \frac{\eta \sqrt{\alpha}}{2(1-A)} \right]} \end{aligned}$$

Modulus of the pole is then,

$$\rho' = \sqrt{\eta^2 + \frac{\eta\sqrt{\alpha}}{2(1-A)}} = \eta \left[1 + \frac{\sqrt{\alpha}}{2(1-A)\eta} \right]^{1/2}$$

and the argument $\theta' = \cos^{-1} \frac{\cos \theta}{\sqrt{1 + \frac{\sqrt{\alpha}}{2(1-A)\eta}}} - \frac{1 + \eta\sqrt{\alpha}}{2(1-A)\eta\sqrt{1 + \frac{\sqrt{\alpha}}{2(1-A)\eta}}}$

Thus with $A > 1000$, error in using the simplified expression (2) is very small, unless, η is very small. Large error will occur in using the simplified expression when η is small, of the order of $\frac{1}{A}$ or less.

(ii) Short circuit transfer admittance function of the network, shown in figure 6, is

$$Y_{12} = \frac{K}{R} \frac{x^3 + \frac{4}{K\beta}x^2 + \frac{4}{K^2\beta}x + \frac{\alpha}{K^3\beta}}{\left(x + \frac{\alpha}{4K}\right)\left(x + \frac{4}{K\beta}\right)}$$

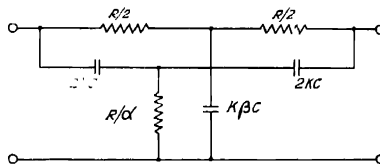


Fig. 6. Network (ii) for complex poles or zeroes.

$$Y_{12} = \frac{x^3 + \frac{4}{K\beta}x^2 + \frac{4}{K^2\beta}x + \frac{\alpha}{K^3\beta}}{\left(x + \frac{\alpha}{4K}\right)\left(x + \frac{4}{K\beta}\right)}$$

Using this as the feedback network with a resistance R/K as the input network as shown in figure 7, the transfer function of the amplifier becomes [using the simplified equation (1)].

$$\frac{E_{out}}{E_{in}} = - \frac{\left(x + \frac{\alpha}{4K}\right)\left(x + \frac{4}{K\beta}\right)}{x^3 + \frac{4}{K\beta}x^2 + \frac{4}{K^2\beta}x + \frac{\alpha}{K^3\beta}} \quad \dots (3)$$

There are two zeroes and three poles in the transfer function. Zeroes lie on the negative real axis. For $K = 1$, the position of the zeroes can be known by calibrating the R/α resistance and βC capacitance dial.

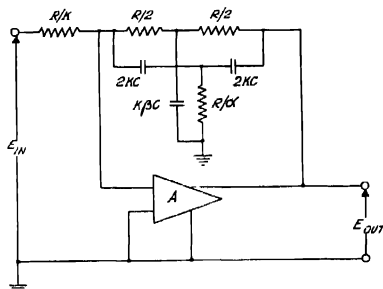


Fig. 7. Feedback amplifier for complex poles using network shown in Fig. 6.

$$\frac{E_{out}}{E_{in}} \approx - \frac{\left(x + \frac{\alpha}{4K}\right)\left(x + \frac{4}{K\beta}\right)}{x^3 + \frac{4}{K\beta}x^2 + \frac{4}{K^2\beta}x + \frac{\alpha}{K^4\beta}}$$

All the three poles may be real or one pole real negative and the other two conjugate complex. Applying Routh's criteria, when $\alpha\beta > 16$, real part of the complex roots of the denominator polynomial of Equ. (3) will be positive. So, using the network of figure 6, a pair of complex conjugate poles may be realised even in the right half of the complex frequency plane.

Let the real root of the denominator polynomial be $-a_0$ and the complex roots $-\xi \pm j\eta$. Modulus of the complex roots is $r = \sqrt{\eta^2 + \xi^2}$

Then

$$a_0 + 2\xi = \frac{4}{K\beta}$$

$$r^2 + 2a_0\xi = \frac{4}{K^2\beta}$$

$$a_0r^2 = \frac{\alpha}{\beta}$$

when $K = 1$, $a_0 + 2\xi = \frac{4}{\beta}$, $r^2 + 2a_0\xi = \frac{4}{\beta}$ and $a_0r^2 = \frac{\alpha}{\beta}$.

All the three roots will be real when $\xi > r$.

If $r = 1$ and $\alpha_0 = 1$ and $\xi < 1$, all the roots will be on a unit circle, and the equations reduce to

$$1 + 2\xi = \frac{4}{\beta} ; \quad 1 = \frac{\alpha}{\beta} \quad \text{i.e. } \alpha = \beta.$$

Root locus of the network becomes a unit circle when $\alpha = \beta$, and to obtain real complex roots, ξ is to be less than 1 or β greater than 4/3.

Argument of the complex roots of unit modulus is

$$\theta = \cos^{-1} \xi \quad \text{and} \quad \alpha = \beta = \frac{4}{1 + 2 \cos \theta} \quad \dots (4)$$

Thus keeping $\alpha = \beta$, and $K = 1$ poles of the transfer function can be located on a unit circle, and argument of the poles can be read from a calibrated dial attached to the α dial.

Keeping argument fixed, modulus of the poles can be varied by giving K a value other than unity. Modulus of the roots then become $1/K$.

Due to the finite gain of the amplifier exact position of the poles will be different from that calculated from equation (3). The exact expression for the transfer function taking the finite gain of the amplifier into account is given by

$$\frac{E_{out}}{E_{in}} = \frac{1}{A \left[1 + \frac{\alpha + 4}{2} \frac{x(x+1)}{\left(x + \frac{\alpha}{4}\right)\left(x + \frac{4}{\beta}\right)} \right] + \frac{1-A}{A} \frac{x^3 + \frac{4}{\beta}x^2 + \frac{4}{\beta}x + 1}{\left(x + \frac{\alpha}{4}\right)\left(x + \frac{4}{\beta}\right)}} \quad \dots (5)$$

From equation (5) it is evident that deviation of the actual pole position from that calculated from equation (3) increase with increasing values of θ and the location of the poles on the imaginary axis requires values of α and β greater than 4. Deviation of the values of θ obtained from equation (4) will be smaller, the greater the value of A .

It may be noted that if the network of figure 6 is used for constructing selective amplifiers, the selectivity of such an amplifier is limited by the finite open-loop gain of the amplifier. From the above discussion, it is seen that a high selectivity can be achieved even with a finite value of open-loop gain by adjusting α and β to a value greater than 4.

4. ROOTS OF POLYNOMIALS

Using the circuit arrangement of figure 8 roots of a polynomial can be found. Let the polynomial be given by

$$f(z) = z^n + a_{n-1}z^{n-1} + \dots + a_0.$$

where the coefficients are all real.

A new function $F(z)$ is formed from $f(z)$, given by $F(z) = \frac{f(z)}{g(z)}$ and $g(z)$ is chosen arbitrarily to have real negative roots of convenient values.

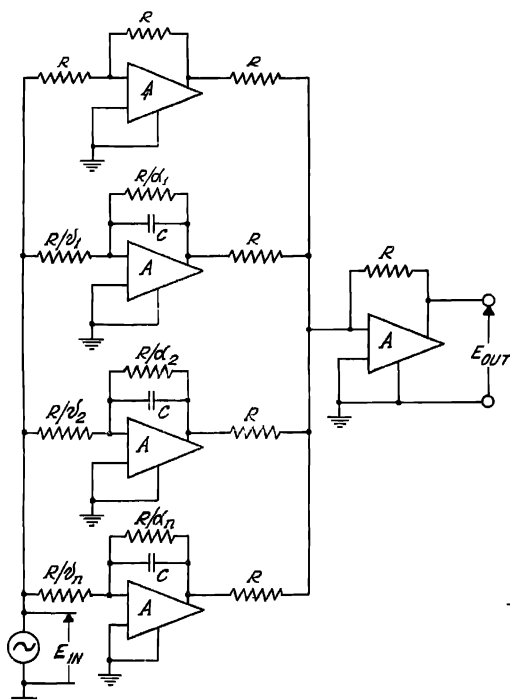


Fig 8. Circuit arrangement for realising the transfer function.

$$F(z) = 1 - \frac{p_1}{z + \alpha_1} + \frac{p_2}{z + \alpha_2} - \dots - \frac{p_n}{z + \alpha_n}.$$

$$\text{i.e. } g(z) = (z + \alpha_1)(z + \alpha_2) \dots (z + \alpha_n).$$

Then

$$F(z) = 1 + \frac{v_1}{z + \alpha_1} + \frac{v_2}{z + \alpha_2} + \dots + \frac{v_n}{z + \alpha_n}.$$

v_1, v_2, \dots, v_n etc. are the real residues at corresponding poles of the function $F(z)$. Individual terms of $F(z)$ can be realised by network configuration of figure 3.

Circuit arrangement for realising $F(z)$ is shown in figure 8.

Supposing that one of the roots of the numerator polynomial lies at $-a + jb$ in the complex plane, the value of the function $F(z)$ will be zero at this point. This point in the complex plane is found out, moving along the imaginary axis by varying the frequency of the oscillator (which is normalised in terms of ωCR) to make the output of the system minimum, corresponding to a value of frequency b and then gradually shifting the imaginary axis towards zero by shifting the poles $\alpha_1, \alpha_2 \dots \alpha_n$ etc., all by the same amount keeping $v_1, v_2 \dots v_n$ etc., fixed. The latter adjustment can be done by keeping all the input coupling network settings fixed and varying all the dials of the feedback network by the same amount. As the zero point in the complex plane is reached the output voltage gradually decreases and finally, at the zero, becomes zero. Dial reading of the oscillator gives b and amount of shift required in the α dial gives α .

Figure 9 shows an alternate arrangement of circuit suitable for finding only the real roots of the polynomial.

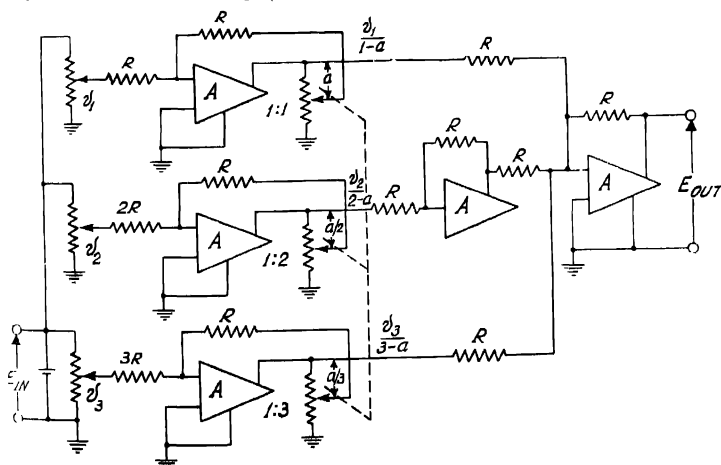


Fig. 9—Circuit arrangement for finding real roots of a polynomial.

It may be noted that in the arrangement shown in figure 8, when $\alpha_1, \alpha_2 \dots \alpha_n$ dials are varied by the same amount to shift the imaginary axis the gain of the

feed back amplifiers become $\frac{v_1}{\alpha_1 - a}, \frac{v_2}{\alpha_2 - a} \dots \frac{v_n}{\alpha_n - a}$. Same can be obtained by

using ganged potentiometers as shown in figure 9. Potentiometers are so ganged that when 1 : 1 potentiometer rotates through an angle θ° , 1 : 2 potentiometer rotates through an angle $\theta^\circ/2$, 1 : 3 potentiometer rotates through $\theta^\circ/3$ and so on.

Hence, if (1 : 1) potentiometer is set to $1 - a$, (1 : 2) is set to $1 - a/2$, (1 : 3) to

$1 - \frac{a}{3}$. D. C. gain of the amplifiers become $\frac{1}{1-a}, \frac{1}{2-a}, \frac{1}{3-a}$.

and
$$\frac{V_{out}}{V_{in}} = \frac{v_1}{1-a} + \frac{v_2}{2-a} + \frac{v_3}{3-a}.$$

Value of a which makes the above zero, gives the values of the real roots of the polynomial.

5 SOME EXAMPLES

1. Circuit arrangement for realising a Butterworth function of 3rd. order.

A Butterworth function of third order has one real pole and a pair of complex poles, all situated on the left half of the complex frequency plane. Modulus of the roots are unity and the argument of the complex roots is 60° . These are realised by the amplifier of figure 7 setting $K = 1, \alpha = \beta = 2$ and the real zeroes are cancelled by using two amplifiers of figure 3 connected in cascade. Resultant system is shown in figure 10.

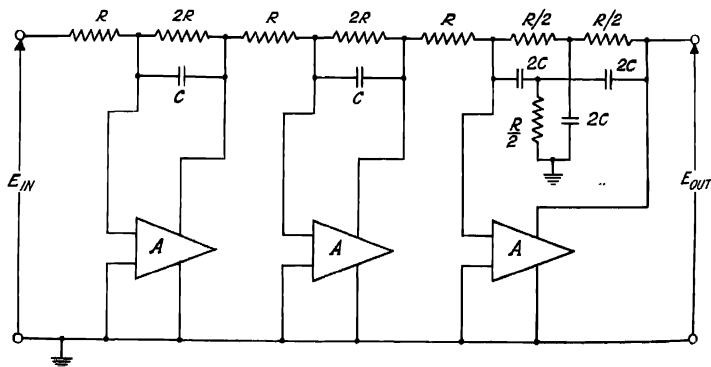


Fig. 10—Circuit arrangement for realising third order Butterworth function.

The overall transfer function is

$$\frac{B_{out}}{B_{in}} = \frac{1}{(x+1)(x+j600)(x-j600)}$$

Transfer function of this system was measured and the experimental plot of the function is shown in the figure 11

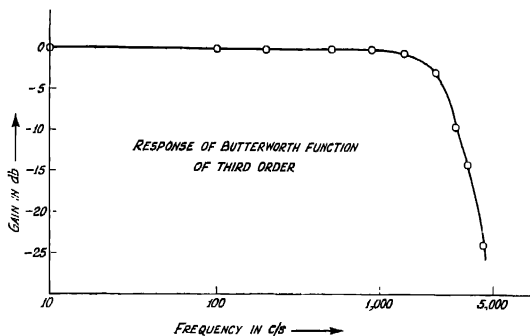


Fig. 11—Experimental plot of third order Butterworth function using circuit arrangement of Fig. 10

2. Circuit arrangement for realising a network having the transfer function

$\frac{x^2+1}{(x+2)(x+3)}$. In figure 12 is shown the amplifier arrangement for obtain-

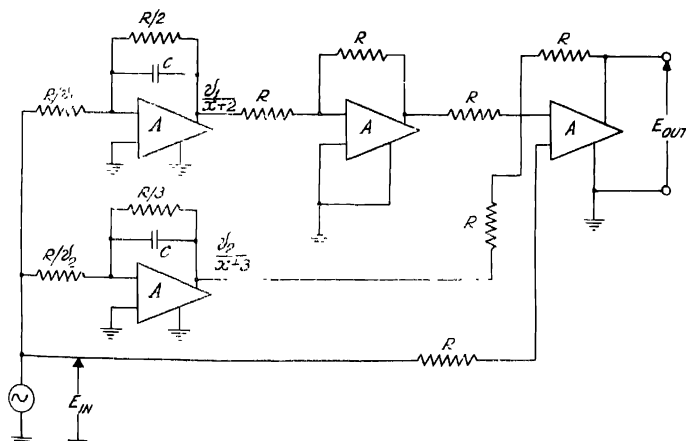


Fig. 12—Circuit arrangement for realising a network having the transfer function $\frac{x^2+1}{(x+2)(x+3)}$

ing the above transfer function. Figure 13 shows the experimental plot of the transfer function.

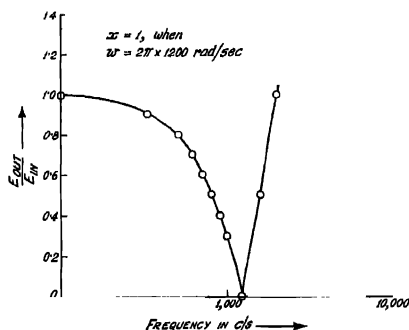


Fig. 13—Experimental plot of frequency response of a network having the transfer function

$$\frac{x^2 + 1}{(x + 2)(x + 3)}$$

ACKNOWLEDGMENT

The authors are deeply indebted to Prof. S. K. Mitra for his constant help and guidance in the work. Thanks are due to Dr. J. N. Bhar, Acting Head of the Department of Radio Physics and Electronics for his kind interest in the work.

REFERENCES

- Boothroyd, A. R., Cherry, E. C. and Makar, R., 1949, *J.I.E.E.*, Part I, **96**, 163.
Guillemin, E. A., 1949, *Journal of Mathematics and Physics*.

ULTRAVIOLET ABSORPTION SPECTRA OF ORTHO- AND PARA-CHLOROANISOLE IN THE LIQUID AND SOLID STATES*

S. B. BANERJEE

OPTICS DEPARTMENT, INDIAN ASSOCIATION FOR THE CULTIVATION OF SCIENCE,
JADAVPUR, CALCUTTA-32

(Received for publication, October 4, 1956)

ABSTRACT. The ultraviolet absorption spectra of ortho- and para-chloroanisole have been studied in the liquid and solid states. The results have been discussed and compared with those for the substances in the vapour state and for other analogous compounds in different states reported by previous workers.

For each compound the ν_0 -band is found to undergo large shift towards longer wavelengths when the vapour is liquefied. In the case of *o*-chloroanisole the spectrum due to the liquid appears to consist of two series of bands separated by about 23 Å U. from each other while the spectrum of the solid shows only one series of narrower bands. The results have been interpreted on the assumption that in the liquid state there are probably two types of molecules corresponding to the *cis*- and *trans*-positions of the methoxy group in the molecule with respect to the chlorine atom.

INTRODUCTION

From the investigations of the ultraviolet absorption spectra of disubstituted benzene compounds containing one or more halogen atoms carried out in this laboratory (Swamy, 1952, 1953a, 1953b) it was observed that in the case of some disubstituted benzenes with a chlorine or bromine atom in the ortho or meta position with respect to another chlorine atom or any substituent group of atoms other than an OH-group, the excited state electronic energy level is split up into more than one components when the substances are solidified and cooled to -180°C , but in the case of compounds having the chlorine or bromine atom in the para position no such splitting takes place. It was concluded that in the ortho or meta compounds in the liquid and solid states the molecules become associated through virtual linkages owing to the presence of a strong permanent electric moment and as a result of such an association the excited state electronic energy level is split up into three components. In the case of the respective para compounds such strong association does not take place owing to the absence of a strong permanent dipole moment and consequently the excited state energy level is not split up with lowering of temperature.

Although the splitting of the energy level mentioned above is observed in the case of chloro- or bromo-toluenes (Swamy 1952, 1953b), no such splitting was observed in the case of *o*-chlorophenol (Swamy, 1953b) or *o*-bromophenol

* Communicated by Prof. S. C. Sarkar.

(Banerjee, 1956b) because the chlorine or bromine atom is attached to the OH-group of the same ring (Pauling, 1939; Ghosh, 1955). It is not known, however, whether molecules having any substituent with rotational freedom other than OH-group behave in the same way as orthochlorophenol molecules. It was, therefore, thought worthwhile to extend the investigations to ortho- and para-chloroanisol. The results of such an investigation have been discussed in the present paper and compared with those for the vapour state reported by previous workers.

EXPERIMENTAL

The chloroanisoles were of chemically pure quality supplied by B.D.H., and were distilled under reduced pressure before use. Very thin films of the liquids of thickness of the order of a few microns were required to obtain the absorption bands. The spectra were photographed on Ilford HP3 films with a Hilger EI spectrograph having a dispersion of 3 A.U. per mm in the 2600 Å region. Iron-arc spectrum was taken on each spectrogram as comparison. Microphotometric records of the absorption bands and iron arc lines were taken with a Kipp and Zonen type Moll microphotometer. The frequencies of absorption bands were determined by a comparison of the records of the absorption bands and iron arc spectrum in the same spectrogram by the method described earlier (Banerjee, 1956a).

RESULTS AND DISCUSSION

The microphotometric records of the absorption bands of the chloroanisoles are reproduced in figures 1 and 2. The wave numbers of the bands and then

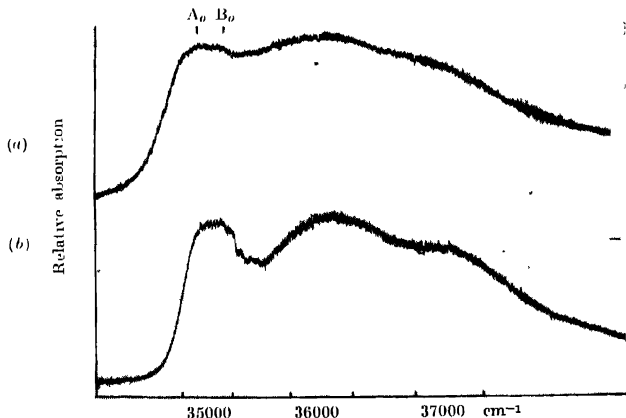


Fig 1 Microphotometric records of the ultraviolet absorption spectra of *o*-chloroanisol.
(a) Liquid at 32°C (b) Solid at -180°C

V. Absorption Spectra of Ortho- & Para Chloroanisole 137.

Arguments are given in Tables I and II. As the spectra of the compounds in vapour state have already been reported by Suryanarayana and Rao (1955, (i)) those data have been included in the tables for comparison.

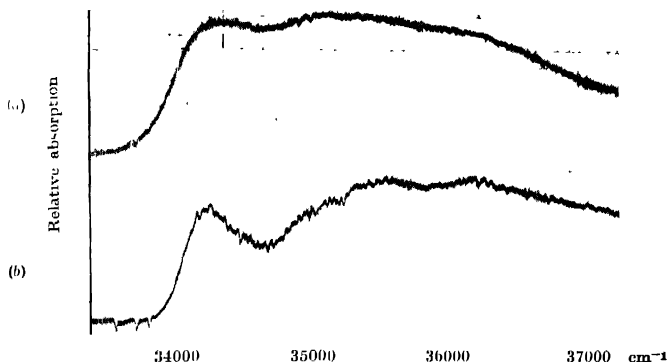


Fig 2. Microphotometric records of the ultraviolet absorption spectra of *p*-chloroanisole.
(a) Liquid at 32°C (b) Solid at -180°C

o-Chloroanisole

The absorption spectrum of *o*-chloroanisole in the vapour state reported by Suryanarayana and Rao (1956) consists of 66 bands with the position of the ν_0 -band at 35760 cm^{-1} . The other bands have been interpreted on the basis of eight fundamental frequencies in the excited state, viz., 357, 518, 614, 767, 948, 1060, 1274 and 1389 cm^{-1} and four other frequencies in the lower state. In the spectrum of the liquid the ν_0 -band is at 35139 cm^{-1} . It is thus displaced towards longer wavelengths by about 600 cm^{-1} from its position due to the vapour. It can also be seen from figure 1 that the ν_0 -band as well as the other three bands appear to be doublets each having a component on the shorter wavelength side, the separation of the components being about 23 Å. or 286 cm^{-1} . When the liquid is solidified and cooled to -180°C the bands become narrower and only one series of bands are observed. The ν_0 -band shifts again towards shorter wavelengths by 223 cm^{-1} on solidification of the liquid.

Anzilotti and Curran (1943) studied the dipole moment of *o*-chloroanisole in very dilute solutions in benzene and concluded that the OMe-group in the molecule is locked in the *trans*-position because of steric repulsion between the methyl group and the halogen atom. Similar conclusions were arrived at by Burawoy and Chamberlain (1952) who suggested from a study of the electronic spectra of the solution of *o*-chloroanisole in ethyl-alcohol that the methyl group is able to turn away from the substituent in the ortho position to avoid steric

TABLE I
Absorption bands of *o*-chloroanisole.

Vapour* (Suryanarayana & Rao, 1956)		Liquid at 32°C Present author		Solid at -180°C Present author	
Wave No. (cm ⁻¹) & Int.	Assign- ment	Wave No. (cm ⁻¹) & Int.	Assign- ment	Wave No. (cm ⁻¹) & Int.	Assign- ment
35070 (w)	$\nu_o - 690$	35130 (s)	A _o	35362 (s)	ν_o
35195 (w)	$\nu_o - 565$	35425 (s)	B _o	36330 (s)	$\nu_o + 977$
35342 (vw)	$\nu_o - 418$	35990 (s)	A _o 860	37316 (ms)	$\nu_o - 2 \times 977$
35481 (m)	$\nu_o - 279$	36285 (s)	B _o 860		
35760 (s)	ν_o	36869 (ms)	A _o + 2 × 860		
36117 (m)	$\nu_o + 357$	37136 (w)	B _o + 2 × 860		
36278 (m)	$\nu_o + 518$				
36401 (s)	$\nu_o + 641$				
36527 (s)	$\nu_o + 767$				
36708 (s)	$\nu_o + 948$				
36820 (ms)	$\nu_o + 1030$				
37034 (m)	$\nu_o + 1274$				
37149 (w)	$\nu_o + 1389$				

* Only prominent bands corresponding to fundamental vibrational frequencies have been included

TABLE II
Absorption bands of *p*-chloroanisole

Vapour* Suryanarayana & Rao (1956)		Liquid at 32°C Present author		Solid at -180°C Present author	
Wave No. (cm ⁻¹)	Assign- ment	Wave No. (cm ⁻¹) & Int.	Assign- ment	Wave No. (cm ⁻¹) & Int.	Assign- ment
34505	$\nu_o - 361$				
34866	ν_o	34389 (s)	ν_o	34318 (s)	ν_o
35203	$\nu_o + 337$	35375 (s,vb)	$\nu_o + 986$	35078 (ms)	$\nu_o + 760$
35645	$\nu_o + 779$	36366 (ms,b)	$\nu_o + 2 \times 986$	35275 (s)	$\nu_o + 957$
35919	$\nu_o + 1053$			35602 (s)	$\nu_o + 1284$
36140	$\nu_o + 1274$			36352 (s)	$\nu_o + 1284 + 760$
				36565 (ms)	$\nu_o + 1284 + 957$

* Only prominent bands corresponding to fundamental vibrational frequencies have been included.

interaction, so that the bands shift towards shorter wavelengths only by about 20 Å U from the position of the band due to *o*-chlorophenol, but when both the ortho positions are filled up the shift is about 100 Å.U. In the vapour state all the molecules of *o*-chloroanisole have the methoxy group fixed in the *trans*-position and thus the substance contains only one type of molecules. In the liquid state the molecules are randomly oriented with respect to each other and in some of the molecules the methoxy group may tend to come to the *cis*-position with the result that the conjugation effect is weakened, so that the bands shift towards shorter wavelengths. This may be responsible for the appearance of the second series of bands on the shorter wavelength side of the main bands in the spectrum of *o*-chloroanisole in the liquid state. When the liquid is solidified and cooled to -180°C all the molecules probably tend to be converted to the *cis*-form owing to the influence of the field due to chlorine atom of neighbouring molecules on the methoxy group giving rise to only one series with the ν_0 -band displaced more towards shorter wavelengths.

If the changes in the spectra observed with change of state are compared with those observed in the case of *o*-cresol it is found that the shifts of the ν_0 -band with the changes from the vapour to the liquid state and from the liquid to the solid state are larger in the case of *o*-chloroanisole than in the case of *o*-cresol. The larger chemical activity of chlorine atom seems to produce this larger influence of intermolecular field on the electronic state.

p-Chloroanisole .

In the vapour state *p*-chloroanisole exhibits a large number of bands which represent transitions involving excited state vibrational frequencies 337, 699, 779, 1053 and 1274 cm^{-1} and a ground state vibrational frequency 361 cm^{-1} as shown tentatively by Suryanarayana and Rao (1955). The band at 34866 cm^{-1} was taken as the ν_0 -band by them. The spectrum due to the liquid consists of three broad bands. The broad band at 34369 cm^{-1} has been taken as the ν_0 -band and the other bands represent progression of a frequency 986 cm^{-1} . The ν_0 -band is thus displaced by 477 cm^{-1} towards longer wavelengths with the liquefaction of the vapour. When the liquid is frozen and cooled to -180°C the absorption bands become a little sharper and bands corresponding to excited state frequencies 760, 957, 1284 cm^{-1} and their combinations are observed. It appears that owing to the smaller value of the dipole moment of the para compound the excited electronic state is not affected by the intermolecular field as much as in the case of ortho compound in the solid state at low temperature. Also, the shift of the ν_0 band is larger in the case of *p*-chloroanisole than in the case of the analogous molecule *p*-cresol probably owing to the greater chemical activity of the chlorine atom.

ACKNOWLEDGMENT

The author is indebted to Professor S. C. Sirkar, D. Sc., F.N.I. for his kind interest and guidance during the progress of the work.

REFERENCES

- Anzilotti, W. F. and Curran, B. C., 1943, *J. Am. Chem. Soc.*, **65**, 607.
Banerjee, S. B., 1956a, *Ind. J. Phys*, **30**, 106.
 ,, 1956b, *Ind. J. Phys*, **30**, 353.
Burawoy, A. and Chamberlain, J. T., 1952, *J. Chem. Soc.*, 2310.
Ghosh, D. K., 1955, *Ind. J. Phys.*, **29**, 450.
Pauling, L., 1939, *The Nature of the Chemical Bond* (Cornell University Press)
Suryanarayana, V. and Rao, V. R., 1955, *J. Sci. and Ind. Res.*, **14B**, 128
 ,, ,, 1956, *Ind. J. Phys.*, **30**, 117
Swamy, H. N., 1952, *Ind. J. Phys.*, **26**, 445.
 , 1953a, *Ind. J. Phys*, **27**, 55.
 ,, 1953b, *Ind. J. Phys.*, **27**, 119

X-RAY ANALYSIS OF STRUCTURE OF FROZEN TOLUENE AND ITS SOLUTION IN ALCOHOL AT -180°C

S. G. BISWAS AND S. C. SIRKAR

OPTICS DEPARTMENT, INDIAN ASSOCIATION FOR THE CULTIVATION OF SCIENCE, JADAVPUR,
CALCUTTA-39

(Received for publication, December 17, 1956)

Plate III

ABSTRACT The crystal structure of frozen toluene at -180°C has been investigated by studying the Debye-Scherrer pattern, and by using Lapson's method, it has been observed that the crystal belongs to orthorhombic system. The dimensions of the unit cell are $a = 7.338 \text{ \AA}$, $b = 8.606 \text{ \AA}$ and $c = 9.20 \text{ \AA}$. The density of the crystal has been determined and found to be 1.061. The number of molecules in the unit cell is 4. The crystal probably belongs to space group $C2_{2v}$.

The Debye-Scherrer patterns due to frozen ethyl alcohol and frozen solutions of toluene of strength 81% and 35% in ethyl alcohol (and also of liquid toluene at -80°C) have been studied and the results indicate that both the solutions in the solid state are amorphous. In the 81% solution cybotactic groups of toluene molecules are present but their number is reduced by alcohol molecules and the latter molecules do not form groups in the frozen solution. In the 35% solution groups due to ethyl alcohol molecules are present and in this case also the number of such groups is reduced by toluene molecules. It has been pointed out that these results explain the Raman spectra in the low frequency region observed by Kastha (1956).

INTRODUCTION

From the results of investigation on the Raman spectra of frozen solutions of toluene in ethyl alcohol at -180°C Kastha (1956) concluded that the low-frequency Raman lines observed in the case of frozen solution of strength 81% are produced by groups of toluene molecules formed by association of the molecules. He further observed that when the strength of the solution is diminished to 35% a continuous wing is produced instead of the discrete band. He concluded that a wing is produced by the groups formed by the association of toluene molecules with alcohol molecules. Both the solutions were found to be transparent like glass. It was not known however whether the frozen masses were crystalline or amorphous. The object of the present investigation was to determine the crystal structure of frozen toluene, if possible, and to find out whether the frozen masses of the mixtures mentioned above are crystalline or amorphous, as such information would be helpful in understanding the origin of the low-fre-

quency Raman lines. For this purpose the Debye-Scherrer patterns of frozen toluene and of solutions of toluene in ethyl alcohol at -180°C have been photographed and the results of the analysis of the patterns have been discussed in this paper.

EXPERIMENTAL

Toluene used in the investigation was of chemically pure quality. Besides the Debye-Scherrer photograph of toluene such patterns due to 81% and 35% solutions of toluene in dehydrated ethyl alcohol at -180°C were also photographed just to find out whether the frozen masses were crystalline or amorphous. Each of these patterns was photographed several times in order to find out whether the results were consistent with each other. The diffraction patterns due to pure alcohol, pure toluene and solutions of toluene in alcohol in the liquid state were also photographed for comparison.

A Seifert X-ray tube running at 32KV and 26mA was used to photograph the Debye-Scherrer patterns. The X-ray tube was provided with a copper target and a nickel filter was used to cut off the $K\beta$ radiation. An exposure of 3 hours was sufficient to record each pattern with moderate intensity.

The patterns at -180°C were photographed by the method used previously by Krishnamurti and Sen (1956). The arrangement was slightly modified so that liquid oxygen was first falling into a funnel and while coming out from the lower end of the funnel it produced a narrow stream surrounding the specimen. As the stream was in the path of X-rays a liquid oxygen halo was produced in each Debye-Scherrer pattern. The radius of the camera was measured accurately by taking a Debye-Scherrer pattern of rock-salt before each exposure.

RESULTS AND DISCUSSION

(a) *Space group of solid toluene*

The Debye-Scherrer pattern due to crystals of toluene at -180°C is reproduced in figure 1, (Plate III). The values of $\sin^2 \theta$ for the rings in the patterns due to toluene were calculated and plotted on a graph paper according to Lipson's (1949) method. It was found that some of the differences were repeated several times. So, it was concluded that the crystal might belong to orthorhombic system. By trial it was found that the spacings could be explained by assuming the values of $\lambda^2/4a^2$, $\lambda^2/4b^2$, and $\lambda^2/4c^2$ to be .0110 .00800 and .00700, respectively. These gave the following dimensions of the unit cell.

$$a = 7.338\text{\AA}$$

$$b = 8.606\text{\AA}$$

$$c = 9.20\text{\AA}$$

The observed values of $\sin^2\theta$, the spacings and the proposed indices of the reflections and also the values of $\sin^2\theta$ and the spacings calculated with the values of a , b , c mentioned above are given in Table I. In order to find out the number of molecules in the unit cell the density of solid toluene at -180°C was required, but it could not be found in the existing literature. So, an attempt was made

TABLE I

Data from the Debye-Scherrer pattern of toluene at -180°C

$\sin^2 \theta$ (observed)	$\sin^2 \theta$ (calculated)	Difference	Spacings observed in Å	Proposed Indices & Intensities
01804	01800	00004	5.730	101 (s)
02574	02600	00026	4.795	111 (ms)
03198	03200	00002	4.30	020 (s)
03894	03900	00006	3.90	021 (w)
04513	04300	00013	3.705	120 (ms)
04669	04700	00031	3.56	112 (w)
04962	05000	00038	3.45	121 (ms)
06017	06000	00017	3.14	022 (s)
07218	07200	00018	2.865	202 030 (ms)
07586	07600	00014	2.795	220 (w)
07916	07900	00016	2.735	031 (w)
08290	08300	00010	2.67	130 221 (ms)
1037	1040	0003	2.39	222 (ms)
1120	1120	0000	2.30	004 (ms)
1314	1310	0004	2.12	320 114 (w)
1393	1390	0003	2.06	140 (ms)
1460	1460	0000	2.015	141 133 (ms)
1644	1640	0004	1.90	214 (ms)
1760	1760	0000	1.835	400 (w)

to determine the density of frozen toluene at -180°C by measuring the contraction of volume of a certain mass of toluene contained in a cylindrical bulb of Pyrex glass joined to a capillary tube taking into account the contraction of Pyrex bulb itself, and assuming the density of toluene in the liquid state at 20°C as

0.866. The density of solid toluene at -180°C was found out to be 1.061. The number of molecules per unit cell calculated with this value of density is 4.033. Hence, actually there are four molecules in the unit cell.

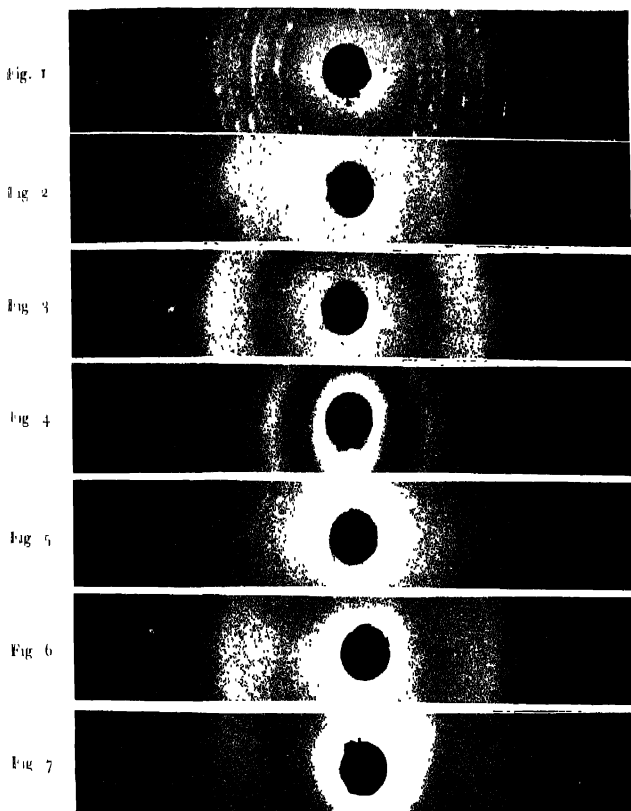
Although reflections from only a few planes have been photographed the results given in Table I indicate that (*h**ol*) planes with (*h*+*l*) odd are absent. So the possible space group is C_{2v}^7 .

(b) *Structure of frozen solutions of toluene in alcohol.*

The patterns due to pure ethyl alcohol in the liquid and the frozen state are reproduced in figures 2 and 3 (Plate I) respectively. In figure 3 the presence of the inner halo in addition to the outer liquid oxygen halo indicates that alcohol is amorphous in the solid state. The mean spacing of the cybotactic groups in the liquid state is 4.12\AA while it changes to 3.78\AA in the solid state. The intensity of the halo due to the solid is larger than that due to the liquid. Evidently, the cybotactic groups are frozen in when the liquid is solidified. The pattern due to toluene in the liquid state at about -80°C reproduced in figure 4 (Plate III) shows two halos, the inner one being very intense. This indicates that the number of cybotactic groups increases at lower temperatures. The pattern due to a 81% mixture of toluene with ethyl alcohol reproduced in figure 5 (Plate III) consists of a fairly intense halo corresponding to a spacing of 5.58\AA superposed on a diffuse halo of larger radius. When this mixture is frozen the other diffuse halo becomes very feeble (figure 6) and only one weak halo corresponding to a spacing of 4.651\AA is observed. Hence the frozen mass is amorphous.

The results observed in the case of the mixture of toluene clearly indicate that some groups of molecules are formed in the frozen mass and these are analogous to cybotactic groups in the pure liquid. The spacing observed is slightly less than that observed in the case of toluene in the liquid state at -80°C . So, probably the cybotactic groups of pure toluene molecules are frozen in when the 81% mixture of toluene in ethyl alcohol is solidified. The feebleness of the halo observed in the case of the frozen mixtures indicates that the number of cybotactic groups is less in the mixture than in the pure liquid at low temperature. This happens probably because the alcohol molecules enter into some of these groups and break them up into smaller groups. Hence the new Raman band observed by Kastha (1956) in the low-frequency region of the Raman spectrum of 81% frozen solution of toluene in ethyl alcohol is produced by the groups of toluene molecules present in the frozen mixture.

The pattern due to frozen mass of 35% solution of toluene in ethyl alcohol reproduced in figure 7 shows one halo corresponding to the spacing of 3.92\AA . This spacing is identical with that observed in the case of frozen ethyl alcohol at -180°C . The intensity of the halo is however much less in the case of the mixture than in the case of pure alcohol in the solid state. So, the number of



Debye-Scherrer patterns
(Radius of the camera = 5.163 cm.)

Fig. 1. Toluene at -180°C

Fig. 2. EtOH at 26°C

Fig. 3. " " -180°C

Fig. 4. Toluene at -80°C

Fig. 5. 70% soln. of toluene at 26°C

Fig. 6. " " " " at -180°C

Fig. 7. 30% soln. of toluene at -180°C

frozen-in cybotatic groups in the mixture is much smaller than that in the case of the pure substance in the solid state. This indicates that groups of pure ethyl alcohol molecules are present in the frozen mixtures, but some of them are broken into smaller groups by toluene molecules used as the solute. The latter molecules do not form groups large enough to produce any diffraction halo. Hence the Raman spectrum in the low-frequency region of 35% frozen solution of toluene in alcohol observed by Kastha (1956) is produced by very small groups of toluene molecules dispersed in ethyl alcohol medium. The explanation offered by him is thus confirmed by the results of the present investigation.

ACKNOWLEDGMENT

The authors are thankful to the Council of Scientific and Industrial Research for financing a scheme under which this investigation was carried out.

REFERENCES

- Kastha, G. S., 1956, *Ind. J. Phys.*, **30**, 313.
Krishna Murti, G. S. R. and Sen, S. N., 1956, *Ind. J. Phys.*, **30**, 242.
Lipson, H., 1949, *Acta Cryst.*, **2**, 43.

TRANSPORT COEFFICIENTS AND FORCE BETWEEN UNLIKE MOLECULES

S. C. SAXENA

INDIAN ASSOCIATION FOR THE CULTIVATION OF SCIENCE, CALCUTTA 32

(Received for publication September 21, 1956)

ABSTRACT Elaborate computations have been performed of the transport coefficients of binary gas mixtures, viz., binary viscosity, diffusion and thermal conductivity, with a view to test the adequacy and appropriateness of the Lennard-Jones 12 : 6 model in representing the like and unlike interactions of the gaseous molecules. So far in such attempts somewhat semi-empirical rules were assumed to assign the interaction energies and diameters for the collision of pairs of unlike molecules. We have used, on the other hand, ϵ_{12}/k values determined from thermal diffusion, a property known to be much sensitive for forces between unlike molecules and r_{12} is calculated by correlating these ϵ_{12}/k values with the theoretical relation developed by Srivastava and Madan connecting the force constants for like and unlike molecules. A fairly reasonable agreement is obtained between the observed and calculated values from theory, which confirms the adequacy of the Lennard-Jones 12 : 6 model as well as the accuracy of the potential parameters.

INTRODUCTION

The general results of the classical kinetic theory for non-uniform gases were developed mainly by Enskog and Chapman and are conveniently summarised by Chapman and Cowling (1952) and Hirschfelder, Curtiss and Bird (1954). The theory, under certain limitations, expresses the transport coefficients in terms of collision integrals which depend upon the nature of the intermolecular field assumed to operate between the two molecules and upon the temperature. Hirschfelder, Bird and Spotz (1948, 1949), Winter (1949) and others have shown that the model most in accord with the observed properties of gases is the Lennard-Jones 12 : 6 model

$$E_{ij}(r) = 4\epsilon_{ij}[(r_{ij}/r)^{12} - (r_{ij}/r)^6], \quad (1)$$

where ϵ_{ij} is the maximum binding energy between the molecules and r_{ij} is the distance at which the attractive and repulsive potentials are equal. On this model Srivastava and Madan (1953) have evaluated the potential parameters for unlike molecules, utilising the temperature dependence of the thermal diffusion factor in view of the greater sensitivity of thermal diffusion towards unlike interactions. In a recent paper, the author (Saxena, 1955a), has improved these calculations and

[Present address : Research Associate, Institute of Molecular Physics, University of Maryland, Maryland, U.S.A.]

... computed the potential parameters for a number of gas pairs to a higher degree of approximation than before. r_{12} can then be determined by substituting these c_{12}/k values in the theoretical relation connecting the potential parameters for like and unlike molecules developed by Srivastava and Maclan (1953). Using these values of c_{12}/k and r_{12} , binary viscosity, diffusion and thermal conductivity have been calculated for a number of gaseous mixtures and compared with the observed values with a view to deriving information about the law of molecular interaction.

2. THEORY AND FORMULAE

For a binary mixture, the first approximation to the coefficient of viscosity is given by the relation

$$[\eta_{mix}]_1 = \frac{1}{X_\eta + Y_\eta} \quad \dots (2)$$

where

$$X_\eta = \frac{x_1^2}{[\eta_1]_1} + \frac{2x_1x_2}{[\eta_{12}]_1} + \frac{x_2^2}{[\eta_2]_1},$$

$$Y_\eta = \frac{3}{5} A_{12}^* \left[\frac{x_1^2}{[\eta_1]_1} \left(\frac{M_1}{M_2} - 1 \right) - \frac{2x_1x_2}{[\eta_{12}]_1} \left(\frac{M_1 + M_2}{4M_1M_2} \right) \left(\frac{[\eta_{12}]_2^2}{[\eta_1]_1[\eta_2]_1} \right) + \frac{x_2^2}{[\eta_2]_1} \left(\frac{M_2}{M_1} \right) \right],$$

$$Z_\eta = \frac{3}{5} A_{12}^* \left[x_1^2 \left(\frac{M_1}{M_2} \right) + 2x_1x_2 \left\{ \left(\frac{M_1 + M_2}{4M_1M_2} \right) \left(\frac{[\eta_{12}]_1}{[\eta_1]_1} + \frac{[\eta_{12}]_1}{[\eta_2]_1} \right) - 1 \right\} + x_2^2 \left(\frac{M_2}{M_1} \right) \right],$$

and

$$[\eta_1]_1 \times 10^7 = \frac{266.93 \sqrt{M_1 T}}{r_{12}^2 \Omega_{12}^{(2,2)*}(T_1^*)},$$

$$[\eta_{12}]_1 \times 10^7 = \frac{266.93 \sqrt{2M_1 M_2 T (M_1 + M_2)}}{r_{12}^2 \Omega_{12}^{(2,2)*}(T_{12}^*)}$$

Here x_1, x_2 are the mole fractions of the species 1 and 2 of molecular weights M_1 and M_2 respectively. A_{12}^* and $\Omega_{12}^{(2,2)*}$ are functions of the reduced temperature T_{12}^* , and are tabulated by Hirschfelder, Curtiss and Bird (1954). The subscripts 1, 2 refer to an interaction between a molecule of species 1 with the other of species 2.

The m -th approximation to the coefficient of mutual diffusion of a binary mixture of gases 1 and 2 is

$$[D_{12}]_m = 0.0026280 \frac{\sqrt{T^3 (\bar{M}_1 + \bar{M}_2) / 2 \bar{M}_1 \bar{M}_2}}{p r_{12}^2 \Omega_{12}^{(1,1)*} (T_{12}^*)} f_{D_{12}}^{(m)}, \quad \dots (3)$$

where D_{12} is the mutual diffusion coefficient in cm²/sec, p is the pressure in atmospheres and the correction factor $f_{D_{12}}^{(m)}$ is best expressed in the determinant notation of Chapman and Cowling (1952) as

$$f_{D_{12}}^{(m)} = a_{00} \cdot A_{00}^{(m)} / A^{(m)} \quad (4)$$

and is unity for $m = 1$. Here $A^{(m)}$ stands for a determinant of $(2m+1)$ -th order whose general element is a_{ij} , with i and j ranging from $-m$ to m . The term $A_{00}^{(m)}$ is the minor of $A^{(m)}$ and is obtained by deleting the row and column containing a_{00} . These elements, a_{ij} , are functions of collision integrals, the molecular weights, and the relative concentrations of the gases in the diffusing mixture and are given by Mason (1954) for i and $j = 2$.

Recently the author (1955b) has calculated the correction factor for $m = 2$ and 3 for the particular case of A-He gas pair and have shown that their contribution is less than 3%. Usually the experimental error in the determination of D_{12} is also of the same order, consequently for our present purpose only the first approximation formula need be considered.

The coefficient of thermal conductivity for a binary mixture of monatomic molecule is given to the first approximation by the formula .

$$[\lambda_{mix}]_1 = \frac{1 + Z_\lambda}{X_\lambda + Y_\lambda} \quad \dots (5)$$

where

$$X_\lambda = \frac{x_1^2}{[\lambda_1]_1} + \frac{2x_1x_2}{[\lambda_{12}]_1} + \frac{x_2^2}{[\lambda_2]_1},$$

$$Y_\lambda = \frac{x_1^2}{[\lambda_1]_1 U^{(1)}} + \frac{2x_1x_2}{[\lambda_{12}]_1 U^{(12)}} + \frac{x_2^2}{[\lambda_2]_1 U^{(2)}},$$

$$Z_\lambda = x_1^2 U^{(1)} + 2x_1x_2 U^{(12)} + x_2^2 U^{(2)},$$

$$[\lambda_1]_1 \times 10^7 = \frac{1989.1}{M_1 r_1^2} \frac{T^{\frac{1}{2}}}{\Omega^{(2,2)*}} (T^*),$$

$$[\lambda_{12}]_1 \times 10^7 = \frac{1989.1}{r_{12}^2} \sqrt{\frac{T(\bar{M}_1 + \bar{M}_2)}{\Omega_{12}^{(2,2)*}}} \frac{\bar{M}_1 \bar{M}_2}{(T_{12}^*)},$$

$$U^{(1)} = \frac{4}{15} A_{12}^* = \frac{1}{12} \left(\frac{12}{5} B_{12}^* + 1 \right) \frac{M_1}{\bar{M}_2} + \frac{1}{2} \frac{(M_1 - M_2)^2}{M_1 M_2},$$

$$\begin{aligned}
 U^{(1)} = & \frac{4}{15} A_{12}^* \left[\frac{(M_1 + M_2)^2}{4M_1M_2} \right] \frac{|\lambda_{12}|_1^2}{|\lambda_{11}|_1|\lambda_{21}|_1} - \frac{1}{12} \left(\frac{12}{5} B_{12}^* + 1 \right) \\
 & - \frac{5}{32 A_{12}^*} \left(\frac{12}{5} B_{12}^* - 5 \right) \frac{(M_1 - M_2)^2}{M_1M_2}, \\
 U^{(2)} = & \frac{4}{15} A_{12}^* \left[\frac{(M_1 + M_2)^2}{4M_1M_2} \right] \left\{ \frac{|\lambda_{12}|_1}{|\lambda_{11}|_1} + \frac{|\lambda_{12}|_1}{|\lambda_{21}|_1} \right\} - 1 \Bigg] \\
 & - \frac{1}{12} \left(\frac{12}{5} B_{12}^* + 1 \right)
 \end{aligned}$$

λ_2 and $U^{(2)}$ are obtained from λ_1 and $U^{(1)}$ respectively by an interchange of subscripts.

The equation correlating ϵ_{12} , r_{12} with ϵ_{11} , ϵ_{22} and ν_{11} , r_{22} and developed by Srivastava and Madan (1953) is

$$\epsilon_{12} r_{12}^6 = 2(\epsilon_{11} \epsilon_{22} \nu_{11}^6 r_{22}^6)(I_1 I_2)/(I_1 + I_2), \quad (6)$$

where I_1 , I_2 are the ionization potentials for the individual components

3. CALCULATION OF TRANSPORT COEFFICIENTS

Recently the author (Saxena 1955a) has evaluated the potential parameter ϵ_{12}/k for a number of gaseous mixtures from the temperature variation of the thermal diffusion factor with the only assumption that the first approximation formula for the thermal diffusion factor gives the correct value. In a subsequent paper he (Saxena 1955b) has critically examined the consequences of this assumption for the particular case of A-He gas pair and has shown that although the second approximation to thermal diffusion factor is approximately three percent higher than the first approximation, yet its effect on the determination of ϵ_{12}/k is insignificant. This is due to the circumstance that the difference in the first and second approximation to the thermal diffusion factor is probably not much dependent on temperature. Hence our ϵ_{12}/k values are preferable to those obtained on the assumption that ϵ_{12} is given by the geometric mean of ϵ_{11} and ϵ_{22} , the $\epsilon\epsilon_{11}$ values being obtained from viscosity, a property more suitable for testing the adequacy of any model rather than to determine the force constants. On the other hand, our ϵ_{12}/k values have been determined from thermal diffusion, a property most sensitive to unlike interactions. Saxena and Srivastava (1955) have also developed a method of finding ϵ_{11} from the temperature variations of the thermal diffusion factor, but its application at present is very much limited due to the lack of reliable experimental data on isotopic thermal diffusion.

Equation (6) has been used to determine r_{12} . The force constants used for like molecules are those obtained from thermal diffusion and viscosity, and are given by Srivastava and Madan (1953). The ionization potentials of the gases used are those reported by Margenau (1939). These when substituted in equation (6) together with ϵ_{12} values obtained from thermal diffusion yield the values for the force constant r_{12} which are listed in Table I, col. 3.

TABLE I
Force constants for unlike molecules

Gas pair	ϵ_{12}/R from Thermal diffusion	r_{12} from equation (6)
He-A	27.91	3.025
Ne-A	67.60	3.079
Ne-Kr	64.88	3.287
Ne-Xe	71.99	3.460
A-Xe	168.9	3.716
H ₂ -A	57.29	3.249
H ₂ -CO	52.45	3.341
H ₂ -O ₂	62.51	3.181
H ₂ -N ₂	48.05	3.377

Tables IIa, IIb and IIc give a comparison between the experimental values of the viscosity and those calculated from the potential parameters of Table I, according to the equation (2). The experimental viscosity data listed in these tables is from Landolt-Bornstein, with the single exception of the H₂-N₂ data of Van Itterbeek *et al.* (1947). In Table III are recorded the calculated binary viscosities for Ne-Kr, Ne-Xe and A-Xe gaseous mixtures for which no experimental data are available.

In Table IV are recorded the values of $[D_{12}]_1$ for those gas pairs for which the experimental data are available. Also shown are the values calculated for the Lennard-Jones 12:6 model according to equation (3). The experimental data for H₂-N₂, H₂-A mixtures is that of Waldmann (1944) while that for H₂-N₂, H₂-O₂, H₂-CO and He-A mixtures have been taken from Chapman and Cowling (1952).

TABLE IIa

Viscosity of binary mixtures (in 10^{-7} gm/cm sec.)

$\% \text{He}$	He-A				Mixture $\% \text{Ne}$	Ne-A			
	Temp. 293°K		Temp. 373°K			Temp. 293°K		Temp. 373°K	
	Theor.	exp.	Theor.	exp.		Theor.	exp.	Theor.	exp.
0	2211	2211	2674	2584	0	2211	2213	2674	2693
38.2	2310	2291	2765	2745	25.8	2403	2401	2882	2885
49.06	2328	2296	2777	2750	39.09	2511	2504	2997	2990
100	1919	1973	2243	2320	73.2	2814	2808	3319	3313
					100	3068	3092	3586	3623

TABLE IIb

Mixture %H ₂	H ₂ -CO				Mixture %H	H ₂ -A			
	Temp. 195°K		Temp. 295°K			Temp. 293°K		Temp. 373°K	
	Theor.	exp.	Theor.	exp.		Theor.	exp.	Theor.	exp.
0	1251	1264	1752	1745	0	2211	2211	2674	2684
19.27	1239	1250	1722	1717	29.42	2128	2140	2561	2586
40.96	1202	1219	1656	1651	44.57	2046	2056	2454	2488
69.47	1080	1081	1464	1449	65.15	1849	1857	2202	2238
100	664	676	876	874	100	872	875	1015	1029

TABLE IIc

Mixture $\% \text{H}_2$	$\text{H}_2\text{-N}_2$				Mixture $\% \text{O}_2$	$\text{H}_2\text{-O}_2$			
	Temp. 82°K		Temp. 292°K			Temp. 300°K		Temp. 400°K	
	Theor.	Exp.	Theor.	Exp.		Theor.	Exp.	Theor.	Exp.
0	571	544	1744	1746	0	2065	2057	2566	2568
25	571	540	1698	1700	18.35	2024	2019	2509	2507
50	560	524	1601	1609	39.45	1939	1925	2394	2381
75	544	493	1389	1396	60.30	1780	1784	2185	2192
100	354	362	871	882	78.08	1529	1494	1803	1858
					100	886	889	1059	1087

TABLE III

(Calculated viscosity of some mixtures (in 10^{-7} gm/cm. sec.)

Mixture % of the lighter component	Ne-Kr		Ne-Xe		Ar-Xe	
	Temp. °K		Temp. °K		Temp. °K	
	200	300	200	300	200	300
0	1715	2526	1546	2311	1546	2311
25	1873	2685	1723	2511	1583	2346
50	2053	2860	1943	2750	1612	2364
75	2243	3028	2203	3008	1623	2370
			2372	3114	1592	2253

Table V gives only the calculated values of the diffusion coefficient for these mixtures, at various temperatures

TABLE IV
[$D_{12}]_1$ in $\text{cm}^2 \text{ sec}^{-1}$

Gas pair	Temperature 273°K			Temperature 293°K	
	Exp.	Cal. (Present Work)	Cal (author)	Exp.	Cal.
He-A	0.641	0.644	0.633		
H ₂ -CO	0.65	0.659	0.662		
H ₂ -A				0.770	0.765
H ₂ -N ₂	0.674	0.657	0.658	0.760	0.739
H ₂ -O ₂	0.697	0.698			

TABLE V
Calculated [$D_{12}]_1$ in $\text{cm}^2 \text{ sec}^{-1}$

Gas pair	Temp. °K.			Gas pair	Temp. °K.	
	100	200	300		200	300
He-A	0.117	0.383	0.752	Ne-A	0.150	0.323
H ₂ -CO	0.112	0.386	0.772	Ne-Kr	0.129	0.260
H ₂ -A	0.113	0.395	0.795	Ne-Xe	0.109	0.221
H ₂ -N ₂	0.113	0.385	0.769	Ar-Xe	0.052	0.113
H ₂ -O ₂	0.115	0.406	0.819			

Table VI gives a comparison of the observed and calculated values of λ_{mix} according to equation (5) for the A-He gas pair for which only the experimental data of Waschmith (1908) are available. Very recently we have completed the measurements of the thermal conductivity of some binary and ternary gas mixtures of inert gases in this laboratory, the results of which are being published elsewhere.

TABLE VI

Calculated and experimental values of λ (in 10^{-7} cal.cm $^{-1}$ sec. $^{-1}$ deg. $^{-1}$) for A-He mixture

Temp. °K	Percentage of the lighter component	Experimental values	Calculated	
			Present author	Hirschfelder, Curtiss & Bird
273.16	0.0	389	389	391
	27.04	742	749	755
	45.37	1077	1093	1102
	84.68	2320	2417	2439
	94.61	2939	3011	3046
	100.0	3386	3418	3466

4. DISCUSSION OF RESULTS

Tables IIa, IIb and IIc give the binary viscosities for monatomic-monatomic, monatomic-diatomic, and diatomic-diatomic gaseous mixtures respectively. It is seen that the agreement between theory and experiment is fairly good, being excellent in certain cases. It reveals that the simple theory developed by Chapman and Enskog for monatomic molecules is also fairly successful in accounting for the transport properties of polyatomic molecules and leads to the conclusion that this assumption of the theory is not very severe and can be neglected for most of the work. The small difference observed may be due to slight errors involved in the force constants for like and unlike molecules and the possible errors in the experimental determination of viscosity. In Table III we have given only the calculated values of the binary viscosities for Ne-Kr, Ne-Xe and A-Xe mixtures, as no experiments with these mixtures have yet been performed, and it is quite curious to confirm these predictions of theory.

In Table IV we have reported the calculated values of the coefficient of inter-diffusion for a few gas pairs for which experimental data are available, together with the calculated values of Winter (1949). It is seen that the agreement between the theory and experiment is very good and is somewhat better than that obtained by Winter (1949), who determined the force constants for unlike mole-

cules from those for like molecules by using the empirical relationships, unfortunately a more detailed comparison could not be attempted due to the lack of elaborate experimental data and awaits the determination of $[D_{12}]$ over a wide range of temperatures. Table V gives some of the calculated values of $[D_{12}]$ for these gaseous mixtures at a few temperatures.

The experimental values of thermal conductivity for the A-He gas pair which are listed in Table VI are in better agreement with the theoretical values obtained from using the force constants given in Table I than the calculated values of the Hirschfelder, Curtiss and Bird (1954). The latter investigators assumed the geometric mean rule for c_{12} and the arithmetic mean for r_{12} .

In a previous publication, the author (Saxena 1955a) has reported a detailed comparison of the calculated and theoretical values of the thermal diffusion factor at various temperatures and concentrations for these nine gaseous mixtures and found an excellent agreement. Here again we find a fairly good agreement for the coefficient of binary viscosity, diffusion and thermal conductivity. This elaborate comparison of theory and experiment for non-equilibrium properties proves the realistic nature of the Lennard Jones 12-6 model. This report also provides a good illustration of the use of force constants obtained from one transport property in predicting the other transport coefficients.

ACKNOWLEDGMENTS

The author is thankful to Prof. B. N. Srivastava, D.Sc., F.N.I., for his valuable guidance throughout the progress of the work presented here. This work has been done under a research project financed by the C.S.I.R., New Delhi, to whom the author is deeply indebted for this award.

REFERENCES

- Chapman, S. and Cowling, T. G., 1951. *The Mathematical Theory of Non-uniform Gases*, Cambridge University Press, England.
- Hirschfelder, J. O., Bird, R. B. and Spotz, E. L., 1948. *J. Chem. Phys.*, **16**, 968.
- Hirschfelder, J. O., Bird, R. B. and Spotz, E. L., 1949. *Chem. Rev.*, **44**, 205.
- Hirschfelder, J. O., Curtiss, C. F. and Bird, R. B., 1954. *Molecular Theory of Gases and Liquids*, John Wiley & Sons, Inc., New York.
- Kihara, T., 1949. *Imperfect Gases*, Japanese Asakusa Book Store, Tokyo.
- Landolt-Bornstein, 'Physikalisch-Chemische Tabellen'.
- Mason, E. A., 1954. *J. Chem. Phys.*, **22**, 169.
- Margenau, H., 1939. *Rev. Mod. Phys.*, **11**, 1.
- Saxena, S. C., 1955a. *Ind. J. Phys.*, **29**, 131.
- Saxena, S. C., 1955b. *Ind. J. Phys.*, **29**, 452.
- Saxena, S. C. and Srivastava, B. N., 1955. *J. Chem. Phys.*, **23**, 1571.
- Srivastava, B. N. and Madan, M. P., 1953. *Proc. Phys. Soc. A.*, **66**, 277.
- Van Itterbeek, A., Van Paemel, O. and Van Lierde, J., 1947. *Physica*, **13**, 88.
- Wachsmuth, J., 1908. *Phys. Z.*, **8**, 235.
- Waldmann, L., 1944. *Naturwiss.*, **32**, 223.
- Winter, E. R. S., 1949. *Trans. Far. Soc.*, **46**, 81.

APPENDIX

In a recent paper, the author (Saxena, 1955a) has reported the computed values of the thermal diffusion factor for several gaseous mixtures using an expression obtained on the approximation scheme of Chapman and Cowling (1952). Kihara (1949) has developed an alternative scheme for approximating the transport coefficients and finds $[\alpha]_1$ to be given by an expression of the same form

$$[\alpha]_1 = (6c^* - 5) \frac{(S_1x_1 - S_2x_2)}{(x_1^2Q_1 + x_2^2Q_2 + x_1x_2Q_{12})},$$

but now Q 's are defined in a different fashion.

As Kihara's approximations are known to be more accurate it will be interesting to note the differences in $[\alpha]_1$ values on the two approximation schemes. Calculations show that in all cases Kihara's values of $[\alpha]_1$ are higher than the corresponding Chapman and Cowling values and let us denote the percentage increase by Z (say). In Table VII are listed the Z values for some inert gas mixtures of equal and limiting concentrations of the two components and refer to a temperature of 327°K. It follows from an examination of these figures that Z increase with increasing content of the heavier component, the increase being more in the beginning though the rate of increase differs from mixture to mixture.

TABLE VII

Values of Z for some inert gas mixtures of equal and limiting concentrations of the two components

% of the heavier component	Ne-A	Ne-Kr	Ne-Xe	A-He	A-Kr	A-Xe
10	2.1	2.3	5.0	3.1	1.6	1.8
50	4	6	9.0	9.8	3.6	5.1
90	6.2	10	11	13	5.8	7.8

TABLE VIII

Values of Z for some inert gas mixtures at a few temperatures

Temp. °K	Ne-A	Ne-Kr	Ne-Xe	A-He	A-Kr	A-Xe	Kr-Xe
117	2	5.8	-	10	—	—	—
185	4.1	6.2	8.2	10	2.8	2.9	—
404	5.0*	7.4	8.5	10	4.0	5.6	3.3
585	5.0*	—	8.5	—	4.2	5.8	—

*These values refer to temperatures 736°K and 1167°K. respectively.

Values of Z for some inert gas mixtures of approximately 50-50 mole percent of the components are listed in table VIII. It follows from an inspection of this table that Z is also somewhat temperatures-dependent, though it tends to a limiting value at high temperatures and varies rapidly at low temperatures.

EMISSION SPECTRA OF MIXED HALOGENS PART I: ICl

P. B. V. HARANATH AND P. TIRUVENGANNA RAO

PHYSICS DEPARTMENT, ANDHRA UNIVERSITY, WALTAIR

(Received for publication, August 14, 1956)

Plates IV A&B

ABSTRACT. The emission spectrum of ICl, as excited in a condensed discharge from a 20 KV. transformer and in a high frequency discharge from a 100 watt oscillator, is photographed on different instruments from the visible down to the vacuum ultraviolet. The spectrum excited in condensed discharge revealed a new system of discrete bands, about 300 in number, in the region from $\lambda 1100$ to $\lambda 3800$. Vibrational analysis of these bands has led to the following quantum formula

$$\begin{aligned} \nu &= 23997.0 + 173.2(\nu' + 1/2) - 1.1\nu' + 1/2; \\ &- 209.7(\nu'' + 1/2) + 1.9(\nu'' + 1/2) \end{aligned}$$

From the equality of the vibrational constants, the lower state of this system is identified as the $^3\Pi_1$ state of the near infrared absorption bands of ICl. A study of the chlorine isotopic effect for some of the bands on the short wavelength end of the spectrum is also made.

Spectra photographed in the vacuum ultraviolet region on an one metre normal incidence vacuum grating spectrograph, revealed two systems in the region $\lambda 1910$ to $\lambda 1670$, known earlier in absorption. Vibrational analyses of these systems proposed earlier, are extended to include some more new bands obtained in emission.

INTRODUCTION

Numerous investigations have been carried out in the absorption spectra of the mixed halogen molecules ICl, IBr and BrCl by different workers Cordes and Sponer (1932), Brown and Gibson (1932), Brown (1932), Darbyshire (1932), Mulliken (1934) and others. A band system in the near infrared region, both in ICl and IBr, in absorption, was interpreted as due to a transition from the normal state $^1\Sigma^+$ to an upper $^3\Pi_1$ state. In addition to this, transitions from ground state to two other upper states $^3\Pi_0$ and 0^+ , in each of the two molecules, were also found to give rise to two band systems in the visible region. The potential energy curves of the latter two states intersect with each other giving rise to predissociation in the visible bands. After intersection, the 0^+ state dissociates into normal $^2P_{3/2}$ iodine atom and an excited $^2P_{1/2}$ chlorine atom while the $^3\Pi_0$ dissociates into normal atoms.

Each of the three molecules ICl, IBr and BrCl gives rise to two sets of absorption continua, one in the visible region and the other in the quartz ultraviolet region. These continua were interpreted as due to the transitions from stable normal state to different repulsive upper states. In the vacuum ultraviolet region, two systems were reported and analysed in the absorption spectra of all the three molecules by Cordes and Spomer (1932). The lower states of these systems were identified as the normal state of the molecule while the upper states were interpreted as belonging to Ω, ω coupling type.

Our knowledge of the emission spectra of the three molecules is rather meagre. While exciting ICl vapour in the presence of nitrogen in fluorescence and high frequency discharges, Fillipov (1928) obtained a single band with intensity maximum at $\lambda 4350$. Similarly, when a mixture of nitrogen and IBr vapour was excited in the high frequency discharge, four maxima at $\lambda 4120$, 3860, 3455 and 3045, and in fluorescence some diffuse bands at about $\lambda 2000$, were observed.

Recently, Asundi and Venkateswarulu (1947) studied the excitation of ICl and IBr vapours in an uncondensed discharge from a transformer. In both cases they obtained a number of broad diffuse bands. In the case of ICl a broad continuous band extending from $\lambda 5640$ to $\lambda 5120$ and a series of diffuse bands in the region lying between $\lambda 4800$ to $\lambda 3700$ were observed. In IBr also they reported similar diffuse bands in the region from $\lambda 5200$ to $\lambda 2300$. The lower states of all these diffuse bands, observed in emission were interpreted by them as repulsive states arising from the combinations of either neutral or excited atoms. The upper states were tentatively suggested as the upper stable electronic levels of the two vacuum ultraviolet band systems observed in absorption by Cordes and Spomer (1932) in each case.

In the course of our attempts to excite the spectra of mixed halogens, it has been found possible to excite new characteristic spectra of ICl and IBr in the visible region. The present paper deals with the results of investigation on ICl molecule, while those in the case of IBr and BrCl are proposed to be discussed in a subsequent communication. A preliminary report of the results obtained in the case of ICl and IBr has already appeared in *Current Science* (1956).

EXPERIMENTAL

The emission spectrum of ICl is excited both in a condensed discharge from a 20 k.w. transformer and in a high frequency discharge from a high power oscillator (100 watts). A pure Merck sample of liquid iodine monochloride, dark-brown in colour, is used in these investigations. When the spectrum is excited in the transformer discharge, the discharge tube employed is made of an ordinary pyrex glass tube of length 30cm. and diameter 20mm. drawn into an adaptor at one end through which it could be evacuated by a system of evacuating pumps.

The other end of the discharge tube is closed with either a quartz or a fluorite window. Two tungsten electrodes are fused into two vertical side tubes of the main discharge tube. The substance is contained in a small bulb which is attached by pressure tubing to a side tube provided near the window of the main discharge tube. The vapour pressure of the substance could be regulated by controlling a pinch-cock fitted to the pressure tubing. The discharge tube is continuously evacuated through one or two liquid air traps by single stage Edwards oil diffusion pump backed by a Cenco Hyvac pump. A large glass condenser of capacity 1.3×10^{-3} mfd. is connected across the two secondary terminals of the high tension transformer. Different high secondary voltages are applied to the two tungsten electrodes of the discharge tube through an auxiliary spark gap included in series in the secondary circuit. As the width of the spark gap is adjusted, it is found that an intense greenish-blue emission due to the atomic line spectra of iodine and chlorine fills the central portion of the discharge tube. When the pressure of ICl vapour is regulated through the pinch-cock, a characteristic bluish emission, weaker in intensity, surrounds the intense line discharge. This characteristic glow, which is of molecular origin, has been photographed when different high voltages are applied across the electrodes and also under various pressure conditions of ICl vapour inside the discharge tube.

In the visible region, spectra are photographed on Fuess and Hilger three-prism glass Littrow spectrographs using Ilford Special Rapid Panchromatic plates. Exposures varying from 5 to 15 minutes are found adequate for good reproductions of the spectra. In the ultraviolet region Hilger medium quartz instrument is employed to photograph the spectrum on Ilford Special Rapid plates. An one metre normal incidence vacuum grating spectrograph having a uniform dispersion of $17.3\text{\AA}^\circ/\text{mm.}$ is employed to record the spectrum in the fluorite region. On this instrument exposures of one to two hours' duration are given on Ilford Q₂ plates. In this region wavelengths of band heads are deduced, taking iodine lines as the internal standards.

When the spectrum of ICl is excited in the high frequency discharge from a 100-watt oscillator, a discharge tube made of pyrex glass of length 30 cm. and diameter 20 mm. drawn into an adaptor at one end and carrying a small side tube at the other flat end is taken. The flat end is closed again either by quartz or fluorite window and the container of the substance is attached to the side tube by pressure tubing. From the adaptor side the discharge tube is continuously evacuated through a liquid air tower by the same system of vacuum pumps. When the R. F. voltage from the oscillator is applied by means of external electrodes bent round the discharge tube, an intense bluish emission, free from all impurities, is observed. This emission is photographed on the same instruments referred to above.

RESULTS

The emission spectrum of ICl as excited in a condensed discharge, consists of a large number of bands in the visible region from $\lambda 4400$ to $\lambda 3800$, in addition to some of the bands belonging to the well known visible systems observed in absorption above $\lambda 5500$. The general appearance of this system taken on Fuess instrument is shown in Plate IVA. To make sure that the emitter of these bands is ICl, the spectra of I_2 and ICl in the region from $\lambda 6400$ — 3800 are reproduced in this plate in juxtaposition. It can be seen that there is an overcrowding of bands on the longer wavelength side and a general fall of intensity towards the short wavelength end. A distinct feature of the spectrum is the occurrence of equispaced prominent red-degraded bands whose intensity gradually falls from longer to shorter wavelengths. Photographs of the spectra taken on the Littrow instrument are reproduced in Plate IVB which correspond to the spectra taken at two different secondary voltages, 10 KV, and 20 KV, respectively. It can be seen from Plate IVB, corresponding to 20 k.v. the bands in the spectrum appear better resolved than in that reproduced in Plate IVB, corresponding to 10 KV. A few more atomic lines also make their appearance in the higher voltage spectrum. In all, about 300 bands have been measured in the region between $\lambda 4400$ to $\lambda 3800$.

In the quartz ultraviolet region, no discrete bands are recorded, but only some of the continuous bands reported earlier by Asundi and Venkateswarulu (1947) are observed. In the vacuum ultraviolet region two systems are observed in the region between $\lambda 1910$ to $\lambda 1670$. These are found to be identical with those obtained by Cordes and Sponer (1932) in absorption. In the present emission pictures some more additional bands belonging to both the systems are obtained. The two systems are reproduced in Plate IVB. Due to self absorption, some of the emission bands appear like absorption bands.

The spectra excited in the high frequency discharge from the 100 watt oscillator reveal the above two systems in the vacuum ultraviolet and a number of continuous bands in the visible and quartz ultraviolet regions, known earlier to occur in the spectrum excited in an uncondensed discharge. The extensive system of discrete bands in the visible region reported, as occurring in the condensed discharge, is absent in this source.

VIBRATIONAL ANALYSIS

New system in the region $\lambda 4400$ to $\lambda 3800$

This system consisting of about 300 bands is not previously reported either in emission or in absorption. Table I illustrates the band head data along with their intensities and assignments. The bands are measured on the plates taken on the higher depression of $7A^\circ/\text{mm.}$ at $\lambda 4000$ of a Hilger throe prism glass Littrow instrument. Under the dispersion of this instrument, the bands appear well resolved.

TABLE I

Wave-length	Wave-number	Int	Assignment ν' , ν''	Wave-length	Wave-number	Int	Assignment ν' , ν''
4424.3	22596	1	4, 10	4339.0	23040	2	
4395.7	22743	0	8, 13	4337.6	23048	2	
4393.6	22754	1	6, 11	4336.4	23054	5	10, 13
4392.8	22758	0	1	4335.1	23064	6	9, 12
4392.0	22762	1	5, 10	4332.6	23074	4	8, 11
4390.3	22771	2	4, 9	4330.4	23086	5	7, 10
4388.2	22782	2	3, 8	4328.9	23094	4	
4385.7	22795	2	2, 7	4327.6	23101	5	6, 9
4383.6	22806	2	1, 6	4325.0	23115	7	5, 8
4381.6	22816	0	1	4323.1	23125	3	1
4379.7	22827	3	0, 5	4322.1	23130	7	4, 7
4377.8	22836	1		4320.8	23137	4	
4374.5	22853	1		4318.8	23148	7	3, 6
4372.1	22866	2		4316.5	23160	3	1
4370.6	22874	3	12, 16	4314.5	23169	6	2, 5
4368.8	22883	3	11, 15	4312.3	23183	2	1
4367.3	22891	3	10, 14	4310.8	23191	7	1, 4
4365.8	22899	2	8, 13	4308.4	23204	4	1
4364.2	22907	3	8, 12	4306.5	23214	8	0, 3
4360.9	22925	2	6, 10	4304.3	23226	2	1
4358.4	22938	3	5, 9	4303.4	23231	6	9, 11
4356.3	22949	4	4, 8	4301.6	23241	3	1
4353.6	22963	1	3, 7	4300.7	23245	3	8, 10
4352.4	22969	2		4298.0	23260	6	7, 9
4350.3	22980	6	2, 6	4296.2	23270	3	1
4348.6	22989	3	1	4294.3	23280	3	6, 8
4346.9	22998	4	1, 5	4292.7	23289	1	1
4341.3	23028	2		4291.5	23295	4	5, 7
4344.1	23013	2	1	4289.6	23306	3	1
4343.0	23019	5	0, 4	4287.8	23315	6	4, 6
4340.2	23034	2	1	4286.1	23315	2	1

TABLE I (Contd.)

Wave-length	Wave-number	Int.	Assign- ment ν' , ν''	Wave-length	Wave-number	Int.	Assign- ment ν' , ν''
4284.5	23333	1		4206.8	23764	3	
4283.6	23338	5	3, 5	4204.4	23778	5	8, 7
4281.8	23348	2	i	4202.3	23790	8	1, 1
4280.1	23357	1		4200.5	23800	6	7, 6
4279.2	23362	5	2, 4	4196.2	23824	10	0, 0
4277.5	23372	2	i	4195.2	23830	5	6, 5
4276.3	23378	2		4189.7	23861	6	5, 4
4274.6	23387	6	1, 3	4188.7	23867	3	
4273.1	23396	2	i	4186.7	23878	3	11, 9
4272.0	23402	2	0, 10	4184.6	23890	4	4, 3
4269.7	23414	8	0, 2	4182.2	23904	4	10, 8
4268.6	23420	3	8, 9	4178.4	23926	4	3, 2
4266.6	23431	2		4177.2	23933	3	9, 7
4264.8	23441	4	7, 8	4175.3	23944	3	
4263.8	23447	2		4172.4	23960	5	2, 1
4261.7	23453	5	6, 7	4171.7	23964	4	8, 6
4258.9	23474	2		3170.2	23973	5	22, 18
4257.7	23480	4	5, 0	4169.2	23979	6	14, 11
4253.2	23505	5	4, 5	4167.4	23989	7	7, 5
4248.0	23529	3	3, 4	4166.4	23995	9	1, 0
4244.0	23556	4	2, 3	4164.7	24004	3	13, 10
4242.4	23565	4		4161.4	24021	4	6, 4
4240.4	23576	4		4160.4	24020	3	12, 9
4238.6	23586	5	1, 2	4159.6	24034	4	
4233.2	23616	7	0, 1	4158.3	24041	4	
4229.0	23640	3	6, 6	4156.3	24053	2	18, 14
4226.3	23655	3		4155.6	24057	3	5, 3
4220.8	23685	2		4154.3	24065	2	
4215.3	23716	2		4152.3	24076	3	17, 13
4213.6	23726	5	3, 3	4150.4	24087	3	10, 7
4209.5	23749	2		4149.5	24091	5	4, 2
4208.1	23757	6	2, 2	4148.2	24100	4	16, 12

TABLE I (Contd.)

Wave-length	Wave-number	Int	Assign-ment w', w''	Wave-length	Wave-number	Int.	Assign-ment v', v''
4146.8	24108	3	23,18	4108.7	24332	3	1
4145.6	24116	4	9, 6	4108.1	24335	8	3, 0
4144.7	24120	5	15,11	4107.3	24340	4	
4144.1	24124	2	1	4106.4	24345	6	8, 4
4143.0	24130	4	3, 1	4105.6	24350	4	19,13
4141.8	24137	2		4104.4	24357	4	13, 8
4141.1	24141	6	21,16	4103.1	24365	4	25,18
4139.9	24148	6	14,10	4101.3	24376	5	18,12
4139.1	24153	6	8, 5	4100.6	24380	3	7, 3
4137.9	24160	5	20,15	4098.7	24391	2	12, 7
4137.1	24165	9	2, 0	4096.7	24403	3	23,16
4135.9	24172	1		4095.7	24400	2	17,11
4134.7	24179	6	13, 9	4094.0	24419	1	6, 2
4133.8	24184	5	7, 4	4093.2	24424	3	11, 6
4133.0	24189	6	19,14	4092.2	24430	3	22,15
4129.7	24208	5	12, 8	4090.8	24438	4	16,10
4129.1	24212	3	1	4089.9	24444	1	j
4128.2	24217	6	6, 3	4088.8	24450	2	i
4126.6	24226	4		4088.0	24455	1	21,14
4124.9	24236	1	24,18	4087.0	24461	5	5, 1
4124.1	24241	5	11, 7	4085.3	24471	4	15, 9
4122.5	24250	7	23,17	4084.8	24474	2	1
4121.3	24257	4	5, 2	4083.3	24483	5	20,13
4119.8	24266	2	16,11	4082.2	24490	3	1
4118.9	24271	4	10, 6	4080.6	24499	5	9, 4
4117.7	24279	2		4079.8	24504	7	4, 0
4116.4	24286	2	1	4078.5	24512	3	19,12
4114.9	24295	5	4, 1	4076.2	24526	2	1
4113.2	24305	3	9, 5	4075.3	24531	4	24,16
4111.2	24317	1	1	4073.6	24541	4	8, 3
4110.4	24322	4	20,14	4072.7	24547	0	1
4109.6	24326	4	14, 9	4070.6	24559	2	23,15

TABLE I (Contd.)

Wave-length	Wave-number	Int.	Assign-ment v', v''	Wave-length	Wave-number	Int.	Assign-ment v', v''
1070.6	24559	2	23, 15a	4024.8	24839	2	i
1068.1	24575	2	12, 6	4023.6	24846	2	24, 14
1067.3	24579	4	7, 2	4022.9	24851	3	10, 3
1066.2	24586	2	22, 14	4021.8	24857	3	10, 10
1064.2	24598	4	27, 18	4020.9	24863	2	
4062.7	24607	2	i	4019.5	24872	3	14, 6
4061.7	24613	4	11, 5	4018.4	24878	2	23, 13
4060.1	24623	5	6, 1	4016.8	24888	0	
4058.2	24634	2	i	4015.7	24895	2	9, 2
4056.9	24642	3	i	4012.7	24914	3	13, 5
4056.0	24648	3	15, 8	4009.0	24937	2	17, 8
4054.8	24655	4	10, 4	4005.4	24959	2	12, 4
4052.7	24668	7	5, 0	4004.2	24967	1	i
4051.2	24677	2	10, 11	4002.4	24978	3	16, 7
4049.5	24687	2	14, 7	4001.2	24985	0	i
4048.3	24695	3	9, 3	4000.6	24989	5	7, 0
4046.1	24708	2	i	3997.7	25007	4	11, 3
4044.3	24719	1	18, 10	3996.0	25018	3	15, 6
4043.3	24725	4	13, 6	3994.5	25027	2	i
4042.1	24733	1	i	3993.8	25032	4	19, 9
4040.9	24740	2	8, 2	3992.7	25039	2	i
4039.7	24747	2	22, 13	3990.9	25050	4	10, 2
4038.5	24755	1		3989.9	25056	2	
4036.8	24765	3	12, 5	3989.1	25061	3	14, 5
4034.7	24778	2	i	3986.7	25076	3	18, 8
4033.7	24784	2	7, 1	3985.8	25084	1	i
4031.8	24796	2	16, 8	3984.1	25093	1	i
4029.3	24811	2	11, 4	3981.8	25071	3	13, 4
4028.5	24816	2	25, 15	3980.5	25115	2	21, 10
4026.4	24829	6	6, 0	3979.9	25119	2	17, 7
4025.4	24835	2	15, 7	3979.3	25123	2	i

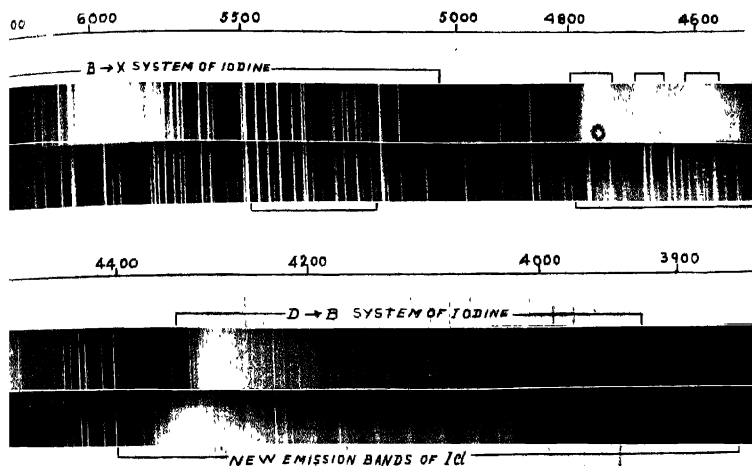
TABLE I (Contd.)

Wave-length	Wave-number	Int.	Assign- ment v', v''	Wave-length	Wave-number	Int.	Assign- ment v', v''
3977.7	25133	2	i	3954.3	25282	2	
3976.6	25140	1		3952.7	25292	4	21, 9
3975.3	25148	4	8, 0	3950.8	25304	4	9, 0
3974.2	25155	2	12, 3	3949.2	25314	1	i
3973.2	25161	1	16, 6	3947.4	25326	1	i
3970.9	25170	0	i	3945.5	25338	4	20, 8
3969.5	25185	0	i	3943.1	25354	2	12, 2
3968.7	25190	0		3939.0	25374	3	23, 10
3966.6	25203	5	11, 2	3937.8	25388	0	
3965.8	25208	2	15, 5	3936.2	25398	1	15, 4
3964.0	25220	1	i	3935.1	25405	2	11, 1
3963.1	25226	1	i	3934.0	25414	0	i
3961.0	25239	0		3931.8	25426	0	i
3960.1	25245	2	22, 10	3929.5	25441	2	18, 6
3958.9	25252	3	10, 1	3926.8	25450	3	10, 0
3957.3	25263	3	18, 7	3925.0	25470	3	21, 8
3955.5	25274	0	i				

Note — The isotopes of the neighbouring bands are marked by the letter (i) in the assignment columns.

The clearly red-degraded prominent bands marked on the reproduction, Plate IVB represents unambiguously a long progression which served as the starting point in the analysis. The order of $\Delta G(v)$ intervals between successive bands in this progression is 170 cm^{-1} and does not appear to coincide with any of the known frequencies of the low excited states of ICl. This suggests the probability that the above progression may be an upper state progression. Some of the fainter bands lying on the long wavelength side of the prominent bands are regarded as sequence members. On this basis, an analysis could be built up with the order of vibrational frequencies of 170 and 210 cm^{-1} for ω'_e and ω''_e respectively. This analysis is displayed in Table II. It can be seen from this table that the prominent bands belong to the v' progression with $v'' = 0$. Most of the bands could be fitted in the scheme. The $\Delta G(v)$ values corresponding to the difference between any two consecutive vibrational levels of either of the two states are found to be consistent throughout the scheme. These differences are also found

BARATH & RAO

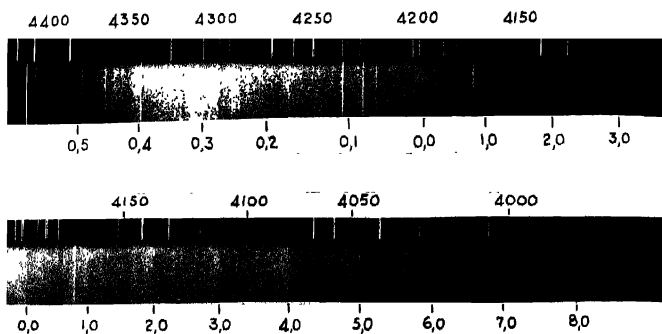


Emission spectra of I_2 and ICl excited in condensed discharge under identical conditions
Fuess spectrograms.

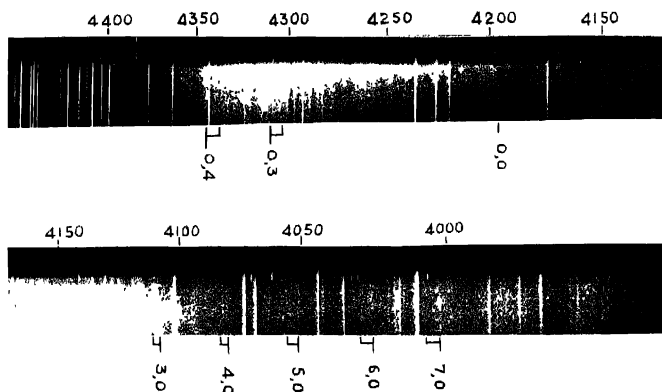
a_1, a_2 — Iodine

b_1, b_2 — ICl .

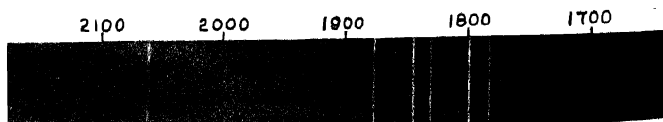
HARANATH & RAO



New emission bands of ICI at 10 kV.
 Littrow Spectrograms



New emission bands of ICI at 20 kV.
 Littrow Spectrograms



Vacuum ultraviolet bands of ICI
 Grating Spectrogram.

TABLE II
Vibrational analysis of ICl emission bands in the region $\lambda \pm 400$ to $\lambda 3900$

v''	0	1	2	3	4	5	6	7	8	9	10	11	12	13	14	15	16	17	18 $\Delta G(v')$
0	23824	23616	23414	23214	23019	22827													172
1	23995	23780	23566	23362	23169	22980	22795												170
2	24165	23960	23757	23556	23362	23178	22990	22795											169
3	24335	24130	23926	23726	23529	23338	23148	22963	22782										167
4	24504	24295	24092	23890	X	23695	23505	23315	23130	22949	22771	22596							165
5	24668	24461	24257	24057	23861	X	23670	23480	23295	23115	22938	22762							163
6	24829	24623	24419	24217	24021	23830	23640	23458	23280	23101	22925	22754							161
7	24989	24784	24579	24380	24184	23989	23800		23641	23460	23286	X							160
8	25148	24940	24740	24541	24345	24153	23964	23778		23620	23445	23264	22907	22743					155
9	25304	X	24895	24695	24499	24305	24116	23933		23741	23554	23364	23064	22898					153
10	25459	25252	25050	24851	24655		24463	24271	24087	23904			22883	22891	23054	22891			151
11	25605	25405	25203	25007	24811	24613	24424	24241	24058				22874						149
12		25554	25354	25155		24959	24765	24575	24391	24208	24029								146
13					25107	24914	24725	X	24557	24379	24204								141
14						25061	24872	24687	24504	24326	24148	23979							143
15					25398	25208	25018	24835	24648	24471		X							142
16							25161	24978	24796	24613	24438	24266	24100						142
17								25119	24937		24766	24609		24076					140
18							25441	25263	25076	24895	24719	24576	24409	24276					137
19										25032	24857	24677	24512	24350	24189				137
20								25338								24141			132
21								25470	25292	25115									131
22										25245									129
23											25574								128
24																			128
25																			129
26																			24816
27																			24481
																			24598
$\Delta G(v')$	206	224	199	196	193	189	184	181	178	175	171	166	163	162	158	156	153	145	

Note. The places marked with (X) are superseded by atomic lines. The bands given in figures occur twice

to fall regularly with increasing vibrational quanta. The following vibrational formula is found to represent most of the bands.

$$\nu = 23997.0 + 173.2(v' + 1/2) - 1.1(v' + 1/2)^2 \\ - 209.7(v'' + 1/2) + 1.9(v'' + 1/2)^2.$$

From equality of the vibrational constants, the lower state of this system is identified as the $^3\Pi_1$, upper state of the near infrared absorption bands of ICl.

In systems of this type, involving higher vibrational quantum numbers, it is natural to expect the chlorine isotope effect, at least for some of the favourable bands. The evidence of the chlorine isotope effect can be seen clearly for some of the bands lying on the short wavelength end of the spectrum taken on the Hilger glass Littrow instrument, (Plate IVB). The isotope separations to be expected for the molecule ICl^{35} and ICl^{37} are calculated from the usual formula

$$\nu' - \nu'' = (\rho - 1)[\omega_e' (v' + \frac{1}{2}) - \omega_e'' (v'' + \frac{1}{2})] - (\rho^2 - 1)[x_e' \omega_e' (v' + \frac{1}{2})^2 - x_e'' \omega_e'' (v'' + \frac{1}{2})^2].$$

Bands for which $\nu < \nu_r$, the isotope head due to the less abundant molecule ICl^{37} lie on the longer wavelength side of the main band head due to the more abundant

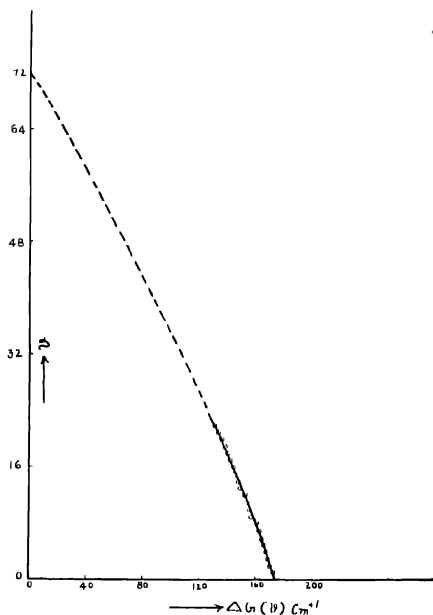


FIG. 1 $\Delta G(v) - v$ Curve of the upper state.

molecule ICl^{35} . For bands lying on the long wavelength side of the system origin ($v < v_e$), the isotope component falls towards the shorter wavelength side of the main head. The isotope heads are detected for about seventy bands. The agreement between the observed and calculated separations can be seen from Table III

The intensities of the bands shown in vibrational matrix, Table IV, are visual estimates on an arbitrary scale of 0 to 10. It is seen that the locus of the bands of maximum intensity is a Condon parabola of the type to be expected for such values of ω'_e and ω''_e as 173.2 and 209.7 cm^{-1} respectively.

In figure 2 are drawn the potential energy curves for the lower and upper states of the above new system. The curves are drawn by using the wellknown Morse's relation. Since the lower state of this system is identified as the $^3\Pi_1$ state,

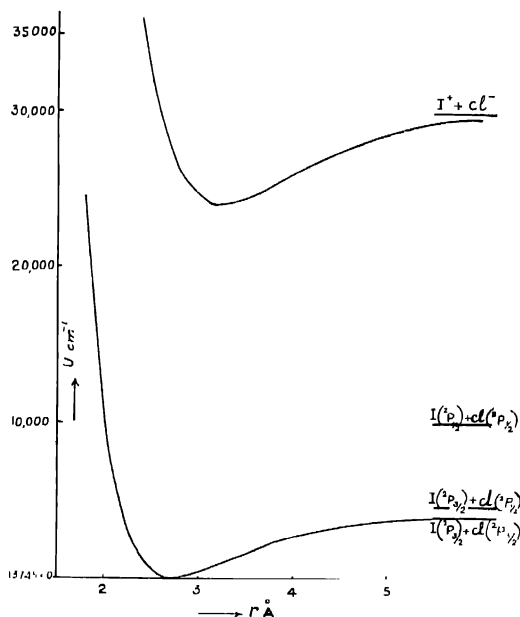


Fig. 2. Potential energy curve of ICl .

the constants B_v , x_e , ω_e , r_e and D_e are taken from the vibrational and rotational analysis of the $^3\Pi_1$ state of the near infrared absorption bands, by previous workers. For the upper state, the value $D_e = 6480 \text{ cm}^{-1}$ is extrapolated graphically by drawing the $\Delta G(v) - v$ curve, (figure 1). The r_e value which is approximately

TABLE III
Isotope effect of ICl bands

I^{127} ν'	Cl^{35} ν''	I^{127} Cal.	Cl^{37} Obs.	I^{127} ν'	Cl^{35} ν''	I^{127} Cal.	Cl^{37} Obs.
10, 0		31.6	33	8, 4		9.6	13
9, 0		28.8	30	2, 4		9.5	10
8, 0		25.9	25	1, 4		13.0	13
7, 0		23.0	22	0, 4		16.7	15
6, 0		19.9	18	15, 5		24.1	23
5, 0		16.8	13	11, 5		14.3	15
4, 0		13.6	14	14, 5		21.8	22
3, 0		12.2	13	3, 5		9.8	10
2, 0		6.8	5	2, 4		13.2	14
11, 1		30.0	31	1, 5		16.7	15
10, 1		27.3	26	0, 5		20.4	*
7, 1		18.7	19	18, 6		26.9	27
6, 1		15.6	16	13, 6		15.9	17
5, 1		12.5	11	9, 6		5.3	5
4, 1		9.3	9	4, 6		9.9	10
3, 1		5.9	6	3, 6		13.8	12
12, 2		28.4	28	2, 6		16.7	18
11, 2		25.8	27	1, 6		20.2	21
10, 2		23.1	23	15, 7		17.2	19
9, 2		20.3	17	5, 7		10.1	11
8, 2		17.4	15	3, 7		16.7	17
7, 2		14.5	*	2, 7		20.1	21
6, 2		11.4	10	20, 8		24.2	24
5, 2		8.3	7	16, 8		16.3	18
0, 2		8.0	6	15, 8		14.1	14
12, 3		24.4	22	6, 8		10.1	99
11, 3		21.8	22	5, 8		13.2	10
10, 3		19.1	22	14, 9		8.7	9
9, 3		16.3	16	7, 9		10.1	10
8, 3		13.4	15	22, 10		21.8	25
6, 3		7.4	5	19, 10		16.5	18
5, 3		4.3	4	9, 11		9.7	10
1, 3		9.2	9	22, 13		14.3	14
0, 3		12.9	12	20, 13		10.8	9
13, 4		23.1	23	8, 13		17.5	15
12, 4		20.6	22	21, 14		10.5	10
10, 4		15.3	13	23, 15		11.6	12

Note—The components marked with * are superposed by atomic lines.

TABLE IV
Intensity distribution of ICl bands ($\lambda 4400$ to $\lambda 3800$)

	0	1	2	3	4	5	6	7	8	9	10	11	12	13	14	15	16	17	18	19
10	10	7	8	8	5	3														
9	10	8	5	6	7	4	2													
8	9	5	6	4	5	6	6	2												
7	8	4	4	5	3	5	7	4	2											
6	7	5	5	4		5	6	7	4	2										
5	7	5	4	3	6		4	4	7	3	1									
4	6	5	4	6	4	5	3	5	3	5	2	1								
3	5	2	4	4	5	7	6		4	6	5									
2	4		2	4	6	6	5	5		3	3	4	3	0						
1	4		2	3	5	3	4	3					6	6	2					
0	3	3	4	3	4		4	3	4					5	3					
		2	2	4	2	4	3	5		3						3				
			2	2		3	2	2	5	3							3			
					3	3	4		4	6	3									
					3	3	2	2	4	0	6									
					1	2	3	2	3	4			5							
							1	3	2		4	2	4							
							2	2				2								
							2	3	3		1		5	3		2				
										4	3	2	3		4	6				
									4					5	4	5				
									3	4	2				1		6			
										2								5		
										2				2	3				3	
										3				2	2	3	7		4	
															2				4	
																2				4

TABLE V
Vibrational analysis of ICl bands in the region $\lambda 1910$ — $\lambda 1800$

ν	0	1	2	3	4	5	6
1	53478 380 (53478) 436	53098 378 (53096)	52720 378 (52723)	52342 (52341) 434			
1	53914 (53910) 429			(52776) 426			
2	54343 (54343) 426			(53202)			
3	54769 378 (54770) 419	(54391) 407			(53250)		
4	55188 390 (55185) 416	54708 383 (54798)	(54415) 375	(54040)			
5	55604 382 (55604)	55222 382 (55225) 420	54840 (54840) 421		(54107)		(53347)
6		55042 381 (55640)	55261 378 (55263)	54883 373 (54885) (55293) 370	(54510) 365 (54023)	(54145)	

Note.—The bands bracketed are newly obtained in the present work.

The bands unbracketed belong to Cordes and Sponer's data.

Letters to the Editor

The Board of Editors will not hold itself responsible for opinions expressed in the letters, published in this section. The notes containing reports of new work communicated for this section should not contain many figures and should not exceed 500 words in length. The contributions must reach the Assistant Editor not later than the 15th of the second month preceding that of the issue in which the Letter is to appear. No proof will be sent to the authors.

3

STUDY OF RECTIFYING CHARACTERISTICS OF FeS_2 AND GERMANIUM POINT CONTACT RECTIFIERS

J. N. DAS

COLLEGE OF SCIENCE, RAIPUR

(Received for publication, November 20, 1956)

Commercially available germanium diodes OA70, OA71, OA74, OA54 and cleaved pieces of FeS_2 crystals with uniform surface were used. Base of the FeS_2 crystals were ground flat and embedded in wood's alloy to establish non-rectifying large area base contact. Pointed tungsten whiskers of 2 to 3 mil diameter were used as metallic point contacts on the crystal surface. The D. C. characteristics of the points were determined with the help of a vacuum tube voltmeter and a multi-range microammeter, after examining them by a C.R.O. in the usual way.

To detect the presence of photo injection with or without bias, the contact was illuminated by a small spot of white light of area 0.01 sq. mm. and the changes in the current were noted by a galvanometer. A typical D.C. characteristics is shown in the figure 1.

The values of the contact potential difference ϕ , and of spreading resistance R_s were determined from the graph by following the method indicated by Gibson (1952); while α was determined from the slope of $\ln(i) - (V_a - iR_s)$ graph. The typical values of ϕ , R_s and α so obtained are shown in Table I.

In the case of FeS_2 no change in current due to illumination was observed.

In the data the value of α is observed to depend on ϕ and is lower for points with high ϕ . A similar observation on galena has been reported earlier by the author and his coworkers (Das 1956). Further the observed values of ϕ are found to vary over the crystal surface and in general are high for FeS_2 than for germanium.

The observations could be explained by taking into consideration the effect produced by trapped immobile electrons in the surface states together with the

TABLE I

Crystal	ϕ volts	R_s ohms	α	Temperature °C
FeS ₂				
IW	0.24	403	30.0	28.0
IIW	1.15	596	9.0-3.2	27.4
IIIW	0.79	563	± 0	27.2
VW	0.40	351	19.0	27.2
VI W	0.32	688	30.0	28.4
Germanium				
OA70	0.22	113.5	29.0	27.2
OA71	0.23	173.0	27.0	27.2
OA74	0.21	126.0	33.0	26.8
OA74	0.17	134.0	42.0	27.2

Results obtained from experiments on photo injection are shown in Table II.

TABLE II

Crystal	Reverse direction current on application of bias	Change in reverse direction current on illumination of contact	Contact pot. diff. inferred from C.R. O. trace
FeS ₂ W contact	20—60 μ A	0.1 μ A	0.5 volts
Ge Rectifiers	6.0 μ A	0.4 μ A	0.2-0.3 volts

usual barrier at metal semi-conductor contact. In the region where the density of trapped electrons is high strong repulsive field for approaching electrons can be assumed to be present, and as a consequence, points situated in this region have a higher contact potential difference. Hence, in general, assuming a certain transmission co-efficient for the electrons that cross the barrier into the metal at the contact, the diffusion equation of Mott (1948) can be written as

$$j = \beta nev F - De \cdot dn/dx \quad \dots (1)$$

which gives

$$j = \beta nev F \cdot \exp. - \beta e \phi / kT (\exp \beta e V / kT) \quad \dots (2)$$

$$\text{and } \alpha = \beta e / kT.$$

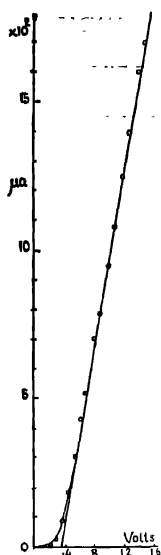


Fig 1. Forward current voltage characteristics of a typical point contact rectifier

where j = current density, β = transmission co-efficient < 1 , k = Boltzmann constant, e = electronic charge, v = mobility of current carriers, D = diffusion constant, V = the voltage across the barrier. To explain the data presented above, β has to vary between 1 and $1/5$ or so.

REFERENCES

- Bhide, V. G., Das, J. N. and Khandekar, P. V., 1956, *Phys. Soc.*, **69B**, 245.
- Gibson, A. F., 1952, *Proc. Phys. Soc.*, **65B**, 196.
- Mott, N. F. and Gurney, R. W., 1948, *Electronic Processes in Ionic Crystals*, Oxford University Press, 183.

NEW EMISSION SPECTRUM OF CHLORINE IN THE SCHUMANN REGION

P. B. V. HARANATH AND P. TIRUVENGANNA RAO

(Received for publication, August 8, 1956)

Following our work on the emission spectra of the halogen molecules I_2 (Haranath & Rao, 1956) and Br_2 (Haranath & Rao, 1956) the emission spectrum of chlorine as excited in high frequency discharge from a 100 watt oscillator was photographed in the Schumann region using an one metre normal incidence vacuum grating spectrograph having a dispersion of 17.3 \AA/mm . Two new extensive band systems were observed, one lying in the region $\lambda 1820$ to $\lambda 1630$ and the other in the region $\lambda 1630$ to $\lambda 1400$.

The first system consists of about 70 bands occurring in different groups. Some of these groups on the longer wavelength side consists of line-like bands lying close to each other, while the bands belonging to the other groups on the short wavelength side appear red degraded. The second system in the region $\lambda 1630$ to $\lambda 1400$ consists of about 80 bands some of which are very intense and are clearly degraded towards red. These bands are found to belong to a few prominent progressions, being separated by a wavenumber interval of 460 cm^{-1} , which is roughly equal to the vibrational frequency of the upper state. The vibrational constants of these two systems are given in Table I, which also contains

TABLE I

Stable electronic levels so far observed in the spectrum of neutral chlorine molecule :

Position of the level, cm^{-1}	Designation	Frequency	Remarks
75000	O	—	A number of continuous bands in the region $\lambda 2565$ — $\lambda 1850$ arise in the levels 0 and 1 and have their lower levels, low repulsive states, (Venkateswarulu, 1947).
67700	I	—	
63975	J	460	J—X gives emission bands in the region $\lambda 1630$ to $\lambda 1400$ analysed in the present work.
58250	H	208	H—X gives emission bands in the region $\lambda 1820$ to $\lambda 1630$ analysed in the present work. Some continuous bands in the far ultraviolet region also arise in this level (Venkateswarulu, 1947).
18310	B	239	X—B gives absorption bands in the region $\lambda 5760$ to $\lambda 4800$ (Elliot, 1930).
0	X	564.0	Ground state.

the data relating to various other electronic states previously identified in the spectrum of chlorine. These levels are designated by analogy with the corresponding levels observed in the case of iodine and bromine.

Details of the analyses and the nature of the electronic states involved in these two systems will be published shortly.

REFERENCES

- Elliot, A., 1930, *Proc. Roy. Soc. (London)*, **127**, 638.
Haranath, P. B. V. and Tiruvenganna Rao, P., 1956, *Curr. Sci.*, **25**, 151.
" " " " 1956, *Curr. Sci.*, **25**, 256.
Venkateswarulu, P., 1947, *Proc. Ind. Acad. Sci.*, **26A**, 22.

ON THE ULTRAVIOLET ABSORPTION SPECTRA OF FROZEN SOLUTIONS OF DICHLOROBENZENES IN ISOBUTYL ALCOHOL

S. B. ROY AND S. C. SIRKAR

OPTICS DEPARTMENT, INDIAN ASSOCIATION FOR THE CULTIVATION OF SCIENCE
CALCUTTA-32

(Received for publication, November 10, 1956)

ABSTRACT. The ultraviolet absorption spectra of different solutions of ortho-, meta- and para dichlorobenzene in isobutyl alcohol frozen and cooled to -180°C have been investigated and compared with those due to the pure substances in the vapour, liquid and solid states. It is found that the splitting of the bands observed in the spectra due to ortho- and meta dichlorobenzene in the solid state by previous workers does not take place in the case of 0.2% frozen solutions of these compounds in isobutyl alcohol. The spectra in the latter case are not exactly identical with those due to the substances in the vapour state. The spectra due to the 25% solutions in the frozen state, however, are more complicated and they can be analysed by assuming that they have been produced by the superposition of the spectrum due to the crystals of the pure substance on that due to the very dilute solution in each case. There are, however, discrepancies between the positions and relative intensities of the bands in the superposed spectrum and that observed in the case of the 25% solution in both the cases.

In the case of 25% solution of para-dichlorobenzene in the solid state at -180°C the spectrum is almost identical with that due to the pure substance at -180°C . The spectrum due to the 0.2% solution at -180°C , on the other hand, is not identical with that due to the vapour, because certain prominent bands observed in the former case are not found in the latter case and some strong bands due to the vapour are almost absent in the spectrum due to the 0.2% solution. These results have been discussed in the light of the existing theories.

INTRODUCTION

It was observed by Swamy (1952, 1953) that in the case of the disubstituted benzene compounds in which one of the substituents is a halogen atom (the other substituent being something other than any hydroxyl group) either in the ortho or in the meta position, the ultraviolet absorption spectra for the solid state at -180°C show splitting of the absorption bands, but when the halogen atom is in the para position, no such splitting is observed. This splitting of the bands was explained on the hypothesis that the molecules of these disubstituted benzene compounds in the solid state get strongly associated with each other through virtual linkages owing to the presence of strong permanent electric moment. When the halogen atom is in the para position, the permanent electric moment

being very small, only weak virtual linkages between the molecules are formed at -180°C , but no such linkages are formed at the room temperature, and such bonds being symmetrically distributed in the molecule, no splitting of the energy level occurs.

Recently, the ultraviolet absorption spectra of the solutions of the isomeric chloro- and bromo toluenes at different temperatures have been investigated (Roy, 1956) to understand the cause of such splitting of the bands. It has been observed that when the solution is very dilute and is transparent in the solid state the ultraviolet absorption spectrum shows no splitting of the bands, but when the concentration of the solution is very high and the frozen mass is translucent the absorption spectrum consists of broad bands which are found to be produced by the superposition of the two systems of bands, one being due to the dilute frozen solution and the other due to the pure substance in the solid state. The absence of the splitting of the absorption bands in the case of the dilute frozen solution was, therefore, explained on the assumption that in dilute solution, the molecules being thinly dispersed in the solvent, the distance between adjacent molecules of the solute is too large to produce associated groups of molecules and so the splitting of the energy level is absent. The dispersed molecules behave like single molecules and absorption spectrum is similar to that of the vapour.

Swamy (1953) also observed similar splitting of the ultraviolet absorption bands of ortho-dichlorobenzene in the solid state, but no such splitting was observed in the case of para compound.

Recently, Sen (1956) observed such a splitting of the absorption bands in the spectrum of meta-dichlorobenzene in the solid state. The number and relative intensities of the components into which the bands are split up, appear to be different for the different molecules. It has not yet been possible to explain why this variation takes place. The study of the absorption spectra of these molecules dispersed in different environments might throw some light on the origin of the these components. The results of investigations on the absorption spectra of the isomeric dichlorobenzenes dissolved in isobutyl alcohol in the solid state have been discussed in the present paper.

EXPERIMENTAL

The experimental arrangement in the present investigation was the same as that described in a previous paper (Roy, 1956). Chemically pure samples of ortho-dichlorobenzene obtained from B.D.H., meta-dichlorobenzene from Theodor Schuchardt-Munchen and para-dichlorobenzene from E. Merck were used in the investigation. All the liquids including the solvent were distilled repeatedly before use. Solutions of different concentrations varying from 0.2% to 30% have been used. The absorption cells used in the present investigations are the same as those described in a previous communication (Roy, 1956). The absorption

spectra of the pure substances in the liquid and solid states were also studied and the nature and positions of the bands in the spectra were found to be the same as those observed by previous workers (Swamy, 1953; Sen, 1956). Only in case of *o*-dichlorobenzene in liquid and solid states there was a deviation of about 3Å. Swamy measured the wavelengths with the help of mercury arc lines and in the present investigation, iron arc spectrum has been used for comparison.

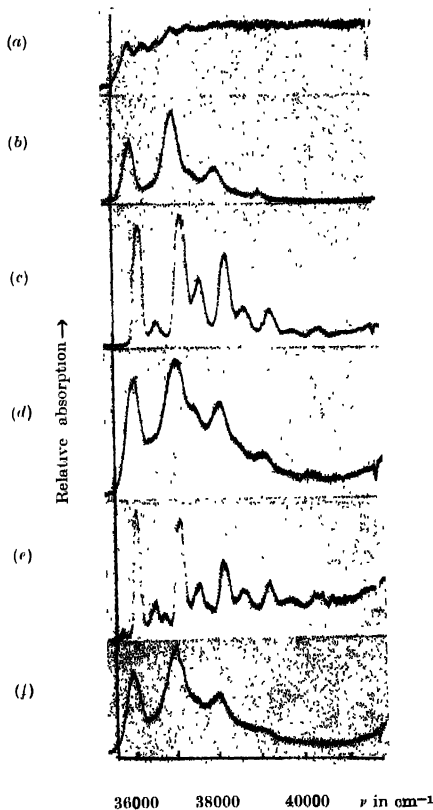


Fig. 1. Microphotometric records of the ultraviolet absorption spectra of *o*-dichlorobenzene and its solution in isobutyl alcohol. (a) Frozen 25% solution at -180°C . (b) 25% solution at 30°C . (c) Frozen 0.2% solution at -180°C . (d) 0.2% solution at 30°C . (e) Pure solid at -180°C . (f) Pure liquid at 30°C .

The frequencies of the absorption bands were measured with the help of microphotometric records as explained earlier (Roy, 1956). Although an Adam Hilger medium quartz spectrograph was used in this investigation, the wavelengths could be measured correct to about 0.5 \AA by this method.

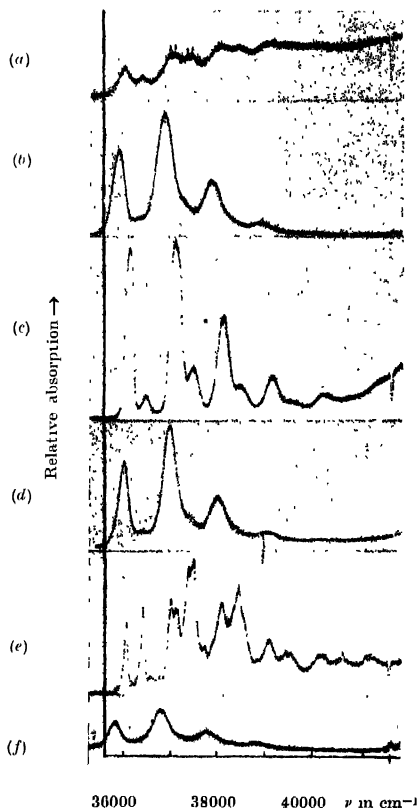


Fig. 2. Microphotometric records of ultraviolet absorption spectra of *m*-dichlorobenzene and its solution in isobutyl alcohol at different temperatures.

(a) Frozen 30% solution at -180°C . (b) 30% solution at 30°C . (c) Frozen 0.2% solution at -180°C . (d) 0.2% solution at 30°C . (e) Pure solid at -180°C . (f) Pure liquid at 30°C .

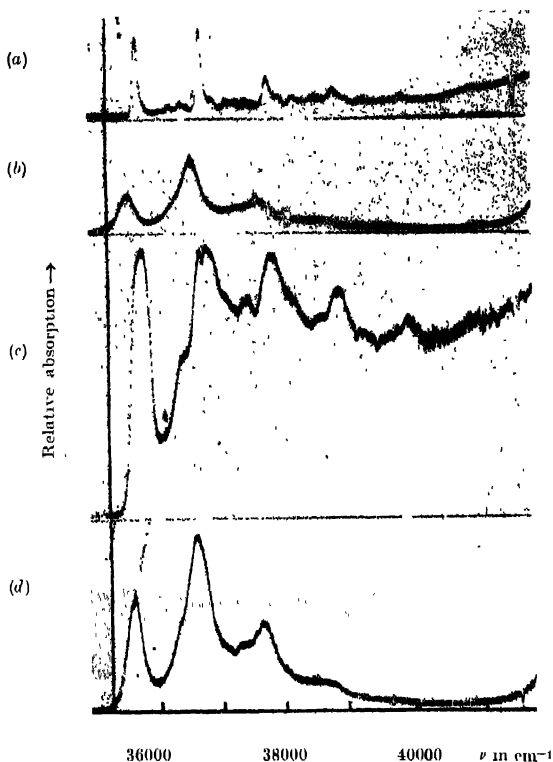


Fig. 3. Microphotometric records of ultraviolet absorption spectra of solution of *p*-dichlorobenzene in isobutyl alcohol at different temperatures.

(a) Frozen 25% solution at -180°C . (b) 25% solution at 30°C .
(c) Frozen 0.2% solution at -180°C . (d) 0.2% solution at 30°C .

RESULTS

The microphotometric records of the spectra are reproduced in figures 1, 2 and 3 and the wave numbers of the bands with approximate intensities and probable assignments are given in Tables I–VI. Some of the prominent bands observed by previous workers in the spectra of these substances in the vapour state are also included in Tables I, III and V.

TABLE I
Absorption spectra of *o*-dichlorobenzene

Vapour (Anno and Matubara, 1955)		Liquid		Solution in isobutyl alcohol at 30°C			
ν in cm^{-1}	Assignment	ν in cm^{-1}	Assignment	ν in cm^{-1}	0 2% Assignment	ν in cm^{-1}	25% Assignment
36232 (vs)	ν_0	35922 (vs) (broad)	ν_0	36050 (vs)	ν_0	35989 (s)	ν_0
36539 (vs)	$\nu_0 + 307$			36480 (vw)	$\nu_0 + 430$	36428 (vw)	$\nu_0 + 428$
36610 (vs)	$\nu_0 + 437 - 59$	36937 (vs) (broad)	$\nu_0 + 1035$	37081 (vs)	$\nu_0 + 1031$	37026 (vs)	$\nu_0 + 1027$
36669 (ms)	$\nu_0 + 437$			37506 (w)	$\nu_0 + 430 + 1031$	37456 (w)	$\nu_0 + 1027 + 428$
36842 (m)	$\nu_0 + 610$						
36951 (mw)	$\nu_0 + 711$			38126 (s)	$\nu_0 + 2 \times 1031$		
37073 (ms)	$\nu_0 + 958 - 2 \times 59$	37997 (m)	$\nu_0 + 2 \times 1035$	38530 (w)	$\nu_0 + 2 \times 1031 - 430$	38054 (m)	$\nu_0 + 2 \times 1027$
37129 (ms)	$\nu_0 + 958 - 59$	39033 (w)	$\nu_0 + 3 \times 1035$	39139 (w)	$\nu_0 + 3 \times 1030$		
37190 (s)	$\nu_0 + 958$						
37259 (ms)	$\nu_0 + 1089 - 24$			39571 (w)	$\nu_0 + 3 \times 1030 + 430$		
37321 (s)	$\nu_0 + 1089$						

TABLE II
Absorption spectra of *o*-dichlorobenzene.

Pure solid at -180°C (Swamy, 1953)		Frozen solution in isobutyl alcohol at -180°C			
		0.2%		25%	
ν in cm^{-1}	Assignment	ν in cm^{-1}	Assignment	ν in cm^{-1}	Assignment
35649 (w)	C_0	36169 (vs)	ν_0	35980 (sb)	ν_0
35999 (vs)	A_0	36599 (w)	$\nu_0 + 431$		
36443 (m)	B_0	37199 (vs)	$\nu_0 + 1030$	36366 (sb)	$\nu_0 + 386$
36686 (w)	C_1	37630 (m)	$\nu_0 + 430$ $+ 1030$	36673 (m)	$\nu_0 + 693$
				37012 (sb)	$\nu_0 + 1032$
37040 (vs)	A_1	38229 (s)	$\nu_0 + 2 \times 1030$		
37481 (m)	B_1	38667 (w)	$\nu_0 + 430 + 2 \times$ 1030	37386 (sb)	$\nu_0 + 1032$ $+ 386$
37730 (vw)	C_2	39249 (w)	$\nu_0 + 3 \times 1030$		
38080 (s)	A_2	39683 (vw)	$\nu_0 + 3 \times 1030$ $+ 430$		
38521 (m)	B_2				
39121 (s)	A_3	40284 (vw)	$\nu_0 + 4 \times 1030$		

DISCUSSION

o-Dichlorobenzene dissolved in isobutyl alcohol

The results in Tables I and II show that in the case of 0.2% solution of *o*-dichlorobenzene in isobutyl alcohol in the liquid state, the ν_0 -band shifts from its position in the vapour state by 182 cm^{-1} towards longer wavelengths. This shift increases to 233 cm^{-1} when the concentration is increased to 25%. In the case of pure liquid, this displacement of the ν_0 -band is 310 cm^{-1} . So, the intermolecular field in the pure liquid has greater influence on the position of the ν_0 -band than in the case of the solution. This is probably due to the chlorine atoms in the molecule. In the case of 0.2% solution the absorption spectrum can be analysed as progressions of excited state frequencies 430 and 1031 cm^{-1} which were also observed in the case of the vapour. The bands due to the pure liquid are slightly broader and only the progression of excited state frequency 1035 cm^{-1} is prominent, the other bands due to the excited frequency 430 cm^{-1} being just perceptible.

On comparing the absorption spectrum due to 0.2% frozen solution with that due to pure substance in the solid state at -180°C , it is found that the splitting of each band into an intense central component and two weak satellites on both sides observed in the latter case, is absent in the case of the frozen solution of strength 0.2%, but the bands due to the frozen 0.2% solution are slightly broader. When the strength of the solution is increased to 25% and the frozen mass

appears to be opalescent, the band system undergoes remarkable changes. Although each band seems to be split up into three components in this case, the relative intensities of the components are different from those observed in the case of the crystals of pure *o*-dichlorobenzene (Swamy, 1953). Also the continuous absorption, starting just on the short wavelength side of the ν_0 -band increasing rapidly towards shorter wavelengths observed in the spectrum due to the 25% solution at -180°C , is not exhibited by the spectra of the pure substance in any state or of the 0.2% solution in the liquid or solid state.

The assignments shown in the last column of Table II have been made assuming the first band on the long wavelength side to be the ν_0 -band, but the excited state vibration frequencies 386 cm^{-1} and 693 cm^{-1} , deduced in this way, are not observed in the spectra of the pure substance in different states. So, an alternative assignment was tried. The positions of the bands at 35980 , 36673 and 37012 cm^{-1} due to the 25% solution at -180°C are almost identical with those of the bands at 35999 , 36686 and 37040 cm^{-1} respectively due to the crystals of the pure substance. Hence, the former three bands may be due to crystals of *o*-dichlorobenzene which might have been formed while the 25% solution was cooled and frozen. In that case, the remaining bands due to this solution should be due to the molecules of the substance dispersed in the rigid glass as in the case of the 0.2% solution at -180°C . It is found, however, that the frequencies of the bands at 36366 cm^{-1} and 37386 cm^{-1} due to the frozen 25% solution are slightly higher than those of the corresponding bands due to the frozen 0.2% solution. Hence the two bands in the former case are not due to single molecules dispersed in rigid glass. They may be due to complex groups of molecules formed by association of the molecules of the solvent and the solute at the low temperature. The continuous absorption increasing towards shorter wavelengths observed in the case of the 25% solution may also be due to those complex groups. Thus the spectrum produced by the 25% solution at -180°C is produced by the superposition of two different spectra, one due to the complex groups and the other due to single molecules dispersed in the rigid glass.

It can be seen from figures 1(c) and 1(d) that the ν_0 -band due to the pure crystals is sharper than that due to the 0.2% solution at -180°C . This shows that irregular distribution of the isobutyl alcohol molecules in the frozen cybotactic groups in the rigid glass produces an intermolecular field varying within certain limits. In the case of the pure crystals of *o*-dichlorobenzene the arrangement of molecules being regular the field has a definite distribution around each molecule. Whether the splitting of the bands in this case is due to asymmetry in the distribution of this field or to some other cause will be discussed after comparing the results obtained in the case of all the three dichlorobenzenes.

Meta-dichlorobenzene :

It was reported previously by Sen (1956) that each band observed in the spectrum due to *m*-dichlorobenzene in the liquid state splits up into three compo-

TABLE III
Absorption spectra of *m*-dichlorobenzene

Vapour (Spencer, 1942) Prominent bands		Liquid (Sen, 1956)		Solution in isobutyl alcohol at 30°C	
				0.2%	
ν in cm^{-1}	Assignment	ν in cm^{-1}	Assignment	ν in cm^{-1}	Assignment
36186 (vs)	ν_o	35826 (sb)	ν_o	35986 (s)	ν_o
36564 (m)	$\nu_o + 378$	36829 (sb)	$\nu_o + 1003$	36379 (w)	$\nu_o + 393$
37147 (vs)	$\nu_o + 960$	37830 (mb)	$\nu_o + 2 \times 1003$	36984 (vs)	$\nu_o + 998$
37276 (vs)	$\nu_o + 1090$	38838 (wb)	$\nu_o + 3 \times 1003$	37380 (w)	$\nu_o + 393 + 998$
37290 (s)	$\nu_o + 1104$			37980 (m)	$\nu_o + 2 \times 998$
38107 (s)	$\nu_o + 2 \times 960$			38370 (w)	$\nu_o + 2 \times 998 + 393$
				38978 (m)	$\nu_o + 3 \times 998$
					$\nu_o + 1004 \pm 399$
					$\nu_o + 1004 + 399$
					$\nu_o + 2 \times 1004$
					$\nu_o + 3 \times 1004$

TABLE IV

Absorption spectra of *m*-dichlorobenzene

Pure solid at -180°C (Sen, 1956)		Frozen solution in isobutyl alcohol at -180°C			
		0.2%		30%	
ν in cm^{-1}	Assignment	ν in cm^{-1}	Assignment	ν in cm^{-1}	Assignment
35853 (m)	C_0	36129 (vs)	ν_0	36025 (sb)	ν_0
36022 (s)	A_0	36512 (w)	$\nu_0 + 383$	36428 (wb)	$\nu_0 + 403$
36418 (s)	B_0	36122 (vs)	$\nu_0 + 993$	37012 (s)	$\nu_0 + 987$
36825 (w)	$C_0 + 972$	37506 (u)	$\nu_0 + 383$ $+ 993$	37122 (m)	$\nu_0 + 1097$
36939 (m)	$C_0 + 1086$	38112 (s)	$\nu_0 + 2 \times 993$	37414 (s)	$\nu_0 + 987$ $+ 403$
36994 (s)	$A_0 + 972$	38494 (w)	$\nu_0 + 2 \times 993$ $+ 383$	37512 (w)	$\nu_0 + 1097$ $+ 403$
37108 (s)	$A_0 + 1086$	39110 (m)	$\nu_0 + 3 \times 993$	38110 (m)	$\nu_0 + 1097$ $+ 987$
37390 (s)	$B_0 + 972$	39495 (w)	$\nu_0 + 3 \times 993$ $+ 383$		
37504 (s)	$B_0 + 1086$	40102 (w)	$\nu_0 + 4 \times 993$	38513 (w)	$\nu_0 + 1097$ $+ 987 + 403$
37796 (w)	$C_0 + 2 \times 972$				
37910 (w)	$C_0 + 972 + 1086$				
37968 (w)	$A_0 + 2 \times 972$				
38080 (m)	$A_0 + 972 + 1086$				
38192 (w)	$A_0 + 2 \times 1086$				
38361 (w)	$B_0 + 2 \times 972$				
38479 (m)	$B_0 + 972 + 1086$				
38590 (w)	$B_0 + 2 \times 1086$				
38883 (m)	$C_0 + 2 \times 972$ $+ 1086$				

nents when the liquid is solidified and cooled to -180°C . As shown in figure 2(c), the first component on the longer wavelength side is hardly visible while the second and third components are much stronger and they are quite sharp. The spectrogram due to the 0.2% solution reproduced in figure (2c) does not show any such splitting of the bands. The second weak band from the left in this spectrogram is due to the excited state vibration frequency 383 cm^{-1} . In the case of the pure crystals the band corresponding to this transition is superposed on the third component of the ν_0 -band. The ν_0 -band due to the 0.2% solution at -180°C is much wider than that due to the pure crystals in this case

TABLE V
Absorption spectra of *p*-dichlorobenzene

ν in cm^{-1}	Vapour (Anno and Matubara, 1955)	Liquid at 60°C (Swamy, 1953)		Solution in isobutyl alcohol at 30°C	
		ν in cm^{-1}	Assignment	0.2%	25%
35750 (vs)	ν_0	35342 (vs, b)	ν_0	35512 (vs)	35488 (s)
36081 (m)	$\nu_0 + 331$	36387 (vs, b)	$\nu_0 \pm 1045$	36242 (w)	36560 (vs)
36278 (m)	$\nu_0 \pm 528$	37430 (m)	$\nu_0 \pm 2 \times 1045$	36565 (vs)	37589 (m)
36475 (s)	$\nu_0 \pm 725$			37294 (w)	$\nu_0 + 2 \times 1052$
36801 (vs)	$\nu_0 \pm 1051$			37615 (s)	
36811 (vs)	$\nu_0 + 1061$			38666 (w)	
37850 (vs)	$\nu_0 + 2 \times 1051$				
37863 (vs)	$\nu_0 + 1051 \pm 1061$				

also and the intermolecular field in the rigid glass varies within wider limits in this case than in the case of the ortho compound. The spectrum due to the 30% solution in the solid state cannot be explained by assuming that it is produced by superposition of the spectra due to the pure crystals and the 0.2% solution. The centres of the bands coincide with those of the prominent bands due to the pure crystal, but the relative intensities and widths of the bands are different in the two cases and the increase of continuous absorption towards shorter wavelengths is absent in the case of the pure crystals. Hence in this case also, the bands may be due to the crystals of the pure substance distorted by the presence of solvent molecules inside the rigid glass. The presence of continuous absorption extending over a wide region, which is observed in this case but is absent in the spectra of

TABLE VI
Absorption spectra of *p*-dichlorobenzene

Pure solid at -180°C (Swamy, 1953)		Frozen solution in isobutyl alcohol at -180°C			
		0.2%		25%	
ν in cm^{-1}	Assignment	ν in cm^{-1}	Assignment	ν in cm^{-1}	Assignment
35593 (vs)	ν_0	35742 (vs)	ν_0	35652 (s)	ν_0
36162 (m)	$\nu_0 + 569$	36092 (w)	$\nu_0 + 350$	36221 (w)	$\nu_0 + 569$
36330 (m)	$\nu_0 + 737$	36459 (w)	$\nu_0 + 717$	36392 (w)	$\nu_0 + 740$
36645 (vs)	$\nu_0 + 1052$	36784 (vs)	$\nu_0 + 1043$	36699 (s)	$\nu_0 + 1047$
36842 (m)	$\nu_0 + 1249$	37134 (w)	$\nu_0 + 1043 + 350$	36916 (w)	$\nu_0 + 1264$
37066 (m)	$\nu_0 + 2 \times 737$	37511 (w)	$\nu_0 + 1043 + 717$	37122 (w)	$\nu_0 + 2 \times 740$
37216 (m)	$\nu_0 + 1052 + 569$	37832 (s)	$\nu_0 + 2 \times 1043$	37316 (w)	$\nu_0 + 1047 + 569$
37382 (m)	$\nu_0 + 1052 + 737$	38183 (w)	$\nu_0 + 2 \times 1043 + 350$	37442 (w)	$\nu_0 + 1047 + 740$
37696 (s)	$\nu_0 + 2 \times 1052$	38546 (w)	$\nu_0 + 2 \times 1043 + 717$	37753 (s)	$\nu_0 + 2 \times 1047$
37896 (m)	$\nu_0 + 1249 + 1052$	38875 (ms)	$\nu_0 + 3 \times 1043$	37965 (w)	$\nu_0 + 1264 + 1047$
38116 (w)	$\nu_0 + 1052 + 737 \times 2$	39918 (m)	$\nu_0 + 4 \times 1043$	38185 (w)	$\nu_0 + 1047 + 2 \times 740$
38435 (w)	$\nu_0 + 2 \times 1052 + 737$			38808 (s)	$\nu_0 + 3 \times 1047$
38608 (vw)	$\nu_0 + 1052 + 737 + 1249$				
38748 (s)	$\nu_0 + 3 \times 1052$				
38950 (vw)	$\nu_0 + 1249 + 2 \times 1052$				
39180 (vw)	$\nu_0 + 1052 + 2 \times 737$				

the pure crystals or of the solution in the liquid state indicates, that the solvent molecules in the solid state produce some fundamental change in the spectrum. Probably, only a small percentage of the molecules crystallise out to form small crystallites and the other meta-dichlorobenzene molecules interpenetrate the cyclohexatic groups of the isobutyl alcohol molecules and form weak bonds with them in the solid state.

Para-dichlorobenzene :

The spectrum due to frozen 25% solution of *p*-dichlorobenzene in isobutyl alcohol, shown in figure 3(a), is identical with that due to the crystals of the pure substance reported by Swampy (1953) and the bands are much sharper than those due to the liquid. The thickness of the cell used in this case is about 0.1 mm and it is quite likely that the major portion of the dissolved *p*-dichlorobenzene is separated out as crystals of the pure substance when such a cell is cooled to

180°C and the absorption due to these crystals being much larger than that due to the other molecules dispersed in the rigid glass, only the spectrum due to the pure substance is observed. The influence of the solvent molecules on the spectrum is to shift the band system towards longer wavelengths by about 262 cm^{-1} from its position in the case of the vapour. This shift increases as the concentration is increased and in the case of the pure liquid the shift is 408 cm^{-1} . When the 0.2% solution is frozen, the bands become still wider unlike those due to the 25% solution and a strong continuous absorption is superposed on the bands. Assignments shown in the fourth column of Table VI have been made taking into consideration only the tops of the peaks. Each of the bands at 36784 , 37832 and 38875 cm^{-1} can, however, be assumed to consist of two bands, one at $\nu_0 + n \times 950\text{ cm}^{-1}$ and another at $\nu_0 + n \times 1050\text{ cm}^{-1}$ ($n = 1, 2, 3$), but in the case of the vapour the frequency 950 cm^{-1} is not observed and at -180°C , the $\nu \rightarrow \nu$ transition is not possible. The spectrum due to the crystals of the pure substance also does not show transitions corresponding to such a vibrational frequency. Hence, the appearance of these extra bands is due to some other cause. Figures 3(a) and 3(c) show that if we assume the ν_0 -band to consist of two bands, one at 35590 cm^{-1} and another at 35490 cm^{-1} , the spectrum due to the frozen 0.2% solution appears to consist of two systems, one similar to that reproduced in figure 3(a) and the other displaced from it by 100 cm^{-1} towards longer wavelengths. The latter spectrum may be due to the single molecules dispersed in the rigid glass and the former due to small groups of the *p*-dichlorobenzene molecules which are present in the rigid glass. This band system due to these groups of molecules differ from that due to the pure crystals in two respects, viz., the continuous spectrum observed in the former case is not present in the spectrum of the pure crystals and the bands due to the crystals are much sharper than those due to the groups of molecules.

There is a significant difference between the spectrum due to the pure crystals and that due to the vapour. The transitions corresponding to the excited state frequency 331 cm^{-1} produce bands much more intense than those due to frequencies 528 cm^{-1} and 725 cm^{-1} in the spectrum due to the vapour (Anno and Matubara, 1955), but such transitions due to the frequency 331 cm^{-1} are absent in the case of the pure crystals, although the other two feebler bands are distinctly observed in figure 3(a). In the Raman spectrum of the crystals at -180°C this line is quite intense (Ray, 1951) and therefore it appears that only in the excited electronic state of the molecule in the crystal the corresponding vibration is restricted

Influence of Davydov splitting on the spectra of the pure crystals :

The influence of environment on the absorption spectra of molecules in crystals was studied theoretically by Davydov (1948, 1952) and the theory has been extended to crystals of anthracene belonging to the space group C_{2h}^s by Craig and Hobbins (1955) and to crystals of naphthalene by Craig and Walsh (1956). In the case of anthracene crystals containing two molecules per unit cell, Craig and Hobbins have calculated the Davydov-splitting of the singlet-singlet absorption system at 2500 \AA . They have shown that for a chosen set of wave vectors k_a and k_b in a sheet of molecules in the ab plane of the crystal and for a chosen molecular excited state, there are two crystal states of energies $E^{\alpha,\beta}(k_a, k_b)$ so that

$$E^{\alpha}(k_a, k_b) - E^{\beta}(k_a, k_b) = 2C\{1 + \cos(k_a \cdot a) + \cos(k_b \cdot b) + \cos(k_a \cdot a + k_b \cdot b)\}$$

where C denotes the value of the interaction integral between the two molecules of a unit cell, a and b being the primitive translations along a and b axes

As the unit cell has a centre of symmetry like the molecule, only the transitions allowed in the case of the single molecule are also allowed in the case of the crystal. The transitions in the crystal which are related to the transitions either along the short axis or along the long axis of the anthracene molecule have then α -component polarised in the ac plane and the β -component along the b -axis. Craig and Hobbins have calculated the shift of each of these components from the position of the band due to the single molecule in the case of both short-axis and the long-axis transition. They have found that for the short-axis transition the calculated mean shift $(\Delta E^{\alpha} + \Delta E^{\beta})/2$ is 5200 cm^{-1} towards lower energies, while for the long axis transition this shift is 4000 cm^{-1} towards higher energies when the value of the oscillator strength f is taken as 2.3. Also, the calculated interval between the a and b components has been found by them to be $16,000\text{ cm}^{-1}$ for the long-axis transition and 1000 cm^{-1} for the short-axis transition. From the experimental results obtained by them they have concluded that the system at 2500 \AA observed in the absorption spectrum of anthracene vapour behaves like that due to the long-axis transition in the molecule.

The crystals of *p*-dichlorobenzene also belong to the space group C_{2h}^6 and the unit cell contains two molecules (Hendricks, 1933). In this case also each transition in the molecule is expected to be split up into two components, one polarised in the *ac* plane and the other along *b*-axis with the change from gaseous to solid state. Also the mean position of the two components is expected to be shifted towards higher energies in the case of a transition along the axis passing through the chlorine atoms and towards lower energies in the case of a transition along the shorter-axis. In the present investigation and also in those by Swamy (1953) only polycrystalline masses were used and the two components are expected to appear simultaneously in the spectrum due to the polycrystalline mass. It can be seen from the spectrograms reproduced in figures 4 and 5 in Plate VA of the paper by Swamy (1953) that no conspicuous change takes place in the spectrum when *p*-dichlorobenzene in the liquid state is solidified and cooled to 30°C except a shift of the system by about 200 cm^{-1} towards higher energies. If the observed system is assumed to constitute one of the two components the other system being at a much shorter wavelength, the same system should also appear at -180°C , because the space group of the crystals remains unaltered at -180°C (Krishna Murti, 1956). Actually, however, the spectrum undergoes changes with the lowering of temperature of the crystals and the bands become much sharper, and a continuous absorption appears in the short wavelength region beyond 2537 Å. Small changes in the intermolecular distance without changes of space group cannot bring about such changes in the influence due to environment according to Davydov's theory, taking into consideration only dipole-dipole interaction. Hence these changes in the spectra are due to some other changes in the π -electrons of the ring which may be produced by formation of weak bonds between neighbouring molecules. The strong continuous absorption appearing in the spectrum due to 0.2% solution in rigid glass at -180°C probably indicates that such changes in the π -electrons take place even when the molecules form very small groups in the rigid glass.

The crystal structure either of *o*-dichlorobenzene or of *m*-dichlorobenzene is not known and therefore the influence of environment on the spectra cannot be estimated applying Davydov's theory. If, however, the splitting of the bands observed in the spectrum due to the pure crystals of these substances be due to the dipole-dipole interaction, it is difficult to interpret the intense continuous absorption observed in the spectra due to frozen 25% solutions of these two compounds. It is, therefore, quite probable that the observed splitting is due to some changes in the π -electrons which take place only at short distances between the molecules and not due to influence of environment expected from Davydov's theory.

REFERENCES

- Anno, T. and Matubara, I., 1955, *J. Chem. Phys.*, **23**, 796.
 Chug, D. P. and Hobbins, P. C., 1955, *J. Chem. Soc.*, 539.

- Craig, D. P. and Walsh, J. R., 1956, *J. Chem. Phys.*, **24**, 471.
Davydov, A. S., 1948, *Zhur. Eksp. Teor. Fiz.* **18**, 210.
Davydov, A. S., 1952, *Akad. Nauk. S.S.S.R.*, Pamyati S. I. Vavilov, 197.
Hendricks, S. B., 1933, *Z. f. Krist.*, **84**, 85.
Krishna Murti, G. S. R. and Sen, S. N., 1956, *Ind. J. Phys.*, **30**, 242.
Ray, A. K., 1951, *Ind. J. Phys.*, **25**, 459.
Roy, S. B., 1956, *Ind. J. Phys.*, **30**, 267.
Sen, S. K., 1957, *Ind. J. Phys.*, **31**, 99.
Sponer, H., 1942, *Rev. Mod. Phys.*, **14**, 224.
Swamy, H. N., 1952, *Ind. J. Phys.*, **26**, 445.
Swamy, H. N., 1953, *Ind. J. Phys.*, **27**, 55.

ON THE DESIGN OF FOUR-TERMINAL INTERSTAGES FOR PULSE APPLICATIONS

ARUN K. CHOUDHURY AND N. B. CHAKRABARTI

INSTITUTE OF RADIOPHYSICS AND ELECTRONICS, CALCUTTA UNIVERSITY

(Received for publication, December 14, 1956)

ABSTRACT The present work is devoted to the design of four-terminal networks having prescribed input and output capacities for a fast transient response with little or no overshoot. The requirements for such a performance are first studied. The conditions that the time response of the network has no overshoot, and the bounds on the time response set by the capacities have been obtained. The pole configurations that may achieve the desired characteristics are described. Methods for realising the required pole distributions are formulated, and some circuit arrangements are suggested.

1 INTRODUCTION

The transmission property desirable of a pulse transmission system is fast response with little or no overshoot and oscillation. Excessive overshoots and oscillations are to be avoided for they cause pulse interference. Filters designed on the basis of flat amplitude characteristics alone cannot meet the requirements. The maximally flat amplifier, for example, has too flat an amplitude response and too non-linear an associated phase shift characteristic to give a monotonic response to a step input. The attendant dispersion in time response can, in some measure, be mitigated by employing all-pass phase correcting networks. But, this adds to the complexity of the system. Our attention here will, therefore, be directed to such minimum phase-shift networks as have an amplitude response decreasing at a proper rate and an associated linear phase shift in the frequency interval of primary interest to ensure a nearly monotonic response.

In this work, a study is first made of the conditions that the step response has little overshoot or oscillation. It is shown that the logarithmic curvature of the impedance function is intimately related to the nature of the response. It is proved that the amplitude function, with all its derivatives, must continuously decrease in magnitude if the response is not to exhibit large overshoots. The bounds set on the time response by the characteristics of the impedance function are then considered. The problem of establishing limits on the gain/rise time ratio is attacked by representing the transfer impedance as the combination of positive and negative impedances, each including a parallel capacity. This leads to the formulation of the optimum impedance characteristics and the necessary general structure for realising it.

A method for realising the pole distributions that achieve the desired characteristics is then formulated and some circuit arrangements are suggested.

2. CONDITIONS FOR A MONOTONE OR SEMI-MONOTONE TIME RESPONSE

Let $g(p)$ be the network function and $f(t)$ its impulse response. Then

$$g(p) = \int_0^{\infty} e^{-pt} f(t) dt \quad \dots (1)$$

If the step response is monotonic, the impulse response is never negative, i.e.

$f(t) \geq 0$, for all $t \geq 0$; and then one gets easily

$$g^{(k)}(p) = (-1)^k \int_0^{\infty} t^k e^{-pt} dt = (-1)^k G^{(k)}(p),$$

where $g^{(k)}(p)$ is the k -th derivative of $g(p)$. $G^{(k)}(p)$ is positive if p is a positive real number. Further

$$G^{(k)}(p) > G^{(k)}(p + \delta) \quad \dots (2a)$$

where δ is a positive number. Along the axis of real frequencies we have similarly for a monotone response

$$|G^{(k)}(i\omega)| < \int_0^{\infty} t^k f(t) dt \quad \dots (2b)$$

and

$$|G^{(k)}(i\omega)| > |G^{(k)}(i(\omega + \delta))| \quad \dots (2c)$$

where δ is positive. The meaning of the above relations is that for a monotone response the network function along the positive real axis and its magnitude function along the axis of real frequencies should with all the derivatives continuously decrease.

We now investigate the necessary and sufficient conditions on the network function such that the time response be monotonic. For this we need an important theorem. A necessary and sufficient condition that the sequence $\{\mu_n\}_0^{\infty}$ should have the expression

$$\mu_n = \int_0^1 t^n f(t) dt \quad \text{is that}$$

$$(-1)^k \Delta^k \mu_n \geq 0 \quad (n, k = 0, 1, 2, \dots) \quad \dots (3)$$

where Δ is the difference operator and its counterpart. The necessary and sufficient condition that $g(p)$ is completely monotonic is that $f(t)$ is bounded and non-increasing.

It can be shown that if $f(t)$ is monotonic and never negative

$$g(p) \geq 0, \quad G^{(1)}(p) \geq 0, \quad \left| \frac{g(p)}{G^{(1)}(p)} - \frac{G^{(1)}(p)}{G^{(2)}(p)} \right| \geq 0, \quad \left| \frac{G^{(1)}(p)}{G^{(2)}(p)} - \frac{G^{(2)}(p)}{G^{(3)}(p)} \right| \geq 0.$$

For this consider the quadratic forms

$$Q_1(p) = g(p)x_0^2 + 2G^{(1)}(p)x_0y_0 + G^{(2)}(p)y_0^2 = \int_0^\infty e^{-pt} (x_0 + ty_0)^2 f(t) dt,$$

$$Q_2(p) = G^{(1)}(p)x_0^2 + 2G^{(2)}(p)x_0y_0 + G^{(3)}(p)y_0^2 = \int_0^\infty e^{-pt} t(x_0 + ty_0)^2 f(t) dt,$$

which by hypothesis regarding $f(t)$ are both positive. Hence one gets

$$g(p) \geq 0, \quad G^{(1)}(p) \geq 0, \quad G^{(2)}(p) \geq 0, \quad G^{(3)}(p) \geq 0 \quad \text{and} \quad G^{(2)}(p)g(p) > [G^{(1)}(p)]^2 \quad \dots \quad (4)$$

$$\text{and} \quad \frac{d^2}{dp^2} \log g(p) = \frac{G^{(3)}(p)g(p) - (G^{(2)}(p))^2}{[g(p)]^2} > 0.$$

The logarithmic second derivative of a network function consisting of m zeroes and n poles (a_r & b_r) can be expressed as

$$\begin{aligned} \psi(p) = \frac{d^2}{dp^2} \log g(p) &= \frac{d^2}{dp^2} \left[\sum_m \log (p + a_r) - \sum_n \log (p + b_r) \right] \\ &= \sum \frac{1}{(p + b_r)^2} - \sum \frac{1}{(p + a_r)^2} \quad \dots \quad (5) \end{aligned}$$

If an a_k (or b_k) be complex, the factors due to each of the complex conjugate pair add up to

$$\psi_k(p) = 2 \cdot \frac{p^2 + 2\alpha_k p + \alpha_k^2 - \beta_k^2}{(p^2 + 2\alpha_k p + \alpha_k^2 + \beta_k^2)^2}, \quad \dots \quad (6)$$

where $a_k = \alpha_k \pm j\beta_k$

which is positive for all real positive p if $\alpha_k > \beta_k$. It may be recalled in this connection that the magnitude function due to a complex pole pair evinces a peak

in the frequency response if the value of the argument of the poles exceeds $\pi/4$. Hence to ensure small overshoot in the time response of an all-pole structure, the arguments of the poles should preferably have values less than $\pi/4$. The first two logarithmic derivatives of the network function of an all-pass quartet ($p_1k = -\alpha_k \pm j\sqrt{\beta_k^2 - \alpha_k^2}$, $p_{2k} = \alpha_k \pm j\sqrt{\beta_k^2 - \alpha_k^2}$) can be written as

$$(1) \quad \frac{g'(p)}{g(p)} = \frac{2\alpha_k[p^2 - (\alpha_k^2 + \beta_k^2)]}{(p^2 - 2\alpha_k p + \alpha_k^2 + \beta_k^2)(p^2 + 2\alpha_k p + \alpha_k^2 + \beta_k^2)} \quad \dots (7a)$$

$$(2) \quad \frac{d^2}{dp^2} \log g(p) = \frac{-4\alpha_k p \cdot [3p^2 + 3\beta_k^2 + \alpha_k^2 + 1] [\alpha_k^2 - (p^2 + \beta_k^2)]}{\{(p^2 - 2\alpha_k p + \alpha_k^2 + \beta_k^2)(p^2 + 2\alpha_k p + \alpha_k^2 + \beta_k^2)\}^2} \quad \dots (7b)$$

The relations show that all-pass structures are all essentially oscillatory; the amount of overshoot and oscillations will be less, the larger the modulus and smaller the real part. (This can be simply understood from a recognition of the fact that the phases of these structures are by premise non-linear).

An examination of the expressions (5) and (6) immediately reveals that (a) a zero on the positive real axis always causes overshoots, (b) the Butterworth and Tchbycheff filters are destined to exhibit overshoots (the later having oscillations also, as its amplitude function shows peaks), the magnitude increases with the order.

The usefulness of the conditions stated above may be appreciated from the ease with which the results with regard to the character of the responses of the following immittance functions are derived

Let us first consider the immittance function $g(p) = \frac{(p+a)(p+b)}{(p+c)(p+d)}$ and let $a > b$ and $c > d$. For a monotonic response we first require that the value of the immittance at $p = \infty$ must not exceed the value at $p = 0$, hence $ab > cd$. We require further that $\left(\frac{1}{c} + \frac{1}{d}\right) > \left(\frac{1}{a} + \frac{1}{b}\right)$ and $\left(\frac{1}{c^2} + \frac{1}{d^2}\right) > \left(\frac{1}{a^2} + \frac{1}{b^2}\right)$, from the conditions on slope and curvature

Let us next consider the function $g(p) = \frac{1}{r + pe^p}$, arising in connection with a servo with a delayed control. Taking the first two derivatives and imposing the conditions stated above we derive that the system will be overshooting unless $r < 0.5$.

3. THE CHARACTERISTICS FOR FAST RISE

In order to be of practical utility, any treatment of a transmission system must take note of the input and output capacities of the component stages and the d.c. resistance, which together set a limit to the band of frequencies the system can transmit, and hence to the minimum possible rise time. Now it is known

that the gain/rise time ratio of a four-terminal network is approximately twice that of a two-terminal network having the same total capacity: the basis of the improvement is that the source and load capacities are separated. And the separation of the capacities results in a delay in the waveform response of the four-terminal network. The improvement can, in fact, be looked upon as resulting from a properly assigned delay.

The delayed square pulse can be considered as the ideal impulse (Cherry, 1949) response of a four-terminal network having a finite bandwidth and the ideal transfer function can be written thus

$$g(p) = \frac{e^{p\tau} (e^{pT/2} - e^{-pT/2})}{p} \quad \dots (8)$$

where τ is the delay and T the time of duration of the square pulse. The real part of the transfer function is then given by

$$R_g g(j\omega) = \frac{\sin \omega (\tau + T/2) - \sin \omega (\tau - T/2)}{\omega} \quad \dots (8a)$$

The approach towards the ideal may be measured by the closeness with which the real part of the actual transfer function simulates such a function with as small a T as possible.

The transfer impedance of a four-terminal network can be expressed as the difference of the two input impedances forming the two arms of an equivalent symmetrical lattice, (figure 1) thus

$$Z_T = \frac{Z_A - Z_B}{2} \quad \dots (9)$$

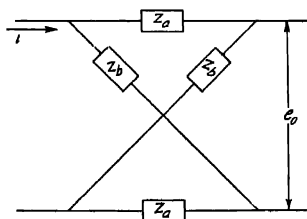


Fig. 1. A four-terminal interstage represented as a symmetrical lattice.

Or, considering ladder networks with input and output capacities C_1 and C_2 , it can be expressed in terms of the input impedances Z_1 , Z_2 and Z_3 looked from the three pairs 1-2, 3-4 and 1-3 (figure 2) thus

$$Z_T = \frac{Z_1 + Z_2 - Z_3}{2} \quad \dots (10)$$

and its real part as
$$R_T = R_1 + R_2 - R_3 \quad (10a)$$

where R_1, R_2 and R_3 are the real parts respectively of Z_1, Z_2 and Z_3 . The step response of the network is obtained from the Fourier integral

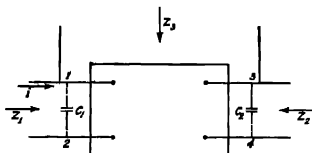


Fig. 2. Four-terminal coupling network having parasitic capacities.

$$F(t) = \frac{2}{\pi} \int_0^{\infty} R_T(\omega) \frac{\sin \omega t}{\omega} d\omega \quad \dots \quad (11)$$

$$\text{Writing } f_1(t) = \frac{2}{\pi} \int_0^{\infty} R_1 \cos \omega t d\omega, f_2(t) = \int_0^{\infty} \frac{2}{\pi} R_2 \cos \omega t d\omega, f_3(t) = \frac{2}{\pi} \int_0^{\infty} R_3 \cos \omega t d\omega,$$

$$\text{and } F_1(t) = \frac{1}{\pi} \int_0^{\infty} \frac{(R_1 + R_2) \sin \omega t}{\omega} d\omega, F_2(t) = \frac{1}{\pi} \int_0^{\infty} \frac{R_3 \sin \omega t}{\omega} d\omega,$$

$$\text{we have } F(t) = \frac{1}{\pi} \int_0^{\infty} (R_1 + R_2 - R_3) \frac{\sin \omega t}{\omega} d\omega = F_1(t) - F_2(t) = \int_0^{\infty} f(t) dt. \dots \quad (11a)$$

$$\text{where } f(t) = \frac{f_1 + f_2 - f_3}{2}.$$

For a fast build-up it is necessary that $f(t) = \frac{f_1(t) + f_2(t) - f_3(t)}{2}$ remains

close to zero for $t \leq \tau - T/2$ and keeps at a high value during $\tau - T/2 \leq t \leq \tau + \frac{T}{2}$

going to zero hereafter $R_3(\omega)$ and hence $F_2(t)$ certainly cannot have a negative d.c. value) thus enabling $F(t)$ to attain values corresponding to $F_1(t)$. This means that the high frequency performance of the components should nearly be identical, and Z_3 should have a stop band centering the zero frequency. The

simplest direct consequence is that $\int_0^{\infty} R_T(\omega) d\omega = 0$ which requires that there

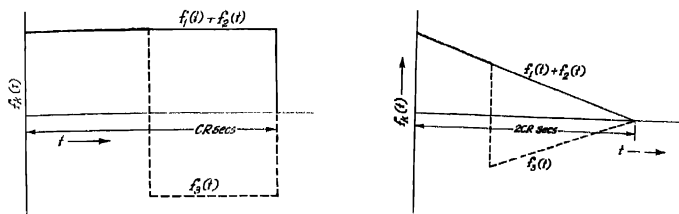
is no capacity path from 1 to 3 except through C_1 and C_2 .

Some bounds on the responses of networks

The maximum bounds of the responses of the impedances $Z_k(p)$ are governed by the theorem:

$$f_k(t) = \frac{2}{\pi} \int_0^{\infty} R_k(\omega) \cos \omega t \, d\omega \leq \frac{2}{\pi} \int_0^{\infty} R_k(\omega) \, d\omega \leq \frac{1}{C_k} \quad \dots (12)$$

where C_k is the capacity appearing across the terminals in consideration. If the charging of the capacitors could be maintained at the maximum possible rate the ideal waveforms of $f_1(t)$, $f_2(t)$ and $f_3(t)$ would be in the symmetrical case as shown



Figs 3 (a) & (b) Ideal impulse responses of the input and transfer impedances of figure 2.

in the figure 3(b). It is to be noted that the maximum value of $f_3(t)$ also occurs at $t = 0$ and the area under the $f_3(t)$ curve equals zero. The general features of the response, if the impulse responses of the two-terminal impedances Z_1 and Z_2 be triangular for a period $0 \leq t \leq 2CR$, are also shown in the figure 3(b). It may be observed that the delay is of the order of $3/2$ times the rise time if the waveform is square and $1/\sqrt{2}$ times if it is triangular, and the rise times are respectively $CR/2$ and $\sqrt{2}CR$ (the corresponding rise times in the two-terminal case are CR and $2CR$ respectively).

The bounds of the step response of a two terminal impedance can be formulated in terms of the real part. Let the ω axis be divided into intervals of separation $\omega_r = \pi/t$ and let the maximum and minimum values of the real part in the interval $(l-1)\pi < \omega < l\pi$ be denoted by $R_{2 \max}$ and $R_{1 \min}$. Then the upper bound of the step response can be found as follows:

$$\begin{aligned} F_k(t) &= \frac{2}{\pi} \int_0^{\infty} R_k(\omega) \frac{\sin \omega t}{\omega} \, d\omega \\ &= \frac{2}{\pi} \left[\int_0^{\omega_r} R_k(\omega) \frac{\sin \omega t}{\omega} \, d\omega + \int_{\omega_r}^{2\omega_r} R_k(\omega) \frac{\sin \omega t}{\omega} \, d\omega + \int_{2\omega_r}^{3\omega_r} R_k(\omega) \frac{\sin \omega t}{\omega} \, d\omega + \dots \right] \\ &= \frac{2}{\pi} \sum_{m=1}^{\infty} \int_{(m-1)\omega_r}^{m\omega_r} R_k(\omega) \frac{\sin \omega t}{\omega} \, d\omega \end{aligned}$$

$$< \frac{2}{\pi} \left[(R_{1 \max} - R_{2 \min}) S_i(\pi) + \dots + (R_{2x+1 \max} - R_{2x+2 \min}) S_i(2x+1)\pi + R_{2n+2 \max} \frac{\pi}{2} \right] \dots \quad (13a)$$

The lower bound is similarly given by the inequality

$$F_k(t) \geq \frac{2}{\pi} \left[R_{1 \min} S_i(\pi) + R_{2 \max} (S_i(2\pi) - S_i(\pi)) + \dots - R_{2n+2 \max} \frac{\pi}{2} \right] \dots \quad (13b)$$

Now $F(t) = F_1 - F_2 = \int_0^t f(t) dt$ is greater, the greater the $R_{1 \max}$ of each component impedance. Further by Schwarz's inequality, one gets

$$|F(t)|^2 \leq \int_0^\infty R_T^2(\omega) d\omega \int_0^\infty \frac{\sin^2 \omega t}{\omega^2} d\omega = \int_0^\infty R_T^2(\omega) d\omega \frac{\pi t}{2} \quad \dots \quad (14)$$

Hence for a fast rise one must ensure that in the useful band $|R_T|$ is as large as possible and $\int_0^{\omega_c} R_T d\omega \approx 0$, where $0 \leq \omega \leq \omega_c$ is the useful band. Therefore,

R_1 , R_2 and R_3 should be such that the cancellation of the components of $R_T(\omega)$ is the irreducible minimum governed by the requirements

$$(i) \int_0^\infty R_T^2(\omega) d\omega \text{ as large as possible,}$$

$$(ii) \quad R_1 R_2 - R_T^2 \geq 0.$$

This requires that the system be externally symmetric, for otherwise the frequency characteristics of Z_1 and Z_2 cannot simultaneously be manipulated to be in proper relation to Z_3 and that R_T be an oscillating function (Bode, 1945).

Let us consider a real part given in the range $0 \leq \omega \leq \omega_c$ by

$$R_T = R_0 \cos \frac{n\pi\omega}{2\omega_c}. \quad \text{Now the integral of the positive component of the real part}$$

given by

$$R_0 \left\{ \int_0^{\frac{\omega_c}{n}} \cos \frac{n\pi\omega}{2\omega_c} d\omega + \int_{\frac{\omega_c}{n}}^{\frac{3\omega_c}{n}} \cos \frac{n\pi\omega}{2\omega_c} d\omega + \dots + \int_{\omega_c}^\infty R d\omega \right\}$$

$$= \frac{2\omega_c}{n\pi} R_0 [1 + 2 + 2 + \dots] + \int_{\omega_c}^\infty R d\omega.$$

is clearly less than $\frac{\pi}{2c_1} + \frac{\pi}{2c_2}$. The level of the impedance can be increased only if the integrals

$$\int_0^{\omega r/n} \cos \frac{n\pi\omega}{2\omega_c} d\omega + \int_{3\omega_c/n}^{5\omega_c/n} \cos \frac{n\pi\omega}{2\omega_c} d\omega + \dots + \int_{\frac{n-1}{n}\omega_c}^{\omega_c} \cos \frac{n\pi\omega}{2\omega_c} d\omega + \int_{\omega_c}^{\infty} R d\omega$$

can be reduced. Therefore the phase-shift in the interval of interest should at least equal π radians. It is, however, to be noted that since the magnitude of the impulse response of each component impedance decreases with time, the delay should not be very large.

4. THE POLE CONFIGURATION

On the basis of consideration of gain alone, the Butterworth and Tchebycheff filters are assuredly desirable. However, the overshoots and the oscillation of the waveform response of these filters tend to be excessive as the order of the network is increased. This is due to the fact that the amplitude characteristics fall more and more to fall at the appropriate rate and hence the phase-shift becomes increasingly non-linear. An approach that immediately suggests itself is to so distribute the poles that the amplitude response decreases continuously at a rate proper to ensure linearity of phase in the frequency band of primary interest.

The 3db point in the amplitude response and the real positive p where the logarithmic curvature of $Z_T(p)$ vanishes can be considered as the two most important design parameters governing the rate of build up and the extent of overshoot.

Now writing the transfer impedance as

$$Z_T(p) = \frac{1}{\prod_{i=1}^n (p^2 + 2b_i p + a_i^2)}$$

we form the logarithmic curvature

$$\psi(p) = \frac{d^2}{dp^2} \log Z_T(p) = \sum 2 \left(\frac{1}{p^2 + 2b_i p + a_i^2} - \frac{2(p + b_i)^2}{(p^2 + 2b_i p + a_i^2)^2} \right) = \sum \psi_i(p) \dots (15)$$

where p is a real variable and $\psi_m(p) = \frac{p^2 + 2b_m p + b_m^2 - a_m^2}{(p^2 + 2b_m p + a_m^2)^2}$. The zero of $\psi_i(p)$ occurs at $p = a_i - b_i$. For a fourth order Butterworth, for example, the zeros occur at $\left(1 - \cos \frac{\pi}{8}\right)$ and $\left(1 - \cos \frac{3\pi}{8}\right)$. The zero of $\psi(p)$ can be moved to the left of the value corresponding to a Butterworth filter by (a) placing the poles on

the ellipse with the real frequency axis as its minor axis, (b) shifting the origin of the circle of figure 4 to the left, (c) or shifting the origin of the Tchebycheff ellipse or the ellipse of figure 4. One consideration governing the choice of contours on which to place the poles is that the centre of gravity of the pole system should be close to the origin if the gain is to remain nearly constant in the band of interest and is not to vary considerably as the order is increased.

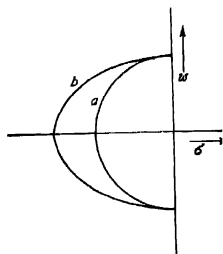


Fig. 4 (a). Geometry of pole-configurations in the p -plane

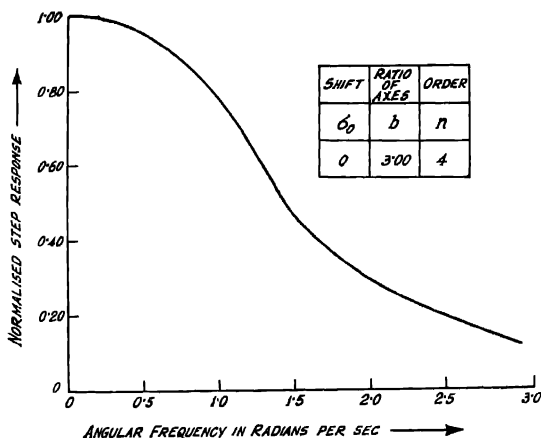


Fig. 4 (b). Normalised amplitude response of a fourth order network with poles situated on an ellipse

All-pole structures only are considered here on grounds of simplicity of design. Such structure are known to realise the largest gain-bandwidth product. It should be emphasised that the incorporation of zeroes in the transfer impedance may result in a better phase-shift characteristic. But the determination of the proper impedance and network realisation of structures having a number of zeroes in the transfer impedance are necessarily more complex. For an all-pole network, on

On the other hand, the process is very simple: it is easy to show that Darlington's method of synthesis (Darlington, 1939) can be directly applied to realise the transfer impedance in the form of a ladder structure.

5. THE RESPONSE FUNCTIONS

The gain function of the system of figure 4(b) is readily calculated by effecting the transformation

$$p = \frac{1}{2} \left(Z + \frac{1}{Z} \right) = \frac{1}{2} \left(r + \frac{1}{r} \right) \cos \theta + j/2 \left(r - \frac{1}{r} \right) \sin \theta \quad \dots (16)$$

where $Z = re^{j\theta}$. The circles in the Z -plane go into ellipses in the p -plane while the unit circle goes into the real axis. If the ratio of the minor axis to the major axis be denoted by b' , then $\frac{1}{b'} = \frac{R_0^2 + 1}{R_0^2 - 1} = b$ say, where R_0 is the radius of the conformally mapped circle in the Z -plane. The magnitude function along the real frequency axis can with a little manipulation be written as

$$F(\omega) = \frac{1}{1 + \left(\frac{e^{\sinh^{-1} \omega}}{R_0} \right)^n} \quad \dots (17)$$

Figure 4(c) depicts the magnitude function for $n = 4$ and $R_0 = \sqrt{2}$. The amplitude function due to poles on the shifted circle is derived by means of the transformations $p = p' - \sigma_0$, $Z = p'^2$. When the total number of poles n , say, is even, the magnitude function in the Z -plane can be expressed as

$$\frac{1}{F(Z)} = R^n - 2a^{n/2} R^{n/2} \cos \frac{n\psi}{2} + a^n$$

where a is the radius of the circle on which the poles are located. Putting $p = \sigma + j\omega = p' - \sigma_0$, one gets $(\sigma - \sigma_0 + j\omega)^2 = Re^{j\theta} = Z$,

whence we derive the amplitude function in the p -plane which is given by

$$\frac{1}{F(\sigma, \omega)} = [(\sigma + \sigma_0)^2 + \omega^2]^{n/2} - 2a^{n/2} [(\sigma + \sigma_0)^2 + \omega^2]^{n/2} \cos \left(\frac{n}{2} \tan^{-1} \frac{\omega}{\sigma + \sigma_0} \right) + a^n \quad \dots (18)$$

The amplitude due to poles on the shifted ellipse can be obtained by means of the transformations $p' = \cosh W$, $p = p' - \sigma_0$, $Z = W^2$... (19)

Configuration (a) of figure (5).

Let the impulse response of the Butterworth filter of order n be denoted by $f_0(t)$ and the step response by $F_0(t)$. Then the impulse response of the system having the pole configuration of figure 5(a) is clearly

$$f_1(t) = e^{-\sigma_0 t} f_0(t),$$

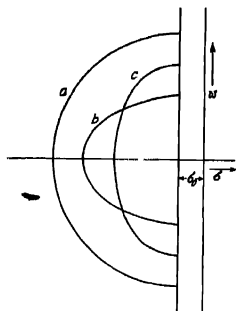


Fig. 5. Geometry of pole configurations with the axis shifted

and the step response $F(t)$ is

$$F(t) = \int_0^t e^{-\sigma_0' t} f_0(t) dt = \left[F_0(t) e^{-\sigma_0' t} \right]_0^t + \sigma_0 \int_0^t F_0(t) e^{-\sigma_0' t} dt = F_0(t) e^{-\sigma_0' t} + \sigma_0 \int_0^t F_0(t) e^{-\sigma_0' t} dt \quad \dots \quad (20)$$

The shift in the frequency axis clearly reduces the contribution due to the later parts of the impulse response and hence the delay and the overshoot. The amount of shift necessary to obtain a satisfactory performance can be determined either from the consideration of the distance of the zero of $\psi(p)$ from the origin or from the expression (20) which utilises the knowledge of the nature of the response of the Butterworth filter. Table I gives the delay and time when the maximum of such filters occurs; it is noted that since both increase with the order the amount of the shift necessary is small for higher orders

Configurations (b) of figure 4 and (b) and (c) of figure 5.

As we have already noted the improved performance of the systems, we discuss, is due essentially to the fact that the phase-shift associated with a gain function is smooth if the change of gain by a given amount is gradual while if

the change of gain is concentrated in a narrow portion of the spectrum, the phase characteristic rises to a sharp peak. In fact, the design of these networks can well be made on the basis of linearity of phase.

TABLE I

For bandwidth—1Mc/s.

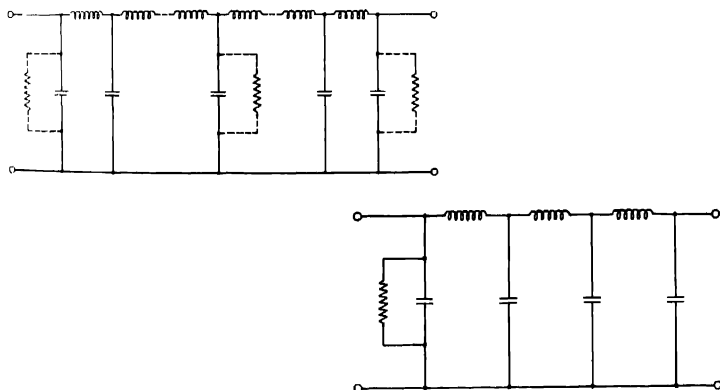
Order n	3	4	5	6	7
Rise time in micro-seconds.	0.36	0.39	0.41	0.42	0.44
Maximum overshoot %	8.15	10.90	12.80	14.3	15.4
Time at which maximum value occurs in μ secs	0.75	0.86	1.00	1.15	1.25

The step response of the systems having the configurations shown in the figures 4(b) and 5(b) and 5(c) with properly chosen eccentricity is likely to have small overshoot. The value of the eccentricity and the shift are to be selected from the considerations of gain conservations and linearity of phase.

There is one practical objection to the employment of the pole configuration of figure 4(b) that the divergence of the configurations for different orders is uncomfortably great. The situations for the cases with the axis shifted are better.

6. CIRCUITS TO REALISE THE DESIRED POLES

The poles can be realised either in a single stage or in the different stages of a multistage amplifier. Every stage is characterised by the input and output capacities which, for the purposes of the design, are to be considered constant and so the load resistance.



FIGS 6 (a) & (b). Network configurations to realise all-pole transfer impedances.

Recalling the discussion in sections (3) and (4), the network structure of figure 6 can be expected to yield in a single stage the desired poles. The system can in fact be designed in the form of a loss-less structure terminated by pure resistance either at any one end or at both. For the latter case, it is convenient to proceed on the basis of reflection coefficients at the two ends. In Table II are given the values of the circuit parameters for the disposition shown in figure 7.

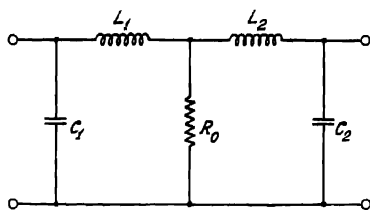
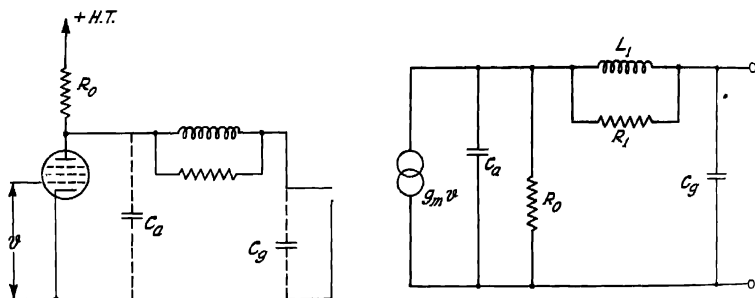


Fig. 7



Figs. 8 (a) & (b). Circuit arrangement for realising a two-pole transfer impedance and the equivalent circuit.

Multistage amplifier

Once the pole configuration and the order of the overall network and the number of stages to be employed are decided upon, it only remains to devise a stage network that gives the response corresponding to each of the factors of the overall response. Figures 8 and 9 show satisfactory stage for realising one pair or two pairs of complex

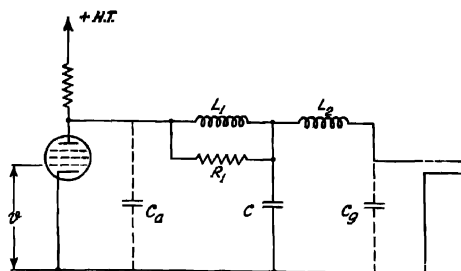


FIG. 9 (a).

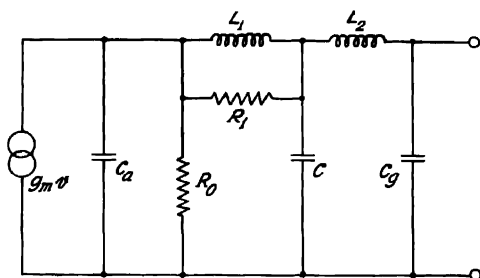


Fig. 9 (b). Circuit arrangement for realising a transfer impedance having five poles and the equivalent circuit.

TABLE II

τ_0	Ratio of axes	$L_1 C_1$	$L_2 C_2$	$R_0 C_1$	$R_0 C_2$
0.3	0.7	0.087	3.663	0.650	2.150
0.3	1.0	0.098	3.536	0.547	2.353
0.3	2.0	0.0285	3.672	0.331	3.154
0	1.0	0.070	3.350	0.740	1.800

poles. We ignore the blocking capacitor which should be large. Setting $R_0 C_a$ $= \frac{L_1}{R_1}$ one obtains the gain functions in the two cases as

$$(1) \quad g(p) = \frac{g_m R_0}{1 + p R_0 (C_a + C_g) + p^2 L C_g} = \frac{g_m R_0}{1 + 2\xi p + p^2 / \omega_1^2}, \quad \dots \quad (21)$$

$$\text{where} \quad R_0 (C_a + C_g) = 2\xi, \quad L C_g = \frac{1}{\omega_1^2}$$

$$(2) \quad g(p) = \frac{g_m R_0}{1 + p R_0 (C_a + C_g + C) + p^2 [L_2 C_g + (L_1 (C + C_g)) + p^3 R_0 L_2 C_g (C_a + C) + p^4 L_1 L_2 C_g]} \quad \dots \quad (22)$$

The first arrangement has the virtue of ease of adjustment, but it does not take the full advantage of the gain-bandwidth product offered by the individual stages.

The design equations for the two cases are listed below. To realise a factor $\frac{1}{1 + 2\xi_1 p + p^2 / \omega_1^2}$ corresponding to a pair of poles one has to set

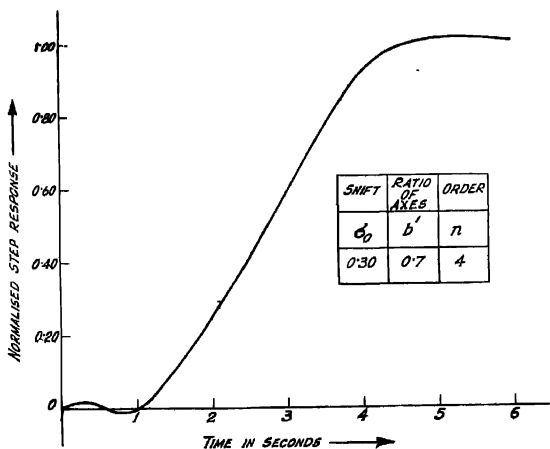
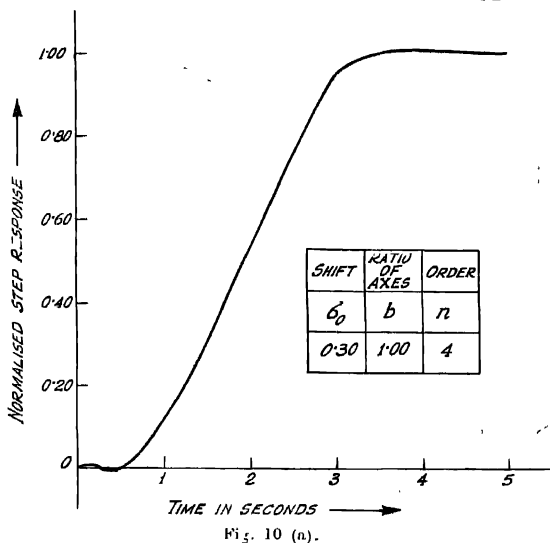
$$\frac{L_2}{R_1} = C_a R_0, \quad 2\xi_1 = R_0 (C_a + C_g), \quad \omega_1^2 = \frac{1}{L_1 C_g}. \quad \dots \quad (23)$$

And to realise a factor $\frac{1}{(1 + 2\xi_1 p + p^2 / \omega_1^2) (1 + 2\xi_2 p + p^2 / \omega_2^2)}$ corresponding to two pairs of poles, one has to set

$$\begin{aligned} \frac{L_2}{R_1} &= C_a R_0, \quad \frac{1}{L_1 C_g} = \omega_1^2, \quad 2(\xi_1 + \xi_2) = R_0 (C_a + C_g + C), \\ 2\left(\frac{\xi_2}{\omega_1^2} + \frac{\xi_1}{\omega_2^2}\right) &= R_0 L_2 C_g (C + C_a), \quad \frac{1}{\omega_1^2} + \frac{1}{\omega_2^2} + 4\xi_1 \xi_2 = L_2 C_g + L_1 (C_g + C) \quad \dots \quad (24) \end{aligned}$$

It will be verified that a system having only four poles on the ellipse defined by $\sigma = 0.3$ and $b = 2.0$ can be realised by setting $R_0 = 1.106$, $L_1 = 1.280$, $L_2 = 0.749$ and $C = 0.150$. The time response is depicted in figure 10(a). The step responses for the cases $\sigma = 0.3$, $b = 0.7$ and $\sigma = 0.3$, $b = 1.0$ are shown in figures 10(b) and 10(c) respectively.

It is advisable in the second arrangement to pair together those roots as have an average damping ratio nearly equal to the average damping of the overall



system: for then the load resistances to be used and the bandwidth of the individual stages will not be widely different.

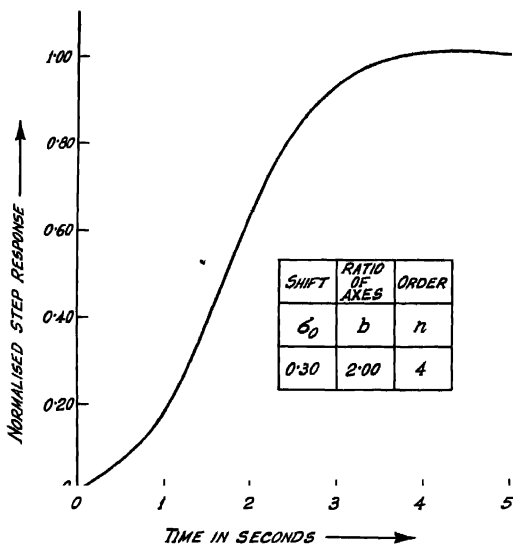


Fig. 10 (c).

Normalised step response of a fourth order network having poles situated on shifted ellipse

ACKNOWLEDGMENTS

The authors are deeply indebted to Prof. S. K. Mitra for constant help and guidance. Thanks are due to Dr. J. N. Bhar, acting Head of the Department, for his kind interest in the work. One of the authors (Chakrabarti) is grateful to the Union Government for the award of Senior Research Scholarship.

REFERENCES

- Bode, H. W. Network analysis and feedback amplifier design, p. 440.
 Cherry, E. C. Pulses and transients in communication circuits, p. 196.
 Darlington, S. 1939*J. Math. Phys.*, **18**, 257-353, 1939.

A NUCLEAR INDUCTION SPIN-ECHO APPARATUS.

B. M. BANERJEE, S. K. GHOSH AND A. K. SAHA

INSTITUTE OF NUCLEAR PHYSICS, CALCUTTA

(Received for publication, October 26, 1956)

ABSTRACT. A very flexible apparatus with Bloch's crossed-coil probe for the detection of spin-echo signals has been described in detail. A fixed one megacycle/sec. master oscillator allows the frequency of the final gated amplifier to be set at different values by proper selection of the harmonic in the harmonic generators. The pulse generators produce a sequence of pulses, the number, durations, intervals and the repetition rates of which can be adjusted independently. Using Hahn's method, both the spin-lattice relaxation time T_1 and the spin-spin relaxation time T_2 have been measured for protons in glycerine as an illustration.

I. INTRODUCTION

Various authors [Hahn (1950); Hahn and Maxwell (1951, 1952), Norberg (1952), Hahn and Herzog (1954), Bloom and Norberg (1954), Carr and Purcell (1954), Bloom *et al* (1955), Holcomb and Norberg (1955)] have reported the application of the spin-echo technique, first introduced by Hahn (1950), in studying the different aspects of nuclear magnetic and nuclear quadrupole resonance. This technique is specially suited for the measurements of both the relaxation times T_1 and T_2 . It is particularly true in the case of liquids where the relaxation times range usually from several milliseconds to a few seconds. A number of authors reported the instrumentation in their papers [Hahn (1950), Norberg (1952), Carr and Purcell (1954), Malling (1954), Bloom *et al* (1955), Holcomb and Norberg (1955)], but in brief. Here, in this paper, we present the details of the apparatus recently set up in the Institute of Nuclear Physics. This apparatus is very flexible and can be set to produce any desired sequence of pulses, of variable width and spacing at suitable repetition rates, at a number of radio frequencies. The final r.f.-amplifier has a high peak power. The output pulses rise to the final amplitude in the first cycle of the r-f and also die out very quickly. Before proceeding to describe the apparatus we shall give a simplified statement of the theory of the phenomenon.

II. THEORY

In the usual nuclear induction experiments, a sample containing nuclei having non-zero spin and magnetic moment, is placed in a strong steady magnetic field \vec{H}_0 . When thermal equilibrium is attained the nuclear ensemble gets distributed among the different spin states according to Boltzmann law of distribution.

As a result there will be a net magnetic moment vector \vec{M}_0 directed parallel to \vec{H}_0 . If we could now deflect \vec{M}_0 by an angle θ from its equilibrium direction along \vec{H}_0 , then \vec{M}_0 will precess about \vec{H}_0 with the circular frequency $\omega_0 = \gamma H_0$, where γ is the gyromagnetic ratio of the nuclei concerned. Due to this precessional motion of \vec{M}_0 , a voltage of magnitude $\omega_0 M_0 \sin \theta$ will be induced in a coil surrounding the sample, the coil axis being normal to \vec{H}_0 . In the nuclear induction experiments, this flipping of \vec{M}_0 is caused by a linearly polarized radio-frequency field applied normally to \vec{H}_0 . The radio-frequency field has the amplitude $2H_1$, where $|H_1| \ll |H_0|$ and has the frequency $\omega \approx \omega_0$, the resonance frequency. Actually, only one of the two circularly polarized components of the linearly polarized r.f. field is effective in producing resonance [Bloch, 1946.] This may be understood if we pass on to a co-ordinate system rotating with a frequency ω about \vec{H}_0 in the sense opposite to that of the r-f field. In such a system the nuclear ensemble will be in an effective field

$$\vec{H}_{eff} = \left(\frac{\omega_0 - \omega}{\gamma} \right) \vec{k} + H_1 \vec{i}$$

where \vec{k} and \vec{i} are the unit vectors along z' and x' axis of the rotating co-ordinate system [Rabi *et al* 1954,1. If the nuclear magnets follow the magnetic field adiabatically then \vec{M}_0 will be directed parallel to \vec{H}_{eff} and hence $\tan \theta = \frac{\omega_0 - \omega}{\gamma H_1}$.

At exact resonance i.e. when $\omega = \omega_0$, θ becomes 90° and the maximum voltage is induced in the coil. This induced voltage decays because of the tendency of the nuclear magnets: (1) to attain thermal equilibrium due to spin-lattice interaction characterized by the spin lattice relaxation time T_1 , and (2) to lose phase coherence with characteristic time T_2^* . Phase incoherence may arise due to (i) the different fixed rates of precession throughout the sample caused by the static "local" field or by an inhomogeneous magnetic field; (ii) processes causing random fluctuations in frequency and phase due to spin-spin coupling or by self-diffusion in an external field gradient, particularly prominent in liquids of low viscosity. In the steady technique, as it is called, the loss in signal voltage due to the above effects is compensated by transitions due to the r.f. field i.e. the precession is maintained by the r.f. field establishing the steady condition.

Contrary to the above technique and the transient technique of Torrey (1949), where the transients are observed in the presence of the r.f. field, Hahn's method consists in observing the induced voltage due to free precession of the nuclei. Here the r.f. field is applied for short durations at certain intervals

and the field inhomogeneity is so chosen that the phase coherence is lost in a time before the application of the next pulse. This loss in phase coherence is due to the isotropic distribution of the moment vectors as they rotate about the steady field H_0 with different circular frequencies caused by the random distribution of the field inhomogeneity over the sample. Still there remains the internal phase coherence having a characteristic decay time T_2 . This will be evident from the simplified picture given below. On the basis of this picture, calculation of the amplitudes of different echoes and free induction signals have been done and their mode of formation is shown here in figure 1. Diffusion effect has not been taken

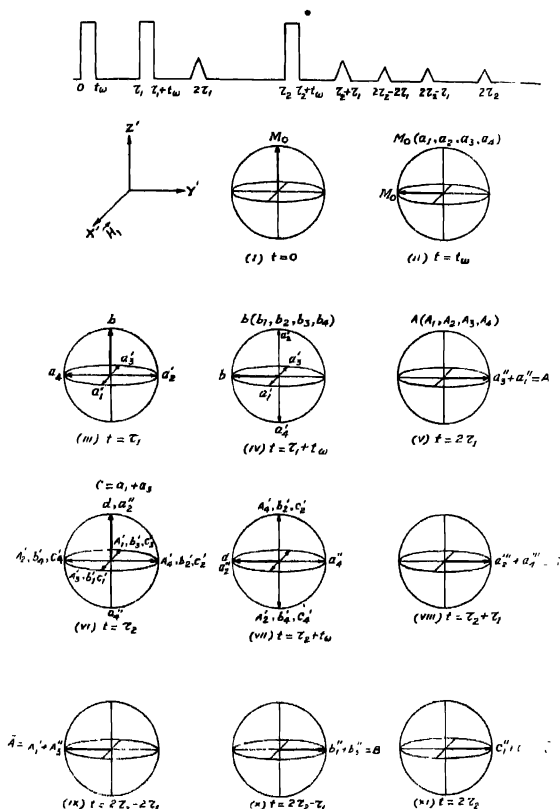


Fig. 1 - Vector diagrams showing the formation of echo pulses and free induction decays. r.f. pulses are applied at $t=0$, τ_1 and τ_2 .

into account. This will simply introduce a damping term to the x and y components of the moment vectors. For simplicity we shall make the following assumptions :

(1) Each r.f. pulse causes a rotation of the moment vectors by an angle $\pi/2$ in the anti-clockwise direction in the rotating co-ordinate system i.e. the nutational angle $\gamma H_1 t_\omega = \pi/2$, where t_ω is the duration of the r.f. pulse.

(2) The r.f. pulses are so short in duration that $t_\omega \ll T_1, T_2$ and T_2^* , where $T_2^* \sim 1/(\Delta H)_{AV}$, $(\Delta H)_{AV}$ being the average field inhomogeneity over the sample volume. T_2^* may be defined as the characteristic time required by the nuclear magnets to distribute themselves isotropically in the $x'y'$ plane.

(3) The condition $T_2^* \ll \tau_1, \tau_2 - \tau_1$, etc., i.e. the signal dies down due to isotropic distribution of the moment vectors before the application of the next r.f. pulse.

(4) $\tau_1, \tau_2 \leq T_2$ and T_1 . The first condition implies that the internal phase coherence may be maintained and the second condition shows that the thermal equilibrium is not attained during the pulse train. T_1 is always greater than T_2 .

(5) During the absence of the r.f. field the moment vector decays with the characteristic time constants T_1 and T_2 . This is true when we can neglect the diffusion damping which damps the x and y components of the moment vectors. T_1 has the effect on the z component only and no effect on the x and y components while T_2 has effect only on the x and y components and no effect on z -component. This is evident from Bloch equations. Bloch equations in the rotating co-ordinate system are given by

$$\left. \begin{aligned} \frac{du}{dt} &= -\frac{u}{T_2} \\ \frac{dv}{dt} &= -\frac{v}{T_2} \\ \frac{dw}{dt} &= -\frac{w - w_0}{T_1} \end{aligned} \right\} \quad (1)$$

The inhomogeneity part has been neglected since this will damp the signal by distributing the nuclear magnets isotropically in the $x'y'$ plane and by introducing a diffusion decay. u, v and w are respectively the x', y' and z' -components of the net magnetic moment vector \vec{M}_0 .

(6) The macroscopic magnetic moment vector \vec{A} , directed parallel to y' -axis, is considered to be composed of a large number of isotropic groups. Different groups will have different circular frequencies determined by the field inhomogeneity at the site of the group. Due to the isotropic distribution of the field inhomogeneity, the groups will be distributed isotropically in the $x'y'$ plane in

a time $\tau > T_2^*$. We can always resolve them along two perpendicular directions, each component having the same magnitude but so directed that the net resultant is zero. Thus, we may consider that the moment vector \vec{A} is originally composed of four components a_1 , a_2 , a_3 and a_4 , all equal in magnitude but having such average circular frequencies that in a time τ they are displaced by $2n_1\pi + \pi/2$, $2n_2\pi + 2\pi/2$, $2n_3\pi + 3\pi/2$ and $2n_4\pi + 4\pi/2$ respectively on the average, from the initial direction, where n 's may be zero or any integer. The subscripts 1, 2, 3 and 4 denote the four cases respectively. In addition, a 's will be damped according to Bloch eqns. (1). Further, it has been assumed that these moment vectors retain their phase memory i.e. they will describe the same angles for the same interval of time at any later time $t \leq T_2$.

The vector diagrams (figure 1) clearly show how the different free induction and echo signals are formed due to the recluster of moment vectors at different times. The system is assumed to be in thermal equilibrium before the application of the pulse train.

\vec{M}_0 is the thermal equilibrium value of the net magnetization and is equal to $\chi_0 H_0$ where χ_0 is the steady magnetic susceptibility and H_0 is the average value of the magnetic field.

In calculating the amplitudes of the different components of the moment vector we have used eqns. (1) which give

$$\left. \begin{aligned} u(t) &= u(t_i) \exp \left[-\frac{t-t_i}{T_2} \right] \\ v(t) &= v(t_i) \exp \left[-\frac{t-t_i}{T_2} \right] \\ \text{and} \quad w(t) &= w_0 \left[1 + \frac{w(t_i) - w_0}{w_0} \exp \left(-\frac{t-t_i}{T_1} \right) \right] \end{aligned} \right\} \quad \dots (2)$$

where

$$w_0 = M_0.$$

The different diagrams of figure 1 are explained as follows

- (i) Initially ($t = 0$) \vec{M}_0 is directed parallel to Z' .
- (ii) At $t = t_\omega$, \vec{M}_0 lies parallel to y' axis due to nutation by angle $\pi/2$. Free induction signal of amplitude M_0 thus occurs at $t = t_\omega$. \vec{M}_0 has four components a_1 , a_2 , a_3 and a_4 where $a_1 = a_2 = a_3 = a_4 = \frac{M_0}{4} = a(\tau_1)$. $a(\tau_1)$ denotes that a 's

will be displaced by $2n_1\pi + \frac{\pi}{2}$, $2n_2\pi + 2\frac{\pi}{2}$, $2n_3\pi + 3\frac{\pi}{2}$ and $2n_4\pi + 4\frac{\pi}{2}$ during τ_1 , due to different precessional frequencies.

(iii) Here $t = \tau_1$, a 's are the values of a 's at $t = \tau_1$. $a_1' = a_2' = a_3' = a_4' = a \exp \left[-\frac{\tau_1}{T_2} \right]$. z -component of the magnetic moment vector will then attain the value

$$b = M_0 \left[1 - \exp \left(-\frac{\tau_1}{T_1} \right) \right]$$

since M_0 is the thermal equilibrium value.

(iv) b has no phase memory at $t = \tau_1 + t_w$. Free induction signal of amplitude $b = M_0 \left[1 - \exp \left(-\frac{\tau_1}{T_1} \right) \right]$ occurs at this time.

(v) At $t = 2\tau_1$, a_3' and a_1' will recollapse on the y' axis and will have the new values a_3'' and a_1'' respectively

$$a_3'' = a_1'' = a_1' \exp \left(-\frac{\tau_1}{T_2} \right) = a \exp \left(-\frac{2\tau_1}{T_2} \right)$$

$$A = a_3'' + a_1'' = \frac{M_0}{2} \exp \left(-\frac{2\tau_1}{T_2} \right).$$

Thus the primary echo forms at $t = 2\tau_1$.

(vi) This is the picture at $t = \tau_2$. Here $a_3'' + a_1'' = A(\tau_2 - 2\tau_1)$ and b may be thought as $b(\tau_2 - \tau_1)$. The components of A , namely A_1 , A_2 , A_3 and A_4 will have values

$$A_1' = A_2' = A_3' = A_4' = \frac{A}{4} \exp \left[-\frac{\tau_2 - 2\tau_1}{T_2} \right].$$

$$\text{Similarly, } b_1' = b_2' = b_3' = b_4' = \frac{b}{4} \exp \left[-\frac{\tau_2 - \tau_1}{T_2} \right].$$

Here we note that since, A 's are due to a_3 and a_1 components of M_0 at $t = t_w$, we may consider $a_1 + a_1 = c(\tau_2)$, say, where $c_1' = A_3'$, $c_2' = A_4'$, $c_3' = A_1'$ and $c_4' = A_2'$.

During the time $\tau_2 - (\tau_1 + t_w)$, a_3' and a_4' have changed to a_2'' and a_4'' respectively, in trying to attain their equilibrium value which is zero for both

$$a_2'' = a_2' \exp \left[-\frac{\tau_2 - \tau_1}{T_1} \right] \quad \text{and} \quad a_4'' = a_4' \exp \left[-\frac{\tau_2 - \tau_1}{T_1} \right].$$

At $t = \tau_1 + t_w$, the z -component was zero and hence it will have the value

$d = M_0 \left[1 - \exp \left(- \frac{\tau_2 - \tau_1}{T_2} \right) \right]$ a_2'' and a_4'' have been separated from d since

they have certain phase memory while d has nothing of the sort at this time.

(vii) Here $t = \tau_2 + t_w$. The free induction decay is caused by d .

(viii) At $t = \tau_2 + \tau_1$, the stimulated echo occurs due to reclustering of a_2'' and a_4'' which have attained respective values of a_2''' and a_4''' . The amplitude is given by $a_2''' + a_4'''$.

$$\begin{aligned} a_2''' + a_4''' &= a_2'' \exp \left[- \frac{\tau_1}{T_2} \right] = a_2' \exp \left[- \frac{\tau_2 - \tau_1}{T_1} - \frac{\tau_1}{T_2} \right] \\ &= a \exp \left[- \frac{2\tau_1}{T_2} - \frac{\tau_2 - \tau_1}{T_1} \right] \\ a_2''' + a_4''' &= \frac{M_0}{2} \exp \left[- \frac{2\tau_1}{T_2} - \frac{\tau_2 - \tau_1}{T_1} \right] = A, \text{ say.} \end{aligned}$$

(ix) Here $t = \tau_2 + \tau_2 - 2\tau_1 = 2\tau_2 - 2\tau_1$. The amplitude of the echo is given by

$$\begin{aligned} A_1'' + A_3'' &= (A_1' + A_3') \exp \left[- \frac{\tau_2 - 2\tau_1}{T_2} \right] \\ &= \frac{A}{2} \exp \left[- \frac{2\tau_2 - 4\tau_1}{T_2} \right] \\ &= \frac{M_0}{4} \exp \left[- \frac{2\tau_2 - 2\tau_1}{T_2} \right] = \bar{A}, \text{ say.} \end{aligned}$$

(x) Here $t = \tau_2 + \tau_2 - \tau_1 = 2\tau_2 - \tau_1$. The amplitude is given by

$$\begin{aligned} b_1'' + b_3'' &= (b_1' + b_3') \exp \left[- \frac{\tau_2 - \tau_1}{T_2} \right] \\ &= \frac{M_0}{2} \left[1 - \exp \left(- \frac{\tau_1}{T_1} \right) \right] \cdot \exp \left[- \frac{2(\tau_2 - \tau_1)}{T_2} \right] \\ &= B, \text{ say.} \end{aligned}$$

(xi) At $t = 2\tau_2$ the amplitude is given by

$$\begin{aligned} c_1'' + c_3'' &= (c_1' + c_3') \exp \left[- \frac{\tau_2}{T_2} \right] \\ &= \frac{c}{2} \exp \left[- \frac{2\tau_2}{T_2} \right] \end{aligned}$$

$$= \frac{M_0}{4} \exp \left[-\frac{2\tau_2}{T_2} \right]$$

$$= C \text{ say.}$$

With all these echo amplitude terms there will be terms indicating the loss of phase coherence due to isotropic distribution of the magnetic moment vectors. This will depend upon the distribution of the field inhomogeneity. For the case of Gaussian distribution this term comes as $\exp \left[-\frac{(t-t')^2}{2T_2^2} \right]$ t' being the time when the signal occurs. Thus we see that in addition to the free induction decays following immediately the r.f. pulses applied at $t = 0, \tau_1$ and τ_2 , echo pulses are formed at $t = 2\tau_1, \tau_2 + \tau_1, 2\tau_2 - 2\tau_1, 2\tau_2 - \tau_1$ and $2\tau_2$ due to constructive interference of the moment vectors. The echoes occurring at $t = 2\tau_1$ and $t = \tau_2 + \tau_1$ are most important and are called primary and stimulated echoes respectively. This constructive interference is possible only when $\tau_1, \tau_2 \leq T_2$ where T_2 is called the 'internal' phase memory time. This causes a damping of the echo signals. In addition to this damping, there is diffusion damping which becomes particularly prominent for the liquids of low viscosity and for the large field inhomogeneity. Table I below shows the echoes with their amplitudes and mechanism of formation when the r.f. pulses have different nutational angles. The superscripts 0, 1 and 2 stand for the free induction, primary and stimulated echo mechanisms respectively. As for example (12)¹ indicates the primary echo formed by the first and the second r.f. pulses. Similarly (123)² denotes the stimulated echo formed by the first, second and the third r.f. pulses. For details of other physical models and mathematical analysis, the reader is referred to the following literatures: [Hahn, (1950, 1953), Carr and Purcell, (1954), Das and Saha, (1954)].

As seen in the Table I, the echo amplitudes at $t = 2\tau_1$ and $\tau_2 + \tau_1$ depend on τ_1 and $\tau_2 + \tau_1$ respectively when the pulse widths are kept constant and the diffusion effect may be neglected. The primary echo amplitudes decay exponentially with T_2 as τ_1 is varied while the stimulated echo amplitudes decay with T_1 as τ_2 is varied. Thus T_2 and T_1 may be measured from the exponential decay envelopes of the primary and stimulated echoes respectively.

But the self-diffusion limits the accuracy of the results. However, modifications introduced by Carr and Purcell (1954) and by Holcomb and Norberg (1955) greatly eliminate this limitation. Even with this limitation, spin echo technique provides a better method of measuring relaxation times than the steady state methods where the field inhomogeneity obscures the actual value of T_2 . This method has another advantage over the steady case such as it needs no special care to minimize the r.f. leakage voltage as the echo signal is observed during the absence of the r.f. field.

TABLE I

PULSES	POSITION	ECHO AMPLITUDE		
		TRIGONOMETRIC PART	RELAXATION DAMPING FACTOR AT THE ECHO MAXIMUM	DIFFUSION DAMPING FACTOR AT THE ECHO MAXIMUM
PRIMARY ECHO (12) ¹	$2\tau_1$	$\sin \xi_1 \sin^2 \xi_2/2$	$\exp \left[-\frac{2\tau_1}{T_2} \right]$	$\exp \left[-\frac{\xi_1^2}{2} \tau_1^2 \right]$
STIMULATED ECHO (123) ²	$\tau_2 + \tau_1$	$\frac{1}{2} \sin \xi_1 \sin \xi_2 \sin \xi_3$	$\exp \left[-\frac{\tau_2 - \tau_1}{T_1} - \frac{2\tau_1}{T_2} \right]$	$\exp \left[-\frac{\xi_1}{3} \{ 3\tau_2^2 \tau_1^2 + 2\tau_1^3 \} \right]$
(13) ³	$2\tau_2$	$\sin \xi_1 \cos^2 \xi_2/2 \sin^2 \xi_3/2$	$\exp \left[-\frac{2\tau_2}{T_2} \right]$	$\exp \left[-\frac{\xi_1}{3} \{ 5\tau_2^3 - 6\tau_2^2 \tau_1 + 3\tau_2 \tau_1^2 + 5\tau_1^3 \} \right]$
(25) ⁴	$2\tau_2 - \tau_1$	$W(\tau_1) \sin \xi_1 \sin^2 \xi_3/2$	$\exp \left[-\frac{2\tau_2 - 2\tau_1}{T_2} \right]$	$\exp \left[-\frac{\xi_1}{3} \{ 5\tau_2^3 - 15\tau_2^2 \tau_1 + 15\tau_2 \tau_1^2 - 5\tau_1^3 \} \right]$
((12) ⁵) ⁵	$2\tau_2 - 2\tau_1$	$-\sin \xi_1 \sin^2 \xi_2/2 \sin^2 \xi_3/2$	$\exp \left[-\frac{2\tau_2 - 2\tau_1}{T_2} \right]$	$\exp \left[-\frac{\xi_1}{3} \{ 5\tau_2^3 - 24\tau_2^2 \tau_1 + 39\tau_2 \tau_1^2 - 17\tau_1^3 \} \right]$

[N.B. Table I. $E = \gamma H_1 t_\omega$ and ξ_1, ξ_2 and ξ_3 represent the values of ξ for three different pulses when their widths are not equal.

$$k = (\gamma G)^2 D$$

where G = average field gradient and D = coefficient of self-diffusion.]

III APPARATUS AND ITS ASSEMBLY

The block diagram of the apparatus required for the observation of the spin-echoes, is shown in the figure 2. The pulse generator generates two, three or more pulses, as may be necessary, with a certain repetition rate determined

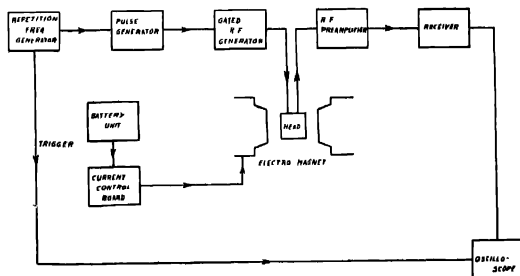


Fig. 2. Block diagram of the nuclear induction spin-echo apparatus.

by the repetition frequency generator. The pulses gate the transmitter and the gated r.f.-output is fed to the transmitter coil of the Bloch type probe by a twin cable. The other coil, called the receiving coil, placed approximately at right

Fig. 5. Circuit diagram of the final pulse stage to drive the r.f. transmitter.

followers. The final pulser stage is d.c. coupled to minimize any distortion in pulse shape. The biases are derived through the cathode followers which normally keep the pulsed stages in the r.f. transmitter (figure 6)—the first amplifier V_2 ,

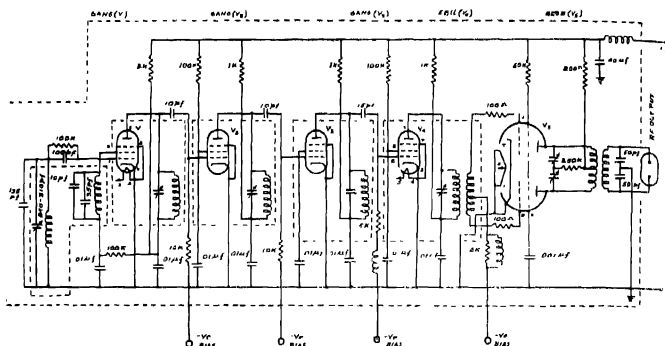


Fig. 6. Circuit diagram of the pulsed r.f. transmitter

the second frequency multiplier V_3 , the second amplifier V_4 and the final power amplifier V_5 beyond cut off. The final pulses are of good square shape with a rise time $\approx 0.1 \mu\text{sec.}$ The decaying tail is of about $1 \mu\text{sec.}$ duration.

(c) R.F. Transmitter

The transmitter starts with an electron-coupled master oscillator of frequency 1 mc/s. This can be set at other frequencies too. A selective circuit in the plate of V_1 (figure 6) selects the desired harmonic (7th harmonic in this preliminary experiment). This is amplified by V_2 and fed to a frequency doubler (V_3) circuit. This is again amplified by V_4 to the level required for adequate drive of the final power amplifier tube V_5 . Excepting the master oscillator, all the stages are pulsed to minimize the stray signal at the working frequency of 14 Mc/s., between pulses, to negligible levels. The pulsed r.f.-output, as seen on the Dumont Model 294 oscilloscope, indicated that the oscillations are established within a cycle and die down rapidly at the tail. The r.f.-output is taken by an inductive coupling link and fed to the transmitter coil by a twin cable. The transmitter coil is series resonated in a symmetrical arrangement to get a large balanced r.f.-voltage at the coil.

(d) The Nuclear Induction Head and other Accessories.

The nuclear induction head, as usual, consists of a transmitter coil split up into two equal sections containing 11-turn coil in each half. The two halves are wound around two perspex forms of 5/8" o.d. with a separation of 3/4" approximately. The perspex forms are made hollow to minimize the r.f.-loss. According to Weaver's model, [Weaver, 1953] one of the sections is held fixed while the

offer is kept movable for v -mode balance. A finer v -mode control is provided with a copper "paddle". The two variable capacitors, used to resonate the transmitter coil, provide the u -mode control by varying the centre voltage. The receiver coil consists of 16 turns of wire wrapped around another perspex form which can accommodate test tubes of 1/4" o.d. This is placed centrally inside the gap between the two sections of the transmitter coil. The transmitter coil is not placed in Helmholtz proportions with the purpose of increasing the r.f.-field impairing comparatively little field homogeneity. In contrast to the steady methods of nuclear induction, spin-echo technique requires very little isolation of the receiver from the transmitter because the nuclear response occurs only when the transmitter is silenced. The purpose of balancing is to prevent the receiver from over-driving during the pulse periods.

Before feeding to the receiver the induced voltage in the receiver coil is amplified by an r.f.-preamplifier to increase the signal to noise ratio. A 6AK5 tube containing the receiver coil with a tuning capacitor at its grid forms this r.f.-preamplifier. The amplified output is fed to the receiver with a single cable by proper impedance matching. The receiver has another r.f.-amplification stage in itself and has a band-width of 160 Kc/s. at 14 Mc/s. The receiver paralysis time is reduced by removing cathode by-pass capacitors at the r.f. amplification and i.f. amplification stages

IV. EXPERIMENTAL RESULTS

Figures 7 and 8 clearly show the effect of field homogeneity on the shape and amplitude of the echo pulse. It is seen that good homogeneity only lengthens

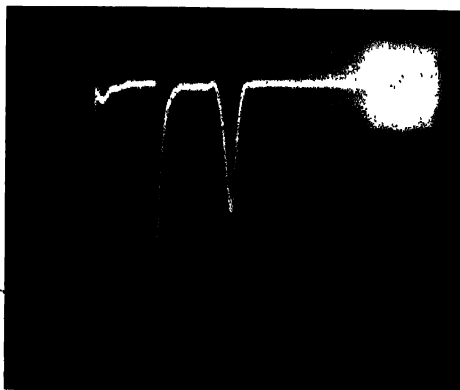


Figure 7. Echo signal of protons in glycerine. Field inhomogeneity $(\Delta H)_{AV} \approx 50$ milligauss. The r.f. pulses are sharp and faintly visible. The free induction decay signals following the pulses are prominent here. The first pulse is of 90° and the second one is 180° pulse. $\tau_1 = 19$ m sec.

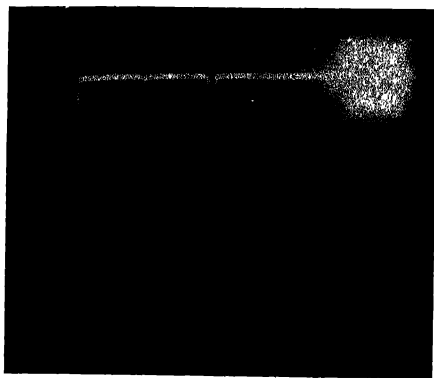


Fig 8. Echo signal of protons in glycerine under the same condition as that of figure 7 excepting the field inhomogeneity which is equal to 0.5 gauss

the decay time instead of appreciably changing the echo amplitude where the condition $H_1 > (\Delta H)_{AV}$ is satisfied and the diffusion effect may be neglected. $(\Delta H)_{AV}$ is the average field inhomogeneity over the sample. The decay time is given by the relation

$$T_2^* = (2 \log e^2)^{1/2} / \gamma (\Delta H)_{AV}$$

$(\Delta H)_{AV}$, calculated with this relation and that measured from the steady experiment

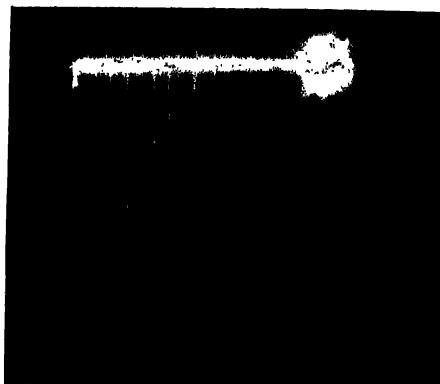


Fig 9. Multiple exposure for each signal of protons in glycerine with two pulse sequence with variation of τ_1 . The first and second r.f.-pulses are 90° and 180° pulse respectively. Field inhomogeneity $(\Delta H)_{AV} = 0.5$ gauss. Sweep period : 110 m sec.

agree quite well within experimental errors. Certain modulation type structures particularly prominent in the free induction signals are probably due to the non-equivalent protons in glycerine and perspex form for the sample holder. We wish to clear this point at some later occasion. Figure 9 is a multiple exposure to show the envelope of the echo signals of protons in glycerine obtained by varying τ_1 . By plotting the logarithm of echo amplitude *vs.* time we get a straight line and its gradient gives the value of 18m sec. for T_2' . Figure 10 represents the

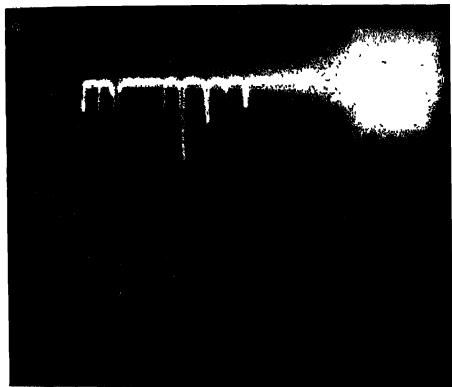


Fig. 10 Echo signals with three 90° rf-pulses. $\tau_1 = 6$ m sec, $\tau_2 = 17.5$ m sec.

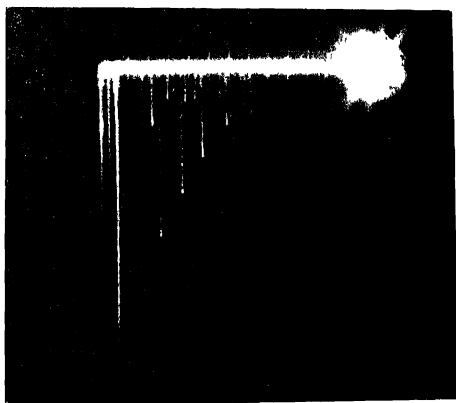


Fig. 11 Multiple exposure for stimulated echo signal of protons in glycerine with variation of τ_2 . $(\Delta H)_{AV} \approx 0.5$ gauss. Sweep period = 110 m sec.

echo pulses observed with three pulses and the figure 11 is the multiple exposure of the stimulated echo pattern with variation of τ_2 . Similarly as before, from a semi-log plot of stimulated echo amplitude vs. time, we can calculate T_1 . This comes out to be 23 m sec. All the measurements were carried at the room temperature

ACKNOWLEDGMENTS

The authors wish to express their sincere gratitude to the late Prof. M. N. Saha, F.R.S. for his constant encouragement during the progress of the work. They also like to thank Messrs T. P. Das, D.K. Roy and Miss T. Ghosh for many illuminating discussions at different times in course of its progress.

REFERENCES

- Bloch, F., 1946, *Phys. Rev.*, **70**, 460.
 Bloom, M., Hahn, E. L. and Herzog, B., 1955, *Phys. Rev.*, **97**, 1699.
 Boom, M. and Norberg, R. E., 1954, *Phys. Rev.*, **93**, 638.
 Carr, H. Y. and Purcell, E. M., 1954, *Phys. Rev.*, **94**, 630.
 Das, T. P. and Saha, A. K., 1954, *Phys. Rev.*, **93**, 749.
 Hahn, E. L., 1950, *Phys. Rev.*, **80**, 580.
 Hahn, E. L., 1953, *Phys. To-day*, **6**, No. 11, 4.
 Hahn, E. L. and Herzog, B., 1954, *Phys. Rev.*, **93**, 639.
 Hahn, E. L. and Maxwell, D. E., 1951, *Phys. Rev.*, **84**, 1246.
 Hahn, E. L. and Maxwell, D. E., 1952, *Phys. Rev.*, **88**, 1070.
 Holcomb, D. E. and Norberg, R. E., 1955, *Phys. Rev.*, **98**, 1074.
 Mulling, L., 1955, *Electronics*, **27**, 134.
 Norberg, R. E., 1952, *Phys. Rev.*, **86**, 745.
 Talm, I. I., Ramsey, N. F. and Schwinger, J., 1954, *Rev. Mod. Phys.*, **26**, 167.
 Saha, A. K., Banerjee, B. M., Das, T. P., Roy, D. K., Ghosh Roy, S. K. and Ghosh, T., 1956, *Ind. J. Phys.*, **30**, 211.
 Torrey, H. C., 1949, *Phys. Rev.*, **76**, 1059.
 Weaver, H. E., 1953, *Phys. Rev.*, **89**, 923.

ULTRASONIC VELOCITY OF SODIUM CHLORIDE SOLUTION IN WATER-DIAXENE MIXTURES.

SRINIBAS PANDA AND BIBHUTI BHUSAN DEO

PHYSICS DEPARTMENT, RAVENSHAW COLLEGE, CUTTACK

(Received for publication, September, 8, 1956)

ABSTRACT. Ultrasonic velocity of sodium chloride solution in water-diaxene mixtures has been measured at 26°C. It is found that the nature of variation of velocity is the same as that in ordinary water-diaxene mixture.

INTRODUCTION

Binary mixtures of non-associated organic liquids have been extensively studied for ultrasonic velocities and absorption by a host of workers. Similar mixtures of associated liquids have also been studied by Willard (1941) and Burton (1948). Their results are very interesting in so far as velocity and absorption maxima are found in intermediate concentrations. They have not yet been successfully explained by any current theory.

Diaxene and water mixture is often used in physical chemistry to vary the dielectric constant of the solvent and it is held that salts, NaCl for instance, depolymerise water. So it was felt worth while to study that variation of ultrasonic velocity in water-diaxene mixture

EXPERIMENTAL METHOD

The determination of the velocities were carried out by the method of photographing the Debye-Seearers diffraction spectra which have been reported in a preceding paper by Mohanty and Deo (1955). However, no great pre-

TABLE I

Percentage by volume of diaxene	Velocity in metres/sec
100	1332
90	1352
80	1400.8
60	1540
50	1565
40	1581
30	1582
20	1565.2
10	1541.5
5	1520
0	1493

caution was taken to maintain the constancy of temperature of the cell containing the solution since we are more interested in relative changes of velocities. The absolute accuracy of each measurement is not as high as the relative changes of velocities. Further, the solution was continuously stirred by a flat stirrer prior to exposure. The time of exposure was sufficiently small to allow any abnormality in temperature during exposure.

TABLE II

Percentage by volume of dioxene Con- centra- tion of NaCl	10%	20%	30%	40%	50%	60%	80%
	velocity in metres/sec						
0.05	1523.1	1544.7	1566.3	1585.1	1587.1	1572.8	1510.4
0.1	1526.3	1548.9	1568.6	1588.5	1590.1	1574.5	1542.7
0.2	1531.8	1552.9	1573.8	1592.4	1593.8	1477.5	1540.0
0.3	1538.0	1559.3	1580.3	1599.0	1597.7	1582.3	1512.7
0.4	1543.1	1565.3	1587.0	1602.7	1601.6	1584.4	1541.8
0.5	1518.4	1569.2	1592.1	1607.1	1607.5	1586.7	1541.9

RESULTS AND DISCUSSIONS

In Table I we report the values of velocities for water-dioxene mixtures. They have been previously measured by Burton (1948) at 23°C. Our values are

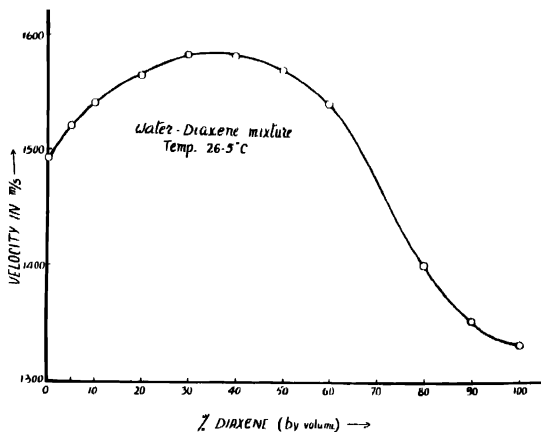


Fig. 1.

for 26°C. Our values agree very well with those of Burton. The concentration for maximum velocity computed from figure 1 is at 33% by volume of diaxene which is .88 m.f. The corresponding value of Burton is the same

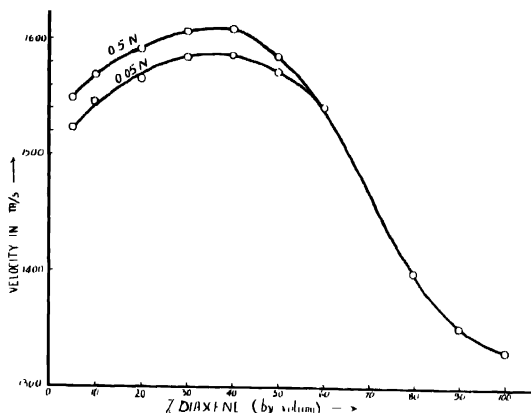


Fig. 2.

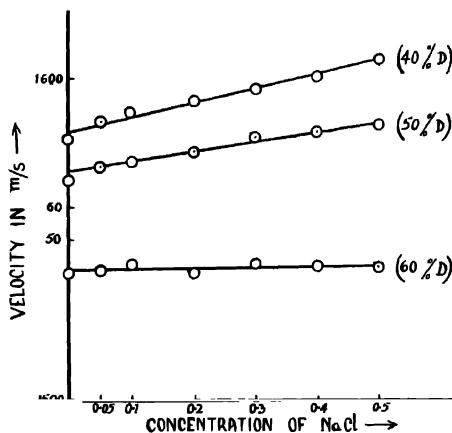


Fig. 3a.

In Table II the velocities for NaCl solutions in mixtures are given. The normalities refer to the strength in the total solution. In figure 2 we have plotted our values of the velocities for strengths 0.05N and 0.5N. To help subsequent discussions and for immediate reference from figure 2 we find the velocity curve

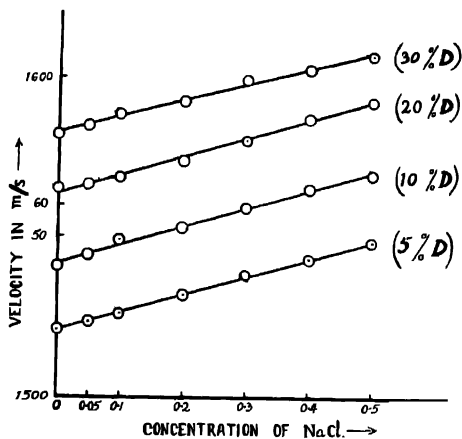


Fig. 3b

to be similar to figure 1 with maximum occurring at very nearly at the same concentration of diaxene. But the values of maxima shift upwards, which is the anticipated result.

Beyond about 60% diaxene by volume, addition of NaCl does not change the velocities at all. It was not possible to take reliable readings beyond this concentration and the solution became syrupy.

We have plotted curves 3(a) and (b) to show the change in slope of velocity and water-NaCl concentration graph with varying amounts of diaxene. The slope slightly increases or is nearly constant till 30% of diaxene and then falls off and at 60% the graph is parallel to the abscissa. Our results therefore, bear out the fact that at this concentration the water-diaxene mixtures behave like a non-electrolyte.

We also conclude that the already high ultrasonic velocities in associated liquids at the maxima (Burton) can be still further raised by addition of salts. In water-diaxene mixture in particular, this result is interesting for naval and radio research since the absorption is not high and does not show a maximum at lower concentration.

ACKNOWLEDGMENT

Authors, thanks are due to Sri B. S. Mohanty for some valuable discussions.

REFERENCES

- Burton, J., 1948, *J. Acous, Soc. Am*, **20**, 186.
- Mohanty, B. S. and Deo, B., 1955, *Ind. J. Phys.*, **24**, 577.
- Willard, G. W., 1941, *J. Acous, Soc. Am.*, **12**, 438.

A NEW METHOD OF DEMODULATION FOR PHASE, FREQUENCY AND AMPLITUDE

P. KUNDU

INDIAN INSTITUTE OF TECHNOLOGY, Kharagpur

(Received for publication, October, 26, 1956)

ABSTRACT. This paper describes a new method of demodulation of angle and amplitude modulated waves. The principle is based on the fact that the distance between the leading edges of the successive pulses obtained by properly limiting and then differentiating a modulated sinusoidal wave is a function of the instantaneous angle. It is also a function of amplitude of the modulated sinusoidal signal if the slicing level is above the zero axis. These variable distance pulses are then converted to variable amplitude saw-tooth waves. The original modulating signal is finally obtained by passing the saw-tooth wave through a low-pass filter.

1. INTRODUCTION

Existing methods of demodulation of angle modulated signal mainly use the principle of frequency discrimination in so far as the response varies linearly with the frequency, while a proper de-emphasis network is required for phase demodulation. Under certain considerations which are quite true for the usual practice, PM is three times better than FM and therefore a direct phase discriminator would have been more advantageous than the present practice of using combined FM and PM to achieve similar results (Starr, 1952). Besides, a perfect limiter and a balanced discriminator are the two essential pre-requisites with the conventional discriminators for improving the signal to noise ratio which is the main advantage of angle modulation. Further, a frequency discriminator is unsuitable for envelope detection required for amplitude demodulation.

2. DESCRIPTION

A method has, therefore, been developed which is essentially a phase discriminator while with slight adjustments it may be used for frequency or amplitude demodulation without having adverse effect on the performance of the system. This method is based on the principle similar to one developed by the author (Kundu, 1955) which consists of utilising the variation of a particular characteristic of a pulse produced by properly limiting a modulated sinusoidal carrier.

When an angle modulated wave is properly clipped near the zero axis, rectangular pulses are produced, the instantaneous frequency of which is a function

of the modulating signal $f(t)$. This information is incorporated in the pulses through the duration of the successive pulses as well as through the distance between them. The method of demodulation then consists in the reconstruction of the original signal $f(t)$ either from the duration or the distance between the pulses.

In case of FM, the frequency of the pulses varies directly (or the instantaneous time period varies inversely) with the modulating signal $f(t)$, while in case of PM it varies directly with rate of change of $f(t)$, i.e. directly as $f'(t)$. When, however, the maximum frequency deviation is a small fraction of the carrier, then the instantaneous time period T_i (i.e. $T_i = \frac{2\pi}{\omega_i}$) may be considered to have a linear relation with $f(t)$ in FM and $f'(t)$ in PM.

By differentiating the leading edges of the rectangular pulses of variable duration, angle modulated pulses of constant duration are produced. These short pulses are then used to switch off a linear saw-tooth generator so that a condenser is charged in the interval between the pulses, but is discharged on their arrival. An angle modulated wave (P.M. or F.M.) is thus translated into a saw-tooth amplitude modulated wave, the amplitude of which is proportional to $f(t)$ in case of FM and to $f'(t)$ for PM. The modulating signal may finally be reproduced by a low-pass filter. The wave emerging from the filter is, however, the original wave integrated in time. If the input is a phase modulated carrier, then the modulating signal is directly reproduced at the output of the filter. But in case of FM wave, a differentiating network is required to produce the original signal.

The same system may also be used for AM by changing the clipping level above the zero axis. In this case, the bias of a clipper diode is so adjusted that a small portion of the AM above the zero axis and below the minimum amplitude (assuming the amplitude modulation less than 100%, which is usually true) is sliced to get width modulated pulses from the AM wave.

If a sinusoidal carrier is given as $A \sin \frac{2\pi t}{T}$ and is sliced as in figure 1,

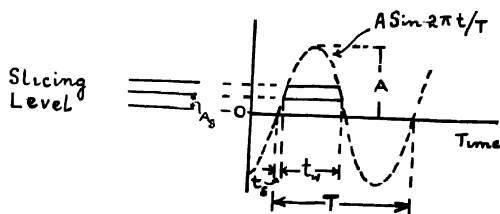


Fig. 1.

then

$$\frac{t_h}{T} = \frac{1}{2\pi} \sin^{-1} \frac{A_s}{A}$$

where A_s is the slicing level above the zero axis

Then the width of the pulse :

$$t_w = \frac{T}{2\pi} \left(\pi - \sin^{-1} \frac{A_s}{A} \right)$$

Or
$$t_w = \frac{T}{2\pi} \left(\pi - \frac{A_s}{A} \right), \text{ when } \frac{A_s}{A} < 1$$

$$t_w \propto m h, \text{ where } m = \frac{A_s}{A}$$

So long as $\frac{A_s}{A} < 1$, the width of the pulses obtained in this manner by slicing the AM signal varies according to the envelope of the AM wave. These duration-modulated pulses are then finally demodulated through the remaining parts of the circuit in the usual way. This demodulation, of course, may be carried out just by passing the width modulated pulses through a low-pass filter. Besides, the usual method of detection may be used here quite conveniently by passing the output of the carrier clipper (which removed the response of one side of the axis) through the low-pass filter.

3 EXPERIMENTAL RESULTS AND DISCUSSIONS

Some preliminary observations have been made with an experimental circuit illustrated in the block diagram. A carrier of low frequency has been preferred here to assure the optimum operation of the pulsing circuits, while a low modulation index was used to avoid any possibility of nonlinearity in the demodulation. A local carrier of 250 Kc/s from a RC oscillator has, therefore, been used with a modulation signal of 400 c/s adjusted to have produced the desired modulation. The demodulated output has been observed on the CRO, and found to be a faithful reproduction of the original modulating signal.

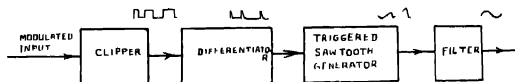


Fig. 2.

This method gives a system for directly demodulating a phase modulated carrier and also the frequency and amplitude modulated signals with a slight readjustment in the circuit. The respective advantages of using each method of

modulation as regards the signal noise ratio is also maintained. Besides, there is a further possibility of reduction of spurious noise due to the fact that limiting is an integral part of the system and that sharp timing pulses are only used to switch off a locally triggered saw-tooth generator. Any transient interference occurring in between the timing pulses will, therefore, produce very small effect. Inherently, this system is less sensitive, but it can be increased by increasing the deviation by translating the i.f. carrier to lower value, which also facilitates the design of the pulsing circuit. On the other hand, linearity of demodulation necessitates a smaller percentage of frequency deviation. A detailed investigation is in progress to study the distortion with deviation, and the noise reduction capability of this method quantitatively. A circuit based on this principle of phase discrimination as discussed above but with a different technique has also been set up by Chatterjee to investigate the performance at comparatively higher frequencies.

As regards the linearity of output with the period, it may be mentioned here that this type of demodulation calls for an investigation of period modulation of a sinusoidal carrier in which the angle is so modulated that the instantaneous period is directly proportional (*i.e.* instantaneous frequency is inversely proportional) to the amplitude of the modulating signal.

ACKNOWLEDGMENT

The author records his grateful thanks to Prof. H. Rakshit, D Sc., for his kind interest in the work and for very valuable discussions.

5. REFERENCES

- Chatterjee, B. Phase-Sensitive Discriminator (unpublished).
- Kundu, P. 1955 *Wireless Engineer* Dec. pp. 337.
- Starr, A. T. 1952 *Radio and Radar, Technique*, pp. 575-584.

AN APPLICATION OF LIPSON'S METHOD IN THE STUDY OF THE CRYSTAL SYSTEM OF BaBOF_3

D. M. CHACKRABURTTY

DEPARTMENT OF GENERAL PHYSICS AND X-RAYS,
INDIAN ASSOCIATION FOR THE CULTIVATION OF SCIENCE, CALCUTTA-32

(Received for publication January 3, 1957)

Plate V

ABSTRACT. An application of Lipson's method to the study of the crystal system of BaBOF_3 is described. The substance was found out to be orthorhombic and the constants A , B and C were directly determined from the difference diagrams. Complete indexing was done, and from the careful observations of extinction of hkl planes the space group was assigned to be $Pnma$. The merits of Lipson's method are also discussed in detail.

INTRODUCTION

A systematic study of BaBOF_3 along with other oxyfluoride compounds was undertaken to find out not only the crystal system of the compound but also to determine the space group, and structure. Full details about the preparation and properties of the substance have been given by Roy (1955).

The sample was obtained in powdered form. As it was difficult to get single crystals of such substances, the X-ray analysis was entirely confined to the powder method. The pictures were taken in a camera of radius 4.13 cm using $\text{CuK}\alpha$ radiation. As usual θ 'd' values and $\sin^2\theta$ were determined from the pictures.

ANALYSIS

The analysis was carried out by Hesse's method (1948). First, search was made to find out systematic relations for cubic systems and as no such relations were obtained, it was concluded that the crystal system is not cubic. Then 1st 9 q s (or $\sin^2\theta$) were taken in order and the systematic relations between the q 's were investigated for hexagonal and tetragonal systems. Even then the occurrence of the ratio m_1/m_2 without a common factor could not be deduced and therefore it was assumed that the system of BaBOF_3 is neither tetragonal nor hexagonal.

Next attempt was made to get relations for orthorhombic system. The method of Hesse (1948) and its extension by Stoeck (1949) was too complicated to be adopted in this case. Moreover, this method requires a very accurate deter-

mination of θ so that an accuracy of usually ± 0.002 in $\sin^2\theta$ values should be obtained. In practice such an accuracy can only be expected from pictures taken in a very good type of focussing camera using crystal monochromator. But with an ordinary camera an accuracy of that extent is difficult to attain. In view of these difficulties the simpler method suggested by Lipson (1949) was taken into account for working out the problem.

For orthorhombic systems

$$\sin^2\theta_{hkl} = Ah^2 + Bk^2 + Cl^2$$

where $A = \frac{\lambda^2}{4a^2}$, $B = \frac{\lambda^2}{4b^2}$, and $C = \frac{\lambda^2}{4c^2}$. The problem here is to find the values

of A , B and C which give the integral values of hkl for all the observed q values. Since $\sin^2\theta_{100} = A$, $\sin^2\theta_{010} = B$, $\sin^2\theta_{001} = C$, we have

$$B + C = \sin^2\theta_{010} + \sin^2\theta_{001} = \sin^2\theta_{011}$$

$$A + C = \sin^2\theta_{100} + \sin^2\theta_{001} = \sin^2\theta_{101}$$

$$A + B = \sin^2\theta_{100} + \sin^2\theta_{010} = \sin^2\theta_{110}$$

In practical analysis, of course, it is not always possible to get the planes 100, 010, 001, 110 etc. because some planes are absent due to vanishingly small amplitudes and some other planes likely due to non-primitive nature of the unit cell. Therefore, to deduce the equations in a more general form we can write,

$$\begin{aligned} A &= \sin^2\theta_{100} - \sin^2\theta_{101} - \sin^2\theta_{001} \\ &= \sin^2\theta_{110} - \sin^2\theta_{010} \\ &= \sin^2\theta_{1kl} - \sin^2\theta_{okl} \end{aligned}$$

Similarly, $4A = \sin^2\theta_{2kl} - \sin^2\theta_{okl}$

$$9A = \sin^2\theta_{3kl} - \sin^2\theta_{okl}.$$

The same type of relations hold good for the constants B and C .

For the purpose of utilising these differences and to find in a straightforward way the constants A , B and C from the observed data, the $\sin^2\theta_{obs}$ values of all the lines are tabulated in one column and in the succeeding columns the differences upto 0.1 between the lines shown at the heads of the columns, and the lines immediately following are noted. A plot is then made showing differences in horizontal lines for each powder line, as shown in the particular case of BaBOF_4 . While plotting, the horizontal lines are a bit elongated thereby including the possible error in the measurement of θ . Where several values are cut simultaneously by a vertical line such points are carefully noted. From these points the



Powder photograph of BaBOF₃

constants are to be deduced. This type of difference diagrams can also be conveniently used in monoclinic cases where β is nearly 90° , and in tetragonal and cubic systems as a rough check to the values of the constants or its multiples obtained by different analytical methods.

From the X-ray pictures of BaBOF₃ all possible differences were calculated in the same way mentioned above. Considering number of lines, a plot was made and vertical lines were run across common points as shown in figure 1. The maximum number that occurred was around .0308. This number divided by 4 gives another number .0077. Around this number too, there were common points.

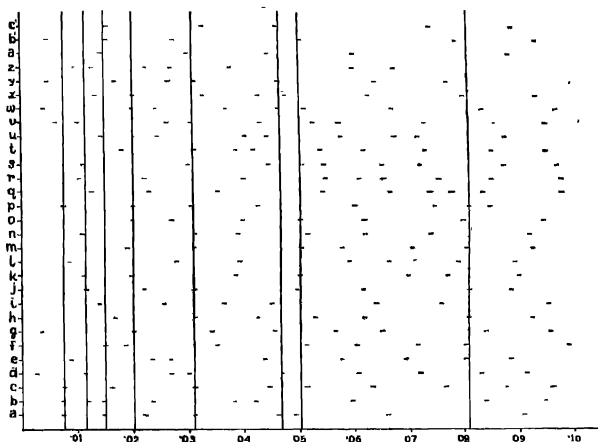


Fig. 1. Diagram of differences in $\sin^2\theta$ (abscissa) for lines (ordinate) on powder photograph of BaBOF₃.

Therefore it was assumed that one constant was .0077. Around slightly greater than .0200 and .0812 other common points were noted and probable value for the second constant was near about .0200. The 3rd constant was deduced to be around .115 from the values .0115 and .0465. From these values of the constants, indexing was tried for each line and for better indexing the constants were modified slightly by trial and error till a good agreement was obtained for $\sin^2\theta_{obs}$ and $\sin^2\theta_{calc}$. The constants after refinement were taken as $A = .0077$, $C = .0116$, and $B = .0203$.

TABLE I
Values of the $\sin^2\theta_{obs.}$ and $\sin^2\theta_{calc.}$ for BaBOF₄

$d(\text{\AA})$	$\sin^2\theta_{obs.}$	$\sin^2\theta_{calc.}$	hkl indices	$I_{obs.}$
4 271	0326	0319	011	m.w
3 856	0399	0396	111	m.w.
3 553	0470	0464	002	v w
3 392	0517	0511	210	s ¹
3 308	0546	0541	102	m.s.
3 067	0632	0627	211	s
2 810	0753	0744	112	m.s
2 702	0815	0813	020	m
2 460	0983	0975	212	w ¹
2 300	1121	1121	220	m w ¹
2 192	1238	1232	400	w
2 100	1347	1348	401	v s.
2 037	1432	1435	410	m w
1 914	1622	1622	321	v w
1 848	1740	1737	303	m
1 752	1936	1944	031	m w
1 721	2008	2021	131	w
1 667	2136	2136	114	m.w
1 629	2240	2244	511	w ¹
1 588	2358	2367	214	m.w.
1 531	2538	2549	304	m w. ¹
1 489	2681	2669	024	m w.
1 472	2744	2746	124	m
1 462	2782	2772	600	w
1 421	2942	2949	133	m
1 411	2984	2977	105	w
1 382	3111	3103	015	m.w.
1 361	3207	3208	205	w ¹
1 352	3253	3250	040	m w.
		3236	602	

TABLE I (contd)

$d(\text{\AA})$	$\sin^2\theta_{obs.}$	$\sin^2\theta_{calc.}$	hkl indices	I_{obs}
1 320	.3409	.3411	215	m.w.
1 288	.3580	.3584	020	m.w.
1 266	.3710	.3714	042	m.w.
1 217	.3992	.3984	514	w ⁺
1 199	.4139	.4132	405	m.w.
1 166	.4332	.4335	415	w ⁺
1 150	.4490	.4484	206	m.w.
1 127	.4681	.4687	216	m.w.
1 100	.4911	.4916	434	m.w.
		.4928	800	
1 081	.5084	.5072	316	w ⁺
1 064	.5255	.5247	811	m.w.
1 052	.5375	.5392	802	w ⁺
		.5387	250	
1 031	.5585	.5609	534	w ⁺
1 019	.5725	.5717	731	w
1 004	.5895	.5887	017	w
9137	.7121	.7120	551	w
9028	.7293	.7281	903	w
8826	.7626	.7628	354	m.w.
8632	.7979	.7979	055	w ⁺
8494	.8239	.8237	028	w.w.

With the help of the different diagram and the constants deduced, complete indexing of all lines were performed. The ' d ' values, calculated on the basis of the wavelength $\text{CuK}\alpha = 1.5418 \text{\AA}$, $\sin^2\theta_{obs.}$ and $\sin^2\theta_{calc.}$ and the intensities of each lines were shown in Table I. The intensities of a few lines at low angle region were greatly affected by a heavy background scattering. Considering this, due care was taken to give the exact nature of their intensities.

DISCUSSION OF THE RESULTS

To get a rough check of the values of the constants, Lipson has given a relation which directly links the number of lines observed in a powder photograph with the constants A , B and C . He deduced for orthorhombic cases, after consi-

dering the effects of extinctions in a photograph likely to be due to non-primitive cell and vanishingly small amplitudes that

$$\sqrt{ABC} \sim \sin^2 \theta_m / 4M \quad \dots (1)$$

where M number of lines observed in the film upto θ_m and A , B and C are the constants. In practice θ_m cannot be taken too large or too small. If θ is large then the expression is altered due to too many extinctions for vanishingly small amplitudes. On the contrary if it is low, the conditions in which the equations are deduced will not hold rigorously. When the magnitudes of A , B and C are of same order,

$$C \sim 0.4 \sin^2 \theta / M^{2/3} \quad \dots (2)$$

In our case θ_m was taken upto $26^\circ.62$ and inserting the values of A , B and C obtained above, M was calculated from equation 1. The value found was ~ 17 which agrees with the observed total number of lines upto such an angle. Again taking the observed number of lines upto $\theta_m = 26^\circ.62$ as 17, the value of one constant was calculated by equation (2) and was found out to be .012. This agrees with the observed C value, namely .0116. These tests confirm indirectly the correctness of the constants.

The axial lengths were calculated from the constants and taking into consideration the tolerance, can be written down as follows :

$$a = 8.78 \pm .03 \text{ \AA}$$

$$b = 5.41 \pm .02 \text{ \AA}$$

$$c = 7.16 \pm .02 \text{ \AA}$$

Search was made for all possible extinctions of the hkl planes and the following conditions seemed to be present.

for hkl planes present : no condition

$$ohl \quad " \quad " \quad : k \neq l = 2n$$

$$hol \quad " \quad " \quad \text{no condition}$$

$$hko \quad " \quad " \quad : h = 2n$$

$$hoo \quad " \quad " \quad : (h = 2n)$$

$$oko \quad " \quad " \quad : (k = 2n)$$

$$ool \quad " \quad " \quad : (l = 2n)$$

The most likely space group for this orthorhombic system is $Pnma$.

From the density observed 4.25 gm/cm^3 the number of molecules per unit cell is 4.

Further work on the above substance will be published shortly.

ACKNOWLEDGMENTS

The author expresses his gratitude to Prof. B. N. Srivastava for his help, suggestions and encouragement during the progress of the work. Sincere thanks are also due to Dr. Grihapati Mitra for supplying the sample

REFERENCES

- Hesse, R., 1948, *Acta Cryst.* **1**, 200.
Stosick, A. J., 1949, *Acta Cryst.* **2**, 271
Lipson, H., 1949, *Acta Cryst.*, 43.
Roy, A. 1955, Thesis, Calcutta University

SOMMERFELD'S FINE-STRUCTURE FORMULA FROM FIVE DIMENSIONAL WAVE-EQUATION

C. C. BANERJEE

DEPARTMENT OF THEORETICAL PHYSICS,

INDIAN ASSOCIATION FOR THE CULTIVATION OF SCIENCE, CALCUTTA-32

(Received for publication November 24, 1956)

ABSTRACT In this paper Sommerfeld's fine structure formula in exact form has been derived from five dimensional wave equation. It appears that the fifth coordinate influences the energy in the same way as the spin.

INTRODUCTION

Sommerfeld (1916) calculated the energy (W_{nl}) corresponding to the quantum numbers n , n_r and l for hydrogen and hydrogen like atoms by extending Bohr's quantisation rules to elliptic orbits for an electron moving in a coulomb field according to the special theory of relativity. According to this calculations,

$$W_{nl} = m_0 c^2 \left[1 + \frac{\alpha^2 z^2}{(n_r + \sqrt{(l+1)^2 - \alpha^2 z^2})^2} \right]^{\frac{1}{2}} \quad \dots (1)$$

$$\approx m_0 c^2 - \frac{R h z^2}{n^2} \left\{ 1 + \frac{\alpha^2 z^2}{n^2} \left(\frac{n}{l+1} - \frac{3}{4} \right) \right\} \quad \dots (1a)$$

where α is the fine structure constant and Z is the nuclear charge number. The equation (1) agrees with experimental data over wide range of wave lengths and the approximate equation (1a) explains experimental results in the optical region within the limits of experimental error.

In wave mechanics, however, the parallel calculation from Klem-Gordon equation, which is the relativistic analogue of the Schrodinger equation, gives

$$W_{nl} = m_0 c^2 \left[1 + \frac{\alpha^2 z^2}{(n_r + \sqrt{(l+\frac{1}{2})^2 - \alpha^2 z^2})^2} \right]^{\frac{1}{2}} \quad \dots (2)$$

$$\approx m_0 c^2 - \frac{R h z^2}{n^2} \left\{ 1 + \frac{\alpha^2 z^2}{n^2} \left(\frac{n}{l+\frac{1}{2}} - \frac{3}{4} \right) \right\} \quad \dots (2a)$$

Heisenberg and Jordan (1926) and Pauli (1927) have made calculations where influences of relativity and spin are taken into account by perturbation method. Their results show that if we take only relativity correction we obtain the approxi-

mate Eq. (2a) and if, further spin correction is added we get the approximate Eq. (1a). Hence to make the theoretical formula conform to the experimental data, it is necessary to take both the influences of relativity and spin, even then they obtain the approximate relation (1a) which is so because perturbation method has been employed to deduce the energy corrections.

The calculations, according to Dirac's theory which incorporates spin and relativity in an inseparable way lead to the exact expression i.e. equation (1).

In the present paper the author shows that Sommerfeld's formula in exact form can be obtained from the relativistic wave equation in five dimensional space-time similar to the Klein-Gordon equation. The spin of the electron does not show up explicitly here, but it appears that the additional momentum component of the space considered may be closely related to the spin.

DERIVATION OF FINE-STRUCTURE FORMULA

According to the special theory of relativity the total energy W of a particle moving in a field of potential V is related to its momentum p and rest mass m by the equation

$$(W - V)^2 - m_0^2 c^2 = p^2 \quad \dots (3)$$

In a five dimensional space-time continuum, the time independent part of the momentum p has got four-components p_x, p_y, p_z and p_s , and hence

$$p^2 = p_x^2 + p_y^2 + p_z^2 + p_s^2 = \frac{W^2 - m_0^2 c^4}{c^2} = \frac{2WV}{c^2} + \frac{V^2}{c^2} \quad \dots (3a)$$

Replacing the components of the momentum by the corresponding Schrödinger operators and putting $V = -\frac{Ze^2}{r}$ we obtain in the usual manner the wave equation

$$\frac{\partial^2 \psi}{\partial x^2} + \frac{\partial^2 \psi}{\partial y^2} + \frac{\partial^2 \psi}{\partial z^2} + \frac{\partial^2 \psi}{\partial s^2} + \left(A + \frac{2B}{r} + \frac{Z^2 \alpha^2}{r^2} \right) \psi = 0 \quad \dots (4)$$

where
$$A = \frac{W^2 - m_0^2 c^4}{\hbar^2 c^2} \quad \text{and} \quad B = \frac{WZe^2}{\hbar^2 c^2}$$

In polar co-ordinates

$$x = r \sin \theta \cos \phi \sin \chi$$

$$y = r \sin \theta \sin \phi \sin \chi$$

$$z = r \cos \theta \sin \chi$$

$$s = r \cos \chi$$

the equation becomes

$$\begin{aligned} \frac{\partial^2 \psi}{\partial r^2} + \frac{3}{r} \frac{\partial \psi}{\partial r} + \frac{1}{r^2} \left[\frac{1}{\sin^2 \chi} \frac{\partial}{\partial \theta} \left(\sin \theta \frac{\partial \psi}{\partial \theta} \right) + \frac{1}{r^2} \frac{1}{\sin^2 \chi} \frac{1}{\sin^2 \theta} \cdot \frac{\partial^2 \psi}{\partial \phi^2} \right. \\ \left. + \frac{1}{r^2} \frac{1}{\sin^2 \chi} \cdot \frac{\partial}{\partial r} \left(\sin^2 \chi \frac{\partial \psi}{\partial r} + \left(A + \frac{2B}{r} + \frac{Z^2 \alpha^2}{r^2} \right) \psi \right) \right] = 0 \quad (4a) \end{aligned}$$

We further maintain that the solution ψ can be written in the form $\psi = \psi_r, \psi_\theta, \psi_\phi, \psi_\chi$ and hence the equation (4a) becomes

$$\begin{aligned} r^2 \psi_r \left[\frac{\partial^2 \psi_r}{\partial r^2} + \frac{3}{r} \frac{\partial \psi_r}{\partial r} + \left(A + \frac{2B}{r} + \frac{Z^2 \alpha^2}{r^2} \right) \psi_r \right] + \left[\frac{1}{\psi_\theta} \frac{1}{\sin^2 \chi} \sin \theta \cdot \right. \\ \left. \frac{\partial}{\partial \theta} \left(\sin \theta \frac{\partial \psi_\theta}{\partial \theta} \right) + \frac{1}{\psi_\phi} \frac{1}{\sin^2 \chi} \frac{1}{\sin^2 \theta} \cdot \frac{\partial^2 \psi_\phi}{\partial \phi^2} + \right. \\ \left. \frac{1}{\psi_\chi} \frac{1}{\sin^2 \chi} \frac{\partial}{\partial \chi} \left(\sin^2 \chi \frac{\partial \psi_\chi}{\partial \chi} \right) \right] = 0 \end{aligned}$$

we may write the above equation as

$$r^2 \psi_r \left[\frac{\partial^2 \psi_r}{\partial r^2} + \frac{3}{r} \frac{\partial \psi_r}{\partial r} + \left(A + \frac{2B}{r} + \frac{Z^2 \alpha^2}{r^2} \right) \psi_r \right] = K$$

and

$$\begin{aligned} \frac{1}{\psi_\theta} \frac{1}{\sin^2 \chi} \sin \theta \cdot \frac{\partial}{\partial \theta} \left(\sin \theta \frac{\partial \psi_\theta}{\partial \theta} \right) + \frac{1}{\psi_\phi} \frac{1}{\sin^2 \chi} \frac{1}{\sin^2 \theta} \cdot \frac{\partial^2 \psi_\phi}{\partial \phi^2} + \\ \frac{1}{\psi_\chi} \frac{1}{\sin^2 \chi} \frac{\partial}{\partial \chi} \left(\sin^2 \chi \frac{\partial \psi_\chi}{\partial \chi} \right) = -K \end{aligned}$$

The equation (4c) admits of single valued solution when $K = l(l+2)$ where l is a positive integer. This gives us

$$\psi_\theta = D_\theta P_l^m(\cos \theta), \quad \psi_\phi = D_\phi e^{im\phi} \quad \text{and} \quad \psi_\chi = D_\chi \sin^l \chi$$

where D_θ, D_ϕ and D_χ are the normalization constants. The value of D_χ is as follows

$$D_\chi = \left[\frac{2^{l+1} (l+1)!}{1 \cdot 3 \cdot 5 \dots (2l+1)} \cdot \left(\frac{2}{\pi} \right) \right]^{\frac{1}{2}}$$

So the radial equation (4b) may be written as

$$\frac{\partial^2 \psi_r}{\partial r^2} + \frac{3}{r} \frac{\partial \psi_r}{\partial r} + \left(A - \frac{2B}{R} + \frac{C}{r^2} \right) \psi_r = 0 \quad (5)$$

where

$$C = \alpha^2 z^2 - l(l+1)$$

To obtain the fine structure formula let us now solve the equation (5) by the well-known polynomial method. In case of hydrogen like atoms $W < 0$ and if we

set $A = -\frac{1}{r_0^2}$ and $\rho = \frac{2r}{r_0}$ the admissible solution of ψ_r is

$$\psi_r = e^{-\frac{\rho}{2}} v$$

where v is a polynomial given by $v = \rho^\gamma \sum a_r \rho^r$ where γ is a constant and $r = 0, 1, 2, \dots, \infty$. Substituting this value of ψ_r in the radial equation (5) we have

$$v'' + v' \left(\frac{3}{\rho} - 1 \right) + \left[\left(\frac{B}{\sqrt{-A}} - 1 \right) \frac{1}{\rho} - \frac{l(l+1) - \alpha^2 z^2}{\rho^2} \right] v = 0$$

Substituting the polynomial expression for v in this equation and equating the coefficient of $\rho^{\gamma-2} = 0$ we finally obtain

$$\gamma + 1 = \sqrt{l(l+1) - \alpha^2 z^2} \quad \dots (6)$$

Limiting the series at $v = n_r$ we have

$$n_r + \gamma + 1 = \frac{B}{\sqrt{-A}} \quad \dots (7)$$

Squaring both sides of equation (7) and substituting the values of A and B , we have for an electron moving in a coulomb field

$$W = m_0 c^2 \left[1 + \frac{\alpha^2 z^2}{(n_r + \gamma + 1)^2} \right]^{-1}$$

Substituting the value of $(\gamma+1)$ from equation (6), we have,

$$W = m_0 c^2 \left[1 + \frac{\alpha^2 z^2}{(n_r + \sqrt{l(l+1) - \alpha^2 z^2})^2} \right]^{-1}$$

This equation is the well known Sommerfeld's fine structure formula.

DISCUSSION

The idea of five dimensions used in this paper was first introduced by Kaluza (1921) to unify gravitational and electromagnetic fields but he did not assign any physical significance to the fifth coordinate.

Flint (1946) has shown that by the introduction of the fifth coordinate in wave mechanics one can obtain the electronic radius $\frac{e^2}{m_0 c^2}$ and the fundamental length $\frac{h}{m_0 c^2}$ as natural consequences of this representation.

In the present paper it is shown that a five dimensional second order wave equation gives us the same energy levels of the hydrogen atom as were obtained from the first order equation of Dirac. In our equation the idea of spin has not been explicitly introduced so far as the energy levels of the bound electron are concerned, the fifth coordinate influences the energy exactly in the same way as the matrices of Dirac.

ACKNOWLEDGMENT

The author wishes to express his sincere thanks to Prof. D. Basu, Ph.D., for his learned discussions and encouragement throughout the progress of the work.

REFERENCES

- Flint, H. T. 1940, *Phil. Mag.*, **29**, 330.
 Heisenberg, W. & Jordan, P. 1926, *Zeit f. Physik.*, **37**, 263.
 Kaluza, T., 1921, *Sitzungsber. d. Preuss. Akad.*, 966.
 Pauli, W. 1927, *Zeit f. Physik.*, **43**, 601.
 Sommerfeld, A., 1916, *Ann. der Physik.*, **51**, 1.

APPARENT SEPARATION AND INTENSITY RATIO OF CLOSE SPECTRAL LINES

K. C. CHATURVEDI

156-D, KAMLA NAGAR, DELHI-6

(Received for publication May 2, 1956)

ABSTRACT. In this paper the author has discussed the relationship between the true separation (a), true intensity ratio (b) and apparent separation (a') and apparent intensity ratio (b') when (i) instrumental line width is negligible and (ii) when natural line width is negligible. Graphs have been drawn, which may be used to correct for shrinkage effect.

INTRODUCTION

In every spectroscopic instrument, the mutual overlapping of intensity patterns of two close spectral lines results in their spurious closing together. Very little work has been done on this important aspect, which introduces considerable error, if disregarded, specially when the instruments are used to the limit of their capacities.

The analysis of the problem becomes extremely difficult when both the instrumental and the Doppler line widths are taken into account. Oldenburg (1922) has discussed the case in which there is partial overlapping of the Doppler distribution of two lines. In his treatment he implicitly assumed that the Doppler width is much larger than the instrumental width for the latter to be disregarded. Thus assuming the intensity distribution to be governed by Doppler effect, Oldenburg (1922) has shown that the shifts x_1 and x_2 , due to shrinkage effect, of the weaker and stronger lines respectively from their true positions are given by

$$x_1 = \frac{ab}{ea^2 + b - 2a^2b}$$

$$x_2 = \frac{a}{bea^2 + 1 - 2a^2}$$

where

$$x = \sqrt{\beta}(v - v_0), \quad a = \sqrt{\beta} \cdot \Delta v, \quad \beta = \mu c_0^2 / 2RTv_0^2$$

and $b (> 1)$ is the intensity ratio of the two component lines.

It is evident that to determine x_1 and x_2 from the above formulae, we must know the true separation a and intensity ratio b of the spectral lines. However,

in practice we can measure only the apparent separation of the two lines a' and apparent intensity ratio b' , given by

$$a' = a - x_1 - x_2$$

and

$$b' = I_2/I_1$$

where I_2 and I_1 are the stronger and weaker maxima respectively of the resultant intensity pattern of the two spectral lines. In this communication, the author has discussed the relationship between a , b , a' and b' , and found that b' is approximately equal to b for all cases of interest. Graphs between $(a-a')$ and a' for various values of b have been given, which may be used to correct for the shrinkage effect.

Moreover Oldenburg's treatment cannot be applied to those cases in which the Doppler width is less than the instrumental width, as has been pointed out by Tolansky (1947). A small gap Fabry Perot etalon is generally employed in the examination of a widespread spectrum and the observable line width is mainly due to the instrument and not due to the line. Similarly, with the prism and the grating and even with high resolving power instruments, when modern hyperfine-structure sources like the atomic beam are used, the condition essential to Oldenburg's treatment that the instrumental width must be less than Doppler width, breaks down.

Sodha (1955) has developed a method of successive approximations to calculate the shift of close spectral lines due to mutual overlapping of intensity patterns, when Doppler width is negligible. To determine the shifts x_1 and x_2 by this method we must know the true separation a and intensity ratio b of the spectral lines. But in actual practice we can measure only the apparent separation a' and apparent intensity ratio b' . In this communication the author has discussed the relationship between a , b , a' and b' for Fabry Perot etalon. It has been found that b and b' are considerably different in this case. Hence the author has finally given a figure illustrating the variation of $(b-b')$ with b' for various values of a' and another figure showing the dependence of $(a-a')$ with a' for various values of b . Using these two figures, it is very easy to obtain the true separation a and true intensity ratio b from the observed apparent separation a' and intensity ratio b' .

NEGLECTIBLE INSTRUMENTAL WIDTH

The intensity distribution of a spectral line of wave number ν_0 due to Doppler effect is given by

$$I' = I_0 e^{-\beta(\nu-\nu_0)^2}$$

where $\beta = \mu c_0^2 / 2RT\nu_0^2$, μ being the mass of radiant atoms.

The intensity distribution of another spectral line of wave number ($\nu_0 + \Delta\nu$) and an intensity b times that of the first is given by

$$I'' = bI_0 e^{-\beta(\nu - \nu_0)^2}$$

if $\Delta\nu$ is small (β same for both the lines)

Putting $\sqrt{\beta}(\nu - \nu_0) = x$ and $\sqrt{\beta} \cdot \Delta\nu = a$, the resultant intensity pattern is given by

$$\frac{I}{I_0} = e^{-x^2} + be^{-(a-x)^2} \quad \dots (1)$$

Now, the value of x for which the maximum of the resultant intensity pattern occurs, is given by

$$\frac{1}{2I_0} \cdot \frac{dI}{dx} = -xe^{-x^2} + b(a-x)e^{-(a-x)^2} = 0$$

$$\text{or} \quad \phi(x) = b\phi(a-x) \quad \dots (2)$$

where

$$\phi(x) = xe^{-x^2}$$

The stronger maximum ($x = a - x_2$), which occurs near $x = a$, can be determined by solving equation (2) by the method of successive approximations.

The weaker and the stronger maxima of the resultant intensity pattern are respectively given by

$$\frac{I_1}{I_0} = e^{-x_1^2} + be^{-(a-x_1)^2} \quad \dots (3)$$

$$\frac{I_2}{I_0} = e^{-(a-x_2)^2} + be^{-x_2^2} \quad \dots (4)$$

The apparent intensity ratio (b') and apparent separation (a') of the two spectral lines are given by

$$b' = \frac{I_2}{I_1} \quad \dots (5)$$

and

$$a' = a - x_1 - x_2 \quad \dots (6)$$

The details of the calculations are given in Table I, which gives the variation of $(a - a')$ and b' with a' for $b = 1, 2, 3, 4$ and 5 . It is seen that in all cases $b' \approx b$.

The variation of $(a-a')$ with a' for various values of b is illustrated figure 1.

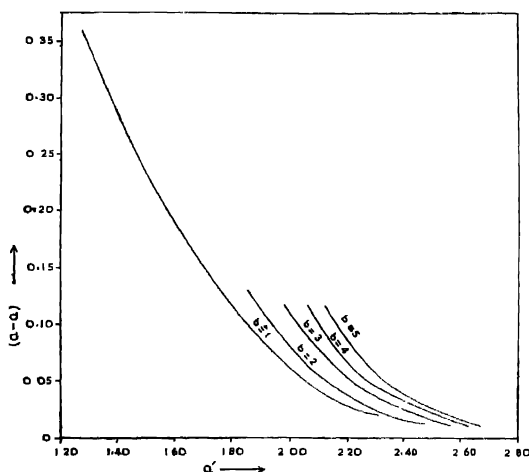


Fig. 1 Variation of $(a-a')$ with a' for $b = 1, 2, 3, 4$ and 5 when instrumental width is negligible

FABRY PEROT ETALON

The intensity pattern of a spectral line in the order (n_0+n) , where n is a fraction and n_0 an integer is given for the Fabry Perot etalon by

$$I' = \frac{I_0}{1 + F \sin^2 \pi(n_0+n)} = \frac{I_0}{1+x^2}$$

where F is the coefficient of fineness and $x = \pi n F^{\frac{1}{2}}$

The intensity distribution of another spectral line, separated by an order Δn and of an intensity b times that of the first, is given by

$$I'' = \frac{bI_0}{1 + F \sin^2 \pi(n_0+n-\Delta n)} = \frac{bI_0}{1+(x-a)^2}$$

where

$$a = \pi \cdot \Delta n F^{\frac{1}{2}}$$

The resultant intensity pattern is given by

$$\frac{I}{I_0} = \frac{1}{1+x^2} + \frac{b}{1+(x-a)^2} \quad \dots (7)$$

TABLE I

Variation of $(a-a')$ and b' with a' for $b = 1, 2, 3, 4$ and 5 when instrumental width is negligible

b	x_1	$a-x_1$	a	$\frac{I_1}{I_0}$	x_2	$\frac{I_2}{I_0}$	$b' = \frac{I_2}{I_1}$	$a-a' = x_1+x_2$	a'
1	0.01	2.336	2.346	1.004	0.0100	1.004	1.000	0.0200	2.3260
1	0.05	1.909	1.959	1.024	0.0500	1.024	1.000	0.1000	1.8590
1	0.10	1.683	1.783	1.049	0.100	1.049	1.000	0.2000	1.5830
1	0.15	1.533	1.683	1.073	0.1500	1.073	1.000	0.3000	1.3830
1	0.18	1.457	1.637	1.088	0.1800	1.088	1.000	0.3600	1.2770
2	0.01	2.492	2.502	1.004	0.0025	2.002	1.994	0.0125	2.4895
2	0.05	2.105	2.155	1.021	0.0107	2.010	1.968	0.0607	2.0943
2	0.10	1.911	2.011	1.042	0.0185	2.018	1.937	0.1185	1.8925
2	0.11	1.883	1.993	1.045	0.0190	2.017	1.930	0.1290	1.8640
3	0.01	2.583	2.593	1.004	0.0011	3.001	2.990	0.0111	2.5819
3	0.04	2.267	2.307	1.016	0.0038	3.005	2.958	0.0438	2.2632
3	0.08	2.091	2.171	1.032	0.0066	3.009	2.917	0.0866	2.0844
3	0.11	2.003	2.113	1.042	0.0084	3.012	2.890	0.1184	1.9946
4	0.01	2.640	2.650	1.004	0.0006	4.002	3.988	0.0106	2.6394
4	0.04	2.336	2.376	1.015	0.0021	4.004	3.943	0.0421	2.3339
4	0.08	2.165	2.245	1.030	0.0037	4.007	3.888	0.0837	2.1613
4	0.11	2.084	2.194	1.040	0.0045	4.008	3.855	0.1145	2.0795
5	0.01	2.680	2.690	1.004	0.0004	5.001	4.982	0.0104	2.6796
5	0.04	2.387	2.427	1.015	0.0014	5.003	4.928	0.0414	2.3856
5	0.08	2.223	2.303	1.029	0.0023	5.005	4.862	0.0823	2.2207
5	0.11	2.143	2.253	1.039	0.0029	5.006	4.819	0.1129	2.1401

*Obtained by trial and error, such that the condition $\phi(x_1) = b\phi(a-x_1)$ is satisfied.

Now, the value of x for which the maximum of the resultant intensity pattern occurs, is given by

$$-\frac{1}{2I_0} \frac{dI}{dx} = \frac{x}{(1+x^2)^2} - \frac{b(a-x)}{(1+(a-x)^2)^2} = 0$$

or

$$F(x) = bF(a-x) \quad \dots (8)$$

where

$$F(x) = \frac{x}{(1+x^2)^2}$$

The stronger maximum ($x = a - x_2$), which occurs near $x = a$, can be determined by solving equation (8) by the method of successive approximations given by Sodha (1955). The weaker and the stronger maxima of the resultant intensity pattern are respectively given by

$$\frac{I_1}{I_0} = \frac{1}{1+x_1^2} + \frac{b}{1+(a-x_1)^2} \quad \dots (9)$$

$$\frac{I_2}{I_0} = \frac{1}{1+(a-x_2)^2} + \frac{b}{1+x_2^2} \quad \dots (10)$$

The apparent intensity ratio (b') and apparent separation (a') of the two spectral lines are given by

$$b' = \frac{I_2}{I_1} \quad \dots (11)$$

and

$$a' = a - x_1 - x_2 \quad \dots (12)$$

The details of the calculations are given in Table 11, which gives the variation of $(a-a')$ and b' with a' for $b = 1, 2, 3, 4$ and 5. The variation of $(a-a')$ with a' for various values of b is illustrated by figure 2. The variation of b' with a' for various values of b is illustrated by figure 3.

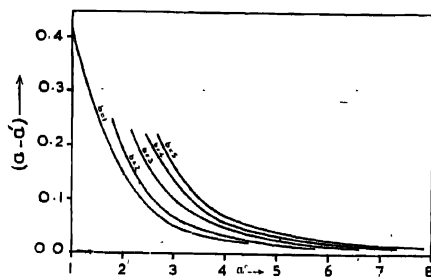


FIG. 2. Variation of $(a-a')$ with a' for $b = 1, 2, 3, 4$ and 5 for Fabry Perot Etalon.

TABLE II

Variation of $(a - a')$ and b' with a' for $b = 1, 2, 3, 4$ and 5 for
Fabry Perot etalon.

b	x_1	$a - x_1$	a	$\frac{I_1}{I_0}$	x_2	$\frac{I_2}{I_0}$	$b' = \frac{I_2}{I_1}$	$\frac{a - a'}{= x_1 + x_2}$	a'
1	0.01	4.46	4.47	1.048	0.0100	1.048	1.000	0.0200	4.4500
1	0.06	2.27	2.33	1.159	0.0600	1.159	1.000	0.1200	2.2100
1	0.11	1.74	1.85	1.236	0.1100	1.236	1.000	0.2200	1.6300
1	0.16	1.44	1.60	1.300	0.1600	1.300	1.000	0.3200	1.2600
1	0.21	1.24	1.45	1.352	0.2100	1.352	1.000	0.4200	1.0300
2	0.01	5.74	5.75	1.059	0.0025	2.029	1.917	0.0125	5.7375
2	0.06	3.00	3.06	1.196	0.0145	2.097	1.753	0.0745	2.9655
2	0.11	2.38	2.49	1.288	0.0240	2.140	1.661	0.1340	2.3560
2	0.16	2.05	2.21	1.359	0.0330	2.172	1.598	0.1930	2.0170
2	0.21	1.84	2.05	1.416	0.0400	2.196	1.551	0.2500	1.8000
3	0.01	6.60	6.61	1.067	0.0011	3.022	2.832	0.0111	6.5989
3	0.06	3.50	3.56	1.223	0.0064	3.073	2.513	0.0664	3.4936
3	0.11	2.81	2.92	1.325	0.0108	3.105	2.343	0.1208	2.7992
3	0.16	2.44	2.60	1.406	0.0146	3.129	2.225	0.1746	2.4254
3	0.21	2.20	2.41	1.472	0.0177	3.148	2.139	0.2277	2.1823
4	0.01	7.30	7.31	1.074	0.0006	4.018	3.743	0.0106	7.2994
4	0.06	3.90	3.96	1.243	0.0035	4.060	3.266	0.0635	3.8965
4	0.11	3.14	3.25	1.356	0.0061	4.087	3.013	0.1161	3.1339
4	0.16	2.73	2.89	1.448	0.0082	4.107	2.836	0.1682	2.7218
4	0.21	2.48	2.69	1.517	0.0100	4.122	2.717	0.2200	2.4700
5	0.01	7.85	7.86	1.080	0.0004	5.016	4.646	0.0104	7.8496
5	0.06	4.23	4.29	1.261	0.0022	5.052	4.006	0.0622	4.2278
5	0.11	3.40	3.51	1.386	0.0040	5.075	3.661	0.1140	3.3960
5	0.16	2.99	3.15	1.478	0.0053	5.092	3.445	0.1653	2.9847
5	0.21	2.72	2.93	1.553	0.0064	5.105	3.286	0.2164	2.7136

*Obtained by trial and error, such that the condition $F(x_1) = bF(a - x_1)$ is satisfied.

The variation of $(b-b')$ with b' for different values of a' is given in Table III which has been tabulated from figure 3.

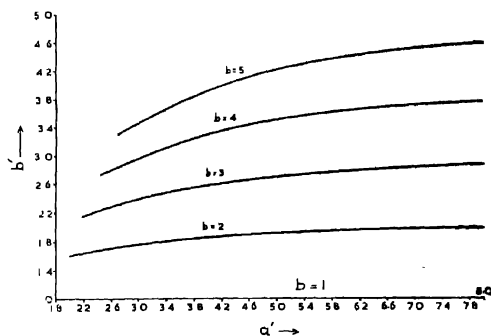


Fig. 3 Variation of b' with a' for $b = 1, 2, 3, 4$ and 5 for Fabry Perot Etalon.

TABLE III

Variation of $(b-b')$ with b' for different values of a' for Fabry Perot etalon

a'	$b=1$		$b=2$		$b=3$		$b=4$		$b=5$	
	b'	$b-b'$	b'	$b-b'$	b'	$b-b'$	b'	$b-b'$	b'	$b-b'$
1.8	1	0	1.55	0.45	—	—	—	—	—	—
2.2	1	0	1.64	0.36	2.15	0.85	—	—	—	—
2.6	1	0	1.71	0.29	2.28	0.72	2.78	1.22	—	—
3.0	1	0	1.76	0.24	2.40	0.60	2.96	1.04	3.46	1.54
3.4	1	0	1.80	0.20	2.49	0.51	3.11	0.89	3.66	1.34
4.0	1	0	1.85	0.15	2.60	0.40	3.30	0.70	3.92	1.08
5.0	1	0	1.90	0.10	2.72	0.28	3.50	0.50	4.24	0.76
6.6	1	0	1.94	0.06	2.84	0.16	3.68	0.32	4.52	0.48
8.0	1	0	1.96	0.04	2.88	0.12	3.78	0.22	4.66	0.34

Table III is illustrated by figure 4.

Figure 4 and figure 2 can be used to determine a and b from a' and b'

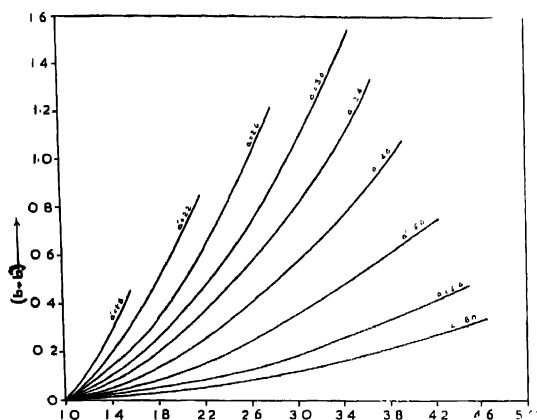


Fig. 4. Variation of $(b - b')$ with b' for different values of a' for Fabry Perot Etalon

ACKNOWLEDGMENT

The author is grateful to Dr. M. S. Sodha for suggesting the problem and to Dr. D. S. Kothari for permission to publish this paper.

REFERENCES

- Oldenburg, 1922, *Ann. der Physik*, **67**, 253.
 Sodha, 1955, *Ind. J. Phys.*, **29**, 161.
 Tolansky, 1947, *High Resolution Spectroscopy* (Methuen and Co. London), 240.

DIPOLE MOMENTS OF SOME SUBSTITUTED BENZENES AND PYRIDINES PART I—FLUOROTOLUENES

C. R. K. MURTY

DEPARTMENT OF PHYSICS, ANDHRA UNIVERSITY, WALTAIR

(Received for publication October 26, 1956)

ABSTRACT. The dipole moments of ortho, meta and para fluorotoluenes were determined in dilute solution in benzene using modified Guggenheim method and Palit's correction. The values were found to agree with those calculated from group moments using Smallwood and Herzfeld's method. The induced effect in halogen substituted toluenes were found negligible.

INTRODUCTION

The dipole moments of ortho, meta and para fluorotoluenes were determined in the vapour state by Moore and Hobbs (1949) and the values were compared with those calculated using the vectorial method. Dipole moments were not determined for these molecules in dilute solutions except for the para compound which was investigated by Myers and Vries (1951) in benzene solution. In the present investigation the dipole moments of ortho, meta and para fluorotoluenes were determined using solution method and benzene as solvent. The present observations complete the dipole moment determination on halogenated toluenes in dilute solutions

EXPERIMENTAL

The experimental arrangement used for measuring the dielectric constants of solutions is similar to that used by Le Fevre, Ross and Smythe (1950) with some minor changes in the circuit and component values. This type of arrangement was used in measurements on gases and changes of the order of 0.0002 *pf* were detected. In the present experiments on dilute solutions the limit of accuracy was set by the precision condenser (G. R. Type 722-D reading to 0.02 *pf*) and not by the detecting device.

The cell for containing solutions is of the Sayce and Briscoe (1925) type modified by Sugden (1933) for the absolute determination of the dielectric constants of benzene and chlorobenzene. The capacity of the cell is 54.4 *pf*. The constant of the cell and leads correction were determined by taking benzene as standard liquid whose dielectric constant and its temperature variation are accurately known.

Dipole Moments of Some Substituted Benzenes and Pyridines 257

The refractive indices of the solutions were measured with a Pulfrich refractometer of the Bellingham and Stanley type.

METHOD OF CALCULATION OF THE DIPOLE MOMENT

Modified Guggenheim method (1951) was used to compute the dipole moments from the experimental observations. In this method the orientation polarisation P_d is given by the equation

$$P_d = \frac{3}{(\epsilon_1 + 2)^2} \cdot \frac{M_2}{d_1} \left\{ \left(\frac{\epsilon_{12} - \epsilon_1}{W_2} \right)_{W_2 \rightarrow 0} - \left(\frac{n_{12}^2 - n_1^2}{W_2} \right)_{W_2 \rightarrow 0} \right\}$$

where ϵ_1 is the dielectric constant of the solvent, d_1 its density and n_1 is its refractive index. ϵ_{12} and n_{12} are dielectric constant and refractive index of the solution; M_2 and W_2 are the molecular weight and weight fraction of the solute respectively. The values for the terms in the brackets are obtained by graphical extrapolation. Then μ is given by the equation,

$$\mu = 0.0128 \sqrt{P_d T} \text{ where } T \text{ is absolute temperature.}$$

A more general equation given by Palit (1952) for the computation of the dipole moment, which reduces to that of Guggenheim under some simplified assumptions, was also used for calculating the μ values and it was found that both methods give the same values when benzene is used as solvent. The final values given were obtained by using Palit's equation (7) of his paper,

$$P_d = \left[\frac{3M_2(\epsilon_1 - n_1^2)}{d_1(\epsilon_1 + 2)(n_1^2 + 2)} \left(1 - \frac{\beta_0}{d_1} \right) \right] + \left[\frac{3M_2\alpha_0}{d_1(\epsilon_1 + 2)^2} \right] - \left[\frac{6M_2n_1\gamma_0}{d_1(n_1^2 + 2)^2} \right]$$

The values of β_0 were calculated from refractive index measurements as indicated by Palit.

The values of dipole moments were also calculated from the group moments using Smallwood and Herzfeld's method (1930) taking inductive effects into consideration and applying Le Fevres' correction (1937) for the dielectric constant of the inter nuclear space. The following values of group moments and polarisabilities were used in these calculations.

Group.	Moment	Polarisability
	m	$\alpha \times 10^{24}$.
F	1.45D	0.57 c.c.
CH ₃	0.40	2.45.

RESULTS AND DISCUSSION

The results (Murty, 1956) of the three fluorotoluenes are given in the following Tables I, II and III. In Table IV are given the consolidated values of the dipole moments along with those for other halogenated toluenes together with calculated values as given by Moore and Hobbs (1949).

TABLE I
p-Fluorotoluene

Sr. No	Π	ε_{12}	$\Delta \varepsilon$	$\Delta \varepsilon / W$	n_{12}	n_{12}^2	Δn^2	$\Delta n^2 / W$
1.	0 00739	2 2809	0 0169	1 512	1 19303	2 22915	0 00150	0 203
2	0 01727	2 2951	0 0311	1 534	1 49280	2 22872	0 00193	0 112
3	0 04303	2 3341	0 0701	1 522	1 49217	2 22657	0 00408	0 095
4.	0 05678	2 3545	0 0905	1 512	1 49202	2 22614	0 00451	0 079
5	0 07839	2 3865	0 1225	1 504	1 19144	2 22410	0 00625	0 080

$\left(\frac{\Delta \varepsilon}{W} \right)_{W \rightarrow 0} = 1.512, \left(\frac{\Delta n^2}{W} \right)_{W \rightarrow 0} = 0.137, P_d = 34.4 \text{ e.v.}, \mu = 1.30 D.$

TABLE II
m-Fluorotoluene

Sl. No	W	ϵ_{12}	$\Delta \epsilon$	$\Delta \epsilon / W$	n_{12}	n_{13}	Δn^2	$\Delta n^2 / W$
1	0.02166	2.3293	0.0653	3.014	1.49256	2.22771	0.00291	0.134
2	0.03356	2.3609	0.0969	2.8888	1.49155	2.22471	0.00504	0.177
3	0.04756	2.3977	0.1337	2.810	1.49148	2.22450	0.00615	0.129
4	0.07331	2.4656	0.2016	2.750	1.49081	2.22250	0.00815	0.111
5	0.10000	2.5361	0.2721	2.723	1.49013	2.22050	0.01015	0.101
6	0.12600	2.6013	0.3373	2.677	1.48975	2.21936	0.01129	0.090

$\left(\frac{\Delta \epsilon}{W}\right)_{W \rightarrow 0} = 2.93$; $\left(\frac{\Delta n^2}{W}\right)_{W \rightarrow 0} = 0.146$. $P_d = 64.2$ c.c. $\mu = 1.78$ D

TABLE III
p-Fluorotoluene

Str. No.	<i>W</i>	ϵ_{12}	$\Delta\epsilon$	$\Delta\epsilon/W$	n_{12}	n_{12}^2	Δn^2	$\Delta n^2/W$
1	0.02984	2.3598	0.0958	3.210	1.49181	2.22551	0.00514	0.172
2	0.04951	2.4198	0.1558	3.147	1.49113	2.22347	0.00718	0.145
3.	0.07513	2.4980	0.2340	3.114	1.49003	2.22019	0.01046	0.139
4.	0.09228	2.5490	0.2850	3.089	1.48998	2.22004	0.01061	0.115
5	0.12660	2.6483	0.3843	3.036	1.48891	2.21684	0.01381	0.109
$\left(\frac{\Delta\epsilon}{W}\right)$ 3.23; $\left(\frac{\Delta n^2}{W}\right)$ - 0.184. $P_d = 11.2$ e.c. $\mu = 1.88$ D								

TABLE IV

Molecule	Ortho		Meta		Para	
	Calcd.	Obs.	Calcd.	Obs.	Calcd.	Obs.
Fluorotoluene (gas)	1.46	1.35	1.82	1.85	1.98	2.01D
Fluorotoluene (sol)	1.32	1.30	1.75	1.78	1.92	1.88 (1.82)
Chlorotoluene (sol)	1.41	1.43	1.79	1.77	1.95	1.94
Bromotoluene (sol)	1.38	1.44	1.76	1.75	1.92	1.93
Iodotoluene (sol)	1.24	1.33	1.61	1.67	1.77	1.80

Table IV shows that the dipole moment increases from ortho to para compounds in all the halogen substituted toluenes. Since the benzene ring is a plane hexagon with its external valencies coplanar, the moment resulting from the symmetric methyl group must act in the direction of the bond between methyl to ring carbon. The moments of halogens in the para position also act in the same direction. The increase of moment from ortho to para substituted toluenes indicate that the methyl to ring line is the plus-minus direction of the dipole since it was established that the C'-Cl link has positive end on the carbon atom. It may be noted that the hyperconjugation of the substituted methyl group also produces a polarity in the same direction.

The solution value obtained for *p*-fluorotoluene from previous investigations, shown in brackets in Table IV, differs from the present value. This difference may arise from the difference in the method of calculation adopted by the previous investigators who used Hedestrand method. The present value is nearer the gas value.

The calculated values using the vectorial method agree with the observed values very closely. The induced effects in substituted toluenes may probably be negligible due to the low moment of the methyl group.

ACKNOWLEDGMENTS

The author is very much indebted to Prof. K. R. Rao for his kind and constant guidance throughout the work. He is grateful to the Council of Scientific and Industrial Research for the award of a Research Assistantship.

REFERENCES

- Guggenheim, E. A., 1951, *Trans. Farad. Soc.*, **47**, 573
Le Fevre, R. J. W., and Le Fevre, C. J. W., 1937, *J. Chem. Soc.* **196**
Le Fevre, R. J. W., and Ross, I. G. and Smythe, B. M., 1950, *J. Chem. Soc.* **276**
Moore, E. M. and Hobbs, M. E., 1949, *J. Am. Chem. Soc.* **71**, 411
Myers, A. L. and Vries, T. D., 1951, *Ibid.*, **73**, 1813
Pahl, S. R., 1952, *Ibid.*, **74**, 3952.
Radhakrishna Murty, C., 1956, *J. Sci. Indust. Res.* **15B**, 260.
Sayce and Briscoe., 1925 *J. Chem. Soc.*, **127**, 315
Smallwood, H. M. and Herzfeld, K. F., 1930, *J. Am. Chem. Soc.* **52**, 1919
Sugden, S., 1933, *J. Chem. Soc.*, **768**

IMPROVED PERFORMANCE OF PHOTOMULTIPLIERS IN SCINTILLATION COUNTERS

A. ASHMORE, B. COLLINGE AND S. K. SEN*

NUCLEAR PHYSICS RESEARCH LABORATORIES, LIVERPOOL

(Received for publication, July 26, 1956)

ABSTRACT. The use of a cathode follower to reduce the effective capacity to earth of the collecting electrode of a photomultiplier, enables bigger voltage pulses to be obtained for the same degree of non-linearity in the photomultiplier. The investigation has been made of the improvement obtained with an E.M.I. 6260 photomultiplier under typical operating conditions.

INTRODUCTION

In a scintillation counter, the height of the pulse produced by the photomultiplier is not necessarily proportional to the light output from the phosphor. Robbins and Raffle (1952) have investigated the behaviour of the E.M.I. 5311 photomultiplier. Non-linearity is apparent for pulse heights exceeding 0.1 volt with anthracene or stilbene crystals, and 1.0 volt with potassium iodide crystals. The effect is thought to be due to current limitation in the later stages of the photomultiplier.

For some purposes these pulse heights are inconveniently small; for example, when pulses from a photomultiplier and an organic phosphor are required to feed into an amplitude discriminator capable of handling pulses of a few tens of millimicroseconds duration, without the addition of a wide band amplifier. The circuit described in this paper reduces the capacity of the collecting electrode of the photomultiplier and hence enables larger pulses to be obtained for the same degree of non-linearity. It has been used in a fast coincidence circuit (Collinge *et al.*, 1956) in which amplitude discrimination of the pulses from the photomultiplier is provided.

Non-Linearity of the E.M.I. 6260 photomultiplier

The behaviour of an E.M.I. 6260 photomultiplier has been examined using polonium alpha particles and stilbene and potassium iodide crystals. The variation of the pulse height at various dynodes was obtained from the peaks of bias curves taken with a single channel pulse analyser. The curves shown in figure 1 were obtained from measurements with a stilbene crystal. The photomultiplier dynodes were supplied through a chain of 100 K resistors, and the potential dif-

* Now at the Institute of Nuclear Physics, Calcutta University.

ference between the 11th dynode and the collector was kept constant at 150 volts. The pulse height ratio for successive dynodes is plotted against the interstage potential. The non-linear behaviour of the 9th, 10th and 11th dynodes is

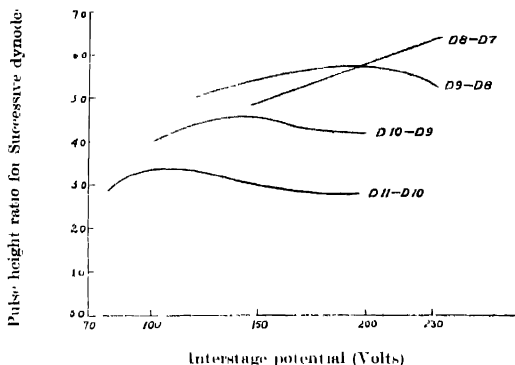


Fig. 1. Curves showing the non-linearity of the photomultiplier

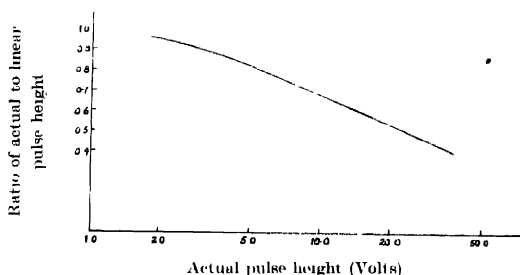


Fig. 2. Variation of the degree of non-linearity of the photomultiplier with pulse height apparent as is the linear behaviour of the 8th dynode. In figure 2, the ratio of the observed pulse height at the 11th dynode to the value of the pulse height calculated on the assumption of linear behaviour, is plotted against the observed pulse height. It is seen that the behaviour is markedly non-linear for pulse heights greater than 2 volts.

Reduction of the effective photomultiplier capacity

The circuit shown in figure 3 causes a reduction of the effective capacity on which the charge produced by the photomultiplier is collected, and hence an increase in the pulse height. As the potentials of the collector and the 10th dynode follow that of the 11th dynode, the capacity between them and the 11th dynode is reduced. The effect of the capacity of the wiring is similarly reduced by

using a co-axial lead to connect the photomultiplier to the cathode follower grid and connecting the outer conductor to the cathode

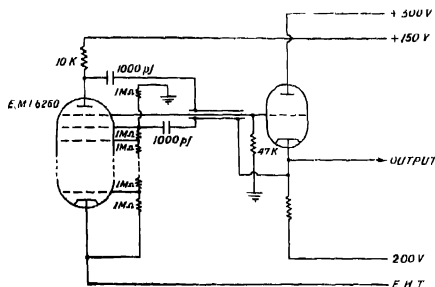


Fig. 3 Capacity-reduction circuit

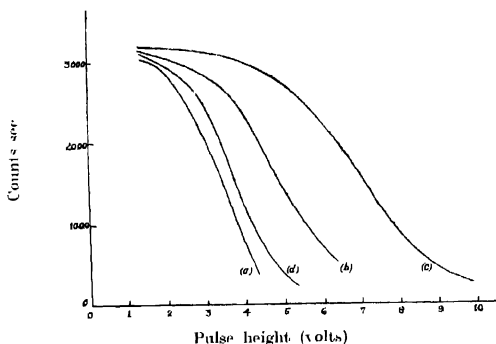


Fig. 4 Curves showing the capacity reduction.

The circuit has been tested using a fast discriminator and alpha particles incident on a stilbene crystal. Figure 4 shows the integral bias curves obtained. Curve (a) was for the usual arrangement in which the collector and 10th dynode are earthed and an unscreened lead connecting the 11th dynode to the grid of the cathode follower. The collector and 10th dynode were then connected to the cathode of the cathode-follower and curve (b) was obtained. The co-axial cable was then introduced and curve (c) was obtained. A progressive improvement in pulse height was noted.

To obtain the value of the effective collecting capacity, a 10pf. condenser was then connected between the cathode-follower grid and earth. Curve (d) was obtained. A correction for the dependence of the pulse height on the collecting time constant was obtained from a separate experiment in which the value of

the cathode-follower grid leak was varied. It was found that the collecting capacity had been reduced from 22.5 pf. to 8 pf. Thus the circuit causes about a threefold increase in pulse height, without a corresponding increase in non-linearity.

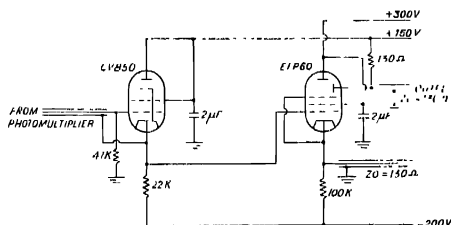


Fig. 5. Head amplifier circuit.

A circuit of a head amplifier which has been used in a fast coincidence circuit (Collinge, Merrison and Eccleshall, 1956) is shown in figure 5. The cathode follower provides the capacity reduction and the drive for the 6FP 60 secondary-emission pentode. Pulse shaping is provided by the open-ended cable in the cathode circuit (Chance, 1949). The output pulses are fed from the dynode into a 130ohm co-axial cable. There is a linear voltage gain of about one and output pulses of 10 volts are obtainable.

ACKNOWLEDGMENT

One of us (S.K.S.) is indebted to the Government of West Bengal for the award of a State Scholarship.

REFERENCES

- Chance, B., 1949 Waveforms, (McGraw-Hill), p. 244.
- Collinge, B. Merrison, A. W. and Eccleshall, D., 1956, *J.S.I.*, **33**, 72.
- Raffle, J. F. and Robbins, E. J., 1952, *Proc. Roy. Soc.*, B **65**, 320.

SPIN ECHOES WITH FOUR AND MORE PULSES†

T. GHOSE*, S. K. GHOSH AND D. K. ROY

INSTITUTE OF NUCLEAR PHYSICS, CALCUTTA

(Received for publication October 26, 1956)

ABSTRACT. The vector model developed in an earlier paper by Banerjee *et al* (1957) for explaining the primary, secondary and stimulated echoes has here been further applied for the explanation of the 'virtual' echo. The model also explains the formation—with positions and relative magnitudes—of all the echoes arising from the four pulse system, including the 'quarternary' echo. In fact, this model shows that with any number of pulses, the resulting echoes can always be explained by the primary, stimulated and virtual echo mechanisms. A tentative explanation of the formation of series echoes with double-pulse system, when the sample is not allowed to come to thermal equilibrium is also given in this paper.

I INTRODUCTION

Extending the spin-echo analysis of Hahn (1950) and of Das and Saha (1954) to the case of four pulses, Das and Roy (1955) showed that of the eighteen echoes that arise in this case, there is one—the 'quarternary' echo as they termed it—occurring at $t = 2\tau_3 - \tau_2 + \tau_1$, which cannot be explained by the usual primary and stimulated echo mechanisms, the four pulses being applied at $t = 0, \tau_1, \tau_2$ and τ_3 respectively (figure 1). Bloom (1955) and Crawford (1955) suggested that this particular echo in the case of four pulses occurs due to primary echo mechanism between the 'virtual' stimulated echo at $t = \tau_2 - \tau_1$, and the fourth pulse at $t = \tau_3$. The 'virtual' echo term which appears in the mathematical analysis for the three pulse system, was so far ignored on account of its physical non-existence. The explanation of the 'quarternary' echo brings out an effect of the virtual echo that can be visualized only after the fourth pulse is applied. The vector model that has been developed explains this effect of the virtual echo, as well as the formation of all the other echoes with the four pulse system, as is discussed in Sec. II. In a short note of Crawford (1955) also, there was a mention about a vector model that can explain the 'quarternary' echo, but no detailed report has yet been published. Sec. III deals with the extension of the procedure to a system of more than four pulses where contradiction arises between the results of this paper and those of Crawford (1955) and of Das and Roy (1954).

*D.A.E. Fellow (Junior).

†A preliminary note on the subject has already been published in the *Nuove Simentio Series* 10 Vol. 5, No. 3, (1957).

II APPLICATION OF THE VECTOR MODEL TO FOUR PULSE SYSTEM

The fundamental basis of the vector model has been developed in the Paper by Banerjee et al (1957)—henceforth referred to as Paper I—where figure 1 explained the formation of the different echoes due to reclustering of the moment vectors in case of three pulse system. The figure 1 of the present paper is a con

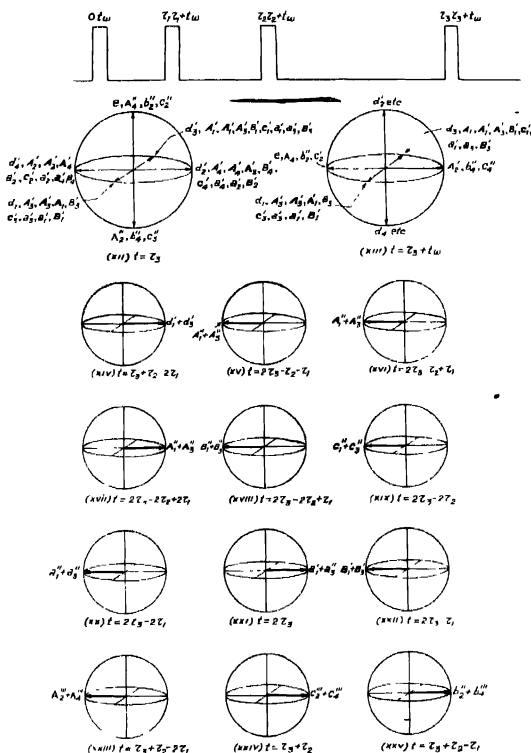


Fig. 1. Vector diagram showing the formation of different echoes for four-pulse system. It should here be noted that τ_3 is taken to be greater than $2\tau_2$, so that all the possible echoes may appear. The detailed explanation of the diagrams giving the positions of the moment vectors at different times is given in the following. The notations here have the same significance as those in Paper I except **A**, **A** and **C** in place of Λ , Λ and Γ respectively of the earlier paper.

Figure 1 (xii) This shows the position of the moment vectors at $t = \tau_3$, i.e. just before the application of the fourth rf-pulse.

$$(1) \quad d = d(\tau_3 - \tau_2) = M_0 \left[1 - \exp\left(-\frac{\tau_2 - \tau_1}{T_1}\right) \right].$$

$$d_1' = d_2' = d_3' = d_4' = \frac{d}{4} \exp\left[-\frac{\tau_3 - \tau_2}{T_2}\right]$$

$$(2) \quad A = A(\tau_3 - \tau_2 - \tau_1) = a_2'' + a_1''' = \frac{M_0}{2} \exp\left[-\frac{2\tau_1}{T_2} - \frac{\tau_2 - \tau_1}{T_1}\right]$$

$$A_1' = A_2' = A_3' = A_4' = \frac{A}{4} \exp\left[-\frac{\tau_3 - \tau_2 - \tau_1}{T_2}\right]$$

$$(3) \quad \mathbf{A} = \mathbf{A}(\tau_3 - \tau_2 - \tau_1)$$

Here \mathbf{A} is considered to take into account the fact that a_2'' and a_4'' which recluster at $\tau_2 - \tau_1$ to form the stimulated echo would have reclustered at $\tau_2 - \tau_1$ had they been in the $x'y'$ plane at that time, which, however, is not physically possible before the application of the third pulse. This is the origin of the 'virtual stimulated echo' which, in spite of its physical non-existence, appears in the mathematical analysis. At time $t = \tau_3$, \mathbf{A}_4 will assume positions $\mathbf{A}_1' = \mathbf{A}_1$, $\mathbf{A}_2' = \mathbf{A}_2'$, $\mathbf{A}_3' = \mathbf{A}_3'$ and $\mathbf{A}_4' = \mathbf{A}_4'$, as shown in the figure.

$$(4) \quad \mathbf{A} = \mathbf{A}(\tau_3 - 2\tau_2 + \tau_1) = \mathbf{A}_1'' + \mathbf{A}_3'' = \frac{M_0}{4} \exp\left[-\frac{2\tau_2 - 2\tau_1}{T_2}\right],$$

$$\mathbf{A}_1' = \mathbf{A}_2' = \mathbf{A}_3' = \mathbf{A}_4' = \frac{\mathbf{A}}{4} \exp\left[-\frac{\tau_3 - 2\tau_2 + \tau_1}{T_2}\right].$$

$$(5) \quad B = B(\tau_3 - 2\tau_2 + \tau_1) = b_1'' + b_3'' = \frac{M_0}{2} \left[1 - \exp\left(-\frac{\tau_1}{T_1}\right) \right] \exp\left[-\frac{2(\tau_2 - \tau_1)}{T_2}\right];$$

$$B_1' = B_2' = B_3' = B_4' = \frac{B}{4} \exp\left[-\frac{\tau_3 - 2\tau_2 + \tau_1}{T_2}\right].$$

$$(6) \quad \mathbf{C} = \mathbf{C}(\tau_3 - 2\tau_2) = C_1'' + C_3'' = \frac{M_0}{4} \exp\left[-\frac{2\tau_2}{T_2}\right];$$

$$C_1' = C_2' = C_3' = C_4' = \frac{\mathbf{C}}{4} \exp\left[-\frac{\tau_3 - 2\tau_2}{T_2}\right].$$

$$(7) \quad \mathbf{a} = \mathbf{a}(\tau_3 - 2\tau_1).$$

Now, from (4), $\mathbf{A}' = \mathbf{A}_2' = \mathbf{A}_3' = \mathbf{A}_4' = \frac{\mathbf{A}}{4} \exp \left[-\tau_3 - \frac{2\tau_2 + 2\tau_1}{T_2} \right]$

$$= \frac{\mathbf{A}_1'' + \mathbf{A}_1'''}{4} \exp \left[-\tau_3 - \frac{2\tau_2 + 2\tau_1}{T_2} \right]$$

$$= \frac{\mathbf{A}_1' + \mathbf{A}_1'''}{4} \exp \left[-\tau_3 - \frac{\tau_2}{T_2} \right]$$

$$= \frac{\mathbf{A}_1 + \mathbf{A}_1'''}{4} \exp \left[-\tau_3 - \frac{2\tau_1}{T_2} \right],$$

we may consider that $\mathbf{a}(\rightarrow \mathbf{A}_1 + \mathbf{A}_1''')$ has accumulated a phase in $\tau_3 - 2\tau_1$ so that \mathbf{a} 's occupy the positions as indicated in the figure 1, where,

$$\mathbf{a}_1' = \mathbf{A}_3, \quad \mathbf{a}_2 = \mathbf{A}_1', \quad \mathbf{a}_3 = \mathbf{A}_1, \quad \mathbf{a}_4 = \mathbf{A}_2'$$

$$\mathbf{a}_1' = \mathbf{a}_2' = \mathbf{a}_3 = \mathbf{a}_4 = \frac{\mathbf{a}}{4} \exp \left[-\tau_3 - \frac{2\tau_1}{T_2} \right]$$

$$(8) \quad \mathbf{a} = \mathbf{a}(\tau_3).$$

from (7),

$$\mathbf{A}_1 = \mathbf{A}_2 = \mathbf{A}_3 = \mathbf{A}_4 = \frac{\mathbf{A}_1 + \mathbf{A}_3}{4} \exp \left[-\tau_3 - \frac{2\tau_1}{T_2} \right]$$

$$= \frac{\mathbf{A}}{8} \exp \left[-\tau_3 - \frac{2\tau_1}{T_2} \right]$$

$$= \frac{\mathbf{a}_1 + \mathbf{a}_3}{8} \exp \left[-\tau_3 \right]$$

Hence, we may consider that $\mathbf{a} \left(= \frac{\mathbf{a}_1 + \mathbf{a}_3}{2} \right)$ which was along the y' axis at $t = 0$ has assumed the values $\mathbf{a}_1', \mathbf{a}_2', \mathbf{a}_3$ and \mathbf{a}_4 at $t = \tau_3$. It is evident that,

$$\mathbf{a}_1' = \mathbf{A}_1', \quad \mathbf{a}_2' = \mathbf{A}_2', \quad \mathbf{a}_3 = \mathbf{A}_3, \quad \mathbf{a}_4 = \mathbf{A}_4;$$

and

$$\mathbf{a}_1' = \mathbf{a}_2' = \mathbf{a}_3 = \mathbf{a}_4 = \frac{\mathbf{a}}{4} \exp \left[-\tau_3 \right].$$

(9) Similarly,

$$\mathbf{B} = \mathbf{B}(\tau_3 - \tau_1),$$

and

$$\mathbf{B}_1 = \mathbf{B}_2 = \mathbf{B}_3 = \mathbf{B}_4 = \frac{\mathbf{B}}{4} \exp \left[-\tau_3 - \frac{\tau_1}{T_2} \right].$$

TABLE I

Figure no.	Time	Amplitude of the echo	Nature of the echo
I.(xiii).	$t = t_1 + t_2$	$M_0 \left[1 - \exp \left(-\frac{T_2 - T_1}{T_1} \right) \right]$ (given by the component c)	Free induction
I.(xiv).	$t = 2T_1 - T_2$	$d_1'' + d_1''' = (d_1' - d_3') \exp \left[-\frac{T_2 - T_1}{T_2} \right]$ $= \frac{M_0}{2} \left[1 - \exp \left(-\frac{T_2 - T_1}{T_1} \right) \right] \exp \left[-\frac{2(T_2 - T_1)}{T_2} \right]$	$P_{3:1}$
I.(xv).	$t = 2T_1 - T_2 - T_1$	$A_1'' + A_1''' = (A_1' + A_3') \exp \left[-\frac{T_2 - T_1}{T_2} \right] = \frac{A}{2} \exp \left[-\frac{2(T_1 - T_2 - T_1)}{T_2} \right]$ $= \frac{M_0}{4} \exp \left[-\frac{2(T_2 - T_1)}{T_1} - \frac{T_2 - T_1}{T_2} \right]$	$P_{(1,2):1}$
I.(xvi).	$t = 2T_1 - T_2 - T_1$	$A_1'' + A_3''' = (A_1' + A_3') \exp \left[-\frac{T_2 - T_1}{T_2} \right] = \frac{A}{2} \exp \left[-\frac{2T_2 - 2T_1}{T_2} \right]$ $= \frac{M_0}{4} \exp \left[\frac{2T_1 - 2T_2 + 2T_1 - T_2 - T_1}{T_2} \right] = \frac{M_0}{4} \exp \left[\frac{2T_1 - T_2}{T_2} \right]$	$P_{(1,2):1}$ (Quaternary echo)
I.(xvii).	$t = 2T_1 - 2T_2 - 2T_1$	$A_1'' + A_3''' = (A_1' + A_3') \exp \left[-\frac{T_2 - T_1}{T_2} \right] = \frac{A}{2} \exp \left[-\frac{2(T_2 - 2T_1 + 2T_1)}{T_2} \right]$ $= \frac{M_0}{8} \exp \left[-\frac{2(T_1 - T_2 - T_1)}{T_2} \right]$	$P_{(1,2):1}$

TABLE (contd)

Figure no.	Time	Amplitude of the echo	Nature of the echo
I. (xxviii)	$t = 2T_1 - 2T_2 - T_1$	$B_1' + B_3' = (B_1' + B_3') \exp \left[-\frac{T_3 - 2T_2 - T_1}{T_2} \right] = \frac{B}{2} \exp \left[-\frac{2(T_3 - 2T_2 + T_1)}{T_2} \right]$ $= \frac{M_0}{4} \exp \left[1 - \exp \left(-\frac{T_1}{T_1} \right) \right] \exp \left[-\frac{2(T_3 - T_2)}{T_2} \right]$	P_{12314}
I. (xxxi)	$t = 2T_3 - 2T_2$	$C_1 + C_3' = (C_1' + C_3') \exp \left[-\frac{T_3 - 2T_2}{T_2} \right] = \frac{C}{2} \exp \left[-\frac{2(T_3 - 2T_2)}{T_2} \right]$ $= \frac{M_0}{8} \exp \left[-\frac{2(T_3 - T_2)}{T_2} \right]$	P_{11314}
I. (xxx)	$t = 2T_1 - 2T_1$	$a_1' + a_3' = (a_1' + a_3') \exp \left[-\frac{T_3 - 2T_1}{T_2} \right] = (A_1' + A_1') \exp \left[-\frac{T_3 - 2T_1}{T_2} \right]$ $= \frac{A}{2} \exp \left[-\frac{2T_3 - 2T_1}{T_2} \right] = \frac{M_0}{8} \exp \left[-\frac{2T_3 - 2T_1}{T_2} \right]$	P_{11214}
I. (xxxi)	$t = 2T_1$	$a_1' + a_3' = (a_1' + a_3') \exp \left[-\frac{T_3}{T_2} \right] = \frac{a}{2} \exp \left[-\frac{2T_3}{T_2} \right] = \frac{M_0}{8} \exp \left[-\frac{2T_3}{T_2} \right]$	P_{11}
I. (xxxii)	$t = 2T_3 - T_1$	$B_1' + B_3' = (B_1' + B_3') \exp \left[-\frac{T_3 - T_1}{T_2} \right] = \frac{B}{2} \exp \left[-\frac{2(T_3 - T_1)}{T_2} \right]$ $= \frac{M_0}{4} \left[1 - \exp \left(-\frac{T_1}{T_1} \right) \right] \exp \left[-\frac{2(T_3 - T_1)}{T_2} \right]$	P_{24}

TABLE (contd.)

Figure no.	T_{im}	Amplitude of the echo	Nature of the echo
1.(xxiii)	$t = \tau_1 + \tau_2 - 2\tau_1$	$A_2'' + A_4'' = (A_2'' - A_4'') \exp \left[-\frac{\tau_2 - 2\tau_1}{T_2} \right] = (A_2' + A_4') \exp \left[-\frac{\tau_2 - \tau_1 - \tau_2 - 2\tau_1}{T_1} - \frac{\tau_2 - 2\tau_1}{T_2} \right]$ $= \frac{A}{2} \exp \left[-\frac{\tau_2 - \tau_1 - 2\tau_1 - 4\tau_1}{T_2} \right] = \frac{M_0}{4} \exp \left[-\frac{\tau_1 - \tau_2 - 2(\tau_2 - \tau_1)}{T_1} - \frac{\tau_2}{T_2} \right]$	P ((12)34)
1.(xxiv)	$t = \tau_1 + \tau_2$	$C_2'' + C_4'' = (C_2'' + C_4'') \exp \left[-\frac{\tau_2}{T_2} \right] = (C_2' - C_4') \exp \left[-\frac{\tau_2 - \tau_1 - \tau_2}{T_1} - \frac{\tau_2}{T_2} \right]$ $= \frac{C}{2} \exp \left[-\frac{\tau_2 - \tau_1 - 2\tau_2}{T_1} - \frac{\tau_2}{T_2} \right] = \frac{M_0}{4} \exp \left[-\frac{\tau_1 - \tau_2 - 2\tau_2}{T_1} \right]$	P (134)
1.(xxv)	$t = \tau_2 + \tau_1 - \tau_1$	$b_2'' + b_4'' = (b_2'' + b_4'') \exp \left[-\frac{\tau_2 - \tau_1}{T_2} \right] = (b_2' + b_4') \exp \left[-\frac{\tau_2 - \tau_2 - \tau_2 - \tau_1}{T_1} - \frac{\tau_2 - \tau_1}{T_2} \right]$ $= \frac{b}{2} \exp \left[-\frac{\tau_2 - \tau_2 - 2(\tau_1 - \tau_1)}{T_1} - \frac{\tau_2}{T_2} \right]$ $= \frac{M_0}{2} \left[1 - \exp \left(-\frac{\tau_1}{T_1} \right) \right] \exp \left[-\frac{\tau_2 - \tau_2 - 2(\tau_2 - \tau_1)}{T_1} - \frac{\tau_2}{T_2} \right]$	P 234

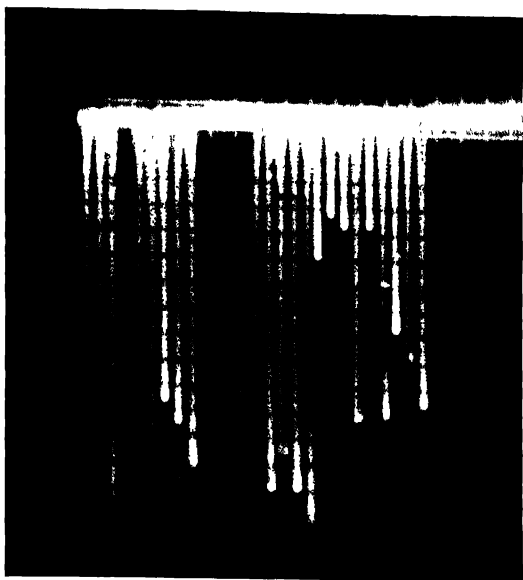


Fig. 3. Photograph of the actual pattern of the echoes observed with four pulses.
(Sample— H^1 in glycerine, $\tau_1 = 0.7$ msec, $\tau_2 = 4\tau_1$, $\tau_3 = 13\tau_1$.)

III. EXTENSION OF THE VECTOR MODEL TO THE CASE OF MORE THAN FOUR PULSES

Sec. II shows the occurrence of eighteen echoes besides the four free induction decays, for the four-pulse system. Of these, the five echoes occurring at $t = \tau_2 + \tau_1$, $\tau_3 + \tau_2$, $\tau_3 + \tau_1$, $\tau_3 + \tau_2 - \tau_1$ and $\tau_3 - \tau_2 - 2\tau_1$ are formed by the stimulated echo mechanism. Corresponding to each of these real echoes, there will be associated one 'virtual' stimulated echo. Thus, in all, there will be five 'virtual' echoes, ($t = \tau_2 - \tau_1$, $\tau_3 - \tau_2$, $\tau_3 - \tau_1$, $\tau_3 - \tau_2 + \tau_1$ and $\tau_3 - \tau_2 + 2\tau_1$), each of which will give rise to one primary echo with the fifth pulse, just as the 'quaternary' echo, previously discussed, arises out of the primary echo mechanism between the virtual echo at $t = \tau_2 - \tau_1$ (occurring before the third pulse) and the fourth pulse. This particular 'virtual' echo at $t = \tau_2 - \tau_1$ will further give rise to a stimulated echo at $t = \tau_4 + \tau_3 - \tau_2 + \tau_1$ with the fourth and fifth pulses due to the flip over of the moment vector from the Z -direction to the $x'y'$ plane as can be visualized from figure 1. According to this vector model there will occur fifty-eight echoes with the five pulse system of which forty will appear after the fifth pulse, if the

condition $\tau_n > 2\tau_{n-1}$, ($n = 1, 2, 3$ and 4) is satisfied. This conclusion has been verified experimentally as can be seen from figure 4. That the 'virtual' echo occurring before the third pulse ($t = \tau_2 - \tau_1$) can give rise to echoes by primary mechanism with the fifth pulse and stimulated mechanism with the fourth and fifth pulses was not taken into account in Crawford's analysis.

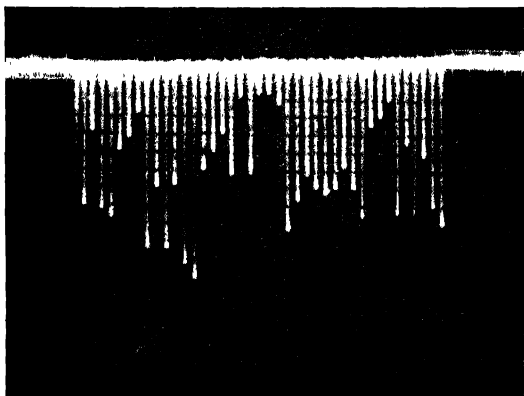


Fig. 4. Photograph of the fifth r.f. pulse and the forty echoes occurring after it (Sample— H_2 in glycerine, $\tau_1 = 0.7$ msec, $\tau_2 = 4\tau_1$, $\tau_3 = 13\tau_1$, $\tau_4 = 40\tau_1$)

The above analysis shows that the virtual echo corresponding to each stimulated echo behave just like the real echoes in forming echoes with subsequent pulses by primary and stimulated echo mechanisms. Only it can have no effect on the pulses responsible for its occurrence. Extending the above procedure, we can find the general formula giving the total number of echoes with n pulses, as follows:

- Total no. of echoes with n pulses. (y_n)
- = Total no. of echoes already existing with $n-1$ pulses and occurring before the n^{th} pulse. (y_{n-1})
 - + no. of primary echoes formed by each of the $n-1$ pulses with the n^{th} pulse. ($^{n-1}C_1$)
 - + no. of stimulated echoes formed between the n -th pulse and any two of the $n-1$ pulses. ($^{n-1}C_2$)
 - + no. of echoes formed by primary echo mechanism between the y_{n-1} echoes and the n^{th} pulse. (y_{n-1})
 - + no. of echoes formed by primary echo mechanism between the total no. of virtual echoes y_{n-1}' for $n-1$ pulses (i.e. occurring before the $(n-1)^{th}$ pulse) and the n^{th} pulse. (y_{n-1}')

- $\left\{ \begin{array}{l} \text{+no. of echoes formed by stimulated mechanism between the } y_{n-2} \text{ echoes} \\ \text{(i.e. total no. of echoes with } n-2 \text{ pulses and occurring before the } (n-1)^{th} \\ \text{pulse), the } (n-1)^{th} \text{ and the } n^{th} \text{ pulses. } (y_{n-2}) \\ \text{+no. of echoes formed by stimulated mechanism between the } y_{n-3} \text{ echoes,} \\ \text{the } (n-2)^{th} \text{ and the } n^{th} \text{ pulses. } (y_{n-3}) \\ \text{+...so on ... + no. of echoes formed by stimulated mechanism between} \\ y_1 \text{ echoes, the } 2^{nd} \text{ and the } n^{th} \text{ pulses. } (y_1). \end{array} \right.$
 $\left\{ \begin{array}{l} \text{+ no of stimulated echoes formed by the total no. of virtual echoes} \\ y_{n-2}' \text{ for } n-2 \text{ pulses (occurring before the } (n-2)^{th} \text{ pulse) with the } (n-1)^{th} \\ \text{and the } n^{th} \text{ pulses. } (y_{n-2}') \\ \text{+no of stimulated echoes between the } y_{n-3}' \text{ virtual echoes, the } (n-2)^{th} \\ \text{and the } n^{th} \text{ pulses. } (y_{n-3}') \\ \text{+...so on... +no of stimulated echoes between the } y_1' \text{ virtual echoes, the} \\ 2^{nd} \text{ and the } n^{th} \text{ pulses. } (y_1') \end{array} \right.$

Or,

$$y_n = y_{n-1} + {}^{n-1}C_1 \{ {}^{n-1}C_2 \{ y_{n-1} + y_{n-1}' + \{ y_{n-2} + y_{n-3} + \dots + y_1 \} \\ + \{ y_{n-2}' + y_{n-3}' + \dots + y_1' \} \}$$

Since, with each stimulated echo there will be associated one 'virtual' echo, the total no. of 'virtual' echoes with n pulses will be

$$\begin{aligned}
 y_n' &= {}^{n-1}C_2 \{ y_{n-2} + y_{n-3} + \dots + y_1 \} + \{ y_{n-2}' + y_{n-3}' + \dots + y_1' \} \\
 &\quad + \text{total no. of 'virtual' echoes already occurring with } n-1 \\
 &\quad \text{pulses } (y_{n-1}') \\
 &= {}^{n-1}C_2 \{ y_{n-2} + y_{n-3} + \dots + y_1 \} + \{ y_{n-2}' + y_{n-3}' + \dots + y_1' \} + y_{n-1}'.
 \end{aligned}$$

On simplification, we get the following general formulae

$$y_n = \frac{1}{2} (3^n - 2n - 1) \quad \dots (1)$$

$$y_n' = \frac{1}{2} (3^{n-1} - 2n + 1) \quad \dots (2)$$

It is to be noted here that

$$y_n - y_{n-1} = \frac{1}{2} (3^{n-1} - 1) = y_{n-1}' - y_n' \quad (3)$$

i.e. the no. of echoes with n r.f. pulses appearing after the n^{th} pulse is always equal to the no. of 'virtual' echoes with $n+1$ r.f. pulses appearing between the n^{th} and $(n+1)^{th}$ pulses. Here it should always be remembered that the time intervals between the pulses are such that no two echoes (either 'virtual' or real) ever superpose on one another. The figure 3 may be referred to as an illustration of eq. (3) for $n = 4$.

Experimentally equation 1 has been verified for $n = 2, 3, 4$ and 5 whence we get $y_n = 1, 5, 18$ and 58 respectively. This is in disagreement with the recursion formulæ given by Das and Roy (1957) where the omission of the 'virtual echo mechanism from the beginning has resulted in an erroneous conclusion.

It is also worth noting that if the *r.f.* pulse separations be so adjusted that

$$\tau_{n-1} = (y_n - y_{n-1})\tau_1,$$

where τ_{n-1} , τ_1 are the time of occurrence of the n^{th} and the 2^{nd} pulses respectively, then the echoes will appear in groups of equi-spaced signals (the spacing in the time scale being τ_1) after each of the n pulses. It is evident that the groups will contain $(y_n - y_{n-1})$ echo-pulses after each of the n *r.f.* pulses. ($n = 1, 2, 3, \dots$). As an illustration, a photograph is reproduced for the case $n = 5$. Here the time intervals are adjusted such that $\tau_2 = 4\tau_1$, $\tau_3 = 13\tau_1$ and $\tau_4 = 40\tau_1$. The forty echoes ($y_5 - y_4$) appearing after the 5th pulse are equally spaced at intervals of τ_1 . ($\tau_1 = 0.7$ msec)

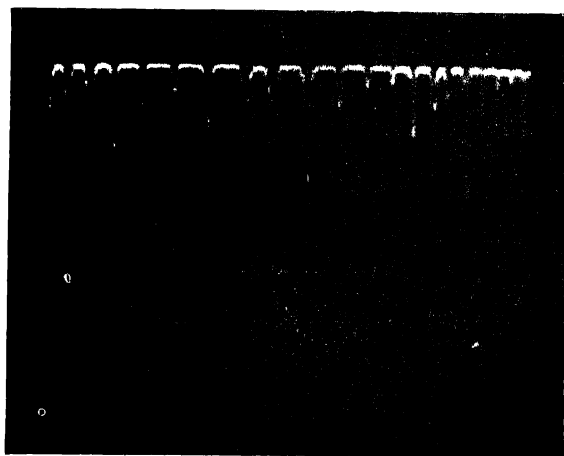


Fig. 5. Photograph of the series echoes with double-pulse system.
(Sample— H^1 in glycerine; repetition time = 25 msec.)

Figure 5 shows the occurrence of a series of echoes with double pulse system when the sample is not allowed to attain thermal equilibrium in between the pair pulses. This also can be explained on the basis of the analysis developed here, supposing the sample to be subjected to a large number of pulses instead of just a two-pulse system. The number and the relative amplitudes of both the series on the two sides of each pair-pulse depend on the repetition time of the pattern and the relaxation time of the sample used.

ACKNOWLEDGMENT

The authors are grateful to Prof. A. K. Saha and Mr. B. M. Banerjee for their encouragement during the progress of the work.

REFERENCES

- Banerjee, B. M., Ghosh, S. K. and Saha, A. K., 1957, *Ind. J. Phys.*, **211**, **31**.
Bloom, A. L., 1955, *Phys. Rev.* **98**, 1105
Crawford, G. J. B., 1955, *Phys. Rev.* **99**, 600.
Das, T. P. and Roy, D. K., 1955, *Phys. Rev.* **98**, 525.
Das, T. P. and Saha, A. K., 1954, *Phys. Rev.* **93**, 749.
Hahn, E. L., 1950, *Phys. Rev.* **80**, 580

SLOTS IN AN IMPERFECTLY CONDUCTING WAVEGUIDE

B. CHATTERJEE

INDIAN INSTITUTE OF TECHNOLOGY, KHARAGPUR

(Received for publication November 11, 1956)

ABSTRACT. A theoretical analysis on the slot radiators in a waveguide has been carried out, taking into account the finite conductivity of the waveguide walls. It has been found that with a slight decrease in conductivity from the perfect conductivity condition, the equivalent shunt conductance of the slot increases by a small amount. But with further reduction in conductivity, it falls off rapidly, almost in direct proportion with the reduced conductivity.

The use of slot antennas for radiating microwave powers is quite common and a detailed treatment on the subject has already been made by Stevenson (1948) and others (Silver, 1949). But all the calculations were made with the supposition that the wave guide is made of a perfect conductor.

Although, in general, the conductivity of copper wave guide is quite high, under certain circumstances (specially below 1 cm) the effective conductivity may be appreciably low with a consequent increase in loss. Chemical impurity and surface roughness lead to low conductivity and the conductivity of a worked surface layer may also be low (Thorp, 1954). In any case, it is worth studying the properties of slots cut in waveguide of low conductivity.

As rectangular waveguides in the H_{01} (or TE_{01}) mode are generally used for propagating microwave powers, we shall consider the slot antennas cut on such waveguide walls only. Any slot in a waveguide wall which obstructs the path of current will radiate some amount of electromagnetic energy in the open space outside the waveguide. The slot may be considered as a shunt or a series element or a combination of both (as the case may be), which consumes a certain amount of power from the wave propagating through the guide. A slot antenna may be cut either on the broad face or on the narrow face of a rectangular guide and may have different orientations as given in standard books on the subject (Fry & Goward, 1950). Depending on its orientation, a slot may be represented as a series or a shunt element in the guide.

In this note, we shall discuss in detail only the case of a narrow slot, cut parallel to the axis and on the broad face of a guide (shunt element). The other cases may be deduced by following a similar line of analysis.

In doing the calculation we shall make use of the well-known Babinet's principle which gives useful relations between the radiation fields of a slot and that of a dipole. The field within the guide in the region behind the face containing the slot is assumed negligible with respect to the field outside the guide. This is equivalent to extending the face containing the slot into an infinite conducting plane. The length of the slot is taken to be equal to half the free space wavelength of the radiated wave (i.e. a half-wave resonant slot) and that the slot is a narrow one [i.e. $2 \log_{10} \left(\frac{\text{length}}{\text{width}} \right) \gg 1$]. It is also assumed that the field in the slot is transverse to its long dimension and varies sinusoidally along the slot.

Now, consider the longitudinal half-wave slot to be at a distance x_1 from the centre line of the broad face as shown in figure 1

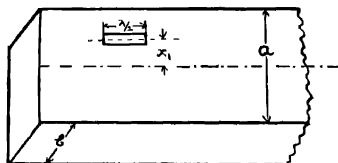


Fig. 1. A longitudinal half-wave slot on the broad face of a rectangular wave guide.

Following the line of analysis of Stevenson and taking into account the losses in the waveguide wall, we get,

$$2A_{01}S_{01} = 2B_{01}S_{01} = \int_{slot} jE_{1\tau} (K_{01})_{\tau} e^{-(a-j\beta_{01})z} ds$$

where A_{01} and B_{01} are the amplitudes of the waves going to the right and left of the slot respectively (the guide is being fed from the left) and S_{01} is twice the Poynting energy flux for a freely propagated mode.

$$S_{01} = Y_0 \frac{ab}{2} \left(\frac{\beta_{01}}{K} \right)^2$$

Y_0 being the normalised conductance of the guide and a and b are the length and the breadth of the cross-section

$$K = \frac{2\pi}{\lambda}; B_{01} = \frac{2\pi}{\lambda_g}$$

where λ is the free space wave length and λ_g is the guide wave length.

$E_{1\tau}$ and $(K_{01})_{\tau}$ are the transverse components of voltage and current given by

$$E_{1\tau} = E_0 \cos \frac{2\pi z}{\lambda}$$

$$(K_{01})_{\tau} = -Y_0 \frac{\pi}{Ka} \sin \left(\frac{\pi x_1}{a} \right) e^{-\alpha z}$$

As the width w of a narrow slot is very small, we may consider the field intensity to be constant across the width.

Hence

$$2A_{01}S_{01} = 2B_{01}S_{01} = -jwE_0Y_0 \int_{-\lambda/4}^{+\lambda/4} \sin\left(\frac{\pi x_1}{a}\right) \cos\left(\frac{2\pi z}{\lambda}\right) e^{-(2\alpha + j\beta_{01})z} dz$$

$$\therefore A_{01} = B_{01} = \frac{wE_0}{ab} \left(\frac{K}{\beta_{01}}\right)^2 \cdot \frac{\pi}{a} \sin\left(\frac{\pi x_1}{a}\right) \frac{e^{(2\alpha + j\beta_{01})\lambda/4} + e^{-(2\alpha + j\beta_{01})\lambda/4}}{K^2 + (2\alpha + j\beta_{01})^2}$$

Now, voltage across the slot $V_0 = wE_0$; and voltage across the guide $V_1 = bA_{01} = bB_{01}$

$$\therefore \left| \frac{V_1}{V_0} \right| = \frac{\pi}{a^2} \left(\frac{K}{\beta_{01}}\right)^2 \sin\left(\frac{\pi x_1}{a}\right) \frac{e^{(2\alpha + j\beta_{01})\lambda/4} + e^{-(2\alpha + j\beta_{01})\lambda/4}}{K^2 + (2\alpha + j\beta_{01})^2} \quad \dots (1)$$

Now, under ordinary circumstances, α is small ($2\alpha \ll 1$), and we may write

$$e^{2\alpha} = 1 + 2\alpha \text{ and } e^{-2\alpha} = 1 - 2\alpha$$

$$\therefore \left| \frac{V_1}{V_0} \right| = \frac{2\pi}{a^2} \left(\frac{K}{\beta_{01}}\right)^2 \sin\left(\frac{\pi x_1}{a}\right) \cdot \frac{\cos\left(\frac{\beta_{01}\lambda}{4}\right) + j2\alpha \sin\left(\frac{\beta_{01}\lambda}{4}\right)}{(K^2 - \beta_{01}^2) + j4\alpha\beta_{01}} \quad \dots (2)$$

If the conductivity of the guide wall is not very poor, the power radiated will not differ much from the perfect conductivity case (for the same field strength at the slot). By the use of Babinet's principle, the power radiated by the slot (for perfect conductivity) $= 73V_0^2 \frac{\epsilon_0}{\mu_0}$ and we may use this expression for our case also.

Using the energy balance equation and with the help of Eq. (2) we finally get the magnitude g of the equivalent normalised shunt conductance of the slot as

$$g = \frac{-2}{1 + |\Gamma|} = \frac{\frac{480\alpha}{73\pi b} \frac{\lambda_g}{\lambda} \sin^2\left(\frac{\pi x_1}{a}\right) \cos^2\left(\frac{\pi\lambda}{2\lambda_g}\right) \left[1 + 4\alpha^2 \tan^2\left(\frac{\pi\lambda}{2\lambda_g}\right)\right]}{1 + 2\alpha^2 \tan^2\left(\frac{\pi\lambda}{2\lambda_g}\right)} \quad \dots (3)$$

[Where Γ is the reflection coefficient of the slot]

For perfect conductivity, the attenuation constant α is zero and the shunt conductance becomes

$$g_p = \frac{480a}{73\pi b} \cdot \frac{\lambda_g}{\lambda} \sin^2 \left(\frac{\pi x_1}{a} \right) \cos^2 \left(\frac{\pi \lambda}{2\lambda_a} \right)$$

and this is identical with the expression derived previously by Stevenson.

For guides of very poor conductivity or of high attenuation constant, the value of $\frac{V_1}{V_0}$ is not given by Eq. (2).

Rather,

$$\left| \frac{V_1}{V_0} \right| = \frac{\pi}{a^2} \left(\frac{K}{\beta_{01}} \right)^2 \sin \left(\frac{\pi x_1}{a} \right) \left[\frac{e^{(2\alpha + j\beta_{01})\lambda/4}}{K^2 + (2\alpha + j\beta_{01})^2} \right]$$

and hence the value of g is also modified. In this case the value of g falls rapidly with increase in α (i. e. decrease in σ) and is approximately given by

$$g = \frac{1}{\alpha^2 \tan^2 \left(\frac{\pi \lambda}{2\lambda_g} \right)}$$

The attenuation constant α for an air-filled rectangular guide of permeability μ and conductivity σ , and carrying the H_{01} wave, is given by (Sarbacher and Edson, 1956).

$$\alpha = \sqrt{\frac{2\pi\mu}{v_1\mu_0^2\sigma}} \cdot a^{-3/2} \left\{ \frac{a/2b(f/f_0)^{3/2} + (f/f_0)^{1/2}}{\sqrt{(f/f_0)^2 - 1}} \right\}$$

where v_1 is the free space velocity $= f\lambda$; μ_0 is the permeability of free space and f_0 is the cut-off frequency for the H_{01} mode in the guide. From the above relation we see that α is proportional to $\frac{1}{\sqrt{\sigma}}$.

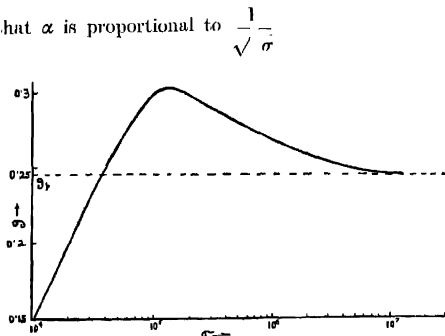


Fig. 2 Variation of shunt conductance g of a longitudinal slot with the conductivity σ of the guide wall.

Figure 2 shows the variation of g with the conductivity σ of the waveguide wall. The particular case considered is that for a 3 cm. wave propagating in a guide of dimensions 2.5 cm. \times 1.25 cm. The slot position taken is half way between the centre line and the edge of the broad face of the guide (i.e. $x_1 = a/4$). It is observed that the equivalent shunt conductance of a slot increases to some extent with a slight reduction in conductivity from the perfect conductivity case. This corresponds to an increased amount of power consumed by the slot. As a result, for this case, the amount of power radiated in free space is not reduced to any appreciable extent. But with further decrease in conductivity, losses in the guide walls become appreciably large and the presence of a small slot has not much effect on the waves propagating inside the guide. The equivalent shunt conductance falls off rapidly and little power is radiated in outside space.

ACKNOWLEDGMENT

The author wishes to express his grateful thanks to Dr. H. Rakshit and Prof. G. S. Sanyal of the Communication Engineering Department for their kind help and interest in the work.

REFERENCES

- Fry, D. W. and Goward, F. K., 1950, Aerials for centimeter Wavelengths, 111.
Saubacher, R. L. and Edson, W. A., 1956, "Hyper and Ultrahigh Frequency Engineering" 220.
Stevenson, A. F., 1948, *Jour. App. Phys.* **19**, 24.
Silver, S., 1949, *Microwave Antenna Theory & Design*, **12**, (Radiation Laboratory Series.) 295.
Thorp, J. S., 1954, *Proc. I.E.E.*, Part III, **101**, 357.

Letters to the Editor

The Board of Editors will not hold itself responsible for opinions expressed in the letters, published in this section. The notes containing reports of new work communicated for this section should not contain many figures and should not exceed 500 words in length. The contributions must reach the Assistant Editor not later than the 15th of the second month preceding that of the issue in which the Letter is to appear. No proof will be sent to the authors.

DIPOLE MOMENTS OF SOME ESTERS

K. V. GOPALA KRISHNA

MICROWAVE LABORATORY, ANDHRA UNIVERSITY, WALTAIR

(Received for publication December 14, 1956)

The dipole moments of ethyl caprylate and butyl stearate are determined in solution in benzene at 24°C, for which data are not available. The dielectric constants at several concentrations are determined at a frequency of 1 Mc/s by resonance method of the type adopted by LeFevre *et al* (1950) in their measurements. The dipole moment values are computed by the method indicated by Palit (1952). The dipole moments in the above cases are also calculated by considering the C—O—C plane 30° out of the Cis plane, as done by Smyth (1955) in the case of other esters. The experimentally observed together with the calculated values are given in Table I.

TABLE I

Compound	Observed	Calculated
Ethyl caprylate	1.86	1.8
Butyl stearate	1.88	1.8

It is found that the calculated values are in satisfactory agreement with those observed.

ACKNOWLEDGMENT

The author is highly indebted to Prof. K. R. Rao for his kind and invaluable guidance throughout the progress of the work.

REFERENCES

- LeFevre, R. J. W., Ross, I. G. and Smyth, B. M., 1950, *Jour. Chem. Soc.* 270.
Palit, S. R., 1952, *J. Amer. Chem. Soc.*, **74**, 3952.
Smyth, C. P., 1955, "Dielectric behaviour and structure", p. 307.

MEASUREMENT OF THERMAL NEUTRON ABSORPTION CROSS SECTION USING SPHERICAL SYMMETRY METHOD

A. M. GHOSH AND N. K. GANGULY

BOSE INSTITUTE, CALCUTTA

(Received for publication, December 4, 1956)

ABSTRACT. An experimental arrangement is described and utilised to measure thermal neutron absorption cross-section of Cf using spherical symmetry method, developed by the present authors. From the measured value it is shown that this method can effectively separate the scattering effects and measure the absorption cross-section directly. Different sources of errors are discussed and their effects are estimated.

1. INTRODUCTION

Critical evaluation of absorption cross-section of thermal neutrons for different materials is of great significance for research on the development of piles and for the production of radio-nuclides. This importance has encouraged a large number of experimenters to develop a number of methods for this purpose and to employ them for the measurement of this important parameter. The absorption cross-section of neutrons, σ_a , is the sum of all the cross-sections for nuclear reactions in which the neutron is not re-emitted. The reactions possible in general for thermal neutrons are, (n, γ) , (n, p) , (n, d) , (n, α) , (n, f) ; more complex reactions are very improbable for thermal neutrons. The principal methods which have been employed for the measurement of σ_a , are the following.

(a) *Pile Reactivity* Danger coefficient method (Anderson *et al*, 1947) and Pile oscillator method (Langsdorf, 1948). The results obtainable from danger coefficient method are affected by various extraneous effects, mainly due to the short time barometric fluctuations. To obviate this the pile oscillator method was developed. This is a very sensitive method and at present the values obtained from experiments employing this method at Argonne, Oak Ridge, and Harwell are the chief sources of data. This method has also various limitations, the important one being the effect on reactivity by the variations of scattering by the samples depending on their positions. Moreover, these methods are not absolute, being dependent on calibration by a standard absorber, which is usually B, Mn, or Au.

(b) *Activation Method* This is also a relative method, requiring a standard absorber to calibrate the neutron beam used for activation. There are many uncertainties in the method. Counting rate should be corrected for gamma rays

and may be affected due to conversion electrons or decay by orbital electron capture. Nevertheless, for absorbers having $\sigma_a \ll \sigma_s$, this method sometimes gives most reliable data by enabling the eliminating of contamination effects from the study of the resulting activities.

(c) *Method based on the local reduction of neutron density* in a solution or mixture due to the presence of the absorber. This is also a relative method (Lapointe and Rasetti, 1940; Coltman and Goldhaber, 1946).

(d) *Method based on the free decay of neutron flux* in a moderator solution containing the absorber. This is also a relative method (Scott *et al*, 1954; Dardel and Sjostrand, 1954)

(e) *Beam attenuation technique*, using velocity selectors or neutron spectrometers. This method yields σ_t , the total neutron cross-section. It is possible to separate σ_t in some cases, into a constant term due to potential scattering, and a term varying as $1/v$, due to absorption. Even for cases $\sigma_a \ll \sigma_s$ there are uncertainties in the measured values owing to the molecular or crystal scattering effects contributing to $1/v$ term. Moreover, this is also a relative method.

(f) *Mass-spectrometric method*. This is a relative method and has only restricted use (Lapp *et al*, 1947).

It should be noted that most of the methods described above are relative methods and so the accuracy of the measured absorption cross-section depends entirely on the accuracy with which the thermal neutron absorption cross-section of a standard $1/v$ absorber such as B, Mn, or Au is known. From the study of the relevant literatures published during the last fifteen years, it is observed that such an important nucleonic constant as the absorption cross-section of boron has changed from time to time depending on the measuring technique (vide Ghosh and Ganguly, 1956).

Although the latest determination of the capture cross-section of boron has removed greatly the difficulty of fixing the capture cross-section of standard absorber, it is obviously desirable to develop an absolute method for determining the thermal neutron absorption cross-section which is even applicable to absorbers having not too large capture cross-section in comparison with scattering cross-section. With this purpose in view the present authors have developed an absolute method (Ghosh and Ganguly, 1956), which successfully separates the scattering part and measures the absorption part of thermal neutron interaction cross-section. To demonstrate the validity and applicability of the theory the present experiment has been conducted. The material chosen for the purpose is chlorine, which has good absorption cross-section with substantial scattering cross-section. The value for the absorption cross-section obtained from the present experiment shows that the absorption cross-section can be measured directly by the present method by eliminating the scattering part.

II. METHOD

When the measurement of transmission is done under "good geometry" condition both scattered and absorbed neutrons fail to reach the detector and as a result, the total absorption cross-section is measured from the transmission. But if the geometry is made "poorer", i.e., if the solid angle submitted by the absorber to the source and to the detector becomes larger, increasing number of scattered neutrons enter the detector system and the resulting cross-section approaches σ_a , the absorption cross-section. The transmission may be expressed in the form,

$$I/I_0 = \exp (-KN\rho S/M) \quad \dots (1)$$

where I_0 and I are the neutron intensities recorded in the detector before and after the introduction of the absorber respectively, N is the Avogadro's number while ρ , M and S are the density, molecular weight and thickness of the absorber along the neutron path respectively. The constant K is dependent on geometry and at "poor" geometry its value lies between σ_t and σ_a . As the geometry is made "poorer" K approaches σ_a and in the extreme case, when the absorber is a spherical shell of small thickness surrounding the source and there is no limiting diaphragm between the source and the detector, K equals σ_a , provided certain condition are satisfied. These conditions are as follows :

(1) The neutron flux distribution is radial so that S in equation (1) is the radial thickness of the absorber.

(2) The thickness of the absorber is so small that the effect of the obliquity of the path of scattered neutrons compared to that of the unscattered neutrons is negligible.

(3) There is no absorber or scatterer between the source and absorber, whose cross-section is under investigation.

(4) We have also tacitly assumed that the absorber does not generate fresh thermal neutrons through slowing down by scattering of epithermal neutrons.

It is evident that the distribution of neutrons emerging out of the moderator is not radial as assumed in condition (1) above. The distribution of neutrons at moderator surface is given by Fermi (Fermi, 1936, Bethe ; 1937) and by Plackzek and Seidel (1947). Taking the distribution given by Plackzek and Seidel the transmission as shown by the present authors (loc. cit.) is modified to

$$\begin{aligned} \psi &= \int_0^1 \mu \phi(\mu) \exp [(-S(\mu)d\mu)] / \int_0^1 \mu \phi(\mu) d\mu \\ &= \int_0^1 \mu \phi(\mu) \exp [-t \cdot \alpha(r, \mu)] d\mu / \int_0^1 \mu \phi(\mu) d\mu \end{aligned} \quad (2)$$

where μ is the cosine of the angle of neutron with the normal to the moderator surface. $\phi(\mu)d\mu$ is the neutron density between directions defined by μ and $\mu+d\mu$;

$$s(\mu) = \frac{S(\mu)}{\lambda} = [\mu^2 a^2 + t(t+2a)]^{\frac{1}{2}} - a\mu$$

where $a = R/\lambda$ and $t = T/\lambda$,

λ = absorption mean free path = $M/N\rho\sigma_a$,

R = radius of the moderator sphere = 8.328 cms.

T = thickness of the absorber shell = 1.899 cms.

Again $s(\mu) = t[\mu^2 r^2 + (1+2r)]^{\frac{1}{2}} - r\mu = t \cdot \alpha(r, \mu)$,

and $\alpha(r, \mu) = [\mu^2 r^2 + 1 + 2r]^{\frac{1}{2}} - r\mu$

where $r = a/t$, is the ratio of inner radius of the absorber shell to thickness of the absorber used.

Equation (2) represents ψ as a function of t and r . r depends upon the geometry of the apparatus. In our previous communication (loc. cit.) universal curves between ψ and r for various t have been given. For any set of experiment, measured value of ψ and r give directly t , from which σ_a is measured using the relation,

$$\sigma_a = \frac{M}{N\rho\lambda} = \frac{Mt}{N\rho T}$$

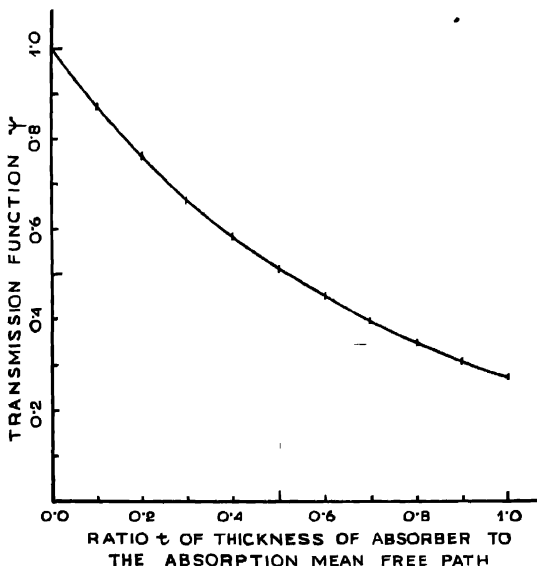


Fig. 1,

For the present experiment, values of ψ for various t are given in Table I and figure 1, the value of r being 4.385.

TABLE I

t	ψ
1.000	0.2711
0.900	0.3077
0.800	0.3494
0.700	0.3971
0.600	0.4518
0.500	0.5144
0.400	0.5864
0.300	0.6689
0.200	0.7639
0.100	0.8735
0.000	1.0000

When a neutron source, such as Ra-Be source, used in this experiment, is placed in a moderator and the moderator is of sufficient quantity to bring the neutrons to thermal equilibrium, the neutron distribution is Maxwellian. In this case the number of neutrons per unit volume in the velocity range dv , at velocity v is given by

$$dn = (4n/v_p^3 \sqrt{\pi}) \cdot v^2 e^{-v^2/v_p^2} \cdot dv$$

where n is the number of neutrons per unit volume, v_p the most probable velocity, is given by,

$$v_p = (2KT/m)^{1/2}.$$

This temperature T , corresponding to v_p of the distribution is known as the "temperature" of neutrons. It is customary to give the thermal neutron cross-sections corresponding to the neutron temperature of 20°C, the corresponding v_p and neutron energy being 2200 m/sec., 0.0252 ev respectively.

Measurement of neutron flux in transmission experiments using $1/v$ detector results in the measurement of neutron density. Since for $1/v$ detector ψ for the transmission is given by

$$\psi = I_x/I_0 = \frac{\int_{v=0}^{v_1} (n_x v) \cdot \frac{K}{v} \cdot dv}{\int_{v=0}^{v_1} (n_0 v) \cdot \frac{K}{v} \cdot dv} = \frac{\int_{v=0}^{v_1} n_x dv}{\int_{v=0}^{v_1} n_0 dv},$$

where I_x is the measured intensity with absorber and I_0 is the measured initial intensity, v_1 is the upper limit of the neutron velocity acceptable by Cd-difference

technique, and n_x is the neutron density after traversing a thickness x of the absorber. Thus the transmission is independent of neutron distribution, as regards the detector is concerned. But this transmission yields average cross-section as the absorber absorbs according to the $1/v$ law. The average cross-section is given by

$$\bar{\sigma}_a = \frac{\int \sigma_a(v) \cdot n(v) \cdot v \cdot dv}{\int n(v) \cdot v \cdot dv}$$

where $n(v)$ is the neutron density per unit velocity interval and $\sigma_a(v)$ is the absorption cross-section for the velocity v . For $1/v$ absorber $\sigma_a(v)$ is K/v . Therefore,

$$\bar{\sigma}_a = (2/\sqrt{\pi}) \cdot K/v_p = 1.128\sigma_a(v_p) \quad \dots \quad (3)$$

where $\sigma_a(v)$ is the cross-section corresponding to most probable velocity. As our experiment yields $\bar{\sigma}$ this formula will be used to get $\sigma_a(v_p)$ corresponding to a temperature $T(v_p)$.

We have hitherto assumed that the velocity of the neutrons attains a Maxwellian distribution, characteristic of the temperature T of the moderator. This is, however, strictly true only in the case of a moderator of infinite dimensions which scatters the neutrons but does not absorb them. As we have taken a moderator sphere of finite dimensions the actual neutron temperature will be different from the moderator temperature (Bacher *et al* 1946, Havens *et al* 1948, Manley *et al* 1946). As shown in our previous paper (*loc. cit.*) the correction necessary for this difference is given by

$$\begin{aligned}\sigma_a(T) &= \sigma_a(T')(T'/293)^{1/2} \\ \sigma_a(T') &= \sigma_a(T')(1.154 \pm .014)\end{aligned}$$

where $\sigma_a(T')$ is the measured absorption cross-section and $\sigma_a(T)$ is the corrected absorption for neutron temperature of 20°C .

III. EXPERIMENTAL ARRANGEMENT

The apparatus consists of an outer copper sphere of diameter about 20 cms. (figure 2). This hollow sphere was constructed by joining two hemispheres pressed out from thin, pure copper sheets. Great care was taken to obtain a regular shape. Within this sphere was centrally placed a round bottom flask of outer diameter of about 16 cms. This inner glass sphere was held fast centrally by three brass pins soldered on the inner surface of the outer sphere. The glass flask was filled with pure paraffin and at the centre was placed a 50 mc Ra-Be source. The Ra-Be source was placed in an aluminium container fixed to a thin, straight alu-

minium rod which was fixed to a stopper. By taking off a thin brass cap fixed on the top of the copper sphere round the neck of the glass flask the absorber could be inserted uniformly in the annular space. This sphere was placed on a vertical ball bearing shaft which could spin freely on the socket of the base plate. A pulley was attached to the shaft which could be rotated by a belting driven by a motor and gear arrangement. The entire arrangement was such that at the time of taking readings the sphere could be rotated about its vertical axis to circumvent any irregularity in the shape of the sphere.

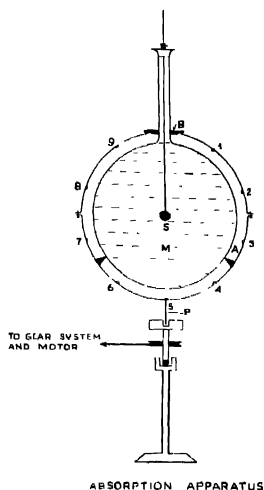


Fig. 2. *S* and *M* are the source and the moderator respectively; *A* is the annular space for the absorber which is introduced by removing the cap *B*. *P* is the fixing pin which determines the axis of rotation of the apparatus. 1 to 9 are the sockets available for the pin *P*.

The method of activation detection was employed for measuring the neutron flux. Indium was selected for an activation detector as it has good activation cross-section in the thermal region and can be obtained in the pure form easily. The activity of the indium foil was measured by using a scintillation beta detector. The phosphor assembly consisted of a thin anthracene crystal of circular cross-section covered on one side by a thin aluminium foil of thickness 4 mgm/cm^2 . On the other side a light pipe made from perspex and ground to fit the photocathode of RCA 5819 tube, was fixed. Magnesium oxide film was deposited around the phosphor to ensure maximum light collection. The window is firmly fixed to a round aluminium shelf so that counts could be taken with strictly reproducible geometry. The photomultiplier dynode voltage divider was fed from an electronically regulated supply. A constant check on the voltage

was kept by means of a bridge circuit whose indicator was a galvanometer and the reference voltage was provided by a RCA 5651 tube. The recorder assembly consisted of a push-pull amplifier and a scalar. The amplifier was constructed with an idea of eliminating isophase noise troubles originating either as high-voltage noise or as pick-up noise. At the tail end of the amplifier was incorporated a modified Schmitt trigger discriminator circuit.

IV. MEASUREMENT OF THE ABSORPTION CROSS-SECTION

An indium foil of radius 3.16 cms was used as the detector. The thickness of the foil was 100 mgm per square centimetre. This thickness of the foil was taken to be the optimum because at this thickness the counting is nearly the maximum, whereas for larger thickness hardening and obliquity corrections become necessary. The activation of indium by thermal neutrons is mainly due to the reaction $I_n^{115}(\alpha, \beta) \text{ Sn}^{116}$ having a half life of nearly 54 mins. Besides this two other activities having half lives 13 secs and 4.5 hrs are produced. The 13 secs half life activity is produced by thermal neutrons and 4.5 hrs activity is due to fast neutrons. Before taking each count, 3 mins were allowed to completely decay out the 13 secs activity. To avoid the 4.5 hrs activity due to any fast neutrons that may be present in the neutron flux the given exposure time of the foil was 54 mins. This exposure time allows the 54 mins activity to reach half the saturation value, whereas the 4.5 hrs activity only attains 13% of the saturation value. For the amount of the moderator used in this experiment the 4.5 hrs activity at the end of a 54 mins exposure will be about 2.6% (Tittle, 1951). Moreover, in the present experiment, the activity of the foil was measured using a scintillation beta counter having low efficiency for gamma counting. Thus the effect of the 4.5 hrs gamma activity was negligible. Under this condition the effective activity can be taken to be due to 54 mins beta activity and saturation counting rate for any set of measurement is given by

$$A_{sat} = (n/\tau) \cdot (e^{-t_1/\tau} - e^{-t_2/\tau})^{-1} \cdot (1 - e^{-t_1/\tau})^{-1}$$

where t is the time of exposure of indium foil and n is the number of counts recorded between time t_1 and t_2 , measured from the end of the exposure. τ is the mean life of the activity ($\tau = T_{1/2}/0.693$) and is equal to about 77.9 mins. While measuring transmission each count rate was reduced to saturation count rate.

Thermal neutron counts were obtained by Cd-difference technique. The thickness of the cadmium foil was 0.02 inch. A cadmium shield not only cuts off thermal neutrons, but also some of the resonance neutrons, the Cd cut-off energy being about 0.4 ev. Due to this fact the effect of resonance neutrons is to be eliminated by subtracting the in-cadmium reading multiplied by a factor F_{cd} given in figure 3 (Tittle, 1951). In our case F_{cd} comes out to be 1.07. The ab-

sorbing material was pure NaCl ground to fine powder and introduced in the annular space uniformly.

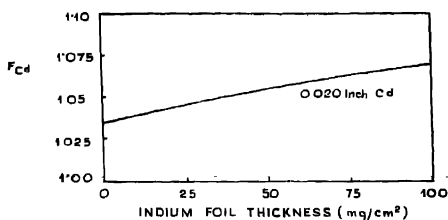


Fig. 3.

Spherical symmetry is the most important condition of this experiment. To verify this, neutron intensity with and without absorber was measured at distances from the source. The resulting values are given in Table II and figure 4. Linear relation between Ω/π and I , where Ω is the solid angle subtended at the centre of the source by the foil, shows that the condition of spherical symmetry has been attained in the present set up.

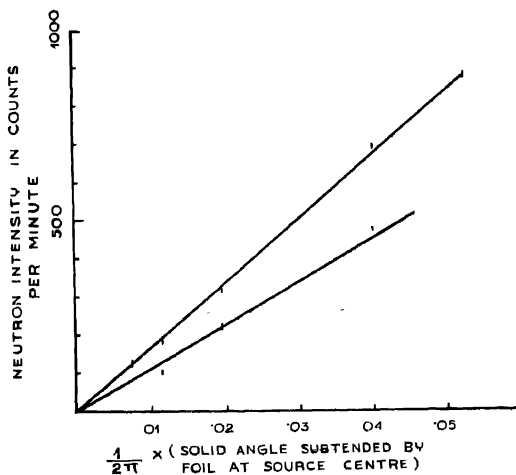


Fig. 4.

l is the distance from the centre of the source to the detector, $I_0(\text{air})$, and $I(\text{NaCl})$ are the intensities without and with absorber respectively.

TABLE II

D (cm)	Ω/π	I_0 (air)	I (NaCl)
13.5	0.0525	891.08 ± 6.09	—
15.5	0.0402	701.80 ± 4.75	487.4 ± 3.2
22.5	0.0194	313.65 ± 3.52	222.46 ± 2.4
29.5	0.0114	187.02 ± 3.00	102.11 ± 1.7
36.5	0.0074	132.45 ± 2.62	—

V. RESULTS AND DISCUSSIONS

Transmission ψ comes out to be equal to $0.4866 \pm .014$ and the corresponding t obtained by interpolation (using Bessel's formula) is 0.544 ± 0.013 . Volume of the absorber 2061 cc and mass of the absorber = 1976 gms

$M = 58.454$, $N = 6.0228 \times 10^{23}$, density of the absorber = 0.9581 gms/cc.

$$\sigma_a(T'') = Mt/N\rho T = 29.02 \pm .075 \text{ barns.}$$

Therefore, $\sigma_a(T) \text{ ex} = \sigma_a(T'')(1.154 \pm 0.0145) = 33.49 \pm 1.2 \text{ barns.}$

This $\sigma_a(T)$ is in effect an average cross-section since any finite amount of absorber changes the distribution of the neutrons in course of absorption. This necessitates a hardening correction. Hardening correction curves for $1/v$ absorber have been given by Bethe, (1937) and Hughes, (1953). From the hardening correction curve it is observed that for a transmission of 0.5, $\sigma(T) \text{ (exp)}/\sigma_a(v_p) = 1$. Therefore for the transmission used in this experiment $\sigma_a(T) \text{ (exp)}$ gives directly the absorption cross-section at v_p , $\sigma_a(v_p)$. So our measured values for $\sigma_a(v_p) = 33.49 \pm 1.2 \text{ barns}$. It should be noted that this hardening correction covers the correction given in Eq (3).

This absorption cross-section is the sum of those of Na and Cl. Absorption cross-section of sodium is 0.49 ± 0.02 (Hughes, 1952, Grineland, 1955). Subtracting this value from our measured value the absorption cross-section of chlorine comes out to be $33.00 \pm 1.22 \text{ barns}$. It has been shown by Hibdon and Muelhaue (1950), Hibdon *et al* (1950) that the absorption and scattering cross-section of chlorine are given by,

$$\sigma_s(E) = 1.43 + \frac{580}{E+75} + \frac{28100}{(E+75)^2}$$

$$\sigma_a(E) = \frac{31.5}{(40E)^{1/2}}$$

From this we get, for thermal neutrons,

$$\sigma_a = 31.5 \text{ barns}$$

$$\sigma_s = 14.2 \text{ barns}$$

Compilation by Hughes gives σ_a equal to $31.6 \pm 1.0 \text{ barns}$.

While comparing these data various other sources of error should be taken into account. The fractional error in estimating σ_a due to multiple scattering and scattering in the moderator can be shown (Ghosh and Ganguly, 1956) to be approximately given by

$$p \simeq 3/4(1 - \psi_0)\sigma_s/\sigma_a$$

where $\psi_0 = \psi - p$, ψ_0 and ψ being true and measured of transmission respectively. In the present experiment the value of p is about 15%. Also the fractional error due to alteration in the efficiency of the detector for scattered neutrons is approximately given by

$$p' \simeq -\frac{1}{2} \frac{\sigma_s}{\sigma_a} \frac{1 - \psi}{\psi} \left(\sec \frac{\theta_m}{2} - 1 \right)$$

where θ_m is the maximum possible inclination for a scattered neutron with the axis of the detector. In the present experiment this correction is of the order of -2%. On the other hand, thermalisation of epithermal neutrons introduces an error which is difficult to estimate. From our data we find that apparently epithermal neutron cross-section for NaCl is vanishing. If we assume that the cross-section is mainly due to 1.44 eV I_n -resonance neutrons, Cl being $1/v$ absorber, the actual cross-section is about 13% of the thermal cross-section. Hence the correction factor for thermal cross-section should be of this order of magnitude. Thus the overall correction factor necessary, covering all these errors, should not be larger than a few percent, the errors more or less compensating each other. Although this correction factors are not very large, the uncertainty inherent in their estimates does not allow us to claim the value to be closer than 10% of the true value. A more accurate estimation of the absorption cross-section may be obtained by using different thickness of absorber and studying the trend of the measured value of σ_a as the thickness of the absorber is made very small. Experiments along this line are in progress in our laboratory. The present experiment however, clearly demonstrates that the spherical symmetry method is sufficient to separate the effect of scattering from that of true absorption of thermal neutrons.

ACKNOWLEDGMENTS

The authors wish to claim equal share in working the problem. Their thanks are due to Dr. D. M. Bose, M.A., Ph.D. F.N.I., Director, Bose Institute, for his kind encouragement throughout the progress of the work.

REFERENCES

- Anderson, Fermi, Wattenburg, Weil and Zinn, 1947, *Phys. Rev.*, **72**, 16.
 Bacher, Baker, McDaniel, 1946, *Phys. Rev.*, **69**, 443,
 Bethe, 1937, *Rev. Mod. Phys.*, **9**, 32.

- Coltman and Goldhaber, 1946, *Phys. Rev.*, **69**, 411.
Dardel and Sjostrand, 1954, *Phys. Rev.*, **96**, 1566
Fermi, 1936, *Ricerca Scient.*, **7**, 13.
Ghosh and Ganguly, 1956, *Ind. J. Phys.*, **30**, 500.
Grimmeland, 1955, *Jour. of Nucl. Energy*, **1**, 231.
Havens, Rainwater, Wu, Dunning, 1948, *Phys. Rev.*, **73**, 733.
Hibdon and Muelhause, 1950, *Phys. Rev.*, **79**, 44.
Hibdon, Muelhause, Selove, Woolf, 1950, *Phys. Rev.*, **77**, 730.
Hughes, D. J., 1953, *Pile Neutron Research*, Addison-Wesley.
Langsdorf, 1948, *Phys. Rev.*, **74**, 1217.
Lapointe and Rasetti, 1950, *Phys. Rev.*, **58**, 554.
Lapp, Van Horn and Dempster, 1947, *Phys. Rev.*, **71**, 745
Manley, Hawroth, Lenleke, 1946, *Phys. Rev.*, **69**, 505.
Plackzok, 1947, *Phys. Rev.*, **72**, 556.
Plackzok and Seidel, 1947, *Phys. Rev.*, **72**, 550.
Scott, Thompson and Wright, 1950, *Phys. Rev.*, **95**, 582.
Tittle, 1951, *Nucleonics*, June.

MODELS OF THE LOWER IONOSPHERE AS MAY BE INFERRED FROM ABSORPTION RESULTS

P. BANDYOPADHYAY

INSTITUTE OF RADIO PHYSICS AND ELECTRONICS, CALCUTTA UNIVERSITY

(Received for publication, February 26, 1957)

ABSTRACT. Values of deviative and non-deviative absorption and their variations with $\cos X$ are calculated for some of the proposed D and E region models. The results obtained are compared with the available experimental data. It is found that so far as the E region is concerned, A. P. Mitra's theoretical model is most consistent with the observed diurnal variation of absorption. For the E region, the model, as proposed by Jones, is found to be unacceptable.

Conditions which are to be satisfied by an acceptable E region model are discussed.

1. INTRODUCTION

It is now well-known that the height variation of ionization in none of the ionospheric layers obeys the simple Chapman distribution. This is obviously due to the highly idealised nature of the assumptions made. Many different models of the ionospheric layers have, therefore, been proposed from time to time to take into account the departures from Chapman distribution. These proposed models have, in many cases, been checked against experimental height measurements. Occasionally these have also been checked against results of absorption measurement. But a general checking of the various proposed models against the available experimental absorption data does not appear to have been made till now. This is done in the present paper for D region models of Nertney (1953), Piggott (unpublished), and Mitra* (1954), and for the E layer model of Jones (1953). The object has been to judge the adequacy of the proposed models for explaining the observed variations of ionospheric absorption. All the calculations are on the basis of the ray theory and by the method of numerical integration.

2. THE MODELS

(i) *Nertney's model* (D region). The model is an empirical one, Chapman-like, with the height of maximum ionization fixed at 79 km (figure 1). It has been claimed that the experimental results of Grace (1951) support this "constant height" idea at least for the hours round noon time. The model has been checked

*The actual model used is a revised one in which S.I.D. observations have been employed to modify the lower portion. The details about this unpublished revised model have been made available to the author by A. P. Mitra.

by Nertney primarily against group and phase heights of reflections of 16, 48, and 150 Kc/s waves, against polarization and wind data, and also against absorption observed of 150 Kc/s waves.

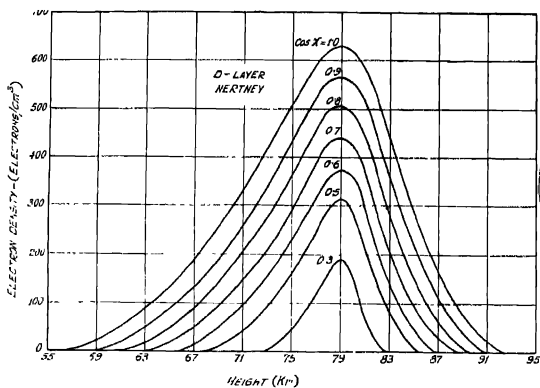


Fig. 1 D-region model (after Nertney)

(ii) *Piggott's model (D region)**. The model is shown in figure 2. It is based on absorption measurements made at Slough with medium and short waves, and on the relaxation times obtained from f_oE and 16 Kc/s phase heights.

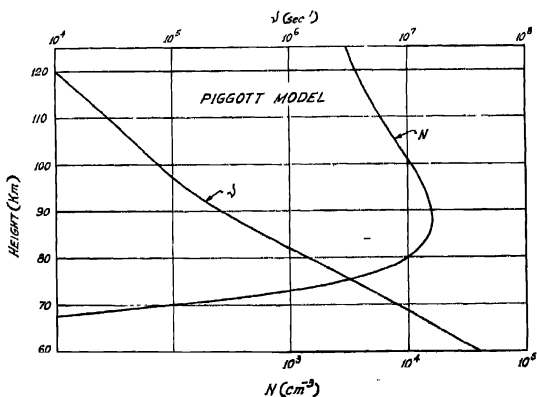


Fig. 2. D-region model and collision frequency model (after Piggott).

*Private communication to A. P. Mitra

(iii) *A. P. Mitra's model (D region).* The model (figure 3) has been proposed from various theoretical considerations regarding the nature and distribution of the atmospheric constituent at the D layer heights, and the height variation of the recombination coefficient. Mitra has checked his model against S.I.D results.

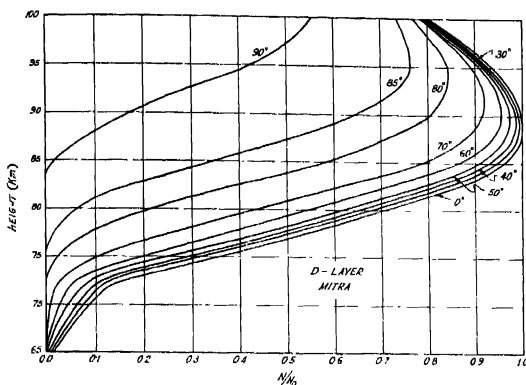


Fig. 3. D region model (after A. P. Mitra)

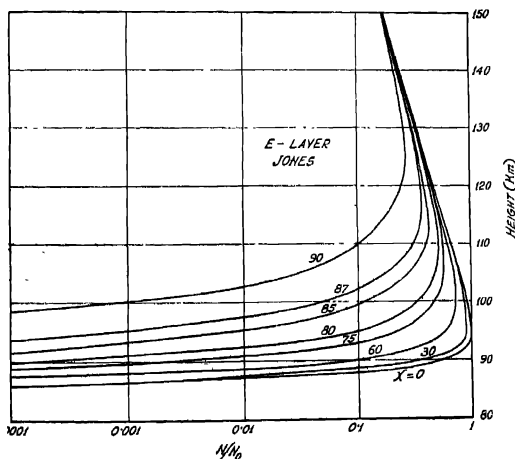


Fig. 4. E-region model (after Jones)

(iv) *Jones' model (E region).* The model (figure 4) has been developed by modifying the Chapman theory so as to include the effects of variable scale height, oxygen dissociation, and variation of recombination coefficient with height. The

model has been checked primarily against the phase height data obtained at Pennsylvania State University on 150 Kc/s.

Calculation of absorption also requires a knowledge of the variation of collisional frequency with height. For this, the height-collisional frequency curve (figure 5), as suggested by Nicolet (1953), has been utilised.

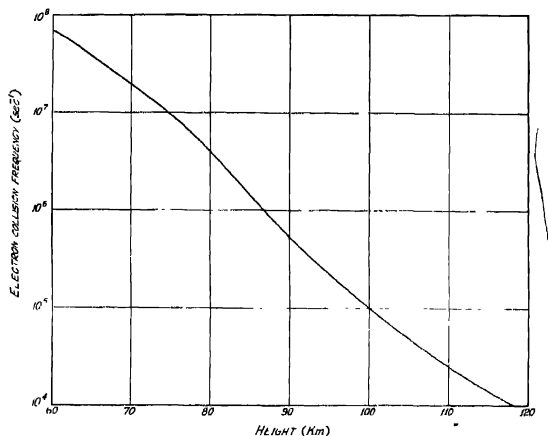


Fig. 5. Collision frequency model (after Nicolet).

3. THEORETICAL CONSIDERATIONS

The total absorption suffered by radio wave along the whole of its direct and reflected ray path is given by

$$\int \kappa ds = -\log \rho \text{ nepers} \quad \dots (1)$$

where κ is the absorption coefficient and ρ is the so-called reflection coefficient. Assuming that the propagation is quasi-longitudinal, we have, according to the approximation of Booker (1935),

$$\mu^2 = 1 - \frac{p_0^2}{(p \pm p_L)^2 + \nu^2} \quad \dots (2)$$

and

$$\kappa = \frac{\nu}{2c} \cdot \frac{1}{\mu} \cdot \frac{p_0^2}{(p \pm p_L)^2 + \nu^2} \quad \dots (3)$$

where ν = collisional frequency,

p = angular frequency of the incident wave

Models of the Lower Ionosphere from Absorption Results. 301.

p_L = angular gyro-frequency corresponding to the longitudinal component of the earth's magnetic field.

and $p_0^2 = \frac{4\pi N e^2}{m}$, N being the electron density and m and e , the mass and the charge of an electron respectively. The upper positive sign refers to the ordinary wave and the lower negative sign to the extra-ordinary one

(a) *Non-deviative absorption*

In the case of non-deviative absorption $\mu \approx 1$. From Eqs. (1) and (3) the total absorption is, therefore, given by

$$-\log \rho = \int \kappa ds = \frac{2\pi e^2}{mc} \int \frac{Nv}{4\pi^2 (f \pm f_L)^2 + v^2} ds \quad \dots (4)$$

where

$$f = \frac{p}{2\pi} \text{ and } f_L = \frac{p_L}{2\pi}$$

Equ. (4) has been utilised for calculating the non-deviative absorption, the evaluation of the integral being carried out by numerical method.

It is seen from (4) that when the collisional frequency v is small compared with the "effective angular frequency" $2\pi(f \pm f_L)$, the total absorption can be put as

$$-\log \rho = \int \kappa ds = \frac{A}{(f \pm f_L)^2} \quad \dots (5)$$

where A is a constant.

The non-deviative absorption becomes thus inversely proportional to $(f \pm f_L)^2$. Hence, if in any special case the absorption is found to vary inversely as $(f \pm f_L)^2$, one may conclude that the absorption is in a non-deviative region.

(b) *Deviative absorption*

In the case of deviative absorption μ is less than unity. From Eqs. (2) and (3) the absorption coefficient κ is now given by

$$\kappa = \frac{v}{2c} \cdot \frac{1 - \mu^2}{\mu} \quad \dots (6)$$

or, substituting the expression for μ as given in (2),

$$\kappa = \frac{v}{2c} \cdot \frac{\frac{p_0^2}{(p \pm p_L)^2 + v^2}}{\sqrt{1 - \frac{p_0^2}{(p \pm p_L)^2 + v^2}}} \quad \dots$$

Putting

$$R = \frac{p_0^2}{(p \pm p_L)^2} \quad \text{and taking} \quad \nu \ll (p \pm p_L)$$

one gets

$$\kappa = \frac{\nu}{2c} R(1-R)^{-\frac{1}{2}} \quad \dots (7)$$

The total deviative absorption of a wave for double traverse of a region is given by

$$-\log \rho = \int_{-s_r}^{s_r} \frac{\nu}{c} R(1-R)^{-\frac{1}{2}} dh \quad \dots (8)$$

where s_r is the height of reflection of the wave given by the condition $\mu = 0$. As for the non-deviative case, the integral in Eqn. (8) has been evaluated by numerical method.

(c) *Variation of non-deviative absorption with the solar zenith angle χ .*

For a Chapman region $N = N_0 \exp \frac{1}{2} (1 - z - \sec \chi e^{-z})$ where z is the height above the datum level expressed in the unit of scale height H_e , N_0 is the electron density at the level of maximum electron production $\chi = 0$, and ν_0 is the collisional frequency at the same level. If we assume that ν decreases exponentially with height, $\nu = \nu_0 e^{-z}$, then substituting for N and ν in Eqn. (4) we get the total non-deviative absorption for a Chapman region. Appleton and Piggott (1954) have calculated this absorption for double traverse of a Chapman region. They have found that when the recombination coefficient α is independent of pressure

$$-\log \rho = \int \kappa ds = \frac{4\pi e^2 N_0 H \nu_0}{mc} \cdot \sqrt{2\pi e} \cdot \frac{\cos^{3/2} \chi}{(p \pm p_L)^2} \quad \dots (9)$$

If α is proportional to pressure, then

$$-\log \rho = \int \kappa ds = \frac{4\pi e^2 N_0 H \nu_0}{mc} \cdot \sqrt{4e} \cdot \frac{\cos \chi}{(p \pm p_L)^2} \quad \dots (10)$$

The total absorption is, therefore, generally of the form

$$\log \rho = \log \rho_0 + \cos^n \chi \quad \dots (11)$$

where $\log \rho_0$ is the absorption for $\chi = 0$. It follows, therefore, that if for a given frequency, ρ is measured for different values of χ , then the plot of the logarithm of $\log \rho$ against logarithm of $\cos \chi$ will be a straight line. The slope of this straight

line should give the value of the index n . Alternatively, n may also be obtained from a comparison of the logarithm of the ratio $\frac{\log \rho_1}{\log \rho_2}$ with the logarithm of the ratio $\frac{\cos \chi_1}{\cos \chi_2}$, where ρ_1 and ρ_2 correspond to χ_1 and χ_2 respectively. Experimental results show that the value of n is slightly below unity. A satisfactory model should, therefore, yield such a value.

4. AVAILABLE EXPERIMENTAL DATA

For checking the proposed models the most useful absorption data are those on the frequency dependence of absorption for different values of χ at some definite epoch of solar activity. Unfortunately the available absorption data are not adequate for this purpose. For checking the value of n the existing data are, however, quite satisfactory.

(a) *Available data for non-deviative and deviative absorptions.*

Extensive series of absorption data are available from Slough. Appleton and Piggott (1954) have utilised these data for studying the variations of absorption with different parameters. They have found that in addition to variations with frequency and with χ , there exist diurnal and seasonal variations of absorption together with a "winter anomaly" (characterised by occurrence of anomalously large absorption on certain groups of days in winter). An effect of solar activity on absorption has also been found.

Due to these anomalies and to the uncertain nature of the dependence of absorption on some of the factors, standard curves of absorption against frequency

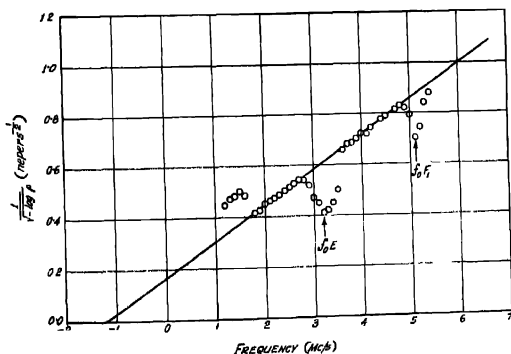


Fig. 6. Variation of absorption given as $(-\log \rho)^{-1/2}$ with frequency (after Appleton and Piggott). Add 1.2 to the values of frequency to get effective frequency ($f \pm f_L$ in Mc/s).

for given values of χ are not available. In the present paper, therefore, the experimental values of Appleton and Piggott (1954) taken on July 11, 1950 and

presented as a plot of $\sqrt{\frac{1}{-\log \rho}}$ against frequency (reproduced in figure 6) are taken to be fairly representative. These are utilised for the purpose of comparison with the theoretically deduced values. We note that the observed values of $\sqrt{\frac{1}{-\log \rho}}$, except those close to the critical frequencies of the E and the F₁ layers, lie on a straight line. From Eqn. (5) we may conclude, therefore that the values on the straight line are non-deviative absorption values.

The values of absorption near the critical frequencies represent mainly the deviative absorption superposed on the non-deviative absorption. The values of the latter are obviously represented by the corresponding points lying on the continuation of the straight line under the total absorption curves. Hence, by subtracting these latter values from the total absorption values, one may obtain pure deviative absorption curves for the E and the F₁ regions. This is shown in figure 7.

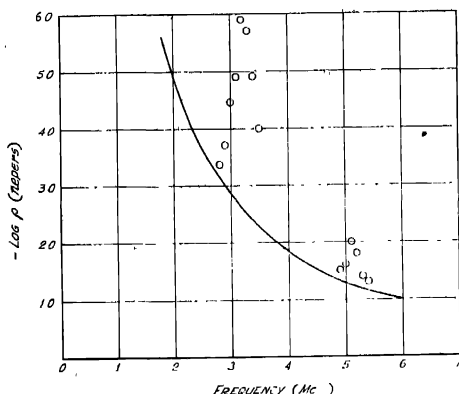


Fig 7 Variation of absorption ($-\log \rho$) with frequency [Add 1.2 to the frequency values to get corresponding effective frequencies in Mc/s]

It is to be noted that each of the models has been represented by its author (or authors) by a number of electron distribution curves for different values of χ . Of these we have selected only the one for $\chi = 30^\circ$ for testing. This is because, as already mentioned, the data available for comparison refer only to this value of χ (at Slough, July 11, 1950).

Besides the absorption values of Appleton and Piggott, those obtained by Mitra and Shain (1953) from measurements of cosmic noise intensity for 18.3 Mc/s are also utilised,

(b) *Available data for the exponent of $\cos \chi$*

A wide range of values has been reported for the $\cos \chi$ exponent (n) of absorption (Eqn. 11). There is a day-to-day variation of n for any given frequency; n also appears to depend on the season and on the magnitude of the absorption. It is also affected by contamination from absorption taking place in a layer or layers besides that under consideration. The investigations of Appleton and Piggott (1954) show that individual values of n normally range from 0.4 to 1.3. The most probable value lies between 0.7 and 0.8.

5. DISCUSSION OF RESULTS

(a) *Non-deviative absorption*

In Table I are given the values of non-deviative absorption for the different D region models as calculated from Eqn (4) for $\chi = 30^\circ$. These may be compared with the experimental values of Appleton and Piggott (for effective frequencies upto 6.0 Mc/s), and of Mitra and Sham (for the operating frequency 18.3 Mc/s; effective frequency 19.7 Mc/s) for the same value of χ .

TABLE I

χ	D region absorption, $\log P$, in nepers						n , the exponent of $\cos \chi$	
	Effective frequency Mc/s	Experimental	Theoretical				Experimental	Theoretical
			Nertney	Mitra	Piggott his p values	using Nicolet's p values		
30°	3.0	5.6	1.1	2.0	5.9	14.1		2.2
	4.0	3.2	0.7	1.4	3.3	8.2		2.3
	5.0	2.0	0.5	0.8	2.1	5.3	7 to 8	2.3
	6.0	1.4	0.4	0.6	1.5	3.7		2.4
	19.7	0.14	0.04	0.06	0.14	0.35		2.7
								0.5
								0.6
								0.7
								0.7
								0.8

It is seen from Table I that the values of absorption for the Nertney model are in every case too low. The values may be improved if the electron densities are increased by a factor of about 5. Even then, however, the 'shape' of the model cannot be regarded as satisfactory, because, the values of n depend on the 'shape' and, as seen from Table I, the n -values are all unusually large.

Absorption values for Mitra's D region model are also too low. Better values of absorption may be obtained if the electron density is increased by a factor of about

2.5. This will raise the maximum electron density N_0 in the model from 2.0×10^3 per cm^3 as recently proposed by Mitra (1955), to about 5×10^3 per cm^3 . One satisfying feature of the model, however, is the close agreement of the values for n with the experimental ones.

Using Piggott's electron density and ν values, the calculated absorption values for D region show also correspondence with the experimental values. This is as expected because the model itself is based on absorption results, and the collision frequency distribution used by him has been chosen to suit the absorption values. The corresponding calculations, using Nicolet's (1953) ν -distribution (figure 5), yield much higher values of absorption. It appears, therefore, that the electron densities in Piggott's model are too high. Values of n for this model, could not, however, be calculated, since its variation with χ has not been specified.

(b) *Deviative absorption*

Values of E region deviative absorption for Jones model for $\chi = 30^\circ$, and for effective frequencies close to and below the critical frequency were obtained by numerical integration. These are given in the last column of Table II and may be compared with the experimental values shown in the second column.

TABLE II

Effective frequency f/f_L Mc/s	Values of deviative absorption, $-\log \rho$, in the E region in nepers	
	Experimental	Theoretical (from Jones's model)
4.0	0.2	9.9
4.1	0.7	9.7
4.2	1.3	10.1
4.3	2.2	12.8
4.4	3.2	13.3

It will be seen that the calculated values for this model differ widely from the observed values. Firstly, the values are too large (larger, for example, by a factor of about 8 for 4.2 Mc/s) and secondly, the rate of variation of absorption with frequency (which depends on the shape of the model) is slower than that actually observed. It may, therefore, be concluded that neither the height nor the shape of Jones model is acceptable. It is possible to retain the shape of the model and yet reduce the absorption values by raising the model bodily up. This, however, is no solution, because, the nature of the frequency variation of absorption will then not agree with the experimental observations.

(c) Conditions to be satisfied by an acceptable E-region model.

In developing an empirical E layer consistent with the various experimental observations, the following points have to be carefully considered

(i) The maximum electron density level should be at a height greater than that of Jones' model. This is in order to reduce the calculated absorption values.

(ii) The bottom part of the layer should behave like the Jones' model. This is to make the layer height consistent with the 150 Kc/s phase height and with the other experimental data on which the model is based.

(iii) For any model, the shape near the peak must not deviate considerably from a Chapman layer, because, observations show that the $\cos \chi$ exponent for $f_0 E$ is normally only slightly different from the Chapman value of 0.25.

Some idea regarding the overall shape of a correct E layer model may be formed from a comparison of the curves of frequency variation of absorption of the proposed models [Jones model and Chapman model, obtained by using the numerical integration results of Jaeger (1947)] with the experimental curve. This is made in figure 8 where the ratio $\frac{\log \rho}{(\log \rho)_{\max}}$ is plotted against effective frequency.

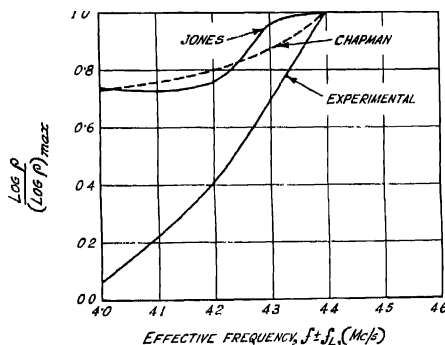


Fig. 8 Variation of $\frac{\log \rho}{(\log \rho)_{\max}}$ with effective frequency.

It will be noted that for both Jones and Chapman models the frequency variation, as compared with the experimental curves, is too slow. This is because the increase of frequency causes comparatively small increase of penetration of the exploring waves into the layer leading to an increase of absorption. The correct layer will have, therefore, to be thicker in the region where it contributes most to the deviative absorption at higher frequencies (*i.e.*, near $f_0 E$).

6. CONCLUDING REMARKS

The study shows that one of the proposed models of the lower ionosphere can cause absorption as demanded by the experimental data. Nevertheless A. P. Mitra's D model is perhaps the most acceptable one, because, its relative variation of absorption with frequency agrees closely with the experimental values. Further the values of the exponent n of $\cos \chi$ for the model fall well within the most frequently observed range.

The study also reveals the dependence of n on frequency—a fact which is significant in the understanding of its wide range of variation as observed by different workers.

Jones E model examined from the point of view of deviative absorption is found to be inadequate. An acceptable E model should not only yield values of deviative absorption agreeing with the experimental, but must also satisfy certain other conditions as outlined in Sec. 5. It is proposed to develop an empirical E-region model along these lines and present the results in a subsequent paper.

ACKNOWLEDGMENTS

The author is indebted to Professor S. K. Mitra for advice concerning the preparation of the paper. He is also grateful to Dr. J. N. Bhar, Head of the Institute of Radio Physics and Electronics, Calcutta University, and to Dr. S. S. Bural of the Institute for helpful discussions.

The author's thanks are also due to Dr. A. P. Mitra of the Radio Research Committee, C.S.I.R. New Delhi for drawing his attention to the problem.

REFERENCES

- Appleton, E and Piggott, W. R., 1954, *J. Atmosph. Terr. Phys.*, **5**, 111.
 Booker, H. G., 1935, *Proc. Roy. Soc. A*, **150**, 267.
 Grace, C. H., 1951, *J. Geophys. Res.*, **56**, 452.
 Jaeger, J. C., 1947, *Proc. Phys. Soc.*, **59**, 87.
 Jones, R. E., 1955, *J. Atmosph. Terr. Phys.*, **6**, 1.
 Mitra, A. P., 1954, *J. Atmosph. Terr. Phys.*, **5**, 28 and Private communication.
 Mitra, A. P., 1955, Progress of the Radio Research Committee, C.S.I.R. (India) March-August, 1955.
 Mitra, A. P. and Shum, C. A., 1953, *J. Atmosph. Terr. Phys.*, **4**, 204.
 Nertney, R. J., 1953, *J. Atmosph. Terr. Phys.*, **3**, 92.
 Nicolet, M., 1953, *J. Atmosph. Terr. Phys.*, **3**, 200.

SOLAR ECLIPSE OF 30TH JUNE, 1954 AND ITS EFFECT UPON THE IONOSPHERE

S. N. MITRA

RESEARCH DEPARTMENT, ALL INDIA RADIO, NEW DELHI

(Received for publication August 24, 1956)

ABSTRACT. Experimental investigations to determine the effect of the total eclipse of the sun on 30.6.54, are described. The investigations were—(1) vertical incidence ionospheric measurements at Delhi, Srinagar and Bombay, (2) recording of the variation of short wave signals from the B.B.C. and Moscow at Delhi, (3) recording of field strength variation of medium wave signals from Jullundur at Delhi, (4) measurement of ionospheric absorption at vertical incidence using pulsed transmissions by means of an automatic absorption recorder at Delhi, and (5) recording of solar radio noise on 204 Mc's at Delhi. The effect of the optical eclipse on the ionospheric layers could not be definitely established, due probably to the eclipse occurring around sunset when most of the optical effect was likely to be obscured. But evidence of three distinct 'corpuscular eclipses' was obtained both on the ionization density of the F-layer and on the absorption in the non-deviating region. These were found to occur 2.4 and 6½ hours before the optical eclipse. Theoretical arguments and past observations indicate that these corpuscular eruptions may have originated from the so-called M-region of the sun.

1. INTRODUCTION

The effect of a solar eclipse on the ionosphere has become a subject of important investigation to the geophysicist and to the communication engineer. This is because the sun exercises a predominant control over the ionospheric characteristics which determine short wave propagation. The sudden withdrawal of solar radiation for a short interval of time during the eclipse offers a rare opportunity of probing into character of these radiations and their accompanying effects.

A decrease in ionization density of the ionospheric layers during the eclipse period has been observed by many workers in the past. This indicates that the ultraviolet radiation from the sun is at least partly, if not fully, responsible for producing ionization of the ionosphere. In addition to the ultraviolet radiation, the corpuscular emission from the sun, known to cause terrestrial magnetic variations and aurorae, has also been found to ionize the ionospheric layers as evidenced from 'corpuscular eclipse' observed from investigations of the ionosphere during solar eclipses. Owing to their slow velocity, the 'shadow' of such corpuscles will be different in its location from that of the optical eclipse and the 'corpuscular eclipse' should precede the optical eclipse at the same location. It may be men-

tioned that there is now sufficient evidence on record to show that the corpuscular emission from the sun produces pronounced effect upon the ionospheric layers. Thus, the F_2 region has been known to possess a geomagnetic control, as shown by Appleton (1946), although it has not been definitely established whether such a control is exercised by corpuscular emission from the sun; the absorption of D and E layers has been found to be influenced by corpuscular emission (Davies and Hagg, 1955), the current systems in the upper atmosphere are caused by the incidence of these corpuscles, even the cosmic ray bursts in times of magnetic storms have been attributed to the ejection of charged particles from the neighbourhood of solar flares (Mixed Commission on Ionosphere, 1949). But little is known about the cause and exact mechanism of the emission of corpuscles from the sun.

In our investigation of the effect of partial solar eclipse of February 25, 1952 (Mitra, 1953) we have observed the occurrence of two corpuscular eclipses. We have later attempted to identify the emission of these corpuscular beams with M-region activity of the sun (Sengupta and Mitra, 1954). The total solar eclipse of 30.6.54 provided us with one of the rare opportunities of studying the corpuscular effects and some experiments were specially planned to investigate the phenomenon. In this paper we shall present the results of our observation and discuss the corpuscular eclipses found in the analysis. Since the eclipse occurred near about sunset, the effect of the optical eclipse was likely to be obscured. On the other hand, since the corpuscular eclipse, if any, would be expected to occur during the day, ionospheric conditions would be quite stable showing little day-to-day variations (as compared with those during night) thus favouring the observation of the corpuscular eclipse. We have, therefore, concentrated on the evidence of any corpuscular eclipse found in the experiment.

2 NATURE OF THE INVESTIGATION

The solar eclipse of 30th June, 1954 commenced at about 1830 I.S.T. and ended at about 2030 IST, the path of totality lying across part of U.S.A., Canada, Southern Greenland and Norway across Russia to Northern India. The eclipse occurred around sunset in the Northern India and it was, therefore, considered necessary to calculate the time of the sunset for different places of observation and for different altitudes. We had fixed Delhi, Bombay and Srinagar as our observing centres. Srinagar is situated at the highest northern latitude at which facilities of measurement were readily available to us. Bombay was chosen as a place of observation where the eclipse would be only partial.

The circumstances of the eclipse at Delhi, Srinagar and Bombay have been calculated and are shown in Table 1.

TABLE I

Circumstances of the solar eclipse of 30.6.54.

	Ground	100 km.(B)	300 km.(F)
<i>Delhi</i> (Lat. 28° 35'N., Long. 77° 5' E)			
Sunset,	1923 IST	2017 IST	2058 IST.
Eclipse begins	1830 "	1831 "	1834 "
Eclipse max.	1923 "	1924 "	1926 "
Eclipse ends	-	2014 "	2013 "
Magnitude	0.93	0.92	0.87
<i>Srinagar</i> (Lat. 34° N, Long. 74° 50' E)			
Sunset,	1946 IST	2044 IST	2131 IST
Eclipse begins,	1823 "	1825 "	1827 "
Eclipse max	1917 "	1919 "	1920 "
Eclipse ends,	—	2019 "	2019 "
Magnitude	0.85	0.83	0.79
<i>Bombay</i> (Lat. 19° N., Long. 73° E.)			
Sunset,	1919 IST		
Eclipse begins	1842 "		
Magnitude at sunset	0.68		

IST — Indian Standard Time is $5\frac{1}{2}$ hours ahead of G.M.T

Our investigations to study the effect of the corpuscular eclipse pertain to the following. The measurement of the critical frequencies permits a direct evaluation of the maximum ionization. Concurrent measurement of the layer heights would indicate the changes in the heights of maximum ionization. Another effect that might be investigated would be the change in the strength of the signals propagated via the ionosphere during the period of the eclipse and this change is likely to indicate the variation in the D and E layer absorption associated with such eclipses. In addition, a direct evaluation of the ionospheric absorption at vertical incidence on pulsed transmissions would usefully supplement the data. The study of the changes in the magnitude of solar radio noise is another pertinent investigation of interest.

To observe any changes during the eclipse period, the conditions for a few days around the day of eclipse are required to be known. We have, therefore, carried out all our observations for five days before and five days after the eclipse—thus providing adequate measurements for the control period of observation. It

can be shown from theoretical considerations that the corpuscular eclipse, if any, will precede the optical eclipse depending upon the speed of the corpuscles. For calculation, one may take that corpuscles having speed of $1600 \text{ km. sec}^{-1}$ will produce a corpuscular eclipse preceding the optical one by about two hours (Chapman and Bartels, 1940). The lower the speed of the particles the greater will be this interval. We have, therefore, conducted all our measurements from 1200 to 2100 I.S.T. each day during this 11-day period.

3. EXPERIMENTAL OBSERVATIONS

To investigate the effect of eclipse on the ionosphere the following observations were made.

(i) Vertical incidence ionospheric measurements at Delhi, Srinagar and Bombay.

(ii) Recording of the variation of field strength of short wave signals from the B.B.C. and Moscow at Delhi.

(iii) Recording of field strength of medium wave signals from Jullundur (Lat. $31^{\circ}25'N.$, Long. $75^{\circ}35'E$) at Delhi

(iv) Measurement of ionospheric absorption at vertical incidence using pulsed transmissions by means of an automatic absorption recorder at Delhi

(v) Recording of solar radio noise on 204 Mc/s at Delhi.

We shall describe these observations separately.

(i) *Vertical Incidence Ionospheric Measurement.*

Measurements at Delhi consisted in photographing the $h'-f$ curves by a panoramic ionospheric recorder constructed at the Research Department of All India Radio. The recorder was capable of sweeping through a frequency range of 0.5 to 20 Mc/s in 7 seconds. The peak power was of the order of 1 kw. The photographs were taken once every 20 minutes on the control days and on the day of the eclipse these records were taken once every 5 minutes. A manually operated ionospheric recorder was kept as a stand-by and measurements by this recorder were also taken once every 20 minutes.

Measurements at Srinagar and Bombay consisted in measuring f_oF_2 , f_oE and h_pF_2 once every half-hour on the control days and once every 15 minutes on the day of the eclipse. Manually operated ionospheric recorders were used for the purpose.

The analyses of the data are shown in figures 1 and 2. Figure 1 shows the variation of $(f_oF_2)^2$ and h_pE_2 for Delhi and figure 2 those for Srinagar. Unfortunately, due to the presence of strong E_s , practically at all times of the period of observation, it was not possible to analyse the data for Bombay and the data for E layer over Delhi and Srinagar.

It will be seen from figure 1 that there is a significant reduction in ionization density at about 1730 I.S.T. The effect of the optical eclipse between 1834 and

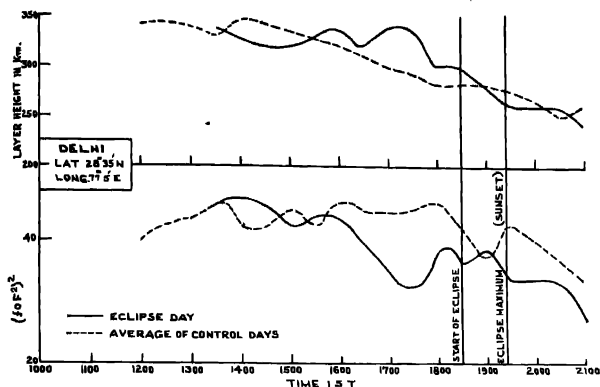


Fig. 1. Vertical incidence ionospheric characteristics at Delhi.

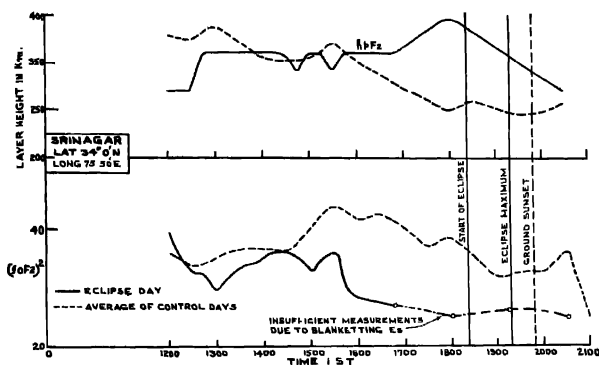


Fig. 2. Vertical incidence ionospheric characteristics at Srinagar

2013 I.S.T. could not be seen as its effect, if any had probably been obscured by the sunset. There was blanketing E_s from 1200 to 1330 I.S.T., on the day of the eclipse and the F_2 layer could not be observed. The reduction in ionization density at 1730 I.S.T. is so pronounced that it could not be explained by day-to-day variations. Moreover, the measurements during control days indicate that the values of f_oF_2 were more or less constant during the period 1530 to 1800 I.S.T. showing slight rising tendency towards the end. The occurrence of a corpuscular eclipse two hours before the optical eclipse could, however, explain this reduction. There is also a small reduction in ionization density at about 1500 I.S.T. but it

is difficult to conclude whether this was due to the effect of corpuscular eclipse. It may, incidentally, be mentioned that we had reported similar two-hour effect from our investigation of the partial solar eclipse of 25th February, 1952 (Mitra, 1953).

At Srinagar, we were able to observe f_oF_2 on the eclipse day right from 1200 I.S.T. But the incidence of strong E_s vitiated our measurements from 1645 to 2030 I.S.T. It will be noted from figure 2 that there was a reduction in ionization density at 1300 I.S.T., a small dip at about 1500 I.S.T. and a gradual but considerable reduction from 1530 I.S.T. onwards. In regard to the dip at 1300 I.S.T., it may be mentioned that the values of f_oF_2 during the control period always showed a rising tendency during the period 1200 to 1400 I.S.T. The reduction on the eclipse day, therefore, appears to be a genuine effect. The two-hour effect, as observed at Delhi, is somewhat obscured by the occurrence of E_s but the depression near 1730 I.S.T. is quite large. Had there been no E_s , the general fall in ionization density from about 1530 I.S.T. onwards would have indicated a large depression in $(f_oF_2)^2$ near about 1730 I.S.T. as could be seen from figure 2. The depression at about 1500 I.S.T. could also be seen at Delhi in figure 1, although not so pronounced. One cannot rule out the possibility of day-to-day variation causing the small depression in $(f_oF_2)^2$ at 1500 I.S.T. but one would hardly expect this coincidence at two independent places of observation if it were due to local variations. We suggest that the small depression in ionization density at about 1500 I.S.T. is likely to be also associated with a corpuscular eclipse.

In regard to day-to-day variation in f_oF_2 over Delhi and Srinagar at any hour during the control period, our data indicate that it was within about 0.4 Mc/s. The accuracy in measuring f_oF_2 was within ± 0.05 Mc/s. The large depressions observed in f_oF_2 on the eclipse day appear to be genuine effects and indicate the occurrence of possible corpuscular eclipses.

We may, therefore, conclude that our vertical incidence ionospheric measurements over Delhi have indicated the presence of two corpuscular eclipses occurring approximately 2 and 4 hours before the optical eclipse. The same has also been observed over Srinagar but with the addition of a $6\frac{1}{2}$ -hour corpuscular eclipse. The last one could not be observed at Delhi due to the absence of measurements of f_oF_2 . But, since the first two are found to occur simultaneously at both the places, we are encouraged to infer that the $6\frac{1}{2}$ -hour corpuscular eclipse could also have been seen over Delhi, if measurements were available. These three corpuscular eclipses would give the velocities of the corpuscles as approximately 1600, 800 and 500 Km/sec., respectively.

(ii) *Recording of Shortwave Signal Intensity from B.B.C. and Moscow.*

Records of field intensities were taken at Delhi on signals from B.B.C. and Moscow on 15070 Kc/s and 15270 Kc/s respectively from 1200 to 2100 I.S.T. on all the days between 25.6.54 and 5.7.54. A communication receiver was used

to receive the signals. The output from the second detector was fed to a d.c. amplifier connected to a pen-recorder. The system was previously calibrated in terms of microvolt signal input by means of a standard signal generator. The recording speed was kept at 3 inches per minute. Continuous recording was made for a duration of 5 minutes on each of the signals once every 15 minutes.

The signals from B.B.C and Moscow were found to be fading quite appreciably. The average strength of the signal during each 5-minute period was arrived at from individual readings of the signal strength at an interval of 2 seconds. All these average values were later grouped together to arrive at an average field

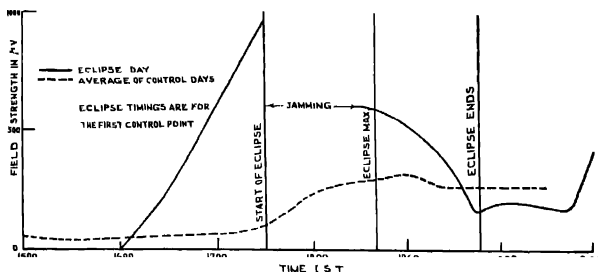


Fig. 3 Field strength variations on signals from B.B.C. on 15070 kc/s (GWC).

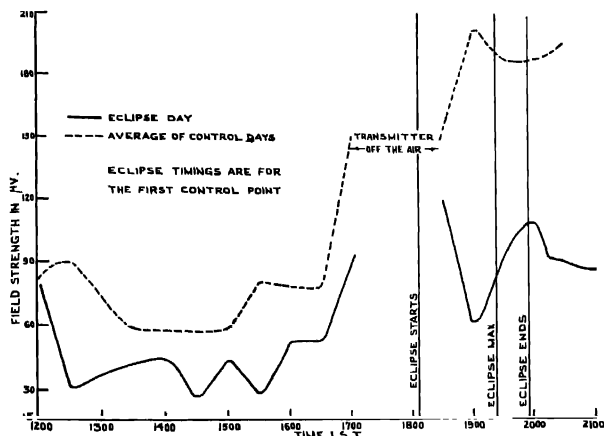


Fig. 4 Field strength variations on signals from Moscow on 15270 Kc/s.

trend variation for the control period of observation and for the eclipse day. The comparison is shown in figures 3 and 4.

It will be noted from figure 3, which also indicates the eclipse timings at the first control point of reflection, that the received strength of the signal on transmission from the B.B.C. on 15070 kc/s went on increasing rapidly on the eclipse day shortly after 1600 I.S.T. and remained high till near the end of the eclipse. The overall increase during the period of the eclipse may be attributed to the optical effect. But the variation of signal strength did not show any significant behaviour so far as a possible corpuscular eclipse was concerned.

Figure 4 shows the signal variation on transmission from Moscow on 15270 Kc/s. The signal on the eclipse day was considerably lower than that on the control days throughout the period of observation. There were depressions in the received signal strength on the eclipse day at 1230, 1530 and 1900 I.S.T. If the eclipse corpuscular or optical, had produced any effect on the propagation of the signal, one would expect a rise in the signal at the corresponding times, provided of course the reduction in ion-density was not sufficient to appreciably alter the MUF. It is difficult to explain the observed overall lowering of signal and the minima at various times.

It may, however, be pointed out that one should be careful in interpreting variation of signal strength on short wave transmissions over large distances. The propagation of the wave is likely to be quite complicated in that a two-hop and or three-hop propagation via F_2 may normally occur, but it is quite certain that some signal will also be propagated through E_s . The combination of these several modes of propagation at the receiving station may produce the variation of a resultant field which does not truly represent the conditions at the control points of reflection for a particular mode of propagation.

(m) *Recording of Medium Wave Signal Intensity from Jullundur.*

During the period of observation, the 50 kw transmitter at Jullundur working on 710 kc/s was made available and continuous recording of its signal strength was made at Delhi from 1200 to 2100 I.S.T. on each day from 25.6.24 to 5.7.54. The same experimental procedure was adopted as in the case with signals from the B.B.C. and Moscow. Separate receivers, aerial and recording systems were used. The analysis of the field strength variation was carried out in the way previously described.

The distance from Jullundur to Delhi is about 350 km. The mode of sky-wave propagation will, therefore, be single-hop E and the received field strength variation is likely to provide a sensitive tool for determining the effect of any corpuscular eclipse on the absorption in the non-deviative region. Figure 5 shows the observed field strength variation and is according to expectation. There is an increase in the signal at 1530 and a bigger increase at 1730 I.S.T. on the eclipse day. These two increases can be identified with two corpuscular eclipses, one at approximately 4 and the other at 2 hours before the optical eclipse. The $6\frac{1}{2}$ -hour effect, as observed from the variation of $(f_oF_2)^2$ over Srinagar

(figure 2), could not be seen here. These two corpuscular eclipses indicate that the corpuscular emission from the sun was also partly responsible for causing variation of absorption in the non-deviative region. There is supporting evidence to

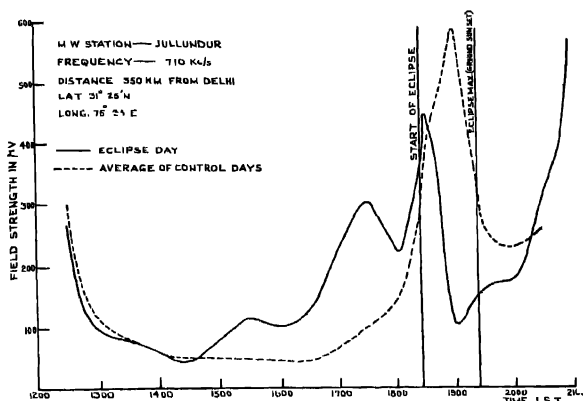


Fig. 5. Medium wave field strength variations.

(this hypothesis which we shall discuss below. The effect due to the optical eclipse between 1831 and 2014 I.S.T. could not be seen probably due to the sunset.

(iv) *Measurement of Ionospheric Absorption by Vertical Incidence Pulsed Transmissions.*

Experiments were conducted on the measurement of ionospheric absorption on 5 Mc/s at vertical incidence employing pulsed transmissions. The period of observation was from 1200 to 2100 I.S.T. each day from 25.6.54 to 5.7.54. The method of measurement is as follows. The apparent reflection coefficient ρ of the ionosphere at vertical incidence is given by

$$\rho = \beta R_1 = \frac{2R_2}{\rho' R_1} \quad (1)$$

where

β = a constant

G = strength of the ground signal.

R_1 = amplitude of the first echo.

R_2 = amplitude of the second echo.

and ρ' = apparent reflection co-efficient of the ground.

$-\log \rho$ is a measure of ionospheric absorption.

The ground pulse and the echo system were received on an ionospheric receiver in the usual way. Since the transmitter and the receiver were located in the same place, to avoid desensitisation of the receiver, the H.T. supply to the first few

stages of the receiver was switched off during the interval occupied by the ground pulse by means of an electronic gate. A pulsed signal from a signal generator adjusted to the same wave frequency was used in place of G . Two electronic gates of independently variable width and delay were made to select the first and the second echoes (or, G and R_1). A difference circuit combined these outputs giving $\log \rho$ and which was recorded by means of a pen recorder. The recording speed was kept at 3 inches per minute. β can, however, be evaluated from consecutive measurement of $\log \frac{R_1}{G}$ and $\log \frac{R_2}{R_1}$ when the second echo is present.

Recording of $|\log \rho|$ was made for 5 minutes or more at each half-hour from 1200 to 2100 I.S.T. on the control days. On the eclipse day, however, these recordings were made at an interval of 15 minutes. The average value of $|\log \rho|$ was calculated in the usual way and the values were grouped to indicate the variation of $|\log \rho|$ on the control days and on the day of the eclipse as shown in figure 6.

During the measurements it was observed that on 5 Mc/s reflection from F alone was not always present. Sometimes E_s and F could be simultaneously seen. At some other times, either a blanketing E_s or a single reflection from F_2 could be observed. Our measurements were taken on whichever echo that was found strongest. The analysis revealed that the value of $|\log \rho|$ either on F or on blanketing E_s at the same time remained more or less the same, indicating that the main absorption was taking place below the level of E_s . In another paper, we have indicated that the main absorption at our latitude during the day takes place in the D region (Mitra and Mazumdar, 1954). But the records of $|\log \rho|$ on partial reflections indicated appreciably different values. Similarly, there were occasions when the downcoming wave consisted in the interference between the two magneto-

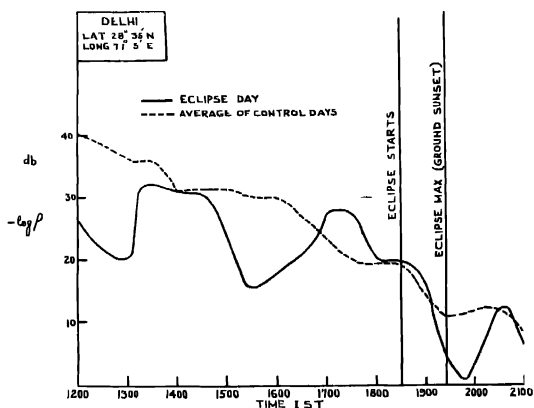


Fig. 6. Variation of absorption at 5 Mc/s.

ionic components and records of $|\log \rho|$ indicated periodic variations (Mitra, 1950). These records were excluded from our analysis.

It will be seen from figure 6 that the variation of $|\log \rho|$ during the control period was according to expectation. But on the eclipse day, there was a large depression in $|\log \rho|$ at about 1300, 1530 and 1945 I.S.T. The reduction in the value of $|\log \rho|$ at these times was quite large and could not be accounted for by day-to-day variations which were within about 7 to 8 db at any hour. These reductions also agree with our other observations as could be seen from figures 1, 2, and 3. The depression at 1945 I.S.T. is probably due to optical eclipse, whereas the minima at about 1300 and 1530 I.S.T. can be attributed to corpuscular eclipses of absorption in the non-deviative region. It is rather surprising that the two-hour effect, as observed in the medium wave field strength variation (figure 5) is absent in our measurement of $|\log \rho|$.

(v) *Recording of Solar Radio Noise on 204 Mc/s.*

Continuous recording of the intensity of radio noise on 204 Mc/s was made from 25.6.54 to 5.7.54 by a pen-recorder. A radar receiver tuned to 204 Mc/s and a 5-element Yagi aerial (fixed) with a reflector oriented 15° west of N with respect to the vertical were employed for the purpose. The beam width of this aerial is about 45° with gain of about 16 db. The noise record showed more or less smooth variation and it was possible to determine the average for a 5-minute period with comparative ease. Bursts and few outbursts were also observed but were left out of the analysis. The average of each 5-minute period was calculated for all the hours and days from 25.6.54 to 5.7.54. These readings were then grouped together and averaged to show the temporal variation of noise from 1700 to 2100 I.S.T. and the corresponding values on the eclipse day were similarly calculated. Figure 7 shows the variation of noise on the control days and on the eclipse day.

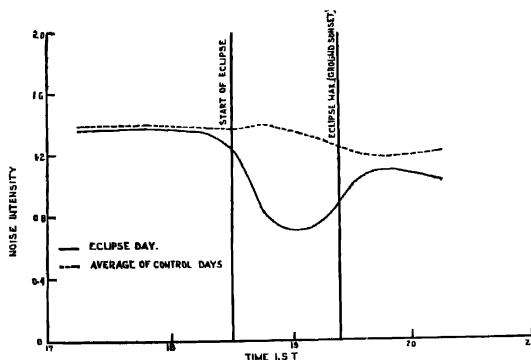


Fig. 7. Solar noise at 204 Mc/s observed at Delhi.

It will be seen from figure 7 that the variation of noise was not appreciable on the control days. The noise intensity started to decrease with the onset of the eclipse and became quite low about 20 minutes before the maximum of the eclipse. This indicates that the noise emission was possibly not distributed homogeneously on the surface of the sun but was due to at least some discrete sources which were occulted before the maximum of the eclipse.

4. DISCUSSION OF RESULTS

The main features of our observation are described below. It may be mentioned here that no ionospheric or magnetic disturbances were reported on 30.6.54.

The vertical incidence ionospheric measurements of the F_2 layer at Delhi and Srinagar indicated the presence of three possible corpuscular eclipses— at 1300, 1500 and 1730 I.S.T. preceding the optical eclipse by approximately 6½, 4 and 2 hours respectively (figures 1 and 2)

The field strength observations of short wave signals from B.B.C and Moscow in the 15 Mc/s band did not indicate the effect of any corpuscular eclipse. This was presumably due to the combination of several modes of propagation at the receiving point obscuring the effect of such eclipse (figures 3 and 4).

The field strength observations of medium wave signals from Jullundur on 710 Kc/s indicated the presence of two corpuscular eclipses, one at 1530 and the other at 1730 I.S.T. The corpuscular eclipse observed at 1300 I.S.T. on the variation of $(f_oF_2)^2$ over Srinagar was not found in the medium wave signal variation (figure 5)

Measurement of ionospheric absorption on vertical incidence pulsed transmission has indicated the presence of two corpuscular eclipses— one at about 1300 and the other at about 1530 I.S.T. (figure. 6).

One would have expected that the medium wave field strength and ionospheric absorption should vary synchronously. The 1530 corpuscular eclipse is common to both. The 1300-hour effect is not observed in the medium wave field strength variation and 1730-hour effect is not seen in the variation of absorption. Strictly speaking, our measurement of $|\log \rho|$ takes into account the absorption in both the D and E layers, although the contribution from E is comparatively less. But the variation of field strength on medium wave transmission will indicate changes almost entirely in the absorption of the D layer. This may be one of the reasons why the same corpuscular eclipses were not observed in the variation of both $|\log \rho|$ and field strength of medium wave transmission. Combining all the observations, we find that the same three corpuscular eclipses observed in F_2 ionization density could more or less be seen in our investigation of the absorption produced by the non-deviating region.

The measurement of solar radio noise indicated a reduction in the noise intensity during the optical eclipse but the minimum occurred about 20 minutes before the maximum of the eclipse. The coronal observation by Muller (1954) on 30th June, 1954, has indicated the presence of some prominences between 0415 and 1327 U.T. These prominences might account for the minimum of the noise occurring about 20 minutes before the maximum of the eclipse.

The effect of the optical eclipse on the characteristics of the ionosphere could not be definitely established from all our measurements, probably because of the sunset coinciding with the maximum of the eclipse.

The evidence of one or more corpuscular eclipses in the F_2 region is an established fact (Harang, 1945; Smith-Rose, 1946; Mitra, 1953). But there is little evidence of a similar effect in the lower layers. The usual experiment in the past has been to concentrate on the measurement of $(f_oE)^2$ and $(f_oF_1)^2$. Since E and F_1 layers are known to behave as simple Chapman layers, the optical eclipse in these layers produces a pronounced effect and greater emphasis has been usually given to this part of the problem. It has also been found that in a good many instances in the past, the observations had not been extended to cover the period when a corpuscular eclipse might have occurred.

We conclude, from our ionospheric measurements, that evidence has been obtained to indicate the presence of three distinct types of corpuscular emission from the sun. Their speeds are 500, 800 and 1600 km sec⁻¹. These corpuscles must have left the sun 3.5, 2.7 and 1.85 days respectively earlier than 30th June, 1954. These corpuscles are found to produce appreciable ionization both in the F_2 and in the lower layers (probably D). The corpuscular emission is known to occur during high sunspot activity associated with solar flares and prominences. But during minimum sunspot activity, as existed in 1954, the mechanism of emission of such particles should be from quite different reasons and is of fundamental importance. This is because that such emission, if it could occur during low sunspot activity, should be a regular phenomenon throughout the sunspot cycle and is likely to produce some sort of a corpuscular control of the ionospheric layers.

Available evidence shows that the corpuscular emission during low sunspot activity could be from the M-region of the sun. The M-region was first identified by Bartels (1932) when he postulated that the 27-day recurrence of mild magnetic storms was associated with M-region activity giving out corpuscular emission. In recent years keen interest has been evinced in the origin, nature and identification of the M-region. Chapman and Bartels (1940) have shown that the activity of the M-region is predominant during minimum of the sunspot cycles. Allen (1944) has associated the M region activity with coronal streamers. Von Klüber (1952) has photographed at Khartoum a long coronal streamer from equatorial regions of the sun at its east limb during the total solar eclipse of Febru-

ary 25, 1952. Kiepenhauer (1947, 1952) has attributed the M-region activity to the increase in filament area near the central meridian of the sun and has shown that the speed of the corpuscles from them is of the order of 350-600 km sec.⁻¹. Babcock and Babcock (1955) have succeeded in recording unipolar magnetic regions by their solar magnetograph and have suggested that these regions may be identified with M-regions.

We have also obtained evidence of corpuscular emission from an apparently undisturbed sun in our analysis of solar flares, radio fade-outs, magnetic storms and sunspot numbers (Mitra and Mazumdar, 1954). We have found that out of 122 fade-outs, 81.2 per cent apparently had no connection with any flare at all. This had encouraged us to link up the "corpuscular" radio fade-outs with M-region activity. We may, therefore, reasonably conclude that both the slower and faster moving corpuscles as observed from the corpuscular eclipses described in this paper presumably originated from the M-region. The exact mechanism of the emission of such particles has, however, not yet been properly understood.

In regard to the nature of these streams, it must be assumed that they are neutral in nature. The corpuscular stream emitted from the sun is mostly ionized with a few neutral atoms. As it travels towards the earth, there may be more neutral atoms created due to recombination between the positively and negatively charged particles in the beam. These neutral particles will be unaffected by the earth's magnetic field and will produce at all geographic latitudes a certain amount of ionization by collision with the gases in the upper atmosphere. A decrease in the ionisation density corresponding to a corpuscular eclipse preceding the effect due to the optical eclipse is likely to indicate the extent to which ionization was being produced by these corpuscles. In regard to the speed of these corpuscles, some of the earlier workers, as well as the present author, have observed different values ranging between 500 and 1600 km sec.⁻¹. But a correlation between solar flares and radio noise outbursts has indicated that the low frequency outbursts may be due to the emission of corpuscles with speeds ranging between 350 and 650 km sec.⁻¹ (Pawsey and Smerd, 1952). The escape velocity of these corpuscles is of the order of 600 km sec.⁻¹. To account for the emission of the corpuscles of velocities lower than 600 km sec.⁻¹, Sengupta and Mitra (1954) have suggested that these corpuscles may travel in an elliptic orbit ultimately falling back on the sun but encompassing the earth in their orbital passage. Kiepenhauer (1952), on the other hand, has indicated the possibility that these particles are being emitted from a distance of three to four solar radii where the escape velocity works out to be quite low (300 km sec.⁻¹).

It is, therefore, possible to obtain evidence of corpuscular emission from the sun by ionospheric investigations conducted during solar eclipses, although considerable work is still to be carried out to understand the nature, origin and ionizing effect of these corpuscles upon the earth's ionosphere. It will then

be merely a question of fact based on observations, and when sufficient evidence is collected, it would be possible to derive a coherent picture of the corpuscular emission and its effect upon the ionosphere.

ACKNOWLEDGMENTS

The work described in this paper forms a part of ionospheric research programme of All India Radio and is published by permission of Mr. B. V. Baliga, the Chief Engineer. The author wishes to express his sincere gratitude to Mr. S. Basu, Director General of Observatories for the loan of Yagi aerial and providing facilities for field strength measurement in his laboratory. The success in the various observations is due to the whole hearted effort of a team of engineers of the Research Department of All India Radio. I am specially indebted to Mr. S. C. Mazumdar and Mr. P. K. Venkatasubramanian for considerable help with the calculation of the circumstances of the eclipse, apparatus and with observations; to Mr. S. Thiruvengatachari, Research Engineer, for helpful discussions and to Mr. B. R. Kapur and late Mr. K. P. Banerjee, for providing facilities of observation at Srirangar and Bombay Stations of All India Radio. Mr. P. R. Desikachar kindly provided special transmissions from Jullundur. The work was conducted under the supervision of Mr. B. V. Nerurkar, past Research Engineer, All India Radio.

REFERENCES

- Allen, C. W., 1944, *Mon. Not. R. Astr. Soc.*, **104**, 43.
Appleton, E. V., 1946, *Nature*, **157**, 691.
Babcock, H. W. and Babcock, H. D., 1955, *Nature* **175**, 296.
Bartels, J., 1932, *Terr. Mag. Atm. Elect.*, **37**, 48.
Chapman, S. and Bartels, J., 1940, *Geomagnetism* (Oxford, Clarendon Press).
Davies, K. and Hagg, E. L., 1955, *J. Atm. Terr. Phys.*, **6**, 48.
Huang, L., 1945, *Terr. Mag. Atm. Elect.*, **50**, 307.
Kiepenhauer, K. O., 1947, *Astrophys. J.*, **105**, 408.
Kiepenhauer, K. O., 1952, *The Sun*, ed. G. P. Kuiper (Chicago University Press).
Mitra, S. N., 1950, *Ind. J. Phys.*, **24**, 197.
Mitra, S. N., 1953, *J. Sci. Indust. Res., India*, **12A**, 349.
Mitra, S. N. and Mazumdar, S. C., 1954, *Ind. J. Phys.*, **37**, 563.
Mitra, S. N. and Mazumdar, S. C., 1957, *J. Atm. Terr. Phys.* **10**, 32.
Mixed Commission on Ionosphere, 1949, (Brussels, Secretariat General de l'U.R.S.I.)
P. 25.
Muller, R., 1954, *Observatory*, **74**, 222.
Pawsey, J. L. and Smeed, S. F., 1952, *The Sun*, ed. G. P. Kuiper, (Chicago University Press).
Sengupta, P. K. and Mitra, S. N., 1954, *Nature*, **873**, 914.
Smith-Rose, R. L., 1946, *Nature*, **153**, 40.
Von Klüber, 1952, *Observatory*, **72**, 207.

X-RAY DIFFRACTION STUDY OF THE HEAT TREATMENT OF KAOLINITE

G. B. MITRA

DEPARTMENT OF PHYSICS, INDIAN INSTITUTE OF TECHNOLOGY, KILARAGPUR.

(Received for publication, January 21, 1957)

Plate VI

ABSTRACT In order to study the crystallographic changes in the structure of kaolinite when it is dehydrated, a sample of kaolinite from Singblum, India, was heat treated for 8 hours at 510°C, 682°C and 1050°C each. The products of heat treatment were examined by the X-ray powder diffraction method and the resulting diffraction patterns were compared with that of the untreated sample. It is observed that certain reflections became extinct while certain other reflections diminished in intensity as dehydration proceeded. The remaining reflections maintained the same relative intensities. In the first two stages, no new reflection appeared nor any one of them had any increased intensity. This has been interpreted as being due to the gradual collapse of various planes on account of dehydration. In the third stage, however, although one of the reflections became extinct and several others became diminished in intensity, several reflections were also increased in intensity. These reflections corresponded to the strongest reflections of mullite indicating the formation of mullite at this stage. A broad band of approximate spacing 4.17 Å also appeared at this stage indicating the formation of fused silica.

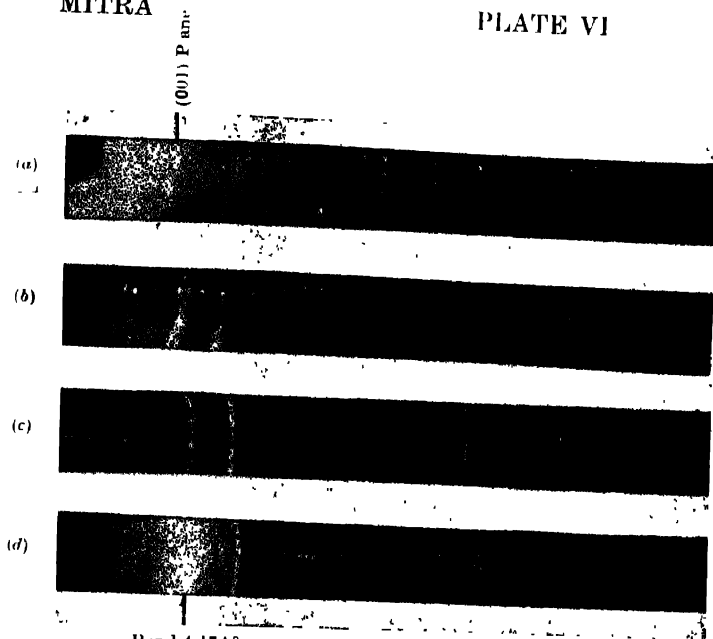
INTRODUCTION

Since the users of clays are generally interested in the products of heat treatment of clays at high temperatures, the bulk of the studies of heat treatment of clays have centred around the high temperature zone. X-ray diffraction studies of the heat treatment of kaolin clays have been confined, so far, mostly in the range 800°C-1400°C, Rinne (1925), Insley and Ewell (1935), Jay (1939), Hyslop (1944) and Richardson (1951) studied by the X-ray methods the products of heating kaolinite in the above range and found that γ - Al_2O_3 appeared in the range 900°C - 1000°C, cristobalite and mullite at 1100°C and at 1400°C only mullite remains. Comerio, Fischer and Bartley (1948) have reported X-ray diffraction study of kaolinite after heat treatment at 525°C but have not drawn any definite conclusion from their studies.

However, the results of the study of kaolinite with the differential thermal analysis method carried out by Spiel, Berkelheimer, Pask and Davies (1945) shows a prominent endothermic effect at approximately 600°C caused by the dehydration of the mineral followed by an exothermic reaction at roughly 1000°C which corresponds to the formation of a new mineral. Ross and Kerr (1931) and Grim and Bradley (1948) presented a series of dehydration curves of kaolinite showing that

MITRA

PLATE VI



Band 4 17A²

X-Ray powder diffraction photographs of kaolinite

- (a) Untreated
- (b) Heat treated at 510°C
- (c) " " 682°C
- (d) " " 1045°C

most of the dehydration takes place between about 400° to 525°C depending on the particle size. A small amount of water was found to have been retained at 525°C and this moisture was found to have been lost gradually upto about 750° to 800°C when dehydration become complete.

It seems, therefore, worthwhile from the X-ray crystallographer's point of view to investigate the structural changes involved when the process of dehydration has fairly advanced, when it is nearly completed and when it is fully completed. With this end in view, a sample of Singbhum kaolinite has been subjected to heat treatment at 510°C, 682°C and 1045°C and the products examined by the X-ray powder diffraction method. A preliminary report of the result obtained is given in this communication.

EXPERIMENTAL

Three samples of kaolinite from Singbhum, India, were heated in a platinum crucible in a controlled electric furnace continuously for eight hours each at 510°C, 682°C respectively. The products of this treatment were examined by the X-ray powder diffraction method. The X-ray tube was run at 60 K V. and 10 ma. and had a copper anticathode. X-rays were passed through a nickel filter before they fell on the sample. The diffraction patterns were received in cylindrical cameras of radius approximately 5 cms. An untreated sample of kaolinite was also similarly irradiated with X-rays for its diffraction pattern. The interplanar distances together with the relative intensities obtained with the help of Kipp and Zonen microphotometer are shown in Table I.

DISCUSSIONS

A critical comparison of the different diffraction patterns obtained experimentally (Plate VI) testify to a gradual change in structure of kaolinite as it is heated to higher and still higher temperatures. In the sample of kaolinite heated at 510°C, the (001) plane is found to have vanished. In the diffraction pattern we find a very weak continuous scattering extending upto the ring corresponding to the (001) plane. The (02 $\bar{1}$), (111), (20 $\bar{1}$), (1 $\bar{3}$ 0), (13 $\bar{4}$), (203), (241), (2 $\bar{2}$ 4) and (300) planes are also found to have disappeared. It can be concluded that these planes are not apparent because of their relatively weak intensities. The (1 $\bar{1}$ 2) plane gives rise to a reflection of relative intensity 2 while the (02 $\bar{1}$) plane gives rise to a reflection of relative intensity 4 and the reflection due to the (20 $\bar{1}$), (1 $\bar{3}$ 0) and (130) planes is of relative intensity 8. In the diffraction pattern of kaolinite heat treated at 510°C, the reflection due to (1 $\bar{1}$ 2) plane has been recorded, while the other two reflections have not been. Obviously it can not be due to weakness of intensity of the reflections because weaker reflections have been recorded. It is therefore certain that these planes have ceased to exist because of the heat treatment. On the other hand, no new lines are found to have appeared. The

TABLE I

X-Ray diffraction patterns of the products of heat treatment of kaolinite

Untreated			Heated at 510°C		Heated at 682°C		Heated at 1045°C	
<i>d</i> A.U.	<i>I</i>	<i>hkl</i>	<i>d</i> A.U.	<i>I</i>	<i>d</i> A.U.	<i>I</i>	<i>d</i> A.U.	<i>I</i>
7.02	10	001	Very weak continuous scattering upto 7.30 A.U.		Imperceptibly weak scattering upto 7.30 A.U.			
4.35	6	110	4.35	6	4.35	6	Broad diffraction band of approximate spacing 4.1 A.U.	
4.17	6	111	4.17	6				
3.80	4	021						
3.54	10	002	3.54	10	3.50	10	3.50	
3.36	4	111						
3.08	2	112	3.08	2				
2.74	2	022	2.77	2				
2.55	8	201, 130, 130						
2.48	9	131, 112, 200	2.48	4	2.49	4		
2.33	10	203, 131, 113	2.33	4	2.33	4	2.33	2
2.28	9	113, 131,	2.23	5	2.23	5	2.23	9
1.98	7	203, 132	2.01	7	2.01	4	2.01	2
1.78	5	004	1.78	5	1.80	5	1.80	4
1.67	8	210, 151, 204 122	1.69	8	1.70	5	1.70	4
1.61	6	133, 242, 310, 151, 242	1.60	6	1.59	6	1.59	5
1.53	5	134, 103, 241, 224						
1.49	9	060, 331, 331	1.49	9	1.49	9	1.50	9
1.38	4	300						
1.34	5	015, 124, 124	1.34	5	1.34	2		
1.28	4	106	1.28	4	1.28	2	1.28	6
1.24	2	033	1.24	2	1.24	2	1.25	6

relative intensities of some of the lines, however, are observed to have changed. The relative intensity of the reflection by (131), (112) and (200) planes in the original sample is 9, whereas in the product of heat treatment at 510°C it becomes 4. Simu-

larly the relative intensity of the reflection due to (202), (1 $\bar{3}$ 1), and (11 $\bar{3}$) planes in the original sample is 10, whereas in the sample heat treated at 510°C it becomes 4. The relative intensity of the reflection due to (1 $\bar{1}$ $\bar{3}$) and (131) planes have also changed from 9 to 5 due to heat treatment. It is interesting to notice the fall in intensity at the various stages of heat treatment. The intensity of the reflection due to (1 $\bar{3}$ 1), (112) and (200) planes have changed from 9 in the untreated sample to 4 in the sample heat treated at 510°C. It remains 4 for the sample treated at 682°C and disappears for heat treatment at 1045°C. The intensity of the reflection due to (20 $\bar{5}$), (1 $\bar{3}$ 1) and (11 $\bar{3}$) planes have changed from 10 in the untreated case to 4 in the case of heat treatment at 510°C, again to 4 for heat treatment at 682°C and to 2 for 1045°C. On the other hand, the intensity of the reflection due to (1 $\bar{1}$ $\bar{3}$) and (131) planes changes from 9 for the untreated case to 5 for heat treatments both at 510°C and at 682°C and again to 9 for heat treatment at 1045°C. This obviously corresponds to the gradual collapse of the structure in the first two stages of heat treatment while it points to the appearance of a new mineral at 1045°C.

On account of the heat treatment at 682°C, there seems to have occurred a further change with respect to heat treatment at 510°C. In this case, the (1 $\bar{1}$ $\bar{2}$) and (022) planes have disappeared. The intensity of reflection due to (20 $\bar{3}$) and (1 $\bar{3}$ 2) planes have diminished from 7 to 4, that due to (2 $\bar{4}$ 0), (1 $\bar{5}$ 1), (20 $\bar{4}$) and (1 $\bar{3}$ 3) planes has altered from 8 to 5 and that due to (015), (124) and (1 $\bar{2}$ $\bar{4}$) planes has changed from 5 to 2. The intensity of the (10 $\bar{6}$) reflection has also diminished from 4 to 2.

Due to heat treatment at 1045°C, the sample seems to have altered considerably. A broad band of approximate spacing 4.17 A.U. appears in the diffraction pattern. This must be due to the formation of fused silica at this stage. Compared to the diffraction pattern of the sample heat treated at 682°C, several reflections have gained in intensity. The reflections at 2.23 A.U., 1.50 A.U., 1.28 A.U. and 1.24 A.U., have increased in intensity. These reflections together with the strong 3.50 A.U. reflection form the first five strongest lines of mullite. The increase in intensity of these lines clearly points to the formation of mullite. The remaining lines, however, have diminished in intensity. This is due to the fact that the entire amount of kaolinite has not been converted to fused silica and mullite. A portion of it still remains although with a collapsed structure.

The crystallographic significances of the collapse of different planes at different stages are still under investigation.

ACKNOWLEDGMENT

Author's grateful thanks are due to Prof. K. Banerjee for helpful discussions and to Prof. H. N. Bose for his kind interest in the work.

REFERENCES

- Comfere, J. E., Fischer, R. B. and Bardley, W. F., 1948, *J. Amer. Ceram. Soc.*, **31**, 254.
Grim, R. E. and Bradley, W. F., 1948, *Amer. Min.* **33**, 50.
Hyslop, J. F., 1944 *Trans. Brit. Ceram. Soc.*, **43**, 40.
Insley, H. and Ewell, R. H., 1935, *J. Res. Nat. Bur. Stand.*, **14**, 615.
Jay, A. H., 1939, *Trans. Brit. Ceram. Soc.*, **38**, 455.
Richardson, 1951, X-ray Identification & Structure of clay minerals, Brindley, Chapter III p. 76.
Rinne, 1925, *Z. Krist.*, **61**, 113.
Ross and Kerr, 1931, *U. S. Geol. Survey Profess. Paper*, **165E**, 151.
Spiel, Berkelheimer, Pask and Davies, 1945, *U. S. Bur. Mines Tech. Paper* 664.

BRANCHING RATIO FOR SLOW NEUTRONS

MADAN LALL SEHGAL

DEPARTMENT OF PHYSICS, MUSLIM UNIVERSITY, ALIGARH

(Received for publication, February 2, 1957)

ABSTRACT. A study of slow neutron reaction with B^{10} has been made with BF_3 proportional counters. The relative probability of the reactions $B^{10}(n, \alpha) Li^7$ and $B^{10}(n, \alpha) Li^{*7}$ is determined by covering the counter with and without cadmium cap.

A study of the reaction of slow neutrons with boron is most important in neutron shields. As reported by Aizenberg and Lauritsen (1952), the first level of Li^7 is at 0.478 Mev from its ground level. Bjørgild (1945) found that the value of the relative probability of the two reactions $B^{10}(n, \alpha) Li^7$ and $B^{10}(n, \alpha) Li^{*7}$ is 6.25 per cent. Hanna (1950) has reported the value of the branching ratio, that is the probability of the reaction going to the ground state as 5.8 per cent. Guer and Lonchamp (1951) from the observation of more than thirty thousands tracks in nuclear plates have reported the value of the branching ratio as 4.27 per cent. Rhodes, Franzen and Stephens (1952) from the study of the ionization produced by the recoil particles of transmutation $B^{10}(n, \alpha) Li^{*7}$ have found the value of the branching ratio as 6.3 per cent. Owing to the difference in value of the branching ratio reported for slow neutrons its study was thought worth while.

Special attention should be paid to the construction of BF_3 proportional counters to study the reaction $B^{10}(n, \alpha) Li^7, Li^{*7}$. The counters employed in this study have internal copper cathode of 1.35 inches in diameter with tungsten wire anode of 0.003 inch diameter. After roasting the counters at 250°C for two hours and removing the impurities from normal boron trifluoride gas (18.8% B^{10} , 81.2% B^{11}) by fractional distillation, the counters were filled at different pressures of BF_3 and argon (spectroscopically pure). A large pressure of BF_3 is desirable for high counting rate, but it is found in the present case that the pulse height resolution decreases as the pressure of BF_3 increases. The half-width of the peak due to $B^{10}(n, \alpha) Li^{*7}$ reaction for counters filled with a pressure of 14.1 cm of Hg of BF_3 gas plus 5.4 cm of Hg of argon, and 35.6 cm of Hg of BF_3 gas plus 16.6 cm of Hg of argon are 68.2 Kev and 254 Kev respectively. Also it is observed that the plateau length increases as the pressure of BF_3 gas is decreased. The spread in pulse height distribution curve may be due to several reasons. When no impurities, like silicon tetrafluoride, hydrogen fluoride, etc, are present in BF_3 gas, that is when no electron capture and negative ion formation takes place, the pulse size should be independent of the distance of the track of α -particle for-

mation from the central wire. In practice it is difficult to remove completely all the impurities from BF_3 gas, hence there will be some inherent spread in pulse height distribution curve which is due to slight impurities present. The end effects, eccentricity of the anode wire, and the presence of some dust particles sticking on the central wire will all increase the spread in the pulse size distribution curve. The last effect was removed by flashing the central wire before filling.

The geometrical arrangement of the neutron source and the counter used in the experiment are as follows. Slow neutrons were obtained from (Ra-Be) source placed inside a howitzer. A cylindrical lead piece of 5.08 cm in thickness and 6.34 cm in diameter is placed in the path of the neutrons inside the howitzer to keep the gamma ray flux minimum. A cylindrical paraffin block of diameter 6.32 cm and length 5 cm which acts as a moderator for fast neutrons is placed just after the lead block. The counter was placed in a cadmium tubing with axis parallel to the beam.

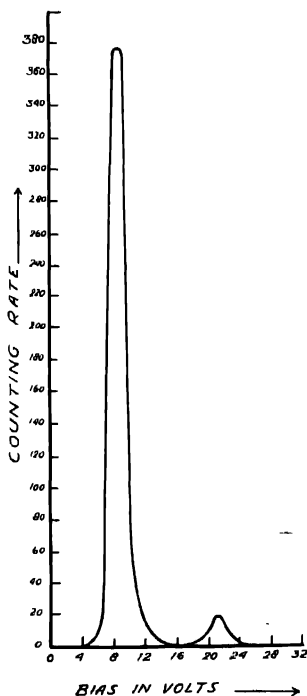


Fig. 1. Pulse height distribution for slow neutron disintegration of boron, when the front face of the counter was covered with a cadmium cap.

The differential pulse height distribution curve for counter filled with a pressure of 14.1 cm of Hg of BF_3 gas and 5.4 cm of Hg of argon is shown in figure 1. The two peaks arise from transitions to the excited state and the ground state of the lithium nucleus. According to Cranshaw and Harvey (1948) the position of a peak is fixed by drawing the central line of the distribution. The Q value of the reaction leading to the excited and ground state is 2.31 Mev and 2.79 Mev respectively. The branching ratio is found equal to 4.0 ± 0.15 per cent. When the front face of the counter, which points towards the beam, is covered with a cadmium cap the branching ratio increases to 4.3 ± 0.15 per cent. Knowing the total cross section for $\text{B}^{10}(n, \alpha)$ reaction and with the help of the branching ratio for the same energy neutrons, the cross sections for the individual reactions $\text{B}^{10}(n, \alpha) \text{Li}^{*7}$ and $\text{B}^{10}(n, \alpha) \text{Li}^7$ respectively can be determined.

ACKNOWLEDGMENTS

The author wishes to express his sincere gratefulness to Professor P. S. Gill for his continuous help and guidance in this work. The support of the Union Education Ministry for the grant of a Senior Research Scholarship is thankfully acknowledged.

REFERENCES

- Ajzenberg, F. and Lauritsen, T., 1952, *Rev. Mod. Phys.*, **24**, 321.
Bjerggild, J. K., 1945, *Kgl. Danske Vid. Sels. Math-Phys. Medd.*, No. 4, 23.
Cranshaw, T. E., and Harvey, J. A., 1948, *Can. J. Research*, A **26**, 243.
Cuer, P. and Lonchamp, J. P., 1951, *Compt. Rend.*, **232**, 1824.
Hanna, G. C., 1950, *Phys. Rev.*, **80**, 530.
Rhodes, J., et al., 1952, *Phys. Rev.*, **87**, 141.

Letters to the Editor

The Board of Editors will not hold itself responsible for opinions expressed in the letters, published in this section. The notes containing reports of new work communicated for this section should not contain many figures and should not exceed 500 words in length. The contributions must reach the Assistant Editor not later than the 15th of the second month preceding that of the issue in which the Letter is to appear. No proof will be sent to the authors.

6. INDUCTION DRAG

K. P. CHOPRA

(Received for publication January 16, 1957)

The problem of induction drag of a sphere of infinite electrical conductivity moving in a conducting fluid, in the presence of a uniform magnetic field has recently been considered. (Chopra, 1956) The author wishes to point out the change in the expressions, if it is assumed that the sphere is of finite electrical conductivity.

Consider a sphere of finite and constant electrical conductivity σ' moving in an incompressible and inviscid fluid of electrical conductivity σ . It is assumed that a uniform magnetic field H is originally prevalent throughout the fluid. Then the magnetic field inside the sphere is given by

$$H^i = \frac{3}{\mu+2} H_0, \quad \dots (1)$$

(the lines of force being parallel to H_0), while the magnetic field outside the sphere is modified to the extent as if a dipole of moment of

$$m = \left(\frac{\mu-1}{\mu+2} \right) H_0 a^3, \quad \dots (2)$$

with the dipolar axis parallel to H_0 , were placed at the centre of the sphere. Here μ is the permeability of the sphere, and the surrounding fluid is assumed of unit permeability. The expressions for induction drag can be obtained by following Chopra, (1956)

(i) *Translational Induction Drag*. If the sphere moves with velocity v in a direction inclined to the dipolar axis at an angle α , the induced electric currents are

$$j^i = j_\varphi = \frac{3}{\mu+2} H_0 \sigma' \left(\frac{v}{c} \right) \sin^2 \alpha \quad \dots (3)$$

inside the sphere, and

$$j^r = j_{\theta}^r = \sigma H_0 \left(\frac{\mu-1}{\mu+2} \right) \frac{v}{c} \left(\frac{a}{r} \right)^3 [3 \sin \theta \cos \theta \cos \alpha + (2-3 \cos^2 \theta) \sin \alpha], \dots \quad (4)$$

outside the sphere, with the result that the translational induction drag R is given by

$$R = 8\pi \left(\frac{1}{\mu+2} \right)^2 H_0^2 a^3 \left[\frac{1}{2} \left(\frac{\sigma'}{c^2} \right) \sin^2 \alpha + \frac{1}{5} (\mu-1)^2 \frac{\sigma}{c^2} \left(1 + \frac{1}{2} \sin^2 \alpha \right) \right] v \dots \quad (5)$$

It is evident that there are no induced currents inside the sphere when v is parallel to H_0 .

(ii) *Rotational Induction Drag* Now consider the sphere to be rotating with uniform angular velocity ω about an axis inclined to the dipolar axis at an angle β , then the induced current inside the sphere is

$$j^i = \left(\frac{3}{\mu+2} \right) \frac{\sigma' H_0 \omega}{c} \dots \quad (6)$$

while outside the sphere the currents is

$$j^r = \sigma H_0 = \left(\frac{\mu-1}{\mu+2} \right) \frac{a^2 \omega}{r^2} [1 - 3 \cos^2 (\theta - \beta)]^{1/2}, \dots \quad (7)$$

It is clear from (6) that the current density j^i is independent of β . Finally, the opposing induction moment D is given by

$$D = 8\pi H_0 \left(\frac{1}{\mu+2} \right)^2 a^3 \left[\frac{9}{10} \left(\frac{\sigma'}{c^2} \right) + (\mu-1)^2 \frac{\sigma}{c^2} \left(1 + \frac{1}{4} \sin^2 \beta \right) \right] \omega. \dots \quad (8)$$

The expressions (5) and (8) are also subject to the limitations discussed in the earlier paper (Chopra, 1956)

REFERENCE

Chopra, K. P., 1956, *Ind. J. Phys.* **30**, 605.

7. DIPOLE MOMENTS OF TRI-SUBSTITUTED BENZENES. PART III

D. V. G. L. NARASIMHA RAO

PHYSICS DEPARTMENT, ANDHRA UNIVERSITY, WALTAIR,

(Received for publication, March 15, 1957)

In continuation of the author's previous work (Rao, 1956, 57) on trisubstituted benzenes, the dipole moments of four other similar molecules are reported in the following table. The observations are carried out in benzene solution at 30°C. The calculated moments are also listed along with the observed values. The agreement between the calculated and observed values is satisfactory.

TABLE

Compound	μ observed	μ calculated
2 Nitro <i>m</i> -xylene	3.39 D	3.40
2 Nitro <i>p</i> -xylene	4.06	4.08
4 Nitro <i>o</i> -xylene	4.82	4.67
4 Nitro <i>m</i> -xylene	4.40	4.34

Full details will be published later.

REFERENCES

- Narasimha Rao, D. V. G. L., 1956, *Ind. J. Phys.*, **30**, 582.
1957, *Ibid.*, **31**, 60.

BOOK REVIEW

RELAXATION SPECTROMETRY—By E. G. Richardson. Pp. i-viii + 140. North Holland Publishing Company, Amsterdam, 1957. Price 20 guilders.

The title of this book would suggest that it might deal with the methods of analysing spectra of relaxation. Actually, however, it describes the methods of determining the acoustical frequencies at which different materials exhibit maximum internal losses or relaxations. Starting from the Maxwell's equation connecting stress and strain in a viscous body the author first describes the experimental results which verified Maxwell's law of relaxation. The relaxational behaviour is then illustrated with the help of two models. Next, the methods of deriving internal friction in solids and liquids in the sonic range are discussed in two chapters. The occurrence of relaxation in the ultrasonic spectrum produced in gases and liquids is then demonstrated with the help of a large number of published experimental results and in another chapter the partial transformation of a particular mode in the ultrasonic range exerted in solids to other types of vibration has been discussed in detail and the relaxations observed in this range in solids have been summarised.

The seventh chapter is devoted to a short discussion on theory and measurement of relaxation in dielectrics during propagation of electromagnetic waves through them and to a comparison between this relaxation and ultrasonic relaxation. The last chapter deals with the delineation of relaxation spectra with the help of Cole and Cole plot of impedance in analogy with the case of complex dielectric constant, and implications of the spectra are also discussed from theoretical point of view.

The book thus deals with results of a very highly specialised line of research in which the author himself has made valuable contributions. As the discussions in each chapter are supported by a list of references, the volume will be a valuable guide to workers in ultrasonics. The price, however, seems to be a little exorbitant.

S.C.S.

PROGRESS IN COSMIC RAY PHYSICS. VOLUME III. Edited by J. G. Wilson. Pp i-xii + 420 with 16 plates. North Holland Publishing Company, Amsterdam, 1956. Price 38 guilders.

This third report on Progress in Cosmic Ray Physics is divided into four long chapters contributed by four different authors. The properties of extensive air showers including its number spectrum, its variation with altitude and time

and also the nature of primary energy spectrum have been discussed in great detail in Chapter I by K. Greisen. The experimental results on charged K-mesons and hyperons have been discussed by H. S. Bridge in the second chapter. Five beautiful plates have been included in this discussion. In the next chapter, R. W. Thompson has discussed the decay processes of heavy unstable neutral particles and has included ten representative photographs of cloud chamber tracks in this discussion. In the last chapter, G. Puppi has dealt with the energy balance of cosmic radiation, taking into consideration the meson component, the electron-photon component and the nucleonic component at 50° geomagnetic latitude.

Important results obtained so far by previous authors in these lines of research have been compiled carefully and presented with utmost precision in a large number of tables. The theoretical implications of the results have also been discussed in all these chapters. There is a long list of references at the end of each chapter.

This volume is meant for active workers in cosmic rays and nuclear physics. Such workers will no doubt be immensely benefited by the huge store of information collected from authoritative sources and embodied in the four chapters mentioned above. The get-up is excellent and if the number of figures and plates and the quality of the paper are taken into account the price seems to be moderate.

S C S

CHARGE TRANSFER REACTIONS

S. N. GHOSH AND W. F. SHERIDAN

CAMBRIDGE RESEARCH CENTRE, BOSTON, MASS., U.S.A.

Received for publication, December 3, 1956

ABSTRACT. An improved method for determining charge transfer cross sections has been applied to symmetric and unsymmetric reactions for a large number of gases. This method shows higher cross sections than the ones originally reported, and also that the variations in cross sections between 150 and 800 ev ion energy are small. Unsymmetric reactions having nearly equal ionization potentials for the reacting particles have been found to possess the character of a symmetric charge transfer reaction. Certain other unsymmetric reactions were found to possess the same character even though the ionization potentials are not equal.

The method has been utilized to determine secondary electron emission from a metal surface by ion bombardment. Relating the variation of emission from a brass plate with the ion mass and energy, it is found that the emission varies inversely as the square root of the ion mass and directly with the energy of ions.

Data for charge transfer cross sections have been applied to certain upper atmospheric phenomena.

1. INTRODUCTION

A charge transfer process, $A^+ + B \rightarrow A + B^+$, or a similar reaction involving negative ions is one of the several types of inelastic collisions that can occur between an ion and a neutral atom or molecule. These reactions have two characteristic features which distinguish them from other inelastic reactions (e.g. ionization, excitation) involving these particles, namely:

- (1) A charge transfer reaction can take place even when the incident ions have very small kinetic energy, for if the particles involved in the reactions are in the ground states, the change of energy in the reaction is just the difference between the ionization potentials of the reacting particles.
- (2) In a charge transfer reaction very small momentum transfer takes place between the incident ions and the bombarded atoms or molecules. In fact, it is found experimentally that newly-created ions have energy much less than one volt even when the incident ions have energy of several kev. Hence the kinetic energy of the neutralized ions is usually much larger than that of the charge transfer ions.

Systematic studies of charge transfer reactions involving mainly positive ions have recently been undertaken by several investigators (Hasted, 1951; Stedeholm and Hasted, 1955; Lindholm, 1954; Potter, 1954; Dillon *et al* 1955; Massey, 1949). These studies have been carried out both from the experimental and theo-

Fig. 1. Ion source and collision chamber

A modified r.f. mass spectrometer provided a collimated beam of ions of varying amounts of energy. The spectrometer was attached to a collision chamber in place of the original ion collector (figure 1). The collision chamber contained three pairs of semi-cylindrical brass plates with electric field between the plates of each pair. The first pair of plates served as guard ring and the second and third as collectors of charge transfer ions and incident ions respectively. In the previous experimental set-up (Dillon *et al*, 1955) one long semi-cylindrical brass plate had been used. By replacing this brass plate by three plates, the apparatus became more versatile. In particular, it afforded separate measurements of the positive charge due to charge transfer, the secondary emission from the Faraday chamber due to ion bombardment, as well as their net charge. These currents were measured by means of vibrating reed electrometers.

Since the secondary electrons emitted from the Faraday chamber due to incident ion bombardment might have sufficient energy to overcome the field across the plates and reach the charge transfer plates, cross sections determined by the net charge measurement were subject to error. In order to avoid this error the positive charge collecting on one of the charge transfer plates was measured. As a check, the negative charge and the net charge were also measured. It was found that the positive charge was essentially equal to the net charge plus the negative charge (Ghosh and Sheridan, 1957).

It should be noted that the greatest source of error in a charge transfer cross section is the determination of pressure. In the operating region of an r.f. mass spectrometer, (usually between 5×10^{-4} to 5×10^{-5} mm Hg) the McLeod gauge does not give accurate results. Furthermore, it cannot be connected close enough to the spectrometer. In order to minimize the error in pressure measurements, two gauges—an ionization gauge (type VG1A) and a McLeod gauge having a capillary tube of 0.717 mm inner diameter and a bulb of 602 cc capacity—were used, and the arrangements were made in such a way that the spectrometer tube was not in the line of flow of the gas. Figure 2 shows the position of the spectrometer

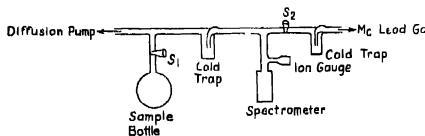


Fig. 2. Position of the spectrometer tube with respect to the ionization and McLeod gauges. Note that the spectrometer tube is not in the line of flow of the gas.

tube with respect to the two gauges and the sample bottle. The gas was diffused into the spectrometer tube so that the pressure at the spectrometer tube (recorded by an ionization gauge situated in the vicinity of the spectrometer tube) was the same as that at the position of the McLeod gauge.

For symmetric charge transfer reactions ($X^+ + X \rightarrow X + X^+$), usually designated by (X^+ , X), the cross section in units of cm^{-1} is calculated from the expression:

$$Q = \frac{1}{pl} \frac{I_x}{I_c + I_x} \quad \dots (1)$$

where,

l = length of the surface on which charge transfer ions are collected

p = pressure in mm Hg

I_x = charge collected at the charge transfer surface

I_c = charge collected at the Faraday chamber

It is to be noted that Eq(1) is a particular case of the more general formula for a gas mixture [Ghosh and Sheridan, 1957].

$$\sum_i^n Q_i P_i = \frac{1}{l} \cdot \frac{I_x}{I_x + I_c} \quad (2)$$

where Q_i and P_i are the cross section and partial pressure of the i -th gas component.

For the unsymmetric reactions ($X^+ + Y \rightarrow X + Y^+$) designated by (X^+ , Y), the cross sections were determined from Eq (2). In such cases, gases were usually mixed in the proportion 10:1 (the gas forming the incident ion being in the lower proportion.)

3. EXPERIMENTAL RESULTS

It should be remembered that a great deal of information concerning charge transfer reactions can be obtained by observing the variation of cross sections with ion energy, instead of determining the cross section for a particular energy. In fact, if the ion energy for which the cross section is maximum is obtained, then by assuming the adiabatic hypothesis, the energy defect of the reaction, and hence, information about the state of the reaction products can be obtained. Another method, which lends itself more readily for the interpretations of experimental results, is that in which the reaction products are analysed. However, in our present experiment, the reaction products were not analysed and the observation was limited to an energy range of 100 to 800 ev.

4. CHARGE TRANSFER CROSS SECTIONS FOR SYMMETRIC REACTIONS

The observed cross sections for symmetric reactions involving inert gases; diatomic gases H_2 , N_2 , Cl_2 , CO, NO; and polyatomic gases CO_2 and certain hydrocarbons are given in figures 3 and 4. In our investigation, the cross sections for

beam energy less than 100 ev was not determined because of the uncertainty concerning the plateau in the saturation curve. (Ghosh and Sheridan, 1957).

The cross sections are about 20 per cent higher than the values previously

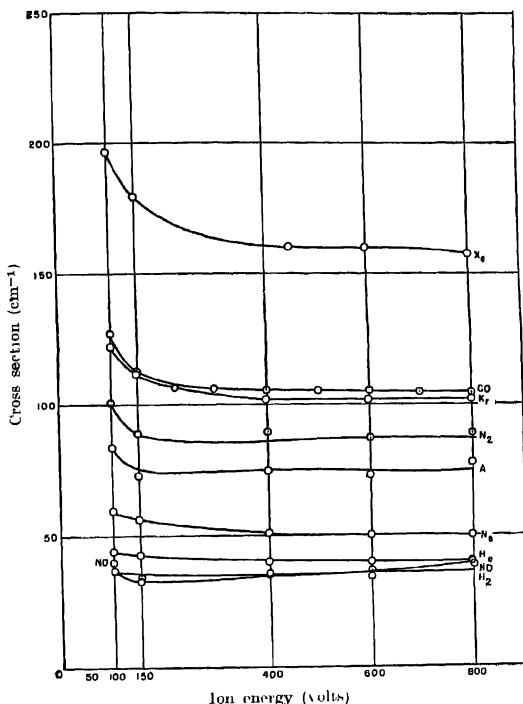


Fig. 3. Symmetric charge transfer cross sections for the inert gases and diatomic gases H_2 , N_2 , Cl_2 , CO and NO .

reported. (Dillon *et al.*, 1955). A plausible explanation for this discrepancy is that in previous experiments, cross sections were determined from net charge measurements which did not take a full account of the secondary electrons collected at the charge transfer plate. This explanation is supported by the fact that the discrepancies were greatest for the light ions for which the secondary emission was large.

A second experimental result is that in contrast to observations made in the previous investigations, very little variation in cross section for inert gases and most of the diatomic gases for beam energy between 150 and 800 ev has been detected.

It is to be noted that the cross sections for hydrocarbons are low and increase with beam energy. This latter fact was also exhibited by NO and CO₂ and may be a consequence of the fact that newly-created ions are dissociated during the process of transfer of charge.

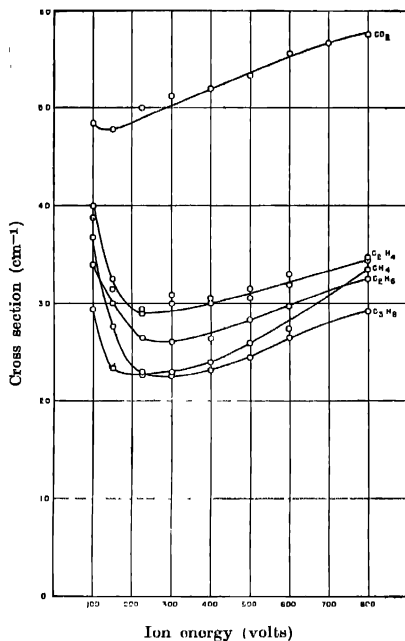


Fig. 4 Symmetric charge transfer cross sections for CO₂ and hydrocarbons.

5. UNSYMMETRIC CHARGE TRANSFER REACTION— SYMMETRIC CHARACTER IN UNSYMMETRIC REACTIONS

Cross sections for the unsymmetric reactions A^+, N_2 , (A^+, H_2) , (N^+, H_2) and their reverse reactions were determined. These gases have nearly equal ionization potentials and hence possess small energy defect ΔE . Therefore, according to the adiabatic hypothesis, maximum cross section should occur at low ion energy and then decrease with increasing energy. In other words, these unsymmetric reactions should have symmetric character above a certain small ion energy.

Figure 5 shows the observed cross sections, indicating maximum cross section at low ion energies. The increasing cross sections with ion energy beyond 400

ev for reactions (N_2^+, A) , (H_2^+, N_2) , and (H_2^+, A) may be explained as being due to the formation of excited states. For example, in the last two reactions H_2^+ ions may be formed in the anti-bonding state $^2\Sigma_u^+$ leading to dissociation of the H_2^+ ion into a proton and a hydrogen atom. This view is supported by the

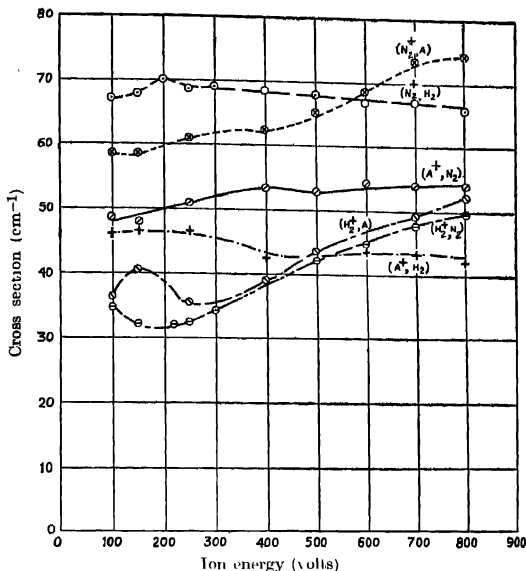


Fig. 5. Charge transfer cross sections for the unsymmetric reactions (A^+, N_2) , (A^+, H_2) , and (N_2^+, H_2) and their reverse reactions

observation of a second maximum at 5000 ev for the reaction (H_2^+, A) , (Stedford and Hasted, 1955).

The interaction distances a were computed from the relation $\frac{a\Delta E}{hv} = 1$ where v is the velocity of the ion, and were found to have values between 9 and 13 Å.

It was found that unsymmetric reactions can have symmetric character even if the ionization potentials of the reacting particles are not equal. In fact, it may be hypothesized that if the neutralized ions or the newly-created ions are excited to proper energy levels or dissociated and at the same time excited so that the energy defect becomes equal to zero, an unsymmetric reaction will behave as a symmetric one (Ghosh and Sheridan, 1956 a, b). We shall now present certain observational facts and shall interpret the results in the light of the above hypothesis.

In figures 6(a) and 6(b) charge transfer cross sections for the reactions (A^+, NO) , (A^+, CO) , (A^+, CO_2) , (A^+, CH_4) , (A^+, C_2H_4) and (A^+, C_2H_6) are given. It is seen

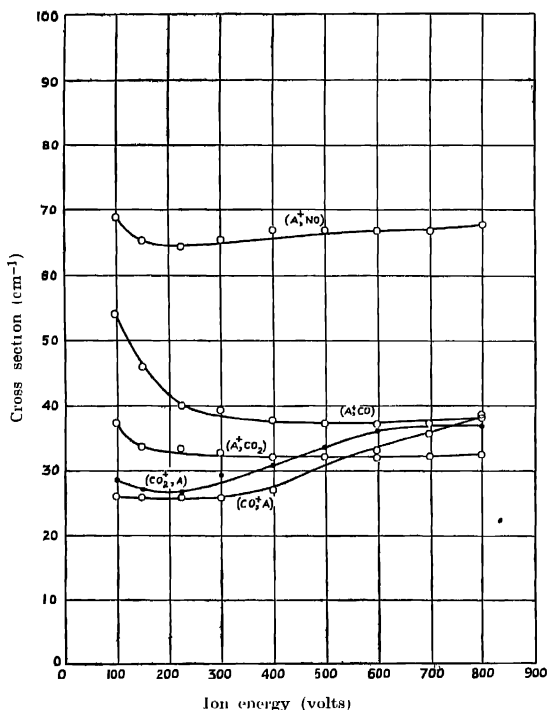


Fig. 6(n)

that these reactions have symmetric character indicating that energy balance has been obtained either through excitation or dissociation of newly-created ions (the neutralized argon ion cannot be excited as the first excited state of A has energy of 11.6 eV which is very large compared to the energy defects of these reactions). The reverse reactions do not possess a symmetric character.

6. SECONDARY ELECTRON EMISSION BY ION BOMBARDMENT

The method described above can be utilized to determine the secondary electron emission due to ion bombardment of a metal surface. Data for secondary electrons emitted by an electropolished brass surface due to ion bombardment have been obtained. (Ghosh and Sheridan, 1957).

It should be noted that the secondary electron emission depends on the mass, charge, energy and electronic configuration of the incident ions. Furthermore, the emission depends on the physical and chemical composition of the target as

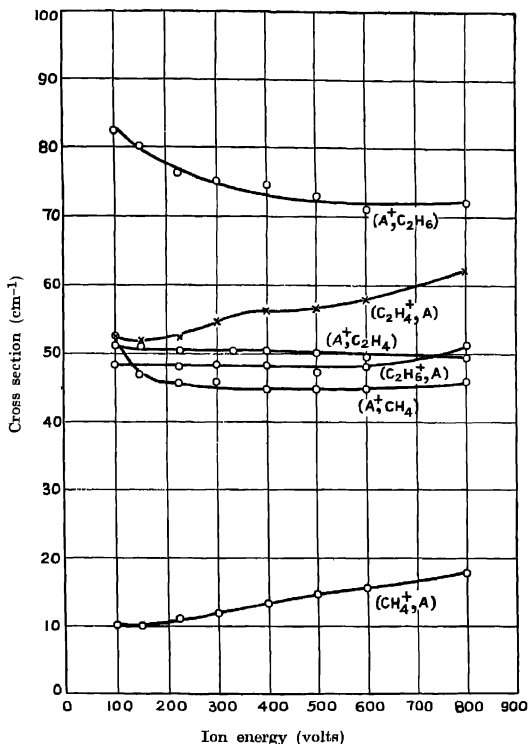


Fig. 6(b). Charge transfer cross sections for the unsymmetric reactions (A^+, NO) , (A^+, CO) , (A^+, CO_2) , (A^+, CH_4) , (A^+, C_2H_4) , and (A^+, C_2H_6) and their reverse reactions.

well as on the angle with which ions are incident on the target. In our experiments, the ions were singly charged and for high energies they were incident essentially at right angles to the brass plate.

The secondary electrons for 100 ions bombardment at different energies is shown in figures 7, 8 and 9. Two facts are predominant from the figures.

(1) For beam energy greater than 300 ev, the secondary electron emission is a linear function of the ion energy. In fact, this linearity extends to even

lower beam energies for light gases. Thus for H_2 and He, the linear rise is observed even at 50 ev.

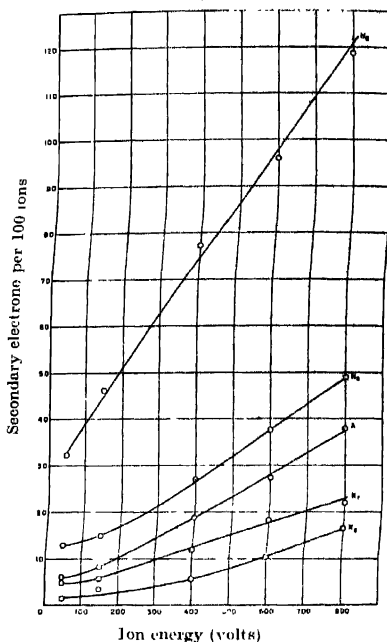


Fig. 7. Variation of secondary electron emission with the energy of ions (of inert gases) for 100 ions bombardment.

(2) For a group of similar gases, the slope of each curve decreases with the mass of the ion. For inert gases, the slope varies from .12 elec/volt to .03 elec/volt; for hydrocarbons and CO_2 between .10 and .06 elec/volt. The slopes for the diatomic molecules are between .14 and .025 elec/volts.

It is found that the relation

$$y = \frac{aV}{\sqrt{M}} + b \quad 225 \text{ ev} \leq V \leq 800 \text{ ev.}$$

where

y = electron emission for 100 ion bombardment

V = energy of the beam

M = mass of the ion,

holds for 225 ev to 800 ev. The values of a and b are given in the Table I below.

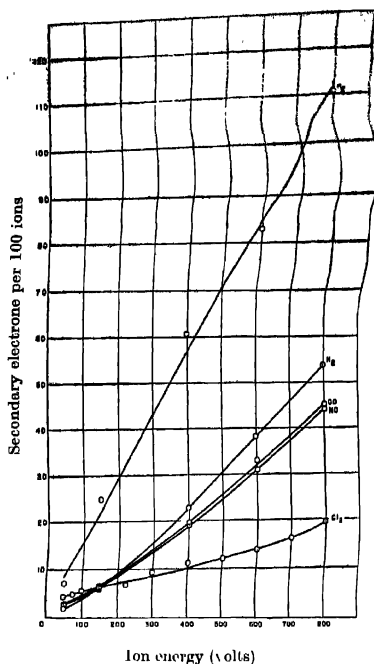


Fig. 8 Variation of secondary electron emission with the energy of ions (of Cl_2 , N_2 , CO and NO) for 100 ions bombardment.

TABLE I

Ions of	a	b
Inert gases	.29	0
Hydrocarbons	.35	+4
H_2	.20	0
N_2	.40	-6
Cl_2	.18	+2
CO	.32	-4
NO	.28	-5
CO_2	.32	-6.5

The deviation of the computed values from the experimental data is seldom in excess of 7 percent, which is well within the scope of experimental error. In general, the maximum deviations are within 20 percent.

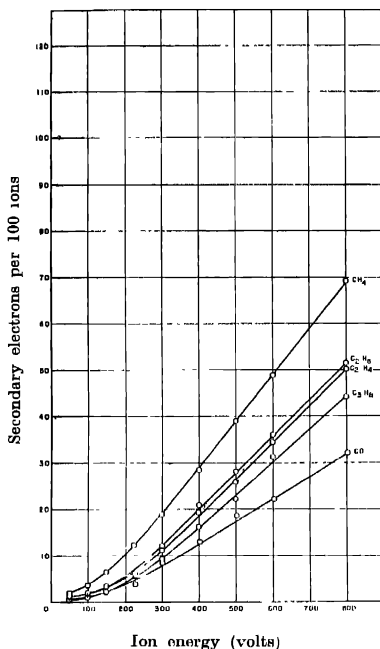


Fig. 9. Variation of secondary electron emission with the energy of ions (of CO₂ and of hydrocarbons) for 100 ions bombardment.

7. APPLICATION TO UPPER ATMOSPHERIC PHENOMENA

Concerning the importance of charge transfer process in the upper atmosphere it should be noted that symmetric reactions occurring within the ionosphere are trivial since no new ions are formed. Furthermore, since ions in the ionosphere have energies of a few tenths of a volt and since during electron exchange very little exchange of kinetic energy takes place, it follows that there is only a small difference of kinetic energies between the original and the newly-created ions. However, such reactions may still be significant for aurora, because, although the incoming charged particles from the sun have large energy, the newly-created ions have small energies.

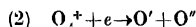
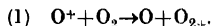
For unsymmetric reactions occurring within the ionosphere new ions are formed, which unlike aurora, have practically no change of kinetic energy.

Thus, due to charge transfer, ions which are not originally produced by the ultra-violet rays of the sun are formed in the upper atmosphere. These reactions increase the heterogeneity of the upper atmosphere because ions of the same atoms or molecules but with different kinetic energies may be present in a layer.

Assuming that the cross section for a charge transfer reaction for energies between 50 eV and 40 keV and at a pressure of 1 mm Hg is 10 cm^{-1} that is, $2.81 \times 10^{-10} \text{ cm}^2$, the coefficient of the reaction for protons of velocity $5 \times 10^5 \text{ cm/sec}$ becomes $1.4 \times 10^{-10} \text{ cm}^3/\text{sec}$. (At low energies, the coefficient is much larger. For instance, Ziegler (1953) has found that for symmetric reactions involving inert gases at thermal energies the coefficient is between 2.5×10^{-9} and $5 \times 10^{-9} \text{ cm}^3/\text{sec}$.) Therefore, the coefficient of a charge transfer reaction is much smaller than that of a dissociative recombination whose value is 10^{-6} to $10^{-7} \text{ cm}^3/\text{sec}$. On the other hand, the rate of a charge transfer reaction is much larger since it involves neutral particle density. A comparison of the rates of collisional process in regions D, E, and F of the ionosphere shows that the charge transfer rate is much larger than any other collisional process in the upper atmosphere (Ghosh, 1956). If the charge transfer reaction occurs in the forward direction only, all the ions formed from ultraviolet rays will be changed to another ion in less than one second.

Considering the F-region, it is found that except for the reaction $\text{O}^+(^4\text{S}) + \text{H}(^1\text{S}) \rightarrow \text{O}(^3\text{P}) + \text{H}^+$, the values of E_a , for which the cross section is maximum, range from several hundred to several thousand volts, and because the energy of ions in the ionosphere is only a few tenths of a volt, the probabilities of these reactions are low. Due to this reaction, the O^+ ions in the F-layer will be neutralized by H-atoms. However, the opposite reaction, namely H^+ ions being neutralized by O atoms is less probable since it involves two processes. The charge transfer processes can take place only after O atoms deliver their kinetic energies to H^+ ions. Because $I(\text{O}) < I(\text{N}_2)$, the other process of removal of O^+ ion the F-layer, namely $\text{O}^+ + \text{N}_2^+ \rightarrow \text{O} + \text{N}_2^+$, has a small probability unless O^+ is in an excited state.

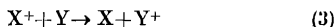
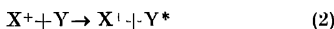
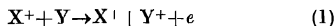
It can be shown by means of the following two equations,



that it is possible to derive both the ratio of the oxygen atomic ion to the oxygen molecular ion density, and the effective recombination coefficient for the F-layer. In addition, it was shown by Nicolet (1954), that the reaction (1) can be a possible source of excitation of the green auroral lines of the air glow. The ratio of O^+ to O_2^+ in the F-region and the effective recombination coefficient were found to be about 10^3 and $5 \times 10^{-10} \text{ cm}^3/\text{sec}$ respectively, (Ghosh, 1956).

Considering the charge transfer process in other ionized regions, it is found that the reactions have high energy defects and hence low probability of occurrence under ionospheric conditions.

With regard to charge transfer reactions between ions from the sun and the upper atmospheric gases, it is to be noted that as the ions penetrate the atmosphere they first ionize, dissociate and/or excite the colliding atmospheric gases and when they have moved deeply into the atmosphere and have sufficiently slowed down, charge transfer reactions take place. In other words, as the incoming particles penetrate into the atmosphere, the following reactions occur successively :



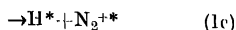
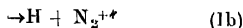
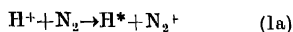
In order to penetrate to auroral height (100 km), a proton must have an initial velocity of 10^4 km/sec, whereas an electron of the same velocity, because of scattering effect, can penetrate only up to 170 km. Since the charge transfer process becomes important when the energy of the particle is less than 1 kev, it follows that the rate of occurrence of this process is highest at the auroral heights.

Table II shows the charge transfer reactions that may occur between H^+ ions with the atmospheric gases, their energy defect ΔE , and the energies E_a of the incident ion which makes $a\Delta E/hv = 1$, where $a = 7 \times 10^{-8}$ cm. It should be noted that for the reaction (3) ΔE is very small. The probability of the reaction is low in high regions of the atmosphere because the incoming protons have high energies before entering the atmosphere. However, it increases as the protons penetrate deeper into the atmosphere and has a large value when these protons have lost practically all of their energy in collisions with the atmospheric gases.

In addition to (1), the following reactions may take place.

TABLE II
Charge transfer reactions between H^+ ions and atmospheric gases

Reaction	$\Delta E(\text{ev})$	$E_a(\text{ev})$
(1) $H^+ + N_2(^1\Sigma) \rightarrow H(^1S) + N_2(^2\Sigma)$	-2.05	649
(2) $H^+ + N(^4S) \rightarrow H + N(^4P)$	-0.95	140
(3) $H^+ + O(^1P) \rightarrow H + O(^1S)$	0.02	0.08
(4) $H^+ + N_a(^2S) \rightarrow H + N_a(^1S)$	8.41	10,874
(5) $H^+ + O_2(^3\Sigma) \rightarrow H + O_2(^2\Pi)$	1.33	272
(6) $H^+ + H_2(^1\Sigma) \rightarrow H + H_2(^2\Sigma)$	-1.81	503
(7) $H^+ + H \rightarrow H + H^+$	0	0



Reactions (1a) and (1c) might lead to the excitation of the $\text{H}\alpha$, $\text{H}\beta$, and $\text{H}\gamma$ lines of the Balmer series of hydrogen (the presence of these lines has definitely been shown to exist in aurora). However, due to the large energy defect, ΔE , the region of maximum occurrence of these reactions is located much above the auroral height. The reactions (1b) and (1c), of which (1b) occurs at the lower height, would lead to the excitation of the first negative bands of $\text{N}^+_{2^+}$ and might explain the increased intensity of $\text{N}^+_{2^+}$ bands with height (height effect).

In Table III, the charge transfer reactions between Ca^+ ions and the atmospheric gases, their energy defects, and the values of E_a are collected.

To estimate the intensity of the first negative bands of $\text{N}^+_{2^+}$ ions excited by reaction (1b), we note that the density of proton streams near the earth's atmosphere is about 20 ions/cc. Assuming the charge transfer process is alone operative, stream velocity of 10^8 cm/sec, and charge transfer cross section of 10^{-16} cm², it can be shown by a simple calculation that even for a thin layer of 10 km thickness, few ions can pass out of the layer. In other words, the rate of production of excited $\text{N}^+_{2^+}$ ions is 2×10^9 ions per cm² column per sec, which is sufficient to produce a strong aurora.

No data concerning the penetration of Ca^+ ions through air is available. A rough estimate can be obtained from the penetration of α -particles through air. It is found that in travelling a distance of 1 cm through air at S.T.P. an α -particle loses about 1 Mev energy. Assuming the penetrating power of Ca^+ ions is ten times greater than that of α -particles, it follows that these ions can penetrate to an altitude of about 80 km.

TABLE III

Charge transfer reactions between Ca^+ ions and atmospheric gases

Reactions	$\Delta E(\text{ev})$	$E_a(\text{ev})$
(1) $\text{Ca}^+(^2\text{S}) + \text{N}_2(^1\Sigma) \rightarrow \text{Ca}(^1\text{S}) + \text{N}^+_{2^+}(^2\Sigma)$	-9.47	547,159
(2) $\text{Ca}^+ + \text{N}(^4\text{S}) \rightarrow \text{Ca} + \text{N}^+(^3\text{P})$	-8.37	427,431
(3) $\text{Ca}^+ + \text{O}(^3\text{P}) \rightarrow \text{Ca} + \text{O}^+(^4\text{S})$	-7.44	337,687
(4) $\text{Ca}^+ + \text{H}(^1\text{S}) \rightarrow \text{Ca} + \text{H}^+$	-7.42	335,885
(5) $\text{Ca}^+ + \text{Na}(^2\text{S}) \rightarrow \text{Ca} + \text{Na}^+(^1\text{S})$	0.99	5 980.
(6) $\text{Ca}^+ + \text{O}_2(^3\Sigma) \rightarrow \text{Ca} + \text{O}_2^+(^2\Pi)$	-6.09	226,276

In the reactions of Table III, the energy defect is large, and therefore they have maximum probability before the incident Ca^+ ions have lost all their energies in collisions with the atmospheric gases, i.e., above the altitude of 80 km.

As in the case of reactions involving protons, the neutralized incident calcium ions or the newly-created ions or both (Table III) may be excited. As regards the Ca line between excited states and ground states, it may be noted that there is an intercombination line, $^3\text{P}_1 - ^1\text{S}_0$ at $\lambda 6573$. In the blue ultraviolet region there is a strong permitted line $\lambda 4227(^1\text{P}_1 - ^1\text{S}_0)$ of Ca, and in the ultraviolet region, there are three lines of Ca namely $\lambda 2735$, $\lambda 2722$, $\lambda 2399$ which are obscured by the ozone layer. A search into the auroral spectrum shows that the line $\lambda 6573$ may be hidden in the high background (as shown in the microphotometer tracing) in the vicinity of H α line. Also, there are two lines at $\lambda 4223$ and $\lambda 4236$ which are thought to be NI and I-2 bands of the first negative system of N_2^+ . It may be that these lines are actually Ca lines.

REFERENCES

- Dillon, J. A., Sheridan, W. F., Edwards, H. D., and Ghosh, S. N., 1955, *Jour. Chem. Phys.*, **23**, 776.
 Ghosh, S. N. and Sheridan, W. F., 1957 *Jour. Chem. Phys.* **26** 480.
 " " " " 1956a *Jour. Chem. Phys.* **25** 1076
 " " " " 1956b, *Proc. Phys. Soc.* (London).
 Ghosh, S. N., 1956, *J. Geophys. Res.* **61**, 193.
 Hasted, J. B., 1951, *Proc. Roy. Soc. A*, **205**, 421; 1952, **212**, 235.
 Lindholm, E., 1954, *Arkiv För Fysik*, **8**, 257; **8**, 433.
 Mussey, H. S. W., 1949, *Rep. Progr. Phys.* **12**, 248.
 Nicolet, M., (1954), *Phys. Rev.*, **93**, 633.
 Potter, R. F., 1954, *Jour. Chem. Phys.*, **22**, 974.
 Stedford, J. B. H. and Hasted, J. B., 1955, *Proc. Roy. Soc., A*, **227**, 466.
 Ziegler, B., 1953 *Z. Physik*, **136**, 108.

THE CRYSTAL STRUCTURE OF *p*-NITROANILINE AT DIFFERENT TEMPERATURES*

G. S. R. KRISHNA MURTI

OPTICS DEPARTMENT, INDIAN ASSOCIATION FOR THE CULTIVATION OF SCIENCE,
JADAVPUR, CALCUTTA-32

(Received for publication April 8, 1957)

Plato VII

ABSTRACT. The crystal structure of *p*-nitroaniline at 90°K has been reinvestigated using Debye-Scherrer method. The cell dimensions $a = 12.16$ A.U., $b = 6.06$ A.U., $c = 8.506$ A.U., and $\beta = 93^{\circ}16'$ are found from the pattern. The coefficient of expansion α_{11} in the direction making an angle $40^{\circ}2'$ to the a -axis in the range 90°K to 301°K is found to be 140×10^{-6} which agrees with the value reported by McKoown *et al* (1951). The coefficients of expansion along the three crystallographic axes a , b and c are found to be 70.15×10^{-6} , -16.06×10^{-6} and 70.69×10^{-6} respectively. The unit cell dimensions of the crystal at 301°K deduced from the pattern are almost the same as those reported by Abrahams and Robertson (1948) except that $b = 6.04$ A.U. instead of 6.02 A.U. reported by them. It is pointed out that the slightly larger value for b and the smaller values for a and c at 90°K indicate the existence of strong intermolecular forces which increase at 90°K and turn the molecules a little in the unit cell as pointed out by previous workers, and that it is desirable to redetermine the positions of the atoms in the unit cell at 90°K as well as at 301°K.

INTRODUCTION

The crystal structure of *p*-nitroaniline at the room temperature was first determined by Prasad and Merchant (1938), who studied the rotation photographs of the crystal about a , b and c axes and reported the unit cell dimensions of the crystal as $a = 15.31$ A.U., $b = 6.085$ A.U., $c = 8.63$ A.U., and $\beta = 126^{\circ}11'$. They found that the crystal belongs to the space group of C_{2h}^5 . Abrahams and Robertson (1948) studied the intensities of reflection from different planes of the crystal by using a moving film camera. Assuming the glide to be along the diagonal axis instead of the c -axis, they found the dimensions of the unit cell to be $a = 12.34 \pm 0.02$ A.U., $b = 6.02 \pm 0.02$ A.U., $c = 8.63 \pm 0.02$ A.U., and $\beta = 91^{\circ}40'$ and the space group to be C_{2h}^5 in agreement with the results reported by earlier authors. They also carried out double Fourier analysis and pointed out that in addition to weak hydrogen bonds between the oxygen atoms of the NO_2 group and the hydrogen molecules of the amino group, there is an exceptionally close approach between one of the oxygen atoms of the NO_2 group and three of the aromatic carbon

*Communicated by Professor S. C. Sarkar

atoms of the next molecule. They concluded that intermolecular attraction of new type was present in the crystal.

McKeown *et al* (1951) determined the spacings of some planes of (*hol*), (*hol*) and of (47 $\bar{1}$) with large values of *h* and *l* at different temperatures ranging from 90°K to 293°K in order to find out whether there was any anisotropic contraction of the crystal with lowering of temperature. They also determined the coefficients of expansion α_{22} along *b*-axis, α_{11} along a direction making an angle 40°2' with *a*-axis and α_{33} along a direction perpendicular to that of α_{11} . They found the values of α_{11} , α_{22} and α_{33} to be 150.3×10^{-6} , 7.5×10^{-6} and 24×10^{-6} respectively. They came to the conclusion that there was a polarisation bond linking the aromatic C-atom *ortho* to the NH₂ group of one molecule to the O-atom of the NO₂ group of an adjacent molecule. They also concluded that the molecules turn a little in the crystal as the temperature changes from 293°K to 90°K.

Recently, Donohue and Trueblood (1956) recalculated the Fourier projections by assuming some orientations of the molecules in the crystal which are quite different from those assumed by Abrahams and Robertson (1948) and found much better agreement with the observed intensities. They concluded that the so-called short intermolecular distances in the crystal as well as the polarisation bonds found out by Abrahams and Robertson (1948) are actually absent.

The abnormal high value of coefficient of expansion α_{11} and the very low value of α_{22} found out by McKeown *et al.* (1956), however, point to some change in orientation of the molecules in the crystal with the lowering of temperature to 90°K and it is difficult to understand how such a change takes place in absence of any strong attraction. It has been observed in the case of anthracene (Krishna Murti, 1956) and diphenyl (Krishna Murti, 1957) that there is no abnormal contraction with lowering of temperature of the crystals. So, in the case of substituted benzenes, if actually such a reorientation of molecules is observed with lowering of temperature, some sort of attraction between the molecules is to be postulated. As the unit cell contains four molecules a slight turning of molecules would lead to some changes in the relative intensities of reflection from certain planes. McKeown *et al.* (1956) did not study such changes in the relative intensities in detail. So, it was thought worthwhile to study the Debye-Scherrer patterns of *p*-nitroaniline at 90°K and also at room temperature (301°K) using the same arrangement to find out whether the Debye-Scherrer patterns indicate any anisotropic contraction observed by McKeown *et al.* (1956) with lowering of temperature to 90°K and whether the relative intensities of reflection from different planes undergo remarkable changes with lowering of temperature.

EXPERIMENTAL

Pure *p*-nitroaniline (m.p. 147°C) was used after being crystallised in alcohol. The crystals were powdered properly and packed tightly in a thin-walled soda

glass tube of diameter of about 0.04 cm to photograph the Debye-Scherrer patterns at the different temperatures mentioned above. The low temperature photographs were taken by the method described earlier (Krishna Murti and Sen, 1956).

A Seifert X-ray tube running at 26 ma, 32KV was used and an exposure of about $2\frac{1}{2}$ hrs. was sufficient to get the patterns recorded with moderate densities. The X-ray tube was provided with a copper target and a nickel filter was used to cut off the Cu, $K\beta$ wavelengths. The distance from the specimen to the film was measured accurately by taking the Debye-Scherrer pattern of rock salt and was found to be 5.228 cms. Several photographs for each specimen were taken under the same conditions to test the genuineness of the results. Spacings were calculated from the diameters of the rings measured with a comparator. The pattern due to the crystal at room temperature was photographed to find out whether the spacings calculated agreed with those calculated from the data of Abrahams and Robertson (1948) and to compare them with those at low temperature.

RESULTS AND DISCUSSION

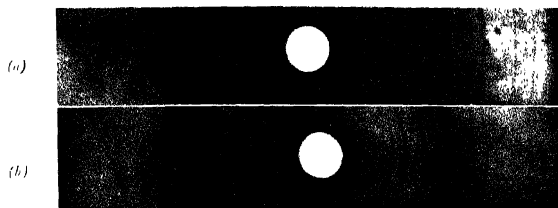
Some of the representative photographs of the Debye-Scherrer patterns obtained at different temperatures are reproduced in Plate VII. The spacings calculated from the Debye-Scherrer patterns of *p*-nitroaniline at different temperatures as mentioned above are calculated and given in Table I along with the spacings calculated from the data of Abrahams and Robertson (1948). The intensities of different rings in the patterns obtained are given along with the spacings in parentheses as very strong (vs) strong (s), medium (m), weak (w) and very weak (vw).

TABLE I
Spacings of *p*-nitroaniline

Planes	At 301°K			At 90°K	
	From the data of Abrahams & Robertson (1948)	Observed	From the refined data (Present author)	Observed	From the data calculated (Present author)
101	7.170	7.170 (m)	7.170	7.150 (m)	7.150
200	6.170	6.170 (w)	6.170	6.170 (w)	6.170
110	5.410	5.423 (ms)	5.424	5.423 (ms)	5.423
011	4.938	4.948 (m)	4.947	4.933 (m)	4.933
111	4.610	4.621 (s)	4.619	4.621 (s)	4.623
111	4.558	4.565 (vw)	4.565	4.519 (w)	4.517
002	4.314	4.315 (vw)	4.313	4.245 (vw)	4.245

TABLE I (contd.)

Planes	At 301°K			At 90°K	
	From the data of Abrahams & Robertson (1848)	Observed	From the refined data (Present author)	Observed	From the data calculated (Present author)
211	3.824	3.830 (s)	3.828	3.770 (s)	3.767
30 $\bar{1}$	3.755	3.755 (w)	3.754	3.735 (w)	3.737
301	3.671	—	3.670	3.573 (w)	{ 3.575 3.575 3.475 3.388 3.386
202	3.585	3.582 (s)	3.583		
012	3.506	3.510 (m)	3.510		
202	3.487	3.485 (vs)	3.486		
112	3.392	3.396 (vw)	3.398	3.390 (s)	
310	3.396		3.397		
31 $\bar{1}$	3.186	3.186 (s)	3.188	3.186 (vw)	3.181
311	3.135	3.134 (m)	3.136	3.080 (s)	{ 3.079 3.079
212	3.080	3.080 (m)	3.081		
020	3.010	3.019 (m)	3.020	3.030 (w)	3.030
120	2.925	2.936 (w)	2.934	2.936 (m)	2.938
121	2.764	2.758 (w)	2.770	—	—
410	2.746		2.750	2.710 (m)	2.714
41 $\bar{1}$	2.635	2.635 (w)	2.636	2.620 (m)	2.622
013	2.594	2.593 (ms)	2.595	2.563 (m)	2.564
50 $\bar{1}$	2.390	2.395 (m)	2.392	2.375 (m)	2.370
222	2.305	2.310 (vw)	2.310	2.310 (vw)	2.311
51 $\bar{1}$	2.222	2.228 (vw)	2.224	2.205 (w)	2.208
004	2.157	2.160 (vw)	2.157	2.125 (w)	2.123
600	2.056	2.054 (w)	2.056	2.023 (w)	2.023
130	1.981	1.986 (w)	1.987	1.990 (w)	1.993
422	1.943	1.946 (w)	1.946	1.946 (w)	1.945
610	1.945		1.946	1.916 (w)	1.919
611	1.887		1.886	1.855 (w)	1.852
521	1.854		1.856	1.835 (vw)	1.832
132	1.795	1.795 (vw)	1.800	1.795 (vw)	1.798
124	1.742	1.740 (w)	1.744	1.732 (vw)	1.732
70 $\bar{1}$	1.737		1.736		
105	1.704	1.705 (vw)	1.704	1.670 (w)	1.668

Debye-Scherrer patterns of *p*-nitroaniline

(a) Specimen at 25° C (Radius of camera = 5.228 cms).

(b) Specimen at -186° C (Radius of camera = 5.228 cms).

Attempt was made first to find out the unit cell dimensions of the crystal at low temperature from the spacings of the planes (10 $\bar{1}$), (200), (011) and (110). The values of b and $c \sin \beta$ were calculated from spacings of planes (110) and (011) with that for $a \sin \beta$ obtained from the spacing of (200). It was found that the unit cell dimensions of the crystal calculated from these planes satisfy the spacings obtained for all other planes. The dimensions of the unit cell thus obtained are:

$$a = 12.16 \text{ A.U.}$$

$$b = 6.06 \text{ A.U.} \quad \text{and} \quad \beta = 93^\circ 16'.$$

$$c = 8.506 \text{ A.U.}$$

The assignment of the indices to different planes for the crystal at room temperature (301°K) was made with the help of the structure factors reported by Donohue and Trueblood (1956). It can be seen from Table I that most of the spacings obtained for the crystal at 301°K, in this investigation, agree fairly well with the data of Abrahams and Robertson (1948) except a few which involve b -axis. The spacings for the planes which contain b dimension, viz., (011), (110), (111) etc. obtained in this investigation are slightly higher than those calculated from the data of Abrahams and Robertson (1948). So if the length of b -edge of the unit cell, as reported by the above authors, is slightly increased from 6.02 A.U. to 6.04 A.U., the other data remaining unchanged, the spacings for the above mentioned planes agree well with those observed in the present investigation. At 90°K the value of b increases a little, while the values of a and c diminish. Also β increases at the lower temperature. These values of a , b , c and β would make some of the spacings smaller than those at room temperature while some other spacings would either remain unchanged or increase slightly. Table I shows that the planes (110), (11 $\bar{1}$), (31 $\bar{1}$), (21 $\bar{2}$), (120), (22 $\bar{2}$), (42 $\bar{2}$) and (132) have the same spacings at both the temperatures and the planes (020), (130) have slightly higher spacings at about 90°K. Thus the observed spacings can be explained satisfactorily with the help of the unit cell dimensions mentioned above. From this it may be concluded that the primitive translation along b axis slightly increases instead of diminishing at 90°K. By comparing the dimensions for the crystal at 90°K with those for the crystal at 301°K, it can be seen that the unit cell contracts in the directions of a and c axis whereas it elongates slightly along b axis which must be due to the slight reorientation of the molecules at the low temperatures.

In order to compare these results with those reported by McKeown *et al.* (1951), the value of coefficient of expansion α_{11} along a direction making an angle of about 40° with a axis was calculated by deducing the spacing of the plane (1609) from the unit cell dimensions of the crystal at 90°K. The spacing was found to be 0.5754 A.U., whereas at 301°K it is 0.5924 A.U. This gives a value of 140×10^{-6} for α_{00} . α_{22} has almost a slightly negative value. These values agree fairly well

with those obtained by McKeown *et al.* (1951). The coefficients of expansion along the three crystallographic axes a , b and c are calculated as 70.15×10^{-6} , -16.06×10^{-6} and 70.69×10^{-6} respectively. It can be seen from the patterns reproduced in Plate VII that the general nature of the pattern obtained for the crystal at 301°K is the same even at 90°K, which clearly indicates that the space group C_{2h}^5 remains unaltered even at low temperatures.

It can be seen from Table I that some significant changes in the relative intensities of reflections from a few planes occur with cooling of the crystal to 90°K. The intensities of reflection from the planes (202) and (311) decrease whereas those from the planes (310) and (120) increase at 90°K. This clearly indicates a change in the structure factor of certain planes at low temperatures (90°K). This change coupled with the slight increase in angle β clearly establishes the fact that the molecules in the unit cell reorient themselves slightly as the crystal is cooled to 90°K.

These results thus confirm similar conclusions drawn by McKeown *et al.* (1951). This reorientation cannot be due to Van der Waals forces, and the existence of some stronger intermolecular forces is to be postulated. Donohue and Trueblood (1956) have proposed a structure in which the intermolecular distances are too large to give rise to intermolecular forces larger than Van der Waals forces. It is found, however, that the structure factor for the plane (301) calculated for the structure proposed by them is only about one tenth of the observed value. This discrepancy might indicate that the structure proposed by them, in spite of being able to explain most of the observed intensities, fails completely to explain the intensities of reflection from a few planes and that slight changes in the parameters might give a better agreement between the observed and calculated values. It would be interesting to calculate the structure factors for the crystal at 90°K for the modified structure in order to find out whether there are abnormally short intermolecular distances at 90°K.

ACKNOWLEDGMENT

The author wishes to express his indebtedness to Prof. S. C. Sirkar, D.Sc., F.N.I. for his kind interest and constant guidance throughout the progress of the work.

REFERENCES

- Abrahams, S. C. and Robertson, J. M., 1948, *Acta Cryst.*, **1**, 252.
- Donohue, J. and Trueblood, K., 1956, *Acta Cryst.*, **9**, 960.
- Krishna Murti, G. S. R. and Sen, S. N., 1956, *Ind. J. Phys.*, **30**, 242.
- Krishna Murti, G. S. R., 1956, *Ind. J. Phys.*, **30**, 537.
- Krishna Murti, G. S. R., 1957, *Ind. J. Phys.*, **31**, 1.
- McKeown, P. J. A., Ubbelohde, A. R. and Miss Woodward, I., 1951, *Acta Cryst.*, **4**, 391.
- Prasad, M. and Merchant, J. M., 1938, *J. Ind. Chem. Soc.*, **15**, 47.

ELECTRONIC SPECTRA OF BENZYLAMINE AND ISO-BUTYL BENZOATE IN DIFFERENT STATES AT DIFFERENT TEMPERATURES*

S. B. BANERJEE

OPTICS DEPARTMENT, INDIAN ASSOCIATION FOR THE CULTIVATION
OF SCIENCE, JADAVPUR, CALCUTTA-32

(Received for publication April 2, 1957)

ABSTRACT. The paper deals with the results of investigations on the ultraviolet absorption spectra of benzylamine and iso-butyl benzoate in all the three states at different temperatures. In the case of benzylamine in the vapour state two systems of bands separated by 57 cm^{-1} have been observed while the spectra due to the substance in the liquid and solid states consist of only one series of broad bands. The results have been explained on the assumption that in the vapour state there are two types of molecules with slightly different electronic energy states due to two different orientations of the CH_2NH_2 -group about the C—C bond.

In the case of iso-butyl benzoate the spectrum due to the vapour exhibits sharp bands whereas in the liquid and solid states broad bands are observed. It is found that the main change in the spectrum takes place with liquefaction of the vapour while with subsequent solidification no further change takes place. Attempts have been made to interpret these results.

INTRODUCTION

Previous investigations on the ultraviolet absorption spectra of substituted benzene compounds showed that remarkable changes in the spectra take place with changes of state, depending on the mode of substitution in the ring. Absorption spectra of a number of monosubstituted benzene compounds with long chains as substituent groups have been studied by Swamy (1952) and Deb (1953). It was observed that in the case of benzyl chloride (Swamy, 1952) the position and structure of bands do not undergo any change with solidification and lowering of temperature of the liquid, while with change from the vapour to the liquid state the ν_0 -band shifts by a large amount indicating the presence of associated groups of molecules in the liquid state. Similar results were obtained by Deb (1953) who studied the ultraviolet absorption spectra of *n*-butyl ester of benzoic acid, but the shift observed with the change from vapour to liquid state was much smaller. He concluded that the molecules of esters do not facilitate formation of virtual bonds in the solid state.

The present work was undertaken to extend these investigations to similar molecules having different substituents in order to find out whether a general

*Communicated by Professor S. C. Sarkar.

conclusion can be drawn from the results obtained with a large number of similar compounds. With this object in view the ultraviolet absorption spectra of benzylamine and iso-butyl benzoate in different states and at different temperatures have been investigated and the results have been compared with those reported by previous workers for similar compounds.

EXPERIMENTAL

Benzylamine and iso-butyl benzoate were of chemically pure quality obtained from Merck's original packing and were distilled under reduced pressure before use. Thin films of the liquids of thickness about a few microns were found to produce bands in the absorption spectra which were photographed on Ilford HP3 films with a Hilger EI spectrograph. Absorption cells of length 50 cm were used for obtaining the spectra of the compounds in the vapour state. In the case of benzylamine the absorption tube containing a small quantity of the liquid was evacuated and heated to two different temperatures, viz., 45°C and 65°C by means of an electric heater to get the spectrograms at two pressures, while in the case of iso-butyl benzoate the temperature of the tube was about 75°C. Iron arc spectrum was recorded on each spectrogram as comparison. Microphotometric records of the spectrograms were taken with a Kipp and Zonen type Moll microphotometer. The absorption spectra were calibrated with the help of microphotometric records of iron arc lines by the method described earlier (Banerjee, 1956).

RESULTS AND DISCUSSION

The microphotometric records of the spectrograms are reproduced in figures 1, 2, 3 and 4. The frequencies of the bands in cm^{-1} and their probable assignments are given in Tables I, II, III and IV. The results for the two compounds have been discussed separately in the following paragraphs.

Benzylamine:

The spectrum due to benzylamine in the vapour state at 45°C consists of a number of bands with the first intense band at 37414 cm^{-1} . It can be seen from figure 1(b) that this band is accompanied by a feeble and slightly broad band at 37471 cm^{-1} on the short wavelength side. If the band at 37414 cm^{-1} were taken as the ν_0 -band due to the vapour, the band at 37471 cm^{-1} would represent a transition ν_0+57 . It is, however, unlikely that 57 cm^{-1} represents an excited state vibrational frequency because the Raman spectrum of the compound does not show any ground state frequency of that order (Sirkar and Bishui, 1946). It can also be seen from figure 1(b) that the strong band at 37927 cm^{-1} is also accompanied by a similar weak band at 37984 cm^{-1} . It is further observed that when the temperature of the vapour is raised from 45°C to 65°C these two bands at 37471 cm^{-1} and 37984 cm^{-1} become appreciably sharper and stronger (figure 1a.) Thus it seems that besides the main system of bands with the ν_0 -band at 37414 cm^{-1} there is a

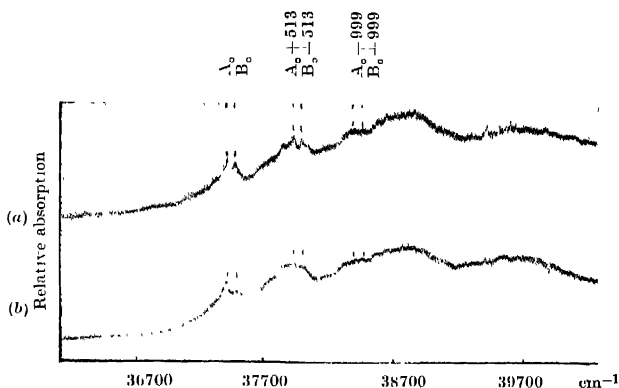


Fig. 1 Microphotometric records of the ultraviolet absorption spectra of benzylamine in the vapour state.

(a) Vapour at 65°C (b) Vapour at 45°C

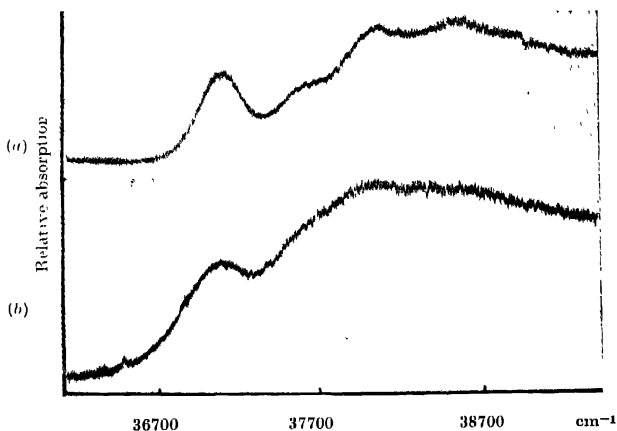


Fig. 2. Microphotometric records of the ultraviolet absorption spectra of benzylamine.

(a) Solid at -180°C. (b) Liquid at 24°C

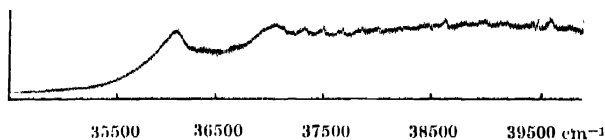


Fig. 3. Microphotometric records of the ultraviolet absorption spectra of iso-butyl benzoate in the vapour state at 75°C

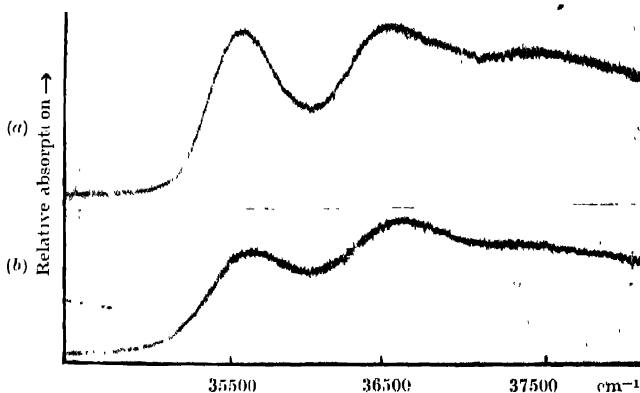


Fig. 4. Microphotometric records of the ultraviolet absorption spectra of iso-butyl benzoate in the liquid and solid states.

(a) Solid at -180°C; (b) Liquid at 24°C.

second system of weaker bands separated from the first system by 57 cm^{-1} with the ν_0 -band at 37471 cm^{-1} and that the intensity of this second system depends on the temperature of the vapour. The bands at 37414 and 37471 cm^{-1} have accordingly been taken as the ν_0 -bands of the two systems and designated as A_0 and B_0 respectively. When the temperature of the vapour is increased to 65°C a few very weak broad bands are observed on the long wavelength side of the band at 37414 cm^{-1} and with reference to this band as the ν_0 -band (A_0) these weak bands can be assigned to ground state vibrational frequencies 168 , 484 and 627 cm^{-1} respectively which agree closely with some Raman frequencies of the substance.

TABLE I

Absorption bands of benzylamine in the vapour state at 65°C

Wave No. (cm^{-1}) and intensity	Assignment	Wave No. (cm^{-1}) and intensity	Assignment
36787 vw	$A_0 - 627$	38214 vw	$A_0 + 800$ $A_0 + 346 + 429$
36930 vw	$A_0 - 484$	38413 s	$A_0 + 999$
37246 vw	$A_0 - 168$	38470 w	$B_0 + 999$
37358 w	$A_0 - 484 + 429$	38574 s	$A_0 + 1160$
37414 ms	A_0	38673 s	$A_0 + 2 \times 633$
37471 ms	B_0	38921 s	$A_0 + 999 + 513$
37760 m	$A_0 + 346$	39311 vw	$A_0 + 3 \times 633$
37843 ms	$A_0 + 429$	39428 vw	$A_0 + 2 \times 999$
37927 s	$A_0 + 513$	39576 w	$A_0 + 999 + 1160$
37984 ms	$B_0 + 513$	39860 w	$A_0 + 2 \times 999 + 429$
38047 m	$A_0 + 633$		

TABLE II

Absorption bands of benzylamine in the liquid and solid states

Liquid at 24°C		Solid at -180°C	
Wave No. (cm ⁻¹) and intensity	Assignment	Wave No. (cm ⁻¹) and intensity	Assignment
37067 s	ν_0	37081 s	ν_0
37596 sb	$\nu_0 + 529$	37588 m	$\nu_0 + 507$
38040 vs	$\nu_0 + 973$	37696 m	$\nu_0 + 615$
38583 sb	$\nu_0 + 973 + 529$	37867 ms	$\nu_0 + 786$
		37953 s	$\nu_0 + 872$
		38069 vs	$\nu_0 + 988$
		38643 vs	$\nu_0 + 2 \times 786$
		38921 s	$\nu_0 + 988 + 872$

The bands on the shorter wavelength side of 37414 cm⁻¹ and 37471 cm⁻¹ can be assigned to transitions involving excited state vibrational frequencies 346, 429, 513, 633, 999 and 1160 cm⁻¹ in the A-system and 513 and 999 cm⁻¹ in the B-system. There is also a very feeble band at a distance of 56 cm⁻¹ on the longer wavelength side of the A₀-band which represents a $\nu \rightarrow \nu'$ transition involving the ground state frequency 484 cm⁻¹ which is reduced to 429 cm⁻¹ in the excited state. A tentative suggestion regarding the origin of the two systems in this molecule is given below.

In benzylamine molecule the CH₂NH₂ group which is attached to the ring through a C-C bond may possess a freedom for two different orientations about that bond. Evidence of such freedom of rotational orientation of substituent groups has been furnished by Ghosh (1954) from a study of absorption of micro-waves in many polar liquids including benzylamine. In the case of benzylamine in the vapour state such freedom of rotation of the substituent group may possibly give rise to two types of molecules with slightly different electronic energy states and the relative population of the two types will be determined by the energy difference between the two configurations. The appearance of the two systems of bands with A₀ and B₀ as the ν_0 -bands may be due to the presence of such two types of molecules in the vapour state. The influence of temperature on the relative intensities of the two systems actually corroborates the view that molecules of two different configurations are present in the vapour.

In the liquid state benzylamine exhibits only one series of broad bands consisting of four bands with centres at 37067, 37596, 38040 and 38583 cm⁻¹ of which the first one has been taken as the ν_0 -band. The ν_0 -band due to the liquid thus

lies at a distance of 347 cm^{-1} on the longer wavelength side of the ν_0 -band (A_0) due to the vapour. In the case of the liquid the bands of each system become broader owing to influence of fluctuating intermolecular field and the corresponding bands of the two systems coalesce with each other to form a single series of broad bands. When the liquid is frozen and cooled to -180°C there is no further shift of the ν_0 -band and again only one system of bands is observed. When benzylamine is cooled to -180°C , the different molecules of the compound might be frozen with the substituent group having any of the two possible orientations. But the bands due to the solid are still broad though they are a little sharper than those due to the liquid. This indicates a fluctuation of the intermolecular field even in the solid state as in the case of iso-butyl benzoate discussed below. In the spectrum due to the solid the excited state vibration frequencies 507 , 615 , 786 , 872 and 986 cm^{-1} are observed. It is found, however, that with solidification and lowering of temperature the intensity of the band representing the excited state frequency 513 cm^{-1} observed in the case of the vapour corresponding to one of the components of $606\text{ cm}^{-1} e_{2g}$ mode of the benzene ring is diminished, while the intensity of the band involving the excited state frequency 999 cm^{-1} due to the breathing vibration of the ring is increased.

Iso-butyl benzoate:

In the vapour state iso-butyl benzoate yields a number of sharp bands of which the first strong band at 36083 cm^{-1} has been assigned as the ν_0 -band. The other bands correspond to excited state vibrational frequencies 151 , 256 , 583 , 970 , 1025 , 1436 cm^{-1} and their harmonics and combinations. There is a weak band at 35921 cm^{-1} representing the ground state frequency 153 cm^{-1} . There is also a band at 36909 cm^{-1} which might be assigned either as ν_0+826 or $\nu_0+970-153$. The second assignment would require the molecules to be initially in the excited vibrational state of frequency 153 cm^{-1} . In that case the intensity of the band in question would be expected to diminish greatly in the case of the solid at -180°C , because the number of molecules present initially in the excited vibrational state would diminish at low temperatures. Actually, such a diminution in the intensity of the band takes place at the low temperature. In the spectrum due to the solid at -180°C reproduced in figure 4(a) the band corresponding to the frequency 970 cm^{-1} is quite intense and does not indicate the presence of another band adjacent to it on the long wavelength side, while in the spectrum due to the liquid (figure 4b) the band corresponding to the frequency 970 cm^{-1} appears to be accompanied by a broad band on the long wavelength side. Thus the frequency 826 cm^{-1} is not a fundamental excited state vibrational frequency.

In the liquid state three very broad bands are observed with the centres of the bands at 35614 , 36565 and 37512 cm^{-1} respectively, the first band being assigned as the ν_0 -band of the system. The other two bands involve transitions ν_0+951 and $\nu_0+2\times 951$. It is thus found that the liquefaction of the vapour results in

TABLE III

Absorption bands of iso-butyl benzoate in the vapour state at 75°C

Wave No. (cm ⁻¹) and Intensity	Assignment	Wave No. (cm ⁻¹) and intensity	Assignment
35030 w	$\nu_0 - 153$	37082 m	$\nu_0 \pm 1025 + 583$
36083 s	ν_0	37804 w	$\nu_0 \pm 970 \pm 583 \pm 151$
36234 vw	$\nu_0 \pm 151$	37874 w	$\nu_0 \pm 2 \times 970 - 153$
36339 vw	$\nu_0 \pm 256$	38028 w	$\nu_0 \pm 2 \times 970$
36666 w	$\nu_0 \pm 583$	38244 w	$\nu_0 \pm 1025 \pm 970 \pm 151$
36909 ms	$\nu_0 \pm \begin{matrix} 826 \\ 970 - 153 \end{matrix}$	38464 m	$\nu_0 \pm 970 \pm 1436$
37053 s	$\nu_0 \pm 970$	38538 w	$\nu_0 \pm 1025 \pm 1436$
37108 s	$\nu_0 \pm 1025$	38598 s	$\nu_0 \pm 2 \times 970 + 583$
37212 w	$\nu_0 \pm 970 \pm 151$	38793 w	$\nu_0 \pm 970 \pm 1436 \pm 256$
37323 m	$\nu_0 \pm \begin{matrix} 1240 \\ 970 + 256 \end{matrix}$	38989 w	$\nu_0 \pm 3 \times 970$
37484 w	$\nu_0 \pm 970 \pm 256 \pm 151$	39389 m	$\nu_0 \pm 3 \times 970 \pm 256 \pm 151$
37519 m	$\nu_0 \pm 1436$	39451 w	$\nu_0 \pm 2 \times 970 \pm 1436$
37632 w	$\nu_0 \pm 970 \pm 583$	39560 ms	$\nu_0 \pm 3 \times 970 \pm 583$

a shift of 469 cm⁻¹ of the ν_0 -band towards longer wavelengths. Evidently, the excited electronic state of the benzene ring is lowered by the influence of the intermolecular field created by the proximity of the COOCH₂CH(CH₃)₂-group. When the liquid is solidified and cooled to -180°C only a small shift of 76 cm⁻¹ in the position of ν_0 -band towards longer wavelengths takes place and except a slight sharpening of the bands the structure of the bands remains the same. This shows that no further change in the intermolecular field takes place with solidification.

TABLE IV

Absorption bands of iso-butyl benzoate in the liquid and solid states

Liquid at 24°C		Solid at -180°C	
Wave No. (cm ⁻¹) and intensity	Assignment	Wave No. (cm ⁻¹) and intensity	Assignment
35614 s	ν_0	35538 s	ν_0
36565 sb	$\nu_0 \pm 951$	36572 s	$\nu_0 \pm 974$
37512 wvb	$\nu_0 \pm 2 \times 951$	37484 mb	$\nu_0 \pm 2 \times 974$

The persistence of large width of the bands in the solid state indicates that the angular oscillations of the molecules responsible for the widening of bands in the case of the liquid persist at low temperatures. The results are similar to those obtained by Deb (1953) for other benzoic acid esters. Probably the presence of a long $\text{COOCH}_2\text{CH}(\text{CH}_3)_2$ substituent in the ring prevents the formation of additional virtual bonds between the benzene rings and consequently the ring is free to execute angular oscillations which are responsible for fluctuation in the intermolecular field even at low temperatures, thus causing a broadening of the bands.

ACKNOWLEDGMENT

The author is indebted to Professor S. C. Sirkar, D.Sc., F.N.I. for his kind interest and guidance during the progress of the work

REFERENCES

- Banerjee, S. B., 1956, *Ind. J. Phys.*, **30**, 106.
Deb, A. R., 1953, *Ind. J. Phys.*, **27**, 457.
Ghosh, D. K., 1954, *Ind. J. Phys.*, **28**, 191.
Sirkar, S. C. and Bisht, B. M., 1946, *Ind. J. Phys.*, **20**, 111.
Swamy, H. N., 1952, *Ind. J. Phys.*, **26**, 233.

EMISSION SPECTRA OF MIXED HALOGENS. PART II

IBr AND BrCl

P. B. V. HARANATH AND P. TIRUVENGANNA RAO

PHYSICS DEPARTMENT, ANDHRA UNIVERSITY, WALTAIR

(Received for publication August 21, 1956)

Plates VIII A & VIII B

ABSTRACT The emission spectra of IBr and BrCl, excited by the same electrical sources used as in the case of ICl, are photographed from the visible down to the vacuum ultraviolet. In the visible, unlike ICl, the spectrum of IBr revealed only a brief system of about 40 bands, in the region λ 3900 to λ 3800. The analysis of these bands has led to the following vibrational constants.

$$\omega_e' = 104.0 \text{ cm}^{-1}, \quad x_e' \omega_e' = 0.8 \text{ cm}^{-1}, \quad \omega_e'' = 140.0 \text{ cm}^{-1}, \quad r_e'' \omega_e'' = 1.9 \text{ cm}^{-1}, \\ r_e = 26076 \text{ cm}^{-1}.$$

The lower state of this system is identified as the $^3\Pi_1$ state of the infrared absorption bands of IBr. The spectrum of BrCl has revealed only six continuous diffuse bands in the region λ 3600 to λ 2500.

In the vacuum ultraviolet, the two systems, known earlier in absorption for each of these molecules, are recorded. In the case of IBr, some more bands have been newly obtained in emission and are assigned to the two systems.

The nature and properties of the new electronic states identified in ICl and IBr are discussed in relation to the term scheme of these molecules.

INTRODUCTION

In continuation of our work on the emission spectra of mixed halogen molecules, the spectra of IBr and BrCl are studied using the same two sources of electrical excitation, a condensed discharge from a 20 k.v. transformer and the high frequency discharge from a 100 watt oscillator, described previously in Part I. Reference to early work on these molecules, both in emission and absorption, has already been made in the earlier paper. In this communication, it is proposed to describe the results of investigation on the spectra of IBr and BrCl, and to discuss the nature of the electronic states of these mixed halogen molecules.

1. IODINE MONOBROMIDE

EXPERIMENTAL

Resublimed iodine crystals and liquid bromine are mixed in equal proportions to their atomic weights. The mixture is heated and the vapour is allowed to condense to give pure iodine bromide crystals which are dark grey in colour.

As a little excess of bromine is added, the crystals become liquified forming probably IBr_3 which is used in the present investigation.

The design of the discharge tube and the system of evacuating pumps are the same as those used for ICl , in each case when the spectrum is excited either in condensed discharge from a transformer or in a high frequency discharge from a high power oscillator. When the spectrum is excited in the condensed discharge, the same type of characteristic bluish glow, surrounding the intense line-like discharge giving rise to the atomic line spectra, is also observed in the case of IBr . The spectra are photographed on the same instruments as for ICl in the visible, quartz and vacuum ultraviolet regions.

RESULTS

The emission spectrum of IBr reveals a new system of about 40 bands lying in the region from $\lambda 3900$ to $\lambda 3800$ in addition to some of the bands belonging to the well known visible absorption systems of IBr above $\lambda 5000$. In addition to the bands, a number of atomic lines due to both bromine and iodine are also recorded on the plates. This new system is not so extensive as the one observed in ICl . As can be seen in Plate VIII A, some of the bands are diffuse while the others appear probably red degraded. Table I gives the band head data in the region $\lambda 3900$ to $\lambda 3800$. In the quartz ultraviolet region a few continuous bands are also observed. These are identical with some of those, reported by Asundi and Venkateswarulu (1947), in an uncondensed discharge through IBr vapour. In the vacuum ultraviolet region two systems lying between $\lambda 1975$ to $\lambda 1740$ are observed. These are found to be the same as those obtained by Cordes and Spomer (1932), in absorption. A few additional bands have been recorded in the present emission spectra.

The spectra excited both in high frequency discharge and in an uncondensed discharge from a transformer, are found to be quite similar. Photographs of the spectra reveal continuous bands in the visible and quartz ultraviolet regions and two discrete band systems in the vacuum ultraviolet, referred above.

VIBRATIONAL ANALYSIS

New system of IBr in the region $\lambda 3900$ to $\lambda 3800$

The general appearance of this system is shown in Plate VIII A. Unlike ICl bands, this system, however, does not appear to consist of bands belonging to long progressions or sequences. A wavenumber interval of 140 cm^{-1} , among some of the prominent bands of this system suggests the possibility of the lower state of this system as the $^3\Pi_1$ state of the visible absorption bands. The vibrational

analysis of the bands shown in Table II has led to the determination of the following approximate constants of the two states. The fact that $\omega_e' < \omega_e''$ is consistent with the red degradation of some of the bands.

TABLE I

Wave length	Wave number	Int.	Assignment v', v''	Wave length	Wave number	Int.	Assignment v', v''
3912.3	25553	2		3847.4	25984	7	6,4
3909.6	25571	2	3,5	3845.2	25990	6	2,1
3904.1	25601	2	2,4	3841.8	26022	4	5,3
3895.4	25664	2	0,2	3840.8	26029	5	
3889.0	25706	2		3839.4	26038	9	1,0
3884.9	25733	3	2,3	3836.2	26060	5	4,2
3880.2	25765	3	1,2	3833.9	26075	4	7,4
3878.0	25779	3		3830.6	26098	4	3,1
3875.0	25799	6	0,1	3828.3	26114	4	6,3
3871.8	25820	6	7,6	3825.9	26130	4	9,5
3870.4	25830	4	3,3	3824.7	26138	4	2,0
3866.9	25853	4	6,5	3822.3	26155	7	5,2
3865.0	25866	7	2,2	3819.1	26177	2	
3863.3	25877	5		3816.4	26195	1	4,1
3859.8	25901	8	1,1	3814.6	26208	1	7,3
3856.1	25926	4	4,3	3812.1	26225	3	
3854.5	25936	10	0,0	3808.4	26250	2	6,2
3853.4	25944	5	7,5	3806.5	26203	2	9,4
3852.2	25952	4		3804.0	26274	3	
3850.5	25963	3	3,2	3802.7	26290	2	

TABLE II

Vibrational analysis of IBr bands in the region $\lambda 3900\text{-}\lambda 3800$

v' \ v''	0	1	2	3	4	5	6
0	25936	25799	25664				
1	26038	25901	25765				
2	26138	25909	25866	25733	25601		
3		26098	25963	25830		25571	
4		26195	26060	25926			
5		26290	26155	26022	*		
6			26250	26114	25984	25853	
7				26208	26075	25944	25820
8					*		
9					26263	26130	

Note. The places marked with (*) are superposed by diffuse bands and hence their measurements are uncertain.

TABLE III

Intensity distribution in $\lambda 3900\text{-}\lambda 3800$ system of IBr

v' \ v''	0	1	2	3	4	5	6
0	10	6	2				
1	9	8	3				
2	4	6	7	5	2		
3		4	3	4		2	
4		1	5	4			
5		2	7	4			
6			2	4	7	4	
7				1	4	5	6
8							
9					2	4	

$$\omega_e' = 104.0 \text{ cm}^{-1}, \quad x_e' \omega_e' = 0.8 \text{ cm}^{-1}, \quad \omega_e'' = 140.0 \text{ cm}^{-1}, \quad x_e'' \omega_e'' = 1.9 \text{ cm}^{-1}, \\ \nu_e = 26076 \text{ cm}^{-1}.$$

The intensity distribution among the bands of this system is shown in Table III. The bands of maximum intensity are found to lie on a typical Condon para-

bola as in the case of ICl. The lower state of this system is identified as the $^3\Pi_1$ state of IBr. According to this analysis the position of the upper level is at $\nu 38306 \text{ cm}^{-1}$.

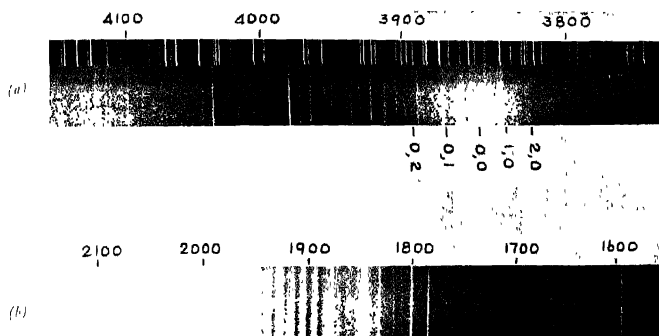
VACUUM ULTRAVIOLET SYSTEMS

These systems are reproduced in Plate VIII B. As in the case of ICl, some of the bands in these systems appear like absorption bands, probably due to self-absorption. The vibrational schemes proposed by Cordes and Sponer (1932), are extended to include some of the additional bands newly recorded in our present emission pictures. These schemes are shown in Tables IV and V, in which the bands marked with "*" are newly obtained and assigned. These two systems are analogous to those of ICl. The upper electronic levels of these two systems are interpreted by Mulliken (1934), as belonging to Ω_c, ω type of coupling, while the lower states of the two systems are identified as the ground state of IBr molecule.

TABLE IV
Vibrational analysis of IBr bands $\lambda 1975\text{--}\lambda 1840$

ν	0	1	2	3	
0	51701	51434	51169	50916	50658
1	52015	51745	51483	51224	50973
2	52315	52051	51784	51529	51359
3	52630	52371	52092	51843*	51562* 51294
4	52931	52666	52400*		51873* 51613*
5	53237	52967	52702	52427*	51648*
6	53533	53264	53000	52731*	52466*
7	53836*	53563	53291	53015	52754* 52500*
8	54148*	53879*	53602*		52798* 52531*
9			53911*	53362*	53083* 52551*
10				53952*	53697* 53416* 52851*
11				53996*	

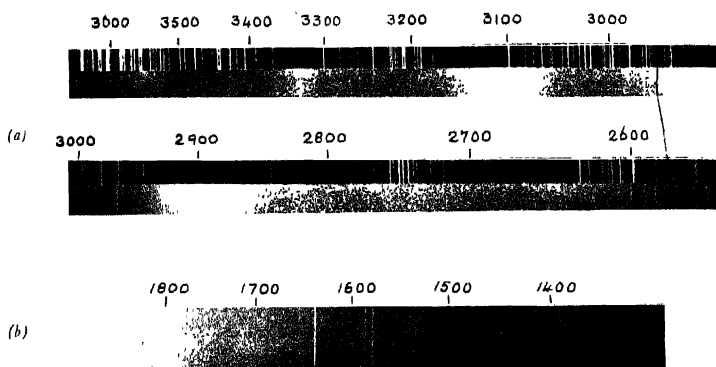
Note. Bands marked with "*" are newly obtained in the present work.



(a) Emission spectra of IBr excited in condensed transformer discharge (Fuss spectrogram)

(b) Vacuum ultraviolet bands of IBr (Grating spectrogram).

HARANATH & RAO



(a) Continuous emission bands of BrCl (Medium quartz spectrogram).
 (b) Vacuum ultraviolet bands of BrCl (Grating spectrogram).

TABLE V

Vibrational analysis of IBr bands in the region $\lambda 1840$ - $\lambda 1740$

ν''	0	1					6	7	8	9
0	56369	56101	55834	55574	55304*	55041*	54788*	54535*	54292*	
1	56673	56406	56158	55884						54354*
2	56970	56712	56449		55935*	55664*		55175*	54903*	
3	57274	57012								
4	57576	57306						55741*	55491*	
5	57875	57610	57336							
6				57369						

Note. Bands marked with "*" are newly obtained in the present work.

2. BROMINE MONOCHLORIDE

EXPERIMENTAL

Unlike ICl and IBr the preparation of a sample of BrCl is not possible as the substance is very unstable at the room temperature. Hence, the design of the discharge tube used in this case, is different from that of ICl and IBr. The tube, made of pyrex glass 30 cm. in length, 20 mm in diameter, is drawn out into an adaptor at one end. The other flat end is closed either with a quartz or a fluorite window. The adaptor is connected to a system of evacuating pumps through one or two liquid air towers as in the case of ICl and IBr. The main discharge tube has two side tubes in the middle. In the horizontal tube on which a heating coil is wound, chlorine is generated from cupric chloride. To the other side tube which is shorter and vertical, is connected a liquid bromine container by a pressure tubing. The pressure of bromine is adjusted by means of a pinch-cock, while that of chlorine is adjusted by regulating the current in the heating coil. When the pressures of chlorine and bromine are suitably adjusted, a characteristic intense bluish glow, different from the individual glows of bromine and chlorine, is observed. The spectra as excited both in a condensed discharge and in a high frequency discharge are photographed in the visible, quartz and vacuum ultraviolet regions employing the same instruments as before.

RESULTS

No discrete band system corresponding to those of ICl and IBr in the visible region is observed for BrCl. In the near ultraviolet, six continuous bands in the regions $\lambda 3600$ to $\lambda 3520$, $\lambda 3390$ to $\lambda 3300$, $\lambda 3190$ to $\lambda 3070$, $\lambda 2950$ to $\lambda 2825$, $\lambda 2750$ to $\lambda 2710$ and $\lambda 2605$ to $\lambda 2550$ are recorded on the plates taken on a medium quartz

instrument. These continuous bands are reproduced in two strips *a* and *b* in Plate VIII B. These bands are attributed to BrCl molecule as they do not bear any relationship with the diffuse bands of either bromine or chlorine. The occurrence of these diffuse bands in BrCl indicates the repulsive nature of some of the low lying excited states of this molecule.

In the vacuum ultraviolet region the emission spectrum of this molecule reveals the two vacuum ultraviolet systems lying in the region $\lambda 1720$ to $\lambda 1560$. These systems are identical with those previously reported in absorption by Cordes and Spomer (1932). These are reproduced in Plate VIII B, strip *c*.

ELECTRONIC STATES IN MIXED HALOGENS

The nature and properties of electronic states to be expected in the spectra of mixed halogen molecules were discussed by Mulliken (1934). Using atomic orbitals for the π electrons, the ground state configuration of ICl molecule can be written as

$$(3p\sigma_{\text{Cl}} + 5p\sigma_{\text{I}}, \sigma)^2 (3p\pi_{\text{Cl}})^4 (5p\pi_{\text{I}})^4 \quad \dots (1)$$

giving rise to the state $^1\Sigma^+$.

The lowest excited states can be obtained by suitable excitation of a π_1 electron to the σ^* antibonding orbital, thus

$$\sigma^2\pi^4_{\text{Cl}}\pi^3_1\sigma^* - ^1\Pi, ^3\Pi \quad \dots (2)$$

The well-known visible and near infrared absorption bands of ICl are attributed to transitions from the normal state to the $^1\Pi_0$ and $^3\Pi_1$ levels arising from configuration (2). These two states are also identified to be the upper states of similar systems in IBr. Above these the following two groups of states belonging to the two configurations are expected to lie higher in energy. Thus,

$$\sigma^2\pi^4_{\text{Cl}}\pi^3_1\sigma^* - ^1\Pi, ^3\Pi \quad \dots (3)$$

$$\sigma^2\pi^4_{\text{Cl}}\pi^2_1\sigma^{*2} - ^1\Sigma^+, ^1\Delta, ^3\Sigma \quad \dots (4)$$

From the term scheme of ICl proposed by Mulliken, these two groups of states are expected to have approximately the same height above the ground state. The states arising from configuration (3) are predicted by Mulliken to be repulsive in character, and transitions from ground state to these levels are explained by him as giving rise to the ultraviolet continua observed in ICl and IBr. The other group of states from configuration (4) are predicted to be stable dissociating into ions of type I^+ and Cl^- . The mean vertical energies of these states arising from configuration (4), above the ground state, are estimated as 4.8 e.v. in the case of ICl and 3.4 e.v. in the case of IBr.

According to the vibrational analysis proposed for the new systems observed in ICl and IBr, the lower state in each case is identified as the $^3\Pi_1$ state of the near infrared absorption bands arising from configuration (2). The heights of the upper levels above the ground state, in ICl and IBr are obtained as $\nu 37742 = 4.66$ e.v. and $\nu 38306 = 4.72$ e.v. respectively. It is reasonable to expect that the electronic terms responsible for these two states might arise from configuration (4). Since the upper level in IBr (4.72 e.v.) lies slightly higher in energy than that of ICl (4.66 e.v.) it is probable that the two upper levels may not belong to the same electronic term. The lower state involved being a $^3\Pi_1$ state, it is probable that the upper level in ICl may arise from $^3\Sigma^-$ term, while that in IBr may be a $^1\Sigma^+$ state, both arising from the same configuration. Thus in ICl the transition involved is

$$\sigma^2\pi^4_{Cl}\pi^2_I\sigma^{*2}, {}^3\Sigma^- - \sigma^2\pi^4_{Cl}\pi^3_I\sigma^*, {}^3\Pi_1$$

in which the type of coupling may belong to either case *A* or *B* or case *C*

In IBr the transition is

may be attributed to, as belonging, only case *C* type of coupling

Transitions from ground state $^1\Sigma^+$ of $\sigma^2\pi^4\pi^4$ to any of the above upper states $^1\Sigma^+$ or $^3\Sigma^-$ from the configuration $\sigma^2\pi^4\Pi^2\sigma^2$, are less likely to occur in absorption as the transition involves a two electron jump. This may probably explain the absence of these systems in the absorption spectra of ICl and IBr

For the vacuum ultraviolet band systems, the upper electronic levels are previously interpreted as $(X^+Y, {}^2\Pi_{3/2})\sigma^x - \Pi_{1,2}$ and $(X^+Y, {}^2\Pi_{1/2})\sigma^x - \Pi_{1,0}$ where *X* represents an iodine atom and *Y* represents either Cl or Br atom in the case of ICl and IBr and for BrCl, *X* represents a Br atom and *Y* represents a Cl atom. The lower state of these systems in the three molecules is identified as the ground state, while the upper states belong to the (Ω_c, ω) coupling type.

REFERENCES

- Asundi, R. K. and Venkateswarulu, P., 1947, *Ind. J. Phys.*, **21**, 76.
 Cordes, H. and Sponer, H., 1932, *Zeit. fur. Phys.*, **79**, 170.
 Haranath, P. B. V., and Tiruvenganna Rao, P., 1957, *Ind. J. Phys.*, **31**, 156.
 Mulliken, R. S. 1934, *Phys. Rev*, **46**, 549.

EXCITATION OF THE SPECTRUM OF THE SUNLIT AURORA

PRABHAT K. SEN GUPTA

DIRECTORATE OF METEOROLOGY, AIR HEADQUARTERS, NEW DELHI

(Received for publication February 13, 1957)

ABSTRACT. In the sunlit aurora certain features in its selective emission spectrum are known to be more intense as compared with the ordinary aurorae. The following mechanisms of the enhancement of these features in the selective emission spectrum of the sunlit aurora have been discussed:

- (i) Photoionisation of atmospheric constituents by solar ultra violet radiation followed by the action of the solar corpuscular stream and secondary reactions.
- (ii) Ionisation of atmospheric constituents by the solar corpuscular stream followed by resonance excitation by sunlight and secondary reactions.

As the particle density in the upper atmosphere at the high altitudes concerned is extremely small, neither process can adequately account for the intensities observed. This difficulty disappears, if we consider that there is an increase in concentration of secondary ions and recombined atoms in columns in the vicinity of the earth's magnetic lines of force. Of the two mechanisms the first one is considered more likely.

I INTRODUCTION

1.1. Of the various forms in which the aurorae are manifested, the rays or streamers have been known to reach the highest altitudes. As a rule most of the ordinary auroral forms, viz., arcs, bands, draperies etc., have bases in the region of 100 Kms., and tops rarely exceeding 300 Kms. The bases of the rays are, however, situated at higher altitudes and tops are also much higher than those of the ordinary aurora. In particular, when the upper regions of the atmosphere are illuminated by the light of the sun (which may be about 20° below the horizon) the auroral rays situated at the highest altitudes seem to become fully exposed. Stormer(1929) who was the first to observe the phenomenon found that the sunlit auroral rays reach as high as 1100 Kms. At the boundary of the earth's shadow separating the sunlit aurora from the aurora in the dark atmosphere below, the aurora appears to become divided. This feature is particularly noticeable in the case of some individual rays, the upper part of which lies in the sunlit region and the lower part in the shadow, with a section missing in between at the boundary of the earth's shadow.

1.2 According to the generally accepted view, the impact of fast corpuscular streams from the sun is responsible for the development of the aurora. The corpuscular stream consists of positive ions and electrons, which together make the

stream neutral in character (Chapman, 1950). The Doppler displacement towards the violet of the H_{α} line (Gartlein, 1951; Vegard, 1952, Memel, 1951) of the aurora shows that protons form the bulk of the positive ions of the corpuscular stream. On approaching the earth, these charged particles are guided by the terrestrial magnetic field towards the auroral zones following more or less direct trajectories, and give rise to the ordinary forms of the aurora. But the rays or streamers are characterised by their alignment to the earth's magnetic lines of force, round which the charged particles spiral and give rise to the cylindrical structure. Vegard (1939) has shown that the angle made by the trajectories with the lines of force determines the depths up to which such helical trajectories penetrate and then turn back. A returning spiral is fully developed provided the energy of the particles has not already been spent up in ionisation and excitation. The spiral trajectory also accounts for the high bases of the auroral rays, as the incident charged particles have to traverse a longer path along the spiral and come to a stop at higher altitudes compared to others following a straight path.

1.3. The rays have diameters of the order of several kilometres, but some are quite narrow with diameters of the order of 300-400 metres (Vegard, 1939). For a spiral trajectory, we get the same order for the radius r , as given by the expression

$$r = mvc/eH$$

where H = intensity of the magnetic field

m = mass of the particle

e = charge

and v = component of velocity normal to H

At an altitude of 200 Kms. in the auroral regions, taking $H = .45$ Gauss, $v = 10^8$ cm/sec for incoming protons, and $m = 1.65 \times 10^{-24}$ gm, r comes out as 230 metres. The electrons rotate in the opposite sense and their orbits have much smaller radii.

1.4. The sunlit aurora is generally greyish-violet in colour due to the admixture of enhanced red auroral lines with the green auroral line of atomic oxygen. At times the enhancement of the first negative bands of nitrogen imparts a blue colour to these rays. The absolute values of intensities of auroral features are not available, but an idea can be formed from the visual estimates of brightness as given by International Coefficients (Mitra, 1952a) which have been classified into four types, I to IV corresponding to the brightness of the Milky Way increasing to that of the full moon. The sunlit aurora belongs to the more intense categories. At λ 3914, of the negative bands at high altitudes, Seaton (1954) has estimated an emission rate of the order of 5×10^{11} photons per square centimetre column in the line of sight per second or $5 \times 10^{11}/10^5 = 5 \times 10^6$ photons $\text{cm}^{-2} \text{sec}^{-1}$, considering emission taking place from rays of 1 Km thickness. The order for the red auroral lines of atomic oxygen will not be much different. For comparison, it may be

mentioned that the absolute intensity of the green auroral line of the night sky light corresponds to only 4×10^8 transitions per cm^2 column per second.

2. ENHANCEMENTS IN SELECTIVE EMISSION SPECTRUM OF THE SUNLIT AURORA.

2.1. In this paper it is proposed to discuss only the main spectral features which get enhanced in the sunlit aurora. Compared to the green line $\lambda 5577$ (S^1-^1D) of atomic oxygen, the enhancements of the following have been reported.

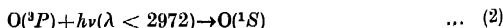
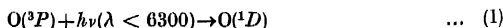
(i) Red lines, $\lambda\lambda 6300, 6363$ ($^1D-^3P$) of atomic oxygen.

The enhancement is considerable (up to 8 times)

(ii) First negative bands $N_2^+(A')-N_2^+(X')$ of nitrogen. The enhancement is up to 6 or 7 times.

The green line $\lambda 5577$ may either weaken (Störmer, 1929) or remain unaffected. The appearance of the negative bands and a similar enhancement of the red auroral lines of atomic oxygen have also been observed in the spectrum of the night sky during "Twilight Flash", when the atmosphere around 100 Km is illuminated by the sun during the morning or evening twilight. Although illumination by the sun is mainly responsible for the enhancements of some of the bands and lines in both cases, the mechanisms which give rise to the excitation and enhancement cannot be comparable; the sunlit aurora is a phenomenon occurring in rather tenuous atmosphere where de-excitation processes are negligible, but the twilight flash occurs in lower and denser atmosphere where de-excitation processes play a prominent part. It has also to be noted that the sunlit aurora is not a day-to-day feature like the twilight flash, and is manifested only during occasions of auroral activity.

2.2. The enhancements in the spectrum of the sunlit aurora have been generally attributed to a simple resonance effect. According to Bates (1949), in the case of resonance excitation of the negative bands, the photon emission even at high altitudes is quite sufficient to account for the observed intensity. In view of the uncertainty in the density of N_2^+ ions and the radiative lifetime of the $N_2^+(A')$ state, it is proposed to examine first the behaviour of the red lines, which show the effect to a much greater extent. For resonance excitation, we have the following processes :



from which the omission of the red and green auroral lines follow. For these processes the number of transitions per illuminated particle per second has been calculated by Bates and Massey (1946) from the expression

$$(\omega_a / \omega_n) \tau^{-1} e^{-h\nu / kT} \cdot f$$

where, ω_e, ω_n = the statistical weights of the excited and ground states

τ = is the radiative lifetime

ν = the frequency of the exciting radiation

$T = 6000^\circ\text{K}$, the temperature of the sun as a black body

and f = dilution factor, 5.44×10^{-5}

The number of transitions/illuminated atom/sec have been given as follows :-

Red lines..... 7×10^{-10}

Green line..... 3×10^{-11}

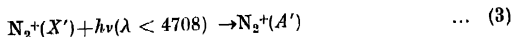
Thus at any height the red lines would be about 20 times more intense than the green line, if excited by resonance. Multiplying the figure given above for red lines, with the values of density we give below the number of photons emitted per cm^3 per sec. for a few representative altitudes.

TABLE I
 $^1D \rightarrow ^3P$ of oxygen

Altitude Kms	Density of oxygen atom/ cm^3 (Mitra, 1952b)	Number of photons emitted per cm^3 per sec
100	1.09×10^{12}	763.0
200	1.75×10^{10}	12.3
400	1.08×10^8	.076
600	8.49×10^6	.006

At high altitudes the photon emission reduces to an extremely small value, but actually we find that high sunlit rays have an emission rate of the order of 10^6 photons $\text{cm}^{-3} \text{sec}^{-1}$ (section 1). Therefore, unless we assume that the density of oxygen atoms increases by several orders of 10 at the regions concerned, the resonance effect utterly fails to account for the observed intensities in the aurora.

2.3. For the resonance excitation of the first negative bands of nitrogen, as suggested by Wulf and Deming (1938), prior presence of $\text{N}_2^+(X')$ ions is assumed in the process,

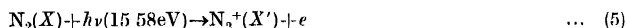
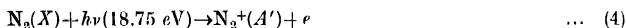


At high altitudes of the sunlit rays, the presence of the $\text{N}_2^+(X')$ ions could only be accounted for by the impact of the charged corpuscles on the nitrogen molecules present there. Now, the particle densities at these altitudes vary from 10^8 to 10^6 cm^{-3} (vide Table 1) of which nitrogen molecules form a small fraction, and the number of N_2^+ ions resulting from bombardment by charged particles still smaller.

On the whole, there will be hardly 10^2 cm^{-3} of such ions at these altitudes. But Seaton (1954) estimated from the intensities of the negative bands of sunlit aurora, that the number of N_2^+ ions are of the order of $2 \times 10^7 \text{ cm}^{-3}$. Thus we again find that the concentration of the particles in the region should be considerably higher to account for the observed intensities

3. MECHANISM OF EXCITATION OF THE SPECTRUM

3.1. Any suggestion as regards the mechanism of excitation of the spectrum of the sunlit aurora has to take account of the fact that the phenomenon occurs only during occasions of auroral activity and that the presence of sunlight in the upper regions of the atmosphere is also necessary. Of the main atmospheric gases, atomic oxygen and in smaller proportion molecular nitrogen form the principal constituents at the altitudes concerned ($\sim 300 \text{ Km}$). Atomic nitrogen is also known to exist, but in rather small quantities. In the region of the sunlit aurora, ultraviolet light of the sun is capable of causing photo-ionisation as follows,



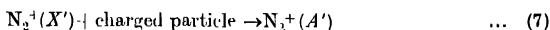
Process (4), first proposed by Saha (1937) to explain the excitation of the first negative bands in the twilight flash holds possibilities for the sunlit aurora also. Assuming that the sun radiates like a black body at 6000°K , the number of solar quanta whose energy exceeds 18.75 eV , entering the earth's atmosphere per cm^2 per sec. is only 7.4×10^4 . Therefore to account for the total ion formation, Saha suggested that the solar ultraviolet light of wavelength $< 660 \text{ \AA}$ (that is, $h\nu > 18.75 \text{ eV}$) is about 10^6 times more intense, thus raising the yield of solar quanta to about $10^{10} - 10^{11}$ per sec. If each photon produces one ion on meeting a molecule, there should be 10^{10} to 10^{11} ions formed per cm^2 column per sec, provided there are as many molecules. At the high altitudes under consideration, however, the density of nitrogen molecules is much smaller (about $1.93 \times 10^6 \text{ cm}^{-3}$ as given by Mitra, 1952b). Therefore, the number of ions formed through photo-ionisation will be too small to account for the observed intensity of the bands. The solution of this problem apparently lies in finding out if there is any mechanism which increases the concentration of the particles at these altitudes to the right values.

In section 1, we have drawn attention to the action of earth's magnetic field in making the incident charged particles spiral round the line of force. The secondary ions from the processes (4) to (6) are also expected to behave in the same manner and cluster round individual lines of force. At the heights under consideration, the temperature is of the order of 1000°K and thermal velocity about 2 Km/sec .

Taking the velocity of ions normal to H as 1 Km/sec (Mitra and Banerjee, 1939), and $H = .45$ and $.32$ Gauss respectively at 200 Km and 1000 Km, we get the radius of the spiral ranging from 1.8×10^2 to 4.5×10^2 cm. If we consider that individual magnetic lines of force draw ions from a distance of 1 Km or so, it follows that in the vicinity of the lines of force, the concentration of ions increases by a factor, $(1 \text{ Km/spiral radius})^2 = 10^6$ to 10^8 nearly. Thus at the high altitudes if we get normally 10^6 to 10^8 ions per cm^3 by photo-ionisation, the concentration of ions in narrow cylinders round the lines of force becomes of the order of 10^{12} to 10^{14} per cm^3 .

3.3. The $\text{N}_2^+(A')$ ions resulting from process (4) will be guided towards the magnetic lines of force in the above manner, but unless the radiative life time is high, all the excited ions will revert to the ground state $\text{N}_2^+(X')$ by the time the ions concentrate round the lines of force. Otherwise we would see the sunlit aurora every day like the twilight flash. Thereafter further excitation will depend upon the action of the solar corpuscular stream in association with secondary reactions on days of auroral activity as follows

- (i) Initial excitation by charged particles :



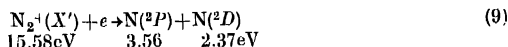
which yields the first negative bands.

- (ii) Radiative recombination with electrons of the corpuscular stream or secondary electrons ,



There may be excited oxygen atoms also. Bates and Massey (1949) have suggested a coefficient $1.5 \times 10^{-12} \text{ cm}^3. \text{ sec}^{-1}$ for this reaction. The value may be much higher, say, $10^{-8} \text{ cm}^3. \text{ sec}^{-1}$ in the denser columns of ions (round individual lines of force).

- (iii) Dissociative recombination (Bates, 1949, Mitra 1952c) :



taking the heat of dissociation of nitrogen as 9.76eV.

- (iv) Two-body collisions between the oxygen and nitrogen atoms from (8) and (9) :



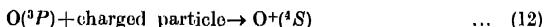
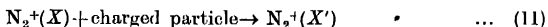
which yields the red forbidden lines of atomic oxygen due to the transition $^1D-^3P$. It may be seen that sufficient energy is not available to excite the green line $^1S-^1D$ (4.17eV) of oxygen by collision of the second kind,

Normally at the high altitudes under consideration recombinations and collisions are rather infrequent, but it has to be borne in mind that above reactions take place in the vicinity of the lines of force, where the concentration has been shown to be high enough to make recombination and collision processes significant.

3.4. The proposed reactions take place in the sunlit regions of the aurora. As we descend towards the base (at the boundary of the earth's shadow) in denser conditions, the oblique rays of the sun passing through the regions of ozone and oxygen absorption have their extreme ultraviolet portions comprising the ionising photons cut off. Hence, the processes (4) to (6) cease to operate and the denser columns of N_2^+ and O^+ ions do not form. In fact, the whole series of reactions (4) to (10) stop functioning. This is most probably the reason why the auroral rays appear to be missing near the shadow line. Further downwards, in the dark atmosphere, the excitation of the aurora takes place in the normal manner. It is beyond the scope of this paper to discuss the excitation processes in the ordinary aurora.

3.5. We may now consider an alternative mechanism in which the initial ionisation is brought about by corpuscular bombardment followed by resonance excitation by sunlight as follows.

(i) Corpuscular bombardment :



(ii) Charge transfer due to encounter with incoming protons:

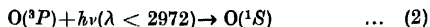
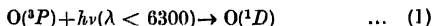
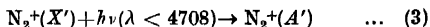


As mentioned in section 3, the ions resulting from (10), (11) and (12) will spiral round the individual lines of force and increase the concentration by about a million times. Thereafter we have the following reactions in the vicinity of the lines of force.

(iii) Radiative recombination :



(iv) Resonance excitation by solar radiation :



The reactions (1), (2) and (3) have been advocated by Wulf and Deming (1938), Bates, (1949), and Mitra (1952d). It has, however, been already shown that in

the tenuous conditions of the regions of the sunlit aurora, adequate photon emission through resonance excitation is not possible unless the concentration of the particles takes place as discussed in section 3.

In the resonance mechanisms (1) and (3) the visible photons of the solar radiation take the most important part. Considering the fact that the visible radiation is capable of penetrating through the boundary of the earth's shadow down to lower altitudes the resonance mechanism is unable to explain why a portion of the auroral rays is found to be completely missing at the shadow line.

R E F E R E N C E S

- Bates, D. R., 1949, *Proc. Roy. Soc. A.*, **196**, 562.
 Bates, D. R. and Massey, H. S. W., 1946, *Proc. Roy. Soc. A.*, **187**, 261.
 Chapman, S., 1950, *J. Geophys. Res.*, **55**, 361.
 Gartlein, C. W., 1951, *Nature*, **167**, 277.
 Meinel, A. B., 1951, *Rep. Prog. Phys.* **14**, 121.
 Mitra, S. K., 1952a, "The Upper Atmosphere" (Asiatic Society of Bengal, Calcutta,) p. 421.
 " 1952b, *Ibid.* p. 582
 " 1952c, *Ibid.* p. 441.
 " 1952d, *Ibid.* p. 442.
 Mitra, S. K. and Banerjee, A. K., 1939, *Ind. J. Phys.*, **13**, 107.
 Saha, M. N., 1937, *Proc. Roy. Soc. A.*, **160**, 155.
 Seaton, M. J., 1954, *J. Atm. Terr. Phys.* **4**, 285.
 Stormer, C., 1929, *Zeit. f. Geophysik*, **5**, 177.
 Vogard, L., 1939, "Terrestrial Magnetism and Atmospheric Electricity" (Edited by J. A. Fleming). McGraw Hill. p. 573.
 " 1952, *Geophys. Publ.* **18**, No. 5.
 Wulf, O. R., and Deming, L. S., 1938, *Terr. Mag. Atm. Elec* **43**, 283.

Letters to the Editor

The Board of Editors will not hold itself responsible for opinions expressed in the letters, published in this section. The notes containing reports of new work communicated for this section should not contain many figures and should not exceed 500 words in length. The contributions must reach the Assistant Editor not later than the 15th of the second month preceding that of the issue in which the Letter is to appear. No proof will be sent to the authors.

8

A NEW PARTICLE ACCELERATOR

YATENDRA PAL VARSHNI

DEPARTMENT OF PHYSICS, ALLAHABAD UNIVERSITY, ALLAHABAD

(Received for publication, February 1, 1957)

Within a few years of the construction of the first cyclotron, it was realized (Bethe and Rose, 1937) that it will not be possible to accelerate ions by means of the cyclotron beyond a certain limit on account of the relativistic increase in mass of the accelerated particles at high velocities and the consequent departure from resonance.

In 1945 McMillan (1945, 1946) and Veksler (1945, 1946) proposed to overcome this difficulty by varying the frequency of the accelerating potential and/or the magnetic field. This led to the construction of synchrocyclotron and electron and proton synchrotrons. In recent years interest is growing on Alternate Gradient Focusing (Livingston 1954, Courant *et. al* 1952, Christofilos 1950).

The present letter suggests a new method that overcomes the relativistic limitation to accelerations by means of cyclotrons by changing the shape of the dees.

The essential principle can be explained as follows (see figure 1):

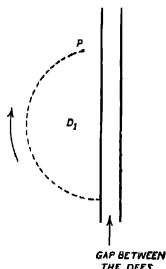


Fig. 1.

Consider the motion of a particle, in a cyclotron, having energy in a region where relativistic effects become important, and is just getting out of phase with the accelerating potential on the other dee D_2 . Let its position in such a situation be P (the effect has been exaggerated in the diagram). Then it is obvious that if it had not to traverse the remaining distance in the dee D_1 it would have been accelerated in the right phase. This can be achieved by changing the shape of the dees. The proposed shape is shown in figure 2. With such a shape of the dees, the

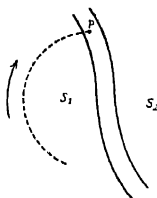


Fig. 2.

particle will be further accelerated in the right phase. During its motion in S_2 there will be a further lag which is compensated in a similar manner by S_1 , and so on. Thus the particle will always arrive in the gap between the dees after exactly equal time intervals. Ultimately the dees will be spiral shaped as shown in figure 3 (only $1\frac{1}{2}$ revolutions of the spirals have been shown; there may be many more). It may be noted that the dees spiral in the direction opposite to the direction of motion of the particle.

Let

$E_0 = m_0 c^2$ rest energy of the particle

$T =$ Kinetic energy

$e =$ Charge of the particle

$B =$ Magnetic field

$r =$ Radius of the path of the particle.

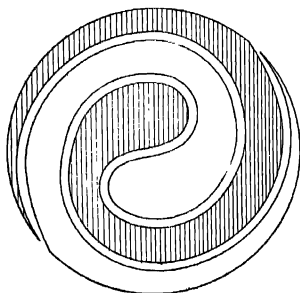


Fig. 3.

Then the angle ϕ made by the particle inside a dee after each acceleration is given by

$$\phi = \frac{\pi}{1 + T/E_0} \quad \dots (1)$$

and the radius r is determined by the equation

$$T^2 + 2TE_0 = c^2 e^2 B^2 r^2 \quad \dots (2)$$

Knowing ϕ and r from equations (1) and (2), the exact shape of the spiral dees can be calculated.

This accelerator will have the advantage that, unlike synchrocyclotron and synchrotron which have a low average ion output (about 1% of the conventional cyclotron), it will give the average output of the same order as a cyclotron.

The suggested accelerator may be called the "Spiratron" (short form of Spiralotron.).

The slanting nature of the spiratron dees may lead to greater radial oscillations of the particle than in the case of cyclotron. This can be countered by the well-known technique of using radially decreasing field:

$$B = B_0(r_0/r)^n \quad \dots (3)$$

where $0 < n < 1$. Equation (2) would be accordingly modified. Such a field provides restoring forces for radial displacements. A high dees voltage would also be helpful in minimising radial oscillations. The details of the focusing conditions are being studied.

ACKNOWLEDGMENT

The author is thankful to Prof. K. Banerjee for his kind interest in the work.

REFERENCES

- Bethe, H. A. and Rose, M. E., 1937, *Phys. Rev.*, **52**, 1254.
 Christofilos, N., 1950, Focusing system for Ions and Electrons and application in Magnetic Resonance Particle Accelerators (Privately printed report).
 Courant, E., Livingston, M. S. and Snyder, H., 1952, *Phys. Rev.*, **88**, 1190.
 Livingston, M. S., 1954, High Energy Accelerators, Interscience Publishers, New York.
 McMillan, E. M., 1945, *Phys. Rev.*, **68**, 143.
 McMillan, E. M., 1946, *Phys. Rev.*, **69**, 534.
 Veksler, V. I., 1945, *J. Phys. U.S.S.R.*, **9**, 153.
 Veksler, V. I., 1946, *Phys. Rev.*, **69**, 244.

9. THE ULTRAVIOLET ABSORPTION SPECTRA OF *o,m,p*-FLUOROiodo-AND BROMOCHLOROBENZENES

S. L. N. G. KRISHNAMACHARI

PHYSICS DEPT. ANDHRA UNIVERSITY, WALTAIR

(Received for publication, April 11, 1957)

In continuation of the work on the ultraviolet absorption spectra of *o,m,p*-fluorochloro and fluorobromobenzenes (author, 1955, 1956), the ultraviolet absorption spectra of *o,m,p*-fluoriodo and bromochlorobenzenes are investigated in the vapour state. The fluoriodobenzenes were kindly presented by Dr. G. C. Emger of the Illinois State Geological Survey and the bromochlorobenzenes were prepared by the author adopting the procedure suggested by Hartwell (1944) for the ortho and meta compounds and that suggested by Fry and Grote (1926) for the para compound. The earlier work on these compounds relates to that of Conrad-Billroth (1936) who studied the ultraviolet absorption spectra of *p*-fluoriodo and *o,m,p*-bromochlorobenzenes in hexane solution, and of Dima and Tintea (1940) who studied the vapour absorption spectrum of *p*-bromochlorobenzene. The latter authors identified only three frequencies in the upper state.

The experimental set up employed was described in the previous reports. In the case of the fluoriodobenzenes the absorption spectra consist of a few diffuse patches in each case, which repeat with approximately 900, 950 and 1000 cm^{-1} intervals in the ortho, meta and para compounds respectively, the one lying on the longest wavelength side (0, 0 band of the system) being at 36670, 36600 and 35820 cm^{-1} for the three compounds in the above order. In the case of the bromochlorobenzenes the absorption spectra consist of a large number of discrete bands. The absorption spectra of the *o,m,p*-compounds resemble those of the corresponding isomers of dichlorobenzene (Sponer, 1942) and Anno and Matubara, 1955). The characteristic features of the absorption spectra are given in Table I and the correlation between the ground and excited state frequencies and their assignments are given in Table II.

For all the six molecules, the long wavelength edge of the continuous absorption spectrum on the lower wavelength side (below 2150 Å) was also observed,

TABLE I

Characteristic features of the ultraviolet absorption of *o*, *m*, *p*-bromochlorobenzenes

	Region of absorption	Number of bands	0, 0 band	Prominent $v-v$ separations	Nature of the electronic transition
Ortho	2850-2600A	120	36178cm	63 cm	A'-A'
Meta	2850-2500A	100	36120cm	66cm	A'-A'
Para	2900-2550A	100	35691cm	23 cm	A ₁ B ₁

TABLE II

Ground and excited state frequencies of *o*, *m*, *p*-bromochlorobenzenes

	Raman data		U.V. abs. data		Assignment
	$\Delta\nu$	Int ρ	Ground	Excited	
Ortho	(Author)		(Author)		
	142 vs, b	.90	—	77 vw	C-Br nonplanar bending
	165 s, sh	.85	166	121 w	C-Br planar bending
	281 ms, sh	.65	282	196 mw, d	C-C-C planar bending
	441 ms, d	.20	—	416 ms, sh	C-Br stretching
	645 s, sh	.30	648	688 m, sh	C-Cl stretching
	1036 vs	.10	1039	955 s, sh	C-C stretching
	1122 s	.20	—	1034 m, sh	C-H planar bending
	1161 ms, sh	.85	—	1069 ms, sh	
Meta	1570 s	.90	—	1481 mw, d	C-Cl stretching
	(Author)				
	167 vs, b	.90	—	96 w, d	C-Br nonplanar bending
	205 s, d	.90	—	181 w, d	C-Br planar bending
	301 vs, sh	.40	—	287 mw, d	C-C-C planar bending
	421 s	.55	430	378 mw	C-Br stretching
	654 s, vsh	.45	654	664 mw, d	C-Cl stretching
	995 vs, sh	.15	996	960 vs, sh	C-C stretching (breathing)
Para	1101 ms, sh	.20	—	1075 s	C-H planar bending
	(Paulsen, 1939)				
	260 (4)	.25	—	223 mw	C-C-C planar bending
	335 (0, 0)	.65	—	283 m	C-Br stretching
	625 (1 $\frac{1}{2}$)	.83	632	526 m	C-C-C planar bending
	733 (5)	.54	735	711 ms	C-Cl stretching
	1087 (6)	.12	1002	1022 vs	C-C stretching
	1168 (1 $\frac{1}{2}$)	.33	—	1056 s	C-H planar bending
	1569 (3b)	.77	—	1409 s	C-C stretching

ACKNOWLEDGMENT

The author wishes to express his grateful thanks to Dr. Finger for the gift of the fluoro compounds. The author is deeply indebted to Prof. K. R. Rao for his kind and valuable guidance.

REFERENCES

- Krishnamachari, S. L. N. G., 1955, *Ind Jour Phys.*, **29**, 603
 ———, 1956, *ibid*, **30**, 151.
 ———, 1956, *ibid*, **30**, 487.
 Conrad-Billroth and Forster, 1936, *Zest Fur. Phy. Chem.* **33**, 311.
 Hartwell, 1944, *Org. Synth*, **24**, 22.
 Fry and Grote, 1926, *J Am Chem Soc.*, **48**, 711.
 Dima and Tinten, 1940, *Bull. Ser. Sci Acad. Rou*, **23**, 34.
 Sponer, 1942, *Rev Mod. Phys*, **14**, 224.
 Anno and Matubara, 1955, *J. Chem Phys*, **23**, 796
 Paulsen, 1939, *Monatsch. Chem* **72** 224

BOOK REVIEW

TECHNIQUES GENERALES DU LABORATOIRE DE PHYSIQUE—By J. Surugue, Vol. I, 2nd Edition (In French). Pp. 671. Centre National de la Recherche Scientifique, 13, Quai Antole-France, Paris 7, 1955, Price 2,400.00 Francs.

As pointed out by Professor Frederic Joliot Curie, N. L. in the Preface this volume gives some information collected by various workers regarding the worth and convenience of different experimental methods by practical experience and published in scientific literature. This book consists of ten chapters written by different authors. The first chapter, dealing with general principles of construction of scientific apparatus, is written by H. Gondet. The second chapter on principles of glass blowing is written by Ch. Amate. In the third Chapter J. Surugue has discussed the vacuum technique. The fourth chapter written by G. Ribaud and A. Moutet deals with production and measurement of high temperature. The fifth chapter on general technique used in optical laboratories is written by A. Arnulf. The sixth chapter written by G. Dupuy deals with light sources and light filters. The seventh chapter by A. Lallemand and M. Munsch deals with photoelectric cells. Chapter VIII dealing with methods of registering is written by H. Gondet. In Chapter IX, M. Demontvignier has discussed various methods of regulation and rectification of voltage and current. The last chapter written by K. R. Huchet covers 134 pages and deals with electric circuits and vacuum tubes. Unlike other chapters, the last chapter includes almost exhaustive theoretical discussions about nature of wireless signals and functions of various parts of wireless circuits.

The language in which the book is written will limit its usefulness, but those engaged in experimental research work in a physical laboratory will no doubt find a store of useful information in this volume.

S. C. S.

A NOTE ON THE VALIDITY OF THE REVISED ROTATIONAL STRUCTURE CONSTANTS OF GREEN-YELLOW SYSTEM OF VO BANDS

N. R. TAWDE AND N. SREEDHARA MURTHY

DEPARTMENT OF PHYSICS, KARNATAK UNIVERSITY, DHARWAR

(Received for publication, October 24, 1956)

ABSTRACT. The intensity distribution of the green-yellow system of VO bands and the transition probabilities studied in terms of the revised rotational structure constants recently announced by Lagerqvist and Selin have proved the untenability of the old constants of Mahanti and the validity of the revised ones. This has been verified from the standpoint of asymmetry of molecules and internuclear separations in electronic states of the band systems of analogous oxides AlO, BO and TiO.

Tawde and Chandratreya (1955) have recently reported some results on asymmetry effect in Hutchisson's theory of transition probabilities by investigating the intensity distribution as a function of mass asymmetry in bands of some analogous oxides AlO ($A^2\Sigma^+ - X^2\Sigma^+$), BO ($B^2\Sigma^+ - X^2\Sigma^+$), TiO ($C^3\Pi - X^3\Pi$) and VO (green-yellow system). This study involved the use of accurate vibrational and rotational analyses constants of the band systems chosen for the molecules. In that paper a very serious misfit of results of VO with other band systems is noticed in respect of the conclusions drawn, regarding the mass asymmetry on transition probabilities. Chandratreya (1953) also had drawn pointed attention to VO, showing its anomaly with respect to other oxides studied in the above series. The anomaly or misfit is in respect of the expected magnitude of agreement of theoretical predictions with experimental results, depending on the asymmetry of the molecule. While $Ti^{48}O^{16}$ with its mass asymmetry 3.0 (defined here as the ratio of the heavier to the lighter atomic mass in the molecule) gave 33% agreement, the molecule $V^{51}O^{16}$ with comparable mass asymmetry 3.2 gave only 17% agreement. The latter should have been generally of the same order as in TiO.

It is now possible to explain this anomaly in the light of the recent revision, by fresh analysis, of the rotational structure constants of VO, by Lagerqvist and Selin (1955). As a result of this revision,* the new constants take the following magnitude (Table 1) against the old ones of Mahanti (1935).

* In a private communication to this laboratory, Dr. Lagerqvist informs that the transition ${}^2\Delta - {}^2\Delta$ of VO (green-yellow system), as reported in their advance announcement of the revision of the structure analysis, may not sustain as a result of their further investigation. The final detailed paper of Dr. Lagerqvist is expected to be out sometime hence.

TABLE I

VO state	Mahanti	Lagerqvist & Selin
Upper r_e'	2.033 Å	1.67 Å
Lower r_e''	1.890 „	1.59 „
Δr_e	0.143 „	0.08 „

The transition probabilities of this system have been recalculated, using the new rotational constants of Lagerqvist and Selin by Hutchisson's (1930) theory and verified at the same time by Manneback's (1951) easier technique. The following Table II gives these calculations, side by side with the earlier data (under Mahanti's constants) and the experimental derivations by Tawde and Chandratreya (1955).

TABLE II

Band ν' ν''	Transition probabilities			Band ν' ν''	Transition probabilities		
	Theoretical		Experimental		Theoretical		Experimental
	Old constants (M)	New constants (L. & S)			Old constants (M)	New constants (L. & S)	
0,0	0.11	<i>0.34</i>	<i>0.35</i>	1,4	0.10	0.15	0.31
0,1	0.27	<i>0.34</i>	<i>0.36</i>	1,5	(0.50)	0.08	(0.61)
0,2	0.67	0.20	0.45	2,0	0.56	<i>0.20</i>	<i>0.23</i>
0,3	0.98	0.09	0.48	2,1	0.26	<i>0.20</i>	<i>0.17</i>
0,4	0.48	0.03	0.20	2,2	0.00 ₁	0.11	0.40
1,0	(0.34)	<i>0.40</i>	(<i>0.41</i>)	2,4	(0.26)	0.10	(0.24)
1,1	0.43	0.00 ₂	0.06	2,5	0.07	0.16	0.39
1,2	0.32	<i>0.12</i>	<i>0.14</i>	3,1	0.04	0.29	0.41
1,3	0.02	0.20	0.51	4,4	0.16	0.11	0.25

Note: (i) M - Mahanti; (L & S) - Lagerqvist and Selin.

(ii) Pairs of values in italics and in parenthesis are to be considered close for agreement respectively in the relevant columns.

It is evident that agreement between the theory and experiment with the use of new constants, goes up from 3 bands under the old constants to 6 bands under the new ones in the whole set of 18 bands measured, thus causing the percentage to increase from 17 to about 33, the same as in TiO as one should

expect. Thus the anomaly indicated disappears. It shows that the old constants were largely in error and supports the correctness of the new analysis of Lagerqvist and Selin. Herzberg (1950), too, had made a note expressing doubt about the earlier analysis of the band system and this doubt now stands verified from the independent considerations of intensity aspects presented through the change from old to revised constants.

Tawde and Chandratreya (1956) have shown another instance of misfit of VO in the intensity distribution, in its dependence on the internuclear separations in the two states of the system. This misfit also disappears on adopting the new constants. The earlier state of affairs and the new situation are given below (Table III) in relation to TiO system which stands comparable with VO in difference in respect of the internuclear separations Δr_e as given by the new analysis.

TABLE III

	TiO	VO	
Δr_e in Å	0.075	0.08 (New)	0.143 (Old)
Percentage agreement	33	33	17

These results on the TiO and VO also fit in fairly well with the other band systems investigated, viz., BO and AlO, except for the incompatibility of the parabola (i.e. its width and disposition) in its dependence on Δr_e . While Δr_e (with the new constants of VO) increases in the order AlO (0.049), TiO (0.075), VO (0.08) and BO (0.1065), the parabola width and the axis change systematically in the order AlO, TiO, BO and VO according to the findings of Chandratreya (1953). That means VO does not keep adjacent to TiO, as it should, from considerations of transition probabilities and asymmetry. Except for this slight incompatibility, the results, in general, favour the untenability of the old constants and the validity of the revised ones from the various independent aspects examined here.

ACKNOWLEDGMENT

One of the authors (N.S.M.) acknowledges his gratitude to the Ministry of Education, Government of India, for the award of a Senior Research Training Scholarship which enabled him to participate in this particular piece of work in the general programme in hand.

REFERENCES

- Chandratroya, P. V., 1953, Ph.D. Thesis (Physics), University of Bombay.
- Herzberg, G., 1950, Molecular Spectra and Molecular Structure, 2nd Edn. P. 579, D. Van Nostrand Co., New York.
- Hutchisson, E., 1930, *Phys. Rev.*, **36**, 410.
- Lagerqvist, A. and Sohn, L. E., 1955, *Naturwissenschaften*, **42**, 65. (Sc. Abs. (Phys.) Abs. No. 4517, 1955).
- Mahanti, P. C., 1935, *Proc. Phys. Soc., Lond.* **47**, 433
- Mannaback, C., 1951, *Physica*, **17**, 1001.
- Tawde, N. R., and Chandratroya, P. V., 1955, *Ind. J. Phys.*, **29**, 388.
- Tawde, N. R., and Chandratroya, P. V., 1956, *Jour. Kar. Univ.*, **1**, 74.

RAMAN SPECTRA OF ISOMERIC PICOLINES IN DIFFERENT STATES AND IN SOLUTIONS OF ETHYL ALCOHOL AT DIFFERENT TEMPERATURES

G. S. KASTHA

OPTICS DEPARTMENT, INDIAN ASSOCIATION FOR THE CULTIVATION OF SCIENCE,
JADAVPUR, CALCUTTA-32

(Received for publication, April 29, 1957)

Plate IX

ABSTRACT. The Raman spectra of α - and γ -picoline and of their solutions in alcohol at different temperatures in liquid and solid states have been investigated and the results have been compared with those obtained by previous workers for benzene, pyridine and toluene in different states. It has been observed that when these compounds are solidified and cooled to -180°C a few new low-frequency Raman lines appear in each case, but they disappear when the molecules are dispersed in frozen ethyl alcohol. Some of the prominent Raman frequencies of both the molecules are found to increase with dissolution of the liquids in alcohol and also with solidification in the case of α -picoline. On comparing these results with those reported earlier for toluene, it has been concluded that the low-frequency lines are produced not by ordinary lattice field but by small groups of molecules present in the crystals. Assignment of some of the prominent Raman frequencies has been made and it has been concluded that the average C-C bond strength in the pyridine ring increases with the substitution of a hydrogen atom by CH_3 group, with dissolution in alcohol and with solidification.

INTRODUCTION

The Raman spectra of pyridine and its solutions in ethyl alcohol at different temperatures and in different states were investigated recently (Kastha, 1956b). It was observed that the four new Raman lines of low frequency-shifts, which appear in the spectrum due to the pure crystals at -180°C , are replaced by a moderately strong band with a frequency shift of 95 cm^{-1} in the case of 38% and 56% frozen solutions of pyridine in alcohol. Similar results were obtained in the case of 81% frozen solution of toluene in alcohol, but when the concentration was reduced to 35% the band at 95 cm^{-1} spread out into a continuous wing. Biswas and Sirkar (1957) observed that when 81% solution of toluene in ethyl alcohol is frozen, the frozen mass is amorphous and also the number of frozen-in cybotactic groups of toluene molecules is very small in comparison with that in the pure liquid. It was concluded from these results that the low-frequency Raman

lines originate from vibrations in associated groups of molecules formed in the pure substances in the solid state and the disappearance of these lines in the case of molecules of the substances dispersed in rigid glass at -180°C is due to the breaking up of these associated groups. The new band at 95 cm^{-1} was thus due to groups formed by the association of toluene molecules with alcohol molecules in the frozen solutions and not due to any crystalline substance. The results obtained with pyridine were also explained on the same hypothesis. In the case of solutions of pyridine in alcohol in the solid state, the formation of pyridine-alcohol complex may be due to the linking of a non-bonding electron of the nitrogen atom with the hydroxyl group of a neighbouring alcohol molecule (Kastha, 1956b).

It would be of interest to extend the investigations to methyl-pyridines (picolines) which are expected to behave like pyridine, because these molecules possess in the ring a nitrogen atom with non-bonding electrons. With this object in view the Raman spectra of α - and γ -picoline and their solutions in ethyl alcohol at different temperatures both in liquid and solid states have been investigated and the results have been compared with those of similar investigations with pyridine and toluene. An attempt has been made to assign the frequencies observed in the spectra due to α - and γ -picoline to the different vibrational modes of the ring. All these results have been discussed in the present paper.

EXPERIMENTAL

Chemically pure samples of α - and γ -picoline were procured from some German firms and were further purified by distillation under reduced pressure. Ethyl alcohol purified in the same way was used as the solvent. The Raman spectra of the pure liquids, of their 25% solutions in ethyl alcohol in the liquid state at 25°C and in the solid state at -180°C were photographed in the same way as in the case of frozen solutions of toluene in ethyl alcohol (Kastha, 1956a). The spectra of pure α - and γ -picoline in the solid state and of 70% solution of γ -picoline in alcohol at -180°C were also photographed using the usual arrangement. A Fuess spectrograph having a dispersion of 11 \AA/mm in the region 4047 \AA and Ilford Zenith plates were used for photographing the Raman spectra.

RESULTS AND DISCUSSION

Spectrograms showing the low frequency Raman lines due to α - and γ -picoline in the solid state at -180°C in the region 4047 \AA are reproduced in enlarged forms in figures 1(a) and 2(a), Plate IX. Spectrograms of the corresponding regions for the frozen 25% solutions of α - and γ -picoline in alcohol are reproduced in figures 1(b), 2(b), Plate IX respectively. The line at 810 cm^{-1} due to the molecules has also been included in the spectrograms for comparison of intensities.

The Raman frequencies for α - and γ -picoline in the liquid state at 25°C and in the solid state at -180°C together with those for the 25% solutions of these compounds in alcohol at different temperatures are given in Tables I and II. The Raman frequencies for pure toluene in the solid state at -180°C have also been included in each table for comparison. In the case of solutions the lines due to the solvent have been excluded. The Raman frequencies observed in the case of α -picoline agree well with those reported by Bonino *et al* (1933) while those for γ -picoline are most probably reported for the first time. These latter frequencies are found to agree with those deduced from the infra-red absorption curve of γ -picoline reproduced by Barnes *et al* (1944).

(a) *Assignment of some of the Raman lines*

It can be seen from Tables I and II that there are great similarities between the spectra of the methyl pyridines and toluene. If the methyl group is treated as a single atom then toluene and γ -picoline both have the symmetry C_{2v} . Pitzer and Scott (1943) have assigned all the frequencies observed in toluene to different vibrational modes in the molecule and have compared these modes with those of the benzene molecule. Similar assignments can be made of the corresponding lines observed in the two substituted pyridine compounds. A comparison of the frequencies in picolines with those obtained in toluene suggests that the lines at 542 and 630 cm^{-1} of α -picoline and the corresponding frequencies 518 and 672 cm^{-1} due to the γ -compound may be assigned to the two modes arising from the e_{2g} vibration of frequency 606 cm^{-1} in the benzene molecule. In either case the smaller frequency may be attributed to that component of the e_{2g} vibration of the benzene ring which is symmetric to the C_2 axis while the higher frequency may belong to the component antisymmetric to the C_2 axis. In the former mode all the atoms in the ring are displaced, whereas, in the latter mode two diametrically opposite atoms remain stationary. The frequency 672 cm^{-1} observed in the case of γ -picoline due to the anti-symmetric mode indicates a larger value of the average C—C bond strength in the ring in comparison with that in the benzene ring. In the case of α -picoline the frequency of this mode is 630 cm^{-1} probably because the heavier nitrogen atom takes part in the displacements. As regards the mode symmetric to the two-fold axis of symmetry mentioned above the situation in γ -picoline is similar to that in toluene except that in the former case there are displacements in opposite directions of a nitrogen atom at the end of a diameter and of a C—CH₃ group at the other end in place of a carbon atom and a C—CH₃ group respectively in these two positions in the toluene molecule. The frequency observed is 520 cm^{-1} in both the case probably because the effect of larger bond strength in the γ -picoline molecule is compensated for by the heavier mass of nitrogen atom. In the case of α -picoline there is a carbon atom at the corner opposite to C—CH₃ group as in the toluene molecule but the larger value of the C—C bond strength increases the frequency of the symmetric

mode to 542 cm^{-1} in the former case. So, these frequencies in the two picolines definitely indicate a larger value of the average C—C bond strength in the ring of the picolines. In the case of pyridine also there are two frequencies at 652 cm^{-1} and 603 cm^{-1} respectively and those may also be attributed to the antisymmetric and symmetric components of the ϵ_{2g} mode mentioned above. In this

TABLE I

 α -Picoline $\Delta\nu$ in cm^{-1}

Liquid α -picoline at 25°C	Solid α -picoline	25% solution in alcohol		Solid toluene at -180°C (Ray, 1950)
		25°C	-180°C	
Continuous wing extending upto 100 cm^{-1}	45 (2) 70 (2) 97 (4)	Continuous wing extending upto 100 cm^{-1}		47 (2) 66 (2) 86 (1) 108 (2) 127 (0)
213 (2b)	216 (1)	212 (2b)	212 (2)	220 (2)
542 (3)	550 (2)	550 (4)	550 (3)	520 (2)
630 (1)	634 (0)	633 (1)	633 (1)	623 (2) 788 (5)
810 (3)	811 (4) 987 (1)	810 (4)	810 (4)	
998 (10)	1005 (5)	1010 (6)	1010 (6)	1005 (10)
1051 (10)	1057 (5)	1053 (6)	1053 (6)	1033 (4)
1239 (3)	1241 (2b)	1240 (3)	1240 (2)	1217 (3)
1298 (1)	1298 (1)			
1380 (2)	1382 (1)	1382 (1)	1382 (1)	1380 (2)
1571 (2)	1572 (2)	1572 (2)	1572 (2)	1592 (3)
1595 (2)	1595 (2)	1595 (2)	1595 (2)	1608 (3) 2865 (0b)
2928 (4)	2928 (6) 2960 (1) 3030 (1)	Other Raman lines in this region have been overlapped by lines due to the solvent		2921 (5) 2980 (0)
3054 (8)	3060 (8)			3030 (3) 3060 (8)
3066 (8)				

TABLE II

 γ -Picoline $\Delta\nu$ in cm^{-1}

Liquid γ -picoline at 25°C	Solid γ -picoline at -180°C	25% solution in alcohol		Solid toluene at -180°C (Ray, 1950)
		25°C	-180°C	
Continuous wing extending upto 100 cm^{-1}	65 (0b) 110 (6)	Continuous wing extending upto 100 cm^{-1}		47 (2) 66 (2) 86 (1) 108 (2) 127 (0)
219 (2)	219 (0)	2190 (0b)	219 (0b)	220 (2)
352 (0)				
518 (2)	518 (0)	523 (2)	523 (1)	520 (2)
672 (3)	673 (2)	673 (2)	673 (2)	623 (2)
812 (5)	812 (4)	810 (4)	813 (3)	788 (5)
	973 (0)			
995 (8)	995 (6)	1005 (6)	1010 (6)	1005 (10)
1060 (0)	1070 (1)			1033 (4)
1224 (4b)	1225 (3)	1224 (1b)	1224 (0b)	1217 (3)
1383 (1)	1383 (0)	1383 (1)	1384 (0)	1380 (2)
1570 (1)	1570 (0)	1570 (0)	1571 (0)	1592 (3)
1608 (3)	1610 (2)	1612 (3)	1612 (3)	1608 (3)
				2865 (0b)
2928 (4b)	2926 (3)	Other Raman lines in this region have been overlapped by lines due to the solvent		2921 (5)
3038 (1)	3038 (1)			2980 (0)
3052 (6b)	3054 (6)			3030 (3)
				3060 (8)

case also the average C-C bond strength is larger than that in benzene ring and less than that in the ring of the picolines. Incidentally, it might be pointed out that Kohlrausch (1935) assigned the frequency 603 cm^{-1} to the symmetric mode but did not assign the line at 652 cm^{-1} which is totally depolarised.

It is observed that in the Raman spectra of both the picolines in the liquid state, there is a line with frequency-shift about 995 cm^{-1} which is slightly higher

than, the frequency of the breathing vibration of the benzene ring. Evidently, the motion of the CH_3 group in the ring during the breathing vibration of the ring compensates for the increased value of the C-C bond strength and the frequency remains almost the same. However, the frequency is slightly higher in the case of α -picoline than in the case of γ -picoline. This difference is apparently due to the different positions of the heavy CH_3 group with respect to the nitrogen atom in the two molecules

Similar arguments will show that in the case of toluene also the C-C bond strength in the ring is greater than that in the benzene ring. Thus the results due to picolines indicate that the C-C bond strength in the picolines is slightly larger than that in toluene and much larger than that in benzene.

The Raman frequency 810 cm^{-1} , which is observed in the spectra due to both the picolines, may be due to a mode corresponding to e_{1u} mode of the benzene ring which has a frequency of 1030 cm^{-1} . As the line is intense it cannot be assigned to the mode b_{1u} of benzene of frequency 1010 cm^{-1} .

The e_{2g} mode involving only C-C stretching of frequency 1586 cm^{-1} in the benzene ring splits up into two equally strong components at 1575 and 1595 cm^{-1} in the case of α -picoline in the liquid state but in the case of γ -picoline these two components are at 1570 and 1608 cm^{-1} respectively, the former component being much weaker than the latter.

It can be seen from Tables I and II that in place of the two Raman frequencies 1051 and 1239 cm^{-1} of α -picoline, γ -picoline shows two lines at 1060 and 1224 cm^{-1} respectively. In the former case the two lines are evidently due to the two modes corresponding to the two components of the e_{2g} mode of benzene of frequency 1178 cm^{-1} in which both stretching of the C-C bond and bending of the C-H bond are involved. One of these increases to 1239 cm^{-1} in α -picoline and to 1224 cm^{-1} in the γ -picoline molecule because the C-C bond strength is larger in these molecules. The heavier CH_3 group in place of the H-atom lowers the frequency of the other components to about 1055 cm^{-1} in both the molecules. In the case of γ -picoline, however, the line due to the latter component has a very small intensity.

As pointed out by previous workers (Pitzer and Scott, 1943) the line in the region 216 cm^{-1} is also observed in the case of toluene and it is due to the mode corresponding to the a_{2u} mode of benzene. Similarly, the faint line at 352 cm^{-1} due to γ -picoline is due to a mode corresponding to a component of the e_{1u} mode of benzene in which both stretching and bending of C-H bond are involved. In this case the heavier CH_3 group lowers the frequency enormously.

As regards the mode corresponding to one of the components of e_{2g} mode of benzene in which only C-H stretching is involved, the C- CH_3 group in place of CH group may reduce the frequency to about 1220 cm^{-1} in γ -picoline as in

the case of toluene (Pitzer and Scott, 1943). This line is then superposed on the line at 1224 cm^{-1} mentioned above to produce a broad band. The line due to the other component is probably superposed on the line 3052 cm^{-1} making the line broad in the case of γ -picoline and in the case of α -picoline it is at 3054 cm^{-1} being just resolved from the line 3060 cm^{-1} due to the totally symmetric C-H stretching oscillation.

It can be seen from Table I that the molecular frequency at 998 cm^{-1} observed in the spectrum due to α -picoline in the liquid state shifts to 1010 cm^{-1} in the case of the 25% solution in alcohol at 25°C , and when the solution is frozen and cooled to -180°C no further shift in the position of this line is observed. In the case of the γ -compound, however, it is found that the line at 995 cm^{-1} due to the pure liquid shifts to 1005 cm^{-1} in the case of the 25% solution in alcohol at 25°C and the line further shifts to 1010 cm^{-1} when the solution is frozen at -180°C (Table II). These changes in the breathing vibration of the ring in the case of both the compounds indicate the influence of a strong perturbation acting on the ring. This perturbation may be due to formation of complexes through the linking of a non-bonding sp^2 electron of the nitrogen atom in the ring of the picoline molecule with an OH group of a neighbouring alcohol molecule in the solution. It appears that the formation of such complexes increases the average C-C bond strength in the ring.

(b) *Molecular frequencies at -180°C*

A comparison of the Raman frequencies given in Table I for α -picoline in the liquid and solid states shows that the frequencies at 542 , 630 , 998 and 1051 cm^{-1} observed in the spectrum due to the liquid shift to 550 , 634 , 1005 and 1057 cm^{-1} respectively when the liquid is solidified and cooled to -180°C . Also, the line at 3054 cm^{-1} of the liquid probably merges into the line at 3060 cm^{-1} in the solid state. Moreover, two new frequencies at 987 and 2960 cm^{-1} appear in the spectrum of the pure solid at -180°C . No such changes are observed in the case of γ -picoline excepting the appearance of a very weak new line at 973 cm^{-1} in the spectrum of the pure crystal. This line is much weaker than the corresponding line at 987 cm^{-1} observed in the case of α -picoline. These two lines may originate from the b_{1u} mode of frequency 1010 cm^{-1} in benzene. Though this mode is forbidden in the Raman spectrum of benzene, it may appear in the Raman spectra of the picolines in the solid state if the rings are distorted in the crystals owing probably to the formation of some virtual linkages through the non-bonding electrons of the nitrogen atom. Such a bond formation would increase slightly the C-C bond strength and the increase in frequencies of the vibration corresponding to the a_{1g} and e_{2g} modes of benzene mentioned above with the solidification of the liquids may be due to such an increase in the bond strength. As pointed out earlier, substitution of the CH_3 group in the pyridine molecule increases some of the frequencies only in the case of α -picoline but not in the case of γ -picoline.

So, even if there is formation of virtual bonds in γ -picoline. So, even if there is a formation of virtual bonds in γ -picoline with solidification not much change is expected to occur in the molecular frequencies of γ -picoline.

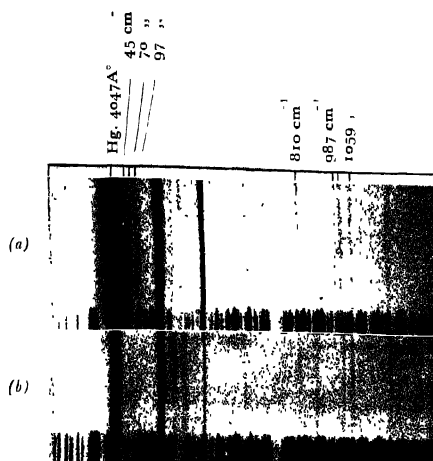
(c) *Low-frequency Raman lines at $-180^{\circ}\text{C}.$*

In the case of α -picoline (figure 1a, Plate IX) three new lines with frequency shifts 45, 70 and 97 cm^{-1} appear when the liquid is frozen and cooled to $-180^{\circ}\text{C}.$ The line at 97 cm^{-1} is strong, its intensity being equal to that of the molecular line at 811 cm^{-1} . In the case of γ -picoline in the solid state at -180°C only two lines are observed at 65 and 110 cm^{-1} respectively (figure 2a, Plate IX). Of these, the line at 110 cm^{-1} is stronger than the line 65 cm^{-1} and also than the molecular line at 811 cm^{-1} . In this connection it would be interesting to compare the number of low-frequency Raman lines observed in the case of benzene, pyridine, methyl pyridines and toluene in the solid state at $-180^{\circ}\text{C}.$ These data are given in Table III, from which it can be seen that the number of low-frequency Raman lines in pyridine is less than that in benzene though they have identical molecular structures and also probably belong to the same crystal system.

TABLE III
Low frequency lines at -180°C

Compounds	$\Delta \nu, \text{ cm}^{-1}$				
Benzene (Sirkar & Ray, 1950)	47 (1)	53 (2)	78 (5)	95 (11)	134 (3)
Pyridine (Kastha, 1956b)		58 (3)	82 (3)	97 (3)	137 (1)
Toluene (Ray, 1950)	47 (2)	66 (2)	86 (1)	108 (2)	127 (0)
α -picoline	45 (2)	70 (2)	97 (4)		
γ -picoline		65 (0b)		110 (4)	

Methyl pyridines which have structures similar to that of toluene yield lesser number of Raman lines than toluene. On the other hand, crystals of toluene at -180°C produce the same number of low frequency lines as benzene at the same temperature. These facts show that the lines cannot be due to angular oscillations in the lattice, because they are not very much dependent on the moment of inertia of the molecule but their number depends on the symmetry of the substituted ring. In the case of pyridine the non-bonding electrons of the nitrogen atom make the ring different from the benzene ring. So only four low-frequency lines are observed in the spectrum due to the crystals of pyridine. On the other hand, results due to the frozen solutions of picolines in ethyl alcohol show that the low-frequency lines disappear when the molecules are dispersed in rigid glass



Fig

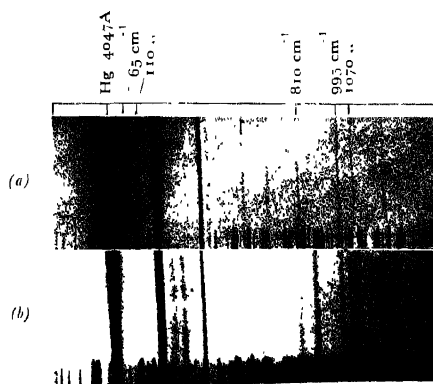


Fig 2.

Raman spectra of picolines

Fig. 1. (a). α -Picoline in the solid state at -180°C Fig. 1. (b). 25% Solution of α -picoline in ethyl alcohol at -180°C Fig. 2. (a). γ -Picoline in the solid state at -180°C Fig. 2. (b). 25% Solution of γ -picoline in ethyl alcohol at -180°C

(figures 1b and 2b, Plate IX). Hence the lines are produced by groups of molecules of picolines. The lines are absent even in the case of 70% solution of γ -picoline in alcohol at -180°C . In this rigid glass there are almost as many picoline molecules as alcohol molecules. So the formation of bonds between the nitrogen atom and the OH group seems to be the cause of producing a rigid glass even at 70% concentration and of the disappearance of the low-frequency lines. Comparing these results with those due to the frozen solutions of toluene (Kastha, 1956a) it is found that it is only small groups of molecules and not crystallites which produce those low-frequency lines.

ACKNOWLEDGMENT

The author is indebted to Professor S. C. Sirkar, D.Sc., F.N.I., for his interest and guidance throughout the progress of the work.

REFERENCES

- Barnes, R. B., Gore, R. C., Liddel, U. and Williams V. Z., 1944 *Infrared Spectroscopy* (Reinhold Publishing Corporation), p. 96.
Biswas, G. S. and Sirkar, S. C., 1957, *Ind. J. Phys.*, **31**, 141.
Bonino, G. B. and Manzoni-Ausideri, 1933, *Mem. Acad. Bologna*, **1**, 1-
Kastha, G. S., 1956a *Ind. J. Phys.*, **30**, 313,
.. 1956b, *Ind. J. Phys.*, **30**, 519.
Kohlrausch, K. W. F., 1935, *Z. f. Phys. Chem.*, **303**, 305-315.
Pitzer, K. S. and Scott, D. W., 1943, *J. Am. Chem. Soc.*, **65**, 803.
Ray, A. K., 1950, *Ind. J. Phys.*, **24**, 111.
Sirkar, S. C. and Ray, A. K., 1950, *Ind. J. Phys.*, **24**, 189.

FORCE CONSTANTS FOR LIKE MOLECULES ON EXP-SIX MODEL FROM THERMAL CONDUCTIVITY

K. P. SRIVASTAVA

INDIAN ASSOCIATION FOR THE CULTIVATION OF SCIENCE, CALCUTTA- 32

(Received for publication, April 25, 1957)

ABSTRACT The Chapman-Enskog theory of non-uniform gases has been utilised in determining the force parameters for some simple non-polar molecules on exp-six model from the observed variation of thermal conductivity with temperature. The method used is an adaptation of the Keenan and Lennard-Jones procedures and has been applied to neon, argon, krypton and xenon. First the parameter α is fixed up and then translations are carried out to determine the parameters ϵ/k and r_m . To test the adequacy of the model, both the equilibrium and non-equilibrium properties of gases have been computed by utilising these experimentally determined potential parameters and the results compared with the observed values over an extensive range of temperatures. The agreement between theory and experiment is found to be quite satisfactory, showing thereby the adequacy of the exp-six model and the appropriateness of the potential parameters used.

INTRODUCTION

Various expressions for the intermolecular potentials have been formulated for calculating the transport properties of fluids. Amongst these, the Lennard-Jones 12-6 model and the modified Buckingham exponential-six model are quite realistic and are consequently widely used, the latter being written in the more convenient form

$$\phi(r) = \frac{\epsilon}{1 - 6/\alpha} \left[\frac{6}{\alpha} e^{\alpha(1-r/r_m)} - \left(\frac{r_m}{r} \right)^6 \right]$$

where $\phi(r)$ is the potential energy existing between the two molecules at a separation distance r , ϵ is the depth of the potential energy minimum, r_m is the separation distance for this energy minimum and α is the parameter which is the measure of the steepness of the repulsion energy. In this potential model, the leading repulsion energy term is described by an exponential form and has better theoretical justification. Recently, Mason (1954) has evaluated the transport property collision integrals for this model and has used them for the determination of potential parameters for a few gases from experimental virial coefficient, viscosity and crystal data. The determination of potential parameters from the property of thermal diffusion will be the most accurate due to its greater sensitivity towards this property, but its usefulness is limited by the difficulty of obtaining accurate experimental data. All the other transport properties are almost equally

sensitive and any one of them can be preferred to the other for the determination of potential parameters depending on the reliability of the experimental data. Generally viscosity data are used for this purpose but unfortunately this cannot be done for krypton and xenon due to lack of sufficient experimental data. Recently, Kannuluk and Carman (1952) have made an extensive and accurate determination of the coefficient of thermal conductivity for some monatomic gases over a large range of temperature and this enables us to utilise this property for the determination of potential parameters. In the present paper we have utilised the observed temperature dependence of thermal conductivity to evaluate the force parameters, for the gases neon, argon, krypton and xenon. To test the correctness of the force constants obtained, both equilibrium and non-equilibrium properties of gases have been calculated and compared with their experimentally observed values.

DETERMINATION OF THE POTENTIAL PARAMETERS

Several different methods are available for the determination of potential parameters from the experimental measurements on compressibilities or transport properties. The method we have used is an adaptation of the Keesom (1912) and Lennard-Jones (1924) procedures and has been more recently utilised by Mason and Rice (1954) for the evaluation of the force constants for a few nonpolar gases on the exp-six model. Srivastava and Srivastava (1957), and Srivastava, (1957) utilised this translation method for determining the force parameters of some binary gas mixtures from the temperature dependence of thermal diffusion factor. Here we have used this method for determining the force parameters of some monatomic rare gases from the observed variation of thermal conductivity with temperature. From Chapman and Enskog theory, the third approximation to the coefficient of thermal conductivity $[\lambda]_3$ of a pure monatomic gas can be written in practical units in the form

$$10^7 \lambda = \frac{1989.1 T^{1/2} f_{\lambda}^{(3)}(\alpha, T^*)}{M^{1/2} r_m^2 \Omega^{(2,2)*}(\alpha, T^*)}, \quad \dots (1)$$

where λ is the thermal conductivity in $\text{cal-cm}^{-1}\text{-sec}^{-1}\text{deg}^{-1}$, M is the molecular weight, r_m is in angstroms, and $f_{\lambda}^{(3)}(\alpha, T^*)$ and $\Omega^{(2,2)*}(\alpha, T^*)$ are dimensionless functions of kT/ϵ and α and have been tabulated by Mason (1954). It is convenient to put

$$T^* = kT/\epsilon, \quad \dots (2)$$

where T^* is called the reduced temperature

Taking logarithms of equations (1) and (2) we obtain

$$\log \frac{10^7 \lambda M^{1/2}}{T^{1/2}} = \log \frac{f_{\lambda}^{(3)}(\alpha, T^*)}{\Omega^{(2,2)*}(\alpha, T^*)} - 2 \log r_m + \log 1989.1 \quad \dots (3)$$

$$\text{and } \log T = \log T^* + \log(\epsilon/k), \quad \dots (4)$$

A plot of the theoretical tabulated quantities $\log [f_{\lambda}^{(3)}(\alpha, T^*)/\Omega^{(2,2)*}(\alpha, T^*)]$ versus $\log T^*$ will give different curves for different values of α , over one of which the plot of the experimental quantities $\log [10^7 \lambda M^{1/2}/T^{1/2}]$ versus T can be superposed by suitable parallel translation of the axes. The amount of translations along the T^* and λ axes determine respectively $\log \epsilon/k$ and $\log r_m$.

In practice, this method can be successfully applied to such gases only which have a sharp bend in the experimentally plotted curves. Hence the gases selected are neon, argon, krypton and xenon. Three or four points are selected on the bend and tangents are drawn at these points of the experimental curve and lines parallel to these tangents are projected on the various theoretical curves so that they may be tangent to them at some point. To determine which theoretical curve would best overlap, the variation of $\log T$ with $\log [10^7 \lambda M^{1/2}/T^{1/2}]$ at any selected point of the experimental curve was calculated for different arbitrary changes in $\log [10^7 \lambda M^{1/2}/T^{1/2}]$. This variation was also calculated for all its corresponding points on the different theoretical curves. The variations in the two cases will be equivalent. That particular theoretical curve was chosen for which the change in T^* is the same as the change in T for the experimental curve. This fixes the parameter α and the necessary translations along the axes will give ϵ/k and r_m .

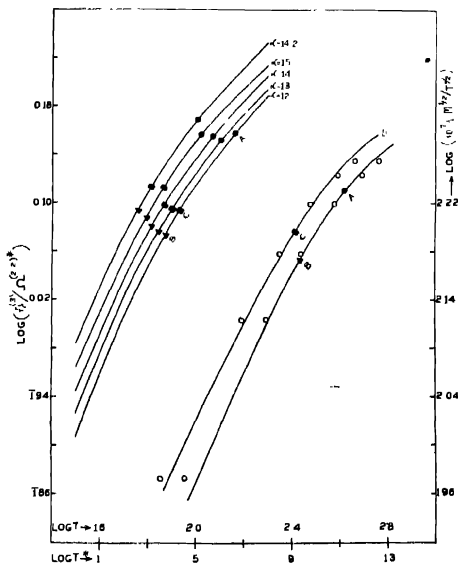


FIG. 1. Theoretical $\log f_{\lambda}^{(3)}/\Omega^{(2,2)*}$ versus $\log T^*$ and experimental $\log (10^7 \lambda M^{1/2}/T^{1/2})$ versus $\log T$ graphs. The curve marked D has been arbitrarily displaced sideways by 0.1

The recent measurements of Kannuluik and Carman (1952) on the thermal conductivity for five rare gases have been utilised for evaluating the force parameters. In figure 1, the experimental and theoretical curves corresponding to the plot of $\log [10^7 \lambda M^3/T^4]$ versus T and the plot of $\log f_{\Lambda}^{(3)}(\alpha, T^*)/\Omega^{(2,2)*}(\alpha, T^*)$ versus T^* are shown for the case of argon. To avoid uncertainty in the drawing of the experimental curve, two different curves 1(a) and 1(b) are drawn from the same set of experimental points and are arbitrarily displaced to prevent overlapping. Theoretical curves are plotted for $\alpha = 12, 13, 14, 15$ and for a few intermediate values where necessary. The curves for $\alpha = 13, 14$ and 15 are displaced upwards by .02, .04 and .06 respectively. A, B and C are the three selected points on the experimental curve and their corresponding points are determined on each theoretical curve by projecting parallel tangents. From each of these projected points, ordinates $y = 15, 20, 25$ small divisions are drawn and from the foot of these ordinates, distances drawn parallel to the x -axis so as to reach the theoretical curves are read. The corresponding value of x for the experimental curve for that y value is noted. Next for a particular point, a graph connecting r and α is plotted for each fixed value of y and the exact value of α corresponding to the x value on the experimental curve is found from each of the plots and mean α taken.

Thus having fixed the value of α , the theoretical curve of $\log [f_{\Lambda}^{(2)}(\alpha, T^*)/\Omega^{(2,2)}(\alpha, T^*)]$ versus T^* corresponding to this value of α is plotted. Points A, B and C are fixed up on this theoretical curve in the way described above and translations carried out to give average c/k and r_m . The values of the force parameters for all the four gases are collected in Table I along with those obtained by Mason and Rice (1954b) from other properties. It is seen that there is marked difference in the force parameters for krypton and this may be the reason why his values of the force parameters for this gas are unable to reproduce all the transport properties satisfactorily.

TABLE I

Exp-six potential parameters for some simple nonpolar molecules

Gas	Parameters determined by the author			Parameters determined by Mason & Rice		
	α	$\epsilon/k^\circ K$	$r_m \text{ \AA}$	α	$\epsilon/k^\circ K$	$r_m \text{ \AA}$
Ne	14.6	36.7	3.157	14.5	38.0	3.147
Ar	14.2	125.5	3.800	14.0	123.2	3.866
Kr	13.1	135.5	4.365	12.3	158.3	4.056
Xe	13.0	235.8	4.575	13.0	231.2	4.450

COMPARISON WITH EXPERIMENT

To test the adequacy of the exp-six model and the accuracy of the experimentally determined potential parameters, it is necessary to see how far these parameters can successfully predict the equilibrium and non-equilibrium properties.

Viscosity. The values of viscosity for different gases were calculated from the potential parameters of Table I, using the formula

$$10^7 \eta = \frac{266.93 (MT)^{1/2} f_{\eta}^{(3)}(\alpha, T^*)}{r_m^2 \Omega^{(2,2)*}(\alpha, T^*)} \quad (5)$$

where η is the viscosity in gm cm⁻¹ sec⁻¹, M is the molecular weight, r_m in angstroms, and $f_{\eta}^{(3)}(\alpha, T^*)$ and $\Omega^{(2,2)*}(\alpha, T^*)$ are dimensionless functions tabulated by Mason (1954). These are compared with experimentally determined values and are given in Table II.

TABLE II
Viscosity of gases ($\eta \times 10^7$ in gm. cm⁻¹ sec⁻¹)

Temp. °K	Neon		Argon		Temp. °K	Krypton	
	$\eta_{\text{Obs.}}(a)$	$\eta_{\text{Calc.}}$	$\eta_{\text{Obs.}}(a)$	$\eta_{\text{Calc.}}$		$\eta_{\text{Obs.}}(d)$	$\eta_{\text{Calc.}}$
80	1198	1193	688	661	273.2	2334	2357
100	1435	1431	839	829	283.8	2405	2433
120	1616	1648	993	995	289.5	2459	2473
140	1841	1848	1146	1144	373.2	3063	3054
160	2026	2033	1298	1320			
180	2204	2210	1447	1478			
200	2376	2379	1594	1630			
220	2544	2541	1739	1774			
					Temp. °K	Xenon	
						$\eta_{\text{Obs.}}(e)$	$\eta_{\text{Calc.}}$
240	2708	2696	1878	1915	289.7	2235	2223
260	2867	2846	2014	2052	293	2260	2240
280	3021	2991	2145	2180	400	3009	3006
300	3173	3134	2270	2315	450	3351	3340
800	5918(b)	6015	4621(c)	4781	500	3652	3653
1000	6800	6972	5302(c)	5558	550	3954	3967

(a) Johnston, H. L. and Gilly, E. R., 1942, *J. Phys. Chem.*, **46**, 948.

(b) Trautz, M. and Zink, R., 1930, *Annalen der Physik*, **7**, 427.

(c) Vasilescu, V., 1945, *Annales de Physik (Paris)*, Series 11, **20**, 202.

(d) Landolt-Bornstein, *Physikalisch-Chemische Tabellen*.

(e) Trautz, M. and Heberling, R., 1934, *Ann. Physik*, (5), **20**, 118.

A glance at the Table II shows that the agreement between theory and experiment is excellent in all the cases except for argon whose calculated values at extremely high and low temperatures exhibit larger deviations from the observed values than the estimated experimental error. Recent experiments by Amdur and Mason (1954) on the scattering of high velocity argon beams in argon gas do not indicate any steep repulsion at short intermolecular distances which these low values of viscosity at high temperatures would imply. It is therefore likely that these experimental results for the viscosity of argon are low at high temperatures and further experiments are desirable to clarify this point. There is much better agreement in the case of krypton and xenon than that found by Saxena (1955) and Mason and Rice (1954b) from their force parameters and this may be due to a better assignment of the potential parameters for these gases.

Self-diffusion. A property more suitable than viscosity for testing the appropriateness of the potential parameters is the coefficient of self-diffusion which is given as

$$D_{11} = \frac{0.0026280 T^{3/2} f_D^{(3)}(\alpha, T^*)}{p \bar{M}^{1/2} r_m^2 \Omega^{(1,1)*}(\alpha, T^*)} \quad (6)$$

where D_{11} is the coefficient of self-diffusion in cm^2/sec , p is the pressure in atmospheres, $f_D^{(3)}(\alpha, T^*)$ and $\Omega^{(1,1)*}(\alpha, T^*)$ are dimensionless functions of α , T^* and the other quantities are as previously defined. In some of the cases the quantity actually measured is D_{12} i.e. inter-diffusion of one isotope into the other and it is converted to give D_{11} from the relation

$$D_{11} = [2M_2/(M_1 + M_2)]^{1/2} [D_{12}], \quad (7)$$

where M_1 and M_2 are the molecular weights of the two isotopes. Experimental measurements on the coefficient of self-diffusion at different temperatures have been reported by Groth and Harteck (1941) (Kr), Wunn (1950) (Ne, A), Hutchinson (1949)(A) and Visner (1951)(Xe). These are compared with the theoretically calculated values and listed in Table III. Considering the uncertainty involved in the accurate measurements of this property, it is seen that on the whole the agreement is quite satisfactory being excellent in the case of argon, krypton and xenon. It may be remarked that unlike us, Mason and Rice (1954b) got poor agreement for the case of krypton and xenon using the force parameters obtained from virial, viscosity and crystal data.

Thermal diffusion: Another property which is most sensitive towards intermolecular interaction is the reduced thermal diffusion ratio $[K_T^*]_m$ which is related to $[K_T]$, the thermal diffusion ratio as

$$[K_T] = [K_T^*]_m \frac{(M_1 - M_2)}{(M_1 + M_2)} x_1 x_2, \quad \dots \quad (8)$$

TABLE III

 D_{11} in $\text{cm}^2 \text{sec}^{-1}$

Temp. °K	Argon		Neon		Temp. °K	Krypton	
	Obs.	Calc.	Obs.	Calc.		Obs.	Calc.
353.2	0.249	0.252	0.703	0.677	250		0.068
298.2	..	.	0.516	0.508	293	0.093	0.094
295.2	0.178	0.182	350		0.131
273.2	0.156	0.158	0.452	0.438	Xenon		
194.7	0.0830	0.0840	0.255	0.246			
90.2	0.0180	0.0184	.		Temp. °K.	Obs.	Calc.
77.7	0.0134	0.0137	0.0492	0.0485	250		0.040
					300.5	0.058	0.057
					350		0.077

where M_1 and M_2 are the molecular weights of species 1 and 2 and x_1 , x_2 are the mole fractions of the two components. Three different theoretical expressions are given for $[K_T^*]_m$, first and second approximations of Chapman and Cowling and the first approximation of Kihara. Kihara's expression for the first approximation of $[K_T^*]$ is much simpler and differs very slightly (not more than the uncertainties involved in the extrapolation) from the second approximation of Chapman and Cowling and is given by

$$[K_T^*]_1 = \frac{15}{16} \frac{(6C^* - 5)}{A^*} \quad \dots (9)$$

the thermal separation ratio R_T is given by

$$R_T = (118/105) K_T^* \quad \dots (10)$$

Equation (10) shows that the thermal diffusion of a simple gas is independent of the parameter τ_m and will therefore provide a better test of the accuracy of the potential parameters as well as the force model used. Experimental data on R_T are given by Nier (1940), Stier (1942) and Mann (1948) for argon and neon but their temperature assignment is open to uncertainties.

In figure 2 the observed values of R_T are plotted against T . For comparison the theoretically calculated values, after Kihara's expression (see appendix), are also indicated by a continuous curve. The agreement is good for the case of argon but poor for neon as observed by several workers.

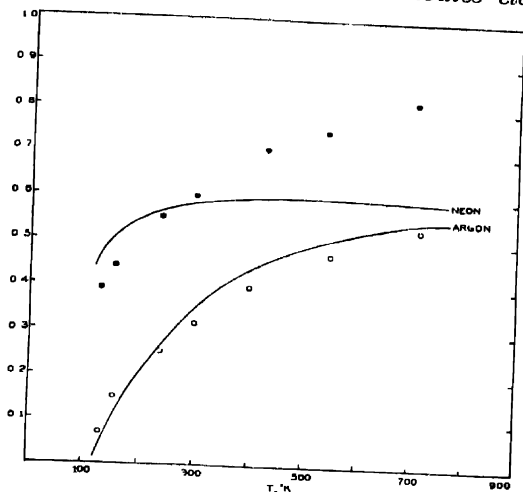


Fig. 2.

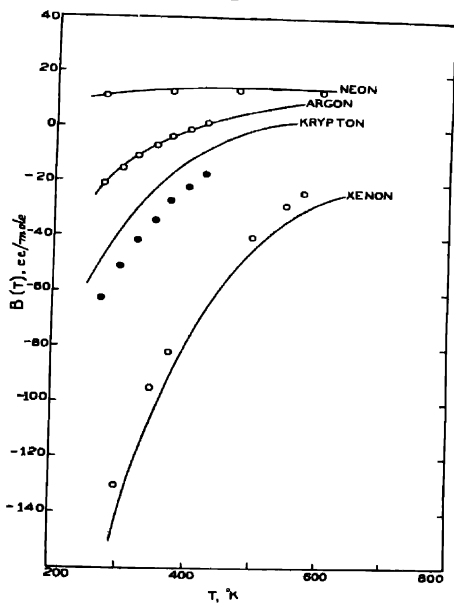


Fig. 3

Second virial coefficient : Figure 3 shows a comparison of experimentally determined second virial coefficient with those calculated from our potential parameters according to the equations :

$$B(T) = b_m B^*(\alpha, T^*), \quad \dots (12)$$

$$b_m = (2\pi/3) N_0 r_m^3$$

where $B(T)$ is the second virial coefficient, $B^*(\alpha, T)$ is a dimensionless quantity tabulated by Rice and Hirschfelder (1954) and N_0 is the Avogadro number. The agreement is not as good as in the case of non-equilibrium properties and is very poor for the case of krypton. It may be perhaps due to the use of the potential parameters, obtained from non-equilibrium property in testing equilibrium property. It is always better to use parameters derived from non-equilibrium measurements for computing transport properties.

ACKNOWLEDGMENTS

The author wishes to express his thanks to Prof. B. N. Srivastava, D.Sc., F.N.I. for many helpful discussions and suggestions throughout the progress of the work. This work has been carried out under a research scheme financed by the Council of Scientific and Industrial Research, New Delhi, to whom the author is grateful for this award.

REFERENCES

- Amdur, I., Mason, E. A., 1954, *J. Chem. Phys.*, **22**, 670.
 Groth, W. and Hartock, P., 1941, *Z. Elektrochem.*, **47**, 167.
 Hutchison, F., 1949, *J. Chem. Phys.*, **17**, 1081.
 Kannuliik, W. G. and Carman, E. H., 1952, *Proc. Phys. Soc. (London)*, **65**, 701.
 Keesom, W. H., 1912, *Leiden Comm. Suppl.*, No. 25.
 Lennard-Jones, 1924, *Proc. Roy. Soc. (London)*, A, **106**, 463.
 Mann, A. K., 1948, *Phys. Rev.*, **73**, 413.
 Mason, E. A., 1954, *J. Chem. Phys.*, **22**, 169.
 Mason, E. A. and Rice, W. E., 1954a, *J. Chem. Phys.*, **22**, 522.
 Mason, E. A. and Rice, W. E., 1954b, *J. Chem. Phys.*, **22**, 833.
 Nier, A. O., 1940, *Phys. Rev.*, **57**, 338.
 Rice, W. E. and Hirschfelder, J. O., 1954, *J. Chem. Phys.*, **22**, 187.
 Srivastava, B. N. and Srivastava, K. P., 1957, *Physica*, **23**, 103.
 Srivastava, K. P., 1957, *J. Chem. Phys.*, **26**, 579.
 Stier, L. G., 1942, *Phys. Rev.*, **62**, 548.
 Visner, S., 1951, *Phys. Rev.*, **82**, 207.
 Winn, E. B., 1950, *Phys. Rev.*, **80**, 1024.

APPENDIX

Values for the thermal separation ratio R_T for a binary mixture of heavy isotopes are calculated from the simple and more accurate first approximation formula of Kihara for $\alpha = 12$ to 17 as a function of T^* . These values are collected in Table IV and were utilised to calculate the thermal separation ratio for neon and argon

TABLE IV

T^*	R_T					
	$\alpha = 12$	$\alpha = 13$	$\alpha = 14$	$\alpha = 15$	$\alpha = 16$	$\alpha = 17$
0.5	-0.0918	-0.0436	-0.0048	0.0244	0.058	0.094
0.6	-0.1162	-0.0689	-0.0286	0.0021	0.038	0.074
0.7	-0.1165	-0.0705	-0.0303	0.0004	0.036	0.072
0.8	-0.1031	-0.0580	-0.0184	0.0118	0.047	0.083
0.9	-0.0793	-0.0365	0.0027	0.0329	0.067	0.102
1.0	-0.0528	-0.0104	0.0283	0.0575	0.091	0.125
1.2	0.0083	0.0488	0.0849	0.1139	0.146	0.178
1.4	0.0680	0.1072	0.1424	0.1699	0.201	0.232
1.6	0.1227	0.1612	0.1950	0.2215	0.251	0.280
1.8	0.1722	0.2087	0.2413	0.2673	0.296	0.325
2.0	0.2138	0.2505	0.2817	0.3080	0.336	0.363
2.5	0.2963	0.3314	0.3612	0.3876	0.414	0.439
3.0	0.3545	0.3885	0.4171	0.4429	0.469	0.493
3.5	0.3941	0.4293	0.4573	0.4833	0.509	0.534
4	0.4228	0.4582	0.4861	0.5113	0.537	0.562
5	0.4603	0.4968	0.5238	0.5512	0.577	0.600
6	0.4805	0.5178	0.5470	0.5715	0.597	0.622
7	0.4905	0.5307	0.5599	0.5857	0.611	0.636
8	0.4976	0.5376	0.5680	0.5934	0.618	0.643
9	0.4991	0.5401	0.5722	0.5995	0.626	0.652
10	0.5005	0.5418	0.5749	0.6016	0.629	0.654
12	0.4998	0.5419	0.5764	0.6047	0.634	0.661
14	0.4966	0.5411	0.5749	0.6047	0.633	0.660
16	0.4914	0.5376	0.5728	0.6046	0.634	0.663
18	0.4881	0.5344	0.5704	0.6027	0.634	0.662

TABLE IV (contd.)

T^*	R_T					
	$\alpha=12$	$\alpha=13$	$\alpha=14$	$\alpha=15$	$\alpha=16$	$\alpha=17$
20	0.4823	0.5306	0.5702	0.6023	0.634	0.664
25	0.4743	0.5231	0.5648	0.5994	0.633	0.664
30	0.4665	0.5178	0.5612	0.5970	0.633	0.664
35	0.4606	0.5141	0.5578	0.5970	0.634	0.667
40	0.4575	0.5109	0.5562	0.5967	0.634	0.669
45	0.4530	0.5096	0.5547	0.5969	0.634	0.670
50	0.4504	0.5076	0.5541	0.5973	0.636	0.672

In Table V are given the values of the quantity B^* for $\alpha=16$ and 17 which occurs in the expressions for the transport properties of mixtures. It is expressed in terms of the ratio of the reduced collision integrals as

$$B^* = \frac{5 \Omega_{12}^{(1,2)*} - 4 \Omega_{12}^{(1,3)*}}{\Omega_{12}^{(1,1)*}}$$

The values of B^* for $\alpha=12$ to 15 are tabulated by Mason (1954). We have extended the tabulations by extrapolation. These extrapolations can involve uncertainties amounting to several per cent.

TABLE V

B^*			R^*		
T^*	$\alpha=16$	$\alpha=17$	T^*	$\alpha=16$	$\alpha=17$
0.1	1.194	1.195	2.5	1.107	1.103
0.2	1.222	1.218	3.0	1.101	1.097
0.3	1.261	1.253	3.5	1.098	1.093
0.4	1.276	1.269	4.0	1.095	1.089
0.5	1.269	1.261	5	1.096	1.093
0.6	1.255	1.250	6	1.093	1.087
0.7	1.237	1.233	7	1.094	1.089
0.8	1.219	1.215	8	1.094	1.087
0.9	1.203	1.199	9	1.096	1.090
1.0	1.189	1.185	10	1.095	1.088
1.2	1.165	1.161	12	1.099	1.093
1.4	1.148	1.145	14	1.098	1.093
1.6	1.135	1.130	16	1.099	1.093
1.8	1.125	1.121	18	1.100	1.094
2.0	1.118	1.114	20	1.101	1.094

n - p AND p - p SCATTERING FROM CASE-PAIS MODEL IN THE ENERGY-RANGE 91 MEV TO 437 MEV

S. MUKHERJEE* AND M. K. PAL

INSTITUTE OF NUCLEAR PHYSICS, CALCUTTA

(Received for publication, January 29, 1957)

ABSTRACT. A two-body potential consisting of even-parity central and tensor interactions with Yukawa radial dependence, and a Case-Pais type spin-orbit interaction with adjustable exchange dependence have been used to calculate n - p and p - p cross-sections in the Born approximation over a wide range of energies and angles. A set of values of parameters in the potential has been obtained corresponding to the best fit with experimental curves. It has been found that though these "best fit" parameters reproduce n - p cross-section satisfactorily from 91 Mev to 400 Mev, they can give the observed isotropy in case of p - p scattering in the range 90° to 35° c.m. angles only upto 345 Mev, beyond which too much forward scattering is predicted.

A deduction of the Born approximation scattering formulae using Racah's tensor operator formalism and Wigner's D-matrix has been appended

1. INTRODUCTION

The phenomenological nuclear two-body potential obtained from deuteron and low energy n - p and p - p scattering data has, in the past, been supplemented in three different ways to extend its applicability to the case of high energy scattering data also. Of these three approaches, the p - p singular tensor force model of Christian and Noyes (1950) gives up charge-independence hypothesis, while singular spin-orbit interaction model of Case and Pais (1950) and Jastrow (1951) hard-core model maintain it. The last named approach distinguishes itself in that it alters the singlet potential as compared with the change of triplet potential in the first two. The following Table I will illustrate the relevant details of the potentials in the above three cases together with the range of angles and energies where their authors originally obtained fit.

After the preliminary success of these authors, Goldfarb and Feldman (1952) have performed exact calculations for p - p scattering at 240 Mev on all the three models. They find that for both the Christian-Noyes and Case-Pais models exact calculations do not reproduce the observed isotropy of p - p scattering at high energy as claimed by the original authors from their Born approximation calculations. The Jastrow model, on the other hand, beautifully gives the isotropy as well as

* In partial fulfilment of his requirements in the Thesis Paper for the Post M.Sc. Associateship Examination of this Institute.

observed high magnitude of p - p cross-section. Goldfarb and Feldman have made calculations also for the percentage of polarisation of an unpolarised beam

TABLE I

	Singular tensor force	Hard-core	L-S force
Singlet potentials	$-V_s, r < r_s$ $0, r \geq r_s$	$a, r < r_0$ $-V_s \exp\left(\frac{-r+r_0}{r_s}\right), r \geq r_0$	$-V_s \frac{\exp(-r/r_s)}{r/r_s}$
Triplet potentials	$V_t S_{12} \frac{\exp(-r/r_t)}{(r/r_t)^2}$	$V_t S_{12} \exp(-r/r_t)$	$V_t \frac{\mathbf{L} \cdot \mathbf{S}}{(r/r_t)} \frac{d}{d(r/r_t)} \left(\frac{\exp(-r/r_t)}{r/r_t} \right)$
r_s in 10^{-13} cm	2.6	0.40	1.14
r_t in 10^{-13} cm	1.6	0.75	1.07
r_0 in 10^{-13} cm		0.60	
V_s in Mev	13.27	375	45.8
V_t in Mev	± 18	-50.8	± 29.8
Range of isotropic scattering predicted in c.m. system			
340 Mev	90° to 40°	90° to 35°	90° to 40°
105 Mev	90° to 35°	90° to 35°	90° to 35°

produced on single scattering. Their results, when compared with the experimental percentage polarisation, show that the Jastrow model is the worst with regard to polarisation.

Above observations imply that the potential model of nuclear interaction, though very promising at the outset, has run into a disheartening plight at the present moment. But, as we notice, in the field of structural problems of light nuclei belonging to the $(2p)$ -shell ($4 < A \leq 16$) it has been a consistent trend to assume a total nuclear potential in the form of a sum over all nucleon pairs of charge-independent two-body potentials comprising of a central part and non-central tensor and spin-orbit parts. (See for example, Elliott (1953)). We have, therefore, thought it worthwhile to examine the Case-Pais model in more details. As we could presume from Goldfarb and Feldman's results that Born approximation results will be more in favour of this model than exact calculations, we preferred to stick to such approximate calculations. Moreover, the energy range to which we have devoted our attention in making the definite conclusions of the

present paper is even higher than the highest energy attended to by Case and Pais and Born approximation results at such high energies may not be very much off from the results of exact calculations. It may be pointed out here that the third order radial singularity of the spin-orbit interaction requires a cut-off to be given near the origin in the exact calculations and thus makes such results also liable to some doubtful uncertainties.

For the theoretical calculation of scattering cross-section from a phenomenological standpoint, one is to be guided by the following principal features of *n-p* and *p-p* scattering.

n-p Scattering

- (1) Total cross-section is small
- (2) There is a small asymmetry of scattering in the centre of mass system about 90° .
- (3) The position of minimum in $d\sigma/d\Omega$ vs. $\theta_{c.m.}$ curve shifts from one energy range to other.
- (4) With the increase of energy there is an increase in backward scattering (Hartzler *et al.* 1954).

p-p Scattering

- (1) Coulomb scattering is predominant at lower angles followed by a Coulomb-interference region, while in the region of 90° (c.m.) scattering is isotropic.

At 30 Mev Coulomb scattering is predominant upto $\theta_{c.m.} \sim 20^\circ$, Coulomb-nuclear interference region extends roughly from 20° to 50° , isotropic nuclear scattering is from 50° to 90° c.m.; (scattering, due to indistinguishability of protons, is necessarily symmetrical about 90° in centre-of-mass system). At 345 Mev. isotropy is produced down to 15° c.m. angle [Chamberlain *et al.* (1951)]. Similar is the situation at still higher energy. (Sutton *et al.* 1955).

- (2) Apart from isotropy, the most noticeable fact in the case of *p-p* scattering is that in the energy range ~ 300 Mev to 450 Mev, scattering at 90° is roughly 4 times larger than the corresponding quantity in *n-p* scattering in that energy interval.

In our attempt to fit the experimental data in the energy range 91 Mev to 437 Mev we have obtained a set of "best fit" parameters in the potential. For *n-p* scattering these parameters give fairly good agreement but for *p-p* scattering they fail to reproduce the observed isotropy beyond an energy value of 345 Mev. The validity of the potential model may be doubted at energies towards the end of the range we have considered but it may yet be maintained because meson production cross-section at 440 Mev is still too small. [Hartzler *et al.* (1954), Sutton *et al.* (1955)].

We have displayed our results on a number of curves and have arrived at two definite conclusions on their strength: (1) The Case-Pais model, as such, is definitely inadequate to describe the results of high energy p - p scattering experiments all over the energy range 91 Mev to 437 Mev. One need not go into painstaking exact calculations to demonstrate this inadequacy; even Born approximation calculations, which are more in favour of this model, show it. (2) With a single potential of the Case-Pais type it is impossible to explain n - p data simultaneously. n - p data seem more amenable to potential description than p - p data.

II FORM OF POTENTIAL AND CROSS-SECTION FORMULAE

We assume the following form of interaction Hamiltonian in the c.m. systems:

(1) Central singlet even-parity potential :

$$V(\mathbf{r}) = V_0 \left(\frac{e^{-r/a}}{r/a} \right)$$

(2) Central singlet odd-parity potential :

$$V(r) = 0$$

(3) Triplet potential .

$$V(\mathbf{r}) = V_0 \left(\frac{1+P_M}{2} \right) [1+g_1 S_{12}] \left(\frac{e^{-r/a}}{r/a} \right) + V_0 g_2 (1+\alpha P_M) \frac{1}{r} \frac{\partial}{\partial r} \left(\frac{e^{-r/a}}{r/a} \right) \mathbf{L} \cdot \mathbf{S} \quad \dots (1)$$

where S_{12} = tensor operator of Rarita and Schwinger (1941). It may be noted that the Serber type $\left(\frac{1+P_M}{2} \right)$ exchange-dependence means that the central and tensor interactions are present only in even parity states. The last term represents Case-Pais type spin-orbit interaction; \mathbf{L} and \mathbf{S} are orbital and spin angular momentum operators respectively of the two-particle system. The radial dependence of this term is easily seen to have third order singularity at the origin. The parameter α in the factor $(1+\alpha P_M)$ determines the relative proportions of even and odd parity S.O. interaction. The parameters g_1 and g_2 determine the strengths of tensor and S.O. interactions relative to the central interaction. V_0 and a are depth and range parameters respectively. We have used the same value of range parameter for all the three types of interactions. Further, it may be noted that we have used the same central interaction in singlet and triplet states. (See Kalos *et al* 1956).

The method of calculating the scattering cross-section formulae for this interaction is shown in the Appendix. In this section we choose to quote simply the results.

$$\frac{d\sigma^{n-p}}{d\Omega} = \frac{U_0^2}{4} \{ [C(\theta) + C(\pi - \theta)]^2 + 6g_s^2 \{ T^2(\theta) + T^2(\pi - \theta) - T(\theta)T(\pi - \theta) \} + 2g_s'^2 \{ K \cos \theta/2 S(\theta) - \alpha K \sin \theta/2 S(\pi - \theta) \}^2 \}$$

$$\frac{d\sigma^{p-p}}{d\Omega} = \frac{U_0^2}{4} \{ [C(\theta) + C(\pi - \theta)]^2 + 2g_s'^2 (1 - \alpha)^2 \{ K \cos \theta/2 S(\theta) + K \sin \theta/2 S(\pi - \theta) \}^2 \}$$

Symbols used in these formulae are explained in the Appendix.

III. RESULTS OF CALCULATION

We have chosen $a = 1.16 \times 10^{-13}$ cm, $V_0 = -48.4$ Mev in conformity with low energy *n-p* and *p-p* scattering data. Best fit is obtained with $g_t = \pm 1$, $g_s = \pm 1.4$, $\alpha = -2.0$. The results are shown in the figures 1-7. It

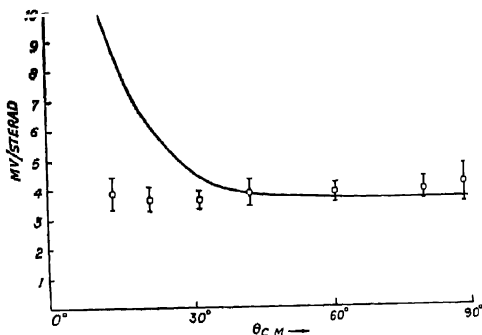


Fig. 1. 345 Mev *p-p* scattering. Experimental points are taken from Chamberlain *et al* (1951).

N.B. In all the figures the ordinates should be read mb/sterad instead of mv/sterad

is found that the experimental uncertainties permit the parameters g_s , α and g_t to be varied in the range $.17 \leq g_s^2(1 - \alpha)^2 \leq .21$, $1 \leq |g_t| \leq 1.5$ without distorting the angular distribution too much. Since in the formula for *p-p* cross-section strength and exchange part of spin-orbit interaction come always in the combination $g_s(1 - \alpha)$, analysis of *p-p* data alone cannot explore the details of spin-orbit force. From the form (1) of interaction Hamiltonian it is easy to see that positive value of α means greater magnitude of even-parity spin-orbit force than that in odd-parity state. It is found (figure 8) that apart from what has been assumed

for even-parity central and tensor force, excess of even-parity spin-orbit over that in odd-parity state means too much of backward scattering. Again even and

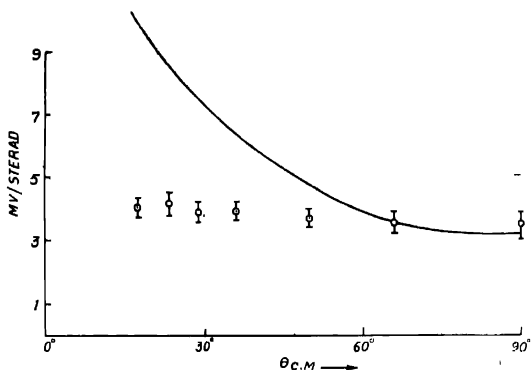


Fig. 2 437 Mev $p-p$ scattering Experimental points are taken from Sutton *et al* (1955)

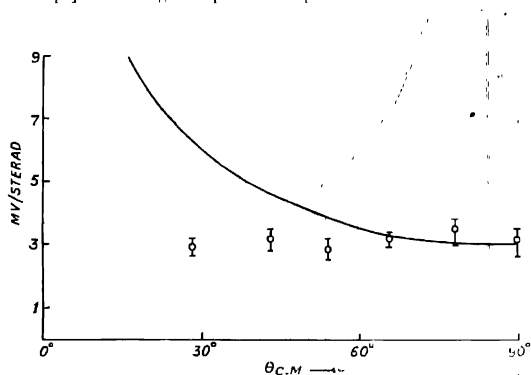


Fig. 3 429 Mev $p-p$ scattering Experimental points are taken from Marshall *et al* (1953)

odd-parity force of comparable proportion gives more forward scattering than what is evidenced experimentally (figure 9). By virtue of tensor and spin-orbit forces, associated Legendre polynomials are introduced in scattering amplitude, which is not necessarily antisymmetrical about 90° in odd parity state. The effect of such an odd-parity force is that apart from producing asymmetry it has the effect of shifting the position of minimum away from 90° . A small magnitude of such a force is thus necessary to get a better fit of $n-p$ data. Figures 4-7 show that, with the above mentioned parameters, quite a good fit is obtained to $n-p$ data from 91 Mev to 400 Mev.

The situation in case of *p-p* scattering is, however, quite different. The desired high value of scattering at 90° is produced and up to 345 Mev isotropy can be predicted from 90° down to 35° c.m. angles. Beyond this range isotropy

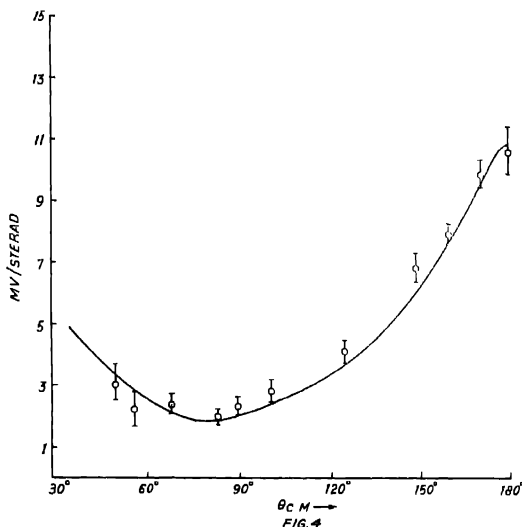


Fig. 4 156 Mev *n-p* scattering. Experimental points are taken from Rundle *et al* (1952)

is lost, and this model predicts too much forward scattering. Again, at still higher energy $\frac{d\sigma}{d\Omega}$ vs. $\theta_{c.m.}$ curve shows a tremendous rise at lower angle ($\theta_{c.m.} \leq 50^\circ$). As a result, it is useless to work with such a model to explain *p-p* scattering at higher energies.

IV. CONCLUSION

It is seen that in spin-orbit force model with Case and Pais type radial dependence it is not possible even in Born approximation to produce isotropy in *p-p* scattering, beyond 90° — 50° range in the energy range ~ 430 Mev. The reason can be seen qualitatively from the following two considerations.

(1) The peak in scattering (in Born approximation) is predicted where $2Ka \sin \theta/2 \simeq 1.2$; so that for a given range parameter "*a*" as the energy increases the peak shifts towards the lower angles (it is also the characteristic of tensor potential scattering in Born approximation). At 345 Mev peak is produced at $\theta_{c.m.} \simeq 35^\circ$ while at 437 Mev peak is produced at $\theta_{c.m.} \simeq 25^\circ$. As a result

the curve fitted to given desired high value of scattering at 90° ($\approx 4\text{mb/steradian}$) shows tremendous rise at lower angles. Due to the shift in the position of peak, the conclusion (Case and Pais) as regards the choice of radial dependence from the ratio of $\frac{d\sigma(30^\circ)}{d\sigma(90^\circ)}$ can be misleading.

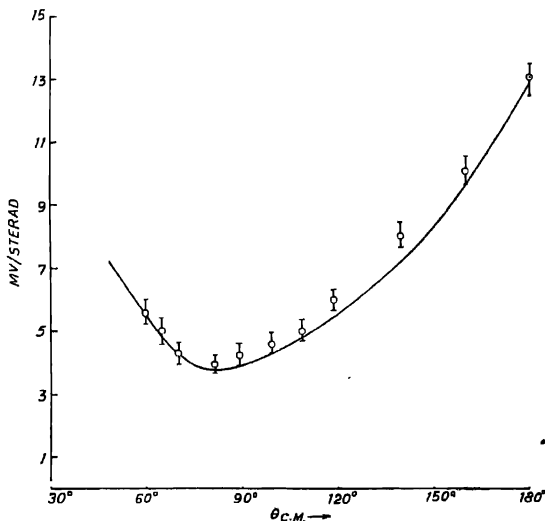


Fig. 5. 91 Mev n - p scattering. Experimental points are taken from Ramsay *et al* (1954).

(2) The dominating part of the Born approximation formula in Case and Pais model is extra $(Ka)^4$ factor in the expression of differential scattering cross-section. With $a = 1.16 \times 10^{-13}$ cm the value of $(Ka)^4$ at 345 Mev and 437 Mev are ≈ 31 and 51 respectively. The effect is that, with the increase of energy, this model begins to give too much of scattering (especially at lower angles), and also makes the peak value greater.

The above two points are sufficient to make it clear that in this model even in Born approximation at higher energy ~ 430 Mev, it is not possible to predict isotropic p - p scattering in the angular range 90° - 15° c.m. angles, which is established experimentally.

In case of n - p scattering, the contribution to the scattering from this model (maintaining charge independence hypothesis), in addition to that from even-parity central potential with Yukawa type radial dependence in both spin states and even-parity tensor Yukawa potential of same depth and range as that of central potential, makes fit of the data quite good. For a good fit it is, however, found that

magnitude of odd-parity force must always be greater than that of even-parity force (apart from what was assumed for central and tensor potential). It is also seen that the above odd parity force must not be stronger than 50% of central even parity force to give a good fit. It seems on the ground of our results that

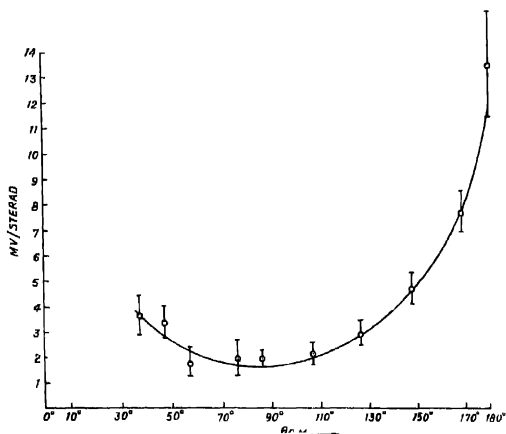


Fig. 6. 260 Mev $n-p$ scattering. Experimental points are taken from Kelly *et al* (1950).

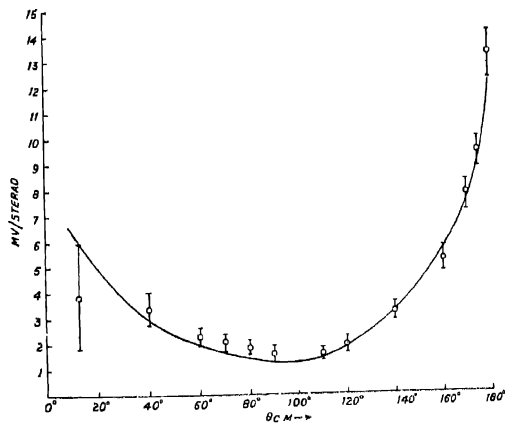


Fig. 7. 400 Mev $n-p$ scattering. Experimental points are taken from Hartzler *et al* (1954).

$n-p$ data is more amenable to description with the Case-Pais potential than $p-p$ data, and that the situation in case of $p-p$ scattering cannot be improved, so

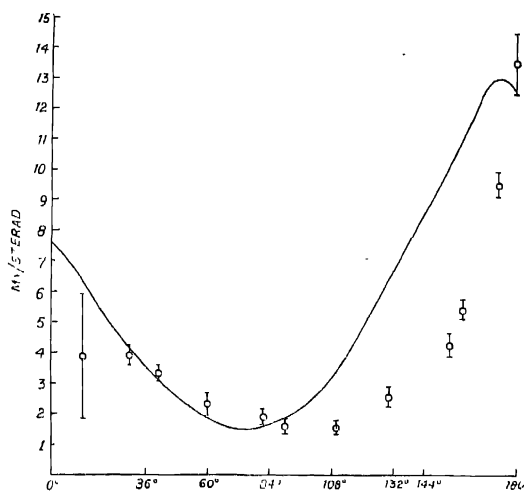


Fig. 8. Solid curve is our theoretical curve with $\alpha = 7.1$ and $g_8 = \pm .07$. Experimental points are taken from Hutzler *et al* (19).

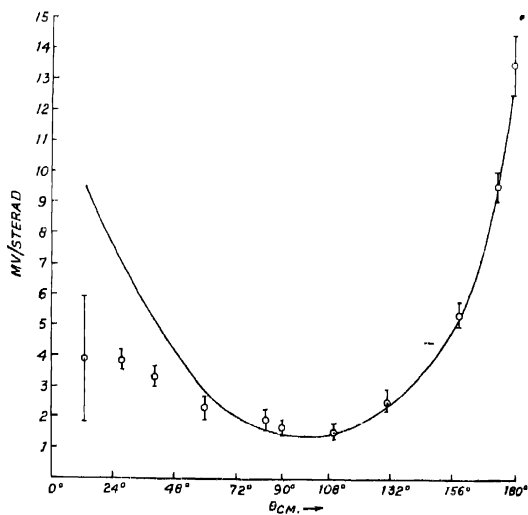


Fig. 9. Theoretical curve is with $\alpha = -.09$ and $g_8 = \pm .4$. Experimental points are taken from the same source as in Fig. 8.

far as isotropy down to low angle is concerned, even in exact theory as the results of Goldfarb and Feldman (1932) and Swanson (1952) show; for at higher energies, at lower angle ($\theta_{c.m.} \leq 40^\circ$) Born approximation underestimates both attractive and repulsive potentials having a high singularity. Relativistic correction Snyder, (1947), however, improves the situation in *p-p* system still further, as observed from our preliminary calculations, but does not help much in *p-p* system. We feel that the attempt to describe *n-p* and *p-p* interaction with same potential may have to be abandoned.

ACKNOWLEDGMENTS

We are indebted to Professor A. K. Saha for many helpful and illuminating discussions during the time we carried out the present work. We would also like to thank Sri P. N. Mukherjee for the valuable helps he rendered in connection with some of the results of rotation group used herein.

APPENDIX

CALCULATION OF CROSS-SECTION FORMULAE

The method of calculating cross-section formula with a combined central and non-central interaction has been given by Ashkin and Wu (1948). They have given formulae for central plus tensor interaction, while Case and Pais have supplemented these formulae with their results for the additional S.O. term. We give here a deduction for the combined central, tensor and S.O. interactions which is more elegant than the above deductions in two respects: (a) we have expressed each of the tensor and S.O. interactions as scalar products of one irreducible orbital tensor into another similar spin tensor of the same rank, the common rank being 2 in the case of tensor interaction and 1 in the case of S.O. interaction. With such expressions for the interactions the evaluation of the spin matrix $U_{M_s'M_s}$ (see below for notations) can be effected by the application of standard results of Racah's (1942) tensor operator formalism. (b) Secondly, in evaluating the volume integral in the expression for $FM_s'M_s$ we have taken the direction of $\mathbf{n}_0 - \mathbf{n}$ as the polar axis, just as is done in the evaluation of the same integral for central interaction alone. This choice requires a transformation of the spherical harmonics $Y_{lm}^i(\theta, \phi)$ ($l = 2$ for tensor and $= 1$ for S.O.) under rotation. This, as is well known, is secured through the representation of the rotation group $D^{(l)}$ (γ_i) (see Wigner, 1931) where $\gamma_1, \gamma_2, \gamma_3$ are the Eulerian angles corresponding to the rotation. $D^{(l)}_{\mu\nu}(\gamma_i)$ being known functions, the actual evaluation of the volume integral becomes much simplified compared to the manner of evaluation of Ashkin and Wu.

Writing $U(\mathbf{r}) = \frac{M}{\hbar^2} V(\mathbf{r})$, where $V(\mathbf{r})$ is given by expression (1) of text, we have to solve the Schrodinger equation

$$\nabla^2 \psi + (K^2 - U(\mathbf{r})) \psi = 0 \quad \dots (i)$$

and express the solution in the form

$$\psi = \sum_{M_s} a_{M_s} e^{ikz} \chi^s_{M_s} + \sum_{M_s, M_{s'}} a_{M_s} F_{M', M_s}(\theta, \phi) \frac{e^{ikr}}{r} \chi^s_{M_{s'}} \quad \dots (ii)$$

We have, for an unpolarised incident beam, the triplet differential cross-section given by

$$\frac{d\sigma_{tr}}{d\Omega} = \frac{1}{3} \sum_{M', M_s} |F_{M', M_s}(\theta, \phi)|^2 \quad \dots (iii)$$

In the Born approximation $F_{M', M_s}(\theta, \phi)$ is given by

$$F_{M', M_s}(\theta, \phi) = -\frac{1}{4\pi} \int \sum_{spin} \exp(-ik\mathbf{n} \cdot \mathbf{r}) \chi^s_{M_s'} U \chi^s_{M_s} \exp(ik\mathbf{n}_0 \cdot \mathbf{r}) d\mathbf{r} \quad \dots (iv)$$

Writing

$$\sum_{spin} \chi^s_{M_s'} U_{trip} \chi^s_{M_s} = \langle SM_s' | U_{trip} | SM_s \rangle = U_{M_s' M_s}$$

and

$$S_{12} = L^{(2)} \cdot S^{(2)}, \quad \begin{cases} L_0^{(2)} = \frac{16}{3} \sqrt{\frac{\pi^3}{10}} Y_0^2 \\ S_0^{(2)} = \frac{3\sqrt{2}}{8\pi} (3\sigma_z^{(1)} \sigma_z^{(2)} - \vec{\sigma}^{(1)} \cdot \vec{\sigma}^{(2)}) \end{cases}$$

$$\mathbf{L} \cdot \mathbf{S} = L^{(1)} \cdot S^{(1)} \quad \begin{cases} L_0^{(1)} = L_z \\ S_0^{(1)} = \frac{1}{2} (\sigma_z^{(1)} + \sigma_z^{(2)}) \end{cases}$$

one establishes with use of the results of Racah's operator algebra, the following Table II for U_{M', M_s}

TABLE II

M_s	1	0	-1
M'_s			
1	$U_0 f(r/a) + 4\sqrt{\frac{\pi}{5}} U_{00} Y_{20} f(r/a) - 4\sqrt{\frac{3\pi}{5}} U_{00} Y_{2-1} f(r/a)$ $+ U_{00} L^1_1 f_1(r/a)$	$U_0 f(r/a) + U_{00} L^1_{-1} f_1(r/a)$	$8\sqrt{\frac{3\pi}{10}} U_{00} Y_{2-2} f(r/a)$
0	$4\sqrt{\frac{3\pi}{5}} U_{00} Y_{21} f(r/a) - U_{00} L^1_{11} f_1(r/a)$	$U_0 f(r/a) - 8\sqrt{\frac{\pi}{5}} U_{00} Y_{20} f(r/a)$	$4\sqrt{\frac{3\pi}{5}} U_{00} Y_{2-1} f(r/a) + U_{00} L^2_{-1} f_1(r/a)$
-1	$8\sqrt{\frac{3\pi}{10}} U_{00} Y_{-22} f(r/a)$	$-4\sqrt{\frac{3\pi}{5}} U_{00} Y_{12} f(r/a) - U_{00} L^1_{11} f_1(r/a)$	$U_0 f(r/a) + 4\sqrt{\frac{\pi}{5}} U_{00} Y_{20} f(r/a) - U_{00} L^1_{11} f_1(r/a)$

where

$$U_0 = \frac{M}{\hbar^2} V_0, g_s' = g_s a^2, f(r/a) = \frac{e^{-r/a}}{r/a}, f_1(r/a) = \frac{1}{r} \frac{\partial}{\partial r} \left(\frac{e^{-r/a}}{r/a} \right) \text{ etc.}$$

To calculate the contribution (4) from tensor operator we have to evaluate the integrals of the type

$$I_m^2 = \int \exp(-ik \mathbf{n} \cdot \mathbf{r}) Y_m^2(\theta, \phi) \exp(ik \mathbf{n}_0 \cdot \mathbf{r}) f(r/a) dr$$

Taking the direction \mathbf{n}_0 of incident beam as z-axis, and direction of momentum transfer $\mathbf{n}_0 - \mathbf{n}$ as z' -axis, we have in a self-explanatory notations,

$$Y_m^2(\theta, \phi) = \sum_q D^{(2)}_{mq}(0, -\frac{\pi-\theta}{2}, -\frac{\pi}{2}-\phi) Y_q^2(\theta', \phi')$$

so that

$$\begin{aligned} I_m^2 &= \sum_q \int \int \int \exp(-ikr \cos \theta') f(r/a) D_m^2(\dots) Y_q^2(\theta', \phi') r^2 \sin \theta' d\theta' d\phi' dr \\ &= -D_{m0}^{(2)}(0, -\frac{\pi-\theta}{2}, -\pi/2-\phi) \sqrt{20\pi} T(\theta) \end{aligned} \quad \dots \text{ (v)}$$

$$\text{where } T(\theta) = \int_0^\infty \left\{ \frac{\sin Kr}{Kr} - 3 \frac{\sin Kr - Kr \cos Kr}{(Kr)^3} \right\} r^2 f(r/a) dr$$

$$= a^3 \left[3 \frac{x - \tan^{-1}x}{x^3} - \frac{1}{1+x^2} \right] \quad \dots \text{ (vi)}$$

with $x = Ka = 2Ka \sin \theta/2$ and

$$D \left(0, -\frac{\pi-\theta}{2}, -\pi/2-\phi \right) =$$

m	2	1	0	-1	-2
	$\frac{\sqrt{6}}{4} \cos^2 \theta/2 e^{2i\varphi}$	$-\frac{\sqrt{6}}{4} \sin \theta e^{i\varphi}$	$\frac{1-3 \cos \theta}{4}$	$\frac{\sqrt{6}}{4} \sin \theta e^{-i\varphi}$	$\frac{\sqrt{6}}{4} \cos^2 \theta/2 e^{-2i}$

when evaluated in right-handed system of coordinates. (N.B. Wigner gives results for the left-handed system).

Similarly for spin-orbit part we have

$$I_m^1 = \exp(-ik\mathbf{n} \cdot \mathbf{r}) f_1(r/a) L_m^1 \exp ik\mathbf{n}_0 \cdot \mathbf{r} d\tau$$

Proceeding as above, it is easy to see that $I_0^1 = 0$

$$\text{for } L_0^1 = -i \frac{\partial}{\partial \phi}, L_{\pm 1}^1 = \pm \frac{e^{\pm i\varphi}}{\sqrt{2}} \left(\pm \frac{\partial}{\partial \theta} + i \cot \theta \frac{\partial}{\partial \phi} \right). \text{ For } m = \pm 1$$

$$I_m^1 = \mp 4\pi k D_{m0}^{(1)} \left(0, -\frac{\pi-\theta}{2}, -\pi/2-\phi \right) \int_0^\infty \frac{Kr \cos Kr - \sin Kr}{(Kr)^2} r^3 f_1(r/a) dr$$

$$= \mp 4\pi k D_{m0}^{(1)} \left(0, -\frac{\pi-\theta}{2}, -\frac{\pi}{2}-\phi \right) S(\theta)$$

$$\text{where } S(\theta) = - \int_0^\infty \frac{Kr \cos Kr - \sin Kr}{(Kr)^2} r^3 f_1(r/a) dr$$

$$= a^3 \frac{x}{1+x^2} \dots \quad \text{(vii)}$$

and

$$D_{m0}^{(1)} \left(0, -\frac{\pi-\theta}{2}, -\pi/2-\phi \right) =$$

m	1	0	-1
	$-\frac{\cos \theta/2}{\sqrt{2}} e^{i\varphi}$	$\sin \theta/2$	$\frac{\cos \theta/2}{\sqrt{2}} e^{-i\varphi}$

The contribution of central potential to (iv) easily comes out to be

$$= 4\pi \int_0^{\infty} \frac{\sin Kr}{Kr} r^2 f(r/a) dr$$

$$= 4\pi \cdot \frac{a^3}{1+x^2} = 4\pi U(\theta) \quad \dots \text{ (viii)}$$

With the above simplification of the integrals occurring in (iv) one finds the following table for the scattering amplitude $f_{M'_s M_s}(\theta, \phi)$ for a pure Wigner force

TABLE III

$M_s \backslash M'_s$	1	0	-1
1	$U_0 C(\theta)$ $-U_0 g t \left(\frac{1-3 \cos \theta}{2} \right) T(\theta)$	$\frac{3}{\sqrt{2}} U_0 g t \sin \theta e^{-i\varphi} T(\theta)$ $+ \frac{U_0 g t'}{\sqrt{2}} k \cos \theta / 2 e^{-i\varphi} S(\theta)$	$-3 U_0 g t \cos^2 \theta / 2 e^{-2i\varphi} T(\theta)$
0	$\frac{3}{\sqrt{2}} U_0 g t \sin \theta e^{i\varphi} T(\theta)$ $- \frac{U_0 g t'}{\sqrt{2}} k \cos \theta / 2 e^{i\varphi} S(\theta)$	$U_0 C(\theta)$ $+ U_0 g t (1-3 \cos \theta) T(\theta)$	$-\frac{3}{\sqrt{2}} U_0 g t \sin \theta e^{-i\varphi} T(\theta)$ $+ \frac{U_0 g t'}{\sqrt{2}} k \cos \theta / 2 e^{-i\varphi} S(\theta)$
-1	$-3 U_0 g t \cos^2 \theta / 2 e^{2i\varphi} T(\theta)$	$-\frac{3}{\sqrt{2}} U_0 g t \sin \theta e^{i\varphi} T(\theta)$ $- U_0 g t' k \cos \theta / 2 e^{i\varphi} S(\theta)$	$U_0 C(\theta)$ $- U_0 g t \left(\frac{1-3 \cos \theta}{2} \right) T(\theta)$

The contribution of tensor force to $f_{M'_s M_s}(\theta, \phi)$ in Table III is exactly the same as that in eqn. (9) of Ashkin and Wu (1948). Actual $F_{M'_s M_s}(\theta, \phi)$ in (iv), as easily seen from (1), is

$$F_{M'_s M_s}(\theta, \phi) = \frac{1}{2} \{ f_{M'_s M_s}^C(\theta, \phi) + f_{M'_s M_s}^C(\pi - \theta, \pi + \phi) \} + \frac{1}{2} \{ f_{M'_s M_s}^T(\theta, \phi) + f_{M'_s M_s}^T(\pi - \theta, \pi + \phi) \} + \{ f_{M'_s M_s}^S(\theta, \phi) + \alpha f_{M'_s M_s}(\pi - \theta, \pi + \phi) \} \quad \dots \text{ (ix)}$$

where superscripts C, T, S in (ix) refers to the contribution to $f_{M'_s M_s}(\theta, \phi)$ from central, tensor and spin-orbit forces respectively.

The appearance of azimuthal angle ϕ in the off-diagonal matrix-elements of Table III assures the axial-symmetry of scattering cross-section (iii) for an unpolarised incident beam, while the vanishing of the interference terms between central, tensors and spin-orbit part in the averaging process (iii) leads to the result that in Born approximation the contribution to the cross-section (iii) of central, tensors and spin-orbit part of (1) is purely additive.

From Table III, (ix) and (iii) one calculates the following expression of differential scattering cross-section for n - p and p - p scattering. In deducing these formulae use has been made of the fact, that the effect of P_M on the cross sections is simply to replace θ by $\pi - \theta$ and ϕ by $\pi + \phi$ as it denotes spatial exchange. Further, for p - p scattering the triplet part (spin symmetric) has been represented by an antisymmetrised $F_{M_s} M_s(\theta, \phi)$ for identity of the two particles.

We get finally

$$\begin{aligned} \frac{d\sigma^{n-p}}{d\Omega} &= \frac{1}{4} \sigma_{sing} + \frac{3}{4} \sigma_{trip} \\ &= \frac{U_0^2}{4} \left[\left\{ C(\theta) + C(\pi - \theta) \right\}^2 + 6g_s^2 \left\{ T^2(\theta) + T^2(\pi - \theta) - T(\theta)T(\pi - \theta) \right\} \right. \\ &\quad \left. + 2g_s'^2 \left\{ k \cos \theta/2 S(\theta) - \alpha \cdot k \sin \theta/2 S(\pi - \theta) \right\}^2 \right] \quad \dots (x) \end{aligned}$$

$$\begin{aligned} \frac{d\sigma^{p-p}}{d\Omega} &= \frac{U_0^2}{4} \left[\left\{ C(\theta) + C(\pi - \theta) \right\}^2 + 2g_s'^2 (1 - \alpha)^2 \left\{ k \cos \theta/2 S(\theta) + k \sin \theta/2 S(\pi - \theta) \right\}^2 \right] \\ &\quad \dots (xi) \end{aligned}$$

REFERENCES

- Ashkin and Wu, 1948, *Phys. Rev.*, **73**, 972.
 Case and Pais, 1950, *Phys. Rev.*, **80**, 203.
 Chamberlain *et al*, 1951, *Phys. Rev.*, **83**, 923.
 Christian and Noyes, 1950, *Phys. Rev.*, **79**, 85.
 Elliot, 1953, *Proc. Roy. Soc. A.*, **218**, 345.
 Goldfarb and Feldman, 1952, *Phys. Rev.*, **88**, 1099.
 Hartzler, *et al*, 1954, *Phys. Rev.*, **95**, 591.
 Jastrow, 1951, *Phys. Rev.*, **81**, 165.
 Kulos, *et al*, 1950, *Nuclear Physics*, **1**, 233.
 Kelley, *et al*, 1950, *Phys. Rev.*, **79**, 96.
 Marshall, *et al*, 1953, *Phys. Rev.*, **92**, 835.
 Ramsay, *et al*, 1954, *Phys. Rev.*, **96**, 1310.
 Randle, *et al*, 1952, *Proc. Roy. Soc. A.*, **213**, 392.
 Rarita and Schwinger, 1941, *Phys. Rev.*, **59**, 436.
 Racha, 1942, *Phys. Rev.*, **62**, 438.
 Sutton, *et al*, 1955, *Phys. Rev.*, **97**, 783.
 Swanson, 1952, *Phys. Rev.*, **87**, 208.
 Snyder and Marshak, 1947, *Phys. Rev.*, **72**, 1253.
 Wigner, 1931, *Gruppentheorie und Quantenmechanik* Frieder. Vieweg & Sohn Publication (1931).

ANALYSIS OF CATHODE-COUPLED FREE RUNNING MULTIVIBRATOR

D. C. SARKAR

DEPARTMENT OF PHYSICS, MUSLIM UNIVERSITY, ALIGARH, U P.

(Received for publication, August 7, 1956)

ABSTRACT. An analysis of the relaxation period of free running cathode-coupled multivibrator is made and the method of finding different electrode potentials at different instants is shown. The theoretical values obtained have been compared with the experimental data.

INTRODUCTION

In plate-coupled multivibrator there are two capacitive couplings, one between the plate of first tube and the grid of the second tube and other, between the grid of first tube and the plate of second tube, in cathode-coupled free running multivibrator there is one capacitive coupling between plate of first tube and the grid of second tube and another coupling is accomplished by placing a resistor between two cathodes of both the tubes joined together and earth. Due to various applications of relaxation oscillators, many authors have attempted to make analysis of these circuits (e.g., Kriebert and Inglis, 1945; Sarkar and Ahamed, 1954; Williams *et al.*, 1950). So far as the plate-coupled multivibrator is concerned, its relaxation periods are calculated most accurately without neglecting the effect of shunting capacitances and the positive drive of the grids of both the tubes (Sarkar and Ahmed, 1954). In cathode-coupled free running multivibrator, one coupling being a common cathode resistor between the two cathodes joined together and earth, its analysis becomes very much complicated. Upto this time a few have explained the operation of the circuit in qualitative way, but none has made any quantitative analysis of free running cathode-coupled multivibrator. In this analysis graphical method using the characteristics of tubes is followed.

OPERATION OF THE CIRCUIT

The circuit of the free running cathode coupled multivibrator is shown in figure 1. Its operation is somewhat different from that of free running plate-coupled multivibrator and explained by several authors (Seely, 1951; Farley, 1955). This circuit gives square wave on each anode, the waveform at the grid of V_2 being a differentiated square wave. Advantages of this circuit are the free grid in V_1 and free anode of V_2 which do not play part in generating the

oscillations. An undistorted square wave output may be taken from the anode of V_2 without disturbing the oscillation and the synchronizing signal may be injected to the grid of V_1 . The typical waveforms are shown in figure 5.

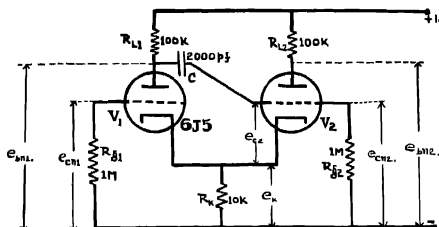


Fig. 1

ANALYSIS

e_{bn1} and e_{bn2} = plate to earth voltage of V_1 and V_2 respectively.

e_{c1} and e_{c2} = grid to cathode voltage of V_1 and V_2 respectively.

e_{gn1} and e_{gn2} = grid to earth voltage of V_1 and V_2 respectively.

e_k = voltage across the cathode resistor R_k .

E_b = plate supply voltage.

E_{gm} = maximum negative grid voltage of V_2 with respect to earth.

E_0 = voltage across the load resistance R_{L1} when e_{gn1} is zero.

The analysis of a free running cathode-coupled multivibrator with the circuit constants given in figure 1 is to be made in the following manner. As the relaxation time is far greater than the switching time, the latter will be neglected in finding time period in order to simplify the analysis.

A 110K load line is drawn with the plate supply voltage of 125 volts as shown in the figure 6. To use the load line with cathode follower is not so simple as with amplifier because the grid-cathode voltage is not known directly. So it is essential to draw input-output characteristics. The values of grid-cathode voltage e_c are assumed and the corresponding values of cathode voltage e_k and input voltage e_i are calculated and plotted.

For example, $e_c = 0$, the point of operation is on the point A on the load line and the plate current $i_b = .95$ mA. So $e_k = 9.5$ volts and $e_i = e_k + e_c = 9.5 + 0 = 9.5$ volts. The point B on the input-output curve is located by it.

Again a cut-off voltage for plate supply voltage of 125 volts is 7.25 volts; so $e_k = 0$ and $e_i = e_k + e_c = 0 - (-7.25) = -7.25$ volts. This point is located

by point C on the curve. In this way few more points are located and the input-output curve CDB is plotted. The points beyond B correspond to positive values of e_g and the grid current must be considered in locating them.

So from input-output curve we get that if e_1 (i.e., e_{cn1}) is equal to zero, then e_k comes out to be 4 volts as shown at the instant τ_1 of the figure 5. Therefore the voltage across the load resistance R_L must be 40 volts and plate voltage e_{bn} at that instant is equal to 85 volts.

Again at the end of the previous cycle when current changes from V_2 to V_1 at the instant τ_1 , e_{cn2} is few volts positive which can be calculated in the following way.

As soon as the voltage across R_k becomes equal to cut-off voltage of V_1 , the current switches on from V_2 to V_1 . From the input-output curve when e_k cut-off voltage = +7 volts, e_{cn2} comes out to be 5 volts. So the maximum negative grid voltage of V_2 at the instant τ_1 will be $(5 - 40) = -35$ volts. Now again cut-off value of V_2 corresponding to plate voltage of $(125 - 4) = 121$ volts is -7 volts. If by the discharge of condenser C the grid to earth voltage of V_2 (i.e., e_{cn2}) becomes equal to -3 volts, then grid to cathode voltage of V_2 is equal to $-3 + (-4) = -7$ volts = cut-off voltage.

Let the time taken for e_{cn2} to change from -35 volts to -3 volts be t_1 . The time constant for the equivalent circuit of discharge as shown in the figure 2 is

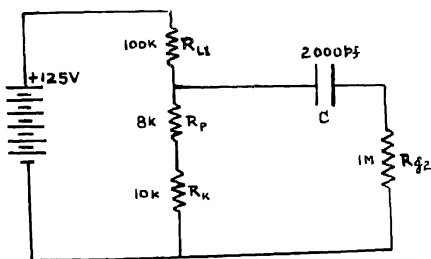


Fig.

$$2000 \times 10^{-12} \left[10^6 + \frac{18 \times 100}{118} \times 10^3 \right] = 2030 \text{ micro-seconds} \approx 2 \text{ milliseconds.}$$

Hence,
$$-3 = -35 e^{-\frac{t}{2}}$$

i.e.,
$$t_1 = 4.87 \text{ milli-seconds.}$$

Now at the instant τ_2 , V_2 starts conducting in a few microseconds and V_1 goes off. As the condenser starts charging towards 125 volts, grid to earth voltage of V_2

becomes few volts positive. The equivalent circuit of charging is shown in the figure 3. Its time constant is $2000 \times 10^{-12} \left[100 + \frac{11 \times 1000}{1011} \right] \times 10^3 = 220$ microseconds = .22 milliseconds.

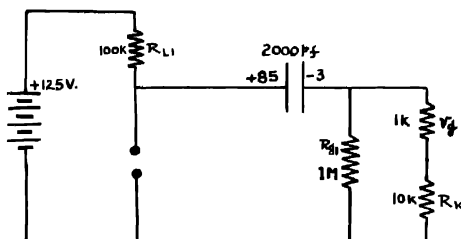


Fig. 3

The voltage across the condenser at the instant τ_2 is $85 - (-3) = 88$ volts; therefore the driving voltage at beginning of the charging is $(125 - 88) = 37$ volts.

So the charging current at the beginning of charging is
$$\frac{37}{100 + \frac{11 \times 1000}{1011}} = .33 \text{ mA}$$

and the amount passing through the branch r_g and R_k is $\frac{.33 \times 1000}{1011} = .33 \text{ mA}$,

which makes the grid-cathode voltage of V_2 equal to .33 volts and the voltage across R_k due to charging current is 3.3 volts. From the load line, if $e_r = .33$ volt, $i_b = 1 \text{ mA}$ which makes the voltage across the resistance R_k due to the space current of $V_2 = 10$ volts; so the total voltage across R_k at the instant τ_2 is 13.3 volts and $e_{cn2} = 13.3 + .33 = 13.6$ volts. Again when $e_{c2} = 0$, $e_{cn2} = e_i = 9.5$ volts. Therefore with the time constant of 220 microseconds, e_{cn2} changes from 13.6 volts to 9.5 volts. Let the time required be t_2 . Then

$$9.5 = 13.6 e^{-\frac{t_2}{.22}}$$

i.e., $t_2 = .07$ milliseconds.

As soon as e_{cn2} becomes 9.5 volts, the equivalent circuit becomes different because static grid-cathode resistance r_g will not be operative and the time constant of the circuit, as shown in the figure 4, is $2000 \times 10^{-12} [10^6 + .1 \times 10^6] = 2.2$ milliseconds,

Again the cut-off voltage of V_1 corresponding to plate-cathode voltage of $(125-4) = 121$ is -7 volts. In order that e_k becomes equal to 7 volts, $e_{c_{n2}}$ should be 5 volts, which is obtained from the input-output characteristics.

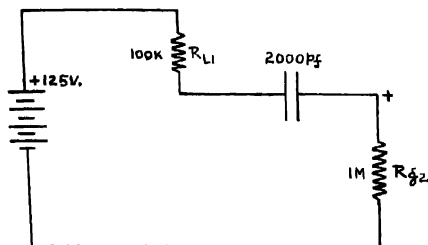


Fig. 4

So $e_{c_{n2}}$ should change from 9.5 volts to 5 volts with the time constant of 2200 microseconds. Let the time required be t_3 .

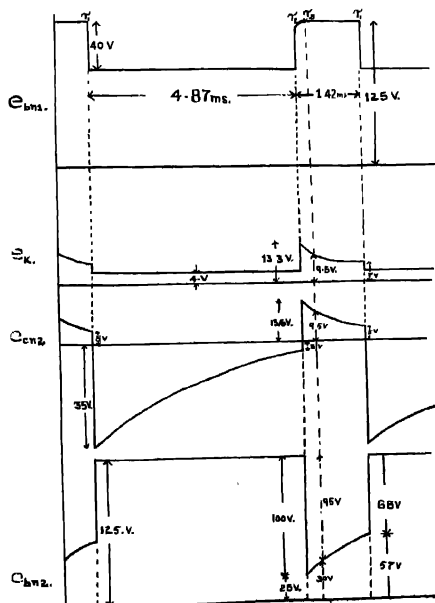


Fig. 5

Then

$$b = 9.5 \frac{t_3}{2.2}$$

$$\text{i.e., } t_3 = 1.35 \text{ milliseconds.}$$

Therefore the time period is $(4.87 + .07 + 1.35) = 6.29$ milliseconds and the experimental value of the same for the circuit is 6.3 milliseconds. In order to

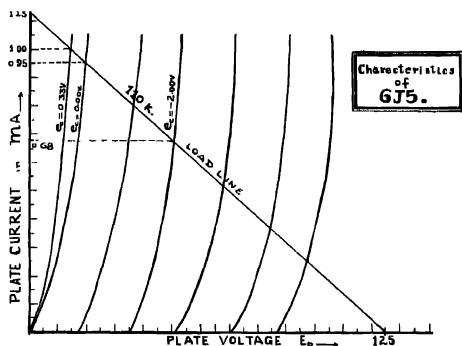


Fig. 6

find out plate voltage waveform of V_2 at any instant we should know the grid to cathode voltage of V_2 at that instant. When e_{c2} is .33 volt at the instant τ_2 , the corresponding current in V_2 is 1 mA. So the voltage drop across R_{L1} is 100 volts and $e_{nb2} = (125 - 100) = 25$ volts.

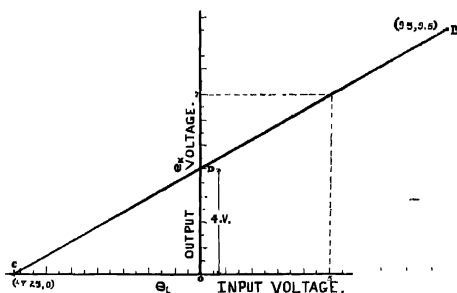


Fig. 7

At the instant τ_3 , e_{cn2} is equal to e_k , so grid-cathode voltage of V_2 is equal to zero and the plate current comes out to be .95 mA from the load line. So the voltage drop across R_{L2} at that instant is 95 volts.

Therefore, $e_{b_{n2}}$ at that instant is $(125-95) = 30$ volts.

Again at the instant τ_1 , $e_k = 7$ volts and $e_{r_{n2}} = 5$ volts, so $e_{c2} = -2$ volts and current corresponding to $e_{c2} = -2$ volts is .68 mA which is obtained from the load line; so the voltage across R_{12} volts is 68 volts and $e_{b_{n2}}$ is equal to $(125-68) = 57$ volts. During the time τ_1 to τ_2 , the tube V_2 was not conducting at all, so its plate voltage is equal to 125 volts.

EXPERIMENTAL RESULTS

A double beam Cossor oscillograph is used to measure the time period and different electrode potentials at different instants. The values of the circuit elements, such as resistances, capacitances are checked by means of RCA senior volt ohmyst and G.R. impedance bridge.

TABLE I

$R_{g1} = R_{g2} = 1\text{megohm}$, $E_b = 125$ volts, $R_k = 10\text{K}\Omega$ $C = 2000$ pf. V_1 and $V_2 = 6\text{J5}$ tube

$R_{L1} = R_{L2}$ in kilo-	t_1 in milliseconds		$t_2 + t_3$ in milliseconds	
			Observed	Calcu
100	4.9	4.87	1.4	1.42
80	4.8	4.7	2.0	2.02
60	4.4	4.45	2.4	2.47
40	4.0	4.2	3.4	3.8

TABLE II

$E_b = 130$ volts, $R_{L1} = R_{L2} = 100\text{K}\Omega$, $C = 2100$ pf, $R_K = 10\text{K}\Omega$, V_1 and $V_2 = 6\text{J5}$ tube.

$R_{g1} = R_{g2}$ in kilo-ohms	t_1 in milliseconds		$t_2 + t_3$ in milliseconds	
	Observed	Calculated	Observed	Calculated
1000	5.5	5.3	1.8	1.68
650	3.7	3.45	1.2	1.18
350	2.0	1.85	0.90	0.74
90	0.5	0.478	0.40	0.355

TABLE III

$E_b = 130$ volts, $R_{g1} = R_{g2} = 1$ megohm, $R_{L1} = R_{L2} = 100$ K Ω ,
 $C = 2100$ pf, V_1 and $V_2 = 6J5$ tube.

R_K in kilo-ohms.	t_1 in milliseconds.		$t_2 + t_3$ in milliseconds.	
	Observed	Calculated	Observed	Calculated
10K	5.5	5.3	1.8	1.68
15K	4.8	5.0	2.8	2.9
25K	4.2	4.4	3.6	4.7

TABLE IV

$E_b = 170$ volts, $R_{g1} = R_{g2} = 340$ K Ω , $R_K = 10$ K Ω , $R_{L1} = R_{L2} = 50$ K Ω ,
 V_1 and $V_2 = 6J5$ tube.

C in pf	t_1 in milliseconds.		$t_2 + t_1$ in milliseconds	
	Observed	Calculated	Observed	Calculated
2000	1.3	1.28	1.1	1.2
1020	.65	.658	.55	.60
510	.32	.329	.29	.30
250	.15	.16	.15	.15

CONCLUSION

It can be concluded from the tables that the method given, can be used reliably to find out time period and different electrode potentials of free running cathode-coupled multivibrator. Still the following points are to be observed very carefully.

1. The effects of shunting capacitances are neglected in this analysis, so the analysis is valid at lower repetition frequency, when the coupling capacitance C is much larger than the shunting capacitances. At fairly high frequency range, the shunting capacitances are of same order as the coupling capacitance; its effects therefore, cannot be neglected. So in case of analysis, at high frequency range, the method should be modified slightly.

2. The analysis is correct, when the circuit is operating like a perfect relaxation oscillator. Thereby it is meant that during the first relaxation period the tube V_1 is off and V_2 is on and during the second relaxation period V_2 is off and V_1 is on. When cathode resistance R_k is very small compared with the plate

resistance R_p and load resistance R_L such that the voltage drop across R_K , even at maximum current, is too small to bring the tube to cut-off. In this case also, the oscillation will also go on and during the one relaxation period V_1 is on and V_2 is off and during the other relaxation period V_1 is on and V_2 is also on with lesser plate current than that it had during the first relaxation period. In those cases slightly modified method should be used.

ACKNOWLEDGMENTS

The author is grateful to Dr. H. Rakshit for going through the manuscript and making valuable suggestions. He also thanks Professor P. S. Gill for facilities given by him for continuing the work in the laboratory of the Department.

REFERENCES

- Farley, F. J. M. 1955, Elements of Pulse Circuits, Methuen & Co
Kiebert, M. V. and Inglis, A. P., 1945, *Proc. I.R.E.*, **33**, 534
M. I. T. Staff, 1946, Principles of Radar, McGraw Hill
Pucko, O. S., 1951, Time Bases, Chapman and Hall
Sarkar, D. C. and Ahmed, R., 1954 *Ind. Jour. Phys.*, **28**, 333.
Seely, S., 1950, Electron tube circuit, McGraw Hill
Williams E. M., Aldrich, D. F. and Woodford, J. B. 1950 *Proc. I.R.E.*, **38**, 65.



SYNONYM OF QUALITY FOR 110 YEARS

**PHYSICAL INSTRUMENTS OF HIGH PRECISION
AND DEPENDABILITY.**

- * ELECTRON MICROSCOPE
- * REFRACTOMETERS:-ABBE, BUTTER & DIPPING.
- * UV SPECTROGRAPH Q 24
- * ALL-AUTOMATIC INFRARED SPECTROPHOTOMETER UR-10
- * ABBE COMPARATOR
- * RAPID PHOTOMETER
- * MONOCHROMATOR
- * PHOTOELECTRIC PHOTOMETER
- * GALVANOMETER, ELECTROMETER & SCHLIEREN EQUIPMENT.
- * MACRO-ELECTROPHORESIS APPARATUS

SOLE AGENTS IN INDIA :

GORDHANDAS DESAI PRIVATE, LTD.

(Telo No. 251418)

**PHEROZESHAH MEHTA ROAD,
BOMBAY I**

**4/2B, ASAF ALI ROAD,
NEW DELHI**

**22 LINGHI CHETTY STREET
MADRAS 1**

**P-7 MISSION ROW EXTENSION
CALCUTTA 1**

A DEVIATION FROM WILKINSON'S THEORY OF DISCHARGE SPREAD IN GEIGER-COUNTERS

SATYAPAL PURI

DEPARTMENT OF PHYSICS, MUSLIM UNIVERSITY, ALIGARH

(Received for publication, April 5, 1957)

ABSTRACT. The measurements of the velocity of propagation of discharge in Geiger counters have been carried out by the method of delayed coincidences. The measurements are interesting only in showing a divergence of results from the theory after the point where the charge generated becomes equal to the charge on the central wire. The spread due to electrons is considered to take a lead over the spread by virtue of ultraviolet photon content of the earlier avalanches after this point.

1. INTRODUCTION

Two highly approximate theories on the mechanism of propagation of discharge in organic vapour rare gas filled counters have been advanced by Alder *et al.* (1947) and Wilkinson (1948). Although their assumptions differ, they both agree that the discharge occurs by a series of photo-ionization processes, each followed by a short radial Townsend avalanche, along the wire, as indicated by the experiments of Stever (1942), and Wilkening and Kanne (1942). The ultraviolet photons which trigger the discharge have energies equal to or greater than the first excitation potential of argon, that is, 11.5 V.

The velocity of propagation of the discharge along a counter wire has been measured by several workers, employing different methods, Hill and Dunworth (1946), Huber *et al.* (1946), Wantuch (1947), Knowles *et al.* (1947), Balakrishnan and Craggs (1950), Saltzmann and Montgomery (1950), Mortier and Roose (1954) and Mortier (1955). Unfortunately all of these reports pertain to the voltages either at threshold or a few volts above it, but none dealt with overvoltages of 200 volts or more.

The present investigation was conducted to see the counter behaviour at and beyond voltages corresponding to $m = \frac{Q}{Q_0} = 1$, the charge formed on the discharge divided by the charge on the wire. A break is expected to occur for voltages beyond $m = 1$, from the theory of Wilkinson.

2. EXPERIMENTAL SET UP

The externally coated maze type counters, filled with petroleum ether and argon as the filling admixture to its total pressure of 10 cm of Hg, were employed. These counters have been described elsewhere, Puri and Gill (1956).

The block diagram of the electronic circuitry is shown in figure 1. A pulse resulting from discharge build-up in one of the short end cylinders (1.5 cm long)

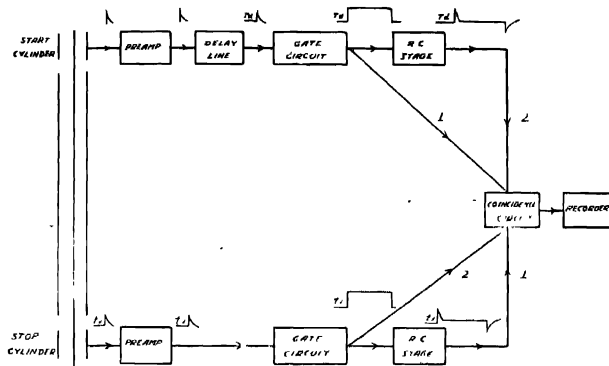


Fig. 1

of the split cathode counters, is put into a square wave-shape by cathode-coupled multivibrator in the direct channel after the pulse has been delayed by an artificial delay T_d , which can be conveniently varied from 0.2 microseconds, by passing it through a network of inductances and capacitances that behave like simulative transmission lines. The discharge then spreads along the counter and the subsequent pulse from the other end cylinder, designated "stop cylinder" as the discharge reaches it, marks the arrival of the discharge after a natural delay t_d , which depends upon the finite speed of propagation of the Geiger discharge, which in its turn depends upon the overvoltage, the nature and composition of the gas filling. This stop pulse is put into the square wave form by the cathode-coupled multivibrator in the delay channel. The two rectangular pulses, the direct (artificially delayed) and the delayed (naturally delayed) were of nearly 15 microseconds duration each. One of them was differentiated and made coincident with the other square pulse.

Two sets of observations were made. In the first set, pulses from the start cylinder remained as square form and the coincidence took place as long as the delay time was within the time due to the spread of the discharge. The results are shown by curve *A* in figure 2. In the second set, the said pulses were differentiated and the coincidence occurred only when the delay time became larger than the spread time. The results are plotted in curve *B*.

The time of spread is determined from the maximum point of curve *C* obtained by superimposing the two curves. This procedure eliminated the finite resolving time of the coincidence circuit and the finite width of the differentiated pulse. The detailed diagram of the whole assembly is shown in figure 3.



cuit. Due to these preamplifiers, the pulses suffer far less distortion or change in shape or size in traversing the delay line.



The delay line was made in the laboratory and consisted of 50 sections of wood-cored inductances of nearly equal value, different points of which were grounded through condensers, making it a multisectioned shaped delay line. The delay

introduced per section was 0.2 microsecond. The cathode coupled multivibrator which was used for putting the pulses into the square shape was constituted by two 6AK5 tubes. The speed of transition depends primarily upon the quantity, as given by Chance and Hughes (1949), g_m^2/C_1C_2 where g_m is the mutual conductance of the tube, C_1 and C_2 are the stray capacities. In the present case, C_1 and C_2 were kept to a minimum by employing miniature tubes, keeping the wiring short and taking the output signal from the multivibrator through a cathode follower. The plate resistances were kept fairly small so that the tubes operated at high current and therefore at high g_m . The rest of the circuit elements were of the conventional types.

It was thoroughly tested with artificial pulses before finally using it for the discharge velocity measurements.

The counter employed was 28 cm long, on either side of which were cathodes of 1.5 cm length. The discharges were initiated in the start cylinder by gamma-rays from a radioactive substance collimated by a small hole in a lead block. The whole counter was shielded from back-ground radiation by placing it in an axially

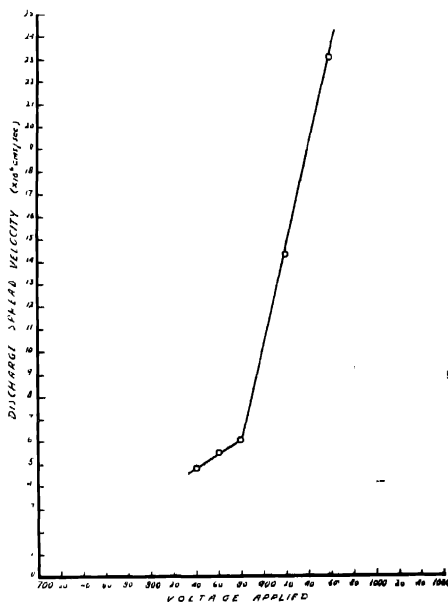


Fig. 4a

bored 1" diameter hole in a lead block of 6"×6" area, except at the place of irradiation.

The results are shown in figures 4(a) and 4(b) for two filling mixtures. The values of propagation velocity at smaller overvoltages are not inconsistent with the results of other workers.

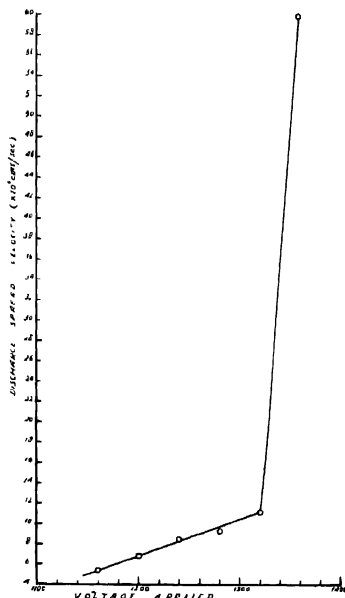


Fig. 4(b)

The earlier parts of the curves of figure 4(a) and 4(b) shows linear increase with overvoltage, whereas at overvoltages of 80 volts and 160 volts for counters 1 and 2 respectively, the curve deviates from the earlier part. The values of discharge velocity are too large to fit the theory. The points of initial divergence correspond to the points $\frac{Q}{Q_0} = 1$, in the two cases.

3. DISCUSSION

Spreading of discharge in Geiger-Muller counters is generally described as occurring through a succession of elementary processes where photons of a primary avalanche release electrons either out of the cathode (in non-self-quenching counters) or out of the filling gas (in self-quenching counters). The secondary electrons initiate the necessary new avalanches. The duration of an elementary process is the sum of the (1) time intervals involved in the production and migration of photons and (2) transit time of the secondary electrons.

With gas mixtures commonly used in counters, for example 9 cm argon plus one cm alcohol vapour, the values of absorption coefficient are of the order of 0.1 cm, (Alder *et al.*, 1947). These values incidentally are also supported by the experiments with glass beads, for a 1 mm bead will in many cases stop a discharge spread. The picture of the progress of the discharge consists in a series of steps, each averaging around one mm in length and then followed by a de-excitation time of around 10^{-8} second. The new electron formed by the absorption of the quantum and resulting photoionization of the organic molecule then originates a new Townsend avalanche. The distance of travel for the electron from the point of formation to the wire being 0.1 cm or less, occurs in a region where the field is high, 10^3 or more volts/cm, and so requires time of the order of 10^{-9} second. Since the duration of single step cannot be much less than 10^{-8} second, the velocity of spread may be as much as 10^{-6} to 10^7 cm/sec. This is supported by the earlier parts of the curves, till the point $m = \frac{Q}{Q_0} = 1$.

After the voltage corresponding to point $m = 1$ reaches, the charge generated being equal to the charge on the wire, there is no resultant pull on the electrons towards the central wire. The wire next to that "Burning out", however, is still active and can pull the electrons, which so far are free in the burnt out part of the wire. The transit time of electron in such high fields requires times of the order of 10^{-9} second, resulting in the propagation velocity of discharge of 10^7 to 10^8 cm/second. The spread by virtue of ultraviolet photons generated in the earlier avalanches is still active, but the spread due to electrons takes a lead, since this process requires comparatively less time.

ACKNOWLEDGMENTS

My sincerest gratitude is due to Professor P. S. Gill, for going through the manuscript and making some very useful suggestions. The financial assistance of National Institute of Sciences of India is also thankfully acknowledged.

REFERENCES

- Alder, F. *et al.*, 1947, *Helv. Phys. Acta*, **20**, 73.
 Balakrishnan, C and Craggs, J. D., 1950, *Proc. Phys. Soc.*, **63A**, 358.
 Chance *et al.*, 1949, "Waveforms" Radiation Laboratory Series.
 Hill, J. M. and Dunworth, J. V., 1946, *Nature*, **158**, 833. ~
 Knowles, A. J. *et al.*, 1948, *Phys. Rev.*, **74**, 627.
 Mortier, P., 1955, *Appl. Sci. Res.*, **5**, Sec. B.
 Mortier, P. A. C. and Roose, J. F., 1954, *Proc. Phys. Soc.*, **67**, 161-3.
 Puri, Satya Pal and Gill, P. S., 1956, *Ind. J. Phys.*, **30**, 62.
 Saltzmann, H. and Montgomery, C. G. 1950, *Rev. Sci. Inst.*, **21**, 548.
 Stever, H. G., 1942, *Phys. Rev.*, **61**, 38.
 Wantuch, E., 1947, *Phys. Rev.*, **74**, 646.
 Wilkinson, D. H., 1949, *Phys. Rev.*, **74**, 1417.
 Wilkening, M. H. and Kanne, W. R., 1942, *Phys. Rev.*, **62**, 534.

ANALYSIS OF THE NEAR ULTRAVIOLET ABSORPTION SPECTRA OF ORTHO, META AND PARA-FLUORO-CHLOROBENZENE VAPOURS

S. L. N. G. KRISHNAMACHARI

DEPARTMENT OF PHYSICS, ANDHRA UNIVERSITY, WALTAIR

(Received for publication, October 26, 1956)

Plate X

ABSTRACT. The ultraviolet absorption spectra of *o,m,p*-fluorochlorobenzene vapours were recorded and analysed. In the spectrum of the ortho isomer about 140 red degraded bands are recorded in the region 2830–2420 Å, with the 0,0 band at 37035 cm⁻¹. These bands are interpreted in terms of 9 upper state and 9 ground state frequencies. For the meta isomer 140 red degraded bands are recorded in the region 2850–2380 Å with the C₁0 band at 37027 cm⁻¹. The bands are interpreted in terms of 8 upper state and 5 ground state frequencies. In the spectrum of the para compound about 240 bands are recorded in the region 2940–2380 Å, the 0,0 band lying at 36276 cm⁻¹. These bands are interpreted in terms of 6 upper state and 9 ground state frequencies. The selected fundamentals in all the three cases are correlated with the Raman frequencies and are assigned to the characteristic normal modes of the molecules. A comparative study of the 0,0 shifts, the prominent *ν*-*r* separations and the intensities of the C–Cl and C–F stretching modes is made in the three compounds.

INTRODUCTION

A number of investigations were carried out on the study of the infrared. (Lecomte, 1938, Parodi, 1941; Kamada, 1952, Milone & Borillo, 1952 and Nielsen, 1953, 1956). Raman effect (Kohlrausch, 1947; Hertz, 1948, 1942 and Sponer & Kirby-Smith, 1941) and the ultraviolet absorption chiefly in solution (Courad-Billroth & Forster, 1936; Dima & Tintea, 1940; Sponer, 1942, 1952, Sreeramamurty, 1951; Cooper, 1954 and Anno Matubara, 1955) of the dihalogenated benzenes of the type ortho, meta, para-C₆H₄XY and C₆H₄X₂ but the ultraviolet absorption in the vapour phase for several molecules of the XY type remain uninvestigated, particularly of those which contain fluorine as a substituent. A comprehensive investigation of these types of substituted benzenes has been planned by the author with a view to arriving at the fundamental vibrational frequencies of the molecules both in the ground and excited states. The author has been enabled to carry out this plan through the generosity of Dr G. C. Finger of the Illinois State Geological Survey who made a gift to the author nine of these compounds (*o*, *m*, *p*-monohalo fluorobenzenes) which were immediately taken up for investigation consisting of the study of the Raman

effect, the infrared and ultraviolet absorption, the last being in the vapour phase. Some of the results have already been reported briefly in letters published in Indian Journal of Physics (Krishnamachari, 1955, 1956) and in Current Science (author, 1955, 1956). The present paper deals with a detailed discussion of the analysis of the ultraviolet absorption spectra of *o*, *m*, *p*-fluorochlorobenzenes. There is no previous work on the absorption of the para compound while the ortho and meta compounds were investigated in hexane solution by Conrod-Billroth (1936). The latest work on the infrared and Raman spectra of these compounds is that of the Nielsen and co-workers (1956).

The experimental set up developed in this laboratory for studies of the kind described here has been already described elsewhere (Krishnamachari, 1956a). The samples of *o*, *m*, *p*-fluorochlorobenzenes supplied by Dr. Finger were vacuum distilled twice before use.

DESCRIPTION OF THE BANDS

o-Fluorochlorobenzene :

The absorption spectrum of this molecule lies in the region between 2830 and 2420 Å. About 140 bands are recorded in various stages of the saturated vapour pressures corresponding to different temperatures. The minimum number of bands are recorded with a 5 cm. cell at -18°C . These are at 37035, 37674, 37833, 37975, and 38111 cm^{-1} . Of these the one lying at the longest wavelength, i.e., 37035 cm^{-1} , was chosen as the 0,0 band of the system. The maximum number of discrete bands are recorded with a 50 cm. cell at -15°C . At higher temperatures the absorption on the violet side grows stronger and becomes continuous, and bands corresponding to the excitation of the higher frequency vibrations in the ground electronic state of the molecule gradually appear on the red end of the continuum. The longest wavelength band near about 2830 Å is recorded at 60°C . The bands are red degraded and almost all the strong bands are accompanied by satellite bands on the long wavelength side with separations 35, 69 and 125 cm^{-1} and their multiples, the 69 cm^{-1} separation being the most pronounced one. The band data are listed in Table I. The intensities are only visual estimates and have the following significance *w* = weak, *mw* = medium weak, *m* = medium, *ms* = medium strong, *s* = strong, *vst* = very strong, *sh* = sharp, *d* = diffuse and *b* = broad. The development of the spectrum under different experimental conditions is shown in figure 1 Plate X.

m-Fluorochlorobenzene :

The meta spectrum lies in the region 2850–2380 Å in which about 140 red degraded bands are recorded. The minimum number of bands observed with a 5 cm. cell at -18°C are 37027, 37663 and 37993 cm^{-1} of which the longest

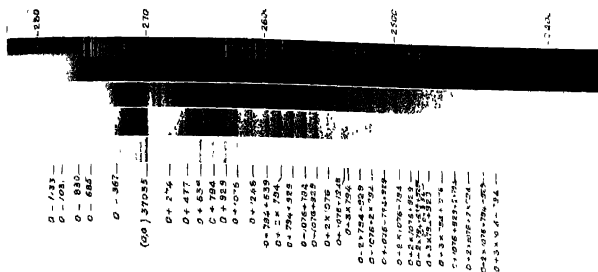


Fig. 1 Ultraviolet absorption spectrum of *o*-fluorochlorobenzene

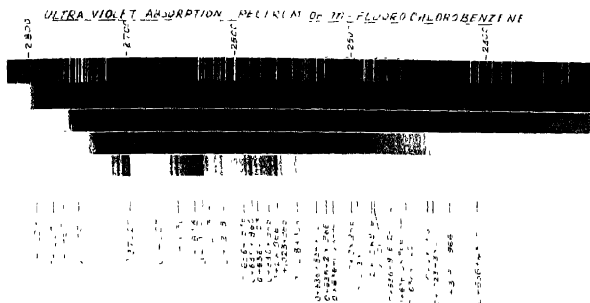


Fig. 2 Ultraviolet absorption spectrum of *m*-fluorochlorobenzene.

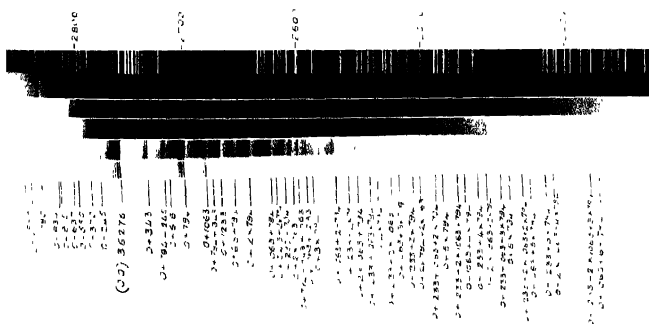


Fig. 3. Ultraviolet absorption spectrum of *p*-fluorochlorobenzene.

TABLE I
Absorption bands of o-fluorochlorobenzene

ν cm^{-1}	Intensity	$\Delta\nu$ cm^{-1}	Assignment
50cm, 60°C			
35315	ew,b,d	-1720	-1031-685 = 1716
35625	ew	-1410	-1031-367 = 1398
35666	vw	-1369	-2 x 685 = 1370
35720	w	-1315	-830-489 = 1319, -1246-69 = 1315
35765	m	-1275	
50cm, 28°C			
35789	m	mw	-1246 0-1246
35796		mw	-1239 -556-685 = 1241
35839		w	-1196 -830-367 = 1197
35902		m,d	-1133 0-1133
35934		w	-1101 -2 x 556 = 1112, -1031-69 = 1100
36004		m,sh	-1031 0-1031
36070		mw,d	-965 -830-2 x 69 = 968, +274-1246 = 972
36105		mw	-930 -367-556 = 923
36026		m,sh	-899 -830-69 = 899
36205		st,sh	-830 0-830
36227		ms,sh	-808 -685-125 = 810
36283		st	-752 +274-1031 = 757, -685-69 = 754
50cm, -15°C			
36350	ms	st	-685 0-685
36441	mw		-594 +651-1246 = 595
36479	w		-556 0-556
36514	m		-521 +513-1031 = 518
36546	w		-489 +639-1133 = 494, 0-489
36586	m,d		-440 +794-1246 = 452
36624	mw,d		-411 +274-685 = 411
36668	st		-367 0-367
25cm, -15°C			
36759	st	vw	-276 +274-556 = 282
36801		w	-234 +794-1031 = 237
36820		mw	-215 +274-489 = 215
36824		mw	-211 477-685 = 208
36837		vw	-198 -3 x 69 = 207
36841		ew	-194 +639-830 = 191
36865		ew	-170 +513-685 = 172, 0-170
36896		m	-139 -2 x 69 = 188
36910		mw	-125 0-125
36933		w	-102 -69-34 = 103, +620-1031 = 102
25cm, -15°C			
36959		st	-76 +474-556 = 79
36966		st	-69 -69
37001		m	-34 +794-830 = 36, +651-685 = 34
37035		vst	0 0,0
37062		vw	27 +513-489 = 24
37134		mw	99 +929-830 = 99, 0+99
37182		w	147 +513-367 = 146
37206		mw	171
37309		mw	274 +639-367 = 272, 0+274
37421		w	386 +940-556 = 384
37440		mw	414 +1248-830 = 418
37512		w	477 0+477
37534		w	499 +639-2 x 69 = 501
37548		mw	513 0 + 513
37557		vw	522 +1076-556 = 520
37606		m	571 +639-69 = 570
37619		w	584 +1076-489 = 587
37639		w	604 639-34 = 605
37674		st	639 0+639

TABLE I (Contd.)

ν cm^{-1}	Intensity	$\Delta\nu$ cm^{-1}	Assignment
37686	ms	651	0-1 651 ?
37727	mw	692	1-1248-556 = 692
37782	ms	727	+794-69 = 725
37798	mw	763	1-1248-489 = 759, -1 794-34 = 760
37829	st	794	0-1 794
37833	st	798	
37896	ms	861	929-69 = 860
37905	m	870	$2 \times 470 - 69 = 871$
37964	st	929	0-1 929
37975	st	940	$2 \times 470 \pm 940$
37984	mw	949	$2 \times 477 = 954$
38040	m	1005	1076-69 = 1005
38077	mw	1042	1076-34 = 1042
38111	st	1076	0-1 1076
38152	vw	1117	477+639 = 1116
38214	w	1179	1248-69 = 1179
38234	w	1199	274+929 = 1203
38283	m	1248	0-1 1248
38283	w	1269	477+794 = 1271
38304	w	1282	$2 \times 639 = 1278$
38317	w	1309	513+794 = 1307
38344	vw	1345	271+1076 = 1350
38380	w	1363	794+639-69 = 1364
38398	w	1433	794+639 = 1433
38468	m	1433	513+929 = 1442
38479	w	1444	1248+274 = 1522, $2 \times 794 - 69 = 1519$
38555	mw,d	1520	639+929 = 1568
38611	m,d	1576	$2 \times 794 = 1588$
38620	mw,d	1591	651+2 \times 470 = 1591
38626	mw,d	1641	639+1076-69 = 1646
38676	w	1641	639+1076 = 1715
38748	m,d	1713	794+929 = 1723
38758	m,d	1723	794+2 \times 470 = 1734
38770	m,d	1735	1076+794-69 = 1801
38835	mw,d	1800	1076+794 = 1870
38906	m,d	1871	639+1248 = 1887
38928	vw	1893	1076+929-69 = 1936
38976	w	1941	1076+929 = 2005
39036	m,d	2001	1076+2 \times 470 = 2016
39049	m,d	2014	1248+794 = 2042
39071	vw	2036	$2 \times 1076 - 69 = 2083$
39107	w	2072	$2 \times 1076 = 2152$
39182	mw	2147	929+1248 = 2177
39209	w,d	2174	1248+2 \times 470 = 2188
39218	w,d	2183	639+2 \times 794 = 2227
39262	w	2227	1076+1248-69 = 2255
39283	vw	2248	
50cm, -15°C			
39356	m	2321	1076+1248 = 2324
39397	m,b,d	2362	929+794+639 = 2362
39417	m,b,d	2382	$3 \times 794 = 2382$
39470	w,d	2435	1076+794+639-69 = 2440
39484	w,d	2440	$2 \times 794+929-69 = 2448$
39434	ms,b,d	2499	794+639+1076 = 2509, $2 \times 1248 = 2496$
39558	ms,b,d	2523	$2 \times 794+929 = 2517$
39608	w,d	2573	639+1076+929-69 = 2575
39628	w,d	2593	$2 \times 794+1076-69 = 2595$
39678	ms,b,d	2643	639+1076+929 = 2644
39694	ms,b,d	2659	$2 \times 794+1076 = 2664$
39761	vw	2726	1076+794+929-69 = 2780
39833	m,b,d	2798	$2 \times 1076+639 = 2791$

TABLE I (Contd.)

ν cm ⁻¹	Intensity	$\Delta\nu$ cm ⁻¹	Assignment
39843	m,b,d	2808	1076 + 794 + 929 = 2799
39903	w,d	2868	1076 + 2 × 929 - 69 = 2865
	50cm, -15°C		
39970	m,b,d	2935	1076 + 2 × 929 = 2934
39977	m,b,d	2942	2 × 1076 + 794 = 2946
40042	w,d	3007	2 × 1076 + 929 - 69 = 3012
40120	m,b,d	3085	2 × 1076 + 929 = 3081
40189	mw	3154	2 × 794 + 639 + 929 = 3156, 0 + 3154
40286	w,b,d	3251	1076 + 1248 + 929 = 3253
	50cm, 20°C		
40351	w,b,d		
	m,b,d	3316	3 × 794 + 929 = 3311
40426	m	3391	2 × 1076 + 1248 = 3400
40474	m,vb,d	3439	2 × 794 + 929 + 929 = 3446 1076 + 929 + 794 + 639 = 3438
40490	m,vb,d	3455	1076 + 3 × 794 = 3458
40551	mw	3516	1076 + 2 × 794 + 929 - 69 = 3524
40620	m,vb,d	3585	1076 + 2 × 794 + 929 = 3593
40632	m,vb,d	3597	
40689	vw,b,d	3654	1076 + 794 + 2 × 929 - 69 = 3659
40761	m,vb,d	3726	1076 + 794 + 2 × 929 = 3728
40772	m,vb,d	3737	2 × 1076 + 2 × 794 = 3740
40826	w	3791	
40904	mw,vb,d	3869	2 × 1076 + 929 + 794 = 3875
40921	mw,vb,d	3886	639 + 1076 + 929 + 1248 = 3892
41054	mw,b,d	4019	2 × 1076 + 794 + 1076 = 4022
41128	mw,b,d	4093	3 × 794 + 929 + 794 = 4105
41187	w,b,d	4152	2 × 1076 + 929 + 1076 = 4157
41264	w,b,d	4229	2 × 929 + 3 × 794 = 4240

wavelength one, the 37027 cm⁻¹ band, is chosen as the 0,0 band of the system. The effect of increasing the temperature and path length is the same as in the case of the ortho compound. The maximum number of discrete bands are recorded with a 50 cm. cell at -10°C and the longest wavelength band is recorded at 100°C. As in the ortho compound satellite bands occur on the long wavelength side of the strong bands, the intervals are 42 cm⁻¹ and 78 cm⁻¹ and their multiples, the latter being more pronounced. The band data are presented in Table II. The development of the spectrum is shown in figure 2 (Plate X)

TABLE II
Absorption bands of *m*-fluorochlorobenzene

ν cm ⁻¹	Intensity	$\Delta\nu$ cm ⁻¹	Assignment
	50cm, 100°C		
35124	vw,b	-1903	-1007 - 895 = 1902
	50cm, 80°C		
35247	m,b	-1780	-2 × 895 = 1790
35332	vw,b	-1695	-1007 - 688 = 1695
	w,b		
	50cm, 70°C		
35447	ew,b	-1580	-688 - 895 = 1583
35571	w,b	-1456	
35600	w,b	-1427	-1264 - 2 × 78 = 1420
	50cm, 50°C		
35640	mw,b	-1387	-1229 - 2 × 78 = 1385
	w,b,d		

TABLE II (Contd.)

	Intensity	$\Delta\nu$ cm ⁻¹	Assignment
35679	w,b,d	-1348	-1264-78 = 1342
35719	mw,b,d	-1308	-1229-78 = 1307
35763	mw,sh	-1264	0-1264
35798	ms,sh	-1229	0-1229
35836	w,sh	-1191	-1007-186 = 1193
35867	ms,d	-1160	-1007-2 × 78 = 1163
35902	w,d	-1125	
35941	s,sh	-1086	-1007-78 = 1085
35977	vw,sh	-1050	-2 × 1007 + 966 = 1048, 0-1050
36020	s,sh	-1007	0-1007
36056	m,b	-971	-895-78 = 973
36132	ms,sh	-895	0-895
36171	ms,b	-856	
36217	vw,b	-810	-1007 + 966 - 688 - 78 = 807
36263	s,b	-764	-688-78 = 766
36275	vw,b	-752	
36295	vw,b	-732	-1007 + 966 - 688 = 729
36339	vs,sh	-688	0-688
36432	s,b	-595	-1229 + 636 = 593
36589	w,b	-438	-895 + 455 = 440
25cm, -15°C			
36673	w,d	s,b	-354
36688	w,sh		-339
36721	mw,b		-306
36742	mw,b		-285
36765	mw,b		-262
36793	m,sh		-234
36799	mw,sh		-228
36807	mw,sh		-220
36814	mw,sh		-213
25cm, -15°C			
36835	mw,sh		-192
36841	mw,sh		-186
36872	ms,sh		-155
36878	m,sh		-149
36905	mw,sh		-122
36949	s,sh		-78
36953	ms,sh		-74
36975	w,b		-52
36979	vw,sh		-48
36985	mw,d		-42
37022	s,sh		-5
37027	vs,sh		0
37030	w,sh		3
25cm, 0°C			
37048	ow	mw,b,d	21
37102		w,b,d	75
37109		w,sh	82
37151		ms,sh	124
37190		ms,sh	163
37231		ms,sh	204
37267		m,sh	240
37345		ms,sh	318
37354		ms,sh	327
37393		m,b,d	366
37427		w,sh	400
37482		ms,b,d	455
25cm, -15°C			
37507	mw,sh	st,b,d	480
37541	w,sh		514
37585	s,sh		558

TABLE II (Contd.)

ν cm ⁻¹	Intensity	$\Delta\nu$ cm ⁻¹	Assignment
37591	m,sh	564	1251 - 688 = 563
37611	w,d	584	2 × 636 - 688 = 584
37621	w,d	594	636 + 966 - 1007 = 595
37663	vs,sh	636	0.636
37666	m,sh	639	
37684	w,b,d	657	2 × 327 = 654
37762	mw,b,d	735	966 - 3 × 78 = 732
37798	m,sh	771	846 - 78 = 768
37806	w,d	779	966 - 186 = 780, 465 + 327 = 782
37838	ms,d	811	966 - 2 × 78 = 810
37873	ms,sh	846	0 + 846
25cm, -15°C			
37915	s,sh	888	966 - 78 = 888
37921	ms,sh	894	
37951	m,sh	924	2 × 966 - 1007 = 925
37987	s,sh	960	
37993	vs,sh	966	0 + 966
37996	w,sh	969	
38050	m,sh	1023	0 + 1023
38086	w,b,d	1059	1218 - 2 × 78 = 1062
38114	w,b,d	1087	636 + 455 = 1091
38167	mw,sh	1140	1218 - 78 = 1140
38172	vw,sh	1145	636 + 514 = 1150
38202	w,b,d	1175	846 + 327 = 1173
38245	ms,sh	1218	0 + 1218
38278	w,sh	1251	0 + 1251
38296	vw,b,d	1269	2 × 636 = 1272
38319	w,b,d	1292	327 + 966 = 1293
38393	vw,b,d	1366	636 + 966 - 3 × 78 = 1368
38444	vw,b,d	1417	966 + 455 = 1421
38471	vw,b,d	1444	636 + 966 - 2 × 78 = 1446
38509	vw,b,d	1482	514 + 966 = 1480, 846 + 636 = 1482
38547	ms,d	1520	636 + 966 - 78 = 1524
38623	s,sh	1596	
38629	vs,sh	1602	636 + 966 = 1602
38688	mw,b,d	1661	1023 + 636 = 1659
38757	w,b,d	1730	966 + 846 - 78 = 1734
38796	mw,b,d	1769	2 × 966 - 2 × 78 = 1776
38839	mw,sh	1812	966 + 846 = 1812
38882	s,sh	1855	2 × 966 - 78 = 1854
38854	s,d	1927	
38950	s,d	1932	2 × 966 = 1932
39013	w,sh	1986	1023 + 966 = 1989
39091	ew,b,d	2064	1218 + 846 = 2064
39130	vw,b,d	2103	1218 + 966 - 78 = 2106
39211	m,sh	2184	1218 + 966 = 2184
39241	w,b,d	2214	1251 + 966 = 2217
39263	w,b,d	2236	2 × 636 + 966 = 2238
39393	vw,b,d	2366	514 + 2 × 966 - 78 = 2368
39471	w,b,d	2444	846 + 636 + 966 = 2448
39516	mw,b,d	2480	636 + 2 × 966 - 78 = 2490
39592	m,b,d	2565	636 + 2 × 966 = 2568
39643	mw,b,d	2616	1023 + 636 + 966 = 2625
39724	w,b,d	2697	846 + 2 × 966 - 78 = 2700
50cm, 0°C			
39758	w,b,d	2731	
39800	w,b,d	2773	846 + 2 × 966 = 2778
39845	mw,b,d	2818	3 × 966 - 78 = 2820
39928	m,b,d	2901	3 × 966 = 2898
40022	mw,b,d	2955	1023 + 2 × 966 = 2955

TABLE II (Contd.)

ν cm ⁻¹	Intensity		$\Delta\nu$ cm ⁻¹	Assignment
40183	ew	mw,b,d	3156	$1218 + 2 \times 966 = 3150$
40218		mw,b	3191	$0 + 3191$
40247		w,b,d	3220	
40325		w,b,d	3298	
40442		ew,b,d	3415	$636 + 848 + 2 \times 966 = 3414$
40507		ms,b,d	3540	$636 + 3 \times 966 = 3534$
40633		m,b,d	3606	$1023 + 636 + 2 \times 966 = 3591$
40777		mw,b,d	3760	$846 + 3 \times 966 = 3744$
40818		m,b,d	3791	$4 \times 966 - 78 = 3786$
40893		m,b,d	3866	$4 \times 966 = 3864$
40959		mw,b,d	3932	$1023 + 3 \times 966 = 3921$
41029		w,b,d	4002	
41077		w,b,d	4050	
41111		w,b,d	4084	
41155		vw,b,d	4128	
41186		w,b,d	4159	$3191 + 966 = 4157$
	50cm, 25°C			
41518	mw,b,d	ew,b,d	4491	$636 + 4 \times 966 = 4500$
41576	mw,b,d		4549	$1023 + 636 + 3 \times 966 = 4557$
41640	w,b,d		4613	
41721	mw,b,d		4694	
41901	w,b,d		4874	$4 \times 966 + 1023 = 4887$

p-Fluorochlorobenzene

The para spectrum lies in the region between 2940 and 2380 Å. About 240 bands are recorded in this region. Many of the strong bands appear to be slightly violet degraded. The least number of bands are recorded with a 50 cm cell at -70°C . These are at 36276, 37070, 37339 and 38133 cm^{-1} , and the one at 36276 cm^{-1} is chosen as the 0,0 band of the system. The effect of increasing the temperature and path length is similar to that for the ortho and meta compounds. The maximum number of discrete bands are recorded with a 50 cm cell at -10°C and the longest wavelength band is recorded at 100°C . with a 75 cm. tube. The satellites occur with separations of 33 cm^{-1} . The band data are collected in Table III and the spectrum is reproduced in figure 3 (Plate X)

In addition to the near ultraviolet electronic spectra discussed above, there is another continuous absorption system below 2150 Å for all the three molecules. We could only observe the long wavelength edge of this system which gradually moves towards the red with increasing temperatures and finally merges with the system on the long wavelength side described above.

ANALYSIS AND DISCUSSION

The ortho and meta-fluorochlorobenzene molecules belong to the C_s point group with the molecular plane as the only element of symmetry. The near ultraviolet absorption spectrum of benzene has been interpreted as due to the forbidden electronic transition ${}^1A_{1g} \rightarrow {}^1B_{2u}$ made allowed by the superposition of the c_g^+ vibrations on any one of the electronic states.

TABLE III

Absorption bands of *p*-fluorochlorobenzene

	Intensity	$\Delta \nu$ cm ⁻¹	Assignment
75cm, 100°C			
34048	ew,b	-2228	-1590 - 637 = 2227
34090	vw,b	-2186	-2 × 1090 = 2180
34131	ew,b	-2145	-1590 - 550 = 2140
34163	vw,b	-2113	
34218	vw,b	-2058	-1239 - 815 = 2054
34256	vw,vb	-2020	
34282	vw,vb	-1994	-1090 - 834 - 2 × 33 = 1990
34312	vw,vb	-1964	-1090 - 834 - 33 = 1957
34346	w,sh	-1930	1090 - 834 = 1924
34379	vw	-1897	-1090 - 815 = 1905
75cm, 85°C			
34537	vw,vb	-1739	
34567	mw,	-1709	-2 × 834 - 2 × 33 = 1734
34600	mw,	-1676	-2 × 834 - 33 = 1701
34629	m,vl	-1647	-2 × 834 = 1668
34663	m,vl	-1613	-815 - 834 = 1649
34686	m,vl	-1590	-1239 - 370 = 1609
75cm, 50°C			
34808	vb,vw	-1468	0 - 1590
34844	vw	1432	-834 - 637 = 1471
34872	vw	1404	-815 - 370 - 245 = 1430
34899	mw,sh	-1377	-1090 - 245 - 33 = 1368
34933	m,sh	-1343	-1090 - 245 = 1335
34971	m,b	-1305	-1239 - 2 × 33 = 1305
35003	m,b	-1273	1239 - 33 = 1272
35037	m,b	-1239	0 - 1239
50cm, 30°C			
35061	mw,b		
35082	vw,b	-1215	-815 - 370 - 33 = 1218
35094	mw,sh	-1194	-1090 - 3 × 33 = 1189
35117	w,b	-1182	-815 - 370 = 1185
35149	mw,sh	-1159	-1090 - 2 × 33 = 1156
35186	ms,sh	-1127	-1090 - 33 = 1123
	st,sh	-1090	0 - 1090
50cm, 10°C			
35216	vw,b		
35267	w,sh	-1060	-815 - 245 = 1060
35289	w,b	-1007	-637 - 370 = 1007
35319	mw,b	-987	
35346	w,b	-957	-370 - 550 - 33 = 953
35353	w,b	-930	-834 - 3 × 33 = 933
35378	mw,sh	-923	-370 - 550 = 920
		-898	-834 - 2 × 33 = 900
50cm, 10°C			
35396	mw,b	-880	-815 - 2 × 33 = 881
35411	m,sh	-865	-834 - 33 = 867
35431	m,d	-845	-815 - 33 = 848
35442	mw,sh	-834	0 - 834
35461	m,b	-815	0 - 815
35482	w,b	-794	-245 - 550 = 795
35497	w,b	-779	
35526	vw,b,d	-750	
35548	vw,b,d	-728	-637 - 90 = 727
35576	vw,b,d	-700	-637 - 2 × 33 = 703
35607	w,b,d	-669	-637 - 33 = 670
35639	m,sh	-637	0 - 637
35657	m,sh	-619	-370 - 245 = 615
35692	m,sh	-584	-550 - 33 = 583

TABLE III (Contd.)

ν cm ⁻¹	Intensity	$\Delta\nu$ cm ⁻¹	Assignment
35726	ms,sh	-550	0-550
	50cm, 0°C		
35788	vw,b	-488	-834+343 = 491
35805	vw,b	-471	-370-3×33 = 469, -815-1 343=472
35818	vw,b	-458	-370-90 = 460
35838	mw,b,d	-438	-370-2×33 = 436
35870	s,sh	-406	-370-33 = 403
35900	vw,d	-376	-370-6 = 376
	50cm, -10°C		
35906	w,sh	-370	0-370
35928	w,sh	-348	-245-3×33 = 344
35941	mw	-335	-245-90 = 335
35960	m	-316	-245-2×33 = 311
35995	m	-281	-245-33 = 278
36023	w,d	-253	-245-6 = 251
36031	ms,sh	-245	0-245, -815+563 = 252
36058	w	-218	-834+618 = 216
36066	w,vb	-210	-550+343 = 207
36097	m,b	-179	-2×90 = 180
	50cm, -30°C		
36119	m,b,d	-157	-90-2×33 = 156
36148	mw,d	-128	-4×33 = 132
36156	mw,d	-120	-90-33 = 123
36180	m,b,d	-96	-3×33 = 99
36186	m,b,d	-90	-90
36212	m,sh	-64	-2×33 = 66
36230	mw,d	-37	-33-6 = 39
36243	ms	-33	-33
	50cm, -30°C		
36270	s,sh	-6	-6
36276	vs,sh	0	0,0
	50cm, -10°C		
36376	mw,b	100	343-245 = 99
36425	w	149	-1090+1233 = 143
36433	mw	157	794-637 = 157
36468	mw,vb	192	563-370 = 193
36493	w,b	217	
36507	mw,b	231	1063-834 = 229
36532	m,vb	256	1063-815 = 248
36564	mw,vb	288	-1090+1382 = 292
36582	m	306	343-33 = 310
36593	m	317	563-245 = 318
36612	m,d	336	343-6 = 337
36619	m	343	0+343
36665	mw,b	389	
36677	w,b	401	1233-834 = 399
36704	mw,vb	428	1063-637 = 426
36797	ms,vb	521	1063-550 = 513, 794-3×90 = 524
36829	ms,vb	553	794-245 = 549
36839	w,sh	563	0+563
	50cm, -30°C		
36894	mw,b,d	618	784-2×90 = 614
36941	m,d	665	794-4×33 = 662
36948	m,d	672	794-90-33 = 671
36963	w,sh	687	2×343 = 686
36974	ms,d	698	794-3×33 = 695
36982	ms,d	706	794-90 = 704
36999	ms,d	723	
37004	ms,sh	728	794-2×33 = 728
37029	ms,sh	753	
37035	w	759	794-33 = 755

TABLE III (Contd.)

ν cm ⁻¹	Intensity	$\Delta \nu$ cm ⁻¹	Assignment
37038			
37059	ms,sh	762	794-33 = 761
37065	vw,d	783	
37070	s,sh	789	794-6 = 788
	s,sh	794	0+794
37089	50cm, -10°C		
	m		
37105	m,b	813	1063-245 = 818
37187	m,vb	889	343+794-245 = 892
37208	mw,b	911	563+343 = 906
37215	mw,b	932	1063-4×33 = 931
37221	mw,b	939	1063-90-33 = 940
37241	m,b	945	
	50cm, -10°C		
37249	m,b	965	1063-3×33 = 904
		973	1063-90 = 973
37273	50cm, -30°C		
	m,sh		
37300	mw,sh	997	1063-2×33 = 997
37306	vw,d	1024	1063-33-66 = 1024
37332	m,sh	1030	1063-33 = 1030
	w,d	1056	1063-6 = 1057
37339	50cm, -10°C		
	s		
37358	w	1063	0+1063
37383	mw,vb	1082	
37415	m,vb	1107	794+343-33 = 1104
37442	w,b	1139	794+343 = 1137
37459	vw,b	1166	1233-2×33 = 1167
37475	m,sh	1183	
37509	ms,sh	1199	1233-33 = 1200
37523	w,sh	1233	0+1233
37543	w,vb	1247	
37582	w	1267	
37604	w,sh	1306	
37621	w,sh	1328	2×794-2×90-2×33 = 1332
37636	vw,sh	1345	1382-33 = 1349
37658	ms,b	1360	2×794-2×90-33 = 1365
		1382	0+1382
37672	vw,vb	1396	2×794-2×90 = 1398
37731	mw,vb	1455	2×794-90-33 = 1456
37702	mw,vb	1486	2×794-90 = 1488
37799	ms,vb	1523	2×794-2×33 = 1522
37828	ms,vb	1552	
37833	ms,vb	1557	2×794-33 = 1555
37866	ms	1590	2×794 = 1588
38003	mw,vb	1727	794+1063-4×33 = 1725
38012	mw,b	1736	794+1063-1×90-33 = 1734
38036	m,b	1760	794+1063-3×33 = 1758
38044	m,b	1768	794+1063-90 = 1767
38066	m,b	1790	794+1063-2×33 = 1791
38091	w	1815	
38096	w	1820	
38102	ms,b	1826	794+1063-33 = 1824
38129	ms,b	1853	794+1063-6 = 1851
38133	ms,b	1857	794+1063 = 1857
38174	w,vb	1898	343+2×794-33 = 1898
38204	mw,b	1928	343+2×794 = 1931
38241	w,b	1965	1233+794-2×33 = 1961
38268	m,vb	1992	1233+794-33 = 1994
38300	50cm, -10°C		
	m		
38330	w,sh	2024	1233+794 = 2027
38365	mw,sh	2054	2×1063-2×33 = 2060
38397	m,sh	2089	2×1063-33 = 2093
		2121	2×1063 = 2126

TABLE III (Contd.)

Intensity		$\Delta\nu$ cm ⁻¹	Assignment
38436	w,b,d	2160	794 + 343 + 1063 - 33 = 2167
38472	w	2196	
38478	mw	2202	794 + 343 + 1063 = 2200
38503	vw,d	2227	1063 + 1233 - 2 × 33 = 2230
38532	mw	2256	1063 + 1233 - 33 = 2263
38569	m,sh	2293	1063 + 1233 = 2296
38617	mw,b	2341	3 × 794 - 33 = 2340
38652	m,vb	2376	3 × 794 = 2382
38728	mw,b	2452	2 × 1233 = 2466
38794	w,vb	2518	1063 + 2 × 794 - 4 × 33 = 2519
38820	mw,vb	2550	1063 + 2 × 794 - 3 × 33 = 2552
38861	mw,b	2585	1063 + 2 × 794 - 2 × 33 = 2585
38892	mw,vb	2616	1063 + 2 × 794 - 33 = 2618
38907	mw,b	2631	
38919	mw,b	2643	
38925	m,b	2649	1063 + 2 × 794 = 2651
39058	mw,b,d	2782	1233 + 2 × 794 - 33 = 2788
39090	mw,b,d	2814	1233 + 2 × 794 = 2821
39125	w,b	2849	2 × 1063 + 794 - 2 × 33 = 2854
39159	mw,b,d	2883	2 × 1063 + 794 - 33 = 2887
39194	m,b,d	2918	2 × 1063 + 794 = 2920
39263	w,b	2987	2 × 794 + 343 + 1063 = 2994
39293	w,b	3017	1233 + 1063 + 794 - 2 × 33 = 3024
39328	m,b	3052	1233 + 1063 + 794 - 33 = 3057
39361	m,b	3085	1233 + 1063 + 794 = 3090
39411	mw,vb	3135	
39421	mw,vb	3145	4 × 794 - 33 = 3143
39452	m,vb	3170	4 × 794 = 3176, 3 × 1063 = 3189
39527	mw,vb,d	3251	794 + 343 + 2 × 1063 = 3263
39554	w,vb,d	3278	
39590	mw,b,d	3314	1233 + 2 × 1063 - 33 = 3326
39624	mw,b,d	3348	1233 + 2 × 1063 = 3359
39676	mw,b,d	3400	1063 + 3 × 794 - 33 = 3412
39716	mw,b,d	3440	1063 + 3 × 794 = 3445
39846	w,b	3570	1233 + 3 × 794 - 33 = 3582
39877	w,b	3601	1233 + 3 × 794 = 3615
39914	vw,d	3638	2 × 1063 + 2 × 794 - 2 × 33 = 3648
39947	mw,b	3671	2 × 1063 + 2 × 794 - 33 = 3681
39983	mw,b	3707	2 × 1063 + 2 × 794 = 3714
50cm, -10°C			
40015	w,vb	3839	1233 + 1063 + 2 × 794 - 33 = 3851
40150	w,vb	3874	1233 + 1063 + 2 × 794 = 3884
40201	w,vb	3925	5 × 794 - 33 = 3937
40234	w,vb	3958	5 × 794 = 3970
40281	ew,vb,vd	4005	794 + 343 + 2 × 1063 + 794 - 33 = 4020
40316	ew,vb,vd	4040	794 + 343 + 2 × 1063 + 794 = 4057
40347	w,b,d	4071	1233 + 2 × 1063 + 794 - 2 × 33 = 4087
40379	w,b,d	4103	1233 + 2 × 1063 + 794 - 33 = 4120
40412	w,b	4136	1233 + 2 × 1063 + 794 = 4153
40465	ew,b	4189	1063 + 4 × 794 - 33 = 4206
50cm, 0°C			
40503	ow,b	4227	1063 + 4 × 794 = 4239
40515		4239	
40528		4252	
40540		4264	
40634		4358	1233 + 4 × 794 - 33 = 4376
40666		4390	1233 + 4 × 794 = 4409
40735		4459	2 × 1063 + 3 × 794 - 33 = 4475
40768		4492	2 × 1063 + 3 × 794 = 4508
40808		4532	
40842		4566	
40892		4616	1233 + 1063 + 3 × 794 - 33 = 4645

TABLE III (Contd.)

ν cm ⁻¹	Intensity	$\Delta\nu$ cm ⁻¹	Assignment
40931	w,b,d	4655	1233 + 1063 + 3 × 794 = 4678
40961	w	4685	
41030	w,b,d	4754	6 × 794 = 4764
41063	w,vb,vd	4787	343 + 3 × 794 + 2 × 1063 = 4814
41100	w,vb,vd	4824	343 + 3 × 794 + 2 × 1063 = 4851
41151	mw,vd,vh	4885	
41198	mw,vb,vd	4922	1233 + 2 × 1063 + 2 × 794 = 4947
41252	mw,b,d	4976	1063 + 5 × 794 = 5000
50cm, 10°C			
41285	s,b,d	5009	1063 + 5 × 794 = 5033
51324	m,vb,d	5048	
41350	ms,vb,d	5083	
41393	m,b,d	5117	
41424	w,b,d	5148	
41461	m,vb,vd	5185	1233 + 5 × 794 = 5203
41546	mw,b	5270	2 × 1063 + 4 × 794 = 5302
41638	mw,b	5362	
41989	m,b,d	5713	1233 + 2 × 1063 + 3 × 794 = 5741
42035	w,b,d	5759	
42068	m,b,d	5792	1063 + 6 × 794 = 5827

For C_s point group the above states become A' states and the transition $A' - A'$ is an allowed one with the transition moment lying in the molecular plane. The para-fluorochlorobenzene molecule, however, belongs to the C_{2v} point group for which the above mentioned states of benzene become A_1 and B_1 states respectively. The transition $A_1 - B_1$ is also an allowed one, the transition moment lying in the molecular plane and perpendicular to the para axis. In conformity with the allowed nature of the electronic transition strong 0,0 bands and progressions and combinations of many totally symmetrical vibrations are observed for all the three molecules. In addition to this allowed transition, a so called forbidden part of the transition of much weaker intensity may also be produced by a vibration moment as in the case of benzene. This moment can be produced in the z-direction (perpendicular to the molecular plane) by an α'' vibration in the case of the ortho and meta compounds and by a β_1 vibration in the y-direction (parallel to the para-axis) or by an α_2 vibration in the z direction in the case of the para-compound.

Ortho-Fluorochlorobenzene.

In ortho-fluorochlorobenzene the two very strong bands 794 cm⁻¹ and 929 cm⁻¹ correspond to the progression forming frequencies in the upper state. These represent totally symmetrical carbon frequencies and are correlated with the ground state frequencies 830 and 1031 cm⁻¹. The corresponding Raman lines at 826 and 1029 cm⁻¹ are strong and polarised.

The strong band 639 cm⁻¹ in the upper state and its counterpart 685 cm⁻¹ in the ground state represent the C—Cl stretching frequency in the two electronic

states. The corresponding Raman line is the strong polarised one at 680 cm^{-1} . This assignment is suggested from a comparative study of the ortho-substituted chlorobenzenes. The following are the excited and ground state frequencies which may be assigned to the C—Cl stretching mode

	Raman	U.V. ground state	U.V. excited state
<i>o</i> -chloroanisole	685	690	641
<i>o</i> -chlorophenol	680	685	635
<i>o</i> -chlorotoluene	678	675	644
<i>o</i> -dichlorobenzene	659	662	610 or 642

Another strong band at 1076 cm^{-1} corresponds to 1133 cm^{-1} in the ground state, correlated with the strong polarised Raman line at 1127 cm^{-1} . These may represent a totally symmetric C—H planar bending mode in the three cases. The medium strong band at 1248 cm^{-1} in the upper state and the weak band 1246 cm^{-1} in the ground state are assigned to the totally symmetric C—F stretching mode, the corresponding Raman line being the strong polarised one at 1237 cm^{-1} . It is interesting to find no appreciable change in the magnitude of this frequency in the two electronic states. This is characteristic of the C—F stretching frequency and has been observed in the other fluorinated benzene derivatives.

	Raman	U.V. Ground state	U.V. excited state
<i>p</i> -difluobenzene	1245	1259	1250
<i>p</i> -fluoroanisole	1249	1275	1280
fluorobenzene*	1218	1218	1218 or 1228
<i>m</i> -difluorobenzene*	1279	...	1269
<i>p</i> -fluorotoluene*	1212	...	1229
<i>m</i> -fluorotoluene*	1254 or 1266	...	1262
<i>o</i> -fluorotoluene*	1233	...	1230
<i>p</i> -fluorobenzotrifluoride*	1231

* In these molecules the assignment has not previously been suggested but bands are observed in the positions indicated in the table and in some cases they are chosen as fundamentals.)

The band at 274 cm^{-1} in the upper state which is of medium intensity, is correlated with the 367 cm^{-1} band in the ground state, the corresponding Raman line being the strong polarised one at 375 cm^{-1} . These are considered to represent the planar carbon bending mode. This forms one of the two components into which the ϵ_g^+ 606 vibration in benzene splits on removal of degeneracy caused by loss of symmetry. The other component may be represented by one of the two medium intensity bands 477 cm^{-1} and 513 cm^{-1} in the upper state. The

corresponding ground state frequencies are 489 and 556, the Raman shifts being 496 and 554. The Raman lines are equally strong and knowledge of the depolarisation factors which are nearly same is not of much help in deciding which of them represents the carbon bending mode. However, the percentage drop in frequency (nearly 8 percent) suggests that the pair 513, 554 might be more probable.

The medium strong band 940 cm^{-1} may not likely represent an upper state fundamental (as was previously considered to be, Krishnamachari, 1955) because a similar band is not observed in *o*-fluorobromobenzene. Instead, this band may represent the two quantum excitation (single excitation of which being too weak to be observed) of a non-planar vibration which might have gained in intensity because of its totally symmetric nature and its proximity to the strong 929 cm^{-1} band.

Of the satellite bands, the 69 cm^{-1} separation is the most pronounced one occurring as 1×69 , 2×69 , and 3×69 . These are generally ascribed to the $v-v$ transitions of some of the low-lying non-totally symmetric vibrations. The very strong Raman line 167 cm^{-1} is classified as a non-planar vibration. In ultraviolet absorption, a weak band 99 cm^{-1} in the upper state and a very weak band 170 cm^{-1} in the ground state are observed. If these are considered to represent the same vibration in the upper and lower states then their difference 71 cm^{-1} may well explain the 69 cm^{-1} satellite bands. The low magnitude of this frequency, 170 cm^{-1} is in conformity with the observed intensity of the satellite bands and this frequency may be assigned to the C—Cl out-of-plane bending mode. The selected fundamentals are given in Table IV.

TABLE IV
Ground and excited state frequencies of *o*-FC₆H₄Cl

$\Delta\nu$	Raman data Int. (Nielsen, <i>et al.</i> , 1956)	ρ	U.V. absorption data		Assignment
			Ground state	Excited state	
167	vs	0.74	170	99 mw	C-Cl out-of-plane bending
375	s,sh	0.41	367	274 mw	components of e_g^+ 606 of benzene.
554	s	0.46	556	513 mw	
496	s,sh	0.48	489	477 w	C-Cl stretching frequency Totally symmetric carbon vibrations.
680	vs,sh	0.13	685	639 s	
826	s,sh	0.18	830	794 s	
1029	vs,sh	0.08	1031	929 s	
1127	s	0.49	1103	1076 s	
1237	s	0.15	1246	1248 m	C-F stretching mode

Meta-fluorochlorobenzene.

In meta-fluorochlorobenzene the very strong band 966 cm^{-1} in the upper state gives the progression forming frequency. The corresponding lower state frequency 1007 cm^{-1} agrees with the very strong polarised Raman line at 1003 cm^{-1} . This definitely represents the totally symmetric carbon ring vibration. The strong band 636 cm^{-1} in the upper state, 688 cm^{-1} in the ground state and the strong polarised line 682 cm^{-1} in Raman effect represent the C—Cl stretching mode as in the case of the ortho compound. The medium strong band 1218 cm^{-1} in the upper state, 1229 cm^{-1} in the ground state and the medium strong polarised Raman line 1221 cm^{-1} represent the C—F stretching mode. Again, the closeness of this frequency in the two electronic states is noticeable. The medium strong band 846 cm^{-1} is also chosen as an upper state fundamental because it accounts for some of the bands and the 966 cm^{-1} progression states on this frequency. The corresponding ground state value is 895 cm^{-1} which can be correlated with the 883 cm^{-1} Raman line. From the magnitude of this frequency, this may be assigned to a non-planar C—H bending mode or to the C—F planar bending mode. The medium intensity band 1023 cm^{-1} in the upper state is also chosen as a fundamental because it is able to explain some of the bands. The corresponding ground state frequency is the very weak band at 1050 and this may be correlated with the 1063 cm^{-1} Raman line and this may probably represent a C—H planar bending mode.

The medium weak bands 327 , 455 , and 514 cm^{-1} are also considered though with less certainty, as the upper state fundamentals. Of these, the first two may represent the two upper state frequencies into which the ϵ_g^+ 606 vibration in benzene splits. The ground state frequencies corresponding to these are not observed but may be correlated with the Raman frequencies 410 and 519 cm^{-1} .

The prominent v - v separation in this case is the 78 cm^{-1} separation, occurring as 1×78 , 2×78 , 3×78 and 4×78 with many of the very strong bands. The high intensity of these bands suggests that they should originate from low frequency vibrations. The difference 82 cm^{-1} between the Raman frequency 245 cm^{-1} and the excited state frequency 163 cm^{-1} probably explains these satellite bands. The selected fundamentals are given in Table V.

Para-fluorochlorobenzene.

In para-fluorochlorobenzene, the two very strong frequencies 794 cm^{-1} and 1063 cm^{-1} in the excited state are the progression forming frequencies. These are correlated with the ground state frequencies 815 and 1090 cm^{-1} respectively which agree well with the strong and polarised Raman lines 815 and 1091 cm^{-1} . These frequencies represent totally symmetric carbon frequencies and the former probably the ring breathing frequency, because of its higher intensity and because of the relatively longer progressions associated with it. The medium

strong frequency 1233 cm^{-1} in the upper state and 1239 cm^{-1} in the ground state represent the C—F stretching frequency in the two states, the corresponding Raman frequency being 1232 cm^{-1} . In this case as well, (as in the case of the ortho and meta derivatives) the C—F stretching frequency remains practically the same in the two electronic states. The medium intensity band 343 cm^{-1} in the upper state is correlated with the 370 cm^{-1} band in the ground state which corresponds to the 376 cm^{-1} Raman frequency. These frequencies represent the planar carbon bending mode in the excited and ground states and in Raman effect. This represents the totally symmetric components of the ϵ_g^+ 606 vibration of benzene. The other component is represented by the weak band 563 cm^{-1} in the upper state and 637 cm^{-1} in the ground state, (Raman value 630 cm^{-1}). The weaker intensity of this component relative to the totally symmetric component discussed above, indicates the decreasing importance of the forbidden part of the transition in producing the spectrum. The weak band 618 cm^{-1} in the upper state can be correlated with the 680 cm^{-1} line in Raman effect in which it is assigned to a C—Cl stretching mode.

TABLE V

Ground and excited state frequencies of *m*-FC₆H₄Cl

$\Delta\nu$	Raman data Int. (Nielsen, <i>et al.</i> , 1956)	$\nu\rho$	U.V. absorption data		Assignment
			Ground state	Excited state	
245	s,b	0.86	—	160 m,s,l	Components of ϵ_g^+ 606 of benzene.
410	s,sh	0.25	—	325 m,s,sh	
519	s,sh	0.47	—	455 m,s,l	
683	s,sh	0.10	688	636 vs,sh	C—Cl stretching
883	w	0.39	895	846 m,s,sh	C—F planar bending or C—H non-planar bend- ing.
1003	vs,sh	0.10	1007	966 vs,sh	Carbon ring breathing
1063	s,sh	0.26	1050	1023 m,sh	C—H planar bending
1221	m,b	0.18	1229	1218 m,s,sh	C—F stretching.

(* determined in the present investigations.)

The prominent ν — ν separation in this case is the 33 cm^{-1} separation which occurs as 1×33 , 2×33 , 3×33 , 4×33 , and 5×33 with many of the very strong bands even at lower temperatures. The intensities of these bands suggest that they should be associated with low frequencies and probably it may be associated with the lowest Raman frequency 267 cm^{-1} which is assigned to a C—Cl out-of-plane bending mode. The selected fundamentals are given in Table VI.

TABLE VI

Ground and excited state frequencies of *p*-FC₆H₄Cl

$\Delta\nu$	Raman data Int. (Nielsen, <i>et al.</i> , 1956)	ρ	U.V. absorption data		Assignment
			Ground state	Excited state	
			245	—	
376	vs,sh	0.45	370	343 m	Totally symmetric component of ϵ_g^+ 606 of benzene.
556	w	dp	550	—	
630	s,sh	—	637	563 w,sh	Non-totally symmetric component of ϵ_g^+ 606 of benzene
680	m,sh	—	—	618 vw	C-Cl stretching.
815	vs,sh	0.20	815	794 s	Totally symmetric carbon vibrations
1091	vs,sh	0.35	1090	1063 ms,sh	
830	s	0.30	834	—	
1232	s,b	0.25	1239	1233 m	C-F stretching.
1596	s,b	0.75	1590	—	

Comparison of the o,m,p-fluorochlorobenzenes

A comparative study of the absorption spectra of the ortho, meta and para isomers reveals a few interesting points.

The shifts of the 0,0 band in the *o,m,p*-fluorochlorobenzenes relative to that of benzene are respectively 1054, 1063 and 1813 cm⁻¹ whereas, according to the additivity rule a shift of 1307 cm⁻¹ is expected for all the three molecules. (the shift for chlorobenzene is 1037 and that for fluorobenzene is 270 cm⁻¹). The ortho and meta compounds show practically the same shift as does chlorobenzene whereas, the para compound shows a markedly larger shift. This abnormal influence of the para positioned fluorine atom on the shift of the 0,0 band is also exhibited in *p*-difluorobenzene in which the shift is 1246 cm⁻¹ compared to that of 180 cm⁻¹ in meta-difluorobenzene; and in para-fluorotoluene in which it is 1213 cm⁻¹ compared to that of 691 cm⁻¹ in meta-fluorotoluene and 513 cm⁻¹ in ortho-fluorotoluene.

It is interesting to observe that whereas the C—F stretching frequency is recorded only with moderate intensity in the ortho, meta and para compounds, the C—Cl stretching frequency is very strong in the ortho and meta compounds while it is very weak (and absent in the ground state) in the case of the para-compound.

The prominent $v-v$ separations also exhibit certain interesting features in the series ortho-meta-para. In the ortho and meta-fluorochlorobenzenes they are 69 and 78 cm^{-1} respectively whereas, in para-fluorochlorobenzene it is 33 cm^{-1} . In ortho and meta-dichlorobenzenes they are 59 and 63 whereas, in para-dichlorobenzene it is 26 cm^{-1} . In meta-difluorobenzene it is 66 cm^{-1} (or 97) whereas, it is 40 cm^{-1} in para-difluorobenzene. The $v-v$ separations in the para compounds are consistently smaller than those of the ortho and meta compounds.

ACKNOWLEDGMENTS

The author is grateful to Dr. Finger for the gift of the samples and to the Government of India for the award of a senior research scholarship. The author is deeply indebted to Prof. K. R. Rao for his valuable guidance.

REFERENCES

- Conrad-Bullroth, H. and Forster, G., 1936, *Zeit. Fur. Phys. Chem.*, **33**, 311.
Cooper, C. D., 1954, *J. Chem. Phys.*, **22**, 503.
Dima, G. A. and Timtea, H., 1940, *Bull. Sect. Sci. Acad. Rou.*, **23**, 34.
Hertz, E., 1946, *Mh. Chem.*, **76**, 1-26.
Hertz, E. and Kohlrausch, K. W. F., 1942, *Mh. Chem.*, **74**, 175.
Hitoshi Kamaeda, 1952, *Jap. Analyst.*, **1**, 141-5.
Kohlrausch, K. W. F. and others, 1947, *Mh. Chem.*, **76**, 200.
Krishnamachari, S. L. N. G., 1955, *Ind. J. Phys.*, **29**, 603.
" 1956a, **30**, 151.
" 1956b, " **30**, 319.
" 1956c, " **30**, 487.
" 1956a *Curr. Sci.*, **25**, 185.
" 1956b, " **25**, 260.
Lecomte, J., 1938, *J. Phys. Riol.*, **9**, 13.
Marino Milone and Enzo Borollo, 1952, *Gazz. Chem. Ital.*, **82**, 79.
Nielsen, J. R. and others, 1953, *J. Chem. Phys.*, **21**, 1457.
" " 1956, " **24**, 420, 433, 1232.
Paciotti, M., 1941, *Compt. Rend.*, **212**, 1138.
Sponer, H. and Kirby-Smith, J. S., 1941, *J. Chem. Phys.*, **9**, 667.
Sponer, H., 1942, *Rev. Mod. Phys.*, **14**, 224.
Sponer, H. and Rao, V. R., 1952, *Phys. Rev.*, **87**, 213.
Sreenivasamurthy, K., 1951, *Curr. Sci.*, **20**, 176.
Tominobu Aino and Ikuro Matubara, 1955, *J. Chem. Phys.*, **23**, 77.

CRYSTAL STRUCTURE AND MAGNETIC SUSCEPTIBILITY OF RECTIFYING CUPROUS OXIDES

K. R. DIXIT AND V. V. AGASHE

GUJARAT COLLEGE, AHMEDABAD.

(Received for publication December 17, 1956)

Plate XI

ABSTRACT. Oxides of copper were prepared in air at 0.5 mm of Hg in the temperature range 200°C to 1030°C. Their composition, rectification, magnetic susceptibility and crystal structure—all these as a function of the thickness of the film and their subsequent heat treatment—have been studied. The films formed at 800°C begin to show an appreciable rectification, which increases rapidly with the temperature of formation of the film. The appearance of an appreciable amount of rectification is accompanied by changes in the crystal structure at the surface and in the body of the film. There is also a characteristic change of the magnetic susceptibility. In a rectifying film the surface layer contains large Cu_2O crystals showing 111 orientation, while in the body of the film, small crystallites of Cu_2O , containing traces of excess oxygen and showing a zinc blende structure, are present. The effect of heat treatment is to reduce the oxygen content and increase the diamagnetic susceptibility. The presence of an additional atom of oxygen, in each crystallite of Cu_2O appears to give the maximum rectification. A mechanism for the formation of these rectifying films is suggested.

INTRODUCTION

We have already reported the properties of oxides of copper formed at atmospheric pressure (Dixit and Agashe, 1955) and also at low pressures (Dixit and Agashe, 1956). We find that at atmospheric pressure and at low temperatures a thin film of Cu_2O is formed. As the temperature and the time of formation increase, Cu_2O gradually changes over into CuO . At temperatures beyond 750°C and with a proper time of formation, it is possible for a Cu_2O film to be formed below the CuO film. Such a composite film shows considerable rectification. At 410°C and pressures up to 75 mm of Hg only Cu_2O can be formed. Oxides formed at pressures up to 5 mm of Hg, and a time of oxidation sufficiently long, show a peculiar under-growth structure of Cu_2O in contact with the copper block. This oxide shows four, rather broad, rings which approximately correspond to 111, 222, 333 and 444 rings of Cu_2O . In the light of these two observations of ours, namely the formation of a Cu_2O film below a CuO film, the composite film showing rectification and the peculiar structure shown by Cu_2O film formed at low pressures, and also in the light of the well-known fact that the rectifying oxide of copper is formed at low pressure, at about 1000°C followed by a suitable heat treatment or annealing, we decided to study the oxides

of copper formed at an air pressure 0.5 mm of Hg in the temperature range 200°C to 1030°C and also to study the effect of the subsequent heat treatment. The following properties of the films so formed were investigated: their crystal structure by the method of electron diffraction and X-ray reflection, the thickness of the films formed and the change of crystal structure with depth; the resistance, rectification and magnetic susceptibility of the films. We also studied the variation of all these properties as a function of the temperature of formation of the films and their subsequent heat treatment.

We find that films formed at 500°C just begin to show rectification, it becomes appreciable at about 800°C, afterwards this increases very rapidly with the temperature of formation. The rectifying films are all cuprous oxide films. The appearance of an appreciable amount of rectification is accompanied by a peculiar change in the electron and X-ray patterns. The electron diffraction pattern is now characterised by the 222 ring of Cu₂O becoming broad and strong at the centre, ultimately changing over to a four arc pattern showing four rather broad arcs which approximately correspond to 111, 222, 333, and 444 arcs of Cu₂O. The corresponding X-ray pattern is characterised by a weakening of the 200 ring which is normally strong and by an increase in the intensity of the 220 ring. This definitely indicates a change of crystal structure accompanying the rectification. The greater the magnitude of rectification the more prominent becomes the change. We measured the magnetic susceptibility of rectifiers formed at 700°C, 800°C, 900°C and 1030°C. We find that rectifiers formed at 700°C, which show only a small rectification, are slightly paramagnetic, and an increase in rectification corresponds to a decrease in the paramagnetic susceptibility. When the rectification becomes about 50, the paramagnetic susceptibility becomes almost zero. An increase in rectification now makes the layer slightly diamagnetic. The diamagnetism increases with rectification and for the best rectifiers with a rectification of about 300, χ is about -9×10^{-8} . By changing the heat treatment it is possible to reduce the rectification of the best rectifiers (rectification about 300). This subsequent reduction of rectification is accompanied by an increase in the diamagnetic susceptibility. All these rectifiers with different values of rectification (>30) and different values of χ , show no appreciable difference in crystal structure as revealed by X-rays and electrons. A small associated diamagnetic susceptibility appears to be an additional criterion for rectification.

EXPERIMENTAL

The copper blocks (except those used for magnetic susceptibility measurements) were prepared and oxidised at a given temperature in the same manner as described earlier (Dixit and Agashe, 1956). In the first series the oxide was formed by keeping the block at a temperature of 1030°C for 60 minutes in air

at a pressure of 0.5 mm of Hg. The blocks of oxide so formed were subsequently cooled in vacuum from 1030°C to 200°C over different intervals of time. In the second series of experiments the oxide was formed on the blocks kept at various temperatures in the range 200°C to 1030°C, and at each temperature air at a pressure of 0.5 mm of Hg were allowed to remain in contact with the blocks for 60 minutes. The oxide blocks formed at each temperature were divided into two groups, one group was suddenly cooled (500°C/min) and the other was slowly cooled (10°C/min) in vacuum. The resistance, rectification, the growth of oxide and its crystal structure (by the method of weighing on a microbalance combined with electron reflection) was determined as before. This time the structure of the films was studied in addition by X-ray reflection. We used Cu K_α radiation, K_β line was eliminated by a suitable nickel filter. The X-ray beam was incident on the film at an angle of 20°, the reflections were recorded photographically, and the relative intensities of these reflections were later determined by a recording microphotometer. A few back reflection photographs were also taken to investigate the $\sqrt{24}$ and $\sqrt{27}$ rings and to ascertain whether the observed changes in structure at 900°C were due to a change in the orientation or a change in the structure. For comparison, X-ray photographs of chemically pure Cu_2O were also taken. In taking these pictures we used tablets of chemically pure Cu_2O prepared with the help of a small amount of gum tagacanth.

MAGNETIC SUSCEPTIBILITY MEASUREMENTS

The magnetic susceptibility was determined by a Guoy balance, with an accuracy in weight determination of 0.01 mgm. The rods required for this work were prepared by melting electrolytic copper in vacuum. The rods were rectangular bars 75 mm long and approximately 5 mm \times 4 mm cross-section. The oxide layer was formed on these rods at the given temperature, pressure and time. The oxide layer was formed on all the five free surfaces of this block. The trace of oxide which may sometimes be formed on the sixth surface in contact with the holder was removed. The oxide layer formed on the two smallest surfaces was also removed. At one time, i.e., at a given pressure, temperature and time, six oxide blocks were prepared. The oxide block so prepared, with the oxide layer on the three cylindrical surfaces, was weighed with and without the magnetic field (6500 Gauss). The oxide film on the three free sides was then removed by slow etching with sodium cyanide. The copper rod (without the oxide film) was also weighed with and without the magnetic field. These four weights, together with the linear dimensions of the block and the density of Cu_2O , enabled us to determine the weight of the oxide film, its susceptibility and on certain plausible assumptions (as given later) the mass of excess oxygen present in the film. Out of the six rods prepared each time, two were utilised for susceptibility measurements, two were utilised for rectification

and electron and X-ray measurements and two were stored up in vacuum and used later for a final check on previous measurements. The susceptibility measurements were carried out with the two series of oxide layers mentioned under the section experimental. In addition we carried out the susceptibility measurements with one more series of oxides prepared as follows. In this series the oxide layer was prepared by heating the block for 60 minutes at 1030°C and 0.5 mm Hg air pressure. The oxide layer was then cooled from 1030°C to 200°C in 300 minutes. The rate of cooling (P) was maintained appreciably constant in the whole range. A small variation was now introduced in the annealing technique. The oxide layer was cooled from 1030°C to 980°C at the given rate of cooling (P). It was kept at this temperature $980^\circ \pm 15^\circ\text{C}$ for a given interval of time (4, 6, 9, 12, 16 and 36 hours) and was then cooled at the same given rate (P) from 980°C to 200°C. The cooling as well as storing at 980°C was done in vacuum. The rectification and crystal structure of all these blocks (cooled and stored) were also determined.

RESULTS

(1) The oxide was formed by keeping the blocks at a temperature of 1030°C for 60 minutes in air at a pressure of 0.5mm of Hg. The blocks of oxide so formed were subsequently cooled in vacuum from 1030°C to 200°C, at a uniform rate. The interval of time for this fall of temperature was changed from 2 minutes to 295 minutes. The resistances R_1 and R_2 in the two directions were measured by applying a D.C. potential of 1.5 volts. The corresponding values of R_1/R_2 the rectification were calculated. The observations are given in Table I. Each value of R_1 and R_2 tabulated is a mean of 8 values. The tabulated values of rectification are the most probable values, the corresponding probable error is also shown. It will be seen that the rectification becomes appreciable (about 10) for a rate of cooling of about 40°C per minute. It goes on increasing as the rate of cooling becomes slower and slower, till we come to a rate of cooling of about 4°C per minute, beyond this stage no large changes in rectification are observed.

(2) The oxide blocks formed at various temperatures in the range 200°C to 1030°C, were divided into two groups, one group was slowly cooled and the other was suddenly cooled. In each case the structure of the topmost layer was studied for the rapidly cooled films, because only such films could be expected to give an idea of the nature of the surface under which the films were formed. These blocks showed the given in properties Table II.

(a) The layers of oxide formed at 200°C, 250°C and 300°C are too thin or too porous to show any resistance or rectification. The electron reflection pictures of the free surface show fairly sharp rings of Cu₂O, with 110 orientation. At

300°C traces of 111 orientation also begin to manifest themselves. This indicates that even in these thin porous films crystallites of appreciable size are present.

TABLE I

Resistance and rectification as a function of the time of cooling (t_c) from 1030°C to 200°C.

Obs No.	t_c minutes	R_1 ohms.	R_2 ohms.	R_1/R_2
1	2	350,000	320,000	1.09 0.05
2	5	144,000	111,000	1.3 ± 0.06
3	10	27,000	11,000	2.4 ± 0.7
4	20	13,000	1,545	8.4 ± 3.2
5	40	9,600	160	53 ± 2.2
6	60	9,000	110	82 ± 1.9
7	75	7,100	75	95 ± 7.0
8	95	7,000	50	140 ± 5.1
9	125	9,400	45	208 ± 10.7
10	165	8,900	39	228 ± 8.1
11	205	9,000	34	264 ± 7.5
12	250	10,000	36	278 ± 10.0
13	295	11,000	38	290 ± 8.0

(b) Films formed at 350°C and 400°C are appreciably thick and show a resistance of about 10 ohms. These films still do not show any rectification. No difference could be detected in the properties of the slowly cooled and the suddenly cooled layers. The electron reflection pattern from the free surface shows rings of Cu_2O with double orientations 110 and 111.

(c) Films formed at 500°C and 550°C are more than a micron thick and show an appreciable resistance. The difference in the slowly cooled and rapidly cooled layers begins to manifest itself. The slowly cooled layer has lower values of R_1 and R_2 than those of the corresponding rapidly cooled layer and begins to show asymmetric conduction. The electron reflection rings from the free surface are those of Cu_2O with a double orientation. A layer at a depth of 1000 Å shows normal rings of Cu_2O . In Cu_2O , the copper atoms lie on a F.C. configuration and the oxygen atoms lie on a B.C. configuration. The diffracting power of the light oxygen atoms is much less than that of heavy copper atoms. Hence normal rings of Cu_2O give the impression of a F.C. lattice arrangement.

(d) The electrical properties of films formed at 600°C are almost similar to those of films formed at 550°C. The free surface, however, shows 111 orienta-

TABLE II

Properties of the oxide formed in air at a pressure of 0.5 mm of Hg for 60 minutes

Temp. °C	Weight of oxide film in mgm	Thickness of oxide films in microns	Resistance of oxide films at 1.5 volts (D.C.)				Electron Reflection		X-ray reflec- tion suddenly and slowly cooled Cu ₂ O
			Suddenly cooled		Slowly cooled		Topmost layer of Cu ₂ O	At a depth of 1000 Å for both, sud- denly and slowly cooled Cu ₂ O	
			R ₁	R ₂	R ₁ /R ₂	R ₁			
200	0.015	0.025	—	—	—	—	(110)	—	—
250	0.035	.058	—	—	—	—	(110)	—	—
300	0.075	0.125	—	—	—	—	(110 & Traces of 111)	—	—
350	0.186	0.310	9	9	1	9	(110 & 111)	—	—
400	0.277	0.482	12	12	1	12	(110 & 111)	—	—
500	0.877	1.46	25	25	1	22	(110 & 111)	—	—
550	1.58	2.63	30	30	1	25	(110 & 111)	Normal Cu ₂ O rings (F.C.)	—
600	2.55	4.24	110	70	1	57	(111) and spots on rings	Normal Cu ₂ O rings (F.C.)	Normal Cu ₂ O
650	6.015	10.0	400	200	2	52	34	Normal Cu ₂ O rings (F.C.)	Normal Cu ₂ O
700	8.5	14.2	2000	1700	1	80	38	222 broad & very strong at centre	Normal Cu ₂ O
800	14.52	24.2	10000	5000	2	400	37	222 broad & very strong at centre	200 weak
900	19.22	32.0	42000	20000	1	1250	41	4 arc pattern	220 stronger & 200 nearly absent
950	26.69	44.5	72000	54000	1	3360	62	Weak (111) & strong spots on rings	..
1000	38.65	64.4	100000	90000	1	6600	88	4 arc patt rn	..
1030	55.69	92.8	150000	135000	1	8080	86	4 arc pattern	..

(h k l) denote preferred orientation h, k, l .

tion. 110 orientation has disappeared. The layer at a depth of 1000 Å shows normal rings of Cu_2O . The X-ray reflection, which is naturally due to all crystallites present in this film 4.25 microns thick, also shows the rings of normal Cu_2O .

(c) The films formed at 650°C and 700°C are thicker and their resistance is greater. The increase in resistances R_1 and R_2 of the rapidly cooled films is much greater than what could be expected from the increase of thickness. This trend continues right upto the films formed at 1030°C. The thickness of the films formed increases from 10 microns at 650°C to 92.8 microns at 1030°C, an increase of thickness by a factor of about 10. The corresponding increase in the value of resistance shows that it has increased by a factor of 375. The resistances R_1 and R_2 of the slowly cooled films and their increase with temperature are much lower than those of the corresponding rapidly cooled films. The increase in R_1 in the temperature range 650°C to 1030°C is, in this case, only by a factor of 160 while the increase in the resistance R_2 (2.5) is much less than would be expected from the corresponding increase in the thickness of the film. This remarkable result indicates a plausible change in the structure of the film. The changes in the crystal structure of the film begin to show themselves at the free surface at 650°C. Signs of 111 orientation are still there, but we see spots on rings indicating an increase in the size of the crystallites of Cu_2O at the free surface. There is no change in the structure at the depth 1000 Å below the free surface at this temperature. At 700°C the structure of the free surface is the same as at 650°C. But now the structure at a depth of 1000 Å begins to show changes. 222 ring has started to become broad and very strong at the centre, showing the presence of small oriented crystallites. The X-ray picture of this film (figure 2b, Plate X) formed at 700°C and which is about 14 microns thick shows normal rings of Cu_2O . This shows that the average structure of this film is still that of normal Cu_2O (Table III).

(f) The films formed at 800°C and 900°C show an additional difference between the slowly cooled and the rapidly cooled films. Both the films, so far, were showing a small asymmetric conduction or rectification. The rectification of the slowly cooled films now becomes appreciable, about 10 at 800°C, this increases to about 30 for a film formed at 900°C. The structure of the free surface at 800°C, is the same as at 700°C, with spots on rings and 111 orientation. The structure at the depth of 1000 Å is also the same as at 700°C and shows a 222 ring very broad and strong at the centre. The X-ray pattern, however, begins to show a change, the 220 ring of Cu_2O begins to increase in intensity and 200 begins to decrease in intensity. This shows that at 800°C the average structure of all the crystallites in the film (as shown by X-rays) has started to change. At 900°C we observed an almost complete change in the structure and if we remember that this is the temperature at which the rectification is 30, the result is very

TABLE III
Relative changes in X-ray reflection intensities

Specimen	Treatment	Relative intensity of X-ray reflection							Resistance ohms		
		110	111	200	211	220	311	222	R_1	R_2	R_1/R_2
Pure Cu_2O Tablet	Prepared with a little gun traucanth	20	100	61	(<5)	32	25	5			
Cu_2O film formed at	550°C	20	100	60	(<5)	31	25	5	22	11	2.0
	700°C	20	100	61	(<5)	33	26	3	80	38	2.01
	900°C	15	100	(<5)	(<5)	50	30	5	1250	42	30.5
	1030°C	13	100	(<5)	8	50	35	(<5)	6600	88	75.0
	1030°C	Suddenly cooled in vacuum	20	100	(<5)	8	50	35	(<5)	10 ³	1.1
Diamond	A. W. Hull, <i>Phys. Rev.</i> 10, 66, (1917)	0	100	0.5	0	50	40	0			
Znchlenide	W. Gerlach, <i>Physik. Z.</i> 23, 114 (1922)	0	VS	W	0	N	S	W			

significant. The electron reflection picture (111 orientation and rings with spots) shows that large oriented crystallites of normal Cu_2O are present in the free surface. The layer at a depth of 1000 Å shows a pattern of four rather broad arcs which approximately correspond to 111, 222, 333 and 444 arcs of Cu_2O (Fig. 1 Plate XI Table IV). This indicates that rather small oriented crystallites of Cu_2O are present at this depth. A similar structure was observed by us at a similar depth in an oxide film formed at lower temperatures and slowly cooled, which just began to show rectification. This leads us to suggest that there is some connection between this structure and rectification. The X-ray picture of the film formed at 900°C (figure 2, Plate XI and Table IV) shows that the 220 ring has become much stronger and the 200 ring has nearly vanished. In the arrangement used by us, 220, 311 and 222 are rather broad and they do not enable us to determine whether the change of intensity is due to a change in orientation or structure. This point was settled by taking a few back reflection photographs and studying rings of higher orders like $\sqrt{24}$, $\sqrt{27}$. These photographs clearly show that the change in intensity is definitely due to a change in the crystal structure.

(g) In the films formed at 950°C, 1000°C and 1030°C we observe a rapid increase in rectification. The changes in structure already observed which accompany an increase in rectification are now more pronounced.

(h) The average rectifier formed at 1030°C is about 90 microns thick. The manner in which its structure changes with the depth is shown in Table IIIa. This film, if it is rapidly cooled, shows at the surface a layer of Cu_2O with large crystallites showing a 111 orientation and rings with spots. But during the process of slow cooling of this film, the topmost layer becomes very uneven, (probably because of ejection of oxygen) and does not show any electron reflection pattern. When this topmost uneven layer (about 1000 Å) is removed we begin to get an electron diffraction pattern. Between 1μ and 80μ we see the four arc pattern indicating the presence of small crystallites of Cu_2O (with excess oxygen), which have 111 orientation and which form a layer like structure. Now at 80 microns we begin to see spots on rings, but these spots are elongated. The spots lie on rings of normal Cu_2O showing that the size of the crystals is now larger. The elongation of the spots is probably due to refraction. The 222 ring of the 4 arc pattern also persists, showing that large normal crystallites of Cu_2O are present side by side (Schottky, 1930 ; Zworykin and Ramberg, 1950) with small ZnS type of crystallites of Cu_2O . At 88μ copper rings begin to appear along with the normal Cu_2O rings and the four arc pattern has completely vanished. At 90μ depth we also see the elongated spots, but now they are present on the copper rings and not on the Cu_2O rings.

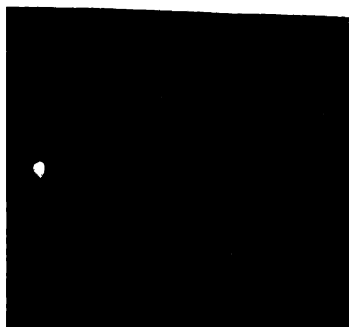


Fig. 1 Shows the four arc pattern, which approximately corresponds (vide table IV) to 111, 222, 311 and 444 arcs of Cu_2O .

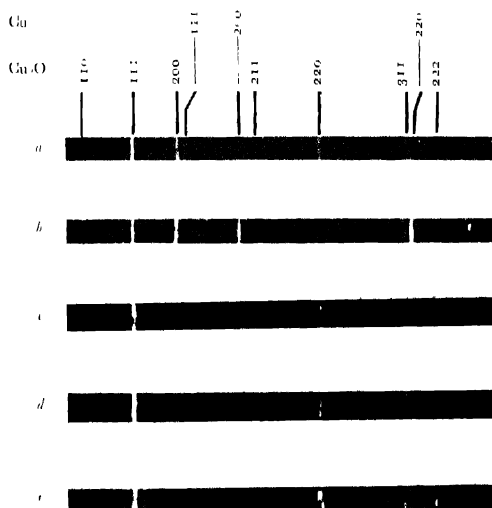


Fig. 2. Shows X-ray reflection from the substances mentioned below.

- Cu_2O powder with small copper impurity
- Cu_2O film formed at 700°C at 5 mm Hg air pressure and slowly cooled
- Cu_2O film formed at 900°C at the same pressure and slowly cooled
- Cu_2O film formed at 1030°C at the same pressure and slowly cooled
- Cu_2O film formed at 1030°C at the same pressure but suddenly cooled

TABLE III(a)

Changes of crystal structure with depth for a cuprous oxide rectifier film formed at 1030°C , and *slowly cooled*. Film thickness about 90 microns. The table gives average values from 7 films.

Depth from the free surface in microns	Electron reflection pattern
0.0	No pattern.
0.1	No pattern.
1.0	The 222 are of the four are pattern visible
5.0	The four are pattern
25.0	-do-
50.0	-do-
60.0	Four are pattern but 222 strong and others weak.
75.0	The 222 are of the four are pattern only
80.0	222 are and elongated spots on normal Cu_2O rings
85.0	-do-
88.0	222 are not visible, but Cu and normal Cu_2O with elongated spots on normal Cu_2O
90.0	Rings of Cu and normal Cu_2O but with elongated spots on Cu and not on Cu_2O

TABLE IV

Intensities and the 'd' spacings of the four are pattern.

Arc. No.	Intensity	d in Å observed	Comparable values for normal Cu_2O	
			h k l	d in Å
1	30	2.4 ± 0.08	1 1 1	2.47
2	100	1.26 ± 0.05	2 2 2	1.24
3	10	0.8 ± 0.03	3 3 3	0.82
4	20	0.6 ± 0.03	4 4 4	0.618

RESULTS (MAGNETIC SUSCEPTIBILITY)

The values of the susceptibilities obtained under various conditions are given in Tables Va, Vb and VI. The greater the change in weight observed, the greater is the accuracy of the susceptibility measurements. For a given susceptibility the change in weight will be a function of the amount of material which could be used. Thus greater the weight of the oxide or greater the thickness of the oxide the greater is the accuracy of the susceptibility measurements. Or, χ cannot be measured very accurately for thin films formed at lower temperatures. This will be seen in Table VI. All the values of the susceptibility so determined along with their corresponding rectifications are plotted in figure 3.

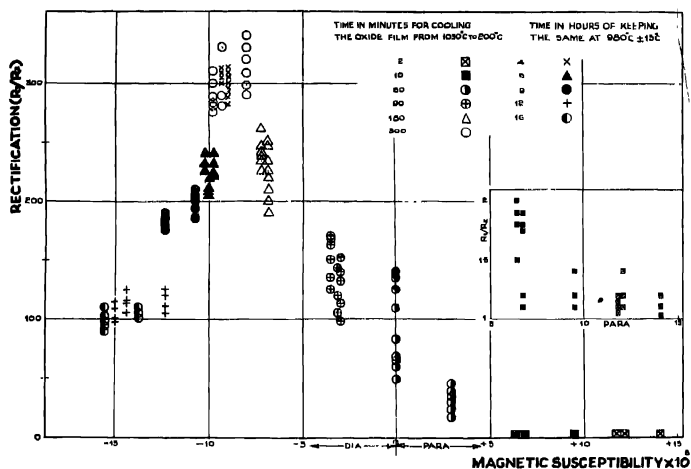


Fig. 3. Shows the relation between the magnetic susceptibility and the rectification for the Cu_2O films prepared at 1030°C followed by different heat treatments

Further understanding of the results will be considerably helped if we recapitulate the general picture of the formation of the Cu_2O barrier layer. At low pressures at which the layers are prepared, small crystallinities of Cu_2O , containing a few extra oxygen atoms, are formed. During the process of slow cooling most of the dissolved oxygen gas is ejected out, retaining only a few oxygen atoms in the crystallite. We know that pure Cu_2O shows (Klemm and Schuth, 1932) a diamagnetic susceptibility (-18.0×10^{-8}), while oxygen gas shows a paramagnetic susceptibility. Assuming that the susceptibility of the solid solution is the sum of the susceptibilities of the two components, it will be possible for us to calculate the amount of oxygen present per 100 molecules of Cu_2O , provided we know the susceptibilities of Cu_2O and oxygen. We made such cal-

culations and in figure 4 we have plotted rectification as a function of the percentage of oxygen atoms present.

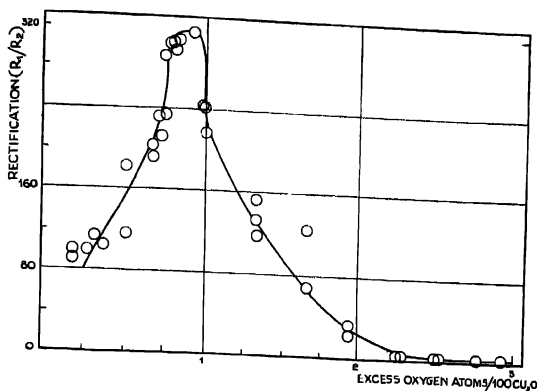


Fig. 4 Shows the relation between the rectification and the percentage excess of oxygen atoms present for all films in Fig. 3

TABLE V(a)

Changes in χ as a function of the time of cooling the oxide film.

Obs No	Cooling time t from 1030° to 200°C min.	Wt. of oxide film m in mgm	Change in (m) due to magnetic field in mgm	Area of cross section sq.cm $\times 10^4$	Magnetic susceptibility $\chi 10^6$	Excess of oxygen atoms per 100 Cu_2O molecules	Rectification R_1/R_2 at 1.5V Mean of 6 readings
1	2	117.99	+ 0.04	26.4	+ 11.91	2.75	1.1
		83.60	- 0.03	19.2	+ 12.07	2.76	1.4
		102.02	+ 0.04	22.7	- 13.7	2.91	1.16
2	10	108.77	+ 0.03	23.4	+ 9.86	2.56	1.10
		103.17	+ 0.02	23.0	+ 6.57	2.26	1.8
		101.59	- 0.02	22.5	- 6.86	2.29	1.58
3	60	113.79	+ 0.01	25.4	+ 3.05	1.94	22 \pm 1.6
		115.40	+ 0.01	25.7	+ 3.00	1.93	32 \pm 2.7
		110.83	0	24.6	0	1.65	68 \pm 4
		94.69	0	21.9	0	1.65	125 \pm 3.5
4	90	111.26	- 0.01	24.6	- 3.14	1.36	118 \pm 4.4
		103.15	- 0.01	22.9	- 3.38	1.34	130 \pm 6.2
		100.21	- 0.01	22.1	- 3.5	1.33	152 \pm 4.6
5	180	101.42	- 0.02	22.6	- 6.85	1.01	215 \pm 5.8
		83.54	- 0.02	18.5	- 7.16	0.99	241 \pm 3.7
		96.00	- 0.02	21.5	- 6.89	1.02	242 \pm 5.0
6	300	114.77	- 0.03	25.4	- 0.34	0.79	302 \pm 4.8
		106.10	- 0.03	23.6	- 0.82	0.75	290 \pm 3.7
		85.59	- 0.02	19.1	- 8.0	0.92	314 \pm 5.3

TABLE V(b)

Same as V(a) but now the oxide films were kept at $980^{\circ}\text{C} \pm 15^{\circ}\text{C}$ for t_c hours and then cooled as in Obs. No. 6 of Table V(a).

Obs. No.	t_c (hours)	Wt. of oxide film m in mgm	Change in (m) due to magnetic field in mgm	Area of cross section $\text{sq. cm} \times 10^4$	Magnetic susceptibility $\chi 10^6$	Excess of oxygen atoms per 100 Cu_2 molecules	Rectification R_1/R_2 at 1.5 V D.C. Mean of 6 readings
7	4	114.77	-0.03	25.4	-8.95	0.83	296 ± 5.0
		110.26	-0.03	24.6	-9.32	0.80	305 ± 7.5
		115.40	-0.03	25.7	-8.9	0.84	306 ± 6.3
8	6	106.10	-0.03	23.6	-9.75	0.76	232 ± 5.3
		101.42	-0.03	22.6	-10.2	0.72	231 ± 6.2
		103.17	-0.03	23.0	-10.0	0.73	211 ± 10.3
9	9	94.69	-0.03	21.3	-10.7	0.67	203 ± 3.2
		83.97	-0.03	18.6	-12.3	0.51	182 ± 2.6
		96.00	-0.03	21.5	-10.7	0.67	191 ± 9
10	12	85.59	-0.03	19.2	-12.2	0.52	116 ± 12
		94.64	-0.03	21.3	-14.4	0.33	114 ± 3.2
		91.00	-0.04	20.3	-15.0	0.28	99 ± 4
11	16	86.97	-0.04	19.3	-15.7	0.20	99 ± 7.2
		85.00	-0.04	22.0	-13.9	0.38	104 ± 5.3
		87.00	-0.04	19.3	-15.7	0.20	91 ± 2

TABLE VI

Average values of R_1/R_2 and χ as a function of the temperature of formation and the time of cooling.

Temperature of oxide formation $^{\circ}\text{C}$	Method of cooling the oxide	Thickness of oxide layer in microns	Rectification R_1/R_2	$\chi \cdot 10^6$	Minimum value of χ that can be determined $\chi \cdot 10^6$
700	Sudden	6	1	+9.4	9.4
700	Slow 700°-200° in 90 min.	6	5	+9.4	9.4
800	Sudden	12	1	+6.4	6.4
800	Slow 800°-200° in 120 min.	12	15	+6.4	6.4
900	Sudden	17	1	+7.8	4.8
900	Slow 900°-200° in 150 min.	17	100	-4.8	4.8
1030	Sudden	20	1	+12.0	3.0
1030	Slow 1030°-200° in 180 min.	20	200	-7.0	3.0

This picture tells us that the suddenly cooled films probably retain enough oxygen, which is paramagnetic, and make the mixture show a paramagnetic susceptibility. Heat treatment in the form of slow cooling ejects oxygen atoms, making the film less and less paramagnetic. This increases the rectification. The optimum conditions we were able to obtain were, a rectification of about 300 with a rate of cooling of about 3°C per minute, the corresponding value of the susceptibility was about -9×10^{-8} . If we could reduce the amount of dissolved oxygen still further, we should be able to obtain an increase in the diamagnetic susceptibility. The question now arises as to what would happen to the corresponding rectification.

We were able to solve this problem by a small variation in the annealing technique. The oxide layer formed at 1030°C, was cooled from 1030°C to 980°C in 18 minutes, it was kept at this temperature of 980°C for various intervals of time (4, 6, 9, 12, 16 and 36 hours) it was then cooled from 980°C to 200°C in 282 minutes. This procedure enabled us to have films with a reduced content of oxygen, increased diamagnetic susceptibility and a reduced rectification (see figure. 3 and 4).

DISCUSSION

We have seen that signs of change of crystal structure at a depth of 1000 Å below the free surface begin to show themselves for films prepared at 700°C and slowly cooled. These films show a small rectification. The X-ray picture of these films shows normal Cu₂O, that is the crystal structure has not changed for the majority of crystallites but has changed only for a few of them present in a layer at a depth of 1000 Å. In the case of the slowly cooled films prepared at 900°C the electron diffraction picture of the layer at a depth of 1000 Å shows a complete change, so also does the X-ray picture. The X-ray picture shows lines in the same position as before but their relative intensities are more like those from a ZnS or a diamond cell. Thus the X-ray pictures suggest that in the rectifying state, the structure of the majority of Cu₂O crystallites changes over to that of zinc blende or diamond type (Table III). The corresponding electron reflection pictures show four broad rings, which are really arcs, about 30° wide and strong at the centre. This picture (figure 1) indicates that a large number of crystallites of Cu₂O are so oriented that the 111 face is parallel to the substrate. Normally with such an orientation (111 of Cu₂O) many other rings are seen (figure 4.) In this case we do not see any other rings or the arrangement is a single crystal arrangement in two dimensions but not in the third. Such a pseudo single crystal structure or a layer structure tends to exhibit effects of surface reflection (Raether, 1932; Dixit, 1933) and also of multiple reflection (Ehlers, 1953; Gottsche, 1956) of the electron beam. The effect of the surface reflection is to make the 222 ring broad and intense. The effect of multiple reflection is more pronounced for the outer rings, 333 and 444.

Thus both, the X-ray pictures (directly) and electron pictures (indirectly) show that the structure of a rectifying layer of Cu_2O is of the zinc blende type. Such a result is not entirely unexpected in the light of the experiments of Welke (1952 and 1953). It also agrees with the observation of Hoffmann and Rose (1953) that the rectifying layer of cadmium selenide has a structure of the zinc blende type. A plausible picture for such a change is already given by one of us (Dixit, 1956). The layer of Cu_2O formed at low pressures contains extra oxygen. These extra oxygen atoms could reasonably be expected to occupy the sites which are occupied by sulphur atoms in a similar zinc blende cell. But as the number of excess oxygen atoms present is small, we may assume that the oxygen atoms, occupy the sulphur atom sites on a time average basis and modify the Cu_2O structure to a zinc blende type.

The magnetic susceptibility measurements (see figure 4) show that for maximum rectification, about 1 oxygen atom is associated with about 110 ± 20 molecules of Cu_2O . But as 2 molecules of Cu_2O are associated with a cell, this indicates that one oxygen atom is associated with about 55 ± 10 cells. Assuming these cells form a crystallite with equal linear dimensions, the width of such a crystallite of Cu_2O will be about 4 cells or 17 Å units. This should be compared with the sizes of crystallites obtained from the width of arcs in the 4 arc patterns (see Table VII). For any particular crystallite the number of associated oxygen atoms will be always integral. The average of such associated oxygen atoms associated with an average crystallite when plotted against rectification gives a curve very much similar to the curve in figure 4. The maximum rectification occurs when the amount of oxygen associated with a crystallite is about one atom (1.0 ± 0.2).

Thus our picture of the formation of a rectifier layer is as follows. During the process of formation of a film of Cu_2O at low pressures and high temperatures, a definite number of extra oxygen atoms (very probably about 3) get associated with a crystallite. This association can be expected to give rise to a modified form of crystal structure of Cu_2O namely a crystal structure of the zinc blende or the diamond type. During the process of annealing, the oxygen gas is gradually ejected out. This reduces the average number of oxygen atoms associated with a crystallite to 2 and then to 1. The association of one oxygen atom (of course as an average) with a crystallite gives us the maximum rectification. A further reduction in the amount of oxygen reduces the rectification till we reach the stage of zero oxygen atom associated with a crystallite. This of course is the stage when we have pure Cu_2O which as is well known is not a rectifier. It is significant to note that when we succeed in removing all oxygen from the rectifier, by suitable heat treatment, the substance is no longer a rectifier and the crystal structure of Cu_2O (as shown by electrons) again changes back from the zinc blende pattern to the normal pattern. The signs of this reversal of crystal structure are seen

in specimens annealed for 36 hours. They show the 4-arc pattern and also some prominent rings of normal Cu₂O ($\sqrt{4}$, $\sqrt{8}$ and $\sqrt{19\sqrt{20}}$).

TABLE VII

The average size of a crystallite in a film formed at 1030°C, calculated from the formula given by Stokes and A. K. Wilson [1942]

Nature of the post oxide treatment	R_1/R_2	Width w of the 2nd arc in the 4 arc pattern in mm	Average thickness t of a crystallite in Å $t = \lambda L/w$
Suddenly cooled (Table I obs. 1)	1.1	1.8 ± 0.1	11.7 ± 0.7
Slowly cooled (Table I obs. 7)	.95	1.6 ± 0.1	13.1 ± 0.8
Slowly cooled (Table I obs. 13)	.290	1.4 ± 0.1	15.0 ± 1.0
Stored for 16 hours at 980°C and slowly cooled	1.04	1.25 ± 0.05	16.8 ± 0.7
Stored for 36 hours at 980°C and slowly cooled	.25	1.1 ± 0.05	19.1 ± 0.9

MECHANISM OF THE FORMATION OF THE RECTIFYING LAYERS

The formation of a layer of Cu₂O below another Cu₂O layer, should be compared with the formation of a Cu₂O layer below a CuO layer already observed by us. We were then working at atmospheric pressure, and now we are working at a low pressure. This results in the present case in the formation of Cu₂O crystals at the surface. The crystals of Cu₂O formed underneath show a peculiar structure. The formation of these peculiar crystals of Cu₂O (Cu₂O with a diamond or zinc blende structure) may be considered as an (epitaxial) undergrowth.

We have seen that with an increase in the time of formation of the oxide film or with an increase of temperature at which the oxide film is formed (vide Table II) there is a tendency for the crystallites in the surface to change over from a double orientation 110 and 111 to a single orientation 111. For a temperature of the film greater than 700°C, the crystallites in the surface show a 111 orientation but an increase in size. Because of this instability a few oxygen atoms or ions are able to diffuse through the interspaces between the crystallites of Cu₂O present at the surface. A thin layer of oxygen will now be formed below the free surface and this will enable new crystallites of Cu₂O to be formed (according to the migration theory of Mott and Cabrera, 1949) below the old, oriented crystallites of Cu₂O present in the surface. We could reasonably expect from the laws of epitaxial growth that the new crystals of Cu₂O, if they grow directly on the oriented

crystals of Cu_2O , should have the same structure and the same orientation. But they are really growing on a thin oxygen layer formed on the oriented crystals of Cu_2O . This introduces a small modification in the structure of Cu_2O crystallites formed. The crystal size is the same, the orientation is the same, but a few more oxygen atoms are virtually incorporated in the 111 plane. This inclusion of a few more oxygen atoms in the 111 planes of a Cu_2O crystal changes its structure to that of the zinc blende type.

The formation of this peculiar undergrowth depends on the presence of oriented crystals of Cu_2O with 111 orientation in the surface. The role of 111 orientation can be understood if we remember that the system of 111 planes in Cu_2O includes copper and oxygen atoms in alternate planes and thus permits the inclusion of a few more oxygen or less copper atoms in this system of planes. This 111 orientation is also helpful, because now the plane of oxygen atoms on which the epitaxial growth takes place becomes the virtual 111 plane of the new crystallites. Thus in this epitaxial growth the new crystal starts with an excess of oxygen atoms in the 111 plane. The excess of oxygen changes a Cu_2O crystallite into a virtual zinc blende crystallite.

Our experiments thus show that the formation of small crystallites of Cu_2O with an excess of oxygen showing a zinc blende or a diamond structure is a necessary condition for rectification. The actual amount of oxygen required for rectification is then adjusted during the subsequent heat treatment.

REFERENCES

- Cabrera N. and Mott, N. F. 1949, *Rep. Progr. Phys.* **12**, 163.
 Dixit, K. R., 1933, *Phil. Mag.* **16**, 980.
 Dixit, K. R., 1956, *Ind. J. Phys.* **30**, 10.
 Dixit, K. R. and Agashe, V. V., 1955, *Z. Naturforsch.*, **10a**, 152.
 Dixit, K. R. and Agashe V. V. 1956, *Z. Naturforsch.* **11a**, 41.
 Ehlers, H. 1953 *Z. Phys.* **136**, 379.
 Gottsche, H. 1956, *Z. Naturforsch.* **11a**, 55.
 Hoffmann A. and Rose, F. 1953, *Z. Phys.* **136**, 152.
 Klemm, W. and Schuth, W. 1932, *Z. Anorgan. Chem.* **203**, 104.
 Raether, H. 1932, *Z. Phys.* **78**, 527.
 Schottky, W. 1930, *Physik. Z.* **31**, 913.
 Stokey A. R. and Wilson, A. K. 1942, *Proc. Comb. Phil. Soc.* **88**, 313.
 Welker, H. 1952, *Z. Naturforsch.* **7a**, 744.
 „ 1953, *ibid* **8a**, 248.
 Zworykin, V. K. and Ramberg, E. G. 1950, Photoelectricity (New York) 198.

ELECTRONIC SPECTRA OF TRICHLOROBENZENES IN THE LIQUID STATE AND IN THE SOLID STATE AT -180°C^* .

S. B. BANERJEE

OPTICS DEPARTMENT, INDIAN ASSOCIATION FOR THE CULTIVATION OF SCIENCE,
JADAVPUR, CALCUTTA-32

(Received for publication May 21, 1957)

ABSTRACT. The ultraviolet absorption spectra of 1,3,5-trichlorobenzene and 1,2,4-trichlorobenzene in the liquid and solid states at different temperatures have been studied and the results have been compared with those reported by previous workers for the vapour state.

In the case of 1,3,5-trichlorobenzene the 0,0 band is forbidden in the vapour state. The bands in the spectra due to the substance in the liquid state at 68°C and in the solid state at 36°C are broad and the frequency differences do not agree with those observed in the case of the vapour. The spectrum due to the crystal at -180°C , however, exhibits a large number of sharp bands and the forbidden 0,0 band is found to appear with weak intensity and with its position shifted by 279 cm^{-1} towards longer wavelengths from its calculated position in the spectrum due to the vapour. The results have been explained on the assumption that the threefold axis of the molecule disappears at -180°C owing probably to the formation of weak intermolecular bonds.

The spectrum due to 1,2,4-trichlorobenzene in the liquid state consists of broad bands with the 0,0 band displaced by 354 cm^{-1} towards longer wavelengths from its position in the spectrum due to the vapour. With solidification and lowering of temperature to -180°C the bands become sharp and on analysis they yield excited state vibration frequencies agreeing with some of those observed in the spectrum due to the vapour.

INTRODUCTION

The ultraviolet absorption spectra of 1,3,5-trichlorobenzene and 1,2,4-trichlorobenzene in the vapour state have been studied by Sponer (1947), Sponer and Hall (1948) and Kohn and Sponer (1949). Sponer and Hall (1948) pointed out that 1,3,5-trichlorobenzene belongs to point group D_{3h} and the near ultraviolet transition is $A'_1-A'_2$ corresponding to the $A_{1g}-B_{2u}$ transition in benzene which has symmetry D_{6h} . This transition would be forbidden according to group theory, as in the case of benzene. The spectrum of the compound in the vapour state reported by Sponer (1947) and Sponer and Hall (1948) accordingly does not exhibit the 0,0 band, but its position was determined from the frequencies of the first strong band and a weak band on the long wavelength side. These two bands correspond respectively to the excited state and ground

*Communicated by Prof. S. C. Sarkar.

state vibration frequencies of a mode corresponding to one of the components of e_{2g} mode of the benzene ring. These two frequencies were found to be 371 cm^{-1} and 425 cm^{-1} respectively. From the results the authors calculated the position of the 0,0 band and found it to be at 35498 cm^{-1} in the same way as was done for benzene.

In the case of benzene it was observed that in the spectrum of the compound in the solid state at -259°C (Kronenberger, 1930) the forbidden 0,0 band appears with weak intensity owing to the influence of intermolecular forces in the solid state (Sponer, Nordheim, Sklar and Teller, 1939) and the bands were shifted by 261 cm^{-1} towards longer wavelengths. It is not known, however, whether in the case of 1,3,5-trichlorobenzene in the solid state at low temperatures the molecule is distorted so that the symmetry of three-fold axis is destroyed and the transition moment does not vanish completely. If such distortion would take place, the 0,0 band would be present in the absorption spectrum. The study of the absorption spectrum of 1,3,5-trichlorobenzene at -180°C was, therefore, undertaken to find out the influence of intermolecular field on the absorption spectrum.

The molecule of 1,2,4-trichlorobenzene has the lowest symmetry C_s and the 0,0 band appears strongly in the spectrum due to the substance in the vapour state (Sponer, 1947; Kohn and Sponer, 1949). This shows that the band system is due to an allowed transition. The influence of intermolecular field in the solid state at -180°C was not known in this case also. So, in the present investigation it was intended to find out whether the absorption spectrum of the compound in the vapour state changed with liquefaction of the vapour or solidification of the liquid. The results of these investigations have been discussed in the present paper.

EXPERIMENTAL

Chemically pure 1,3,5-trichlorobenzene was supplied by Eastman Kodak Co. and was purified by crystallisation from solution in alcohol. 1,2,4-Trichlorobenzene of similar purity was obtained from B.D.H. and was distilled under reduced pressure before use. Absorbing films used were of thickness of the order of a few microns. Spectrograms were taken on Ilford HP3 films with a Hilger E1 spectrograph. Iron arc spectrum was taken on each spectrogram as comparison. Microphotometric records were taken with a Kipp and Zonen type Moll microphotometer. The absorption spectra were calibrated with the help of microphotometric records of iron arc lines by the method described earlier (Banerjee, 1956).

RESULTS AND DISCUSSION

The microphotometric records of the spectrograms are reproduced in figures 1 and 2. The frequencies of the bands with their probable assignments are

given in Tables I and II. The visual intensities are given as very strong (vs), strong (s), etc. The data for 1,2,4-trichlorobenzene in the vapour state reported by Kohn and Sponer (1949) have been included in Table II for comparison.

1,3,5-Trichlorobenzene

It can be seen from figure 1(a) that the first band at 35219 cm^{-1} on the long wavelength side of the absorption spectrum of 1,3,5-trichlorobenzene in the solid state at -180°C is much weaker than the next stronger band at 35602 cm^{-1} , and the interval between the two bands is only 383 cm^{-1} . In the absorption spectrum due to this substance in the vapour state, there is a feeble band at a distance of 796 cm^{-1} from the first intense band at 35869 cm^{-1} on the long wavelength side. These two bands are assumed to be due to coupling of $1 \rightarrow 0$ and $0 \rightarrow 1$ vibrational transitions with the electronic transition, the ground state and excited state vibrational frequencies being 425 cm^{-1} and 371 cm^{-1} respectively (Sponer, 1947; Sponer and Hall, 1948). In the case of the solid at -180°C the first band at 35219 cm^{-1} cannot be due to $1 \rightarrow 0$ transition, because there is no corresponding stronger band on the short wavelength side of the second band at 35602 cm^{-1} . Hence it appears that the first weak band at 35219 cm^{-1} in this case is to be assigned as the $0,0$ band. In that case the band at 35602 cm^{-1} would represent the $0 \rightarrow 1$ band involving the excited state vibrational frequency 383 cm^{-1} . A very weak band at a distance of 423 cm^{-1} on the long wavelength side of the band at 35219 cm^{-1} is just visible in the spectrogram, and this confirms the correctness of the assignment of the $0,0$ band. Thus the symmetry of the molecule is disturbed in the solid state at -180°C and the $0,0$ band appears with small intensity. These results, therefore, prove the correctness of the assumption made by Sponer and Hall (1948) that the $0,0$ band is absent in the spectrum due to the vapour state.

There is another strong evidence supporting the assignment made by Sponer and Hall (1948). They observed a progression $0 \leftarrow 371 + n \times 963$, but no such progression as $0 \leftarrow n \times 963$, which showed that the totally symmetric vibration coupled to the electronic transition was also forbidden. In the case of the crystals at -180°C a progression of $0 \leftarrow n \times 975$ is observed in the present investigation. This shows that the symmetric oscillation coupled to the $0,0$ electronic transition is allowed at -180°C . Hence, the electronic transition itself is allowed and the threefold symmetry of the molecule is not present at -180°C .

As regards the change in the frequency of the $0,0$ band with change of state it can be seen that the frequency changes from 35498 cm^{-1} (calculated) to 35219 cm^{-1} with solidification of the vapour and lowering of temperature to -180°C . Thus the band shifts by 279 cm^{-1} towards longer wavelengths with the solidification of the vapour.

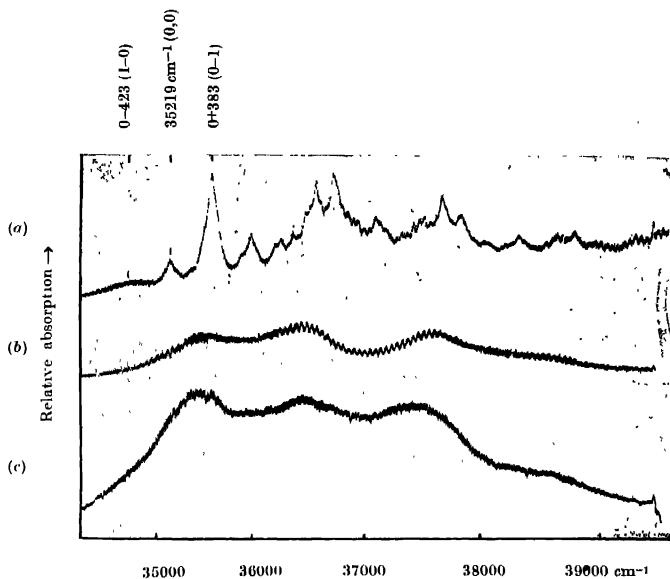


Fig. 1. Microphotometric records of the ultraviolet absorption spectra of 1, 3, 5 trichlorobenzene.

(a) Solid at -180°C (b) Solid at 36°C (c) Liquid at 68°C

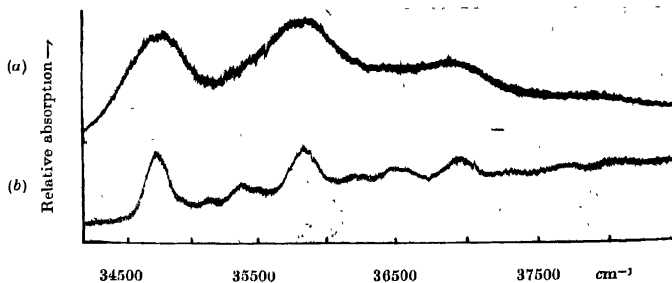


Fig. 2. Microphotometric records of the ultraviolet absorption spectra of 1,2,4 trichlorobenzene.

(a) Liquid at 38°C (b) Solid at -180°C .

TABLE I

Absorption bands of 1,3,5-trichlorobenzene

Liquid at 68°C		Solid at 36°C		Solid at -180°C	
Wave No. (cm ⁻¹) & intensity	Diff. between successive bands	Wave No (cm ⁻¹) & intensity	Diff. between successive bands	Wave No (cm ⁻¹) & intensity	Assignment
35513 s	925	35564 m	908	34769 vvw	0 + 423
36438 s	1004	36472 m		35219 m	0,0
37442 s	1149	37618 m		35412 vw	0 + 193
38501 w		38568 vw		35602 vs	0 + 383
				35883 w	0 + 604
				35978 m	0 + 2 × 383
				36194 m	0 + 975
				36260 m	0 + 1041
				36046 m	0 + 1127
				36460 w	0 + 193 + 1041
				36531 w	0 + 193 + 1127
				36565 vs	0 + 383 + 975
				36713 vs	0 + 1494, 0 + 1127 + 383
				36930 w	0 + 2 × 383 + 975
				37094 m	0 + 1494 + 383
				37177 w	0 + 2 × 975
				37330 vvw	0 + 975 + 1127
				37525 vvw	0 + 383 + 2 × 975
				37667 m	0 + 1494 + 975
				37824 m	0 + 1494 + 1127
				38040 w	0 + 2 × 383 + 2 × 975
				38151 vvw	0 + 3 × 975
				38605 w	0 + 3 × 1127
				38793 w	0 + 975 + 1127 + 1494

TABLE II
Absorption bands of 1,2,4-trichlorobenzene

Vapour* (Kohn and Sponer, 1949)		Liquid at 38°C (Present author)		Solid at -180°C (Present author)	
Wave no. (cm^{-1}) & intensity	Assignment	Wave No. (cm^{-1}) & intensity	Assignment	Wave No. (cm^{-1}) & intensity	Assignment
35565 s	0-543	34754 s	0, 0	34736 s	0, 0
35908 s	0-200				
35004 s	0-104	35825 s	0 + 1071	35120 w	0 + 384
35010 s	0-98			35356 m	0 + 620
		36896 m	0 + 2 \times 1071		
35048 vs	0-60			35500 w	0 + 764
35108 vs	0, 0			35825 s	0 + 1089
35472 w	0 + 364			36208 w	0 + 384 + 1089
35737 ms	0 + 629			36261 w	0 + 2 \times 764
36075 s	0 + 967			36450 m	0 + 620 + 1089
36105 vs	0 + 997			36579 w	0 + 764 + 1089
36154 s	0 + 1046			36916 s	0 + 2 \times 1089
36208 vs	0 + 1100			37302 w	0 + 384 + 2 \times 1089
36228 s	0 + 1120			37540 w	0 + 620 + 2 \times 1089
36236 s	0 + 1128			38004 w	0 + 3 \times 1089

*Only prominent bands involving the fundamental frequencies have been included

The absorption spectra due to the substance in the liquid state at 68°C and in the solid state at 36°C reproduced in figures 1(c) and 1(b) show that in each of them there are four broad bands and that the bands do not undergo any change with solidification of the liquid and cooling down to 36°C. The bands due to the liquid and the crystals at 36°C are broad and the frequency differences do not agree with those observed in the case of the vapour or the solid at -180°C. This shows that each broad band consists of several broad bands overlapping each other. The bands due to the liquid are broad because of fluctuation of the intermolecular field caused by motion of the molecules. In the case of the crystals at 36°C this motion may be angular oscillation about the axes of the molecules.

These results show that when the crystals of 1,3,5-trichlorobenzene are cooled to -180°C some new strong intermolecular forces are developed and the symmetry of the molecules is partially destroyed. The symmetry, how-

ever, can be disturbed only when there is formation of some virtual bonds between the molecules at certain points. These results show conclusively that such bonds are formed only at the low temperature in this case.

1,2,4-Trichlorobenzene

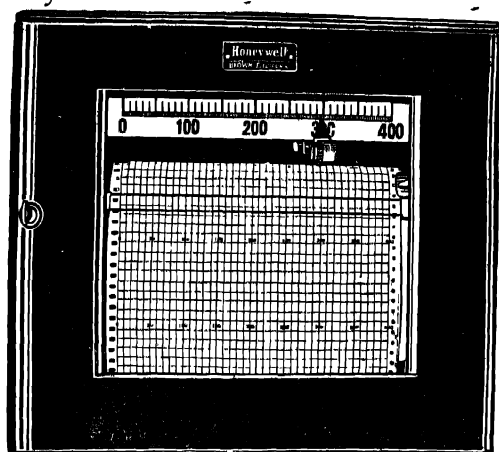
The molecule of 1,2,4-trichlorobenzene belongs to the point group C_s and the near ultraviolet transition which is $A'-A'$ is allowed. The vapour spectrum of 1,2,4-trichlorobenzene reported by Kohn and Sponer (1949) shows a strong 0,0 band at 35108 cm^{-1} and a large number of bands involving different vibrational frequencies. In the liquid state the compound yields three broad bands with the positions of maximum intensities approximately at 34754 , 35825 and 36896 cm^{-1} respectively. The bands are broad and probably bands due to the $v \rightarrow v$ transitions merge into one another to produce these broad bands. Of the three bands due to the liquid the first band has been taken as the 0,0 band. The three bands are separated from each other by 1071 cm^{-1} . It can be seen that the 0,0 band of the liquid is displaced by 354 cm^{-1} towards longer wavelengths from its position in the vapour state. The shift is larger than that observed in the case of 1,3,5-trichlorobenzene at -180°C , probably because in the present case the molecule is more asymmetric and possesses a permanent electric moment. When the liquid film is frozen and cooled to -180°C , the individual broad bands become sharp and some of the frequencies are resolved. This sharpening of the bands is partly due to weakening of the $v \rightarrow v$ transitions and partly to cessation of angular oscillation of the molecules. The position of the 0,0 band, which is quite intense, remains almost unchanged at -180°C and the bands can be assigned to transitions involving excited state vibrational frequencies 384 , 620 , 764 and 1089 cm^{-1} of which the bands corresponding to the frequency 1089 cm^{-1} are most prominent.

ACKNOWLEDGMENT

The author's grateful thanks are due to Professor S. C. Sirkar, D.Sc., F.N.I. for his kind interest and guidance during the progress of the work

REFERENCES

- Banerjee, S. B., 1950, *Ind J Phys.*, **30**, 106
- Kohn, H. and Sponer, H., 1949, *J Opt. Soc. Am.*, **39**, 75.
- Kronenberger, A., 1930, *Zeits. f. Physik.*, **63**, 494
- Sponer, H., 1947, *Chem. Rev.*, **41**, 281.
- Sponer, H. and Hall, M. B., 1948, *Contribution a l'Etude de la Structure Moléculaire*, (Deosor, liege), p. 211
- Sponer, H., Nordheim, G., Sklar, A. L. and Teller, E., 1939, *J Chem Phys.*, **7**, 207.



Price \$700 to \$1700
Size A little larger than
a standard typewriter.

This instrument produces up to 20
different records of laboratory or production
variables on a single chart. It is an
ElectroniK Recorder used in industry
to measure and control hundreds of
variables such as temperature, pressure,
or flow. Honeywell ElectroniK
Recorders are produced for thousands
of industrial applications.



Honeywell
MINNEAPOLIS
BROWN INSTRUMENTS

First in Controls

Exclusive Distributors

BLUE  **STAR**

BLUE STAR ENGINEERING CO. (Calcutta) PRIVATE LTD.

7 HARE STREET, CALCUTTA I

Also at BOMBAY, DELHI, MADRAS

THEORETICAL CALCULATIONS OF TRANSITION PROBABILITIES IN THE FIRST NEGATIVE ($b^4\tilde{\Sigma}_g \rightarrow a^4\Pi_u^-$) BANDS OF O_2^+

P. S. RAO AND J. D. RANADE

DEPARTMENT OF PHYSICS, UNIVERSITY OF SAUGAR, SAUGAR (M.P.)

(Received for publication, January 1, 1957)

ABSTRACT. Transition moments and transition probabilities have been calculated using the methods of Manneback, Manneback and Rahman for the first negative ($b^4\tilde{\Sigma}_g \rightarrow a^4\Pi_u^-$) bands of O_2^+ , as some of the bands of this system have been identified in the spectrum of aurorae recently. Our results are compared with those of Jarman, Fraser and Nicholls.

INTRODUCTION

Hutchisson (1930) first gave the method of evaluation of the Condon's overlap-integral (1926, 1928) for the transition moments of vibrational spectra in electronic bands of diatomic molecules for the case of a harmonic oscillator; later he (Hutchisson, 1931) extended the same to anharmonic oscillator also. His results are in the form of a finite series of expansion but of complicate forms and lengthy for evaluation. Also the greatest difficulty in his method is the lack of check on the results computed. Nevertheless, his method has been successfully applied by many workers to several molecules of astrophysical importance.

Many other authors (Bates, 1952; Fraser and Jarman, 1953; Fraser, 1954) have tried to improve upon the method of Hutchisson, analytically, by taking into account of the anharmonicity of the oscillator. But then treatments are also quite complicated.

Manneback (1951) developed a comparatively easier method of evaluating the transition-moments arriving at very simple recurrence formulac. These could be used independently to compute step-wise the overlap integrals. This method has been successfully used by Voreycken (1932, 1935).

Later, Manneback and Rahman (1954) improved the earlier method of Manneback (1951) by taking into account the electrical anharmonicity while preserving the mechanical harmonicity of the electric potentials involved in the transition.

Interest has been aroused among astrophysicists by the identification of O_2^+ (first negative) bands in the spectrum of aurorae by Nicolet (1948) and Nicolet and Digniaux (1950). This identification has been confirmed by Vegard (1950) Dahlstrom and Hunter (1951), Gartlein and Sherman (1952) have also identified the bands of O_2^+ (first negative) system in the region 3800–7000Å. However, many bands could not be identified because of their inherent weakness in intensity.

We have calculated the transition moments and hence transition probabilities of O_2^+ (first negative) bands using both the methods of Manneback (1951) and Manneback and Rahman (1954) and compared our results with those of Jarmin, Fraser and Nicholls (1955) who have calculated the p -values on the basis of first order perturbation theory, to find out how far the results evaluated by the easier methods agree with those of the complicated ones.

2 SYNOPSIS OF THE METHODS USED HERE AND THAT OF JARMIN, FRASER AND NICHOLLS

The transition moments for an electronic vibrational transition is given by Condon's "overlap integral"

$$\int_0^{\infty} \psi_1^{(n')}(r) \psi_2^{(n'')}(r) \cdot dr \quad \dots (1)$$

where r means the internuclear distance, n' the vibrational quantum number in the state 1, n'' the vibrational quantum number in the state 2, the transition taking place $1 \rightarrow 2$. The ψ 's represent the corresponding normalised vibrational eigenfunctions. The observed intensities in the vibrational spectrum are proportional to the square of the overlap-integral, to the fourth power of the line frequency, and to the number of molecules in the initial state.

The transition probability can be defined as

$$p(n', n'') = \left| \int_0^{\infty} \psi_1^{(n')}(r) \cdot \psi_2^{(n'')}(r) \cdot dr \right|^2 \quad \dots (2)$$

This transition probability or p -value (as it may be called) is of interest in astrophysical applications.

In the calculation of intensities of vibrational spectrum of electronic bands, there are two important factors which control, to a certain extent, the intensities predicted on the basis of a pure "Condon parabola". This parabola can be considered to be arising from Condon's overlap-integral when

- (i) both the electronic states under consideration are taken as perfectly harmonic,
- (ii) the purely electronic transition probability between the excited and the ground state is independent of the internuclear distance.

In the method of Fraser and Jarmin (1953) both the above mentioned factors (i) and (ii) have been assumed to be tacitly correct. Fraser (1954) has improved the method of Fraser and Jarmin (1953), based on the first order perturbation theory by introducing the mechanical anharmonicity of the oscillators. This later improved method was used by Jarmin, Fraser and Nicholls (1955) in evaluating the p -values.

In the method of Manneback (1951) also, both the above mentioned factors (i) and (ii) have been assumed to be perfectly true, and he has given the following formulae for the computation of the $C(n', n'')$ matrix elements. For the (0, 0) band he gives :

$$C(0, 0) = e^{-\frac{1}{2}M^2} (k^+)^{\frac{1}{2}} \quad \dots (3)$$

where

$$k^+ = 2(v' v'') / (v'' + v')$$

$$M = 0.172205 \mu^{\frac{1}{2}} (r' - r'') [v' v'' / (v' + v'')]^{\frac{1}{2}}$$

For the evaluation of the other elements of the matrix, the following recurrence formulae are given :

$$\begin{aligned} C(n'+1, n'') = & - [n' / (n' + 1)]^{\frac{1}{2}} k C(n' - 1, n'') \\ & + [n'' / (n'' + 1)]^{\frac{1}{2}} k^+ C(n', n'' - 1) \\ & - (n' + 1)^{-\frac{1}{2}} a C(n', n'') \end{aligned} \quad \dots (4)$$

$$\begin{aligned} C(n', n''+1) = & + [n'' / (n'' + 1)]^{\frac{1}{2}} k C(n', n'' - 1) \\ & + [n' / (n' + 1)]^{\frac{1}{2}} k^+ C(n' - 1, n'') \\ & + (n'' + 1)^{-\frac{1}{2}} b C(n', n'') \end{aligned} \quad \dots (5)$$

$$\text{where} \quad k = (v'' - v') / (v' + v'')$$

$$a = M[2v'' / (v' + v'')]^{\frac{1}{2}}$$

$$\text{and} \quad b = M[2v' / (v' + v'')]^{\frac{1}{2}}$$

With the aid of the above formulae one can proceed computing successively lines parallel or perpendicular to the initially chosen one; in each case either of the formulae can be used. There is, at each step, a check of orthogonality. However, since this check applies strictly to an infinite series of terms, we have calculated the elements of the $C(n', n'')$ matrix twice making use of both the formulae (4) and (5) for a check. In this particular case of O_2^+ (first negative) transitions are such that the conditions are opposite to that of "normal cases" mentioned by Manneback (1951). Here $r' < r''$, $v' > v''$, and hence all the constants k , a , and b are negative. Therefore following the method suggested by him in such cases by interchanging the meaning of n' and n'' but keeping the formulae unaltered with positive k , a , and b , no difficulty was experienced in evaluating the matrix elements.

In the improved method of Manneback and Rahman (1954) the purely electrical transition probability was assumed to vary linearly with the internuclear distance r , while the oscillators were assumed to be harmonic. This aspect was already mentioned by Schuler (1950) that at least for low lying vibrational levels, the transitional probabilities do not change as much with the introduction of a

mechanical anharmonicity of the vibrational potential as they do on the inclusion of a term which produces a linear variation of the purely electronic transition probability with the internuclear distance. With the improvement the overlap-integral now becomes

$$D(n', n'') = \int \bar{\psi}_1^{(n')} (r) \cdot r \cdot \psi_2^{(n'')} (r) \cdot dr \quad \dots (6)$$

Manneback and Rahman (1954) have solved this integral and developed a simple formula as :

$$D(n', n'') = X C(n', n'') + Y n' C(n' - 1, n'') + Z n'' C(n', n'' - 1) \quad \dots (7)$$

where

$$X = (r'v' + r''v'')/(v' + v'')$$

$$Y = 2\rho' \sin^2 \theta$$

$$Z = 2\rho'' \cos^2 \theta$$

and

$$\rho' = (\hbar/4\pi^2\mu v')^{\frac{1}{2}}; \quad \rho'' = (\hbar/4\pi^2\mu v'')^{\frac{1}{2}} \\ \tan \theta = (v'/v'')^{\frac{1}{2}}.$$

This formula enables us to evaluate the elements of $D(n', n'')$ matrix when once we know the values of the elements in $C(n', n'')$ matrix.

3. RESULTS AND DISCUSSION

The results of the $C(n', n'')$ and $D(n', n'')$ matrices are given in Tables I and II respectively. The p -values calculated from these two methods along with those of Jarmin, Fraser and Nicholls (1955) (abbreviated as J.F.N.) are given in Table III.

It can be seen that the results of the p -values obtained by Manneback's method agree quite well with those of J.F.N. except for a few higher vibrational levels. But a noticeable difference can be seen from the values calculated by the method of Manneback and Rahman and the other two sets. This marked difference in the values calculated by Manneback's method and also the values of J.F.N. with those by Manneback and Rahman's method, and the close resemblance of the results by the Manneback's method with those of J.F.N., only confirms the earlier view expressed by Schuler (1950).

Therefore, in order to ascertain the validity of the results derived theoretically, experimental studies of determining the integrated intensities of the bands produced in the laboratory by the technique of photographic photometry are undertaken. Work in this direction is in progress,

TABLE I

 $C(n', n'')$

$O_2^+(b^4\Sigma_g^- \rightarrow a^4\pi_u)$				
$\nu' = 1196.77 \text{ cm}^{-1}$ $r' = 1.27953\text{\AA}$ $\mu = 7.99986$ $M = -1.167523$ $\nu'' = 1035.69 \text{ cm}^{-1}$ $r'' = 1.38126\text{\AA}$ $k = 0.9973926$ $a = -1.124612$ $k = 0.0721530$ $b = -1.20881$				
$\downarrow n' \begin{smallmatrix} \rightarrow \\ n'' \end{smallmatrix}$	0	1	2	3
0	0.504946	-0.567868	0.425821	-0.243028
1	0.610433	-0.182875	-0.286273	0.441905
2	0.547577	0.245407	-0.465123	0.015634
3	0.418144	0.475858	-0.099778	0.367123

*The values of the constants have been taken from "Molecular Spectra and Molecular Structure I—Spectra of diatomic molecules" by G. Herzberg (1953).

TABLE II

 $D(n', n'')$

$O_2^+(b^4\Sigma_g^- \rightarrow a^4\pi_u)$				
$X = 1.320725$; $Y = 0.0636516$; $Z = 0.0592137$				
$\downarrow n' \begin{smallmatrix} \rightarrow \\ n'' \end{smallmatrix}$	0	1	2	3
0	0.699245	-0.723546	0.497697	-0.246780
1	0.842022	-0.182455	-0.374308	0.519964
2	0.804194	0.335741	-0.544874	0.004981
3	0.659324	0.702954	0.153386	0.472332

TABLE III

 $p(n', n'')$ values.

(n', n'')	J.F.N.	Manneback's method	Manneback & Rahman's method
(0,0)	0.208	0.255	0.449
(0,1)	0.296	0.323	0.524
(0,2)	0.209	0.181	0.248
(0,3)	0.119	0.059	0.061

Table III (Contd.)
 $p(n', n'')$ values

(n', n'')	J.F.N.	Munneback's method	Manneback & Rahman's method
(1,0)	0.429	0.373	0.709
(2,0)	0.243	0.300	0.647
(3,0)	0.058	0.175	0.435
(1,1)	0.022	0.033	0.033
(2,1)	0.182	0.061	0.112
(3,1)	0.351	0.226	0.494
(1,2)	0.043	0.082	0.140
(2,2)	0.143	0.164	0.297
(3,2)	0.026	0.010	0.024
(1,3)	0.130	0.195	0.270
(2,3)	0.006	0.000 ₂	0.000
(3,3)	0.160	0.135	0.223

ACKNOWLEDGMENTS

One of the authors (P. S. R.) is grateful to the Government of India, Ministry of Education, for the award of a Senior Research Scholarship. The authors are also grateful to the Head of the Department of Physics for the facilities provided here to carry out this work.

REFERENCES

- Bates, D. R., 1952, *Mon. Not. Roy. Astr. Soc.*, **112**, 615.
 Condon, E. U., 1926, *Phys. Rev.*, **28**, 1182.
 ———, 1928, *Phys. Rev.*, **32**, 358.
 Dahlstrom, C. E. and Huntan, D. M., 1951, *Phys. Rev.*, **84**, 378.
 Fraser, P. A. and Jarmun, W. R., 1953, *Proc. Phys. Soc. (Lond.)*, **A66**, 1145.
 Fraser, P. A., 1954, *Proc. Phys. Soc. (Lond.)*, **A67**, 939.
 Fraser, P. A., Jarmun, W. R. and Nicholls, R. W., 1955, *Astrophys. J.*, **122**, 55.
 Garlton, C. W. and Sherman, D. F., 1952, *Mem. Soc. Roy. Sci. Belg'c*, **12**, 87.
 Hutchisson, E., 1930, *Phys. Rev.*, **36**, 410.
 ———, 1931, *Phys. Rev.*, **37**, 45.
 Munneback, C., 1951, *Physica*, **17**, 1001.
 Munneback, C., and Rahman, A., 1954, *Physica*, **20**, 497.
 Nicolet, M., 1948, The emission spectra of night sky and aurora. Gassiot Committee Report, (London Phy. Society), 105.
 Nicolet, M. and Digniaux, R., 1950, *J. Geophysical Res.*, **55**, 21.
 Schuler, K. E., 1950, *J. Chem. Phys.*, **18**, 1221.
 Vegard, L., 1950, C. R. Acad. Sci. Paris, **280**, 1884.
 Veroycken, F., 1932, Thesis, University of Louvain.
 Veroycken, C., 1935, Thesis, University of Louvain.

ANALYSIS OF THE NEAR ULTRAVIOLET ABSORPTION SPECTRA OF α -AND β -FLUORONAPHTHALENES

S. RAMAMURTY, M. JAGANNADHA RAO AND V. RAMAKRISHNA RAO

PHYSICS DEPARTMENT ANDHRA UNIVERSITY, WALTAIR

(Received for publication, December 8, 1956)

Plate XII

ABSTRACT. The near ultraviolet absorption spectra of α - and β -fluoronaphthalenes were found to consist of two systems one in the region 3100–2900Å and another in the region 2800–2500Å. The first systems were analysed on the basis of five and four upper state fundamentals in α - and β -fluoronaphthalenes respectively and two lower state fundamentals in β fluoronaphthalene. Only one upper state fundamental could be found in System II. Both the systems correspond to allowed transitions of the type ${}^1A' \rightarrow {}^1A'$.

INTRODUCTION

While considerable work on substituted benzenes has been in progress for some time, work on condensed ring system, like naphthalene and its derivatives, is still in its very early stages. Both the electronic and the vibrational spectra of these compounds are yet to be satisfactorily explained. The electronic absorption spectra of naphthalene have been the subject of extensive investigation but there is controversy among various workers, from both the theoretical and the experimental point of view. Complete references to earlier work on both the electronic and vibrational spectra of naphthalene can be gathered from the paper by Sponer and Cooper (1955) and the papers mentioned therein.

The near ultraviolet absorption spectrum of naphthalene is found to have two regions of discrete absorption: one in the region 3300–2900Å, consisting of sharp and narrow bands and a second in the region 2900–2500 Å, consisting of broad and diffuse bands. The long wavelength absorption has been severally attributed to ${}^1A_{1g} \rightarrow {}^1A_{1g}$, ${}^1A_{1g} \rightarrow {}^1B_{3u}$ and ${}^1A_{1g} \rightarrow {}^1B_{2u}$. The first transition ${}^1A_{1g} \rightarrow {}^1A_{1g}$ is a symmetry forbidden type of transition, being allowed by interaction with a β_{2u} or a β_{3u} type of vibration. The two other possibilities are transitions of an allowed type. The second system is generally attributed to an allowed transition of one or other of the two types mentioned above depending on which we choose for the first system. It is not at this stage necessary for our work to specify which transition is characterized by which set of symmetry states in naphthalene, particularly because all the above mentioned states reduce to the A' type of state in the C_s point group.

Some work appears to be available in literature on substituted naphthalenes. The relevant results of such investigations are summarised below.

Ferguson *et al* (1954) have investigated the infrared spectra, the ultraviolet absorption spectra in solution and the phosphorescence spectra of a large number of halogen derivatives including α and β fluoronaphthalenes. Sidman (1956) published the fundamentals of β halonaphthalenes and arrived at substantially different conclusions from Ferguson *et al*. According to Sidman, all these fundamentals are derived from the α_g fundamentals in naphthalene and so must be totally symmetric (α'). Deb (1954) investigated the α chloro and the α bromo-naphthalenes.

No work on the ultraviolet absorption spectra of α and β fluoronaphthalenes in the vapour state appears to have been done. The Raman spectrum of β fluoronaphthalene also is not available in the literature. The depolarisation factors of the Raman lines of α fluoronaphthalene are also not available in the literature. The authors have taken up these investigations and the detailed results are published below. The work on α fluoronaphthalene was carried out by S. Ramamurty and V Ramakrishna Rao and a preliminary note has been published in the Journal of Scientific and Industrial Research (1956) while that of β fluoronaphthalene has been published by M. Jagannadha Rao and V. Ramakrishna Rao (1955).

EXPERIMENTAL

Ultraviolet absorption in vapour.

Both the compounds are supplied by Eastman Kodak Co. α Fluoronaphthalene is a colourless liquid with melting point of -13°C while β fluoronaphthalene is a crystalline solid with a melting point of 61°C . The specimens were distilled in vacuum thrice before they were used for the experimental work.

Full details of the absorption tube and the experimental set-up for taking the absorption spectrum were given by Suryanarayana and Rao (1955) in their paper on *o*-chloroanisole. Absorption path lengths of 25 and 75 cms. were used. As the specimens were sealed under dark space vacuum conditions in the absorption tube, we can expect them to be under the saturated vapour pressures corresponding to the temperatures of the containers. By altering these temperatures we obtained various vapour pressures in the absorption columns and spectra were taken under these conditions. α Fluoronaphthalene was investigated in the temperature range -15° to 200°C while β fluoronaphthalene was investigated in the range 0° to 110°C . The higher temperature limit was indicated with the continuous absorption setting in all through. Hilger's hydrogen arc lamp was the source of the continuum. Hilger's quartz Littrow, medium quartz and small quartz were used to record the spectra with Ilford Special Rapid plates. Exposures of 5 to 10 minutes were given on the smaller

instruments while exposures of about one hour were used on the Littrow instrument. The bands were measured with reference to standard iron arc lines, using Hartmann's dispersion formula. Each band was measured at least 8 times and the mean value of the wavelength was taken. Wavelength data of the sharper bands are accurate within 0.3 Å. Diffuse bands cannot, however, be accurate to within less than 2 to 3 Å.

Experimental for Raman spectra

Mercury 4358 radiation, filtrated through Rhodamine 5GD Extra in para-nitrotoluene-alcohol solution, was used for exciting the Raman spectrum. The Raman spectrum of β fluoronaphthalene was obtained by a CCl_4 solution while that of α fluoronaphthalene was obtained in a liquid condition. The depolarisation factors of the Raman lines of α fluoronaphthalene were determined with the aid of a double image prism. The actual procedure was an approximate one and the values obtained may be treated as only semi-quantitative.

RESULTS

Ultraviolet absorption

Both the isomers give two regions of discrete absorption like naphthalene. The long wavelength region 3154 to 2943 Å in α fluoronaphthalene and 3154 to 3000 Å in β fluoronaphthalene consists of a number of well defined bands with sharp edges, degraded towards the red and occurring in distinct groups. Each group consists of 3 to 6 bands. In α fluoronaphthalene the most intense group appears to be at 3136 Å. In β fluoronaphthalene the corresponding group is at 3143 Å. The bands resemble, in their appearance and region, very closely those of naphthalene (3300–2900 Å). Also their appearance is quite distinct from the bands of the shorter wavelength region and hence we might refer to these long wavelength bands as System I hereafter.

System II in α fluoronaphthalene consists of 11 very broad and diffuse bands in the region 2838–2598 Å, while in β fluoronaphthalene the corresponding system consists of only 6 similar bands in the region 2770–2630 Å. The corresponding system in naphthalene is in the region 2900–2500 Å.

At room temperatures, System II appears with maximum clarity while only a few bands are recorded in System I, primarily those on its longer wavelength sides. As the temperatures is increased, System II is lost in continuous absorption while System I develops on the shorter wavelength side. The maximum number of bands are recorded in System I at 70°C in β fluoronaphthalene and at 75°C in α fluoronaphthalene. At still higher temperatures, continuous absorption moves towards longer wavelength side while some additional and weak bands develop on the long wavelength side. At about 110°C there is complete absorption of System I in β fluoronaphthalene with the corresponding phenomenon taking

place at 140°C in α fluoronaphthalene. At lower temperatures, ranging between the room temperature and -15°C , the second system becomes more hazy, with the bands showing no improvement in their definition.

TABLE I
Absorption bands of α -fluoronaphthalene
System I

Int	Wave-number (cm^{-1})	Assignment	Int.	Wave-number (cm^{-1})	Assignment
1	2	3	4	5	6
	31686			32778	0 + 1046 - 149
	31723	0 = 149		32818	0 + 1046 - 109
10	31763	0 - 109		32852	0 + 1046 - 73
8	31799	0 - 73		32883	0 + 1046 - 36
8	31826	0 - 36		32918	0 + 1046
7	31872	(0, 0)		33158	0 + 2 \times 673 - 73
	32087				0 + 1435 - 149
	32130	0 + 409 - 149	7	33189	0 + 2 \times 673 - 36
1	32174	0 - 409 - 109			0 + 1435 - 109
2	32210	0 + 409 - 73	6	33236	0 + 2 \times 673
3	32247	0 + 409 - 36			0 + 1435 - 73
4	32281	0 + 409	6	33269	0 + 1435 - 36
2	32333		4	33307	0 + 1435
5	32371			33340	0 + 673 + 838 - 36
6	32434	0 + 673 - 109		33377	0 + 673 + 838
5	32470	0 + 673 - 73		33415	
5	32507	0 + 673 - 36		33447	
5	32545	0 + 673		33487	
	32564	0 + 838 - 149		33638	0 + 1435 + 409 - 73
	32601	0 + 838 - 109		33678	0 + 1435 + 409 - 36
	32625	0 + 838 - 73	1	33709	0 + 1435 + 409
	32672	0 + 838 - 36	1	33856	0 + 3 \times 673 - 36
1	32710	0 + 838	2	33899	0 + 3 \times 673
	32747		2	33937	0 + 1435 + 673 - 36
			1	33975	0 + 1435 + 673

TABLE II
Absorption bands of β -fluoronaphthalene
(System 1)

Int	Wave-number ν (cm ⁻¹)	Assignment	Int	Wave-number ν (cm ⁻¹)	Assignment
1	2	3	4	5	6
1	31030	0 - 774	1	32748	0 972 - 29
0	31245		2	32758	0 972 - 29
2	31282	0 - 522	4	32776	0 972
1	31636	0 - 2 \times 82			
2	31683	0 - 2 \times 62	0	32796	
2	31693	0 - 2 \times 54	1	32845	0 446 710 - 2 \times 6
			0	32883	0 466 710 - 82
2	31701	0 - 62 - 41	1	32964	0 446 - 710 or
2	31711	0 - 54 - 41			0 710 - 972 - 522
3	31722	0 - 522 - 416	0	33166	0 2 \times 710 - 62 or
1	31742	0 - 774 710			0 446 972 - 62 or
		or			0 1441 - 82
3	31750	0 - 41 - 22	0	33177	0 2 \times 710 - 54 or
3	31763	0 - 41 - 13			0 446 972 - 54 or
3	31782	0 - 22			0 1441 - 62
1	31791	0 - 13	5	33188	0 2 \times 710 - 41 or
0	31804	0,0			0 446 972 - 41 or
2	31818				0 1441 - 54
0	32173	0 446 - 82	5	33206	0 2 \times 710 - 22 or
0	32195	0 446 - 54			0 446 972 - 22 or
1	32210	0 446 - 41			0 1441 - 41
1	32230	0 446 - 29	8	33226	0 2 \times 710 or
3	32250	0 446			0 446 972 or
1	32282				0 1441 - 22
0	32353	0 710 - 2 \times 82	2	33237	0 1441 - 13
1	32402	0 710 - 2 \times 54	2	33245	0 1441
2	32435	0 710 - 82	0	33313	
1	32453	0 710 - 62			
2	32462	0 710 - 54	0	33373	0 710 972 - 2 \times 62
2	32474	0 710 - 41	1	33409	0 710 972 - 82 or
2	32485	0 710 - 29			0 2 \times 416 710
2	32495	0 710 - 22	2	33488	0 710 972
0	32505	0 710 - 13	0	33670	0 446 2 \times 710 or
0	32514	0 710			0 2 \times 446 + 972
	32533		1	33896	0 3 \times 710 - 41
	32578		2	33919	0 3 \times 710 - 22
	32578		3	33939	0 3 \times 710
	32622	0 972 - 2 \times 82			
	32680	0 972 - 54 - 41	1	34183	0 2 \times 710 + 972 - 22
	32697	0 + 972 - 82	1	34205	0 + 2 \times 710 + 972
		or	0	34617	0 + 4 \times 710 - 22
		0 2 \times 446			
	32727	0 972 - 54	0	34646	0 4 \times 710
	32736	0 972 - 41	0	34792	

Figures 1 and 2 (Plate XII) represent the two systems in α and β fluoronaphthalenes along with their microphotometer curves. Tables I and II give the wavenumber data of Systems I in α and β fluoronaphthalenes. Tables III and IV give the same data for Systems II.

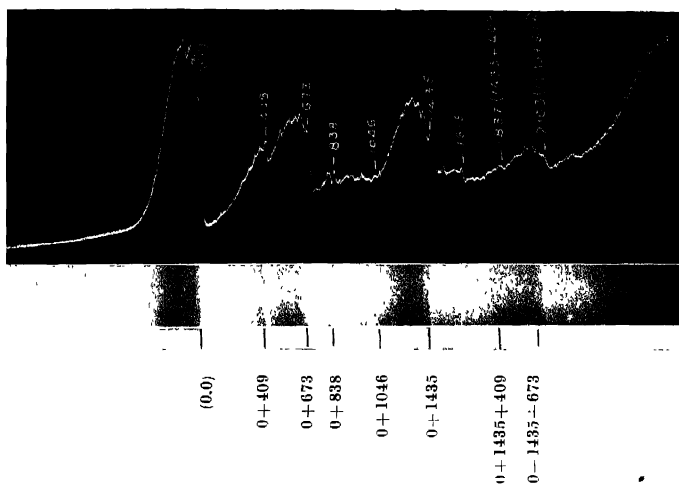


Fig. 1(a). Absorption spectrum of α -fluoronaphthalene, System I.

TABLE III

Absorption bands of α -fluoronaphthalene, System II

Wave-number (cm^{-1})	Sepp. from 0, 0 ($\Delta\nu$)
35222	0
35399	177
25683	461
36053	831
36341	1119
36598	1376
36807	1585
37075	1853
37512	2290
38026	2804
38481	3259

TABLE IV

Absorption bands of β -fluoronaphthalene (System II)

nt.	Wave-number ν (cm^{-1})	Assignment
10	36050	0, 0
3	36308	
10	36502	0 + 464
5	36959	0 + 2 \times 464
8	37418	0 + 3 \times 464
8	37908	0 + 4 \times 464

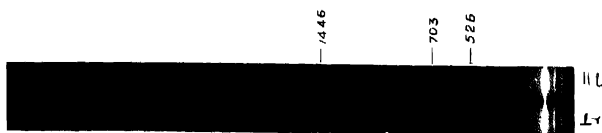


Fig. 3. Depolarisation picture of the Raman spectrum of α -fluoronaphthalene.

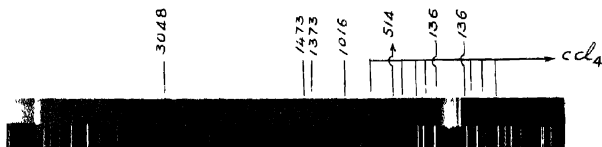


Fig. 4. Raman spectrum of β -fluoronaphthalene

Raman Spectrum.

On comparison with the earlier work on Raman frequencies by Luther (1948) we find satisfactory agreement with our values for α fluoronaphthalene.

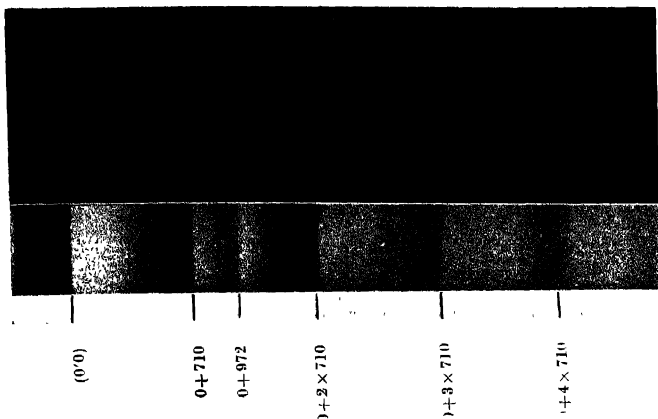


Fig. 1(b) Absorption spectrum of β -fluoronaphthalene

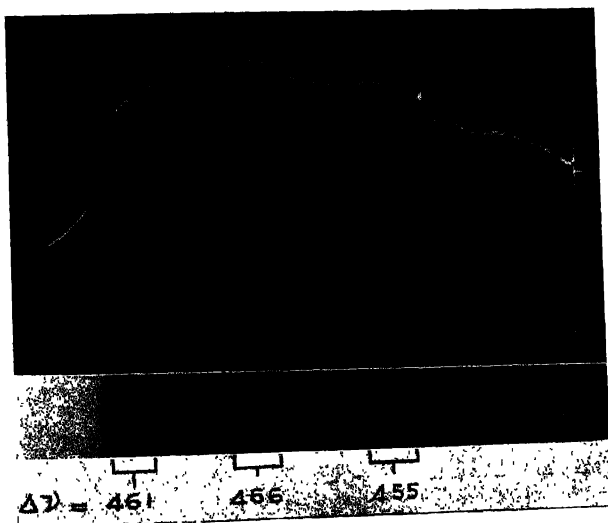


Fig. 2(a). Absorption spectrum of α -fluoronaphthalene. System II

Our semi-quantitative depolarisation factors for some of the Raman lines are given in the column 1 of the assignment Table V. Figure 3 gives the depolarisation picture of α -fluoronaphthalene

β -Fluoronaphthalene in CCl_4 solution gave only six Raman lines which are shown in figure 4. The frequency shifts are marked in the figure. Their values are tabulated in Table V and used for correlation of fundamentals

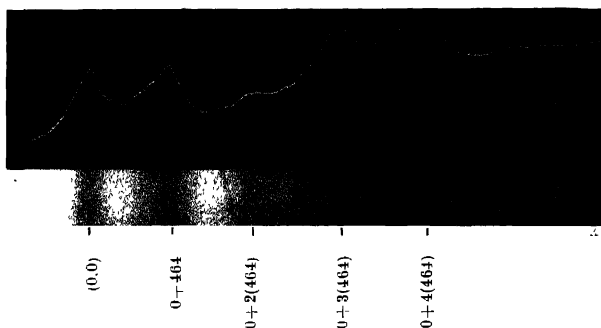


Fig. 2(b). Absorption spectrum of β -fluoronaphthalene System II

ANALYSIS

Both the isomers belong to the point group C_s (C_{1h}) derived on a monosubstitution in naphthalene (point group V_h). The character table for C_s is given below :

C_s	E	σ_h			
A'	1	1	T_x	T_y	R_z
A''	1	-1	T_z	R_x	R_y

There are only two types of electronic wavefunctions and modes of vibration A' and A'' , the former totally symmetric and the latter antisymmetric with respect to reflection in the plane of the molecule (xy). The electronic transitions whether $A' \rightarrow A'$, $A' \rightarrow A''$ or $A'' \rightarrow A''$ are all of an allowed type. From the correspondence of the regions of absorption and the appearance of the bands, we can say that Systems I in both the isomers correspond to the largest wavelength transition in naphthalene. Whatever might be the exact assignment of this transition in naphthalene, all the suggested states reduce themselves to the A' type in the point group C_s . So, the Systems I in the monosubstituted naphthalenes must be due to allowed transitions of the type ${}^1A' \rightarrow {}^1A'$.

Of the 48 independent modes of vibration, 33 would be totally symmetric, of the α' type. The other 15 would be of the α'' type, constituting out-of-plane bending modes. In the Raman spectrum, therefore, the frequencies corresponding to the α' vibrations would be polarized ($\rho < 0.8$).

In the electronic absorption spectrum we expect for an allowed transition the (0,0) band to be either the strongest or one of the strongest bands. Most of the strong bands in the spectrum would form a long series conforming to the Franck-Condon principle and belong to the totally symmetric vibrations, their overtones and their combinations. Non-totally symmetrical vibrations do not generally occur as fundamentals but their even overtones and their difference frequencies may appear with appreciable intensity.

The Systems II also definitely correspond to the short wavelength system in naphthalene in region 2900–2500 Å. Here also the controversy about this transition in naphthalene does not affect our present considerations and the Systems II may be taken as due to an allowed transition of the type ${}^1A' \rightarrow {}^1A'$.

Where the Raman data are available with depolarization factors, the identification of the totally symmetric vibrations is rendered easy as they are polarized. However, there is one drawback in the case of Raman lines with doubtful or marginal depolarisation factors. The probability of their being polarized or depolarized within experimental error is just the same. It is also a general experience that the totally symmetric vibrations among the Raman lines are also frequently the strongest. It appears that an analysis of the ultraviolet spectrum is more reliable in determining the totally symmetric vibrations than some doubtful depolarization data. Thus the depolarization data is only of a confirmatory nature, when available.

System I.

Spectra taken at the lowest temperatures resulting in the minimum number of bands in System I help picking out the (0, 0) band. As the transition is of an allowed type, the largest wavelength band consistent with the greatest intensity is chosen as the (0, 0) band. In α fluoronaphthalene it is 31872 cm^{-1} and in β fluoronaphthalene it is 31804 cm^{-1} , thus showing a shift of 68 cm^{-1} to the red with respect to the α fluoronaphthalene. Frequency shifts of 446, 710, 972, 1160, 1422, 1684, 1684, 2135, 2842 cm^{-1} are obtained with strong and medium strong bands in β fluoronaphthalene. In α fluoronaphthalene similar intervals 409, 673, 838, 1064, 1435 and 2103 cm^{-1} are found. Some of these would be totally symmetric fundamentals in the upper state while the others may be their overtones and combinations. In α fluoronaphthalene 409, 673, 838, 1046 and 1435 cm^{-1} are taken as fundamentals, while the corresponding values in β fluoronaphthalene are 446, 710, 972, 1441 cm^{-1} . We find all the fundamentals in α fluoronaphthalene have smaller values than those in β fluoronaphthalene.

TABLE V
Fundamentals in the α - and β -fluoronaphthalenes

α -fluoronaphthalene				β -fluoronaphthalene					
Vapour absorption (Authors)				Vapour absorption (Authors)					
Raman (Luther)	Infrared (Ferguson)	Ground state	Excited state	Solution absorption (Ferguson)	Raman (authors)	Infrared (Ferguson)	Ground state	Excited state	Solution absorption (Ferguson)
526 (mst. p)	567 st	—	409	433	514	—	522	446	455
703 (st. p)	709 m	—	673	679	—	738	774	710	721
—	—	—	838	857	—	—	—	972	972
—	—	—	1046	1060	—	—	—	—	—
1446	1456	—	1435	1400	1473	—	—	1441	1419

nm, mst = medium strong. st = strong. p = polarized. All frequencies are in cm⁻¹.

m, mst = medium strong, st = strong, p = polarized, All frequencies are in cm^{-1} .

lene. The additional fundamental 1046 cm^{-1} in α fluoronaphthalene has no counter part in β fluoronaphthalene. In α fluoronaphthalene itself this fundamental is very weak and has to be taken as such for want of any other interpretation. All the other prominent bands could be interpreted in α and β fluoronaphthalenes in terms of these fundamentals. If we accept the (0, 0) band of System I in naphthalene to be 32080 cm^{-1} then the α and β fluoronaphthalenes have their (0, 0) bands shifted by 208 and 276 cm^{-1} to the red side.

System II.

System II in β fluoronaphthalene consists of about 6 bands, five of which have a mean separation of 464 cm^{-1} (See Table IV & figure 2b). In α fluoronaphthalene there are about 11 bands, some of which show a mean separation of 461 cm^{-1} . A few other frequency shifts, like 1376 cm^{-1} may correspond to additional upper state fundamentals. If we take the longest wavelength bands in these systems as the (0, 0) band, we find in α fluoronaphthalene a shift of 828 cm^{-1} to the red of β fluoronaphthalene. Thus the shifts of the (0, 0) band between the isomers appear to be in opposite directions in Systems I and II. In naphthalene itself the (0, 0) band for this system has been suggested by Sponer and Cooper (1956) to be at 35910 cm^{-1} . We thus find, with respect to naphthalene, a red shift of 688 cm^{-1} in α fluoronaphthalene and a violet shift of 140 cm^{-1} in β fluoronaphthalene.

The fundamentals observed in both the systems are correlated with Raman data and presented in Table V. A discussion of these fundamentals is presented below.

DISCUSSION

The fundamentals from various sources, Raman spectra, infra red spectra and ultraviolet absorption spectra in vapour and solution for lower and upper states, are given for both the isomers in the Table V. We find that the upper state fundamentals of α fluoronaphthalene are always less than the corresponding ones in β fluoronaphthalene. We have not been able to obtain the ground state frequencies of α fluoronaphthalene in ultraviolet absorption but in β fluoronaphthalene 2 such ground state fundamentals could be found. They are 522 and 774 cm^{-1} . Of these the 522 cm^{-1} frequency agrees with the Raman line 514 cm^{-1} . Correspondingly in the upper state there is a frequency 446 cm^{-1} which is able to explain about 14 bands and occurring with medium intensity. It occurs in combination with other upper state frequencies 710 , 972 cm^{-1} etc.,. It is seen from the analysis of System II that a mean value of 464 cm^{-1} is the frequency difference between successive bands. This is of the same order of magnitude as the value of the fundamental in System I and may probably correspond to the same mode of vibration in the two different excited electronic

states. Except for one weak band in System II, all others are explained in terms of this frequency shift. In α -fluoronaphthalene similar upper state fundamentals from the first and second systems are 409 and 461 cm^{-1} respectively. In System I, the 409 cm^{-1} fundamental is a medium intensity band explaining 8 bands and combining with the fundamental 1335 cm^{-1} . The value 461 cm^{-1} in System II is the mean value of the differences between the extreme bands of 3 groups as indicated in Table III. The corresponding ground state frequency may be 526 cm^{-1} which is a medium strong and polarized Raman line. Similar frequencies are found in β methyl, 2, 6 dimethyl, α chloro, α bromo naphthalenes with values 425, 485, 508 and 496 cm^{-1} respectively. Thus the above set of frequencies may represent a common mode of vibration of the α' type in the various states for the two isomers. In Table V the above frequencies are given in mutual correspondence along with the value obtained from infrared and solution work of Ferguson (1954).

Another pair of fundamentals in β fluoronaphthalene appears to be 774 cm^{-1} in the ground state and 710 cm^{-1} in the excited state. The band representing 710 cm^{-1} appears to be the most intense of all the fundamentals. (The higher intensity of 1422 cm^{-1} group will be discussed at a later stage.). This pair of frequencies explains about 30 bands. The corresponding Raman line was not found. But Ferguson records an infrared band at 738 cm^{-1} . In α fluoronaphthalene the corresponding fundamental seems to be 673 cm^{-1} which is represented by a very prominent band in the spectrum. It explains about 12 bands, occurring also in overtones. The corresponding Raman line is strong and polarized 703 cm^{-1} . In β methyl and 2, 6 dimethylnaphthalenes the corresponding frequencies are 711 and 706 cm^{-1} respectively. In the halogen substitutions these vibrations were not found. These frequencies may possibly represent the α' type of vibration in the two isomers.

Another upper state fundamental in β -fluoronaphthalene is 972 cm^{-1} , slightly more intense than 446 cm^{-1} and much less intense than 710 cm^{-1} . The corresponding ground state frequency has not been found. In α fluoronaphthalene this fundamental appears to be given by the weak band 838 cm^{-1} . This is not very prominent in α fluoronaphthalene. The ground state frequencies could not be identified with certainty. There are a number of fundamentals in the region 870—1173 cm^{-1} obtained in various sources, like the Raman and infrared spectra, which may possibly contain the corresponding ground state frequencies.

In α -fluoronaphthalene a fundamental 1046 cm^{-1} in the excited state is found. A corresponding fundamental is not found in β -fluoronaphthalene. In the spectrum the band corresponding to this fundamental is very inconspicuous, but this and its associates can not be interpreted in any other manner. The justification for this is found from Ferguson's data where we find a frequency

shift 1060 cm^{-1} . The possible ground state value is 1077 cm^{-1} represented by a medium strong and polarized Raman line.

We now take up the fundamental 1435 cm^{-1} in the upper state for α fluoronaphthalene for which the ground state frequency may be 1446 cm^{-1} (strong and polarized Raman line). This is easily the strongest fundamental in the spectrum, as may be seen from the microphotometer curve (figure 1a). It is also conspicuous in the analysis combining with the fundamentals 409 and 673 cm^{-1} and explains in all 8 bands. The corresponding ground state frequency may be 1443 cm^{-1} (strong and polarized Raman line). In β fluoronaphthalene the corresponding frequency 1441 cm^{-1} is represented actually by a weak band accompanying a very strong group of bands at 1422 cm^{-1} . The choice of this fundamental is forced on us by a lack of interpretation of this band. Besides, the band 1422 cm^{-1} is an overtone of the fundamental 710 cm^{-1} and has an intensity greater than any other band excepting those in the $(0, 0)$ group. In fact the intensity of this group of bands is an anomaly that has to be explained. The 1422 cm^{-1} band can also be a combination band $0 + 972 + 446 = 1418\text{ cm}^{-1}$. This double assignment may probably account for part of the high intensity of the band. Still another factor may possibly contribute to the abnormal intensity of this band. We find in naphthalene, and its α -chloro, α -bromo, β -methyl, and 2, 6 methyl substitutions, upper state fundamentals of about 1400 cm^{-1} . In spite of the low intensity of the band 1441 cm^{-1} we take it as a fundamental, we might expect Fermi resonance between this and $2 \times 710\text{ cm}^{-1}$. It is possible in the process that part of the intensity of the fundamental is stolen by the overtone. This explains not only the low intensity of 1441 cm^{-1} but also the abnormally high intensity of 1422 cm^{-1} already given a double assignment. As the unperturbed value of 1441 cm^{-1} is not definitely known, we cannot locate its overtones and combinations. The absence of any such phenomena in the case of α -fluoronaphthalene has enabled us to identify the frequency 1435 cm^{-1} and thus confirm the above views in case of β -fluoronaphthalene. Its ground state frequency in β -fluoronaphthalene may be given by the Raman line 1473 cm^{-1} . The above values may therefore be a totally symmetric mode of vibration, possibly occurring in the ring itself as we do not find much variation in the value of the frequencies with various substitutions.

We are now finally left with the low frequency bands lying to the long wavelength side of the main bands with shifts between 13 and 150 cm^{-1} in α and β -fluoronaphthalenes. Some of these low frequencies also occur in their combinations and overtones. The intensity of some of these bands indicates very high Boltzmann factors which can be associated only with low frequencies. Thus they may be due to difference frequencies (ν' , ν'') transitions of several low lying vibrational levels of a non-totally symmetrical character.

ACKNOWLEDGMENTS

This work was taken up under the research scheme "Fluorescence and Absorption Spectra of Organic Molecules" granted by the Council of Scientific and Industrial Research to one of us (Dr. V. Ramakrishna Rao). Our thanks are due to Prof. K. R. Rao for his interest in this work.

REFERENCES

- Deb, A. R., 1954, *J. Chem. Phys.*, **28**, 21.
Ferguson, J., 1954, *J. Chem. Soc.*, 304.
Ferguson, J., Iredale, T. and Taylor, J. A., 1954, *J. Chem. Soc.*, 3160.
Ferguson, J. and Werner, R. L., 1954, *J. Chem. Soc.*, 3645.
Jagannadha Rao, M. and Ramakrishna Rao, V., 1956, *J. Sci. Inds. Res.*, **14**, B, 547.
Luther, H., 1948, *Zeits. f. Electrochem.*, **52**, 210.
Ramamurty, S. and Ramakrishna Rao, V., 1956, 1956, *J. Sci. Res.*, **15B**, 262.
Sidman, J. W., 1956, *J. Chem. Phys.*, **25**, 229.
Spencer, H. and Cooper, C. D., 1955, *J. Chem. Phys.*, **23**, 646. (and the references given there).
Suryanarayana, V. and Ramakrishna Rao, V. 1956, *Ind. J. Phys.*, **30**, 717.

ON THE p - p SCATTERING AT HIGH ENERGIES

A. DAS

DEPARTMENT OF THEORETICAL PHYSICS,
INDIAN ASSOCIATION FOR THE CULTIVATION OF SCIENCE,
JADAVPUR, CALCUTTA-32

Received for publication, May, 24, 1957

ABSTRACT. The nature of p - p scattering is studied with a phenomenological potential of the form $(\tau^{(1)} \cdot \tau^{(2)}) (\sigma^{(1)} \cdot \nabla) (\sigma^{(2)} \cdot \nabla) e^{-\lambda r/r^2}$.

1 INTRODUCTION

The experimental results on p - p scattering at high energies indicate that the differential cross section is almost isotropic between 15° and 90° and its value is 4.5 mb/std. (cf. Chamberlain and Wiegand, 1950).

The expression for the nuclear interaction, as derived from the pseudoscalar meson field theory, consists of two parts, the central and the tensor potentials. The differential scattering cross section due to the central part depends strongly on the angle, whereas the same due to the tensor part does not change much with angle as pointed out by C. C. Banerjee (1953 & 1954) and Basu (1954).

Further, P. Banerjee (1953) has shown how the terms with different orders of singularity in the tensor part contribute to the scattering cross section. He has found that the differential cross section obtained from term containing $1/r^3$ singularity decreases very slightly with angle and the isotropy so obtained is better than that due to any other potential.

We now propose to take a phenomenological potential of the form $(\tau^{(1)} \cdot \tau^{(2)}) (\sigma^{(1)} \cdot \nabla) (\sigma^{(2)} \cdot \nabla) e^{-\lambda r}/r^2$. The central part of this interaction gives infinite scattering cross section, and so we consider the tensor part alone and see whether the introduction of higher singularity gives more isotropic scattering than the ordinary pseudoscalar tensor term. The calculation with pseudoscalar tensor part has already been done by C. C. Banerjee, (1954).

2. THE INTERACTION

The derivative coupling of the potential $U(r)$ is given by

$$(\tau^{(1)} \tau^{(2)}) (\sigma^{(1)} \cdot \nabla) (\sigma^{(2)} \cdot \nabla) U(r) = 1/3 (\tau^{(1)} \cdot \tau^{(2)}) \left[(\sigma^{(1)} \cdot \sigma^{(2)}) \left(\frac{d^2 U}{dr^2} + 2/r \frac{dU}{dr} \right) \right. \\ \left. + S_{12} \left(\frac{d^2 U}{dr^2} - 1/r \frac{dU}{dr} \right) \right].$$

where

$$S_{12} = 3 \frac{(\sigma^{(1)} \cdot \mathbf{r})(\sigma^{(2)} \cdot \mathbf{r})}{r^2} - (\sigma^{(1)} \cdot \sigma^{(2)})$$

If we choose $U(r) = -1/4\pi[(f/\chi)^2 e^{\chi r}/r^2]$, and consider only the tensor part, the interaction assumes the following form

$$V_T = -1/3(f^2/4\pi)(\tau^{(1)} \cdot \tau^{(2)}) S_{12}(1+5/\chi r+8/\chi^2 r^2)e^{-\chi r}/r^2 \quad \dots (2.1)$$

We shall drop $(\tau^{(1)} \cdot \tau^{(2)})$ subsequently, because in the charge-symmetric proton state its value will be 1.

3. CALCULATION OF THE DIFFERENTIAL CROSS SECTION

Since the operator S_{12} representing the tensor force between the nucleons gives zero value when applied to any singlet spin-function, we need consider only the triplet scattering. In the relative coordinate system, the wave-function representing the initial incident proton beam will be of the form

$$\psi_{inc} = e^{ik\mathbf{n}_0 \cdot \mathbf{r}} \sum_{m_s=-1}^1 a_{m_s} \chi_{m_s} \quad \dots (3.1)$$

where χ_{m_s} 's are the normalised spin functions and a_{m_s} 's are the corresponding amplitudes. In an unpolarised beam, three possible orientations ($m_s = \frac{1}{2}, 0, -1$) of the total spin are equally probable, so that averaging over the phases of amplitudes a_{m_s} 's we get

$$\overline{a_{m_s} a_{m_s'}} = 1/3(\delta_{m_s m_s'}) \quad \dots (3.2)$$

The Born's approximation gives a simple expression for the asymptotic scattered wave namely,

$$\psi_{scatt} \sim -e^{ikr}/r \left(\frac{M}{4\pi\hbar^2} \right) \int e^{-ik\mathbf{r}' \cdot \mathbf{n}} V_{\mathbf{r}'} \psi_{inc} d\tau' \quad \dots (3.3)$$

Substituting (3.1) into (3.3) we obtain

$$\psi_{scatt} = e^{ikr}/r \sum_{m_s'} \chi_{m_s'} \sum_{m_s} S_{m_s' m_s} a_{m_s} \quad \dots (3.4)$$

where

$$S_{m_s' m_s} = - \frac{M}{4\pi\hbar^2} \int e^{-ik\mathbf{r}' \cdot \mathbf{n}} V_{m_s' m_s} e^{ik\mathbf{r}' \cdot \mathbf{n}} d\tau' \quad \dots (3.5)$$

In (3.5), $V_{m_g'm_g}$'s are given by

$$V_{r'} \chi_{m_g} = \sum_{m_g'} V_{m_g'm_g'} \chi_{m_g'} \quad \dots \quad (3.6)$$

Substituting $V_{r'}$ from (2.1) into (3.6), we can easily calculate the matrix elements $V_{m_g'm_g}$'s; these elements have already been tabulated by Ashkin and Wu (1948), Burhop and Yadav (1949) and C. C. Banerjee (1954). For a particular element $m_g' = 1, m_g = 1$ we can write

$$V_{11} = (3 \cos^2 \xi - 1) W(r')$$

where $W(r')$ denotes the radial part in $V_{r'}$. Therefore, from the equation (3.5)

$$S_{11} = -\frac{M}{4\pi\hbar^2} \int_0^\infty \int_0^\pi \int_0^{2\pi} e^{ikr' \cos \xi} (3 \cos^2 \xi - 1) W(r') r'^2 dr' \sin \xi d\xi d\beta. \quad \dots \quad (3.7)$$

The integration of the above leads to

$$S_{11} = 2/3 \left(\frac{Mf^2}{4\pi\hbar^2} \right) \left[\frac{10}{3\chi} - \frac{\chi}{4k^2 \sin^2 \theta/2} + \left(\frac{3}{k \sin \theta/2} - \frac{2k \sin \theta/2}{\chi^2} \right) \right. \\ \left. + \frac{3\chi^2}{4k^3 \sin^3 \theta/2} \right] \tan^{-1} \left(\frac{2k \sin \theta/2}{\chi} \right) = S(\theta) \quad \dots \quad (3.8)$$

Similar calculations yield the following matrix,

	$\begin{smallmatrix} m_g' \\ m_g \end{smallmatrix}$	1	0	-1	
	1	$S(\theta)$	0	0	
$S_{m_g'm_g}$	0	0	$-2S(\theta)$	0	$\dots \quad (3.9)$
	-1	0	0	$S(\theta)$	

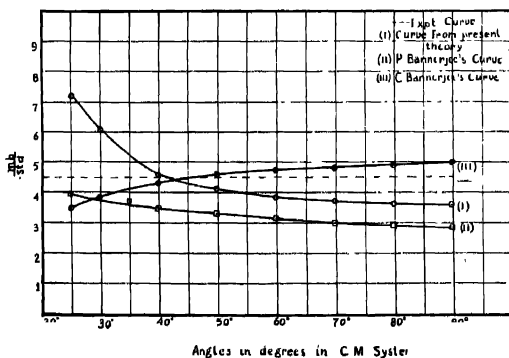
The off-diagonal elements vanish because of the β -integration.

Now, to find the scattering cross section per unit solid-angle, we take the square of modulus of the scattered amplitude in (3.4) and average over the phases of three amplitudes. Making use of (3.2) we obtain for the scattering cross section

$$\sigma(\theta) = 1/4 \sum_{m_g'} \sum_{m_g''} |S_{m_g'm_g''}|^2 \quad \dots \quad (3.10)$$

Making use of the table (3.9), and utilising the symmetry property of the total wave function the cross section ultimately becomes

$$\begin{aligned}
 \sigma(\theta) = & 3/2 \left[|S(\theta)|^2 + |S(\pi-\theta)|^2 + |S(\theta)| |S(\pi-\theta)| \right] \\
 = & \frac{2}{3} \left(\frac{Mf^2}{4\pi k^2} \right) \left[\left\{ \frac{10}{3\chi} - \frac{\chi}{4k^2 \sin^2 \theta/2} + \left(\frac{3}{k \sin \theta/2} - \frac{2k \sin \theta/2}{\chi^2} + \frac{3\chi^2}{4k^3 \sin^3 \theta/2} \right) \right. \right. \\
 & \left. \left. \tan^{-1} \left(\frac{2k \sin \theta/2}{\chi} \right) \right\}^2 \right. \\
 + & \left\{ \frac{10}{3\chi} - \frac{\chi}{4k^2 \cos^2 \theta/2} + \left(\frac{3}{k \cos \theta/2} - \frac{2k \cos \theta/2}{\chi^2} + \frac{3\chi^2}{4k^3 \cos^3 \theta/2} \right) \right. \\
 & \left. \left. \tan^{-1} \left(\frac{2k \cos \theta/2}{\chi} \right) \right\}^2 \right. \\
 + & \left\{ \frac{10}{3\chi} - \frac{\chi}{4k^2 \sin^2 \theta/2} + \left(\frac{3}{k \sin \theta/2} - \frac{2k \sin \theta/2}{\chi^2} + \frac{3\chi^2}{4k^3 \sin^3 \theta/2} \right) \right. \\
 & \left. \left. \tan^{-1} \left(\frac{2k \sin \theta/2}{\chi} \right) \right\} \times \right. \\
 & \left. \left\{ \frac{10}{3\chi} - \frac{\chi}{4k^2 \cos^2 \theta/2} + \left(\frac{3}{k \cos \theta/2} - \frac{2k \cos \theta/2}{\chi^2} + \frac{3\chi^2}{4k^3 \cos^3 \theta/2} \right) \right. \right. \\
 & \left. \left. \tan^{-1} \left(\frac{2k \cos \theta/2}{\chi} \right) \right\} \right] \quad \dots (3.11)
 \end{aligned}$$



In our calculations, we have taken the value of $f^2/\hbar_c = .7$ (cf. Fox *et al* 1950). The numerical values of the differential cross section from the equation (3.11) for 340 Mev are given in Table I and figure 1 gives a comparison of the theoretical results with experiment.

TABLE I

Angles in degrees	in mb/std
20°	8.50
30°	6.12
40°	4.52
50°	4.03
60°	3.75
70°	3.60
80°	3.52
90°	3.49

DISCUSSION

The value for the differential cross section as calculated from equation (3.11) slowly decreases with angles, whereas C. C. Banerjee (1954) has shown that the same expression for the tensor part of the pseudoscalar meson field shows slight increase. The differential cross section with the interaction of P Banerjee (1953) decreases with increasing angle at a rate slower than that obtained by us. In conclusion it may be mentioned that the scattering due to the present potential with higher singularities is less isotropic than that due to the pseudoscalar tensor potential.

ACKNOWLEDGMENT

The author wishes to express his sincere thanks to Prof. D. Basu, Ph.D. for his kind interest throughout the progress of the work

REFERENCES

- Ashkin, J., Wu, T., 1948, *Phys. Rev.*, **73**, 973.
 Burhop, E. H. S., Yadav, H. N., 1949, *Proc. Roy. Soc.*, **197**, 63.
 Banerjee, C. C., 1953, *Ind. J. Phys.*, **27**, 173.
 Banerjee, C. C., 1954, *Ind. J. Phys.*, **28**, 221.
 Banerjee, P., 1953, *Ind. J. Phys.*, **27**, 557.
 Basu, D., 1954, *Ind. J. Phys.*, **28**, 201.
 Chamberlain and Wiegand, 1950, *Phys. Rev.*, **79**, 81.
 Fox, Leith, Wouters & Mackenzie, 1950, *Phys. Rev.*, **80**, 23.

SOLAR TIDAL EFFECTS IN THE F_2 -REGION OF IONOSPHERE OVER DELHI*

C. S. RAGHAVENDRA RAO,

RESEARCH DEPARTMENT, ALL INDIA RADIO, NEW DELHI

(Received for publication March 1, 1957)

ABSTRACT. The object of this paper is to discuss the solar tidal effects in the F_2 region of the ionosphere over Delhi. Ionospheric data collected at Delhi over the period 1946-1955 have been analysed for these effects. The method developed by Martyn and extended by Mitra has been utilised for the purpose. The magnitude and phase of the drift velocities for the different seasons and the relative importance of the drift velocity are determined. While the seasonal velocities have been found to be of the order of 20, 18 and 33 kns/hr for summer, winter and equinox months, the ratio of the seasonal to semi-diurnal velocity has been obtained to be of the order of 1.5. This agrees well with the result obtained by Martyn.

The observed variations in N_m have been explained in terms of the phases of the drift velocities. The values of the attachment coefficient for the three seasons of the year have also been determined taking the tidal effects into consideration. These are found to agree fairly well with the recent results of Ratcliffe and others.

1. INTRODUCTION

It is now well established that solar semi-diurnal components of tidal origin influence the structure of the F_2 region of the ionosphere (Martyn, 1947-1948; Mitra, 1951; Weiss 1953a,b). The object of this paper is to deduce the characteristics of these tidal components for Delhi ($28^{\circ}35'N$, $77^{\circ}5'E$, $42^{\circ}.44N$ magnetic dip) from the ionospheric data over this station collected during the period 1946-1955. The following parameters are desired to be determined:

- (i) The magnitude and phase of the solar tidal drift velocity.
- (ii) The separation of the semi-diurnal and seasonal components of the drift velocity and determination of the relative importance of the two.
- (iii) Vertical distortion of the F_2 layer due to the drift.
- (iv) Calculation of the attachment coefficient taking into account the effect due to the tide.

2. ANALYSIS OF DATA: EVIDENCE OF TIDAL EFFECT:

The basic equation is

$$-\frac{\partial N}{\partial t} = I - \alpha N^2 + \frac{\partial}{\partial z}(Nv)$$

*Communicated by Mr. S. N. Mitra.

where I is the ion production term,

α , the recombination coefficient,

N , the electron density,

and v the resultant drift velocity measured vertically upwards (Z).

This can also be written as

$$\frac{\partial N}{\partial t} = I - \beta N + \frac{\partial}{\partial z}(Nv) \quad \dots (1)$$

where β is the attachment coefficient.

Martyn in his treatment has neglected both the ion production and recombination terms. Mitra (1951) has extended the analysis by taking into account the recombination term. The latter analysis has been followed in the present paper. It may, however, be mentioned that, while Mitra and others treat the subject in terms of recombination, the present analysis uses attachment throughout instead of recombination; for it has been shown recently by Ratcliffe and others (1956), that the behaviour of the F_2 layer of the ionosphere appears to be more consistent if attachment, rather than recombination, is considered.

Hourly values of the ionospheric parameters f_0F_2 and h_pF_2 recorded at Delhi over the years 1946 to 1955 are used in this analysis which reveals the following effects:

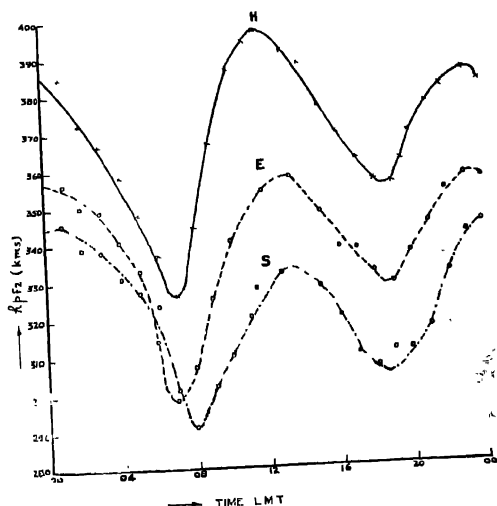


Fig. 1 Average diurnal variation of $h_p F_2$ for Delhi (1945-1955)

Diurnal variation of $h_p F_2$ for all the seasons of the year indicates a 12-hourly periodicity with one maximum near noon and another near midnight, as shown in figure 1.

(a) It will be noticed from figure 1, that the semi-diurnal variations are different for the different seasons. The amplitudes are higher in summer than in winter and the phase also varies. A more rigorous and quantitative study of the semi-diurnal oscillation is afforded by its harmonic analysis. Table I shows the results of this analysis giving the first three harmonics where the amplitudes are represented by A_1 , A_2 and A_3 in km and the times of maximum by T_1 , T_2 , T_3 in local time.

Table I shows the results of harmonic analysis of the diurnal variation of $h_p F_2$ at Delhi for different months :

TABLE I

	A_1	A_2	A_3	T_1 H-M	T_2 H-M	T_3 H-M
Jan.	10.28	18.93	5.37	14 04	01 20	04 28
Feb.	9.16	16.34	3.89	17 48	01 30	04 28
Mar.	5.17	17.58	1.77	15 40	01 08	01 08
April	13.16	19.40	6.90	13 16	00 34	04 00
May	12.29	19.34	4.58	12 00	23 56	03 00
June	10.67	20.88	1.18	08 08	00 24	02 52
July	10.76	24.72	5.12	06 16	00 00	00 52
August	5.64	22.72	6.77	14 32	00 08	03 40
Sept.	10.69	20.22	7.84	15 32	00 28	02 56
Oct.	9.05	18.95	4.63	15 00	00 40	02 56
Nov.	9.85	14.99	3.82	16 44	01 08	02 52
Dec.	13.20	17.16	4.12	14 25	01 40	04 08

It will be observed from the above table that the amplitude of the semi-diurnal component (A_2) is considerably and consistently larger than the diurnal one (A_1).

At Delhi, the times of maxima for $h_p F_2$ are near local noon and local midnight. There is, however, a small seasonal variation in the time of maximum, noticeable in figure 1 and given in detail in Table II. In summer, the noon time maximum tends to occur round about 12.00 hours local time; in winter, it occurs about an hour and a half after noon. However, a difference of about 12 hours is generally maintained throughout the year between the midday and midnight

maxima, as is seen from the last column in the Table II. This is in further support of the semi-diurnal tidal effect.

Table II shows the times of maxima for $h_p F_2$ for different months.

TABLE II

Month	Local time of midday maximum		Local time of mid-night maximum		Difference in hours between the two maxima (observed)
	From analysis	From observed data	From analysis	From observed data	
January	13-20	13-00	01-20	01-00	12-00
Feb	13-30	14-00	01-30	01-00	13-00
March	13-08	13-30	01-08	01-00	12-30
April	12-34	12-00	00-34	00-00	12-00
May	11-56	12-00	23-56	23-30	12-30
June	12-24	12-30	00-24	00-30	12-00
July	12-00	12-00	00-00	00-00	12-00
August	12-08	12-00	00-08	00-00	12-00
Sept.	12-28	13-00	00-28	00-00	13-00
Oct.	12-40	13-00	00-40	00-00	13-00
Nov.	13-08	13-00	01-08	00-30	12-30
Dec.	13-40	13-00	01-40	00-30	13-00

(b) The critical frequency ($f_0 F_2$) data is next examined for the evidence of semi-diurnal harmonic components. The solar diurnal variation, which overshadows the tidal effect in day time, is removed in the usual way by taking the difference in the $f_0 F_2$ values at Delhi and at another station for which the $\cos \chi$ variations are not much different but where tidal effects may be expected to differ. The places so chosen are Calcutta ($22^\circ 33' N$, $88^\circ 21' E$), Ahmedabad ($23^\circ 2' N$, $72^\circ 38' E$) and Kodaikanal ($10^\circ 14' N$, $77^\circ 28' E$). For the Delhi-Calcutta pair, the data cover the period 1950 to 1954, for Delhi-Ahmedabad 1953 to 1955, while for the Delhi-Kodaikanal the data cover a period of six months from September, 1955, to February, 1956. Figure 2 shows the diurnal variation of the difference in the $f_0 F_2$ values for all the three pairs of stations. It is clear from this figure that there is a large semi-diurnal harmonic which is indicative of the tidal effects. Results of the harmonic analysis of the diurnal variation in the difference $f_0 F_2$ values are shown in Table III. It will be noticed that the amplitude of this semi-diurnal variation is larger for larger difference in latitudes.

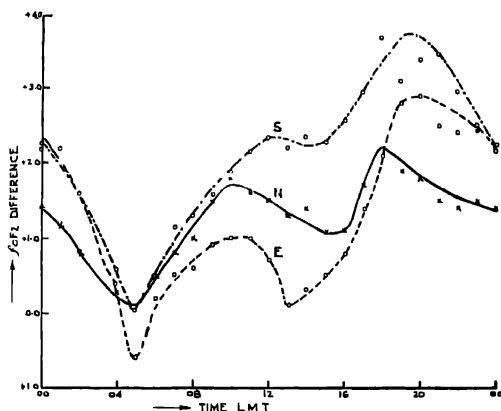


Fig. 2. Difference between mean hourly values of $f_o F_2$ at Delhi and other stations

Table III shows the amplitude and phase of $f_o F_2$ differences.

TABLE III

Station	Difference Amplitude in geomag Lat.	(Mc/s)	Time of max. after local midnight	
			<i>h</i>	<i>m</i>
Delhi-Ahmedabad.	5 1°	0.34	08	00
Delhi-Calcutta	6.3°	0.60	00	40
Delhi-Kodaikanal	18.1'	1 20	01	30

(c) In addition to the semi-diurnal effects described above, there is a seasonal semi-diurnal harmonic component evident from the following results.

(i) The time of occurrence of maximum $h_p F_2$ for all the months of the year shows a seasonal variation (Table II) which can be explained only by the existence of a seasonal tidal effect.

(ii) The difference between the average diurnal variation for the period 7th March to 22nd March 1955 and the same for the succeeding fortnight shows a considerable change in the semi-diurnal harmonic during this period (figure 3).

(iii) There is a change in the phase of the difference in $f_o F_2$ values for the pairs of stations considered in section 2(b). Figure 4 illustrates this for the Calcutta-Delhi pair for the different seasons of the year.

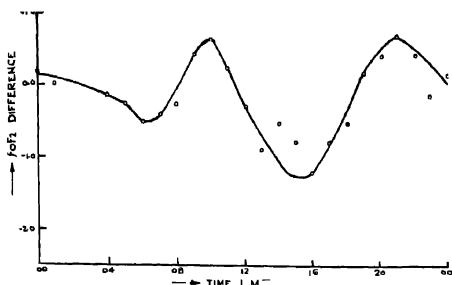


Fig. 3. Difference between average diurnal variation of $f_o F_2$ at Delhi for 7th to 21st. March, 1955 and the same quantity for 22nd March to 5th April, 1955.

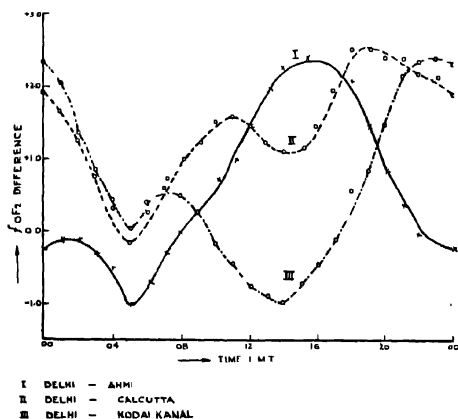


Fig. 4. Difference between mean hourly values of $f_o F_2$ for Delhi Calcutta for the N, S and E stations.

3 DETERMINATION OF THE AMPLITUDE AND PHASE OF THE TIDAL DRIFT OVER DELHI

(a) Having obtained clear evidence about the existence of semi-diurnal and seasonal tidal effects from analysis of the data, the magnitudes of the tidal velocities that produce these effects during different seasons are determined in the following way :

Assuming a continuity equation of the type

$$\frac{\partial N}{\partial t} = -\beta N + \frac{\partial}{\partial z}(Nv) \quad \dots (2)$$

where v is the resultant drift velocity measured positively upwards, and denoting the semi-diurnal and seasonal velocities by v_1 and v_2 respectively, where

$$v_1 = v_{10} e^{-y'/z} \sin(\omega t + \sigma z) \quad \dots (3)$$

$$v_2 = v_{20} e^{-y'/z} \sin(\omega t + \sigma z + \lambda t + \phi), \quad \dots (4)$$

Mitra (1951) has shown that the resultant velocity can be represented by

$$v = v_0 e^{-y'/z} \sin x \quad \dots (5)$$

where

$$x = (\omega t + \sigma z + \delta)$$

and

$$\tan \delta = \frac{v_{10} \sin(\lambda t + \phi)}{v_{10} + v_{20} \cos(\lambda t + \phi)} \quad \dots (6)$$

The attachment coefficient and the value of v_0 in equation (5) can be determined from the following expression

$$\beta = 9.3 \times 10^{-5} \log \left(\frac{f_{\psi}^{\circ}}{f_{\psi+180^{\circ}}^{\circ}} \right) \quad (7)$$

$$G = \frac{A v_0}{\omega} e^{-y'/z} - \log \frac{f_{\psi}^{\circ}}{f_{\psi}^{\circ}} \cdot \frac{f_{\psi+180^{\circ}}^{\circ}}{f_{\psi+180^{\circ}}^{\circ}}, \quad \dots (8)$$

where f_{ψ}° and $f_{\psi+180^{\circ}}^{\circ}$ are the values of the critical frequencies corresponding to $x = \psi$ and $x = \psi + 180^{\circ}$ where $\psi = n \cdot 90^{\circ}$, n being odd.

(b) In this section the amplitude and phase of the drift velocity for different seasons are obtained from analysis of the N_m variations at Delhi. The f_oF_2 data for the period 1946-54 are grouped together for the summer, winter and equinox months which are respectively denoted as N (northern solstice), S (southern solstice) and E (equinox) months. The average diurnal variations of N_m for the F_2 region for each of these seasons are shown in figure 5. It can be observed from this figure that the largest daytime value of N_m occurs in E months and that the maximum N_m values occur in the afternoon in all seasons, the times being 1430, 1330 and 1300 hrs local time for N, S and E months respectively.

It has been shown that the value of y' , which denotes height gradient of the drift velocity, is near unity at places where there is generally high level of ionisation in N months. The same, therefore, applies for Delhi where such a high level is observed in practice. In such a case, the time at which maximum N_m occurs leads the drift by nearly 90° , so that the maximum value of the resultant down-

ward drift will occur in Delhi at 1730, 1630 and 1600 hours in the N, S and E months respectively.

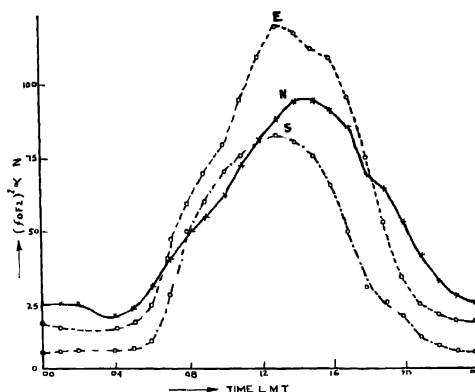


Fig. 5, Average diurnal variation of $(f_o F_2)^2$ at Delhi (1940-1954) for N, S and E Stations.

Now, if we assume the same phases for the downward drift at Delhi, as those given by Martyn for the low latitudes viz., 1200 hrs for the semi-diurnal, 0300 and 0900 hrs for the summer and winter seasonal velocities, we obtain the values of δ for the seasons as follows

$$\delta_N = -165^\circ, \quad \delta_S = -135^\circ, \quad \delta_E = -120^\circ.$$

Equ. (6) will be valid for the above values of δ 's only if

$$\frac{v_{20}}{v_{10}} \simeq 1.5$$

Martyn has obtained theoretical distribution of the semi-diurnal and seasonal tidal velocities as arising from the sectorial (semi-diurnal) and tesseral (seasonal) harmonics. From this we obtain, for the geomagnetic latitude and longitude of Delhi, a ratio of 1.5 for the magnitude of the seasonal to semi-diurnal velocities, which is the same as obtained above from an analysis of N_m variations. This means that the magnitude of the seasonal drift velocity is nearly 50% more than the semi-diurnal drift at Delhi.

(c) Having obtained the relation between the seasonal and semi-diurnal velocities, the actual magnitudes of the velocities are determined as follows :

The values of G for different seasons are determined with the help of equation.

(8). The values of G , so determined, are 0.06 for summer, 0.08 for winter and 0.09 for equinox months.

By substituting these values in equation (8) and by knowing the values of Z , σ and y' , we can obtain the values of the resultant velocity v_0 for different seasons. y' , as already mentioned, is of the order unity and is assumed to be 0.7 (Mitra 1951). σ is assumed, after Martyn, to be 0.3 radians. We therefore obtain:

$$G = 1.2 v_0 e^{-0.7z}$$

$$\text{For N months, } 1.2v_0 = 0.06e^{0.7z}$$

$$\text{For S months, } 1.2v_0 = 0.08e^{0.7z}$$

$$\text{For E months, } 1.2v_0 = 0.09e^{0.7z}$$

Z values for the N, S and E months are 4.0, 2.9 and 3.7 respectively.

Therefore,

$$v_{0N} = 20 \text{ kms/hr.}$$

$$v_{0S} = 18 \text{ kms/hr.}$$

$$v_{0E} = 33 \text{ kms/hr.}$$

An idea of the order of the velocities may also be obtained from the height variations discussed in Sec. 2.

Assuming a velocity of the type

$$v = v_0 \sin(\omega t + \sigma z),$$

Martyn (1947) has obtained the relationship

$$\delta z_m = \frac{v_0}{\omega} \cos x_m$$

where $x_m = (\omega t + \sigma z_m)$.

Making use of this relationship, the values of v_0 are obtained to be of the order of 20, 20 and 30 km/hr. for the N, S and E months respectively.

(d) The observed variations in N_m , as shown in figure 5, can now be explained.

In summer, the phase of the drift is upwards in the morning and starts downwards as late as 1430 hrs. The loss of ions by the attachment process is small. The general level of ionization is, therefore, uniformly high throughout the day and rises above Chapman value. It starts falling only towards the evening.

In winter, the phase of the drift is again upwards in the morning and remains so till 1300 hrs. The ionization level is, therefore, high throughout the morning. The loss due to attachment becomes large only in the afternoon when the phase of the drift is downwards and reaches a maximum at 1600 hrs.

The conditions at equinox are similarly explained.

4. DETERMINATION OF THE ATTACHMENT COEFFICIENT

Usual calculation of this coefficient neglects the tidal effects. Here, it is determined for the different seasons by taking these effects into consideration, by using eqn. (7).

The values of β are found to be as follows :

$$\beta = 0.6 \times 10^{-5}/S \text{ for N months}$$

$$= 0.8 \times 10^{-5}/S \text{ for S months}$$

$$= 1.1 \times 10^{-5}/S \text{ for E months.}$$

These values of β , when taken in conjunction with the corresponding heights, compare favourably with the values recently obtained by Ratcliffe and others (1956).

CONCLUSION

Definite results about the existence of solar tidal effects in the F_2 region over Delhi are obtained.

The resultant vertical drift velocities producing these effects are 20 km/hr in summer, 18 km/hr in winter and 33 km/hr in equinox months. The observed variations in the ionization are explained in terms of the tidal effects.

Attachment coefficient is obtained for the different seasons taking tidal effects into account and it is of the order of $10^{-5}/S$.

ACKNOWLEDGMENTS

The work described in this paper forms apart of a programme of ionospheric research of All India Radio and is published by permission of Mr. B. V. Baliga, Chief Engineer, All India Radio. My grateful thanks are due to Dr. A. P. Mitra, for a critical scrutiny of the paper and helpful suggestions. I am indebted to Mr. S. Thiruvengkatachari, Research Engineer, All India Radio and to Mr. S. N. Mitra, Assistant Research Engineer, All India Radio, for their keen interest during the progress of the work.

REFERENCES

- Martyn, D. F., 1947, *Proc. Roy. Soc. A*, **189**, 214.
 " 1947, " **190**, 273.
 " 1948, " **194**, 429.
 " 1948, " **194**, 445.
 Mitra, A. P., 1951, *Jour. Atmos. Terr. Phys.*, **1**, 286.
 Ratcliffe, J. A. et al, 1950, *Phil. Trans. Roy. Soc.*, **248**, 609.
 Weiss, A. A., 1953, *J. Atmos. Terr. Phys.*, **3**, 30.
 Weiss, A. A., 1953, *J. Atmos. Terr. Phys.*, **4**, 175.

ANOMALOUS MAGNETIC MOMENTS OF PROTON AND NEUTRON

S. K. KUNDU

DEPARTMENT OF THEORETICAL PHYSICS,

INDIAN ASSOCIATION FOR THE CULTIVATION OF SCIENCE, CALCUTTA-32

(Received for publication, May 1, 1957)

ABSTRACT In the present paper, the proton and the neutron magnetic moments, have been calculated with a classical model consisting of spatially extended core charge and a meson cloud charge, both having spherical symmetry.

INTRODUCTION

In calculating the magnetic moment of the nucleon we propose to separate the contributions due to the charge of the core and the mesonic cloud surrounding it. For this purpose we take a classical model with spherically symmetric charge distribution. The contribution due to the mesons is evaluated from the usual expression for the meson charge density in the theory of extended source as proposed by Pauli (1946). The observed magnetic moment of the proton is a sort of time average of two states : the state of being a proton and the state of dissociation into a neutron plus positively charged pseudoscalar meson. From a similar idea the magnetic moment of the neutron comes out only from its state of dissociation into a proton core and negatively charged pseudoscalar meson. The charge distribution of the proton core is assumed to be proportional to the source function and the constant of proportionality is related to the probability that the core charge is present.

METHOD OF CALCULATION

It is here assumed that the mesons give rise to a charge cloud rotating about an axis and as such contribute to the magnetic moment of the nucleon. According to the classical theory the magnetic moment for this kind of motion is given by

$$\mu_{\pi^-} = \int \frac{A i}{c} \quad (1)$$

where $A = \pi(r \sin \theta)^2$, $i = \rho_{\pi^-}(r)rdr \sin \theta d\theta d\phi \omega/2\pi$, ω = angular velocity of the motion, $\rho_{\pi^-}(r)$ = meson charge distribution function and c = velocity of light.

To eliminate ω , we use the condition that $I\omega = \hbar$ (I being the moment of inertia of the meson shell about the rotating axis), then the above expression reduces to

$$\mu_{\pi^-} = \frac{\hbar}{3cm_\pi a^2} \int r^2 \rho_{\pi^-}(\mathbf{r}) d\mathbf{r} \quad \dots (2)$$

where we have put $m_\pi a^2$ for I .

The density matrix of the meson charge is

$$\rho_{\pi^-}(\mathbf{r}) = \langle \psi_N | \rho_{\pi^-}[\phi](\mathbf{r}) | \psi_N \rangle \quad \dots (3)$$

where

$$\rho_{\pi^-}[\phi](\mathbf{r}) = -ie(\pi^* \phi - \pi \phi)$$

Using the extended source model, the value of $\rho_{\pi^-}(\mathbf{r})$ as given by Salzman (1955) has the form

$$\rho_{\pi^-}(\mathbf{r}) = -\frac{4e}{(2\pi)^5} (f/m_\pi)^2 \int d\mathbf{k} \int d\mathbf{k}' -\frac{v(\mathbf{k})v(\mathbf{k}')\sigma \cdot \mathbf{k} \sigma \cdot \mathbf{k}'}{(e+\epsilon')\epsilon'} e^{i(\mathbf{k}-\mathbf{k}') \cdot \mathbf{r}} \quad \dots (4)$$

where $\epsilon = \sqrt{k^2 + m_\pi^2}$, $\epsilon' = \sqrt{k'^2 + m_\pi^2}$ and the cut-off function $v(k)$, defined by

$$v(\mathbf{k}) = \int d\mathbf{r} S(\mathbf{r}) e^{i\mathbf{k} \cdot \mathbf{r}} \quad \dots (5)$$

is a function of the length of \mathbf{k} , because $S(\mathbf{r})$ which is the source function is assumed to be spherically symmetric.

Now substituting (4) in the expression for the meson contribution (2) and performing \mathbf{r} integration we find

$$\mu_{\pi^-} = \frac{e}{3\pi^2 m_\pi a^2} (f/m_\pi)^2 \int d\mathbf{k} \int d\mathbf{k}' \frac{v(k)v(k')}{\epsilon\epsilon'(\epsilon+\epsilon')} \mathbf{k} \mathbf{k}' \dots \nabla \mathbf{k} \nabla \mathbf{k} \delta(\mathbf{k}-\mathbf{k}') \quad \dots (6)$$

where ... means the dyadic inner product.

Using the property of spherical symmetry of $v(k)$ and after partial integration of the term involving d^2v/dk^2 the expression (6) becomes

$$\mu_{\pi^-} = -\frac{e}{3\pi m_\pi a^2} (f/m_\pi)^2 \int_0^\infty dk \frac{k^4}{\epsilon^7} \left[2\epsilon^4 \left(\frac{dv}{dk} \right)^2 + 5(3\epsilon^2 - 2k^2)v^2 \right] \quad \dots (7)$$

Since the integral on the right hand side of (7) involves dv/dk , a square cut-off is unsatisfactory and so following Salzman (1955) we choose for the cut-off the short tailed Gaussian

$$v(k) = B e^{-\frac{k^2}{D^2}} \quad \dots (8)$$

where B and D are constants to be evaluated.

From (5) and (8), we find on using the normalising property of the source function $S(r)$,

$$v(0) = 1 = B$$

The constant D is determined ($D = 5.6\sqrt{2} m_\pi$) from the condition that in meson nucleon scattering, the value of the cross section evaluated from the above Gaussian cut-off should be same as obtained from a square cut-off of the form

$$v(k) = 1 \text{ for } k < k_{max} = 5.6 m_\pi$$

$$= 0 \text{ otherwise.}$$

The numerical integration with the Gaussian cut-off (eqn. 8) gives for the meson cloud contribution to the nucleon magnetic moment as [from (7)]

$$\mu_{\pi^-} = -\mu_0(2/3)(M_p/m_\pi)f^2\left(\frac{1}{m_\pi a}\right)^2 \quad (7.2) \quad \dots (9)$$

where we put $\mu_0 = e/2M_p$, M_p is proton mass.

The value of a is taken from that used by Pauli (1946) to find the exact nucleon magnetic moment using weak coupling theory with the idea of extended source. Further, the meson nucleon scattering data give very good fit when $f^2 = .058$ (Chew, 1954). Thus the meson contribution finally reduces to

$$\mu_{\pi^-} = -4.75 \mu_0 \quad \dots (10)$$

where we use $(1/m_\pi a) = 2.85$, $M_p/m_\pi = 6.6$.

The core contribution to the nucleon magnetic moment, which is supposed to be due to the spin motion of the core particle having spherically symmetric charge distribution $\rho_c(r)$, may be expressed as before by the relation with $\hbar = c = 1$

$$\mu_c = \frac{10\pi}{3} \sigma \frac{1}{M_p a^2} \int r^4 \rho_c(r) dr \quad \dots (11)$$

where σ is spin quantum number and $(2/5) M_p a^2$ is the moment of inertia of the core particle about its spin axis.

Assuming the core charge density $\rho_c(r)$ to be proportional to the source function $S(r)$, we write

$$\rho_c(r) = F e S(r) \quad \dots (12)$$

where F is the constant of proportionality.

Now, on using the normalising property of the source function, we find from (12)

$$F = (1/e) \int \rho_c(r) dr \quad \dots (13)$$

and since $\int \rho_c(r) dr$ represents the total charge the core can have, the relation (13) indicates that F should correspond to the fraction of time the core charge may exist.

It is well-known that

$$S(r) = \frac{1}{(2\pi)^3} \int v(k) e^{-i\mathbf{k}\cdot\mathbf{r}} d\mathbf{k}$$

and from its spherically symmetric property, the above expression reduces to

$$S(r) = -\frac{1}{2\pi^2 r} \frac{d}{dr} \left\{ \int_0^\infty v(k) \cos kr dk \right\} \quad \dots (14)$$

And with the cut-off as that of eqn. (8.), we find from (14)

$$S(r) = \frac{D^3 \sqrt{\pi}}{8\pi^2} e^{-\frac{D^2}{4} r^2} \quad \dots (15)$$

The core contribution thus finally reduces to (from eqns. 11, 12 and 14)

$$\begin{aligned} \mu_c &= \frac{5}{6} \mu_0 \sigma \frac{FD^3}{a^2 \sqrt{\pi}} \int_0^\infty r^4 e^{-\frac{D^2}{4} r^2} \\ &= \frac{40}{3\sqrt{\pi}} \mu_0 \sigma F \frac{1}{(aD)^2} \Gamma(5/2) \end{aligned} \quad \dots (16)$$

where $\Gamma(5/2)$ is the Gamma function.

Taking $(1/m_\pi a) = 2.85$ and $\Gamma(5/2) = (1.5) (.88659)$, we find from eqn. (16)

$$\mu_c = F(1.295) \mu_0 \sigma \quad \dots (17)$$

It is of importance to mention that the relation (17) represents the magnetic moment due to the core charge for the fraction of time F . Accordingly we write for the magnetic moment of the proton and the neutron as

$$\mu_P = (1 - F) \mu_0 + F \mu_{\pi^+} \quad \dots (18)$$

and

$$\mu_N = 1.295 \mu_0 F + F \mu_{\pi^-} \quad \dots (19)$$

respectively, where $(1-F)$ is the fraction of time the nucleon exists as a physical proton (neutron) and the rest F seconds as neutron (proton) core plus a positively (negatively) charged pseudoscalar meson.

Taking $F = 0.5$, we find from (18) and (19)

$$\mu_P = 2.875 \mu_0$$

and

$$\mu_N = -1.727 \mu_0$$

whereas the experimental values for μ_p and μ_N are respectively $2.79\mu_0$ and $-1.91\mu_0$. The ratio of the anomalous part of the neutron magnetic moment to that of the proton is found to be 0.92 (experimental value 1.07).

ACKNOWLEDGMENT

The author is grateful to Professor D. Basu, for suggesting the problem and for his constant help and guidance.

REFERENCES

- Chew, G. F., 1954, *Phys. Rev.*, **95**, 1660.
Pauli, W., 1946, Meson Theory of Nuclear Forces.
Salzman, G., 1955, *Phys. Rev.* **99**, 973.

DESIGN OF CONTINUOUS BAFFLE IN A SHORT LENS BETA-RAY SPECTROMETER

P. N. MUKHERJEE, M. K. PAL, M. K. BANERJEE AND
A. K. SAHA

INSTITUTE OF NUCLEAR PHYSICS, CALCUTTA

(Received for publication, May 14, 1957)

ABSTRACT. A short lens beta-ray spectrometer has been set up following the calculations of Banerjee and Saha (1953). The spectrometer can measure upto 4 Mev electrons. The performance of the spectrometer is checked up using $C_{K^{147}}$ source. A new and simple method of alignment of the spectrometer is proposed. Ring focussing is investigated by photographic method, and from the observed nature of the caustic envelope of the electron trajectories a continuous baffle is designed. With this new baffle system a resolution of 1.47% at a transmissions of 0.56% is obtained.

1. INTRODUCTION

A short lens beta-ray spectrometer is generally classed as a low resolution spectrometer. Up till now the usual procedure to get optimum resolution is to place an annular slit at the position of the circle of least confusion of the electrons in such a way that it just allows the electrons to pass. The resolution obtained by this method is 2.2% at a transmission of 0.56% [Deutsch *et al* 1944]. Perkins and Solbrig (1951) showed that if the outer baffle of the above annular slit is replaced by two circular slits of proper dimensions on its two sides, then the resolution is much improved (2%) without any appreciable loss in transmission. Following this idea, Banerjee and Saha (1953) have deduced that if the number of the outer stops is increased then the line shape becomes more sharp, finally when a continuum of such baffles is used, an optimum resolution of 1.56% at a transmission of 0.56% is obtained. The baffle, known as "Continuous Baffle", is so designed that it follows the caustic envelope of the electron trajectories inside the spectrometer.

Following this new idea we have designed a continuous baffle in a way which will be presented here.

2. THE SPECTROMETER

The short lens beta-ray spectrometer of the Institute was first designed and fabricated by one of us (M. K. Banerjee) in 1954. Since then it has undergone many improvements. It is shown in figure 1 in its final form. It has the following characteristics:

Length of the chamber = 120 cm; diameter of the chamber = 17.8 cm; outer diameter of the lens coil = 52 cm; inner diameter of the lens coil = 20.9 cm; breadth of the coil = 16 cm; number of turns of the coil = 2245; maximum current that the coil can carry = 25 amp.

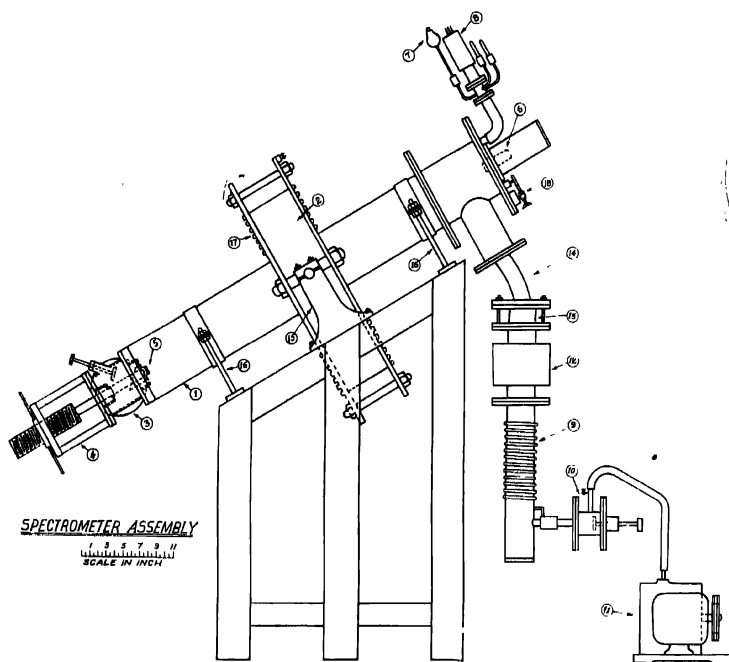


Fig. 1. Short lens beta-ray spectrometer.

1—Chamber; 2—Lens coil; 3—Air lock; 4—Gamma counter; 5—Source; 6—Beta counter; 7—Pirani gauge; 8—Penning gauge; 9—Diffusion pump; 10—Air dock; 11—Mechanical pump; 12—Oil trap; 13—Silphon; 14—Bent joint; 15—Coil support; 16—Chamber support; 17—Lens cooling coils; 18—Baffle adjuster

The current is stabilized to within 0.1% by means of a stabilizing circuit using galvanometer photocell type of error detector (Sen, 1950). Current is measured with the help of a precision potentiometer.

The beta particles are detected by means of a stilbene crystal, grown at the Institute (Bhattacharyya, 1956) followed by perspex light pipe, 6262 photo-multiplier and related amplifier and scaler. The control desk is shown in figure 2.

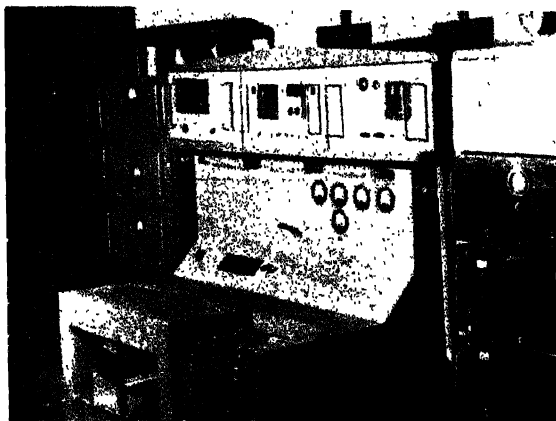


Fig. 2 The control desk

3 DESIGN OF THE CONTINUOUS BAFFLE

The performance of the spectrometer was checked with Cs^{137} source, taking advantage of the strong K -conversion electrons of 0.61 Mev energy. It was found that for a current setting of 4.00 amp, the K -peak was focussed on the detector. The initial line-shape (before the design of the baffle) was found to correspond to 12% resolution.

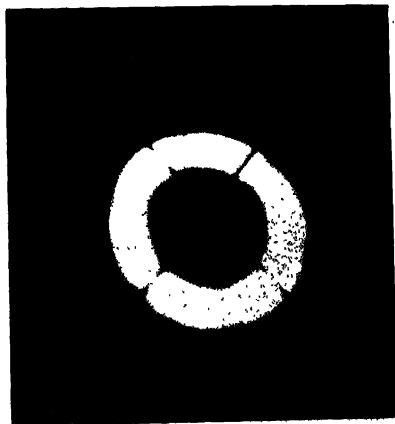


Fig. 3. The elliptical ring.

Maintaining the current at 4.00 amp. photographs of the beta rings had been taken placing Ilford X-ray films inside the chamber. Exposures ranging from three to nine hours had been given. Initial photograph (figure 3) showed that the rings were not circular, but elliptical. This indicated that the field was not symmetric about the axis. After laborious trials the ring was made circular (figure 4) by properly shaping the field.

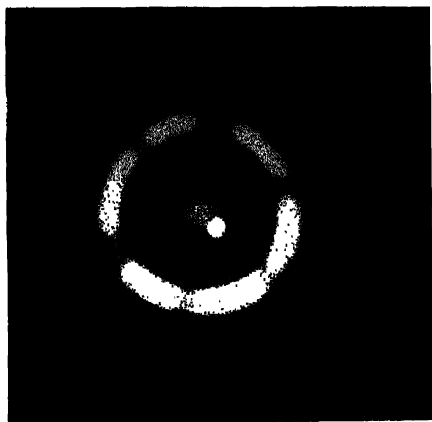


Fig. 4. Circular ring before the alignment of the spectrometer

Next the axis of the chamber and that of the lens were made coincident following a new and simple method. This is indicated in figures 4 and 5. It will be noticed that at the centre of the ring there is a faint spot. This is due to the continuous beta spectrum of C_{x}^{137} . We assume that this corresponds to the to the magnetic axis. In the photographic plate holder, which exactly fit the chamber, there was a narrow bore ($1/32''$) exactly at the centre of the holder. The bright spot in figure 4 was made by light leaking through this hole. This naturally corresponds to the chamber axis. It will be noticed that in figure 4 these two spots are not coincident indicating that the chamber is not aligned. By shifting the position of the chamber the two spots had been made to coincide (figure 5).

Then photographs were taken at different positions along the chamber axis, and the data of the caustic envelope were thus collected. With the help of this data a baffle was designed which was composed of ten outer stops of aluminium and a central stop.

Using this baffle the K conversion line was measured again. A resolution of 1.54% at 0.56% transmission was obtained.

Having assured that a substantial improvement did occur after using a compound baffle, we next proceeded to construct a true continuous baffle. But this requires more accurate data of caustic envelope. Previously photographs

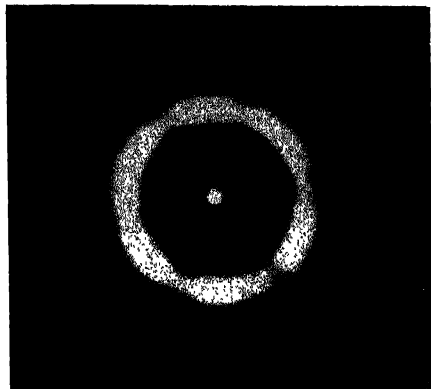


Fig. 5 Circular ring after the alignment

were taken at one cm interval. So the error in placing the baffle was large. We, therefore, introduced some mechanical improvements by means of which photographs at an interval of 2 mm could be taken.

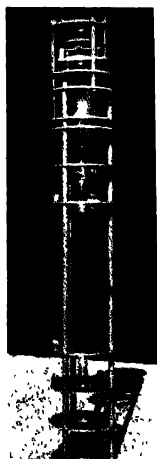


Fig. 6. The complete baffle system.

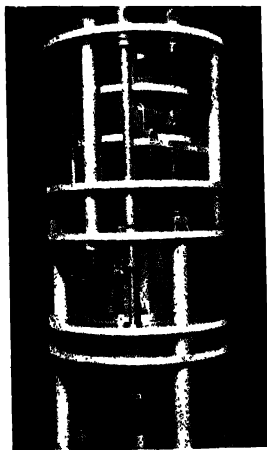


Fig. 7 The continuous baffle

The complete baffle system is shown in figures 6 and 7. The continuous baffle, which is a solid cone of aluminium is divided into two parts, mounted on two brass cylinders (figure 7). These cylinders can be moved along the chamber axis by rack and pinion arrangements, which can be operated from outside the chamber. By this arrangement the baffle can be easily and accurately placed so that it follows the caustic envelope of the electron trajectories. The central stop is also movable, and can be placed at any position on the axis in the neighbourhood of the focussed ring within an accuracy of 0.01 cm.

4 EXPERIMENTAL RESULTS

Figure 8 indicates the influence of the baffles on the line shape of *K*-conversion electrons. Curve *A* corresponds to the line shape without any baffle system. The resolution is 12%. Curve *B* is obtained after the adjustment of

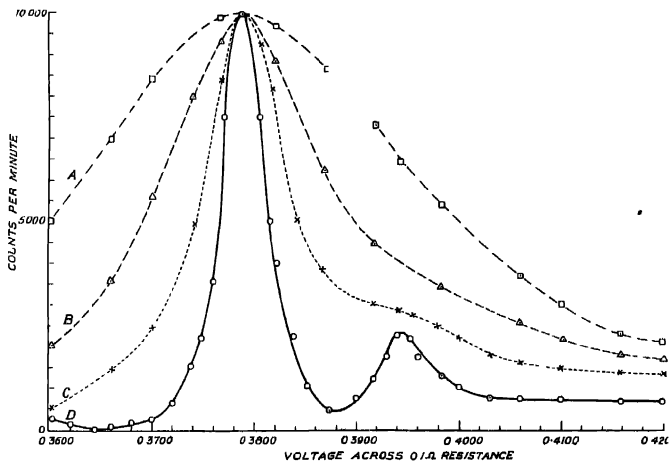


Fig. 8. Influence of continuous baffle on the line shape.

the first outer baffle (i.e. the outer baffle which is away from the detector). Curve *C* gives the line shape when both the outer baffles are in proper positions. It will be seen that a remarkable improvement has occurred after the introduction of the outer baffles (resolution 2.5%). Finally, in curve *D* a resolution of 1.47% is obtained when the central baffle is placed just at the position of the circle of least confusion. The transmission at this region is 0.56%. It will be seen that both the *K* and *L* conversion lines are resolved.

In figure 9 the complete spectrum of Cs^{137} is presented at a moderate resolution (2.2%). The positions and intensity ratios of the conversion lines agree

well with the standard values and this agreement ensures the reliability of our spectrometer. The data are presented in Table I, together with the performance of some other short lens spectrometers reported so far.

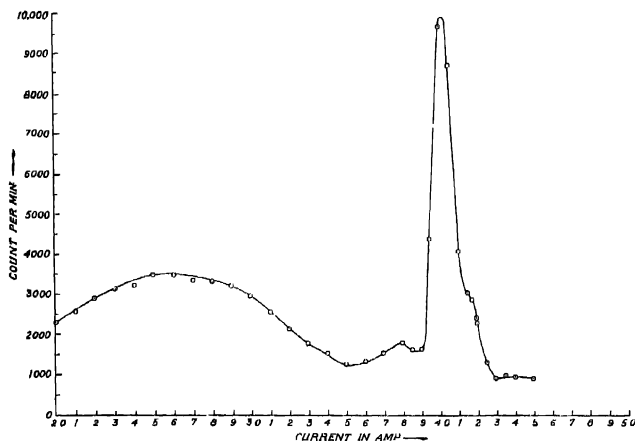


Fig. 9. The spectrum of Cs^{137}

TABLE I
Data on some short lenses

Author	Reference	Resolu- tion α_0	Trans- mission α_0
Siegbahn	1942 <i>Ark. Mat. Astr. Fys.</i> 28, A. 4 No. 17-27	1.0	0.075
Deutsch	1944 <i>R. S. I.</i> 15, 178	1.7	0.18
Müller	1947 <i>J. Res. Nat. Bur. St.</i> 58, 359	2.0	-
Pral	1952 <i>R. S. I.</i> 22, 92	2.0	0.5
The present spectrometer		1.47	0.56

ACKNOWLEDGMENTS

The authors express their deep gratitude to the Late Prof. M. N. Saha, F.R.S. for the kind interest he used to take in this work.

One of the authors (P. N. Mukherjee) is thankful to the Department of Atomic Energy, Government of India, for the award of a Research Fellowship, which enabled him to carry out the work.

The authors acknowledge with pleasure the ungrudging help they have received from Sri R. L. Bhattacharyya, Sri A. K. Sen Gupta and Sri A Chatterjee in setting up some of the electronic equipments concerning the detector. Finally, it is a pleasure to acknowledge the contributions of Sreemati Uma Banerjee to the fabrication of the vacuum chamber of this instrument.

REFERENCES

- Banerjee, M. K. and Saha, A. K., 1953, *Proc Phys. Soc.*, **66**, 937.
Banerjee, M. K. 1955, D. Phil Thesis, Calcutta University.
Bhattacharyya, R., *et al.* 1956, *Ind. Jour. Phys.*, **30**, 585.
Deutsch, *et al.* 1944, *R. S. I.* **15**, 1944.
Perkins and Solbrig, 1951, *R. S. I.* **22**, 173.
Sen, S. 1950, D. Phil Thesis Calcutta, University.

Letters to the Editor

The Board of Editors will not hold itself responsible for opinions expressed in the letters, published in this section. The notes containing reports of new work communicated for this section should not contain many figures and should not exceed 500 words in length. The contributions must reach the Assistant Editor not later than the 15th of the second month preceding that of the issue in which the Letter is to appear. No proof will be sent to the authors.

10 ON OPTICAL METHOD OF MEASURING CONVECTIVE AIR VELOCITY

H. N. PATIL

PHYSICS DEPARTMENT, INSTITUTE OF SCIENCE, BOMBAY

(Received for publication, June, 1 1957).

An interferometer method used to measure temperature of air film is discussed by Kennard (1941). The same can be used to measure velocity v in the plume of hot air, rising vertically from a hot source.

A change of temperature in the plume of air, caused by a change of velocity is revealed by a shift of interference fringes.

A relation between air velocity and shift of fringes is derived as follows. The expression for heat output along the centre line of an interference fringe (Kennard 1941) is

$$Q = \frac{K\lambda_0 T_2}{L(n_1-1)} \cdot \frac{N}{y} \cdot \tan \theta. \quad (1)$$

where T_2 is the temperature of heat source, L , the length of source, y , the distance measured parallel to source and N is the number of fringes contained in y , $\tan \theta$ is the slope of fringes at the surface of the source, λ_0 , the wavelength of light in vacuum, and n_1 is the refractive index of air at room temperature.

The hot air jet rising vertically from the source takes the shape of a cone, (Sutton, 1950). The heat output Q spreads over the cross section of the jet, and is put equal to $H\pi r^2$; where H is the heat flux and r , the radius of the cross section of the jet. Heat flux can be expressed as

$$H = \int C_p \rho_0 v \Delta T \cdot dy = C_p \rho_0 v \Delta T L. \quad (2)$$

where ΔT is the excess of temperature over room temperature and C_p and ρ_0

have usual meanings. The relation between r and Z , the distance of the cross-section from the source as established by Railston (1954), is $r = 0.40, Z^{0.85}$. Using this relation and eqns. (1) and (2) the expression for v becomes

$$v = \frac{KZ^{-1.7}}{0.16\pi C_p \rho_0 L} \cdot \frac{1}{\Delta N} \cdot \frac{N}{y} \cdot \tan \theta.$$

This shift in fringes ΔN , $\frac{N}{y}$ and $\tan \theta$ can be determined experimentally. The difference between ρ and ρ_0 is ignored for smaller values of ΔT . K is put equal to $K_s \left(\frac{T}{T_s} \right)^{0.78}$, where K_s is the thermal conductivity of air at standard pressure and temperature T_s .

REFERENCES

- Railston, W., 1954, *Proc. Phys. Soc. B*, **67**, 42.
 Sutton, O. G., 1950, *Amer. J. Met.*, **7**, 307.

"Temperature its measurement and control in Science and Industry" American Institute of Physics, 1941.

AN ACCURATE PHASEMETER FOR FOUR-TERMINAL NETWORKS

B. CHATTERJEE

INDIAN INSTITUTE OF TECHNOLOGY, Kharagpur,

(Received for publication, May 5, 1957)

ABSTRACT. This paper is a continuation of a previous one [Chatterjee, 1956] in which the principle of working of an accurate phase-meter for four terminal networks was discussed. The present paper gives the details of measurement with such a phase meter at audio and radio frequencies. Arrangements for both balanced and unbalanced types of networks are explained and the circuit diagrams are also given. The absolute accuracy of measurement is about 1° and a small change in phase can be measured with an accuracy of about 0.1° . Modifications necessary for making different types of measurement as well as the high-frequency limit of the meter are also discussed.

1. INTRODUCTION

Though phase is one of the fundamental parameters in circuit techniques, there is no readily available means for the accurate measurement of phase changes produced by a given network. A simple and accurate phase meter has been devised in our laboratory for measuring the phase changes produced by a given network, active or passive. As the method is a very simple one, it can be easily constructed and calibrated. Accuracy of this simple device, specially for measuring small changes in phase, is much greater than any other readily available method. The technique is applicable both at radio and at audio frequencies, almost with equal accuracy. Some typical examples with schematic circuit diagrams and observed results are given to illustrate its applications.

2. THEORY OF OPERATION

The principle of phase measurement, as described in this paper, is based on the fact that an oscillator is capable of giving a stable oscillation only at that particular frequency at which the total phase shift in the feedback loop is 2π or an integral multiple thereof. Thus any four terminal network, introducing a phase change $\Delta\phi$ in the loop, will change the frequency of oscillation in such a manner that the phase of the remaining circuit (mainly the tuned load) changes by an equal magnitude in the opposite direction.

Hence, the phase change produced by the given network may be written as

$$\Delta\phi = \left(\frac{\partial\phi}{\partial\omega} \right) \Delta\omega \quad \dots (1)$$

where $\left(\frac{\partial\phi}{\partial\omega}\right)$ is the rate of change of phase with frequency in the whole loop.

For ordinary oscillator circuits, $\left(\frac{\partial\phi}{\partial\omega}\right)$ for the tank circuit near resonant frequency is very much greater compared to that in other parts of the loop and for all practical purposes, the value of $\left(\frac{\partial\phi}{\partial\omega}\right)$ for the tank circuit, may be taken as equal to that for the whole loop.

Thus, knowing $\left(\frac{\partial\phi}{\partial\omega}\right)$ from the constants of the tank circuit, we can determine $\Delta\phi$ by measuring the frequency change $\Delta\omega$. As the change in frequency can be very accurately measured by a good frequency meter, the measurement of the phase also becomes accurate.

$\left(\frac{\partial\phi}{\partial\omega}\right)$ for an LC tank circuit (as generally used in the radio frequency range) is given by

$$\left|\frac{\partial\phi}{\partial\omega}\right| = 2CR \cos^2 \phi = 2(Q_0/\omega_0) \cos^2 \phi \quad \dots (2)$$

where C is the effective tuning capacity, R is the equivalent parallel resistance, Q_0 is the effective Q value of the tank circuit at resonance $\left(Q_0 = \frac{R}{\omega_0 L} = \omega_0 CR\right)$ and ϕ is the phase angle of the tank circuit at the changed frequency of oscillation. In such a case

$$\left|\Delta\phi\right| = 2Q_0 \cos^2 \phi \cdot \frac{\Delta\omega}{\omega_0} = 2Q_0 \cos^2 \phi \cdot \frac{\Delta f}{f_0} \quad \dots (3)$$

A universal phase change curve for such a phase meter, plotted in terms of Q_0 times fractional change in frequency ($\Delta f/f_0$) is given in figure 1. Knowing the value of Q_0 (from the resonance curve or by a Q -meter), and measuring the frequency change Δf by a good frequency meter, accurate determination of phase change in a given network is possible with the help of the curve of figure 1.

A Wien-bridge type of R - C oscillator circuit may be used for measuring phase changes in the audio frequency range. For such a circuit, $\left|\frac{\partial\phi}{\partial\omega}\right| = \frac{2}{3} CR \cos^2 \phi$, when the series and parallel branches of the Wien bridge circuit have the same values of capacitances (C) and resistances (R). In this case

$$\left|\Delta\phi\right| = \frac{2}{3} CR \cos^2 \phi \cdot \Delta\omega = \frac{2}{3} \cos^2 \phi \cdot \frac{\Delta\omega}{\omega_0}, \quad \left(\because \text{in a Wien bridge oscillator } \omega_0 = \frac{1}{CR}\right) = \frac{2}{3} \cos^2 \phi \cdot \frac{\Delta f}{f_0} \quad \dots (4)$$

Comparing with equation (3), we see that in this case also we can make use of the curve of figure 1 for determining $\Delta\phi$, if we take $Q_0 = 1/3$ for that curve.

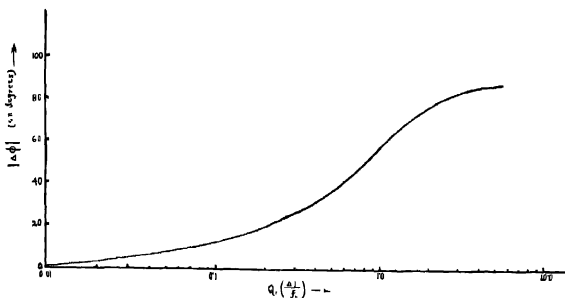


Fig. 1. The Universal calibration curve for the given type of phase meter, determining phase change ($\Delta\phi$) with $Q_0 \frac{\Delta f}{f_0}$, where $\frac{\Delta f}{f_0}$ is the fractional change in frequency and Q_0 is the tank circuit Q at resonance.

Thus, in this case there is no necessity for determining any tank circuit parameter (like Q_0 for the L oscillator) and only a measurement of the relative change in frequency $\frac{\Delta f}{f_0}$ will determine the phase change.

3. SOME TYPICAL EXAMPLES

The general schematic arrangement for measuring phase changes was illustrated with block diagrams in the previous paper. Here we shall show some typical experimental results at different frequency ranges.

(A) At Radio frequencies

Observations were made in the radio frequency range with four terminal networks of resistance-capacitance type and also with co-axial transmission lines, and the results were compared with theoretical calculations.

The circuit connections of the equipment, as built up in this laboratory, is shown schematically in figure 2. V_1 is a tuned amplifier and V_2 acts as an inverter. V_3 and V_4 are cathode followers to isolate the network under test from the rest of the circuit, so that it does not affect the system in any way excepting introducing the phase change. Feedback from V_4 to V_1 forms the closed loop for oscillation. All the coupling condensers are of sufficient value to introduce negligible phase change in the circuit. The normal frequency of oscillation is determined by the parallel resonant frequency of the tuned load (the tank circuit) at the plate of V_1 . Its parallel resonant frequency was set to the particular range of frequencies where we want to study the phase change in the given network. The effective

Q value of the tank circuit (Q_0) was measured by plotting the frequency response curve of the tuned amplifier and by measuring its half-power bandwidth. If the

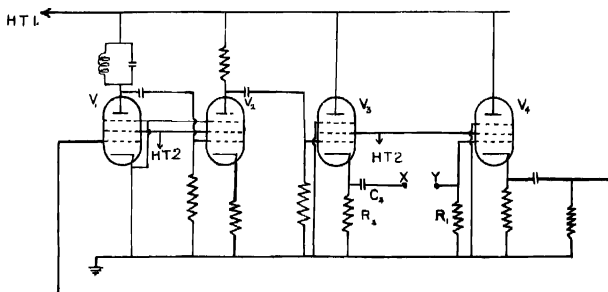


Fig. 2 Schematic circuit diagram of the phase meter for the r.f. range and for unbalanced type of four-terminal networks. The network under measurement is to be connected between the points X and Y .

bandwidth for the half-power points be δf and f_0 be the resonant frequency, then $Q_0 = f_0/\delta f$. While measuring Q_0 , care was taken to have the same grid-drive for the amplifier, as it gets under the oscillating condition.

The network under test is put between V_3 and V_4 at the points X and Y . If the network contains any d.c. voltage at its output, then it is advisable to put a blocking condenser before terminal Y . Each blocking condenser should have sufficient capacitance to act as a complete by-pass.

In order to check the accuracy of measurement, known phase changes were introduced in the loop, at the point XY , by a standard variable capacitor C_0 (figure 3). The effective capacitance between terminal Y and ground is the sum of the standard capacitor and the stray capacitance (C_s):

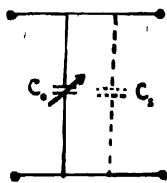


Fig. 3. Position of the standard variable capacitor (C_0) to produce known phase changes in the circuit of Fig. 2.

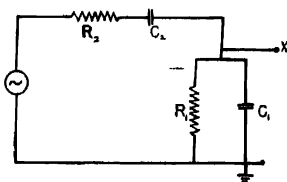


Fig. 4 The equivalent circuit of the phase changing networks at r.f. as used with the circuit of Fig. 2.

The phase shifting network actually forms a Wien bridge circuit as shown in figure 4, the phase (θ) of which is given by

$$\tan \theta = \frac{1 - \omega^2 C_1 R_1 C_2 R_2}{\omega C_2 (R_1 + R_2) + \omega C_1 R_1} \quad \dots (5)$$

where $C_1 = C_0 + C_s$ and C_2 , R_1 and R_2 are as shown in figure 2.

In the experiment mentioned above, nominal values of $R_2 = 4.7K$, $R_1 = 20K$, $C_2 = 0.2\mu F$ and C_1 varied from $25\mu\mu F$ to $200\mu\mu F$. $\omega \approx 3.35 \times 10^6 r/s$.

Taking even the minimum value of C_1 , $\omega^2 C_1 R_1 C_2 R_2 = 5.27 \times 10^3$ and hence for any setting of C_1 we have $\omega^2 C_1 R_1 C_2 R_2 \gg 1$. Also, for the maximum value of C_1 , $\omega C_1 R_1 = 1.68$ and $\omega C_2 (R_1 + R_2) \approx 1.68 \times 10^3$ and hence $\omega C_2 (R_1 + R_2) \gg \omega C_1 R_1$. Hence under these conditions, we can safely put

$$\tan \theta \approx - \frac{\omega C_1 R_1 R_2}{R_1 + R_2} \approx - \omega C_1 R_0 \quad \dots (6)$$

where $R_0 = \frac{R_1 R_2}{R_1 + R_2}$ i.e. the parallel combination of R_1 and R_2

The effective values of R_0 and C_s were measured by an r.f. bridge with all tubes placed in their respective sockets. The values found in the cold condition were $1/R_0 = 268\mu\Omega$ and $C_s = 32\mu\mu F$. But in the hot condition (when the circuit was on), the values found were $1/R_0 = 250\mu\Omega$ and $C_s = 25\mu\mu F$.

This reduction in the effective values of conductance and capacitance in the hot condition is due to the cathode-follower action. When the tube is on, the grid and cathode of a cathode-follower are practically at the same potential and the effect of the shunt path through C_{gk} (as shown in figure 5) is practically elimi-

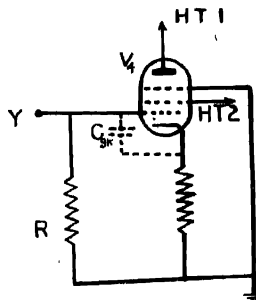


Fig. 5. Illustrating the reduction in the shunt admittance across R_1 , for the cathode follower action in tube V_4 of Fig. 2.

nated. This is responsible for reduction in the effective values of capacitance and conductance. In our calculation, we took the effective values for the hot condition, viz., $R_0 = 1/250\mu\Omega = 4K\ \Omega$ and $C_s = 25\mu\mu F$.

The calculated values of phase shift for different values of the standard capacitance (C_o) is shown in Table I. The same are also experimentally determined by noting the corresponding frequency changes and the results are given in Table II. This table also shows the calculated values of phase shifts and it will be noted that there is a good agreement between the calculated and observed values within the limits of experimental errors.

TABLE I

$$\omega_0 = 3.35 \times 10^6 \text{ radians/sec.}$$

$$C_s = 25\mu\mu F.$$

$$R_0 = 4K\ \Omega.$$

Ex. cap. C_o	Total cap. = $C_o + C_s$	ϕ	$\Delta\phi$	$\cos^2\phi$
0 $\mu\mu F$	25 $\mu\mu F$	18°.5	0	0.899
40 „	65 „	41°.1	22°.6	0.569
70 „	95 „	51°.9	33°.3	0.381
100 „	125 „	59°.1	40°.6	0.263
140 „	165 „	65°.7	47°.1	0.197

TABLE II

$$Q_0 = 35$$

Ex. cap.	Δf	$\Delta\phi$ (measured)	$\Delta\phi$ (calculated)
0 $\mu\mu F$	0	0	0
40 „	5.1 Kc/s.	22°	22°.6
70 „	11.4 „	32°.6	33°.3
100 „	20.5 „	40°	40°.6
140 „	30.9 „	46°.4	47°.1

The standard variable capacitors at our disposal had a minimum value of $40\mu\mu F$ and the minimum phase shift obtainable with this capacitor was 22°. As the above instrument was specially well-suited for giving small changes in

phase accurately, a few measurements on small phase changes produced by transmission lines of different lengths placed between the points *X* and *Y* in figure 2, were carried out. The results are shown in Table III and they reveal a very good agreement with the theoretical values. The transmission line was effectively terminated at both ends by its characteristic impedance.

TABLE III

$$Q_0 = 35 \qquad f_0 = 533 \text{ Kc/s.}$$

Line length (electrical)	$\Delta\phi$ (calculated)	$\Delta\phi$ (measured)
2.8 m ($\lambda/120$)	3"	3.3"
4.2 m ($\lambda/80$)	4.5"	4.9"
7 m ($\lambda/48$)		8.0"

Measurements on a balanced network

The experimental observations discussed in the previous paragraphs were for a four terminal network of the unbalanced type. To determine the phase shift in a balanced network such as shown in figure 6, the circuit arrangement is to be modified. A circuit arrangement of the type as shown in figure 7 (and

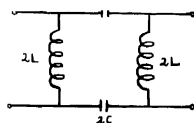


Fig. 6 The balanced filter arrangement used for illustrating the measurement of phase change produced by a balanced network.

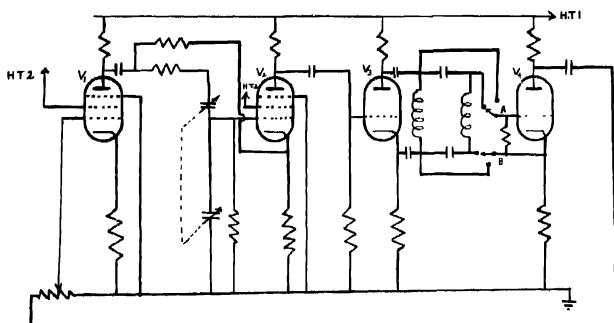


Fig. 7. Schematic circuit arrangement for measuring the phase change produced by a balanced filter (in its pass band) in the audio frequency range.

discussed in detail under measurements in the audio frequency range) may be used. Or, in some cases, balanced to unbalanced transformer coupling may be used to separate the balanced network from the unbalanced tube-circuits.

For making measurements over a range of frequency, a variable condenser may be used in the tank circuit and the resonant frequency varied over the range. To give a further variation, separate tank coils may be used. Measurements on active networks like amplifiers may also be done in a manner described below for the audio frequency range.

(ii) *At Audio frequencies*

For making measurements in the audio frequency range, a Wien bridge type of audio oscillator was used. This is not only easy to make and gives sinusoidal oscillations easily, but also variation of the tuning condenser only can give a frequency range of about 1 : 10 (the corresponding case for LC oscillator being about 1 : 3). As most of our measurements in the audio frequency range are carried out over a band of frequency, this method of R - C tuning gives an important advantage. The resistances in the tuning network may be changed for further variation of frequency.

Firstly, we shall discuss the measurements on a balanced high-pass filter of the constant K type as shown in figure 6. This will not only provide an example of phase measurement with this instrument in the audio frequency range, but it will also illustrate a method of phase measurement in a balanced network.

The circuit connections were made as shown in figure 7 with arrangements to switch on or off the filter in the closed loop of the oscillator. V_1 and V_2 comprise the oscillator portion and V_3 and V_4 separate the balanced filter from the unbalanced circuit. Oscillation frequencies were noted for the filter in or out of the circuit, and the phase changes were calculated from these measurements with help of equation (4) and figure 1. Frequency measurements were carried out by comparing the oscillation frequencies with those of a standard audio oscillator capable of giving small changes in frequency and noting the Lissajous patterns on a cathode ray oscillograph. The results of phase measurements, together with the calculated values, are plotted graphically in figure 8. The values of the condensers and inductances in the filter section (of the constant K type) were $L = 50\text{mH}$ and $C = 0.1\mu\text{F}$, having cut-off frequency $\approx 1\text{Kc/s}$.

The phase measurements were carried out in the pass band sufficiently above cut-off frequency. The network was effectively terminated by its nominal characteristic impedance (characteristic impedance at infinite frequency) at both ends and as such there was some mismatch at the low frequency end (near cut-off). The effect of mismatch is to lower the phase shift in those frequency ranges as is evident from figure 8. It shows that the measured phase change is practically

identical with the calculated phase change (calculated on the supposition that the network is properly matched) for frequencies sufficiently above the cut-off. But as the cut-off is approached, the measured value falls short of the calculated value

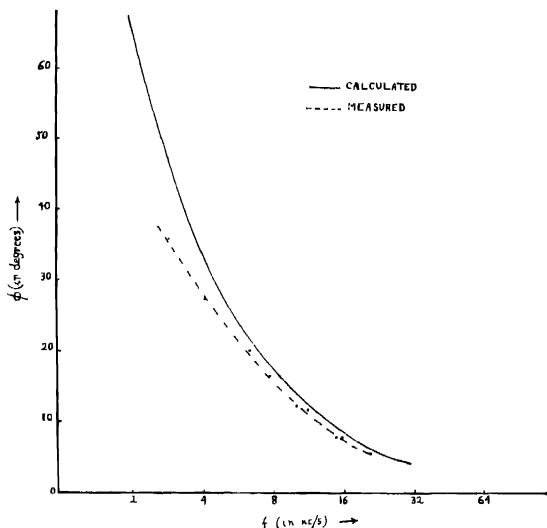


Fig. 8 Variation of phase change with frequency of the filter circuit of Fig. 6, as measured by the phase meter. The experimental curve is shown by dotted line and a calculated curve is also shown in the same graph by solid line.

due to the mismatch effect. For measuring phase changes in the range 90° to 180° , the connections at the points *A* and *B* should be interchanged so as to keep suitable phase relations in the loop for the maintenance of oscillation. The same effect may also be accomplished by introducing another amplifier stage. This is further discussed in section 4.

Phase shift in an active network.

We now consider the measurement of phase change produced by an active network (an amplifier) in the audio frequency range. The circuit connection is shown in figure 9. The Wien bridge oscillator portion is as in figure 7. V_1 is the amplifier under test and V_2 is an inverter. It is to be noted that a phase inverter has to be put in the closed loop as a single stage amplifier of the type shown inverts the signal on amplification. The phase-frequency response of the given *R-C* coupled amplifier was plotted in figure 10 for the high frequency range. A similar phase frequency characteristic for the low

frequency range may also be plotted by changing the values of R in figure 9, and making the Wien bridge oscillator to oscillate in the low frequency band.

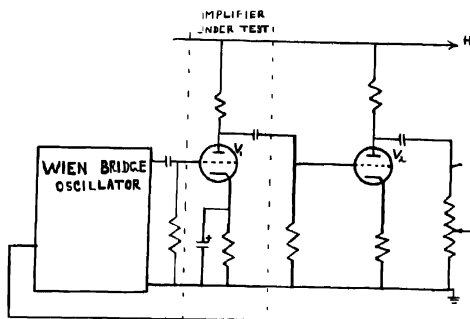


Fig. 9. Schematic circuit diagram for measuring the variation of phase with frequency of an R-C coupled A. F. amplifier.

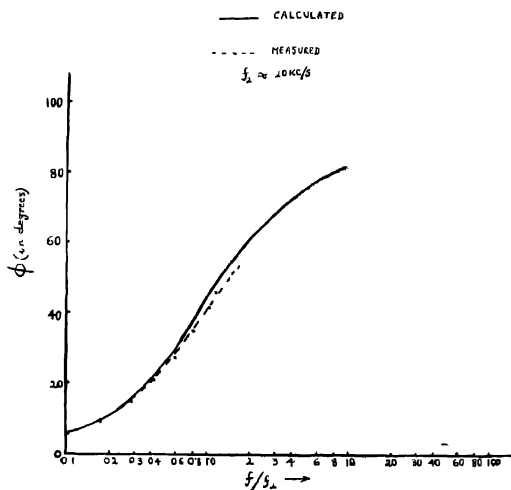


Fig. 10. The variation of phase with frequency for the high-frequency region of an R-C coupled amplifier, as shown in Fig. 9. The solid line shows the calculated curve and the dotted line gives the measured phase variation by the given phase meter.

The phase-frequency curve of figure 10 shows a good agreement with theory and such types of phase meters may conveniently be used for these and similar applications. It gives a ready method of phase measurement and the accuracy

is also sufficiently good. Deviation of the measured phase characteristic from the calculated one at higher frequency (above half-power frequency f_2) is due to the fact that our measurement is based on the assumption of negligible phase change in the rest of the loop (excepting the given network and the tuning circuit). This is no longer valid accurately in the high frequency range, where some small phase changes also occur in the loop at points other than the Wien bridge.

It may be mentioned in this connection that phase changes produced by active networks (such as amplifiers) in the radio frequency range may be measured in an identical manner. Only difference is that the oscillator portion is made for the radio frequency band. Precautionary measure should however be taken to prevent distortion due to over-driving of the tubes, as shown in figure 9.

The typical examples of the application of the phase meter under discussion clearly show that the meter can be used for various measurements at audio and radio frequencies as are commonly encountered in any electronics laboratory.

4 DISCUSSIONS

For phase measurements in the radio frequency range, the measurement of frequency can be done very accurately by using a heterodyne type of frequency meter. The accuracy of such frequency meters is about one part in ten thousands, though some experience and training may be required to get a sharp null. As such the accuracy of phase measurement in this range is mainly determined by the accuracy with which Q_0 is known. As Q_0 can generally be determined with an accuracy of about one part in a hundred, the accuracy of phase measurement is also of the same degree. From figure 1, we see that measurement of phase with the above type of circuit arrangement is limited to the range of $\pm 90^\circ$. With an accuracy of 1% it is obvious that maximum uncertainty takes place for phase change near 90° and is about 1° . The uncertainty is proportionately less for smaller values of phase changes. It may be noted, however that Q_0 remains practically constant for small changes in frequency and thus for noting small relative changes in phase values, the accuracy may be much higher, of the order of 0.1° .

As frequency measurements cannot be made in general, with so much accuracy in the audio frequency range, small relative changes in phase in the audio frequency range cannot be measured with an accuracy of 0.1° . But even then, the absolute accuracy remains in the order of 1° , as audio frequencies can easily be measured (by Lissajous figures or bridges) with an accuracy of one part in one hundred.

It is to be noted that before taking any measurement, the apparatus should be kept on for a sufficient time to attain temperature stability. This precaution is a common one for making any accurate measurement and need not be discussed in detail. The components of the tuning circuit should be as insensitive to temperature changes as possible.

Any phase change lying within the range $\pm 90^\circ$ to $\pm 180^\circ$ can only be measured by introducing an additional phase shift of 180° in the circuit. With this modification in the circuit, the actual phase angle (in magnitude) of the network is equal to 180° minus the phase angle as measured by the apparatus. It is easy to introduce a phase shift of 180° by taking out the inverter stage or adding another amplifier, which ever is found to be more convenient. The sign of the phase angle is determined by noting the direction in which the frequency changes.

If the measurements are to be carried out only at a given frequency in the radio frequency range, then one can conveniently use a frequency discriminator circuit (as for example a ratio detector) to measure the frequency change. A meter giving the discriminator output may then be directly calibrated in phase angles.

The high frequency limit of operation of this phase meter in the radio frequency range is governed by the stray capacitances shunting the load resistances or the terminating resistances (in case of transmission lines). At frequencies for which the reactance of these shunt capacitances becomes comparable with the resistances shunted by them, large phase changes are introduced in all these points of the circuit and the results are vitiated. One such observation with transmission lines shows that for a calculated phase change of $30^\circ.5$, the observed phase change becomes about 34° at a frequency of 5 Mc/s. This reduction in accuracy is due to extra phase shift caused by the shunt capacitance across the terminating resistance of the transmission line. A measurement on this stray capacitance showed that it is responsible for an extra phase shift of about 3° . Thus when this extra phase shift is taken account of, the calculated value agrees very well with the measured value (within an accuracy of 1°). For higher frequencies, the amount of these additional phase shifts will increase, thus increasing the error of observation. Accurate measurement at higher frequencies is possible if the stray capacitances are reduced or they are of known value and remain constant. In that case the observed phase shifts may be corrected, for these stray effects and accurate results obtained.

It may be mentioned that if the given network introduces high loss or high gain in the loop, it may either stop the oscillation or give wrong results by producing distorted (non-sinusoidal) wave shapes. Under such circumstances, the amplifier gains are to be properly adjusted and it is convenient to have a gain control as shown in figures 7 and 9.

ACKNOWLEDGMENT

The author wishes to express his grateful thanks to Dr. H. Rakshit, Head of the Dept. of Electronics & Electrical Communication Engineering, Indian Institute of Technology, for his guidance, help and interest in the work.

REFERENCE

Chatterjee, B., 1956, *Jour. Inst. Telecomm. Eng.*, **2**, 93.

SCATTERING OF 9.5 MEV PROTONS BY NITROGEN

ANWAR HOSSAIN AND A. N. KAMAL

PHYSICS DEPARTMENT, DACC A UNIVERSITY, DACC A.

(Received for publication, March 5, 197)

ABSTRACT. The paper deals with the results obtained by the work on the scattering of 9.5 Mev protons by nitrogen. Nuclear emulsion technique has been employed for the detection of scattered particles. The exposure was made in 1952 at the Birmingham cyclotron using nitrogen target. The scanning of the plates was done, however, in the Physics laboratory of the Dacca University.

Levels in N^{14} nucleus has been obtained at $2.36 \pm .03$, $3.93 \pm .05$, $4.91 \pm .03$, $5.15 \pm .02$, $5.49 \pm .02$, $5.77 \pm .03$, $6.05 \pm .02$, $6.20 \pm .03$, $6.48 \pm .05$, $6.75 \pm .03$ and $7.01 \pm .05$ Mev.

The angular distribution of the elastically scattered protons by N^{14} has been obtained. An asymmetric angular distribution has been obtained for the protons inelastically scattered by N^{14} leading to the formation of the 3.9 Mev level.

INTRODUCTION

In autumn 1952 a series of exposures using 9.5 Mev protons was made at Birmingham by the members of the Physics departments of Bristol and Birmingham universities and that of St. Bartholomew's Hospital, London. The beam obtained from the 60-inch Birmingham cyclotron was made to strike gaseous targets within the scattering camera. Ilford C-2 emulsions were employed for the detection of particles. The plates on nitrogen, which were studied here form a part of the series of exposures, and were kindly lent to us by Dr. D. J. Prowse of H. H. Will's Laboratories, University of Bristol.

METHOD OF ANALYSIS

Burrows, Powell and Rotblat (1951) and Prowse (1954) gave details of the exposure and technique involved in the present investigation. They also discussed the method of measurement in the determination of the energy levels and the scattering cross-sections.

The plates were scanned in this laboratory under a Reichert monocular microscope with a maximum magnification of 1,200. The lengths of all the tracks originating at the surface of the emulsion and starting within a rectangular region, defined by a rectangular mesh in the eyepiece, were measured with the help of an occlumeter previously calibrated with a stage micrometer. Measurements were made from 30° to 60° at intervals of 5° , a smaller angle, where background tracks number was high, being impossible to investigate with the present microscope.

RESULTS

Before proceeding to give our results, it will be worthwhile to make a survey of the results obtained so far.

Studying the inelastic scattering of 15 Mev protons by N^{14} , Fulbright and Bush (1948) found levels at 5.1 and 6.7 Mev in N^{14} . Using 8 Mev deuterons, Burrows, Powell and Rotblat (1951) determined levels at 3.98 and 5.06 Mev employing the $O^{16}(d, \alpha)N^{14}$ reaction. The same reaction yielded levels at 3.95, 5.01 and 5.70 Mev to Ashmore and Raffle (1951) and at 3.95, 4.93 and 5.98 Mev to Sperduto and Fader (1953) who used 8 Mev deuterons.

With the help of magnetic spectrograph Bockelman *et al.* (1953) detected levels at 2.31, 3.95, 4.91 and 5.01 Mev studying the inelastic scattering of 6.92 and 7.56 Mev protons. Freeman *et al.* (1954) reported levels at 2.31, 3.95, 4.91 and 5.10 Mev studying the inelastic scattering of 9.5 Mev protons by N^{14} .

Mackin *et al.* (1955) obtained levels at 3.91, 4.93, 5.13, 5.73 and 6.45 Mev employing the $C^{13}(d, n)N^{14}$ reaction. The same reaction employed by Bent and Bonner (1955) yielded levels at 3.42, 3.71, 4.48, 4.96, 5.12, 5.74, 6.53, 7.09 and 7.34 Mev. They, however, are not certain about the level at 3.71 Mev, which, according to them, may belong to C^{13} .

Miller *et al.* (1956) studied the inelastic scattering of 22 Mev alpha particles using a point focussing 180° magnetic spectrograph and reported levels at 3.95, 5.12, 5.79, 6.47 and 7.02 Mev. The levels at 2.31, 7.40 and 7.70 Mev reported by other authors were not obtained

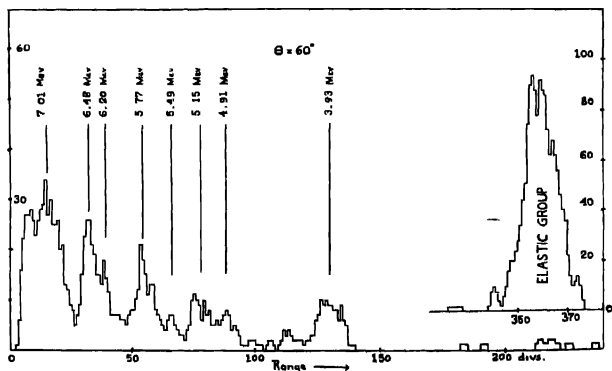


Fig. 1 Histogram of the tracks obtained at $\theta = 60^\circ$. Each division is equal to 1.19 nucleons. The distribution has been smoothed out by adding to each ordinate the mean of its neighbours. The ordinate represents the number of tracks obtained.

PRESENT LEVEL DETERMINATION

The levels observed in the present investigation are quoted in Table I. Of these levels Ajzenberg and Lauritsen (1952) mention all except the ones at 5.49 and 6.75 Mev. In order to show the levels obtained at a certain angle the histogram of the tracks observed at $\theta = 60^\circ$ has been reproduced in figure 1.

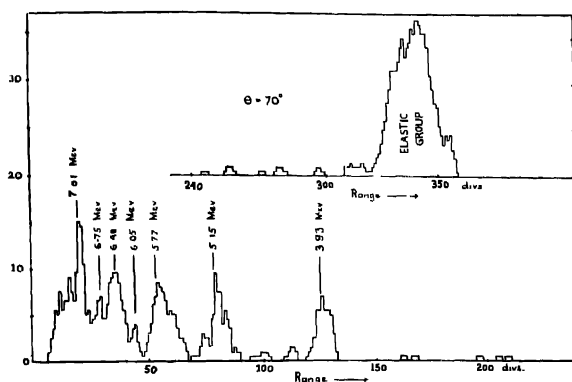


Fig. 1(u) Histogram at $\theta = 70^\circ$ showing clearly a level at 6.75 Me

TABLE I

Ajzenberg and Lauritsen 1955	Present Authors
2.31 Mev	2.36 \pm .03 Mev
3.95 Mev	3.93 \pm .05 Mev
4.91 Mev	4.91 \pm .03 Mev
5.10 Mev	5.15 \pm .02 Mev
—	5.49 \pm .02 Mev
5.69 Mev	5.77 \pm .03 Mev
5.83 Mev	—
5.98 Mev	6.05 \pm .02 Mev
6.23 Mev	6.20 \pm .03 Mev
6.44 Mev	6.48 \pm .05 Mev
—	6.75 \pm .03 Mev
7.02 Mev [*]	7.01 \pm .05 Mev

The levels at 5.49 and 6.75 Mev, though observed at only a few angles of scattering (see figure 1a) stand out quite prominently. All that can be said at the moment is that there is a likelihood of the levels at 5.49 and 6.75 Mev to exist, though their existence has yet to be confirmed by more elaborate work in this direction.

It was not always possible to resolve the 4.91 and 5.15 Mev levels due to the low cross-section of the 4.91 Mev component. A figure of $2.7 \pm .6$ has been obtained for the ratio of the cross-sections for scattering leading to the formation of the 5.15 and 4.91 Mev levels. The resolution of the levels was observed to be the best at the intermediate angles and poor at both forward and backward angles of scattering.

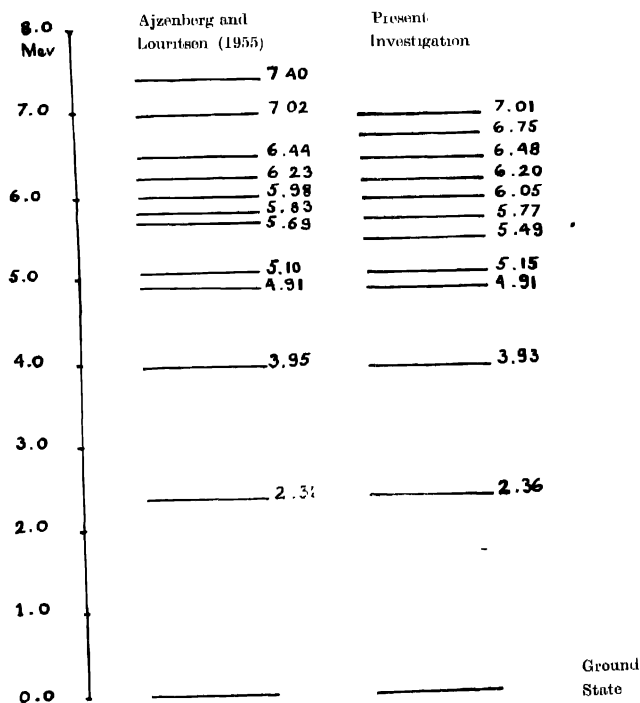


Fig. 2. A comparative study of the level schemes for N^{11} proposed by Ajzenberg and Lauritsen and observed in the present investigation.

The level obtained at 5.77 Mev might be doublet, as suggested by Ajzenberg and Lauritsen (1952), but it was not possible to resolve it into the components. The accompanying diagram (figure 2) shows the levels quoted by Ajzenberg and Lauritsen along with those obtained in the present investigation.

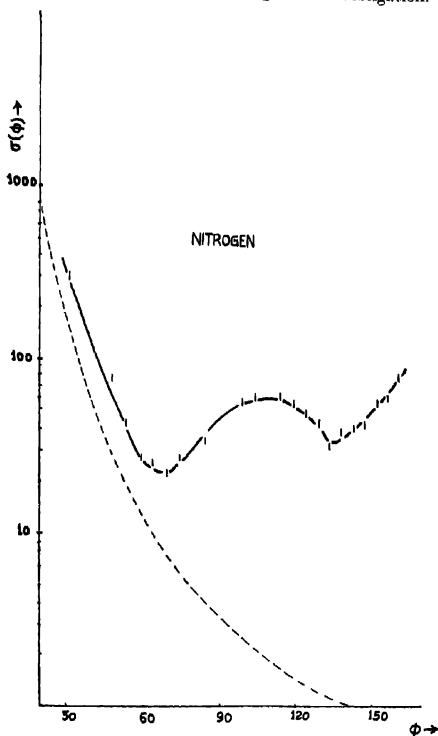


Fig. 3. Angular distribution in the c.m. system of protons elastically scattered by nitrogen. $\sigma(\phi)$ is expressed in millibarns per steradian. The dotted curve gives the Rutherford scattering cross sections.

ANGULAR DISTRIBUTION

The angular distribution of the protons elastically scattered by N^{14} is shown in figure 3. It can be seen that the experimental points fall amiably on a smooth curve. This is slightly different from the findings of Freemantle *et al.* (1954) who obtained an irregular curve. Thus in the present case the cross-section falls

to a minimum at $\phi = 68^\circ$, rises to a blunt maximum at $\phi = 110^\circ$ before falling again to a minimum at $\phi = 137^\circ$. Unlike the distribution for C^{12} and O^{16} , the cross-section rises to a high value at backward angles. The dotted curve represents the cross-section as expected from the Rutherford scattering. As is evident the departure from Rutherford scattering occurs at a centre-of-mass angle less than 30° , thus agreeing with the finding of Freemantle *et al.* (1954).

ANGULAR DISTRIBUTION OF INELASTICALLY SCATTERED PROTONS LEADING TO THE FORMATION OF 3.9 MEV LEVEL.

Freemantle *et al.* (1954) obtained the angular distribution of 9.5 Mev protons scattered inelastically from the 3.9 Mev level of N^{14} . They reported symmetry about 90° with a minimum at this angle and rise of cross-section at both forward and backward angles. The angular distribution obtained in the present investigation is shown in figure 4. The shape of the curve follows the same pattern as

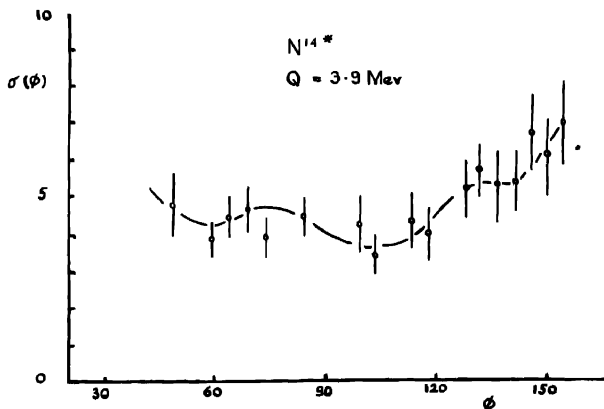


Fig. 4. Angular distribution in the c.m. system of protons inelastically scattered by nitrogen leading to the formation of the 3.9 Mev state. $\sigma(\phi)$ is expressed in millibarns per steradian

that of Freemantle *et al.* but symmetry about 90° is not observed. The curve has a shallow central minimum at $\phi = 111^\circ$.

ACKNOWLEDGMENT

It is our pleasure to thank Dr. D. J. Prowse for making the plates available to us.

REFERENCES

- Ajzenberg and Lauritsen, 1952, *Rev. Mod. Phys.*, **24**, Jan.
Ashmore and Raffle, 1951, *Proc. Roy. Soc., A* **64**, 754.
Bent and Bonner, 1953, *Phys. Rev.*, **98**, 1237.
Bockelman *et al.*, 1953, *Phys. Rev.*, **92**, 665.
Burrows, Powell, Rotblat, 1951, *Proc. Roy. Soc., A* **209**, 461.
Freemantle *et al.*, 1954, *Phys. Rev.*, **96**, 1268.
Fulbright and Bush, 1948, *Phys. Rev.*, **74**, 1323.
Mackin *et al.*, 1955, *Phys. Rev.*, **98**, 43.
Miller *et al.*, 1956, *Phys. Rev.*, **101**, 740.
Prowse, D. J., 1954, Ph.D Thesis, Bristol University,

ULTRASONIC VELOCITY IN COBALT AND CADMIUM SULPHATE SOLUTIONS AT DIFFERENT TEMPERATURES AND CONCENTRATIONS

SRINIBAS PANDA AND BRAJA SUNDAR MOHANTY

DEPARTMENT OF PHYSICS, RAVENSHAW COLLEGE, CUTTACK.

(Received for publication, December 21, 1956)

ABSTRACT. Ultrasonic velocity in cobalt and cadmium sulphate solutions have been measured over a concentration range 0.05 to 0.5 molar (m) and over a temperature range 30°C to 50°C. The values of adiabatic compressibilities have been computed.

INTRODUCTION

In a survey of electrochemical applications of ultrasonic waves in electrolytic solutions by Yeager and Hovorka (1953) it has been pointed out that, although there has been in the past, some amount of work regarding the structure of strong as well as weak electrolytes, still many aspects regarding them have remained unexplained. Measurements of ultrasonic velocities and adiabatic compressibilities may help to solve some of the difficulties. In this connection the sulphates of zinc and magnesium have been studied by Mohanty and Deo (1955). They have found that both velocity and adiabatic compressibility of the above two sulphates vary linearly with concentration (from 0.05 to 0.5 molar), and temperatures (25°C to 45°C). Since the ultrasonic study of bi-valent sulphates have gained some interest in physico-chemical research in the present work, the authors planned to study the same for sulphates of cobalt and cadmium.

EXPERIMENTAL METHOD

Both the sulphate solutions were prepared at room temperature from G.R.E. Merc samples.

The velocities were determined by the usual method of photographing the Debye-Seearer's diffraction spectra. The experimental technique was the same in the work of Mohanty and Deo (1955).

TABLE I

Velocity and adiabatic compressibilities of cobalt sulphate

Temp. in "C	Concen- tration (2m)	Velocity metres/sec.	Density gm /cc.	$\beta \times 10^{12}$
30	0.1	1511	1.0041	43.63
	0.2	1514	1.0119	43.12
	0.4	1530	1.0280	41.50
	0.6	1538	1.0416	40.54
	0.8	1548	1.0557	39.53
	1.0	1560	1.0697	38.42
35	0.1	1526	1.0034	42.8
	0.2	1530	1.0112	42.25
	0.4	1540	1.0272	41.05
	0.6	1544	1.0405	40.31
	0.8	1560.5	1.0542	38.96
	1.0	1578	1.0679	37.61
40	0.1	1535	1.0027	42.33
	0.2	1538	1.0105	41.84
	0.4	1546	1.0264	40.76
	0.6	1552.6	1.0394	39.94
	0.8	1568	1.0527	38.65
	1.0	1581	1.0661	37.53
45	0.1	1542	1.0020	41.98
	0.2	1545	1.0098	41.93
	0.4	1555	1.0250	40.34
	0.6	1566	1.0383	39.20
	0.8	1575.5	1.0512	38.32
	1.0	1586	1.0643	37.35

TABLE I (contd.)

Velocity and adiabatic compressibilities of cobalt sulphate.

Temp. in °C	Concen- tration (2m)	Velocity metres/sec.	Density gm./cc.	$\beta \times 10^{12}$
50	0.1	1550	1.0013	41.58
	0.2	1554	1.0091	41.05
	0.4	1563	1.0248	39.96
	0.6	1570	1.0372	39.11
	0.8	1580.5	1.0497	38.14
	1.0	1590	1.0625	37.23

TABLE II

Velocity and adiabatic compressibility of cadmium sulphate.

Temp. in °C	Concen- tration (2m)	Velocity metres/sec.	Density gm./cc.	$\beta \times 10^{12}$
30	0.1	1511	1.0056	43.56
	0.2	1513	1.0154	43.01
	0.4	1519	1.0350	41.87
	0.6	1526	1.0543	40.75
	0.8	1530	1.0737	39.78
	1.0	1535	1.0928	38.84
35	0.1	1520	1.0043	43.09
	0.2	1523	1.0140	42.52
	0.4	1526.4	1.0335	41.50
	0.6	1533	1.0528	40.42
	0.8	1538	1.0723	39.42
	1.0	1546	1.0915	38.33
40	0.1	1531	1.0029	42.54
	0.2	1533	1.0127	42.01
	0.4	1535	1.0321	41.10
	0.6	1538	1.0514	40.20
	0.8	1542	1.0709	39.26
	1.0	1549	1.0901	38.20

TABLE II (contd.)

Velocity and adiabatic compressibility of cadmium sulphate

Temp. in °C	Concen- tration (2m)	Velocity metres/sec.	Density gm./c.c.	$\beta \times 10^{12}$
45	0.1	1540.5	1.0015	42.08
	0.2	1543	1.0113	41.53
	0.4	1546	1.0307	40.60
	0.6	1548	1.0501	39.74
	0.8	1551	1.0696	38.88
	1.0	1554	1.0888	38.04
50	0.1	1545	1.0001	41.85
	0.2	1547	1.0100	41.35
	0.4	1551	1.0293	40.39
	0.6	1555	1.0487	39.44
	0.8	1558	1.0682	38.60
	1.0	1560.5	1.0875	37.78

RESULTS AND DISCUSSIONS

The results obtained are contained in the preceding tables. The values of the densities at different temperatures and concentrations were computed from the data given in the International Critical Tables, Vol. III. The adiabatic compressibility (β) was calculated from $\beta = 1/v^2\rho$, where v = ultrasonic velocity and ρ is the density. On plotting graphs between adiabatic compressibilities and concentrations, it was found that the adiabatic compressibilities vary linearly with concentrations at all temperatures.

REFERENCES

- Mohanty, B. S. and Deo, B. B., 1955, *Ind. J. Phys.*, **29**, 62.
 Yeager, E. and Hovorka, F., 1953, *J. Acoust. Soc. Am.*, **25**, 443.

PHOTOIONIZATION VERSUS PHOTOELECTRIC EFFECT FOR DISCHARGE SPREAD AND OUTPUT PULSE MEASUREMENTS IN G-M COUNTERS

P. S. GILL AND S. P. PURI

DEPARTMENT OF PHYSICS, MUSLIM UNIVERSITY, ALIGARH.

(Received for publication, June 17, 1957)

ABSTRACT. The probability of discharge spread *versus* overvoltage has been measured in a multicathode, single-anode counter, by keeping dead the space across which the discharge spreads. The pulse size *versus* voltage curves for the externally coated counters reveal that the operation of soft glass type is analogous to that of the conventional counter, whereas in case of pyrex counter, the deposition of the positive ions across the inner glass surface develops an opposing e.m.f., which varies linearly with the overvoltage.

Besides, discharge spread probability has been studied as a function of overvoltage in a multicathode, segmented counter, making use of beads sealed on to the wire. The beads suppress the photoionization contribution by reducing the field around them, thus eliminating altogether the photoionization near the immediate vicinity of the wire, which in normal operation, contributes to the stepwise discharge spread. The photoelectric effect responsible for discharge spread remains negligibly feeble but constant over an overvoltage of about 400 volts in the case of present counter with the rare gas-organic vapor admixture.

INTRODUCTION

There is a lack of an established theory of the mechanism of spread along the wire of a self-quenching counter, but it seems generally agreed that the mechanism is probably akin to the streamer mechanism of spark breakdown (Meek, 1940), *i.e.* photons released in the initial avalanche produce nearby ionization in the counter gas, which is amplified by the radial field and which eventually spreads the discharge to both ends of the counter. Recent investigations of discharge between a positive wire and a cylinder in pure argon have shown that photoelectric emission from the cathode is the important secondary mechanism, (Colli and Facchini, 1954). No photoionization in the volume is observed in pure argon or molecular gases (Huber, 1955). The experiments of Craggs and Jaffe (1947) showed that in the case of organic vapour quenched counters, an appreciable photoemission from the cathode cylinder is always operative. Balakrishnan and Craggs (1950) analysed their results of discharge spread velocities in Geiger counters, to separate these two mechanisms, but no decision seemed possible.

The present experiments were designed to separate these contributory processes, by rendering the photoionization mechanism inoperative by the use of glass beads sealed on to the wire, (Stever, 1942; Wilkening and Kanne, 1942). A detailed

investigation of the properties of counters with beads on the wire, due to Curran and Rae (1947), has shown that the main action of beads in localising the discharge is due to the reduction of the electric field strength in the vicinity of the beads. Field plots in the electrolytic tank were made and substantiated the experiments with the counters. No electrostatic charge need be invoked since conducting beads were found to be as efficient as insulating beads in securing localization.

The charge generated per unit length of the counter is called Q . It is compared with Q_0 , the charge per unit length of the counter required to charge it to its operating potential. Let m be the ratio Q/Q_0 . For the organic vapour-rare gas-filled self-quenching counters the following facts were theoretically predicted by Wilkinson (1948) and experimentally verified by Fenton and Fuller (1949):

- (1) For small overvoltages, the charge generated per unit length of counter depends almost linearly on the overvoltage, which is the difference between operating voltage and the threshold,
- (2) At a well defined voltage, corresponding approximately to $m = Q/Q_0 = 1$, a break in the $Q - V$ curve occurs and the slope drops to half of its previous value.

The present investigation was undertaken to determine the picture of the processes responsible for discharge spread after the limit $m = 1$, whether the very multiplication process is affected or the decrease in slope results from the partial neutralization of the positive space-charge by the electrons generated in the preceding avalanche, since at $m = 1$, no field is present any more at the "burning out" part of the wire. This is accomplished by employing a multi-cathode single anode counter, by initiating the discharges in one of the cathodes and detecting the discharge in the next cathode, the intervening space was kept at the wire potential unlike the experiments of Craggs and Jaffe (1947), who maintained these cathodes at voltages a little lower than the Geiger threshold. The present procedure ensures that what passes across the intervening space are photons only. The method of experiment was to irradiate an extreme cathode by carefully collimated gamma-rays from radium and to determine the probability of discharge spread by counting coincidences between the irradiated cathode and the next cathode versus overvoltage. Indicating α as spread probability, we get

$$\alpha = \frac{\text{Number of coincidences in } A \text{ and } B}{\text{Impulses in } A \times \text{impulses in } B} = \frac{\text{coincidences in } A \text{ and } B}{\text{impulses in } A \times \text{impulses in } B}$$

Then α was measured as a function of the overvoltage across the counter.

The second part of the present investigation consists of the report of pulse size versus overvoltage in case of externally coated counters, both soft glass and pyrex types, to find the role of glass wall on the counter operation.

EXPERIMENTAL SET-UP

The counters employed are the externally coated soft (Puri and Gill, 1956) and pyrex glass counters (Yasin *et al.*, 1951). One megohm quenching resistor was used with the external counters. The scales employed were arbitrary and did not show the absolute values.

The block diagram of the electric circuitry for the measurement of double coincidences is given in figure 1. A pulse resulting from discharge build up in

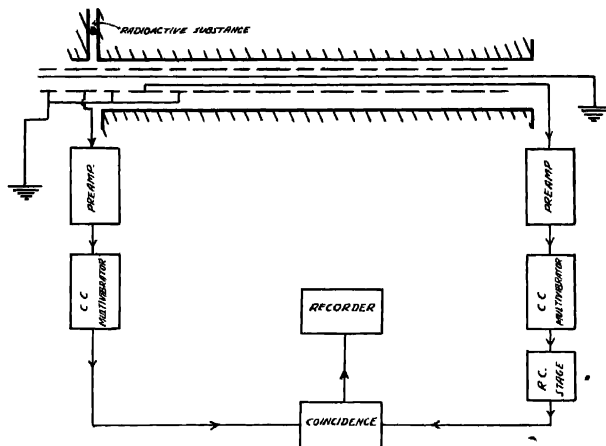


Fig. 1 Block diagram for discharge spread velocity measurements.

one of the short end cylinders (2 cm. long) of the split cathode counter, is put into the square wave-shape by cathode coupled multivibrator in the direct channel. It was about 15 microseconds in duration. The discharge then spreads and in one split cathode there is a substantial number of excited and ionized atoms $\sim 10^8$. The excited atoms will return to the ground state, emitting one or more quanta, which traverse the gas for a distance determined by an exponential absorption coefficient. The next small cathode (3 mm. long) is at the wire potential, the discharges in the succeeding cathodes only result from the passage of energetic photons, since spurious discharges due to scattering and diffusion of electrons along a dead-space of 3 mm are absent. The pulse resulting from the third cathode was put into square wave shape and then differentiated. The coincidences were sought at the output of the diode-coincidence circuit and recorded by the scaler. The counter was shielded from background radiation by placing it in an axially bored 1" diameter hole in a lead block of 6" \times 6" area, except at the place of irradiation.

The multicathode, segmented counter employed for separating the photoionization from the photoelectric effect, was identical with the above mentioned multicathode counter, but for the fact that each of the 2 cm. long cathodes was preceded and followed by 5mm cathodes, which were graphitized over a bead of 1.5 mm diameter. These alternate small cathodes (5mm) were kept at the wire potential.

It has been shown by Curran and Rae (1947) that the lines of force between the cylinder and the bead cover a length of the cylinder more than three times the diameter of the bead. Thus with beads of 1.5 mm diameter separated at 2.7cm, lines of force from only 2.2 cm of the cathode, per section finish on the bare wire, any electron or negative ion formed within the volume bounded by the limiting lines of force will be drawn to the bead and not the wire. In this event since the field near the bead never reaches as high a value as that at the thin wire, no appreciable avalanche is formed and the tube does not give a detectable pulse. Thus the use of beads eliminated altogether all the discharges resulting from the axial motion of the ultraviolet radiation generated in the discharge.

Subsidiary experiments were made to assess the importance of random coincidences which turned out to be negligible. The usual counter tests were applied to individual cylinders and their operation was found to be satisfactory over an overvoltage of 400 volts.

The double coincidences between two cylinders represent besides the showers and the chances, the coincidences due to a photoelectric effect of unabsorbed photons from one section to the other.

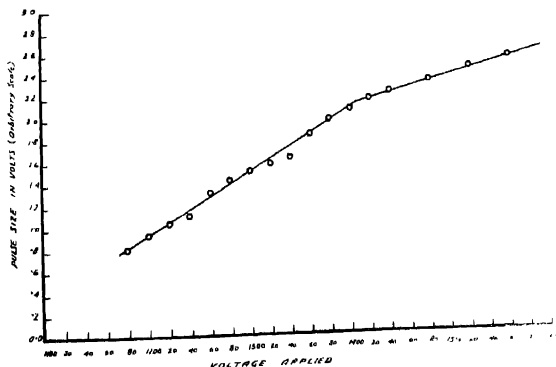


Fig. 2. Pulse size vs voltage applied for soft glass counter.

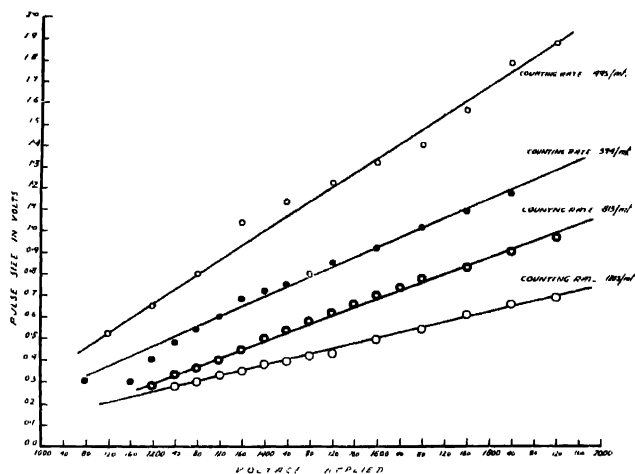


Fig. 3 Pulse size vs voltage applied for Pyrex Maze counters

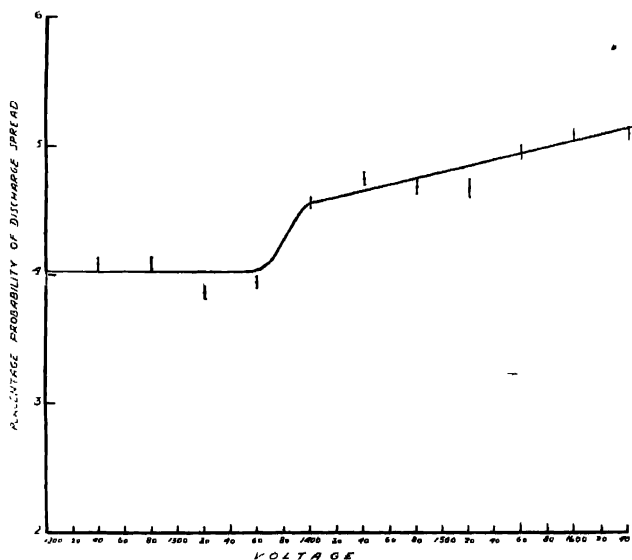


Fig. 4 Discharge spread probability vs voltage for multicathode, single anode counter.

OBSERVATIONS AND DISCUSSION

The curves of figures 2 and 3 give the pulse sizes *versus* overvoltage for the soft glass and pyrex Maze counters respectively. The probability of discharge spread *versus* overvoltage is given in figure 4 for the soft glass counter.

The curve of figure 2 is exactly analogous to the $Q-V$ curve of conventional type, showing that the soft glass envelop has no effect upon the firing and subsequent discharge characteristics of it.

The bend in the discharge spread probability *versus* overvoltage curve, (figure 4,) is coincident with the bend in the pulse size *versus* overvoltage at the same overvoltage of 200 volts. Moreover, α begins to increase after this point corresponding to $m = 1$. As the photoelectric contribution from the cathode remains the same throughout the voltage region of the plateau, as shown by the authors, the observed increase can result only from photoionization from the gas since the latter process requires ultraviolet photons for its operation; these may have arisen from the recombination of the positive ions with their counterpart electrons after the point $m = 1$. The recombination loss can set in only at or after the overvoltage corresponding to $m = 1$ where momentarily there is no pull on the electrons, as the electrostatic shielding by the positive ion sheath effectively reduces the field at the wire to zero till the shielding effect gets decreased with the outward motion of the positive ions.

The curves of figure 3 show the following marked deviations in the behaviour of an externally coated pyrex counter, firstly, it shows the intensity dependence of the pulse size, the product $n \frac{dQ}{dV}$ remaining constant, where n is the counting rate and V is the overvoltage, secondly, the bend in the $Q-V$ curve, corresponding to $m = 1$, is absent, upto an overvoltage of 800 volts.

Both these anomalies from the behaviour of conventional counters suggest the lowering of the applied voltage by the opposing e.m.f. set up by the accumulation of the positive ions over the inner surface of the glass wall. It follows from the curves of figure 3 that $n \frac{dQ}{dV} = \text{constant}$. This leads to $nQ = CV$ where C is a constant. The opposing e.m.f. due to the deposition of positive ions, $n \cdot QR = RCV = C_1 V$ where R is the resistance of the glass envelop and C_1 is another constant. Thus the opposing e.m.f. due to the deposition of positive ions varies linearly with the overvoltage and the point corresponding to $m = 1$ is never reached.

The percentage of α *versus* overvoltage is plotted in figure 5 at three distances between the cathodes, between which the coincidences were studied. It follows from the curves of figure 5 that

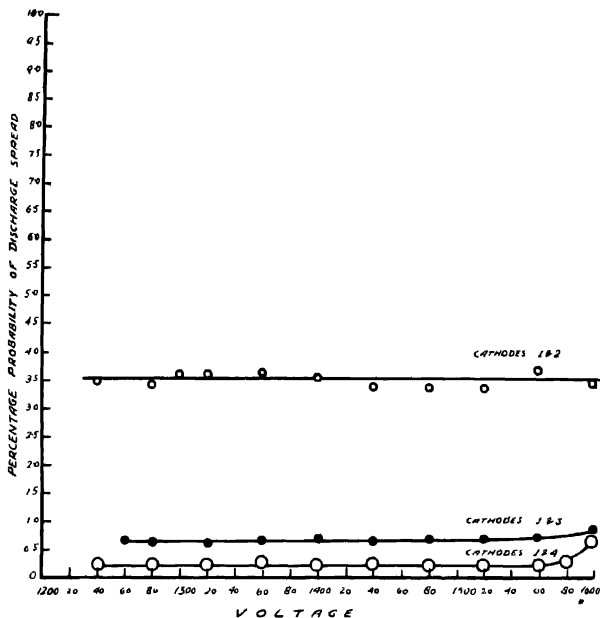


Fig. 5 Discharge spread probability vs. voltage for multicathode, segmented counter.

- (i) the value of α keeps the same steady value throughout the plateau length of 400 volts,
- (ii) the value of α decreases with distance between the cathodes.

As the voltage is increased, the ultraviolet photons generated per avalanche increases. As the photons are generated either from de-excitation or recombination, both these processes become more probable as the overvoltage is increased. These ultraviolet photons are highly absorbable. Along the wire, however, they cause the stepwise propagation of discharge. The absorption coefficient as measured by Alder *et al* (1947) gave the value 640 cm^{-1} , which simply means that in a counter with an admixture of 15mm Hg of alcohol, the number of photons have sunk down to $1/e$ of their original flux, after 0.8 mm of the path. As the photons form in the immediate neighbourhood of the wire, they are practically completely absorbed at 5 mm distance from the wire, the distance along the wire which is dead.

The photons which are responsible for the spread of discharge in the present case are not those that are readily absorbable, but those to which the filling gas is transparent. These photons being less energetic cannot ionize the gas, but can

liberate the electrons from the glass wall. Thus those discharges which result by such photons across a space of 5 mm. have photoelectric origin. The present observations indicate that the probability of generation of such photons remains constant throughout the plateau length, as obvious from the constant value of α . The value of α falls with distance across the two active cathodes, since photons are subject to an exponential absorption by the filling gases. The glass wall of the external cathode counter gives rise to a photoelectric effect.

The absorption of ultraviolet radiation through photoionization of the gas is the predominantly effective process responsible for discharge spread. The photoelectric contribution continues to be feeble throughout the plateau length.

ACKNOWLEDGMENTS

One of the authors (S.P.P.) is grateful to the National Institute of Sciences of India for the award of I.C.I. Research Fellowship. The authors are thankful to Mr. Ajit Singh for constructing the counters.

REFERENCES

- Alder F. *et al.*, 1947, *Helv. Phys. Acta*, **20**, 73.
 Balakrishnan, C. and Craggs, J. D., 1950, *Proc. Phys. Soc.* **63**, 1, 358.
 Coll, L. and Facechi, U., 1954, *Phys. Rev.* **96**, 1.
 Coll, L. *et al.*, 1954, *J. App. Phys.* **25**, 429.
 Craggs, J. D. and Jaffe, A. A., 1947, *Phys. Rev.* **72**, 784, *Nature* **159**, 360.
 Curran, S. C. and Rae, E. R., 1947, *J. Sci. Inst.* **24**, 233.
 Fenton, A. G. and Fuller, E. W., 1949, *Proc. Phys. Soc.*, **62**, 4, 32.
 Hubber, E., 1955, *Phys. Rev.* **97**, 267.
 Meek, J. M., 1940, *Phys. Rev.* **57**, 722.
 Puri, S. P. and Gill, P. S., 1956, *Ind. Jour. Phys.* **30**, 62.
 Steyer, H. G., 1942, *Phys. Rev.* **61**, 38.
 Wilkening, M. H. and Kaune, W. R., 1942, *Phys. Rev.* **62**, 531.
 Wilkinson, D. H., 1948, *Phys. Rev.* **74**, 1417.
 Yasin *et al.*, 1951, *Ind. J. Phys.* **25**, 182.

ON THE X-RAY DIFFRACTION PATTERN AND MICELLER DIMENSIONS OF SOME SUBSTITUTE OF JUTE FIBRE

S. K. CHOWDHURY

TECHNOLOGICAL RESEARCH LABORATORIES, INDIAN CENTRAL JUTE COMMITTEE,
TOLLYGUNGE, CALCUTTA-40

(Received for publication, June 5, 1957)

Plates XIII

ABSTRACT. The X-ray diffraction patterns of Mesta, Abutilon, Dhanchya and Altissima fibres used as jute substitute have been studied in detail. The intrinsic strength and the dimensions of the micelles in these fibres have been determined and it has been observed that they are practically of the same order of magnitude as those in jute. Of these, Dhanchya fibres having higher average intrinsic strength have greater micellar length and this is in agreement with the conclusion obtained by Chowdhury and Sirkar (1948). The orientation of the crystallites of Mesta and Altissima fibres, about the fibre axis, have been found to be the same as that of jute fibre, whereas Abutilon has a poorer orientation. In the case of Dhanchya the orientation seems to be better than that of jute.

INTRODUCTION

Next to cotton, jute is the most widely used fibre in the world. From technological point of view the bast fibres, Mesta (*Bimlipatam jute*, *Hibiscus Cannabinus*), Altissima (*Hibiscus sabdariffavar altissima*), Abutilon (*Abutilon Indicum*) and Dhanchya (*Sesbania Aculeata*) are the nearest approach to jute fibres, so far as their yarn quality-ratios, intrinsic strengths and other spinning qualities are concerned.

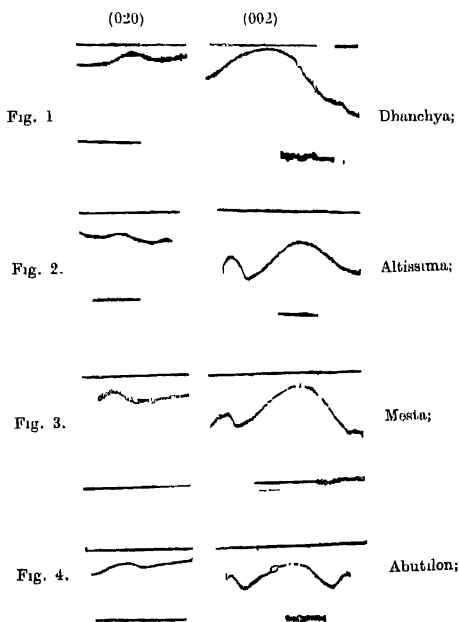
Banerjee and Roy (1941), Sirkar, Saha and Rudra (1944), Chowdhury and Sirkar (1948) determined the size of micelles in jute fibre and Chowdhury (1955) observed some correlation between the intrinsic strengths and lengths of the micelles, in the directions of the fibre axis. It is not known, however, whether any such relation exists in the case of other bast fibres mentioned above, on whose X-ray diffraction pattern no work has yet been done.

The present investigation was, therefore, undertaken to find out the width and length of the micelles and whether there is any correlation between the length of the micelles and the intrinsic strength of the fibres, in the case of the four bast fibres mentioned above. The wide angle X-ray diffraction pattern and orientation of the micelles with respect to the fibre axis of these substitute fibres were also compared with those of jute fibres.

EXPERIMENTAL

The middle portion of all the fibres were taken and well-dried after proper washing with water. The cleaned fibres were separated as far as possible into individual filaments by proper combing and splitting. The intrinsic strength or the substance strength of the fibres were determined by breaking a bundle of fibres weighing 4 mg/cm and containing approximately 100 to 200 filaments depending on the nature of the fibre. Single thread strength testing machine with a special clamp was used for the purpose. The distance between the two jaws of the clamps was kept at 7.5 cm. Strength of the bundle (F) divided by its weight (M) per unit length gave the intrinsic strength of the fibre.

X-ray diffraction photographs of intensities suitable for photometry of all the samples were taken in a flat-film type camera, with a narrow slit of diameter 0.2 mm bore and length 5 cm. CuK radiation filtered by nickel-foil from a Hadding type X-ray tube was used. X-rays were incident normal to the length of a narrow bundle of fibres each containing 12 to 15 strands made parallel by combing. These



Microphotometric records of the interference spots due to (020) and (002) reflecting planes. (magnification = 8)

strands were collected from the same regions of samples wherefrom were obtained the filaments for determining the intrinsic strengths. Experimental conditions for all the samples were made identical as far as practicable. For each sample two photographs of the X-ray diffraction pattern were obtained, one with such a moderately short exposure that the (002) reflection was not over-exposed and the other with a longer exposure to get sufficient blackening due to the (020) reflection.

Microphotometric records of the (002) and (020) reflections were obtained with a Moll-type self-recording microphotometer and on each record the deflection corresponding to infinite density and the unexposed portion of the film were recorded. The intensity at any point in the spot was determined by first determining the total intensity at that point and then subtracting from it the intensity of the background with respect to the unexposed portion of the film. Care was taken to allow the spot of light focussed on the film to move along the equatorial direction. It was also necessary to draw a density-log intensity curve. This was done by the method explained earlier by Chowdhury and Sirkar (1948). The width and length of the micelles in each case were determined by the usual method from the width of the (002) and (020) reflections at the positions having intensities equal to half of that at maximum. The observed half-widths on the record were reduced to radians by taking into account the magnification of the microphotometer, the value of the Bragg angle for the particular reflection and the distance of the film from the irradiated sample. The values of m which denotes the number of times the unit cell is repeated in different directions, were obtained from Laue's formulae (Laue, 1926) used for rhombic lattice. Although the lattice of cellulose crystallites in these fibres is monoclinic, yet the above equation had been applied, because the monoclinic angle β (82°) is almost equal to 90° . The equation used was, therefore,

$$B \cos \chi_m / 2 = .9\lambda \left(\frac{h^2/m_1^2a^4 + k^2/m_2^2b^4 + l^2/m_3^2c^4}{h^2/a^2 + k^2/b^2 + l^2/c^2} \right)^{\frac{1}{2}}$$

where B is the half intensity width of the (hkl) reflection in radian and χ_m is the angle between the incident and reflected X-rays. m_1 , m_2 and m_3 denote the number of times the unit cell is repeated along a , b and c axes respectively.

$$\text{For (002)} \quad m_3 = \frac{.1777}{B_3}$$

and

for (020) reflection,

$$m_2 = \frac{.1361}{B_2}$$

X-Ray Diffraction Pattern of Substitutes of Jute Fibre 575

where B_3 and B_2 are the half widths of (002) and (020) reflections in radian. Both B_2 and B_3 were corrected for instrument width, according to the technique used earlier by Chowdhury (1955), using Warren's formula (Warren, 1938).

The width and length of the micelles were obtained by multiplying these corrected values of m_3 and m_2 by 7.9\AA and 10.3\AA respectively.

RESULTS AND DISCUSSION

The X-ray diffraction photographs of all the samples studied are reproduced in Plate XIII and the microphotometric records from which the values of the half-widths of the reflections (002) and (020) planes were determined are also reproduced in figures 1—4. The curves were smoothed out while these half-widths were measured. The results obtained are given in Table I. The intrinsic strengths of the substitute fibres as determined and the length and width of the micelles are given in Table II.

TABLE I

Corrected half-widths of (020) and (002) reflections of the samples and the values of m_2 and m_3

Sample studied	B_3 in radian	Corrected B_3	m_3	B_2 in radian	Corrected B_2	m_2
Dhanchya	.05	.048	4	.014	.013	11
Mesta	.04	.038	5	.018	.017	8
Atlissima	.04	.038	5	.016	.015	9
Abutilon	.04	.038	5	.018	.017	8

TABLE II

Width and length of the micelles in the different substitute fibres and the corresponding intrinsic strengths as obtained from bundle test

Sample studied	Width of the micelles in \AA U.	Length of the micelles in \AA U.	Intrinsic strength F/M $10^6 \frac{\mu\text{m}}{\text{gm/cm}}$
Dhanchya	32	113	1.6
Mesta	40	82	1.1
Atlissima	40	93	1.2
Abutilon	40	82	1.0

It can be seen from Table II that the width and length of the micelles of these substitute fibres are practically of the same order of magnitude as those in jute. Of these fibres Dhanchya has the micelle-length 113\AA slightly larger than that in the other fibres. The average intrinsic strength of Dhanchya fibres is also higher than those of other fibres studied and from Table II it can be seen that Mesta and Abutilon fibres of lower intrinsic strength have got smaller micelle lengths. This fact corroborates the conclusion drawn in the case of jute fibres by Chowdhury and Sirkar (1948) that the length of micelle is partly responsible for the strength of the fibres. The width of the micelles, however, seems to be almost the same in all the cases. The X-ray diffraction patterns of all the samples studied and reproduced in Plate XIII are typical cellulose I diagrams with an enhanced background scattering except in the case of Dhanchya. The (101) and (10 $\bar{1}$) reflections are composite as in the case of jute fibre. The number of spots and their positions are identical in all the photographs. Visual examination shows that the orientation of the crystallites about the fibre-axis of Mesta and Altissima is practically the same as that in jute, but Abutilon has a poorer orientation. In the case of Dhanchya fibre the orientation seems to be better than that in jute and the background is so clear that spots on the first layer line appear and for small exposures (101) and (10 $\bar{1}$) reflections are slightly resolved, its X-ray diagram may be compared with that of ramie, a comparatively purer cellulosic fibre.

ACKNOWLEDGMENT

The author is deeply grateful to Prof. S. C. Sirkar, D. Sc., F. N.I. for his generous advice and for providing necessary facilities for the microphotometric work, in his laboratories at the Indian Association for the Cultivation of Science, Jadavpur, Calcutta. He is also indebted to Dr. P. B. Sarkar, D. Sc., F.N.I., Director of the Institute and to Dr. R. K. Sen, D.Sc., for their keen interest and constant encouragement. Thanks are also due to Mr. S. B. Bandyopadhyay, M.Sc., for his help in the strength measurements.

REFERENCES

- Banerjee, K. and Roy, A. K., 1941, *Proc. Nat. Inst. Sc.*, **7**, 377.
Chowdhury, S. K., 1955, *Science & Culture*, **21**, 334.
Chowdhury, S. K. and Sirkar, S. C., 1948, *Ind. J. Phys.*, **22**, 39.
Laue, M. V., 1926, *Z. Krist.*, **64**, 115.
Sirkar, S. C., Saha, N. N. and Rudra, R. M., 1944, *Proc. Nat. Inst. Sc.*, **10**, 325.
Warren, 1938, *J. Am. Ceram. Soc.*, **21**, 49.

Fig. 1.

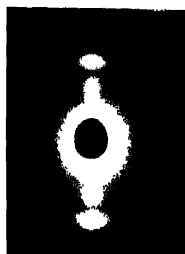


Fig. 2.

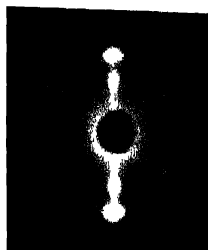


Fig. 3.

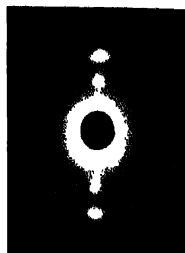


Fig. 4.

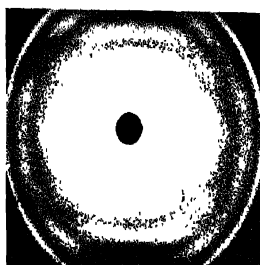
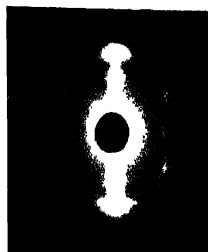


Fig. 5.

X-Ray diffraction photographs

Fig. 1 Dhanchya.

Fig. 2. Altissima

Fig. 3 Mesta

Fig. 4. Abutilon

Fig. 5. Raw jute fibre
mixed with Al-powder.

ABSORPTION SPECTRA OF CHLOROANILINES

P. B. V. HARANATH AND K. SREE RAMAMURTHY*

PHYSICS DEPARTMENT, ANDHRA UNIVERSITY, WALTAIR

(Received for publication, December 8, 1956).

Plate XIV A & B

ABSTRACT. The absorption spectra of the three isomers meta, ortho and para chloroanilines have been photographed in the ultraviolet region under different experimental conditions. The ortho bands are diffuse and fragmentary, whereas the meta isomer gives a large number of sharper bands, as distinct from the other similar cases where the reverse is the case. All the intense bands in the spectrum of the para substance are double headed with a separation of about 18 cm^{-1} , each of these heads consisting of complexes of close lying band heads in intervals of about 10 cm^{-1} , giving the appearance of a rotational structure as in dibromobenzene.

Band heads are measured and analyses are tentatively suggested on the basis of a number of upper state frequencies as enumerated below :

<i>Isomer</i>	<i>0, 0 band</i>	<i>Upper state frequencies</i>
Meta chloroaniline	33661	272, 488, 761, 958, 1157, 1240, 1448, 1883, 2015, 2116
Ortho chloroaniline	33650	155, 261, 343, 493, 611, 818, 998, 1300.
Para chloroaniline	32578	290, 356, 762, 809, 948.

In each case a number of ground state frequencies are identified on the red side of the 0, 0 band, which are compared with the Raman data. A few interesting remarks on the correlation of the frequencies have been made.

INTRODUCTION

Among the disubstituted benzene derivatives so far investigated a considerable number possess a halogen atom at least as one of the substituents, namely dichloro benzenes, dibromo benzenes, fluoro benzenes, chloro toluenes, bromo toluenes, etc. Chloroanilines also belong to this type of molecules. The substitution is by a chlorine atom and a NH_2 radical in the three different isomer positions meta, ortho and para. The experimental investigation on these three derivatives, the results obtained and their interpretation are reported in this paper.

EXPERIMENTAL

For the meta and ortho isomers which are liquids at laboratory temperature, the same experimental technique reported in the case of 3-chlorothionaphthene

* Now in the Department of Physics, Sri Venkateswara University, Tirupati.

by the authors (1954), is adopted. For the para isomer which is a solid at laboratory temperature, a simpler arrangement is adopted which avoids the need of maintaining the container and the absorption column at different temperatures. A small quantity of the pure recrystallised substance itself is contained in a quartz to pyrex absorption tube which is evacuated and sealed. For higher temperatures the tube is mounted inside a coaxial heating coil wound over an outer pyrex tube. The windows of the absorption tube are heated by separate heating coils in order to prevent the condensation of the substance on them. The spectra are photographed on Hilger medium quartz spectrograph using Hilger low voltage hydrogen arc lamp fed by stabilized power unit, as the source of continuous ultraviolet radiation. Table I indicates the type of study of the three spectra under different experimental conditions.

TABLE I

Isomer	Length of the column	Temperature range °C	Region of the spectrum Å ^u	Plate	0, 0 band cm ⁻¹	Shift from benzene 0,0 cm ⁻¹
Meta chloro-aniline	35cm	0 to 100	3020--2790	XIVA	33661	4428
Ortho chloro-aniline	40cm	30 to 100	3010 -2860	XIVA	33650	4439
Para chloro-aniline	50cm	30 to 120	3119--2958	XIVB	32578	5511

META CHLOROANILINE

The molecule meta chloroaniline, $m\text{-ClC}_6\text{H}_4\text{NH}_2$, has one element of symmetry, namely, the plane of the molecule σ_h , assuming NH_2 as a single atom and whole molecule planar. Then the molecule belongs to the point group C_s . From an application of group theory, twentyfive A' vibrations and eleven A'' vibrations belonging to symmetrical and antisymmetrical classes respectively are possible. In view of the lowering of the symmetry of the molecule, the selection rules of the transition in benzene no longer hold good, and the near ultraviolet band system should show the characteristics of an allowed transition. Restrictions on the permissibility of the appearance of certain vibrations become less. Consequently, this spectrum should exhibit a complicated appearance. This is evident from Plate XIV. The spectrum represents the electron transition $A' \rightarrow A'$. It contains a larger number of sharper bands degraded towards red. About 95 bands are measured and the wavenumber and assignment data of the bands are given in Table II.

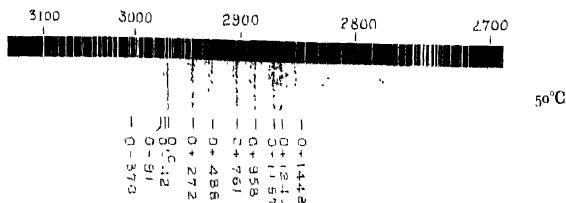


Fig. 1

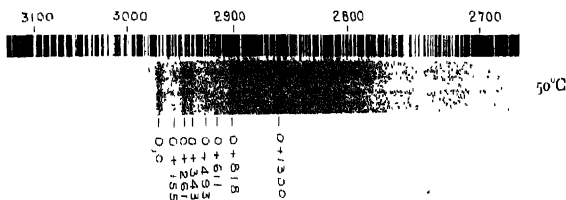


Fig. 2

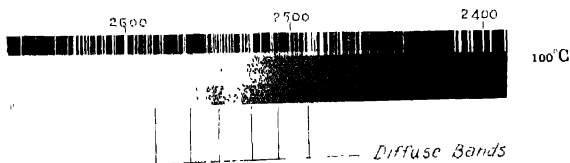


Fig. 3

Fig. 1. Absorption spectrum of meta-chloroaniline

Fig. 2 & 3. Absorption spectrum of ortho-chloroaniline.

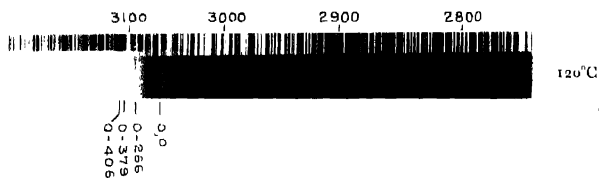


Fig. 4

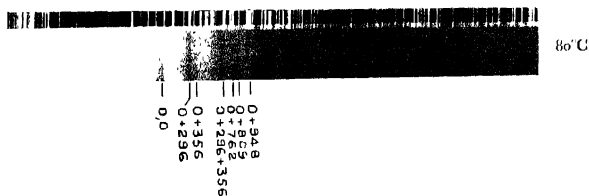


Fig. 5

Fig. 4 & 5. Absorption spectrum of para-chloroaniline.

The 0,0 band is located at $\nu 33661$. It is the most intense and persists to appear even at the lowest temperature of the container and the shortest path lengths. This is accompanied on the red side, apart from others, by two bands separated from this by 42 and 91 cm^{-1} which give a characteristic appearance to the group. This repeats with all other intense bands on the violet side. A frequency of 131 cm^{-1} occurs superposed on some of these bands. These may represent $\nu-\nu$ transitions. The band at $\nu 33474$ on the red side of the 0,0 band with a frequency difference 187 cm^{-1} corresponds to the Raman frequency (193). Taking fairly intense bands on the violet side which are accompanied by the above mentioned pattern, as representing distinct vibrations, the following have been identified as the upper state frequencies: 272, 488, 761, 958, 1157, 1240, 1448, 1883, 2015, 2116. Some of these frequencies are correlated with the Raman frequencies (Kohlransch and Pongratz, 1935). This correlation is shown in the assignment column of Table II where the Raman frequencies are represented by 'R'. Out of the above upper state frequencies 958 and 1157 probably represent totally symmetric carbon vibrations. 761 gives a fairly strong band at $\nu 34422$. A frequency of this order (762), in the case of other similar molecules e.g. in para chlorotoluene is assigned to the totally symmetric C-Cl valence vibration. No other frequency is observed in this region.

The benzene e_g^+ (606) vibration, which splits up in the substituted molecules, is known to give two components, one totally symmetric and the other nontotally symmetric in the case of all mono-substitutions which belong to the symmetry class C_{2v} . The nontotally symmetric component is not supposed to alter much in frequency and is independent of the nature of the substitution. The other is strongly influenced and hence changes in magnitude considerably. In the disubstituted benzenes the influence of the substituents on each of the components may be quite large and both may differ from 606. Further, in molecules belonging to C_s symmetry this benzene e_g^+ vibration splits into two components which are both totally symmetrical, unlike the splitting in other disubstitutions of the C_{2v} type of symmetry.

488 and 272 may be the two components 530 and 408 in the ground state. Regarding the difference frequencies 42, 91 and 131 the following correlations of the vibrations in the two states may be noted. 530 with 488 gives a difference of 42 and 408 with 272 gives a value 136.

All the intense bands are observed to be double headed and the components are bracketed in Table II. The components are separated by an average interval of about 5 cm^{-1} . This feature is reported earlier in some other substances, both singly and doubly substituted molecules, namely, aniline, chlorotoluenes, bromotoluenes etc.

TABLE II

Wavenumber	Intensity	Separation from 0,0	Assignment
33083	vw	578	
33122	w	539	
33141	vw	520	
33197	vw	464	
33233	vw	428	
33240	vw	421	
33286]	vw bd	375	0-370
33291]	w	370	
33335	w	326	
33386	w	275	
33433]	m	228	0 226, 0 131-91
33435]	m	226	
33474	m st	187	0-193 (R)
33489	mw	172	0-131 42
33526]	m	135	0-131, 0-91-42
33530]	m st	131	
33560]	m st	95	0-91
33570]	st	91	
33579	w	82	0-2 x 42
33616]	m st	45	0-42
33619]	st	42	
33658]	st	3	0, 0
33661]	v st	0	
33712	w	51	
33749	w	88	0+272-131-51
33799	w	138	0+272-131
33834	vw	173	
33846	m st	185	+272-91, 193 (R)
33864]	vw	203	
33868]	vw	207	
33893]	m st	232	0+272-42, 244 (R)
33895]	m st	234	
33930]	st	269	0+272
33933]	st	272	
33949	vw	288	
33956	w	295	
33970	vw	309	
33999]	vwv	338	
34002]	vwv	341	

TABLE II (contd.)

Wavenumber	Intensity	Separation from 0,0	Assignment
34057	m	396	
34066	vw	405	0 + 488 - 91
34106)	m bd	445	0 + 448 - 2 x 42, 408 (R)
34108)	m bd	447	
34119	m st	458	0 + 488 - 42
34145)	st	481	
34149)	st	488	0 + 488, 530 (R)
34208	w bd	547	
34245	w bd	584	0 + 2 x 272
34293	m st	632	
34327	m st	666	0 + 761 - 91, 694 (R)
34344	m	683	
34384	m st	723	0 + 761 - 2 x 42
34418)	st	757	0 + 761 - 42
34422)	st	761	0 + 761, 771 (R)
34443	vvw	784	
34488	w	829	0 + 958 - 131
34527	m	866	
34557	m	896	0 + 958 - 91
34577	m	916	0 + 958 - 42
34616)	st	955	
34619)	st	958	0 + 958, 990 (R)
34655	vw bd	994	0 + 761 + 272 - 42
34690)	m	1029	
34693)	m	1032	0 + 761 + 272, 1072 (R)
34735	w bd	1074	
34746	w bd	1085	0 + 1157 - 2 x 42
34776	m bd	1115	0 + 1157 - 42
34814)	m bd	1153	
34818)	m bd	1157	1157, 0 + 1240 - 2 x 42, 1207 (R)
34856	m bd	1195	
34891	m st bd	1230	0 + 1240 - 42
34901	m st	1240	
34965	m bd	1304	0 + 1240, 1300 (R)
34991	vw	1330	
35011	w	1350	0 + 1448 - 91
35060)	w	1399	
35064)	w	1403	0 + 1448 - 42

TABLE II (*contd.*)

Wavenumber	Intensity	Separation from 0,0	Assignment
33109 35116	m vw	1448 1455	0 + 1448, 1597 (R)
35164 35201	vw w	1503 1510	
35374 35451	w bd w	1713 1790	0 + 958 + 761 0 + 1883 - 91
35462 35506	w w	1801 1815	0 + 1883 - 2 + 42 0 + 1883 - 42
35544 35592	w w	1883 1931	0 + 1883 0 + 2015 - 2 + 42
35636 35676	w w	1975 2015	0 + 2015 - 42 0 + 2015
35700 35738	w w	2039 2077	0 + 2116 - 2 + 42 0 + 2116 - 42
35777 35821	mw mw	2116 2163	0 + 2116

ORTHOCHLOROANILINE

Unlike the meta spectrum, this contains a small number of very diffuse bands superposed by a fairly strong continuum. This feature is contrary to the observation made in the other similar molecules, ortho chlorotoluene (Viswanath, 1953), ortho chlorophenol (Ramasastry, 1951) where the corresponding spectra contained a large number of bands sharper than the meta isomer. About twenty band heads are measured and an analysis is suggested in the last column of Table III.

Orthochloroaniline, like the meta isomer, belongs to the symmetry class C_s , but differs in the direction of migration moment, and it is expected to possess all the characteristics of the group C_s . The band at ν 33650 is taken as 0,0. The band on the red side at ν 33283 giving a frequency value 367 is correlated to the Raman frequency 372. From the analysis, the following upper state frequencies are identified on the violet side of the 0,0 band - 155, 261, 343, 611, 818, 998, 1300. These upper state frequencies are compared with the ground state frequencies reported in Raman effect (Herz, 1943), in the assignment column of Table III.

An observation to be noted is a set of a few diffuse bands at about λ 2580. These are followed on the violet side by strong continuum. The wavelengths of these are estimated as

$$\lambda \text{ 2580, 2555, 2545, 2525, 2500 and 2480.}$$

These bands are indicated in Plate XIVA & B. These may relate to a system corresponding to the $\lambda 2400$ system of benzene

PARA CHLOROANILINE

The spectrum in the first photographs contained also the bands characteristic of the meta isomer at the violet end. Thorough purification of the substance and careful manipulation of the experimental conditions resulted in their elimination. In general, the spectrum resembles that of para dibromobenzene or para dichlorobenzene rather than any other similar molecules, para chlorotoluene, para chlorophenol. The band head data and their assignment are represented in Table IV.

Parachloroaniline is a disubstituted derivative of benzene obtained by a substitution of a chlorine atom and the NH_2 radical in the para position. This possesses an axis of symmetry along the para positions in addition to the operations characteristic of the other two isomers. The symmetry is hence reduced and the molecule belongs to the symmetry class C_{2v} . The spectrum corresponds to the allowed electronic transition $A_1 \rightarrow B_1$. It is expected to show the forbidden part also to a greater extent than the other two isomers.

The 0,0 band is represented by the band at $\nu 32578$. Though the band at $\nu 32874$ is the most intense in the spectrum (0 + 296) this is adopted, since it persists even at low temperatures and facilitates the analysis. This feature is reported earlier in a number of cases, dibromobenzene, para xylene, etc. Each strong band is accompanied by a satellite of almost equal intensity on the red side by an average separation of about 18 cm^{-1} . These components are bracketed in Table IV. On the red side of the 0,0 band a number of bands giving frequencies which correspond to the Raman frequencies are observed. Over almost all of those, two small frequencies 45 and 84 appear as progressions and combinations. These may be the $\nu-\nu$ transitions. Bands on the violet side are interpreted in terms of five upper state frequencies namely, 296, 356, 762, 809 and 948. The ground state frequencies which can be probably associated with these upper state frequencies and the Raman frequencies are collected in Table V., which includes the polarization data as well. This data is obtained from Kohdrausch and Paulsen (1939).

A few remarks may be made regarding the frequencies observed. Combinations between frequencies are frequent, whereas overtones are rare. The carbon vibrations at about 1000 cm^{-1} are found to be very weak, if at all they appear in that region. 948 probably represents one such. 762 is suggested as one frequency, since it compares well with the value of C-Cl valence vibration of other similar molecules. In some cases it is observed with similar faintness.

TABLE III

Wavenumber	Intensity	Separation from 0, 0	Assignment
33208	vw	442	
33232	vvw	418	
33283	vw	367	0-367 (372 R)
33300	vvw	350	
33338	vw	312	
33428	vvw	222	
33445	vw	205	
33503	w	147	
33519	mw	131	
33540	w	110	0-367+261
33619	st	31	
33650	v st	0	0,0
33699	vw	49	
33798	w	148	
33805	m	155	0+155
33834	vvw	184	
33911	st	261	0+261 (261 R)
33993	m st	343	0+343 (372 R)
34002	m	352	
34143	m	493	0+493 (559 R)
34261	m	611	0+611 (677 R)
34334	vvw	684	0+2×343
34423	w	773	
34468	st	818	0+818 (836 R)
34523	w	873	0+611+261
34648	w	998	0+998 (1023 R)
34888	w	1238	
34950	m st	1300	0+1300 (1305 R)

TABLE IV

Wavenumber	Intensity	Separation from 0, 0	Assignment
31750	w	828	0-828 (829 R)
31770	vvw	808	
31795	vvw	783	0-697-84
31836	vvw	742	0-697-45
31881	w	697	0-697 (705 R)
31894	w	684	

TABLE IV (contd.)

Wavenumber	Intensity	Separation from 0, 0	Assignment
31007	mw	671	0-632-15
31925	mw	653	
31946	w	632	0-632 (637 R)
31977	vw	601	
31994	vw	584	
32039	vw	539	0-406-84-45
32051	vw	527	
32073	vw	505	
32089	mw	489	0-405-84
32103	mw	475	
32123	mw	455	0-406-45
32134	mw	444	
32153]	m	425	
32172]	m	106	0-406 (407 R)
32184]	w	394	
32199]	w	379	0-379 (379 R)
32236	m	342	
32239	m	339	0-4 x 81
32246]	w	332	
32264]	w	314	0-314 (318 R)
32300]	vw	278	
32312]	vw	266	0-266 (268 R)
32324	vvw	254	
32327	vvw	251	0-3 x 84
32348	vvw	230	
32357	vvw	221	0-142-84
32370	w	208	
32382]	w	196	
32399]	w	179	
32407	w	171	0-2 x 84
32415	w	163	
32425	w	153	
32436	mw	142	0-142 (145 R)
32450	mw	128	0-84-45
32479]	m	99	
32494]	m	84	0-84
32517]	m	61	
32533]	m	45	0-45
32561]	st	17	
32578]	st	0	0, 0

Wavenumber	Intensity	Separation from 0, 0	Assignment
32630	w	52	
32661	w	83	
32796	w	218	0 + 296 - 84
32853	st	275	0 + 356 - 84
32874	v st	296	0 + 296
32914	m	336	
32934	m	356	0 + 356
33149	w	571	0 + 356 + 296 - 84
33216	m st	638	
33233	m st	665	0 + 356 + 296
33298	w	720	0 + 809 - 84
33340	w	762	0 + 762
33370	w	792	
33387	mw	809	0 + 809
33431	w	853	
33476	w	898	
33526	vw	948	0 + 948
33676	w	1098	0 + 809 + 296
33707	vw	1129	
33739	mw	1161	0 + 809 + 356
33757	mw	1179	
33794	w	1216	

TABLE V

Raman fre- quencies	Depolarization factor	Ground state u. v. Abs	Upper state u. v. Abs.
145		142	
268		266	
318	1.01	314	296
379	0.41	370	356
407	(0.98)	406	
637	0.55	632	
705		697	762?
828	0.10	828	809
889			
939			
1002	0.24		948
1090 (o)	0.11		
1092 (ef)	0.34		

An examination of the difference between the upper and lower state frequencies, suggests a correlation of 84 with 379–296. It is interesting to note that 828–809 is 19 which is the average separation of the components of the intense bands, as remarked earlier.

Further, all intense bands are complexes of close lying bands in intervals of about 10 cm^{-1} giving the appearance of rotational structure. This phenomenon is observed in para dibromobenzene as well.

REFERENCES

- Horz, 1943, *Mh. Chem.*, **76**, 1.
Kohlrausch and Paulsen, 1939, *Mh. Chem.*, **72**, 268.
Kohlrausch and Pongratz, 1935, *Mh. Chem.*, **65**, 199.
Ramaswamy, 1951, *Pro. Nat. Inst. Sci. India*, **17**, 349.
Sree Ramamurthy, K. and Hanumanth, P. B. V., 1954, *Pro. Nat. Inst. Sci. India*, **20**, 318.
Viswanath, G., 1953, Thesis for D. Sc. degree of Andhra University.

ULTRAVIOLET ABSORPTION SPECTRA OF 1, 3, 5-TRICHLOROBENZENE AND 1, 3, 5-TRIMETHYLBENZENE IN DIFFERENT SOLVENTS AND AT DIFFERENT TEMPERATURES*

S. B. ROY

OPTICS DEPARTMENT, INDIAN ASSOCIATION FOR THE CULTIVATION OF
SCIENCE, JADAVPUR, CALCUTTA.

(Received for publication, August 6, 1957)

ABSTRACT The ultraviolet absorption spectra of solutions of 1, 3, 5-trichlorobenzene and 1, 3, 5-trimethyl benzene, in isobutyl alcohol, CCl_4 , CHCl_3 and cyclohexane in the liquid state and those of frozen solutions in isobutyl alcohol at -180°C have been investigated. The forbidden 0, 0 band is found to appear with moderate intensity in the spectra due to the solution in isobutyl alcohol, both in the liquid and in the solid state. The 0, 0 band also appears weakly in the spectra due to solutions of 1, 3, 5-trichlorobenzene in chloroform and cyclohexane and in those due to solutions of 1, 3, 5-trimethyl benzene in chloroform and carbon tetrachloride. The 0, 0 band, however, is absent in the spectra due to solutions of 1, 3, 5-trichlorobenzene in carbon tetrachloride and in the spectra due to the solution of 1, 3, 5-trimethyl benzene in cyclohexane.

It is concluded from the results that the symmetry of the molecule is disturbed owing to the formation of weak bonds between the chlorine atom of one molecule and hydrogen atom of the neighbouring molecule.

INTRODUCTION

The near ultraviolet absorption spectra of solutions of the trichlorobenzenes and 1, 3, 5-trimethyl benzene in hexane were first studied by Conrad-Billroth (1932) and later by Wolf and Strasser (1933). The absorption coefficients of these substances, except those of 1,2,4-trichlorobenzene, were found to have small values like that of benzene under similar conditions. They did not, however, analyse those absorption spectra.

The ultraviolet absorption spectrum of 1,3,5-trichlorobenzene in the vapour state was first analysed by Sponer and Hall (1948). They pointed out that as the molecule possesses the symmetry of the point group D_{3h} , the ultraviolet electronic transition $A'_1 - A'_2$ corresponding to $A_{1g} - B_{2u}$ in benzene with the symmetry D_{6h} , is forbidden and so the 0,0 band in the spectrum due to 1,3,5-trichlorobenzene in the vapour state should not appear. They ascribed the first strong band at 35869 cm^{-1} to $0 \rightarrow 1$ vibrational transition coupled to the electronic

* Communicated by Prof. S. C. Sirkar.

transition and a much weaker band at 35073 cm^{-1} to such a coupling of the $1 \rightarrow 0$ transition. The position of the forbidden $0,0$ band was calculated and found to be at 35498 cm^{-1} . Recently, Banerjee (1957) has observed that in the electronic spectra of 1,3,5-trichlorobenzene in the solid state at -180°C the forbidden $0,0$ band appears with weak intensity. He concluded that the three-fold axis of 1,3,5-trichlorobenzene is destroyed in the solid state at -180°C . It has been pointed out by Banerjee (1957) that probably formation of intermolecular bonds may be responsible for the deterioration of symmetry of the molecule in the solid state.

The hypothesis put forward by Banerjee (1957) could be tested by studying the influence of environment on the absorption spectrum of the molecule. The object of the present investigation was to study the influence of the field due to molecule of different solvents on the absorption spectra of solutions of 1,3,5-trichlorobenzene in liquid and solid states.

Spencer and Stallecup (1948) also analysed the absorption spectrum of 1,3,5-trimethyl benzene in the vapour state and the $0,0$ band was found to be absent, as in the case of 1,3,5-trichlorobenzene. Sen (1957) has observed that in this case also the $0,0$ band appears when the substance is frozen and cooled to -180°C . This molecule does not contain any chlorine atom and therefore, it would be interesting to find out whether different environments have the same influence on the absorption spectra in this case as in the case of 1,3,5-trichlorobenzene. The absorption spectra of solutions of 1,3,5-trimethyl benzene in different solvents have, therefore, been studied to find out the influence of different environments on the spectra.

EXPERIMENTAL

The experimental arrangement in the present investigation was the same as that described in a previous communication (Roy, 1956). Chemically pure samples of 1,3,5-trichlorobenzene obtained from Eastman Kodak Co., N. Y. and of 1,3,5-trimethyl benzene (mesitylene) from B D H. were used in the present investigation. The solvents used were isobutyl alcohol, CCl_4 , CHCl_3 and cyclohexane. The purity of the solvents were tested by studying their ultraviolet absorption spectra. The 1,3,5-trichlorobenzene was recrystallised from the solution in ether and the other liquids were distilled under reduced pressure before use. The absorption cell used was similar to that described in an earlier paper (Roy, 1956) and was 3 mm. thick in this case. The concentration of the solution was .01% by weight in each case. Spectrograms were obtained with a Huger medium quartz spectrograph. An iron arc spectrum was used for comparison. The frequencies of the absorption bands were measured with the help of microphotometric records explained earlier (Roy, 1956).

RESULTS

The microphotometric records of the spectra are reproduced in figures 1 and 2 and the wave number of the bands with approximate intensities and probable assignments are given in Tables I—IV.

DISCUSSION

1. 3, 5-Trichlorobenzene :

It can be seen from Table II and figure 1(a) that the first strong band at 35782 cm^{-1} in the spectrum due to the .01% solution in isobutyl alcohol in frozen state at -180°C is accompanied by two much weaker bands on the long wavelength side at distances 370 and 791 cm^{-1} respectively. If this strong band at 35782 cm^{-1} were assumed to be due to 0,0 transition, then distances 370 and 791 cm^{-1} of the two bands on the red side would represent ground state vibration frequencies. The band at the distance 370 cm^{-1} would then represent $1\rightarrow 0$ vibrational transition of a particular mode and in that case we would expect a stronger band on the short wavelength side at a distance less than 370 cm^{-1} due to the corresponding $0\rightarrow 1$ transition. As no such band is observed, the band at 35782

TABLE I
Absorption spectra of 1,3,5-trichlorobenzene at 30°C

.01% Solution in carbon tetrachloride	01% Solution in cyclohexane	01% Solution in chloroform	01% Solution in isobutyl alcohol	Assignment
ν in cm^{-1}	ν in cm^{-1}	ν in cm^{-1}	ν in cm^{-1}	
35665 (s)	34950 (vw)	34845 (vw)	34979 (vw)	0—421
36051 (w)	35372 (vw)	34263 (vw)	35400 (w)	0, 0
36619 (vs)	35742 (s)	35663 (s)	35770 (s)	0+370
37639 (s)	36129 (w)	36010 (w)	36142 (w)	0+742
	36609 (s)	36600 (s)	36370 (m)	0+970
	7767 (s)	37570 (s)	36521 (m)	0+1121
	38420 (vw)		36736 (vs)	0+370+970
	38733 (vw)		37710 (m)	0+370+970 $\times 2$
			37857 (m)	0+370+970+1121
			38600 (vw)	0+370+970 $\times 3$
			38970 (vw)	0+370 $\times 2$ +0 $\times 970$

TABLE II
 Absorption spectra of 1,3,5-trichlorobenzene

Vapour (Sponer and Hall, 1948)	Frozen solution in isobutyl alcohol at -180°C	
	0.1%	
ν in cm^{-1} (prominent bands)	ν in cm^{-1}	Assignment
35073 (ms) $1 \rightarrow 0$	34991 (vs)	$0 \rightarrow 421$
35498 (calculated 0, 0)	35412 (m)	0, 0
35869 (vs) $0 \rightarrow 1$	35782 (s)	$0 \rightarrow 370$
36742 (vs)	36155 (m)	$0 \rightarrow 370 + 2$
36774 (sd)	36372 (w)	$0 \rightarrow 970$
36832 (vs)	36458 (w)	$0 \rightarrow 1046$
36904 (sd)	36533 (w)	$0 \rightarrow 1121$
36993 (sd)	36752 (s)	$0 \rightarrow 370 + 970$
	36903 (s)	$0 \rightarrow 1491$
	37273 (w)	$0 \rightarrow 370 + 1491$
	37722 (m)	$0 \rightarrow 370 \rightarrow 970 + 2$
	37865 (s)	$0 \rightarrow 1491 + 970$
	38464 (m)	$0 \rightarrow 3 \rightarrow 370 + 2 \rightarrow 970$
	38914 (m)	$0 \rightarrow 1491 \rightarrow 970 + 1046$

cm^{-1} cannot be the 0,0 band. In the spectrum due to the vapour the 0,0 band is forbidden (Sponer and Hall, 1948) and the first strong band is due to a $0 \rightarrow 1$ vibrational transition coupled to the electronic transition. So, the first strong band at 35782 cm^{-1} corresponds to a similar $0 \rightarrow 1$ transition in the present case. In the spectrum due to .01% solution at low temperature an extra weak band at 35412 cm^{-1} is observed at a distance 370 cm^{-1} on the longer wavelength side of the band at 35782 cm^{-1} . If this band at 35412 cm^{-1} is taken as the 0,0 band in the present case, the strong band at 35782 cm^{-1} has to be assigned as $0 \rightarrow 1$ vibrational transition and in that case the weak band at 34991 cm^{-1} would be due to the corresponding $1 \rightarrow 0$ transition of ground state frequency 421 cm^{-1} . Sponer and Hall (1948) also observed such a weak band at a distance of 796 cm^{-1} on the red side of the first strong band and a similar assignment was made. So, it appears that in the spectrum due to .01% solution in isobutyl alcohol at low temperature, the 0,0 band is not totally forbidden, but it appears with weak intensity. When the spectrum is analysed with the band at 35412 cm^{-1} as the 0,0 band, a progression of frequencies $370, 970, 1046, 1121$ and 1491 cm^{-1} is obtained and it is similar to that observed in the case of vapour.

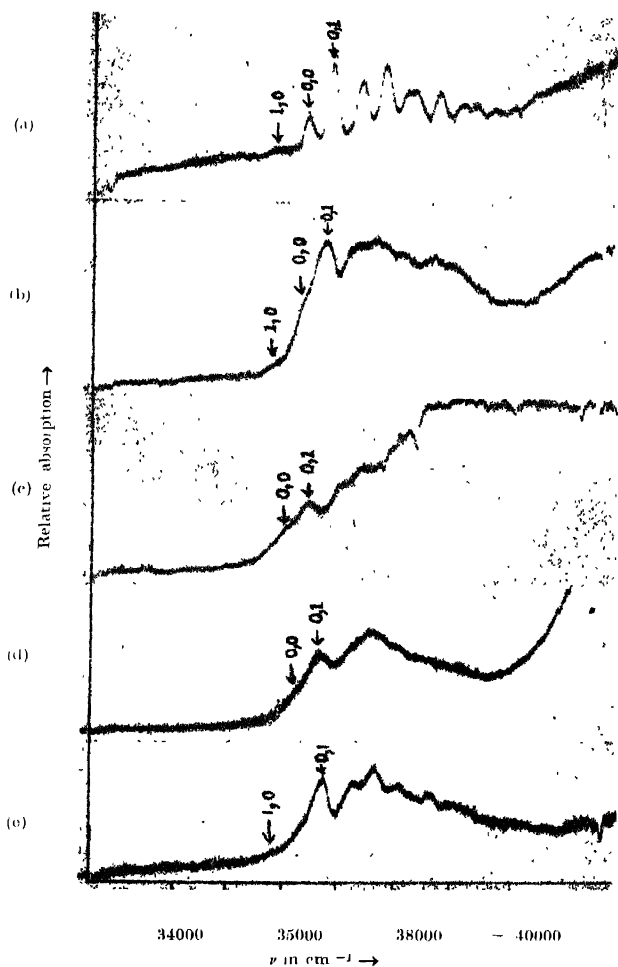


Fig. 1. Microphotometric records of ultraviolet absorption spectra of, 1,3,5-trichlorobenzene in different solvents and at different temperatures

(a)	Frozen	01%	Solution in isobutyl alcohol at -180°C .
(b)	Liquid	01%	Solution in isobutyl alcohol at -30°C .
(c)		01%	CCl_4 at -30°C .
(d)		01%	CHCl_3 ..
(e)		01%	cyclohexane ..

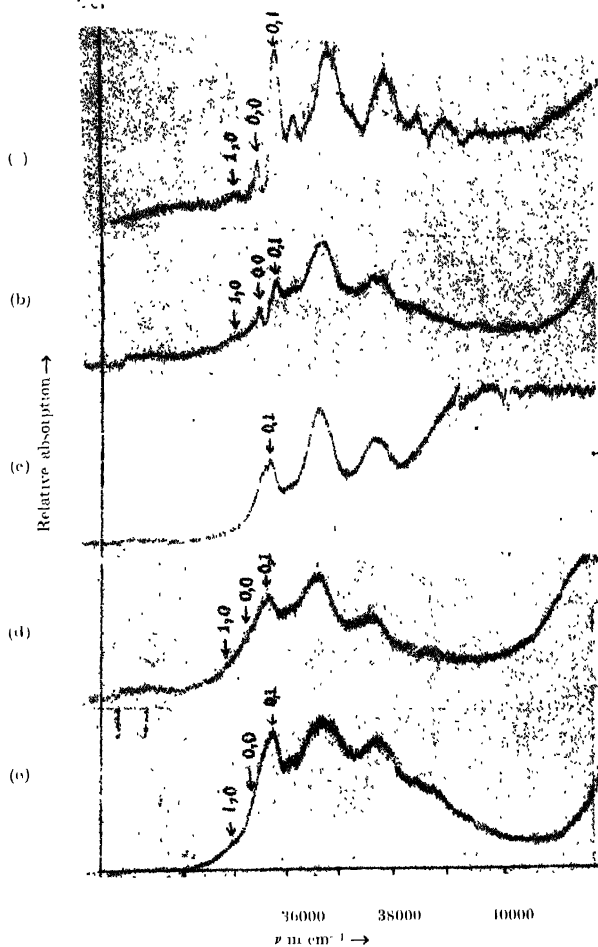


Fig. 2 Microphotometric records of ultraviolet absorption spectra of solutions of 1, 3, 5 trimethylbenzene in different solvents and at different temperatures

(a)	Frozen .01 %	Solution in isobutyl alcohol	at -180°C .
(b)	Liquid .01 %		at -30°C .
(c)	. . .01 %	. . . ClC_4	at -30°C .
(d)	. . .01 %	. . . CHCl_3	at -30°C .
(e)	. . .01 %	. . . cyclohexane	at -30°C .

It can be seen from figure 1(b) that the spectrum due to .01% solution in isobutyl alcohol in the liquid state is almost identical with that due to the frozen solution, but the 0,0 band is at 35400 cm^{-1} . So, in the former case, when the solution is frozen, the 0,0 band shifts only by 12 cm^{-1} towards shorter wavelengths, but when the substance is dissolved in isobutyl alcohol, the 0,0 band, which is absent in the spectrum due to vapour, appears with moderate intensity and its position is shifted by about 98 cm^{-1} towards red side from its position in the spectrum due to vapour. Recently, Banerjee (1957) reported the appearance of the forbidden 0,0 transition with weak intensity in the spectrum due to 1,3,5-trichlorobenzene in the solid state at -180°C . He concluded that the symmetry of the three-fold axis in 1,3,5-trichlorobenzene molecule is disturbed by the intermolecular force in the solid state at -180°C . The results of the present investigation show that such deterioration of the symmetry of the molecules takes place even when the molecule is dissolved in isobutyl alcohol at the room temperature. This indicates that probably this molecule forms weak bond with the isobutyl alcohol even in the liquid state.

On comparing the spectrum due to this solution with the spectra due to solutions in CCl_4 , CHCl_3 and cyclohexane reproduced in figures 1(c), 1(d) and 1(e), it is found that the 0,0 band is absent in the spectrum due to the solution in CCl_4 , but it just appears with very low intensity in the spectra due to other two

TABLE III
Absorption spectra of 1,3,5-trimethyl benzene at 30°C

.01% Sol. in carbon tetrachloride		01% Sol. in cyclo- hexane		01% Sol. in chloroform		01% Sol. in isobutyl alcohol	
ν in cm^{-1}	Assignment	ν in cm^{-1}	ν in cm^{-1}	Assignment	ν in cm^{-1}	Assignment	
36096 (w)	0, 0	35849 (vw)	36268 (w)	0, 0	35849 (vw)	0—517	
36538 (s)	0+442		36713 (s)	0+445	36386 (w)	0, 0	
37065 (m)	0+971	36807 (s)	37224 (m)	0+958	36807 (vs)	0+441	
37512 (s)	0+442+971	37246 (m)	37681 (s)	0+958+445	37246 (m)	0+441×2	
					37330 (m)	0+964	
		37330 (m)	38127 (m)	0+445×2 +958	37767 (s)	0+441+964	
		38767 (s)	38628 (w)	0+2×958 +445	38294 (m)	0+964×2	
		38294 (m)			38744 (m)	0+964×2 +441	
					39185 (w)	0+964×3	
		38744 (m)					

TABLE IV
Absorption spectra of 1,3,5-trimethyl benzene

Vapour (Spencer and Stallcup).	Frozen solution in isobutyl alcohol 0.1% at -180°C	
ν in cm^{-1} (Prominent bands)	ν in cm^{-1}	Assignment
36041 (vw) $1 \rightarrow 0$	35922 (w)	$0 - 523$
36557 (calculated 0, 0)	36415 (m)	$0, 0$
37000 (s) $0 \rightarrow 1$	36889 (vs)	$0 + 144$
37968 (s)	37414 (s)	$0 + 969$
38300 (ms)	37858 (vs)	$0 + 969 + 444$
	38288 (m)	$0 + 444 + 2 + 969$
	38376 (m)	$0 + 969 + 2$
	38820 (m)	$0 + 969 + 2 + 144$
	39346 (m)	$0 + 969 + 3$
	39796 (w)	$0 + 969 + 3 + 444$

solutions. It seems, therefore, that when the solvent molecule does not contain any hydrogen atom, the 1,3,5-trichlorobenzene molecule dissolved in it, retains its three-fold axis of symmetry. This fact indicates that the weak bonds mentioned above, are formed through the chlorine atom of the 1,3,5-trichlorobenzene molecule and the hydrogen atom of the solvent molecule. The bond becomes stronger in the case of the solution in isobutyl alcohol because of the presence in the solvent molecule of OH group which reacts strongly with the chlorine atom of the trichlorobenzene molecule.

It is also probable that when such a bond is formed with one chlorine atom of the molecule, the reactivity of the other two chlorine atoms to form such bond diminishes so that an asymmetry is introduced in the molecule.

1,3,5-Trimethylbenzene :

The near ultraviolet absorption spectrum of 1,3,5-trimethyl benzene in the vapour state was also studied by Spencer and Stallcup (1948). They pointed out that if the methyl group in the molecule were considered as a big atom, the molecule of 1,3,5-trimethyl benzene would also belong to the symmetry D_{3h} and the 0,0 band would be forbidden. They observed that the 0,0 band was actually absent in the spectrum and from the positions of the bands due to $1 \rightarrow 0$ and $0 \rightarrow 1$ transitions of a certain vibrational mode, they calculated the position of the

0,0 band and found it to be at 36557 cm^{-1} . It can be seen from Table IV and figure 2(a) that the first three bands in the spectrum due to .01% frozen solution of 1,3,5-trimethylbenzene in isobutyl alcohol are similar to the corresponding bands in the spectrum due to frozen solution of 1,3,5-trichlorobenzene. Hence, in this case also the second band from the red side is to be assigned as the 0,0 band as in the case of 1,3,5-trichlorobenzene. Analysis of the spectrum made with the assumption that the second band is the 0,0 band is given in Table IV.

The spectra due to .01% solution of the substance in isobutyl alcohol, CCl_4 and CHCl_3 in the liquid state at 30°C which are reproduced in figures 2(b), 2(c) and 2(d) respectively show the presence of the 0,0 band, although this band is rather weak and diffuse. In the spectrum due to the solution in cyclohexane figure 2(e) the 0,0 band is totally absent. It, therefore, appears that when the molecule of the solvent contains a chlorine atom or an OH group, the symmetry of the trimethyl benzene molecule dissolved in these solvents is slightly disturbed and so the 0,0 band appears with a small intensity. The formation of weak intermolecular bonds in the solution is thus definitely established by the results of the present investigation.

ACKNOWLEDGMENT

The author is indebted to Prof. S. C. Sirkar, D.Sc., F.N.I., for his kind interest and guidance during the progress of the work.

REFERENCES

- Banerjee, S. B., 1957 (private communication).*
- Conrad-Billroth, H., 1932, *Z. f. Phys. Chem.*, **B19**, 76.
- Roy, S. B., 1956, *Ind. J. Phys.*, **30**, 267.
- Sen, S. K., 1957 (unpublished results).
- Spencer, H. and Hall, M. B., 1948 "Contribution à l'Etude de la structure Moléculaire", (Desour-lege), p. 211.
- Spencer, H. and Stallcup, M. J., 1948, *Ibid*.
- Wolff, K. L. and Strasser, O., 1933, *z. f. Phys. Chem.*, **B21**, 389.
- * Since published, *Ind. J. Phys.*, **31**, 483.

THERMAL CONDUCTIVITY OF BINARY AND TERNARY MIXTURES OF HELIUM, ARGON AND XENON

S. C. SAXENA†

INDIAN ASSOCIATION FOR THE CULTIVATION OF SCIENCE, CALCUTTA-32

(Received for publication, June 3, 1957)

ABSTRACT. The thermal conductivities of the binary gas mixtures A—He, A—Xe and He—Xe have been determined for various concentrations by using the 'hot wire' method. The experimental values of thermal conductivity are in good agreement with the values calculated on the Chapman-Enskog theory for the Lennard-Jones 12-6 model. The experimental data over the entire range of concentration for each mixture have been formulated by means of an empirical equation containing two constants. These expressions will be of great use for gas analysis in the usual experiments on diffusion and thermal diffusion. A simple modification of the Lindsay-Bromley formula suggested by Srivastava and Saxena is found to reproduce the experimental data extremely well. The thermal conductivities of the ternary mixtures of argon, helium and xenon have also been measured. The experimental values are found to be in good agreement with those calculated on the basis of a simple formula suggested by Srivastava and Saxena. The latter is obtained as an extension of the formula suggested by Lindsay and Bromley for binary mixtures.

1. INTRODUCTION

Recently Srivastava and Saxena (1957a) have reported the thermal conductivity data for the binary and ternary mixtures of neon, argon and krypton. Two different types of hot wire cells were used by them which differed from each other essentially in the details of insulating the wire from the metal body of the cell. In one design a commercial metal to glass seal was used, while in the second a perspex seal served to insulate the axial wire from the metal tube. In the present investigation the latter design of the conductivity cell has been adopted in view of the fact that the accuracy in the construction of this type of cell is relatively larger as perspex can be worked on a lathe with precision. The method of preparing the mixture and of measuring the conductivity is exactly the same as described in a previous paper by Srivastava and Saxena (1957a).

The present report deals with the measurement of thermal conductivity of the binary mixtures : A—He, A—Xe and He—Xe; and the ternary mixtures

†Present address : Research Associate, Institute of Molecular Physics, University of Maryland, Maryland, U.S.A.

of A—He—Xe. This work has been primarily undertaken with a view to testing the scheme proposed by Srivastava and Saxena (1957b) for predicting the ternary conductivities when the binary ones are known. These measurements will also serve to check the appropriateness of the Lindsay-Bromley formula and of its modification suggested by us (1957a) for the thermal conductivity of a binary mixture.

2. EXPERIMENTAL RESULTS

The gases used in the present investigation were supplied by the British Oxygen Co., England; argon and helium were quoted as spectroscopically pure while xenon contained traces of krypton. The current through the conductivity cell was determined this time by measuring the potential difference across a standard 0.1 ohm resistance of manganin manufactured by Leeds and Northrup Co., U.S.A. The constants of the cell were determined as explained by Srivastava and Saxena (1957a) and are recorded in Table I.

TABLE I

Constants of the conductivity cell

Length of the cell wire ($2l$)	..	5 301 cm
Radius of the cell wire (r_1)	.	0.01006 cm.
Internal diameter of the tube ($2r_2$)	.	0.3036 cm.
External diameter of the tube ($2r_3$)	.	0.5969 cm.
Resistance of the cell wire at the bath temperature, 38°C (R_0)	.	0.20065 ohm.
The temperature coefficient of resistance of platinum wire (α)	..	0.003150°C ⁻¹
The mean thermal conductivity of the platinum wire (λ) in cal. cm ⁻¹ sec. ⁻¹ deg. ⁻¹	.	0.168
The cell constant ($1-C$)	..	0.9955.

The theory of the hot wire method, as developed by Kannuliik and Martin (1934), has been utilised to calculate the thermal conductivity of gases and gaseous mixtures. These apparent values of the thermal conductivity are found to be independent of pressure in the range from 6 to 20 cm. of mercury indicating a complete absence of convection and negligible temperature jump effect in this range of pressure. We have, therefore, taken the observation at a pressure of 10 cm. of mercury. The conductivity values were then reduced to the bath temperature and corrected for radial flow, radiation and wall-effect to give the conductivity, K' . To correct for any possible asymmetry in the construction of the cell, the cell constant, C , occurring in the relation

$$K = K'(1-C)$$

was determined by assuming as standard the conductivity of argon given by Kannuliuk and Carman (1952). The values of conductivity K , after applying all corrections, are given in the last column of Tables II, III, and IV for A—He, A—Xe and He—Xe gas mixtures respectively at 38°C and plotted in figure 1.

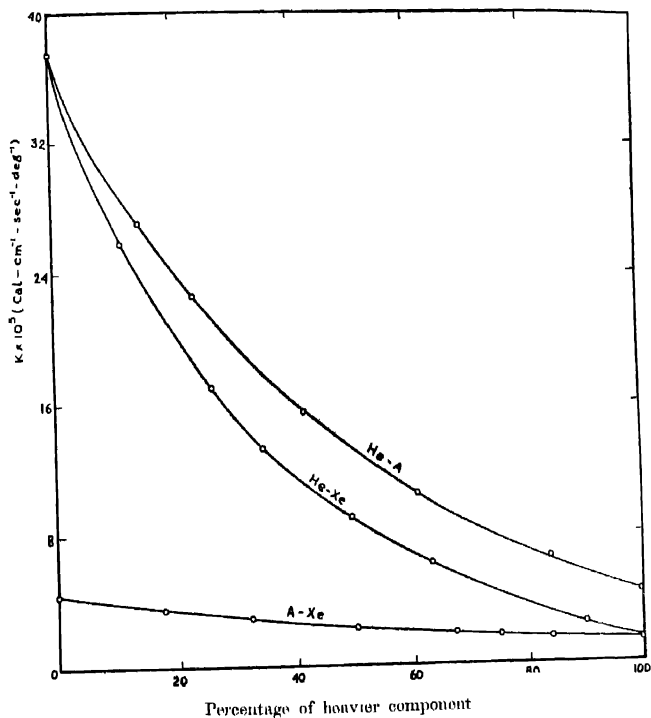


Fig. 1. Observed conductivity of gas mixtures of different composition.

TABLE II
A—He mixture

% of the heavier component	Current I (in milli-amp.)	$R - R_0$ (in milli-ohms)	$K_u \times 10^5$ cal. cm ⁻¹ sec. ⁻¹ deg. ⁻¹	$K'_u \times 10^5$ at bath temperature.	$K' \times 10^5$	$K \times 10^5$ cal. cm ⁻¹ sec. ⁻¹ deg. ⁻¹
0.0	513.25	1.72	38.20	30.05	37.70	37.53
14.12	513.95	2.36	27.51	27.36	27.05	26.93
23.02	512.89	2.78	23.00	22.86	22.57	22.47
41.64	512.06	3.96	15.82	15.68	15.45	15.38
60.84	511.36	5.05	10.69	10.55	10.42	10.37
83.98	510.80	8.51	6.81	6.68	6.60	6.57
100.0	359.60	5.87	4.51	4.45	4.40	4.38

TABLE III
A—Xe mixture

% of the heavier component	Current I (in milli-amp.)	$R - R_0$ (in milli-ohms)	$K_u \times 10^5$ cal. cm ⁻¹ sec. ⁻¹ deg. ⁻¹	$K'_u \times 10^5$ at bath temperature.	$K' \times 10^5$	$K \times 10^5$ cal. cm ⁻¹ sec. ⁻¹ deg. ⁻¹
0.0	359.60	5.87	4.51	4.45	4.40	4.38
17.57	355.71	6.96	3.58	3.53	3.49	3.47
32.31	286.30	5.12	3.00	2.97	2.93	2.92
50.23	286.42	6.04	2.42	2.39	2.35	2.34
67.27	291.25	7.22	1.99	1.96	1.93	1.92
75.17	290.54	7.65	1.82	1.79	1.76	1.75
83.30	238.40	5.37	1.68	1.66	1.64	1.63
100.0	279.92	8.41	1.41	1.38	1.36	1.35

TABLE IV
He—Xe mixture

% of the heavier component	Current I (in milli- amp.)	$R - R_0$ (in milli- ohms)	$K_H \times 10^5$ cal. cm ⁻¹ sec. ⁻¹ deg. ⁻¹	$K'_H \times 10^5$ at bath tempera- ture.	$K' \times 10^5$	$K \times 10^5$ cal. cm ⁻¹ sec. ⁻¹ deg. ⁻¹
0.0	513.25	1.72	38.20	38.05	37.70	37.53
11.39	529.73	2.61	26.40	26.24	25.93	25.82
26.03	528.81	3.85	17.41	17.26	17.01	16.94
34.60	530.01	4.87	13.62	13.47	13.26	13.20
49.63	530.43	6.93	9.29	9.15	9.02	
63.33	530.62	9.76	6.41	6.27	6.19	6.16
89.91	528.43	20.72	2.65	2.53	2.493	2.48
100.0	279.92	8.41	1.41	1.38	1.36	1.35

3. COMPARISON OF THEORY AND EXPERIMENT

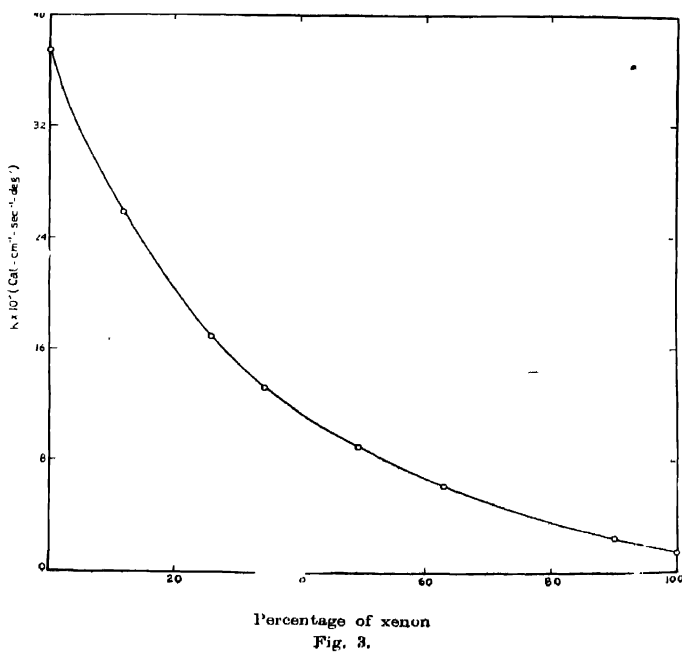
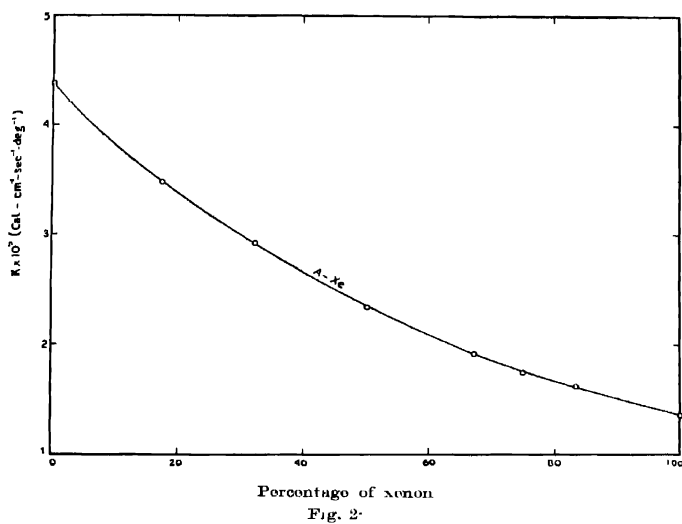
On Chapman-Enskog theory the thermal conductivity of a binary mixture of monatomic gases to the first approximation $[K_{mix}]_1$ can be written in the form

$$[K_{mix}]_1 = \frac{1}{X + Y} \quad \dots (1)$$

The expressions for X , Y and Z have been given by Hirschfelder, Curtiss and Bird (1954) in a form suitable for computation and these have been utilised to calculate the thermal conductivities of the binary mixtures. For theoretical computation the Lennard-Jones 12-6 model

$$E_{ij}(r) = 4\epsilon_{ij}[(r_{ij}/r)^{12} - (r_{ij}/r)^6], \quad \dots (2)$$

has been utilised, where the terms have their usual meaning. For like interactions the values of the potential parameters given by Hirschfelder, Bird and Spotz (1948) were used. For unlike interactions the values given by Saxena (1955) were utilised except for He—Xe, for which the usual combination rules, viz., geometric mean rule for ϵ_{12} and arithmetic mean rule for r_{12} have been used. Figures 2, 3 and 4 show a comparison between calculated and observed values



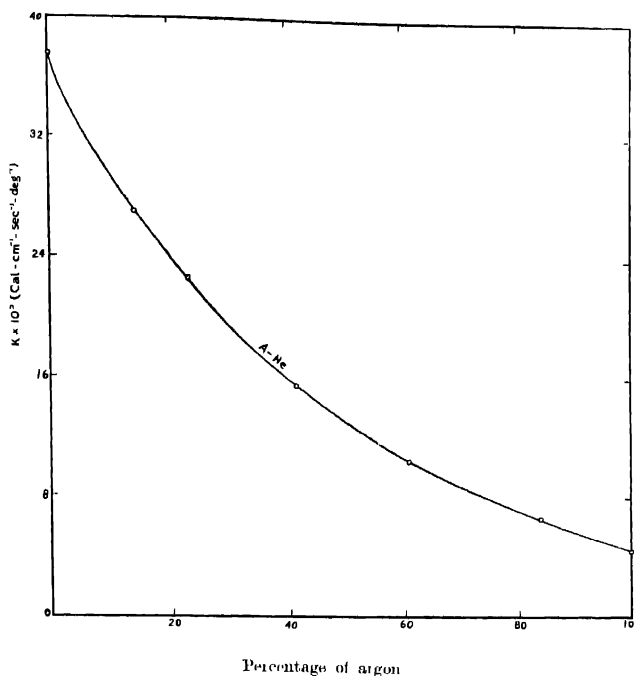


Fig. 4

of conductivity as a function of composition for A-He, A-Xe, and He-Xe gas mixtures respectively. Observed values are denoted by circles and calculated values by full line curves. The agreement between theory and experiment is seen to be very close. In general, the deviation is nowhere greater than one per cent and is of the same magnitude as the difference between the experimental and calculated values of the thermal conductivity for pure gases. Thus on the whole these measurements confirm the validity of the Chapman-Enskog theory and the adequacy of the Lennard-Jones 12-6 model together with the potential parameters used.

4. DISCUSSION OF RESULTS ON BINARY MIXTURES

Srivastava and Saxena (1957a) found that an equation of the type originally suggested by Wassiljewa (1904).

$$K_{mix} = \frac{K_1}{1 + A_{12} \frac{x_2}{x_1}} + \frac{K_2}{1 + A_{21} \frac{x_1}{x_2}} \quad \dots (3)$$

is adequate to represent the data on Ne-A, Ne-Kr and A-Kr gas mixtures over the entire range of concentration within one per cent if the constants A_{12} and A_{21} are properly chosen. Equation 3 is also very convenient for finding the composition of a mixture from its measured conductivity as is often required in gas analysis. From our experimental data we have found the following expressions for the three mixtures investigated here

$$\text{A-Xe} \quad \dots \quad [K]_{mix} = \frac{1.35}{1 + 1.116 \frac{x_2}{x_1}} + \frac{4.38}{1 + 1.553 \frac{x_1}{x_2}}$$

$$\text{A-He} \quad \dots \quad [K]_{mix} = \frac{4.38}{1 + 0.0842 \frac{x_2}{x_1}} + \frac{37.53}{1 + 3.243 \frac{x_1}{x_2}}$$

$$\text{He-Xe} \quad \dots \quad [K]_{mix} = \frac{1.35}{1 + 0.101 \frac{x_2}{x_1}} + \frac{37.53}{1 + 3.870 \frac{x_1}{x_2}}$$

which are accurate and better than one per cent

Lindsay and Bromley (1950) have given an empirical formula for the binary thermal conductivity of the form of Eq. 3 where A_{12} is given by

$$A_{12} = \frac{1}{2} \left[1 + \left\{ \frac{\eta_1}{\eta_2} \left(\frac{M_2}{M_1} \right)^{3/4} \frac{(1+S_1/T)}{(1+S_2/T)} \right\}^{1/2} \right]^2 \frac{(1+S_{12}/T)}{(1+S_1/T)}, \quad \dots (4)$$

and η_1 , η_2 and S_1 , S_2 are the viscosities and Sutherland constants of the two components respectively. S_{12} is assumed to be the geometric mean of S_1 and S_2 . A_{21} is obtained from A_{12} by interchanging the subscripts. Actual calculation using equations 3 and 4 shows a discrepancy of the order of five per cent for A-He and A-Xe, while ten per cent for He-Xe. From a close examination of the Enskog's formula for the binary thermal conductivity, Srivastava and Saxena (1957a) suggested the following modification to the Lindsay-Bromley formula.

$$K_{mix} = \frac{K_1}{1 + A_{12} \frac{x_2}{x_1}} + \frac{K_2}{1 + A_{21} \frac{x_1}{x_2}} + \frac{C'(K_1 K_2)^{1/2}}{\left(1 + A_{12} \frac{x_2}{x_1} \right) \left(1 + A_{21} \frac{x_1}{x_2} \right)} \quad \dots (5)$$

where C' is a constant which can be calculated if the conductivity at one composition is known. From our experimental data we find the values of the constant C' for the three gas pairs A-He, A-Xe and He-Xe as -0.299, -0.263, and

Thermal Conductivity of Binary and Ternary Mixtures 605

1.025 respectively. Values of the conductivity calculated from equation (5) together with (4) are found to agree with the observed values to within one per cent.

5. EXPERIMENTS WITH TERNARY GAS MIXTURE

Recently, Srivastava and Saxena (1957a) have reported the thermal conductivity of the ternary gas mixture Ne-A-Kr. They (Srivastava and Saxena, 1957b) found that if the constants A_{12} and A_{21} of equation 3 be determined experimentally, then the ternary conductivities can be predicted with considerable accuracy by the simple formula obtained by generalising equation 3.

$$K_{mix} = \frac{K_1}{1 + A_{12} \frac{x_2}{x_1} + A_{13} \frac{x_3}{x_1}} + \frac{K_2}{1 + A_{23} \frac{x_3}{x_2} + A_{21} \frac{x_1}{x_2}} + \frac{K_3}{1 + A_{31} \frac{x_1}{x_3} + A_{32} \frac{x_2}{x_3}} \dots (6)$$

The computed values of the thermal conductivity from equation 5 were found to be in good agreement with the observed values for the case of neon, argon and krypton gas mixtures. In the present report we have measured the thermal conductivity of the ternary mixtures of helium, argon and xenon with a view to collecting additional information on the suitability of equation 5.

The experimental data on the ternary gas mixtures of helium, argon and xenon are recorded in Table V for different compositions of the mixture. Each mixture was prepared afresh and no fixed order of mixing the gases was followed.

TABLE V

Thermal conductivity of ternary gas mixtures of argon, helium and xenon.

%He	%A	%Xe	Current <i>I</i> (multi- amp.)	<i>R</i> - <i>R</i> ₀ (milli- ohms)	<i>K</i> _u × 10 ⁵ cal. cm ⁻¹ sec. ⁻¹	<i>K</i> ' _u × 10 ⁵ at bath temperature	<i>K</i> × 10 ⁵	Calcu- lated <i>K</i> × 10 ⁵ from equation (5) cal. cm ⁻¹ sec. ⁻¹ deg. ⁻¹
11.38	14.95	73.67	524.65	18.36	3.011	2.889	2.836	2.827
19.07	18.00	62.33	524.03	13.79	4.119	4.072	4.004	3.986
39.01	36.75	24.24	523.12	7.13	8.75	8.61	8.45	8.36
32.02	60.65	7.33	522.52	7.13	8.73	8.59	8.43	8.36
68.01	18.80	13.19	523.13	3.83	17.10	16.95	16.62	16.44

The conductivity values reduced to the bath temperature (38°C) are recorded in column 7 of Table V while those corrected for radiation, radial flow, wall effect and for any asymmetry in the construction of the cell, are listed in column 8. Utilising the values of A_{12} and A_{21} for these mixtures given in section 4 the thermal conductivities of the ternary mixtures have been calculated from equation 5 and the values so obtained are listed in the last column of Table V.

In Table V there is one very interesting point to notice. The mixtures three and four, though of widely different compositions, have the same conductivity. It will be a fairly critical test of equation 5 to see whether or not it also gives the same value of conductivity for these two mixtures. Calculation from equation 5, however, fully confirmed this prediction. For the remaining mixtures also the agreement between theory and experiment is fairly good, the deviations between the two sets of values being always within the limits of experimental error. Thus here again we find in conformity with our previous conclusion that equation 5 can be utilised with considerable reliance and is probably the simplest way of readily finding the thermal conductivity of multicomponent gas mixtures. As the rigorous theory of multicomponent systems is very complicated and tedious for numerical computation, our generalisation will be extremely useful in the absence of computational assistance.

ACKNOWLEDGMENTS

The author is thankful to Prof. B. N. Srivastava, for his valuable guidance throughout the progress of the work and to the Council of Scientific and Industrial Research, New Delhi, for financial assistance.

REFERENCES

- Hirschfelder, J. O., Bird, K. B. and Spotz, E. L., 1948, *J. Chem. Phys.*, **16**, 968.
Hirschfelder, J. O., Curtiss, C. F. and Bird, R. B., 1954, *Molecular theory of gases and liquids*, John Wiley and Sons, Inc., New York.
Kannuluik, W. G., and Carman, E. H., 1952, *Proc. Phys. Soc. (London)*, **65**, 701.
Kannuluik, W. G., and Martin, L. H., 1934, *Proc. Roy. Soc. A*, **144**, 496.
Lindsay, A. L., and Bromley, L. A., 1950, *Ind. Eng. Chem.*, **42**, 1508.
Saxena, S. C., 1955, *Ind. Jour. Phys.*, **29**, 131.
Srivastava, B. N. and Saxena, S. C., 1957a, *Proc. Phys. Soc. (London)*, **70**, 369.
Srivastava, B. N. and Saxena, S. C., 1957b, *J. Chem. Phys.*, **27**, 583.
Wassiljewa, A., 1904, *Phys. Zeit.* **5**, 737.

OPTICAL AND ELECTRICAL METHODS OF MEASURING THICKNESSES OF THIN METALLIC FILMS

Y. G. NAIK AND E. M. BALSARA

GUJARAT COLLEGE, AHMEDABAD

(Received for publication, May 5, 1957)

ABSTRACT Measurement of thickness of chemically deposited thin films of silver are made from (i) the study of the absorption of light and (ii) from the electrical conductivity of these films. It is shown that the thicknesses determined by the two methods are of the same order.

INTRODUCTION

Thin films of metals, oxides and other substances are finding increasing applications in laboratory and in industry. Since the properties of thin films are dependent on their thickness, various methods have been used for measuring their thickness. In the present paper we describe two methods - optical (absorption of an electromagnetic wave) and electrical, which we used successfully for determining the thicknesses of chemically deposited silver films thinner than $\lambda/10$ of Na light.

EXPERIMENTAL

The silver films under investigation were all prepared by reduction of silver by formaldehyde, from the solution of its salt. The thickness of the deposit depends on the time of action of formaldehyde and very fine thin films of silver are obtained, if the solution is thrown off quickly. The above formaldehyde process gives uniform and bright films. The uniformity of the films was tested by measuring the intensity of a normally transmitted light which remained the same for various portions of the film. The films were deposited on optically flat glass plates and the deposit on the back side of the plate was gently removed by HNO_3 .

The polarimetric measurements for the determination of refractive index (n) and absorption index (k) for the thin films were made with a polarisation spectrometer. The theory of the measurement of the thickness of the films is based essentially on the absorption of an electromagnetic wave through a conducting medium (Abraham and Becker, 1932, or Drude, 1902). All that we have to do is to determine the coefficient of absorption for some standard films of silver of known thickness. Then we plot the reduction in intensity and the change of phase of the electric vector with respect to the magnetic vector (rotation of the plane of polarisation of the incident wave) as a function of the thickness. These standard curves were used for measuring the thicknesses of all the silver films.

DISCUSSIONS

It will be seen that, when an electromagnetic wave travels perpendicularly through a thin layer of absorbing material of thickness t , its amplitude will diminish in the ratio $1 : e^{-2\pi kt/\lambda}$. If I_0 and I are intensities of the incident and the emergent light respectively, then as the intensity is proportional to the square of amplitude, we get

$$I = I_0 e^{-4\pi kt/\lambda}.$$

This can be written as :

$$t = \frac{(\log_{10} I_0 - \log_{10} I) \lambda_0}{4\pi nk \times 0.4343}$$

where

I_0 = intensity of incident light,

I = intensity of emergent light,

and λ_0 = wave-length of light in vacuum.

The intensities of light transmitted by the films were measured by a photo-electric photometer, consisting of a photo cell —a gas filled tube No. 868 R C.A. —and a modified D.C. amplifying circuit of the bridge amplifier type, originally described by Wynn Williams (1928).

The incident intensity I_0 and the transmitted intensity I , were measured for four films, for normal incidence, and the thickness t of each of the films was calculated (Table I).

TABLE I

Wavelength of light in vacuum = $\lambda_0 = 5900^\circ \text{A.U.}$

Number of silver film	Intensity incident on the film I_0 micro-amps	Intensity transmitted by the film I micro-amps.	$\log_{10} \frac{I_0}{I}$	$K_0 = (nk)$	Thickness of silver film
F_1	315	220.00	0.1559	1.761	96 Å.
F_2	230	90.00	0.4075	1.972	223 Å.
F_3	210	40.00	0.7201	2.543	306 Å.
F_4	275	15.31	1.2543	2.732	495 Å.

Wood (1947) has shown that correction for reflection would be necessary while measuring the transmission only if the thickness is greater than 1000Å. As the thicknesses under investigation were all below 500Å. , no such correction is necessary here. This was further confirmed by the straight line plot, through origin, of t versus $\log_{10} \frac{I_0}{I} \times \frac{1}{nk}$

To correlate the thickness of these film smeasured by the transmission (optical) method, electrical conductivity method was employed to determine the thickness. In this method, the resistance x of the film for a surface area $=L \times b$ was determined accurately by a Kohlrausch universal bridge. A special holder for holding the films was prepared to ensure perfect electric contact. The electrical conductivity of the film is then given by $\sigma = \frac{L}{xbl}$, where bl is the cross-sectional area of the film; and $\frac{\sigma}{\sigma_0} = \frac{L}{571400xbl}$ where $\sigma_0 = 571400$ the electrical conductivity of silver in bulk at the temperature of the experiment.

Fuchs (1938) has derived two formulae for the conductivity of thin metallic films, which are

$$(i) \quad \frac{\sigma_0}{\sigma} = 1 + \frac{3}{8K} \quad \text{for thicker films } (K \gg 1)$$

$$\text{and (ii)} \quad \frac{\sigma_0}{\sigma} = -\frac{4}{3K \left(\log \frac{1}{K} \right)} \quad \text{for thinner films } (K < 1)$$

where, $K = \frac{\text{thickness } l \text{ of the film}}{\text{Mean free path } l \text{ of electrons in the metal at the given temperature}}$

These are modified by Dingle (1950) who does not assume that there is a diffuse scattering of electrons at the surface of the films. According to him

$$\frac{\sigma_0}{\sigma} = 1 + \frac{3}{8K} (1-P) \quad (K \gg 1)$$

$$\text{and} \quad \frac{\sigma_0}{\sigma} = \frac{4}{3} \cdot \frac{(1-P)}{(1+P)} \cdot \frac{1}{K \log \frac{1}{K}} \quad (K < 1)$$

where P is the probability of an electron being scattered elastically at the surface.

The values of the ratio $\frac{\sigma}{\sigma_0}$, for different values of K , for a thin metallic film, have been calculated from the last two equations by Dingle (1950) for $P = 0$ and by Sondheimer (1952) for $P = \frac{1}{2}$, (Table II).

TABLE II

K	Theoretical	value of $\frac{\sigma}{\sigma_0}$
	for $P = 0$	for $P = \frac{1}{2}$
0.1	0.212	0.382
0.2	0.333	0.524
0.5	0.526	0.713
1.0	0.684	0.820
2.0	0.819	0.901

The experimental equation for $\frac{\sigma}{\sigma_0}$ is modified by putting

$$t = K \times l = K \times 520 \times 10^{-8},$$

assuming the value of the mean free path of electrons in silver to be 520\AA .

The values of $\left[\frac{\sigma}{\sigma_0} \times K\right]$ were calculated for all films for different values of K , and graphs of experimental values of $\frac{\sigma}{\sigma_0}$ against K were plotted. On the same graph theoretical values of $\frac{\sigma}{\sigma_0}$ against K were also plotted (i) for $P = 0$ and (ii) for $P = \frac{1}{2}$, by using the values given by Dingle (1950) and Sondheimer (1952) from Table II. The points of intersection of the experimental curves with the theoretical curves, gave the values of K , for which both the theoretical and experimental values of $\frac{\sigma}{\sigma_0}$ were identical for a given film. For these values of K , the thickness of the films was determined (Table III).

TABLE III

Film No	Values of K corresponding to the point of intersection		$t = K \times l = K \times 520\text{\AA}$		Thickness of film by transmission method from Table I \AA
	for $P = 0$	for $P = \frac{1}{2}$	for $P = 0$	for $P = \frac{1}{2}$	
F_1	0.245	0.167	127	87	96
F_2	0.337	0.255	175	133	223
F_3	0.542	0.440	282	229	306
		0.687			495

It will thus be seen that the values of the thicknesses determined by the two methods appear to be comparable.

REFERENCES

- Abraham, M., and Becker, R., *The Classical Theory of Electricity and Magnetism*, pp. 189 Blackie & Son, Ltd., 1932.
 Dingle, R. B., 1950, *Proc. Roy. Soc. (London)*, **201A**, 545.
 Drude, P., 1902, *The Theory of Optics*, 358-66.
 Fuchs, K., 1938, *Proc. Camb. Phil. Soc.*, **34**, 100.
 Sondheimer, E. H., 1952, *Adv. Phys.*, **1**, 1.
 Wood, R. W., 1947, *Physical Optics*, 567, Macmillan Co.
 Wynn-Williams C. E., 1928, *Phil. Mag.*, **6**, 324.

THE CRYSTAL STRUCTURE OF ANTHRANILIC ACID AT DIFFERENT TEMPERATURES

G. S. R. KRISHNA MURTI

OPTICS DEPARTMENT, INDIAN ASSOCIATION FOR THE CULTIVATION OF SCIENCE,
JADAVPUR, CALCUTTA-32

(Received for publication, September 27, 1957)

Plate XV

ABSTRACT. Debye-Scherrer patterns of crystals of anthranilic acid obtained (a) by cooling the hot solution in alcohol slowly, (b) by evaporating a saturated solution at room temperature, and (c) from the melt, have been photographed. It has been found that the three methods give three different modifications, the first two belonging to the orthorhombic system and the third one to the monoclinic system. The unit cell dimensions of the first modification are: $a = 12.80$ A.U., $b = 10.78$ A.U. and $c = 9.40$ A.U. The number of molecules in the unit cell has been found to be $8.02 \sim 8$, the measured value of the density being 1.41. The space group is found to be Q_h^{16} . Modification II has the unit cell of dimensions, $a = 16.05$ A.U., $b = 11.65$ A.U. and $c = 7.20$ A.U. The density is found to be 1.36. The number of molecules in the unit cell is $8.02 \sim 8$. The space group in this case is Q_h^{15} . It has been found that modification III is produced by slight distortion of the unit cell of the second modification and the dimensions of the unit cell are: $a = 15.85$ A.U., $b = 12.31$ A.U., $c = 6.81$ A.U. and $\beta = 97^\circ 10'$. The density of this crystal was found to be 1.40. These data give the number of molecules in the unit cell as $7.982 \sim 8$. The space group C_{2h}^{13} explains the observed reflections from different planes of this crystal.

Debye-Scherrer patterns of the three modifications cooled to -180°C show that only slight contraction of the unit cell takes place in the case of each modification. The dimensions of the unit cell for the crystal at -180°C and the coefficients of expansion α_a , α_b and α_c along the three crystallographic axes a , b and c respectively, in the range 30°C to -180°C , have been calculated and given for all the three modifications.

INTRODUCTION

It was well known that anthranilic acid (*o*-aminobenzoic acid, $\text{NH}_2\text{-C}_6\text{H}_4\text{-COOH}$) crystallises ordinarily in two habits (Groth, 1917), both of which belong to orthorhombic system. The crystal structure was determined by Prasad and Kapadia (1935) who obtained the two modifications of the crystal by slowly evaporating the solution in alcohol. They took oscillation photographs of the crystals about the a and c axes. The unit cell dimensions of the two modifications reported by them are: $a = 16.16$ A.U., $b = 11.77$ A.U., $c = 7.17$ A.U. and $a = 12.77$ A.U., $b = 10.80$ A.U., $c = 9.403$ A.U. respectively. They further reported that the first modification belongs to the space group of Q_h^{11} and the second to Q_h^5 .

KitaiGorodskij (1948) redetermined the crystal structure of the compound and reported that only one form belonging to the orthorhombic system was present with the cell dimensions $a = 9.40$ A.U., $b = 10.80$ A.U., $c = 12.80$ A.U. He found the space group to be either C_{2v}^8 or D_{2h}^{16} . This form is the same as the second modification reported by Prasad and Kapadia (1935) with the interchange of a and c axes.

Later, McCrone *et al.* (1949) investigated the problem more thoroughly and obtained three modifications of the crystal at the room temperature. The first form, obtained from a solution in aniline, is orthorhombic with the unit cell dimensions $a = 10.19$ A.U., $b = 12.87$ A.U., and $c = 9.32$ A.U. They have listed 16 powder lines and reported the space group to be either C_{2v}^8 or D_{2h}^{16} , which agrees with the results reported by the previous workers. The second form obtained from aqueous solution was also reported to be orthorhombic with the unit cell dimensions $a = 11.66$ A.U., $b = 16.04$ A.U., $c = 7.18$ A.U. which was the same as the first modification reported by Prasad and Kapadia (1935). These authors listed 22 Debye-Scherrer lines but did not find the space group of this form of the crystal. The third form obtained from the melt was found by them to belong to the monoclinic system and the morphological data were reported by them. They, however, did not find out the unit cell dimensions in this case.

The present investigation was undertaken to find out whether the structures of the first two modifications remained the same when the crystals were cooled to -180°C and also to find out the space group to which the third modification belongs. With this object in view the Debye-Scherrer patterns of the three modifications both at 30°C and at -180°C have been photographed and compared with each other. It has also been possible to find out the space group of the third modification, as will be evident from the following sections.

EXPERIMENTAL

Pure anthranilic acid (m.p. 145°C) supplied by B.D.H. was used in the investigation. The crystals were powdered well and packed tightly in a thin walled soda glass capillary tube of bore about 0.03 cms and this capillary tube filled with the powder was used to photograph the Debye-Scherrer pattern. The low temperature photographs were taken by the same method as described in an earlier paper (Krishna Murti and Sen, 1956).

The substance was crystallised from a solution in alcohol in order to get modification II. When it was crystallised at different constant temperatures in different solvents, the same modification was obtained in all these cases. Then the substance was crystallised from hot solution in alcohol by slow cooling which gave the crystals belonging to the modification I. Next, the substance was allowed to melt and then to cool down to the room temperature. The solid mass obtained in this way was found to belong to modification III, as its Debye-Scherrer pattern was different from that due to the other two modifications.

TABLE I
Debye-Scherrer rings of anthranilic acid—Modification I

At 30°C				At -180°C			
Sin ² θ		Indices		Sin ² θ		Indices	
Spacings in A.U.		From McCrone et al. (1949)		Spacings in A.U.		Spacings in A.U.	
Observed	Calculated	Observed	Calculated	Observed	Calculated	Observed	Calculated
0.00870	0.00871	110	8.26 (w)	0.00880	0.00879	110	8.210 (w)
0.01440	0.01444	200	6.410 (m)	0.01450	0.01452	200	6.390 (m)
0.01560	0.01542	111	6.250 (m)	0.01560	0.01550	111	6.250 (m)
0.02040	0.02040	020	5.380 (wm)	0.02065	0.02056	020	5.365 (wm)
0.02670	0.02684	002	4.730 (ms)	0.02670	0.02684	002	4.710 (ms)
0.03080	0.03072	121	4.390 (vw)	0.03095	0.03090	121	4.380 (vw)
0.03490	0.03484	220	4.120 (vw)	0.03510	0.03508	220	4.110 (vw)
0.03760	0.03759	210	3.970 (vw)	0.03790	0.03781	310	3.955 (vw)
0.04175	0.04159	221	3.770 (vw)	0.04200	0.04179	221	3.760 (vw)
0.04440	0.04430	311	3.655 (s)	0.04480	0.04452	311	3.640 (s)
0.04740	0.04724	022	3.525 (vw)	0.04760	0.04740	022	3.530 (vw)
0.05120	0.05085	122	3.400 (vw)	0.05146	0.05103	122	3.395 (vw)
0.05780	0.05776	400	3.205 (m)	0.05800	0.05808	400	3.195 (m)
0.06950	0.06937	411	2.920 (ms)	0.07020	0.06987	411	2.910 (ms)
0.08500	0.08521	140	2.640 (w)	0.08600	0.08587	140	2.635 (w)
0.09620	0.09604	240	2.480 (vw)	0.09670	0.09677	240	2.475 (vw)
0.11420	0.11408	340	2.280 (wm)	0.11480	0.11491	340	2.270 (wm)
0.12300	0.12288 {0.12325	242 413	2.200 (w)	0.12360	{0.12360 0.12361	242 413	2.190 (w)
0.13000	0.12996	600	2.140 (w)	0.13040	0.13068	600	2.135 (w)
0.13950	0.13936	440	2.060 (w)	0.14020	0.14032	440	2.050 (w)

TABLE III
Debye-Scherrer rings of anthranilic acid—Modification III

At 20°C			At -180°C		
Spacing in A.U.		Indices	Spacing in A.U.		Indices
Observed	Calculated		Observed	Calculated	
$1/d^2$					
7.810 (m)	0.01640	200	7.670 (m)	0.01700	200
6.150 (s)	0.02640	020	6.020 (s)	0.02760	020
5.785 (w)	0.03040	111	5.590 (w)	0.03190	111
5.310 (w)	0.03540	111	5.210 (w)	0.03680	111
4.820 (w)	0.04310	220	4.730 (w)	0.04440	220
4.535 (vw)	0.04860	021	4.440 (vw)	0.05070	021
4.060 (s)	0.06050	221	3.985 (s)	0.06300	221
3.795 (vs)	0.06940	221	3.715 (vs)	0.07340	221
3.360 (s)	0.08800	002	3.280 (s)	0.09280	002
3.200 (vs)	0.09780	401	3.150 (vs)	0.10080	401
3.075 (w)	0.10580	040	3.010 (w)	0.11040	040
2.800 (w)	0.12800	510	2.980 (vw)	0.11200	510
2.680 (vw)	0.13940	421	2.800 (vw)	0.12800	421
2.600 (m)	0.14780	041	2.735 (w)	0.13360	041
2.520 (w)	0.15740	241	2.625 (vw)	0.14500	241
2.490 (w)	0.16140	132	2.550 (m)	0.15380	132
2.395 (w)	0.17440	132	2.470 (w)	0.16380	132
2.345 (m)	0.18200	422	2.445 (w)	0.16740	422
2.260 (m)	0.19630	402	2.360 (w)	0.17970	402
		621	2.310 (m)	0.18740	621
		531	2.220 (m)	0.20280	531

A Seifert X-ray tube running at 26 ma, 32KV was used and an exposure of about $2\frac{1}{2}$ hrs. was sufficient to get the patterns with moderate densities. The X-ray tube was provided with a copper target and a nickel filter was used to cut off the $K\beta$ radiation. The distance from the film to the specimen was measured accurately by taking a powder photograph of rock salt and it was found to be 5.20 cms. Spacings were calculated from the rings in the pattern by measuring the diameters accurate up to 0.05 mm. Several photographs under the same conditions were taken to test the genuineness of the results.

RESULTS AND DISCUSSION

Some of the representative photographs of the Debye-Scherrer patterns obtained at different temperatures for the three modifications of the crystal are reproduced in Plate XV. The values of the spacings along with those of $\sin^2\theta$ and $1/d^2$ for the Debye-Scherrer rings are given in Tables I, II and III. The spacings reported by McCrone *et al.* (1949) are also included in Tables I and II for comparison. The visually estimated intensities of different rings in the patterns are given in parentheses as very strong (vs), strong (s), medium (m), weak (w) and very weak (vw).

Modification I :

The values of the spacings and $\sin^2\theta$ for different planes of reflections of the crystal at 30°C given in Table I show that the results agree quite well with those reported by McCrone *et al.* (1949). By applying Lipson's method (1949) the crystal is found to belong to orthorhombic system, the dimensions of the unit cell being $a = 12.80$ A.U., $b = 10.78$ A.U. and $c = 9.40$ A.U. The number of molecules per unit cell calculated with 1.41 as the density, which was measured is found to be $8.02 \sim 8$. It can also be seen from Table I that the rules for the extinctions of the reflections are :

- (i) (*h*0*l*) planes are halved if *h* is odd.
- and (ii) (*okl*) planes are halved if (*k+l*) is odd.

The space group is found to be Q_h^{16} . The space group reported by Prasad and Kapadia (1935) is Q_h^5 and that by McCrone *et al.* (1949) and by KitaiGorodskij (1948) is C_{2v}^9 or D_{2h}^{10} . The space group C_{2v}^9 applies to a crystal having 4 molecules per unit cell. The restrictions apply both to this space group and to Q_h^{16} but as the number of molecules per unit cell is found to be 8, the space group is to be taken as Q_h^{16} and it is neither C_{2v}^9 nor Q_h^5 . It can be seen from the Table I and from the patterns reproduced, that no change in the crystal structure occurs when the crystal is cooled to -180°C except a small change in the dimensions of the unit cell. It can be seen from the table that $\sin^2\theta$ value for the plane (002) remains the same, whereas for the remaining reflections the values increase slightly showing thereby that the primitive translation along *c* axis remains the same, whereas a slight contraction takes place in the remaining two directions *a* and *b*.

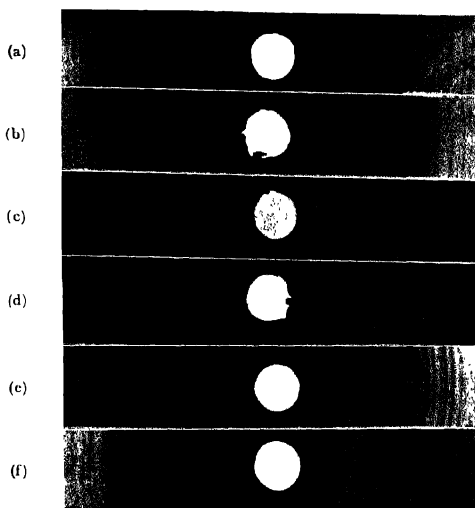


Fig. 1. Debye-Scherrer patterns of anthranilic acid.

- | | | |
|-----|-------------------|----------------------------------|
| (a) | Modification I. | Crystals at 30°C |
| (b) | " | " -180°C |
| (c) | Modification II | Crystals at 30°C |
| (d) | " | " -180°C |
| (e) | Modification III. | Crystals at 30°C |
| (f) | " | " -180°C |

The unit cell dimensions of the crystal at -180°C calculated by Lipson's method (1949) are $a = 12.77$ A.U., $b = 10.74$ A.U., and $c = 9.40$ A.U. The reflections from all the planes observed for the crystal at 30°C are also present in the pattern due to the crystal at -180°C . So the space group is again Q_h^{10} . The coefficients of expansion α_a , α_b , α_c along the three crystallographic axes, in the range 30°C to -180°C , are found to be 11.76×10^{-6} , 17.73×10^{-6} and zero respectively.

Modification II :

The values of the spacings and of $\sin^2\theta$ for the crystal at 30°C are given in Table II. It can be seen from the table that the results agree well with those reported by McCrone *et al.* (1949). By applying Lipson's method (1949) the crystal is found to be orthorhombic, the dimensions of the unit cell being $a = 16.05$ A.U., $b = 11.65$ A.U., and $c = 7.20$ A.U. The density was measured and was found to be 1.36. The number of molecules in the unit cell is found to be $8.02 \sim 8$. It can be seen from the Table II that the extinction in the reflections from the planes are as follows :

- (i) (*h**o**l*) planes are halved if *l* is odd
- (ii) (*h**k**o*) planes are halved if *h* is odd
- and (iii) (*o**k**l*) planes are halved if *k* is odd.

So, the space group is Q_h^{15} . Prasad and Kupaia (1935) reported the same extinctions in the reflections, but they assigned the space group as Q_h^{11} . Evidently, this was not correct and the correct space group is Q_h^{15} .

It can be seen from the Table II and from the patterns that only contraction of the spacings takes place in the crystal when it is brought down to -180°C . So, the space group is not changed by the lowering of temperature. The dimensions of the unit cell of the crystal at -180°C are $a = 15.85$ A.U., $b = 11.46$ A.U., and $c = 7.09$ A.U. The coefficients of expansion α_a , α_b , and α_c along the three crystallographic axes *a*, *b*, *c*, in the range 30°C to -180°C , are found to be 60.1×10^{-6} , 79.0×10^{-6} and 73.9×10^{-6} respectively. The coefficients of expansions are almost the same in all the three directions.

Modification III :

The values of spacings and $1/d^2$ for the rings produced by this modification at 30°C are given in Table III. According to the morphological data given by McCrone *et al.* (1949) this modification belongs to monoclinic system. The dimensions of the unit cell were not determined by any previous worker. It can be seen from the pattern reproduced in Plate XV that it is different from the other two patterns due to the orthorhombic modifications.

This form is taken to belong to monoclinic system and in finding out the unit cell dimensions it was assumed that one of the two orthorhombic forms is slightly distorted to give the monoclinic variety. By trial it is found that if the

spacings 7.810 A.U., 6.150 A.U. and 3.350 A.U. are taken to be those of (200), (020) and (002) planes respectively and the spacing of 5.735 A.U. is taken as that of the (11 $\bar{1}$) plane, on these assumptions the unit cell dimensions of the crystal (monoclinic) are found to be $a = 15.85$ A.U., $b = 12.31$ A.U., $c = 6.81$ A. U. and $\beta = 97^\circ 10'$.

With those values of the unit cell dimensions of the crystal, it is found that all the reflections obtained in the pattern can be indexed. Next, to find out the space group to which the crystal belongs, search is made to find out the rule for the extinctions of the planes. It can be seen from the Table III that all (hkl) planes for which ($h+k$) is odd are missing. The density of the crystal was found to be 1.40 and the number of molecules per unit cell comes out as $7.982 \sim 8$. So, the space group C_{2h}^3 is assigned to the crystal.

It can be seen from the Table III that when the crystal is cooled to -180°C no change in the crystal system takes place; but the spacings of the planes diminish a little. From the patterns reproduced, it can be seen that the pattern produced by the crystal at -180°C is similar to that at 30°C and the restrictions for reflection are also the same. So, when the crystal is cooled to -180°C only a contraction takes place. The unit cell dimensions of the crystal maintained at -180°C calculated from the spacings 7.670 A.U., 6.020 A.U., 5.590 A.U. and 3.280 A.U. which are due to the planes (200), (020), (11 $\bar{1}$) and (002) respectively, are $a = 15.55$ A.U., $b = 12.04$ A.U., $c = 6.62$ A.U. and $\beta = 97^\circ 17'$. The angle β is almost the same as that for the crystal at 30°C . The coefficients of expansion α_a , α_b , α_c along the three crystallographic axes a , b , c respectively are calculated and found to be 9.19×10^{-5} , 10.68×10^{-5} and 13.67×10^{-5} respectively. When the different modifications of the crystal are brought back to room temperature (30°C) after once being cooled to -180°C they all come back to the original form.

ACKNOWLEDGMENT

The author is indebted to Prof. S. C. Sirkar, D.Sc., F.N.I. for his kind interest and guidance during the progress of the work.

REFERENCES

- Groth, P., 1917, *Chemische, Krist.*, **4**, 508.
- KitaiGorodskij, A. I., 1948, *Izv. Akad. Nauk, S.S.S.R., otdel. Khim. Nauk.*, **3**, 278.
- Krishna Murti, G. S. R. and Sen, S. N., 1956, *Ind. J. Phys.*, **30**, 242.
- Lipson, H., 1949, *Acta. Cryst.*, **2**, 43.
- McCrone, W. O., Corvin, I. and Whitney, J., 1949, *Anal. Chem.*, **21**, 1016.
- Prasad, M. and Kapadia, M. R., 1935, *Ind. J. Phys.*, **9**, 239.

ANALYSIS OF THE NEAR-ULTRA-VIOLET ABSORPTION SPECTRUM OF PARA-CHLOROANISOLE

V. SURYANARAYANA AND V. RAMAKRISHNA RAO

PHYSICS DEPARTMENT, ANDHRA UNIVERSITY, WALTAIR

(Received for publication, March 26, 1957)

Plate XVI

ABSTRACT. The near ultraviolet absorption spectrum of para-chloroanisole has been studied. The discrete bands were analysed as due to an allowed transition 1A_1 to 1B_1 . Out of the 100 observed bands 88 bands could be explained on the basis of five fundamentals in the upper state (341, 621, 779, 1053, and 1271) and four fundamentals in the ground state (361, 641, 802, and 1111). The above fundamentals were correlated mutually and with Raman data and possible assignments discussed. The occurrence of CH_3 bending frequency in all substituted anisoles was discussed and established.

INTRODUCTION

In continuation of our earlier work on the near ultraviolet absorption spectra of substituted anisoles, we are now reporting in the following pages the results of our detailed investigations in the case of para-chloroanisole.

Raman data with depolarization factors were given for para-chloroanisole by Paulsen (1939). The Raman spectrum was also taken by us (see figure 3) and frequencies measured and compared with earlier data. Jean Lecomte (1938) gave a plot of the infrared frequencies in the region $500-1400\text{ cm}^{-1}$, but the actual frequency data were not tabulated. Data on fluorescence and ultraviolet absorption do not appear to have been worked out. We find that like orthochloro and para-fluoroanisoles (Suryanarayana and Rao, 1956) para-chloroanisole also does not fluoresce.

EXPERIMENTAL

Full experimental details were given elsewhere (Suryanarayana and Rao, 1956). The substance para-chloroanisole was obtained from B.D.H. Its boiling point is 198°C at 760 m.m. pressure. This was purified by distilling thrice in vacuum sealed tubes at about 65°C . This distilled product was used for further work. Two path lengths, 50 cms. and 150 cms, were found suitable for the development of the bands. Spectra were recorded at saturated vapour pressure corresponding to the reservoir temperature range 18°C to 180°C . Spectrograms were taken both on Hilger's medium quartz instrument (E315) and Littrow E 1 spectrograph employing a slit width of 3 to 5 microns.

RESULTS

The absorption was found to consist of two regions as in other substituted anisoles (a) a continuous absorption below 2350 A.U. and (b) a discrete one between 2900 and 2530 A.U. The two regions of absorption merge into one at a vapour pressure corresponding to 120°C with 75 cm. tube and 60°C with 150 cms. path length.

At the saturated vapour pressure corresponding to -18°C only two bands were recorded distinctly at 2867.3 A.U. (34866 cm^{-1}) which can be taken as the (0,0) band, and at 2804.6 A.U. and traces of bands at 2783.2 A.U. More bands develop to the short wavelength side with higher temperatures and the maximum bands are obtained at 27°C with 75 cms path length (see figure 1). At higher temperatures the region gets under continuous absorption and a few bands develop on the long wavelength side. To develop more bands in this region before the continuous absorption sets in the 150 cms. tube was used and by varying the container temperature in the region 40°C-60°C about 10 bands more could be recorded (see figure 2, Plate XVI). Above 60°C-120°C, the region below 2900 A.U. is completely absorbed up to the limit of quartz instruments.

The bands are red-degraded. There is a certain amount of width for each strong band. The maximum intensity of absorption appears to be in the region 2720 to 2860 A.U. (see figure 1). The long wavelength side bands developed with the 150 cms. tube are extremely weak. The wavenumber and intensity data are given in Table I. Intensities are only visual estimates in the scale 1 to 10. Our final measurements give some frequency values slightly different ($3\text{-}4\text{ cm}^{-1}$) from those given in our earlier note (Suryanarayana and V. R. Rao, 1955). These are accurate to 1 cm^{-1} in the case of sharp bands and 3 to 4 cm^{-1} in diffuse and broad bands.

ANALYSIS AND DISCUSSION

Para-chloroanisole, like other para substitutions in benzene, approximates to the point group C_{2v} and is subject to all the well-known selection rules. The transition is an allowed one A_1-B_1 .

The intense band at 2867.3 A.U. (34866 cm^{-1}) is taken as the (0, 0) band. This is shifted by 894 cm^{-1} to the long wavelength side from the (0, 0) band in ortho-chloroanisole. This is in conformity with the general behaviour of para and ortho substitutions (c.f.) fluoro toluenes (Cave and Thompson, 1950), bromo toluenes, chloro toluenes, dichloro benzenes (Sponer and Teller 1941), fluoro-chloro benzenes (Krishnamachari, 1955, 56), etc.. Frequency shifts of various bands from the (0, 0) band are given in column 4 of Table I. The identified fundamentals in both the states with corresponding Raman data and probable assignments are given in Table II. The obvious fundamentals in the upper state are 341, 621, 779, 1053 and 1271. These frequencies occur in progressions and

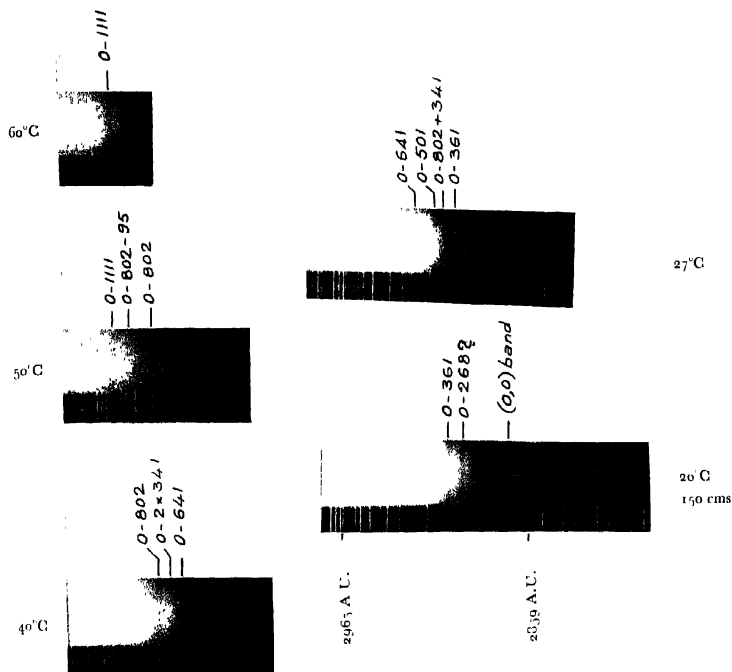


Fig. 2 Ground state frequencies in the absorption spectrum of para-chloro anisole.

Near Ultraviolet Absorption Spectrum of *p*-Chloroanisole 621

combinations between themselves and with other fundamentals in both states. The lower state fundamentals observed are 361, 641, 802 and 1111. On the basis of these fundamentals 88 bands out of a total of 100 observed bands could be interpreted. The uninterpreted bands do not include any intense bands. In the light of the selection rules and other features a detailed discussion of the fundamentals follows.

The (0, 0) band at 34866 is followed on the longwave length side by half a dozen bands by -7 , -12 , -18 , -54 and -79 cm^{-1} (figure 1). This pattern is found to repeat itself fully at the frequency 779 and partly at the frequencies 341, 621, 1053 and 1271. This is a usual characteristic of the spectra of substituted benzenes.

The frequency 341 in the upper state is a very intense band and is found to occur in combination with many other fundamentals. In the ground state its value is 361 cm^{-1} represented by a fairly intense band. The corresponding Raman frequency is 365 cm^{-1} which is strong and has a depolarisation factor of 0.30. This frequency was also obtained as an anti-stokes Raman line which explains the intensity of the band in the ground state even at room temperatures. These frequencies 365 (Raman), 361 (ground state) and 341 (upper state) can be easily attributed to the totally symmetric component of the $606E_g^+$ vibration in benzene. The considerable fall in the value from that in benzene is to be anticipated. The corresponding values in ortho-chloroanisole are 410 (Raman), 418 (ground state) and 357 (upper state). We observed a definite fall in these values from the ortho to para substitution. The other component of E_g^+ vibration, possibly, is observed at 565 (ground state) and 518 cm^{-1} (upper state) in ortho-chloroanisole (A' in C_s) need not necessarily be expected in para-chloroanisole (C_{2v} point group) on account of its non-totally symmetric character (B_1). The value of the lower state frequency is found to be lower than that in para-fluoroanisole (428 cm^{-1}) and higher than those in para-bromoanisole (324 cm^{-1}) (Suryanarayana and Ramakrishna Rao, 1956) showing the effect of the atomic weight on the frequencies when the symmetry is the same. The intensity of this E_g vibration component 341 in para-chloroanisole as compared with that of in ortho-chloroanisole probably indicates that this vibration plays a more important role in the production of the spectrum in para-chloroanisole than in ortho-chloroanisole. Further, this intensity of 341 in para-chloroanisole may be considered to have been shared by the two components 357 and 518 in ortho-chloroanisole in which case the transition probability may be considered to be the same for both.

We now take up the frequency 621 which is represented by a medium intensity band. This replaces the fundamental 699 mentioned in our earlier note (Rao and Suryanarayana, 1955). In the ground state its value is 641 cm^{-1} . In the Raman spectrum there is a close doublet of strong lines at 625 and 636 cm^{-1} with a depolarisation factor of 0.51. Of the two, 636 cm^{-1} is nearer the ground

state value of 641 cm^{-1} . Corresponding values in upper and lower states of ortho-chloroanisole are 641 and 690 (ground state) 685 cm^{-1} (Raman). The upper state value in para-chloroanisole shows the expected fall from that in ortho-chloroanisole. So, if we take 636 cm^{-1} as the Raman value for this vibration the relationship holds. That is why the still another possibility of the Raman line at 700 cm^{-1} is rejected. Other reasons for this rejection are the considerable difference between 641 and 700 (as ground state values) and the low intensity of 700 cm^{-1} in Raman spectrum. Thus we might conclude that the frequencies 621, 641, 636 cm^{-1} represent the same mode of vibration in para-chloroanisole. In our discussion on para-fluoroanisole (Suryanarayana and Ramkrishna Rao, 1957) we presented reasons for regarding the corresponding frequencies as due to C-Cl symmetric stretching mode of vibration.

The fundamental 779 in the upper state is of the greatest intensity in the spectrum. It occurs with the (0, 0) band at the lowest temperature (-18°C), thus showing a high transition probability. It is traced up to 5 overtones and in combination with other fundamentals. The pattern with (0, 0) band is very completely repeated with this fundamental 779. The corresponding ground state frequency appears to be 802 which begins to develop at vapour pressures corresponding to 30° to 40°C with a 150 cms. tube. From the appearance of the band we can easily fix it up as a fundamental. It is also able to explain some bands as difference frequencies. The corresponding Raman line is 796 cm^{-1} with $\rho = 0.07$ which is probably the strongest Raman line and extremely polarised. We observe in the Raman spectra such a strong line as a common factor in most of the substituted anisoles, 755 in guaicol (Reitz and Ypsilante, 1935), 831 in para-fluoroanisole, 796 in para-chloroanisole, 793 in para-bromoanisole (Paulsen, 1957) and 796 in ortho-chloroanisole (Herz, 1946). All are very strong lines and polarised. It is possible that this Raman line may represent a common vibration to all these molecules. So, it may be C-OCH_3 symmetric vibration (our earlier assignment of this to C-Cl vibration in ortho-chloroanisole is shown by us to be subject to correction). If this is so, then the peculiar feature is as follows. In anisole (Sreerama Murty, 1950) the frequency in upper state is 755. On substitution we have 721 (guaicol) 810 in para-fluoroanisole, 767 in ortho-chloroanisole, 779 in para-chloroanisole and 771 in para-bromoanisole. The values come down from anisole to guaicol. But there is a sudden increase in the halogen substitutions, namely, ortho-chloro, para-chloro and para-bromoanisoles. This is strange. In fact that is why we chose the other set of frequencies 641 etc. in our earlier work as representing the C-OCH_3 vibrations. But their presence is only in chloro substitutions, though their behaviour with respect to anisole etc., is satisfactory. Thus we are inclined to doubt our earlier assignment and consider the 779 (upper state value) as due to C-OCH_3 vibration consistent with all other molecules in spite of the anomalous behaviour of the frequencies in bromo and chloro substitutions. While in ortho-chloroanisole the C-Cl vibra-

Near Ultraviolet Absorption Spectrum of *p*-Chloroanisole 623

tion is very strong, in *para*-chloroanisole C-OCH₃ vibration appears to be the strongest in the spectrum.

The upper state fundamental 1053 is less intense than the 779. It is followed on the long wavelength side by a part of the pattern -7, -18, -54 etc. Its ground state value appears to be 1111, the band developing at about 50°C with 150 cm. tube as may be expected from the lower Boltzmann factors corresponding to that high frequency. The corresponding Raman line is at 1092 cm⁻¹ with $\rho = 0.09$, a strong line next in intensity and polarisation to the 796 Raman line. Thus its totally symmetric nature is beyond doubt. From the order of magnitude it could be attributed to a C-C valence vibration in the phenyl radical. The corresponding upper state value in *ortho*-chloroanisole is probably 1060 and the ground state value is 1183 (from Raman spectrum). In *ortho*-chloroanisole two C-C vibrations are found while in *para*-chloroanisole only one could be observed.

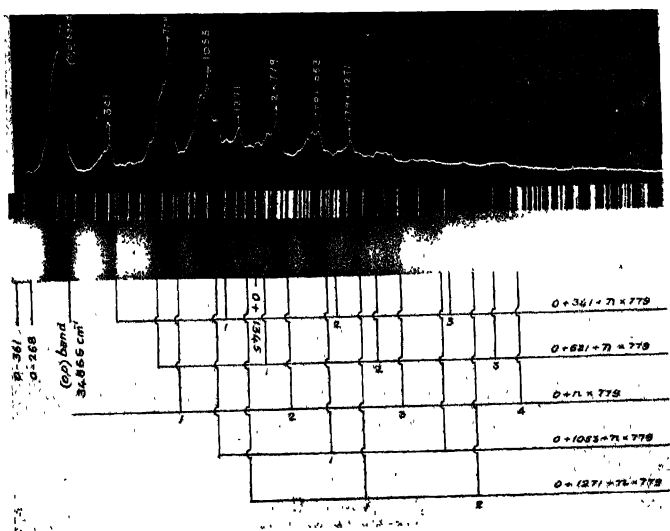


Fig. 1. Ultraviolet absorption spectrum of *para*-chloroanisole.

The frequency 1271 is represented by a lone band (figure 1) of medium intensity. On this is superposed a progression of 779. The corresponding ground state frequency could not be found even with 150 cm. tube heated up to 80°C. The Boltzmann factors may be forbiddingly low. The corresponding Raman line is at 1291 cm⁻¹ with a depolarisation factor of 0.19. As pointed out in our

earlier work on substituted anisoles (Suryanarayana, 1956), this frequency is found characteristic of all molecules containing a CH_3 unit with a phenyl radical like toluenes, and anisoles. The values do not change considerably from ground state to upper state values. For these and other reasons mentioned earlier this frequency was attributed to the CH_3 bending mode in OCH_3 unit. Additional evidence is from benzo-trifluoride (Sponer and Lowe, 1949) where CH_3 is replaced by CF_3 in which a frequency like this does not occur. This also proves that 1271 cm^{-1} does not belong to the phenyl radical as assumed by Sponer in xylenes (Cooper and Spone, 1952; Cooper and Sastry, 1952),

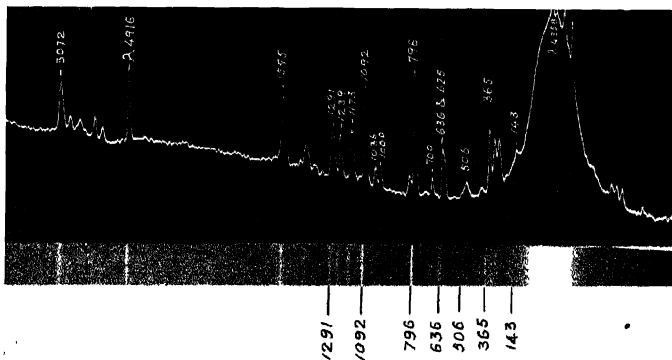


Fig. 3. Microphotometric curve of the Raman spectrum of para-chloroanisole

In ortho-chloroanisole and para-fluoroanisole the aliphatic C-O frequency in OCH_3 was suggested to be 1389 and 1367 cm^{-1} respectively. A corresponding frequency could not be traced with certainty in para-chloroanisole. There is one band 1345 cm^{-1} in this region, but it could be interpreted also as $0 + 621 + 779 - 54$ (see Table I). This frequency was found to be in all cases rather weak. It is possible that in spite of its low intensity this band can be interpreted also as a fundamental. It combines with the other fundamentals 1272 and 341 (though these can be given other interpretations). Corresponding ground state frequency was not found as the spectrum did not develop thus far. In the Raman spectrum it is difficult to suggest a proper corresponding line.

In Table II we have taken 501 as a fundamental in the ground state and this agrees well with the weak Raman line 506 . This line has a depolarisation factor of 0.68 . This line most probably corresponds to the B_1 component of E_g^+ (606) vibration in benzene. We have mentioned earlier in connection with the high intensity of 341 (α_1 component) that E_g^+ vibration in parachloroanisole plays a fairly important role. We find 501 also combining with the 341 vibration.

Near Ultraviolet Absorption Spectrum of *p*-Chloroanisole 625

TABLE I

Para-Chloroanisole : Ultraviolet absorption bands

Wave-numbers (cm^{-1})	Intensity	Shift from (0, 0) band (cm^{-1}) obs. value	Assignment	Difference between observed and calculated values
33755	3	-1111	0-1111	
33975	$\frac{1}{2}$	- 891	0-802-95	6
34004	2	- 802	0-802	
34148	$\frac{1}{2}$ D	- 718	0-2 \times 361	
34225	2	- 641	0-641	
34305	$1\frac{1}{2}$	- 501	0-501	
34404	$1\frac{1}{2}$	- 462	0-802+341	1
34440	$1\frac{1}{2}$	- 417	0-361-54	2
34505	3	- 361	0-361	
34520	1D	- 346		
34548	2 V.D	- 318	0-641-361+2 \times 341	2
34598	3	- 268	0-268 ?	
34640	1D	- 226	0-641-361+779	3
			0-95-74-54	3
35663	$1\frac{1}{2}$	- 203		0
34706	2	- 160	0-501-341	0
34734	$1\frac{1}{2}$	- 132	0-79-54	1
34771	2 Sh	- 95	0-2 \times 361+621 ?	6
34787	2 Sh	- 79	0-79	
34812	2 Sh	- 54	0-54; 0-1111+1053	4
34848	2 Sh	- 18	0-18; 0-361+341	2
			0-641+621	2
34854	2 Sh	- 12	0-12	
34859	2 Sh	- 7	0-7	
34866	8	0	(0,0)	
34890	1D	+ 24		
34913	$\frac{1}{2}$ V.D	+ 47	0+2 \times 341-641	6
34932	1D	+ 66	0+779-2 \times 361 ?	9
35020	$\frac{1}{2}$ D	+ 154	4+1271-1111	6
35075	1D	+ 209	0+621-361-54	3
35118	1D	+ 252	0+1053-802	1
			0+1053-802	1
35156	2	+ 290	0+341-54	3
35199	$2\frac{1}{2}$	+ 324	0+341-18	1
			0+2 \times 341-361	3
			0+341+621-641 ?	3
35207	7	+ 341	0+341	
35231	$1\frac{1}{2}$ D	+ 365	0+779-361-54	1
35279	3	+ 413	0+779-361	5
			0+1053-641	1

TABLE I-(Contd.)

Wave-numbers (cm ⁻¹)	Intensity	Shift from (0, 0) band (cm ⁻¹) obs. value	Assignment	Difference between observed and calculated values
35344	3	+ 478	0 + 2 × 779 - 3 × 361	3
35409	1	+ 543	0 + 621 - 79	1
35487	4	+ 621	0 + 621	
35549	2 Sh	+ 683	[0 + 779 - 95	1
35587	2 Sh	+ 761	0 + 2 × 341	1
35593	2 Sh	+ 727	0 + 779 - 79	1
			0 + 779 - 54	2
35627	2 Sh	+ 761	[0 + 779 - 18	0
35633	2 Sh	+ 767	0 + 779 - 361 + 341	2
35639	2 Sh	+ 773	0 + 779 - 12	0
			0 + 779 - 7	1
35645	6	+ 779	0 + 779	
35701	$\frac{1}{2}$	+ 835	0 + 2 × 779 - 2 × 361	1
35769	1	+ 903	0 + 1271 - 361	7
35848	1½D	+ 982	0 + 1053 - 54 - 18	1
35865	3	+ 999	0 + 1053 - 54	0
35900	2 Sh	+ 1034	0 + 1053 - 18	1
35913	2 Sh	+ 1047	0 + 1053 - 7	1
35919	4	+ 1053	0 + 1053	
35945	1 V.D	+ 1079		
35987	5	+ 1121	0 + 341 + 779	1
36038	2	+ 1172	[0 + 2 × 779 - 2 × 361 + 341	5
			0 + 1271 - 95	4
36120	2	+ 1254	0 + 1271 - 18	1
36137	4	+ 1271	0 + 1271	
36211	2	+ 1345	[0 + 341 + 1053 - 54	5
			0 + 621 + 779 - 54	1
36266	3	+ 1400	[0 + 341 + 1053	0
			0 + 621 + 779	0
			0 + 779 + 2 × 341	5
36332	4	+ 1466	0 + 1053 + 779 - 361	5
			0 + 2 × 779 - 95	3
36390	1	+ 1524	0 + 2 × 779 - 2 × 18	2
36405	2 Sh	+ 1539	0 + 2 × 779 - 18	1
36426	6	+ 1560	0 + 2 × 779	2
36479	2	+ 1613	0 + 341 + 1271	1
36552	3	+ 1636	[0 + 1271 + 779 - 361	3
			0 + 1345 + 341	0
36643	2	+ 1777	0 + 779 + 1053 - 54	1
36648	1½	+ 1780		
36699	5	+ 1833	0 + 779 + 1053	1

Near Ultraviolet Absorption Spectrum of *p*-Chloroanisole 627

TABLE I (Contd.)

Wave-numbers cm ⁻¹	Intensity	Shift from (0, 0) band (cm ⁻¹) obs. value	Assignment	Difference between observed and calculated values
36763	2½	+1897	$\begin{cases} 0+341+2 \times 779 \\ 0+621+1271 \\ 0+1271+1053-361 \\ 0+2 \times 341+1271 \\ 0+779+1271-96 \end{cases}$	2
36822	2½	+1856		5
36918	5	+2052		7
36978	2	+2112		3
37043	2	+2177	$\begin{cases} 0+779+1271 \\ 0+2 \times 1053 \\ 0+779+341+1053 \\ 0+621+2 \times 779 \end{cases}$	1
37085	2			2
37144	2	+2219	0+2×341+3×779-802 ?	2
37201	3½	+2278	0+3×779-3×1854	5
		+2335	0+3×779	2
37261	2	+2395	0+341+779+1271	4
37340	3½	+2474	0+1279+2×779-361	2
37411	1½	+2545	0+2×1271	3
37479	2½	+2613	0+1053+2×779	2
37505	½ V.D	+2639		16
37528	½ D	+2662	0+341+3×779 ?	
37600	½	+2734	0+1271+2×799-95	0
37692	3½	+2826	0+2×779+1271	3
37752	1½	+2886	$\begin{cases} 0+341+2 \times 1271 \\ 0+779+2 \times 1053 \end{cases}$	3
				1
37809	1	+2943	$\begin{cases} 0+341+2 \times 779+1053 \\ 0+621+3 \times 779 ? \end{cases}$	9
37859	—	+2993		15
37908	D	+3042		
37974	3	+3108	0+4×779	8
38033	2	+3167	0+341+2×779+1271	3
38095	1	+3229	$\begin{cases} 0+779+341+2 \times 1053 \\ 0+2 \times 341+2 \times 1271 \end{cases}$	3
				5
38204	½	+3428		
38369	1	+3503		
38454	1½	+3588		
38527	1	+3661	$\begin{cases} 0+341+779+2 \times 1271 \\ 0+2 \times 1053+2 \times 779 \end{cases}$	1
38610	5 Sh	+3744	0+2×1271+2×779-361	3
38747	—	+3881	0+5×779	5
				14
39235	—	+4369		
39380	2	+4514	$\begin{cases} 0+621+5 \times 779 \\ 0+2 \times 1271+3 \times 779-361 \end{cases}$	2
				4
39479	—	+4613		
39534	3	+4668	$\begin{cases} 0+6 \times 779 \\ 0+3 \times 1271+2 \times 779 \\ -2 \times 361 ? \end{cases}$	6
40457	2	+5591	0+4×1271+2×779	19
			-3×361 ?	32

Probably this β_1 component is obtained in the forbidden part of the transition. We find a similar occurrence of β_1 component in both states in benzonitrile (Sponer and Lowe, 1949).

There is a band at -268 in the ground state which has an intensity behaviour the same as -361 . It could not be explained as any combination band. It does not have a counter part in the Raman spectrum or in the upper state frequency. In ortho-chloroanisole a similar intense band was found at 279 cm^{-1} . We are not able to offer an interpretation for this band.

We are now left with the satellite bands that follow the (0, 0) band and some of the outstanding fundamentals. Similar satellites are found to be a general characteristic feature of all substituted benzenes. Of the five satellite bands -7 , -12 , -18 , -54 and -79 , the one -18 could be interpreted as the difference between 361 and 341 fundamentals and also 641 and 621 fundamentals. The double assignment explains possibly the intensity of the band. Some of these frequencies are also attributed to the difference frequency of low lying non-totally symmetric vibrations (Sponer). The reasoning for this view is that in an allowed transition we can get the difference frequencies of non-totally symmetric vibrations by the operation of Franck Condon principle and the high intensity for the bands indicates large Boltzmann factors which, at the room temperatures, can be obtained only for low frequencies. As the fundamentals themselves are forbidden it is not possible to ascertain which particular frequency gives rise to the difference frequency. In our interpretation the -18 frequency was attributed to difference

TABLE II

Identified frequencies and their assignment Para-chloroanisole

Raman data with depolarisation factors	U. V. Absorption data		Assignment.
	Lower State	Upper State	
	268		
365 (0.30)	361	341	Totally symmetric component of $606 E_g^+$ vibration in benzene.
506 (0.68)	501	—	β_1 component of $606 E_g^+$ vibration in benzene.
636 (0.51)	641	621	C-Cl valence vibration.
796 (0.07)	802	779	C-OCH ₃ stretching.
1092 (0.00)	1111	1053	C-C.
1201 (0.19)	—	1271	CH ₃ bending.
		1345	Aliphatic O-C frequency in OCH ₃ unit.

Near Ultraviolet Absorption Spectrum of *p*-Chloroanisole 629

frequency of totally symmetric vibration. In view of the fact that both the fundamentals are obtained at room temperature, the assignment may be justified.

ACKNOWLEDGMENTS

This work was carried out under the C.S.I.R. scheme on 'Fluorescence and Absorption Spectra of Organic Molecules' granted to one of us (V. R. Rao). The authors wish to express their thanks to Prof. K. R. Rao for his kind interest in the work.

REFERENCES

- Cave, W. T. and Thompson, H. W., 1950, A General Discussion of the Faraday Society, page, 35.
- Cooper, C. D. and Sastry, M. L. N., 1952, *Jour. Chem. Phys.* **20**, 607.
- Cooper, C. D. and Sponer H., 1952, *Jour. Chem. Phys.* **20**, 1248.
- Herz, E., 1946, *Monat. F. Chemie*, **76**, 1.
- Krishnamachari, S. L. N. G., 1955, *Ind. Jour. Phys.*, **29**, 603.
- " 1956, *Ind. Jour. Phys.*, **30**, 320.
- Lecomte, Par. Joan, 1938, *Le Jour. De Physique Et Le Radium.*, **9**, 26.
- Paulsen, O., 1939, *Monat F. Chemie.*, **72**, 244.
- Ramakrishna Rao, V. and Suryanarayana, V., 1955, *Jour. Sci. Indust. Research.* **14B**, 470.
- Reitz, A. W. and Prinz Ypsilant, Y. R., 1935, *Monat. F. Chemie.*, **66**, 299.
- Sponer, H. and Lowy, D. S., 1949, *Jour. Opt. Soc. America.* **39**, 840.
- Sponer, H. and Toller, E., 1941, *Rev. Mod. Phys.*, **13**, 120.
- Sriramanurthy, K. 1950, *Ind. Jour. Phys.*, **24**, 421.
- Suryanarayana, V., 1956, Thesis submitted to the Andhra University for the award of D.Sc. degree.
- Suryanarayana, V and Ramakrishna Rao, V., 1955, *Jour. Sci. Indust. Research.* **14B**, 128.
- Suryanarayana, V. and Ramakrishna Rao, V., 1956, *Ind. Jour. Phys.*, **30**, 117.
- Suryanarayana, V and Ramakrishna Rao, V., 1956, *Jour. Sci. Indust. Research.* **15B**, 260.
- Suryanarayana, V. and Ramakrishna Rao, V., 1957, *Spectro Chemica Acta*, **9**, 252.

MEASUREMENT OF THERMAL NEUTRON ACTIVATION CROSS-SECTION

M. L. SEHGAL

DEPARTMENT OF PHYSICS, MUSLIM UNIVERSITY, ALIGARH.

(Received for publication June 17, 1957)

ABSTRACT. The various errors involved in measuring the activation cross-sections for thermal neutrons are discussed. Error due to 'Self-protection', is specially considered and a semi-empirical relation is given for its correction. Thermal neutron activation cross-sections for In^{115} , Ag^{107} and Ag^{109} are measured taking into account these correction. Design of a signal pile is given.

INTRODUCTION

It is intended to measure thermal neutron activation cross-section for certain cases. Before embarking on the actual programme, the desirability of making measurements for standard substances is self-evident, so that the standard procedure for measurement and obtaining the minimum errors is established.

Quite comprehensive measurements of these cross-sections have been reported by Rasetti (1940), O'Neal and Goldhaber (1941), and then by Seren *et al.* (1947). Generally, they quote their errors up to about $\pm 20\%$. We have measured $\sigma(n, \gamma)$ for In^{115} , Ag^{107} , and Ag^{109} taking $\sigma(n, \gamma)$ for Mn^{55} as standard, employing nearly the same method, but taking into account the various possible errors involved as carefully as possible. The effect of self-protection has been studied in detail and a semi-empirical relation has been found.

METHOD OF MEASUREMENT

Evidently, the disintegration rate $\frac{dN}{dt}$ from an irradiated substance at time t_2 after irradiation is given by the well-known equation (Hughes, 1953).

$$\left(\frac{dN}{dt} \right)_{t_2} = nv \cdot \sigma_{act} \cdot N \cdot (1 - e^{-\lambda t_1}) e^{-\lambda t_2} \quad \dots (1)$$

where nv = flux of the neutrons at the place of irradiation.

σ_{act} = activation cross-section for the substance under study.

N = total number of nuclei in the irradiated substance.

λ = decay constant.

and t_1 = time of irradiation.

$$\text{Also} \quad \frac{dN}{dt} = G \epsilon \quad \dots (2)$$

where G is the counting rate as found experimentally ; ϵ is the over-all efficiency

factor for the geometry used, and ϵ is the ratio of the radiations passing into the counter over the number of radiations emitted by the substance, which were heading towards the detector.

Isotopes studied are all β -emitters. So a β -counter was used as a detector. Indium, silver and manganese were available in spectrographically pure form (99.99% from Johnson Matthey and Co, London, (U.K.)). While the indium foils were directly irradiated, silver and manganese powder was first sandwiched uniformly between two thin celloctapes on a well-defined area and then irradiated. It was ascertained that the celloctape itself did not develop any activity. The foils used had approximately half the area of the window of the β -counter, and were placed right at the centre of the window. This kept G constant. ϵ is apparently given by $e^{-\mu_m d}$, where μ_m is the mass absorption co-efficient in cm^2/gm , and d is the effective thickness in gms/cm^2 , which a β -particle has to traverse before entering the counter. The value of d was taken equal to the window thickness plus half the foil thickness. μ_m was measured as a function of the energy with the help of β -emitters of known strength and energy i.e. Co^{60} , Tl^{204} , Bi^{210} , and Pa^{234} available from Baird-Atomic Instrument Co, U.S.A. The curve for μ_m versus the end energy of β -particles got in this way was exactly the same as given by Hughes (1953). The thickness of the window of the β -counter was measured in the same way as done by Seren *et al.* (1947) by making use of two β -sources of known strength. The measurement of the thickness of the foil involved actual weighing by an analytical balance which was sensitive up to 0.1 mgm.

Because in some of these cases, the activity produced emits more than one β -particle, different values of μ_m for each energy of β -particle were used, taking into account the proper branching ratio of the β -particles. As for example, In^{116m} emits three β -particles of energy 1 Mev (51%) with $\mu_m = 19 \text{ cm}^2/\text{gm}$, 0.87 Mev (28%) with $\mu_m = 23 \text{ cm}^2/\text{gm}$ and 0.60 Mev (21%) with $\mu_m = 39 \text{ cm}^2/\text{gm}$. The

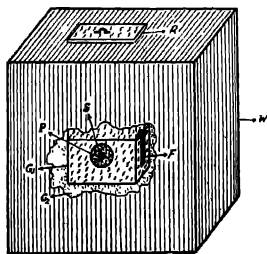


Fig. 1. Details of the Sigma Pilo. S is the (Ra-Be) source, P is the paraffin sphere; F is the pocket for irradiation of foils; G_1 is the solid graphito block G_2 is graphito powder; R is the removable upper graphito block and W is the wooden box.

percentage ratio of the β -particles is taken as given by Slatis, Toit and Siegbahn (1950). ϵ in this case was taken to be $1/100[51e^{-10d} + 28e^{-23d} + 21e^{-39d}]$. Seren *et al.* (1947) have used only a single value of μ_m in such cases, which is not justified.

For irradiating the foils, the arrangement used is shown in figure 1. A 100 milligram Ra-Be source is kept at the centre of a paraffin sphere of 6.5 cms in radius which is further kept at the centre of a cubical graphite block with each side equal to 62.5 cms. The results of Amaldi *et al.* (1935), and Fink (1936) were used in getting the dimensions of the above pile. A pocket of size 10.5 cm \times 6.5 cm \times 3.0 cm, as shown in figure 1, was built in the pile at a distance of 11.5 cm from Ra-Be source to facilitate irradiation of the foils and to keep the place of irradiation exactly the same in all the cases. It is well-known that such a pile contains a certain fraction of resonance neutrons besides the thermal neutrons. To avoid the effect of the resonance neutrons usual cadmium ratio method was employed. By a preliminary experiment with manganese it was estimated that the resonance neutron flux at the pocket was about 7% of the thermal neutron flux.

DISCUSSION OF ERRORS

The errors involved in σ_{act} will be due to the errors in the various quantities given in Eqs. (1) and (2). Errors in the counting rate C due to fluctuation in the electronic instruments, and counter efficiency changes were estimated to be 1%. It was felt justifiable to take into account no error due to changes in the surrounding conditions as they were kept the same throughout the experiment. Half-life, which enters in the equation through the term $e^{-\lambda t_2}$, was actually measured with an estimated accuracy of about 5%, introducing an error of less than 1 per cent in $e^{-\lambda t_2}$. The saturation factor $(1 - e^{-\lambda t_1})$ was always nearly unity within less than 0.05%, introducing little error in the final result. The value of the mass absorption co-efficients for β -particles and of d are estimated to be correct up to 4% to give us an error of about 1% in $e^{-\mu_m d}$. Error, if any, introduced due to the counting of γ -rays, should not exceed 1%, because the β -counter used had a sensitivity to γ -rays of less than 1%. The error in the determination of the value of N is expected to be less than 1%, because the weighing could be done with an accuracy of 0.1 mgm in 40 mgms. The position for irradiation was fixed in the pocket to less than a millimetre and hence no error is expected due to any change in the position of irradiation.

Though cadmium ratio method takes care of most of the effect of resonance neutrons, yet a further correction is needed to take into account the fact that cadmium absorbs a small percentage of resonance neutrons also. This correction has been studied by Rush (1948), Kunstadter (1950) and Tittle (1951) in detail. This correction amounts to about 4%, and when taken into account should leave back only a small error.

When a foil of appreciable absorption cross-section is introduced in a diffusing medium, it will introduce a general depression in the neutron density around the foil. A theory for depression has been put forward by Bothe (1943) and verified by Tittle (1951) and Klema and Ritchie (1952). But apart from the above effect one should also take into account the effect due to self-protection. This effect is there, because when a foil is exposed to neutrons the nuclei at the surface will be in a higher flux as compared with those in the centre of the foil. Marshak (1947), and Plumber and Lewis (1955) have studied this effect for a sphere having dimensions small compared to the mean free path of neutrons in the diffusing medium, which is not applicable to our case. To study the above effect we irradiated a stack containing an odd number of indium foils at the usual place of irradiation in the pile, and the 53 minutes saturation activity of the central foil was studied as a function of the thickness of the stack. In figure 2, curve C

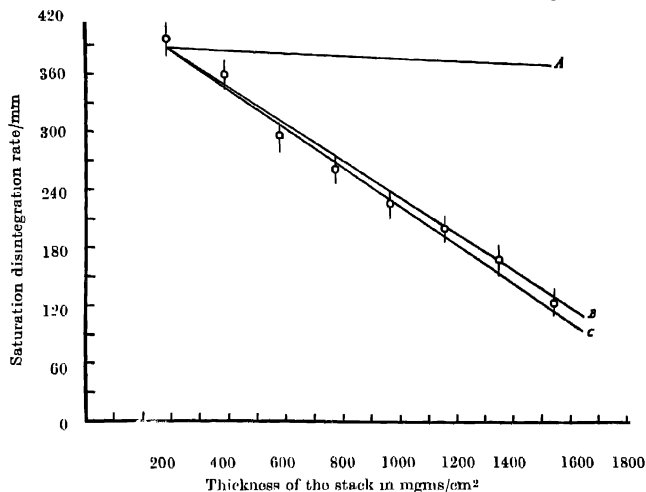


Fig. 2. Points represent the saturation disintegration rate of the central foil of the stack as a function of the total thickness of the stack in mgms/cm².

shows the relation between the saturation disintegration rate and the total thickness of the stack in mgm/cm². In the same figure curve A shows the effect due to depression. The latter curve is drawn from Bothe's theory as given by Tittle (1951) and is normalised at a thickness of 289.2 mgms/cm² of the stack. Normally curve C contains both the depression and the self-protection effects. Therefore, the difference-curve B should give only the self-protection effect. But as is clear from the figure 2, both curves B and C fall with in the statistical fluctuation of the experimental points. These readings were also re-

peated for silver foils with the same area. From these two sets of readings the curve B seemed to obey a semi-empirical relation.

$$\frac{\text{Disintegration rate of the foil for thickness } x}{\text{Disintegration rate of the foil for zero thickness}} = 1 - K\sigma_a N$$

where N is the total number of nuclei per cm^2 of the foil of thickness x , σ_a is the absorption cross-section for thermal neutrons and K is a constant having the value 0.47 ± 0.03 . The correction due to this effect for indium is about 5%. When taken into account, this should introduce little error in the value of the activation cross-section.

The errors discussed in the last two paragraphs are calculable and in the measurement of $\sigma(n, \gamma)$ for most of the case, as reported in the literature, they have not been applied. The application of these errors, and also the use of different values of μ_m for various β -particles in a radioactive isotope, are expected to give us somewhat better results.

The above procedure gave the thermal neutron activation cross-section for In^{115} as 134.7 ± 10 barns. The half-life of In^{116m} measured is 53.3 minutes. For Ag^{107} and Ag^{109} the values of σ_{act} measured are 45.7 ± 4.5 barns and 113.5 ± 13 barns respectively. The half-lives measured for Ag^{108} and Ag^{110} are 2.2 minutes and 24.2 seconds respectively.

ACKNOWLEDGMENTS

The author wishes to express his sincere gratefulness to Professor P.S. Gill for his continuous help and guidance in this work. The author is also thankful to Dr. H. S. Hans for the helpful discussions and valuable suggestions during the course of this work. The support of the Union Education Ministry for the grant of a Senior Research Scholarship is thankfully acknowledged.

REFERENCES

- Amaldi, E. *et al.*, 1935, *Proc. Roy. Soc. (London)*, **149**, 522.
- Bothe, W., 1943, *Z. Physik*, **120**, 437.
- Enk, A., 1936, *Phys. Rev.*, **50**, 738.
- Hughes, D. J., 1953, *Pile Neutron Research*, pp. 186 and 22.
- Kloma E. D. and Ritchie, R. H., 1952, *Phys. Rev.*, **87**, 167.
- Kunstadter, J., 1950, *Phys. Rev.*, **78**, 484.
- Marshak, R. E., 1947, *Phys. Rev.*, **71**, 443.
- O'Neal, R. D. and Goldhaber, M., 1941, *Phys. Rev.*, **59**, 102.
- Plumber, R. C. and Lewis, J. E., 1955, *Nucleonics*, **13**, 8, 42.
- Rasotti, F., 1940, *Phys. Rev.*, **58**, 869.
- Rush, J. H., 1948, *Phys. Rev.*, **73**, 271.
- Seron, L. *et al.*, 1947, *Phys. Rev.*, **72**, 888.
- Slatin, H. *et al.*, 1950, *Phys. Rev.*, **78**, 498.
- Tittle, C. W., 1951, *Nucleonics*, **8**, 6, 5.
- Tittle, C. W., 1951, *Nucleonics*, **9**, 1, 60.

RAMAN SPECTRA OF FROZEN SOLUTIONS OF SOME MONOSUBSTITUTED BENZENE COMPOUNDS IN ETHYL ALCOHOL

G. S. KASTHA

OPTICS DEPARTMENT, INDIAN ASSOCIATION FOR THE CULTIVATION OF SCIENCE,
JADAVPUR, CALCUTTA

(Received for publication September 18, 1957)

Plate XVII

ABSTRACT Investigations on the Raman spectra of ethyl benzene, chlorobenzene and bromobenzene in solutions of ethyl alcohol in the frozen state at -180°C have been carried out and it has been observed that in the case of the last two compounds when the solutions form transparent homogeneous masses, the low-frequency lines exhibited by the pure crystals disappear completely. In the case of frozen 80% and 35% solutions of ethyl benzene, these discrete lines are replaced by a continuous band extending up to 93 cm^{-1} from the Rayleigh line. It has been further observed that when the strength of the chlorobenzene solution is increased from 25% to 40% the frozen mass becomes opaque and the low-frequency lines appear with their intensities with respect to the molecular Raman lines the same as in the spectrum due to the pure crystals. From these results it has been concluded that at the 40% concentration the molecules form small groups which produce the low frequency lines and that as all the molecules cannot be precipitated as crystallites the new lines are not due to such crystallites. In the case of the ethyl benzene solution, such groups contain molecules of both the constituents. It is further pointed out that in the case of the 10% solution of bromobenzene, the concentration being low, all the molecules are present as single molecules, and since the low-frequency Raman lines are absent in this case, these lines are produced only by groups of molecules.

INTRODUCTION

From recent investigations on the Raman spectra of benzene and toluene in frozen solutions of ethyl alcohol and other aliphatic solvents at -180°C (Kastha, 1956) it was observed that the low-frequency Raman lines exhibited by crystals of pure benzene appear with unchanged frequency-shifts and undiminished intensities, but the low frequency lines observed in the spectrum of pure toluene in the solid state at low temperature are replaced by a moderately strong band of frequency-shift 95 cm^{-1} in the case of frozen 81% solution in ethyl alcohol. Further, when the strength of the solution is reduced to 35%, this band is transformed into a weak continuous wing extending up to 95 cm^{-1} .

These results indicate that the nature of the influence of environment is different for benzene and its methyl derivative. It was observed by Ray (1951) that the number and frequency-shifts of low frequency Raman lines exhibited

by ethyl benzene in the solid state at -180°C were almost identical with those observed in the spectrum of toluene crystals at the same temperature, while from a comparison of the Raman spectra of chlorobenzene (Ray, 1950) and bromobenzene (Biswas, 1955) it was pointed out by Biswas (1955) that the number and frequency-shifts of the low-frequency Raman lines depend on the nature of the substituent atom in the benzene ring. It would, therefore, be interesting to find out how the low-frequency Raman lines exhibited by various substituted benzene compounds in the solid state are affected when they are dissolved in alcohol at -180°C . The results of such an investigation on the Raman spectra of chlorobenzene, bromobenzene and ethylbenzene have been reported in the present paper.

EXPERIMENTAL

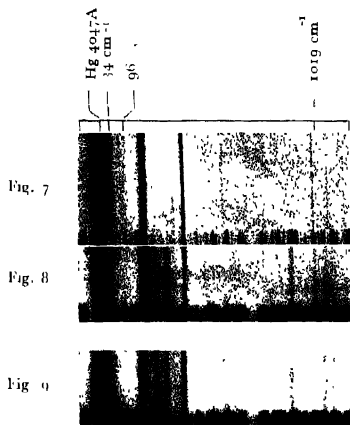
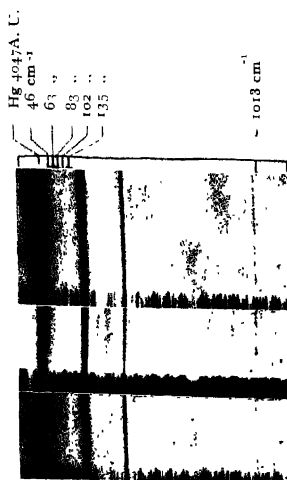
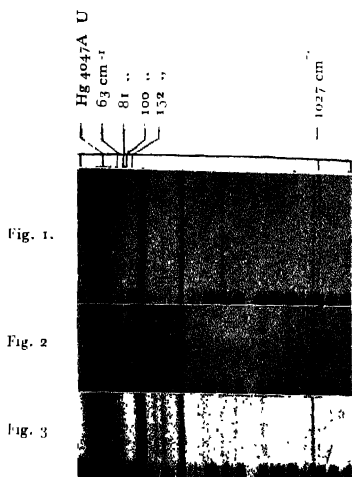
The liquids mentioned above were of chemically pure variety and were distilled under reduced pressure before use. Chemically pure ethyl alcohol used as the solvent was similarly distilled repeatedly to make it free from dust. Transparent homogeneous masses were obtained when 25% solution of chlorobenzene, 35% and 80% solutions of ethyl benzene and 10% solution of bromobenzene in alcohol were frozen and cooled to -180°C . The Raman spectra due to these transparent masses were recorded with the arrangement described earlier (Kastha, 1956). The spectra of the pure substances and of a 40% solution of chlorobenzene in the solid state at -180°C were photographed by the usual method. A Fuess glass spectrograph having a dispersion of 11 A.U./mm. in the region of 4047 A.U. and Ilford Zenith plates were used to photograph the Raman spectra. The time of exposures varied from 2 to 14 hours.

RESULTS AND DISCUSSION

Enlarged spectrograms due to ethyl benzene, chlorobenzene and bromobenzene in the solid state and in solutions of ethyl alcohol at -180°C are reproduced in figures 1–8, Plate XVII. The spectrum of ethyl alcohol in the frozen state at -180°C is given in figure 9, Plate XVII, for comparison.

(a) *Ethyl benzene* :

The Raman spectrum of ethyl benzene in the solid state at -180°C exhibits five low-frequency Raman lines at 48, 63, 81, 100 and 130 cm^{-1} , the intensity of the lines at 63, 81 and 100 cm^{-1} being the same as that of the molecular line at 1027 cm^{-1} (Ray, 1951). A comparison of the Raman spectrum of ethyl benzene in the solid state (figure 1) and frozen 80% solution at -180°C shows that the discrete lines observed in the spectrum of the pure crystals are replaced by a continuous wing extending up to 93 cm^{-1} from the Raleigh line with a band at about 88 cm^{-1} in the latter case. This band becomes extremely weak in the case of 35% frozen solution. A careful examination of the spectrogram due to



Raman spectra

Fig. 1. Ethylbenzene in the solid state at -180°C Fig. 2. 35% Soln. of $\text{C}_6\text{H}_5\text{C}_2\text{H}_5$ in EtOH at -180°C

Fig. 3. 80% " " " " " " " "

Fig. 4. Chlorobenzene in the solid state at -180°C Fig. 5. 25% Soln. of $\text{C}_6\text{H}_5\text{Cl}$ in EtOH at -180°C

Fig. 6. 10% " " " " " " " "

Fig. 7. Bromobenzene in the solid state at -180°C Fig. 8. 10% Soln. of $\text{C}_6\text{H}_5\text{Br}$ in EtOH at -180°C Fig. 9. Ethyl alcohol in the solid state at -180°C

frozen ethyl alcohol (figure 9) reveals that there is no such band in the vicinity of the Rayleigh line, and hence the bands observed in the cases of 35% and 80% frozen solutions are not due to alcohol molecules. Similar band was observed in the case of toluene dispersed in alcohol solution at -180°C (Kastha, 1956) which was assigned to vibrations in groups containing molecules of both alcohol and toluene. Therefore, it can similarly be concluded that the band at 93 cm^{-1} observed in the case of frozen 80% solution of ethyl benzene in alcohol may originate from vibrations in groups of complex molecules formed between ethyl benzene and alcohol molecules and the partial breaking up of these groups is responsible for the weakening of the band in the case of 35% solution. The disappearance of the discrete lines is evidently due to the dissolution of the groups containing molecules of ethyl benzene alone. The disappearance of the band at 88 cm^{-1} with increase of dilution up to 35% shows that the existence of more than one ethyl benzene molecule in the group containing molecules of both the constituents is necessary for producing the band, because at lower dilution the ethyl benzene molecules are separated from each other and the band disappears.

(b) *Chlorobenzene* .

Ray (1950) reported five new low frequency lines at 46, 63, 83, 102 and 135 cm^{-1} in the Raman spectrum of chlorobenzene in the solid state at -180°C . The intensity of these lines is greater than that of the molecular line at 1013 cm^{-1} . A comparison of the spectrum of the pure crystal (figure 4) with that due to a frozen 25% solution of chlorobenzene (figure 5) shows that the discrete lines observed in the spectrum of the pure solid are absent in the case of the frozen solution. When the concentration of the solution is increased to 40%, however, the prominent low frequency lines at 63, 83 and 102 cm^{-1} appear in the spectrum almost with the same intensity as in the case of the pure crystals (figure 6), although the light scattered from the upper half of the frozen mass was photographed. It is difficult to interpret this result on the assumption that crystals of pure chlorobenzene precipitated in the frozen 40% solution produced the low-frequency lines, because formation of glass at 25% concentration shows that at 40% concentration about 60% of the molecules remained in the solution. Hence it is to be concluded that at the higher concentration when the chlorobenzene molecules come closer together, very small groups are formed and it is these small groups and not crystallites which are responsible for the origin of the low-frequency lines. This particular result thus conclusively proves that those low-frequency Raman lines due to these substances in the solid state are produced by small groups of molecules.

(c) *Bromobenzene* :

Bromobenzene in the solid state at -180°C exhibits strong low-frequency lines at 34, 96 and 130 cm^{-1} and two feeble fluorescence bands at 22940 and 21380 cm^{-1} respectively (Biswas, 1955). The lines at 34 and 96 cm^{-1} are more intense

than the molecular line at 1019 cm^{-1} . It can be seen from the spectrograms due to the pure crystals and a frozen 10% solution of bromobenzene in ethyl alcohol reproduced in figures (7) and (8) that there is no trace of low-frequency lines in the spectra of the frozen solution though the weaker line at 1019 cm^{-1} has been recorded with appreciable intensity. The fluorescence bands at 22940 and 21380 cm^{-1} observed in the spectrum of solid bromobenzene at -180°C (Biswas 1955) are also found to be absent in the spectrum of the frozen solution. The fluorescence bands were believed to arise from the distortion of the ring itself in the solid state (Biswas, 1955). Such a distortion might result from the formation of virtual bonds amongst neighbouring molecules in the solid state at -180°C . The disappearance of the bands in solution probably indicates that the distortion of the rings is removed because of the breaking up of these links. Incidentally, it may be pointed out that the non-appearance of the low-frequency lines in the spectrum of the frozen 10% solution may be accounted for by assuming that the groups responsible for the appearance of the low-frequency lines break up completely in the frozen solution. In a 10% solution there is very little likelihood of the existence of groups of bromobenzene molecules and, therefore, the single molecules dispersed in the rigid glass do not produce any low-frequency Raman lines as in the case of chlorobenzene discussed above.

Thus all the results obtained in the case of the three mono-substituted benzene compounds mentioned above point to the fact that the low-frequency Raman lines exhibited by the crystals of these substances at -180°C are due to oscillations in groups of associated molecules and not due to any vibration in the lattices of the respective crystals.

ACKNOWLEDGMENT

The author's thanks are due to Professor S. C. Sankar, D.Sc., F.N.I. for his kind interest and helpful suggestions during the progress of the work.

REFERENCES

- Biswas, D. C., 1955, *Ind. J. Phys.*, **29**, 503.
Kastha, G. S., 1956, *Ind. J. Phys.*, **30**, 313.
Ray, A. K. 1950, *Ind. J. Phys.*, **24**, 131;
1951, *Ind. J. Phys.*, **25**, 111.

ON THE STRUCTURE OF ALPHACELLULOSE AND HOLOCELLULOSE OBTAINED FROM JUTE FIBRES

S. K. CHOWDHURY

TECHNOLOGICAL RESEARCH LABORATORIES, INDIAN CENTRAL JUTE COMMITTEE,
TOLLYGUNGE, CALCUTTA

(Received for publication, June 5, 1957)

Plate XVIII

ABSTRACT The structure of alphacellulose obtained from jute fibres by the modified American Chemical Society's method has been determined. Hologellulose from jute fibres and holocellulose treated with 9.3 per cent NaOH solution to remove about 93% hemicelluloses also have been studied by X-rays. It has been observed that alphacellulose, by the very method of its extraction from jute fibres, gives a typical cellulose II diagram. Unlike hydrated jute fibres this hydrate transformation is complete. The dimensions of the unit cell of this alphacellulose from jute are $a = 8.06 \text{ \AA}$, $b = 10.3 \text{ \AA}$, $c = 9.02 \text{ \AA}$ and $\beta = 62^\circ 30'$. This structure of alphacellulose is quite different from that of hydrated jute fibres. This difference has been ascribed to the lignin present in jute fibres. On the other hand, the structure is very similar to that of hydrated cellulose obtained from cotton and ramio fibres by previous workers. In purity this alphacellulose from jute fibres is of very high order. The diffuse ring passing through the (002) reflection of jute diagram which is due to lignin, is not visible in the pattern due to holocellulose. The X-ray diffraction pattern due to holocellulose treated with 9.3 per cent NaOH solution is very clear and sharp and the (101), (101) reflections are clearly resolved. The composite nature of these reflections and the imperfections of crystallinity of raw jute fibres has been ascribed partly to the presence of hemicelluloses.

INTRODUCTION

Jute fibre is obtained from the inner bark of two species of jute plants *C. capsularis* (white jute) and *C. olitorius* (tossa jute). The plant tissues are built up of cells enclosed within strong cell-walls.

The most important constituents of the mature cell-wall of jute fibre are cellulose, hemicelluloses and lignin and they remain in closest association in the fibres. Lignin has got a stiffening effect on the wall as a whole.

The cellulose proper or alpha-cellulose with hemicelluloses forms the cellulosic frame-work of jute fibres and is called holocellulose. Some other constituents e.g., fat wax, nitrogenous, colouring and mineral matter giving ash, are also present in small amounts.

The average composition of jute fibre has been determined by a large number of workers, but the most recent one is that of Sarker *et al.* (1948) and may be given as follows (on over-dry basis) :

Alpha-cellulose	...	50.7 to 60%
Hemicelluloses		
(Ash and nitrogen free)	...	27.8 to 31.5%
Lignin (Ash free)	..	10.3 to 13.8%
Protein matter	...	1 to 2.8%
Fat and wax (including		
extractible colouring matter)	...	0.5 to 1.6%
Ash	...	0.4 to 1.6%

Alphacellulose, the chief constituent of jute fibres is chemically very similar in all essentials to cotton and ramie cellulose on whose structure and properties an extensive work has been done.

It was first pointed out by Banerji and Ray (1941) that the structure of cellulose in raw and delignified jute fibre is exactly the same. Later Sirkar and Chowdhury (1946) observed that when lignin is partially removed from jute fibre, the faint ring passing through the (002) reflection becomes much weak. They also observed that some of the diffraction spots become sharper indicating a change in the micellar size with bleaching of jute fibres. Sen and Hermans (1949) using monochromatic X-rays, CuK radiation, studied the pattern due to holocellulose and alphacellulose prepared from jute fibre by the method of Sarker *et al.* (1948) and found that the ring through the (002) reflection did not disappear completely. They concluded that this ring was partly due to disoriented cellulose. Since these results are not in agreement with those reported by Sirkar and Chowdhury (1946) that the ring through the (002) reflection of jute fibre diminishes considerably in intensity when the fibre is partially delignified, it was thought worth while to reinvestigate the diffraction pattern of holocellulose, holocellulose treated with 9.3% NaOH solution and alpha cellulose obtained by the method of Sarker *et al.* (1948).

EXPERIMENTAL

According to the method of Sarker, Mazumder and Pal (1948) clean jute fibres free from bark were cut into small pieces ($\frac{1}{2}$ ") and extracted in a Soxhlet with alcohol-benzene (1:1) for six hours. Samples were then air-dried. Holocellulose was prepared by treating the above sample with 0.7% sodium chlorite (Textone) with acetic acid on boiling water bath for two hours (1:50). For complete oxidation the fibres were frequently stirred with a glass-rod. The samples were then washed with water and then with sulphur dioxide solution, and then again with water until acid free. Holocellulose thus prepared was then treated

with 9.3% NaOH solution, which removed about 93% of hemicelluloses. For the preparation of alpha-cellulose, holocellulose was triturated with 17.5% NaOH solution (W/W) in the cold in a mortar, liquor ratio 1 : 25. The samples were spread in the mortar and half the calculated amount of NaOH solution was added and triturated for 5 minutes. The remaining half was then added in four equal instalments in ten minutes, the trituration being continued all the time. The mixture was then allowed to stand for thirty minutes after which an equal amount of water was added. The whole was then filtered in a glass-filter. The samples were then washed gradually with NaOH solution of decreasing strength 5%, 2%, 1% etc. and were then made alkali free by washing with water. Then they were treated in the cold with 10% acetic acid for some time, washed with water and finally with hot water until free from acid.

Alpacellulose thus prepared lost its fibrous form. X-ray diffraction photographs of holocellulose, holocellulose treated with 9.3% NaOH solution and that of alphacellulose were taken in a flat-film type camera with a very narrow slit of bore diameter 0.2 mm and of length 5 cm. In the case of holocellulose treated with 9.3% NaOH solution the fibres were made parallel with extreme difficulty yet the parallelism was not perfect but alpha-cellulose was practically in form of powder. Nickel filtered CuK radiation from a Hadding type X-ray tube was used. The specimen size, exposure time and photographic technique were maintained uniform for all the samples as far as practicable. The tube was run at 45 K V., 5 m a. The samples were intimately mixed with aluminium powder, so that sample to film distance could be measured very accurately from the Al-lines. The relative humidity while taking the photographs varied from 65% to 78%.

RESULTS AND DISCUSSION

X-ray diffraction photographs are reproduced in Plate XVIII. In the case of alpha-cellulose obtained from jute fibres the spacings of the reflecting planes (101), (101) and (002) as identified are given in Table I, along with those obtained by Audreess (1929) for dry hydrated cellulose and hydrated jute by Sirkar and Saha (1947). The dimensions of the unit cell in alpha-cellulose were determined from the relation,

$$d_{hkl} = \left(\frac{h^2}{a^2 \sin^2 \beta} + \frac{l^2}{c^2 \sin^2 \beta} - \frac{2hl \cos \beta}{a.c. \sin^2 \beta} + \frac{k^2}{b^2} \right)^{1/2}$$

where h, k, l are the Miller indices of the planes, d_{hkl} = spacing of (hkl) planes,

a, b and c are the axial lengths and β is the angle between a and c axes. The values of a, b, c and β obtained are shown in Table I.

For the reflections due to other planes the relation

$$\frac{4 \sin^2 \theta}{\lambda^2} = \left[.0203h^2 + .0162k^2 - .0178hl + .00943k^2 \right] \times 10^{16}$$

has been found to be satisfied.

TABLE I

Spacing of 101, 10 $\bar{1}$ and 002 reflections of hydrated cellulose, hydrated jute and alphacellulose with the corresponding dimensions of the unit cell

	Hydrated cellulose dried (Andress)	Hydrated jute (Sarkar and Saha)	Alpha cellulose from jute (Present author)
101	7.52 Å	7.96 Å	7.20 Å
10 $\bar{1}$	4.45 Å	4.42 Å	4.40 Å
002	4.03 Å	4.03 Å	4.00 Å
(a)	8.14 Å	8.80 Å	8.06 Å
(b)	10.30 Å	10.30 Å	10.30 Å
(c)	9.14 Å	9.50 Å	9.02 Å
β	62°	57°-54'	62°-30'

Study of the X-ray diffraction photograph (Plate XVIII, figure 4) and the spacings of the (002), (101) and (10 $\bar{1}$) reflections (Table I) clearly indicate that alphacellulose gives a typical cellulose II diagram. It is also seen that this hydrate transformation is complete and the structure of alphacellulose, as shown in Table I, is very similar to that of dried hydrated cellulose (Andress, 1929). It may be concluded that alphacellulose from jute fibre becomes an allotropic modification of cellulose due to its very method of preparation. It is comparable, if not exactly the same, in purity with pure cellulosic fibres. It is also interesting to note that this structure of alphacellulose from jute fibres, differs from the structure of hydrated jute fibres, as determined by Sirker and Saha (1947). This difference may be mainly due to the presence of lignin and partly due to the presence of that portion of hemicelluloses which cannot be completely removed from jute fibres without removing lignin.

It thus appears that alphacellulose, studied by Sen and Hermans, was not really alphacellulose, because they did not observe such a change in the structure and also crystallinities were found to be highly oriented along the fibre axis, whereas in the present investigation almost a powder pattern is obtained. The

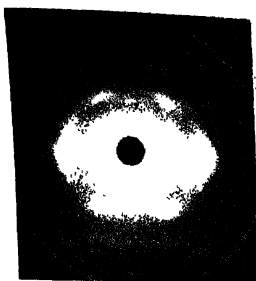


Fig. 1.

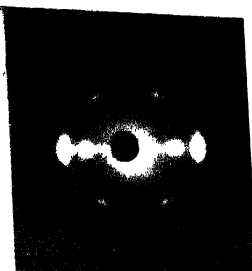


Fig. 2.

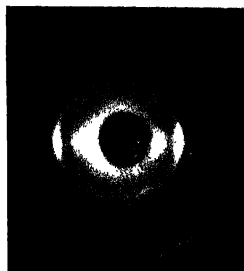


Fig. 3

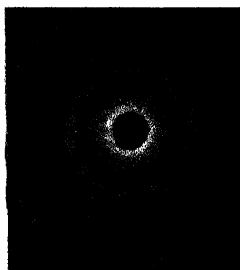


Fig 4.

X-ray diffraction photographs taken in a flat-film camera.

Fig. 1. Raw jute fibres mixed with Al-powder

Fig. 2. Holocellulose.

Fig. 3. Holocellulose treated with 9.3 % NaOH solution. Fibre mixed with Al-powder.

Fig. 4. Alpha-cellulose mixed with Al-powder.

pattern due to holocellulose (Plate XVIII, figure 2) shows that the structure is the same as in raw jute fibre having a monoclinic unit cell with $a = 8.35 \text{ \AA}$, $b = 10.3 \text{ \AA}$ (fibre-period), $c = 7.9 \text{ \AA}$ and $\beta = 84^\circ$ and the space group is P_{21} . The ring through the (002) reflection is not visible, so it can be concluded that this ring is mainly due to lignin. On the other hand, when holocellulose is treated with 9.3% NaOH solution to remove about 93% of hemicelluloses the X-ray diffraction photograph (Plate XVIII figure 3), a cellulose I diagram, becomes very clear and sharp, comparable to ramie diagram. (101) and $(\bar{1}01)$ reflections are also resolved, and this is not observed in the diffraction pattern of holocellulose. So this composite nature of 101 and $\bar{1}01$ reflections of jute X-ray diagram may be partly due to the presence of hemicelluloses. It is more probable as pointed out by Astbury, Preston and Norman (1935) that the imperfections of crystallinity in bast fibres are largely due to the incorporation within the cellulose crystallites some portion of hemicelluloses in a state of mixed crystallisation.

ACKNOWLEDGMENTS

The author is deeply grateful to Prof. S. C. Sirkar, D.Sc., F.N.I. for his generous advice and helpful discussions during the progress of the work. He is also indebted to Dr. P. B. Sarker, D.Sc., F.N.I., Director of the Institute and Dr. R. K. Sen, D.Sc. for their keen interest in the work. Thanks are also due to Mr. K. B. Pal for his assistance in the chemical treatments.

REFERENCES

- Andross, K. R., 1929, *Z. Phys. Chem. B*, **4**, 190.
 Astbury, Preston and Norman, 1935, *Nature*, **136**, 391.
 Banerjee K. and Roy A. K., 1941, *Proc. Nat. Inst. Sci. India*, **7**, 377.
 Sarker P. B., Mazumder A. K. and Pal K. B., 1948, *J. Textile Inst.*, **39**, T 49.
 Sirkar, S. C. and Chowdhury S. K., 1946, *Ind. J. Phys.*, **20**, 31.
 Sirkar S. C. and Saha N. N., 1947, *Proc. Nat. Inst. Sci. India*, **13**, 1.

Letters to the Editor

The Board of Editors will not hold itself responsible for opinions expressed in the letters, published in this section. The notes containing reports of new work communicated for this section should not contain many figures and should not exceed 500 words in length. The contributions must reach the Assistant Editor not later than the 15th of the second month preceding that of the issue in which the Letter is to appear. No proof will be sent to the authors.

11. SPACE GROUP OF ANTHRONE

S. N. SRIVASTAVA

PHYSICS DEPARTMENT, ALLAHABAD UNIVERSITY.

(Received for publication September 27, 1957)

Anthrone ($C_6H_4COC_6H_4CH_2$) is crystallised from a solution in ethyl alcohol. From goniometric measurements it is found to have faces developed very similar to anthraquinone and was found practically isomorphous with anthraquinone. From rotation photographs about three crystallographic axis it was found to be monoclinic with the following axial lengths and angle.

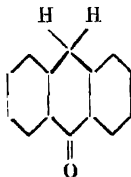
$$a = 15.56 \text{ A.U.}$$

$$b = 3.98 \text{ A.U.}$$

$$c = 7.84 \text{ A.U.}$$

$$\beta = 101^\circ 40'$$

The density of anthrone is 1.33 gms/c.c. and the molar weight is 194 and the number of molecules calculated in the unit cell is two. The melting point of anthrone is 153°C . The structural formula is as given below.



Rotation and Weissenberg photographs about all the three axes were taken. From the Weissenberg photographs of $k = 0$, $l = 0$, $h = 0$ were revealed the two systematic absences.

- (1) In $h0l$ reflection h odd absent, showing glide along a axis
- (2) In $0k0$ reflection k odd absent showing screw axis along b axis.

The space group that corresponds to these absences is $P2_1/a$. As there are two molecules per unit cell, this space group requires that there should be the molecular centre of symmetry. The structural formula, however, shows that the molecule can have no centre of symmetry. So there might be two possibilities :

(1) One of these systematic absences is spurious. Since $0k0$ reflections are much fewer than $h0l$ planes it is more natural to expect that this may be spurious and the space-group is Pa . (2) The axial length is double (7.96 A.U.) so that a unit cell contains 4 molecules instead of 2, and the space group is $P2_1/a$ as indicated above. The two possibilities as detailed above are being more critically examined.

REVIEW

PHYSICOCHEMICAL CALCULATIONS

E. A. GUGGENHEIM AND J. E. PURE

This volume, unlike most other publications of a similar nature, is more than a mere physicochemical data book. In each section the authors have given due emphasis on the practical handling of experimental data in a lucid manner. Procedures for calculations have been discussed on a theoretical basis, followed by actual calculations using the experimental data available in literature, due attention being given to the units. This is followed by a concise but critical discussion of the results and their correlation to other work reported in literature. Original and relevant literature references have been cited all through, and graphical methods of evaluation have been illustrated with neat diagrams. In the Introductory portion the authors have nicely presented the inter-relationship between the various units of measurement and the conversion from one scale to another. This book will be of great help to those workers who might have to start work in a field not quite familiar to them. The entire classification has been subjectwise and includes the various problems connected with atomic and molecular weights, Avagadro's number, molecular velocities, interatomic distances, moments of inertia, characteristic frequencies, electric moments and polarizabilities, entropies, heat capacities, equation of state, mixtures of non-electrolytes, electrolytic solutions, conductance and diffusion of electrolytes, gaseous equilibria, chemical equilibria involving solids, solution equilibria, acid-base equilibria, general electrolytic equilibria, solid surfaces, liquid surfaces, gas mixtures, solution kinetics, and radioactivity.

P.R